www.dmu.ac.uk
DE MONTFORT UNIVERSITY
LEICESTER • BEDFORD • MILTON KEYNES

Faculty of Computing Sciences and Engineering
Leicester

COMPUTER AIDED ANALYSIS AND DESIGN OF A NEW SERVO CONTROL FEED DRIVE FOR ELECTRO DISCHARGE MACHINING USING PIEZOELECTRIC ULTRASONIC MOTOR

Mahmoud Shafik Hassan Abd Alla

PH.D. THESIS

2003

DE MONTFORT UNIVERSITY

FACULTY OF COMPUTER SCIENCES AND ENGINEERING

DEPARTMENT OF ENGINEERING AND TECHNOLOGY

The undersigned hereby certify that they have read and recommend to the Faculty of Graduate Studies for acceptance a thesis entitled **"Computer Aided Analysis and Design of a New Servo Control Feed Drive for Electro Discharge Machining Using Piezoelectric Ultrasonic Motor"** by **Mahmoud Shafik Hassan Abd Alla** in partial fulfilment of the requirements for the degree of **Doctor of Philosophy.**

Dated: **January 2003**

External Examiner: _____

Dr Perry Armstrong
Queens University
Belfast

First Supervisor: _____

Professor Jeffery G A Knight
De Montfort University
Leicester

Second Supervisor: _____

Professor Philip Moore
De Montfort University
Leicester

Examining Committee: _____

Dr J Pu
DeMontfort University
Leicester

DE MONTFORT UNIVERSITY

FACULTY OF COMPUTER SCIENCES AND ENGINEERING

DEPARTMENT OF ENGINEERING AND TECHNOLOGY

Date: **January 2003**

Author: **Mahmoud Shafik Hassan Abd Alla**

Title: **Computer Aided Analysis and Design of a New Servo Control Feed Drive for Electro Discharge Machining Using Piezoelectric Ultrasonic Motor**

Faculty: **Computer Sciences and Engineering**

Degree: **Ph.D.** Convocation: **January** Year: **2003**

Permission is herewith granted to De Montfort University to circulate and to have copied for non-commercial purpose at its discretion, the above title upon the request of individuals or institutions.

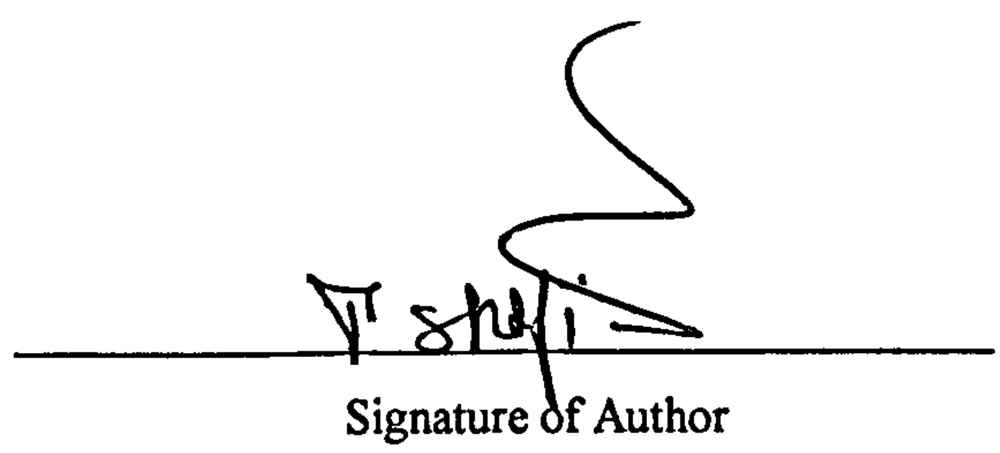

Signature of Author

ABSTRACT

Keywords: *Servo Control, Piezoelectric Ultrasonic Motor, Ultrasonic Motor Modelling and Analysis, Ultrasonic Motor Drivers, Finite Element Analysis, Design for Servo Control, Electro Discharge Machine, Electro Discharge Texturing.*

The thesis presents an innovative servo control feed drive that uses piezoelectric ultrasonic motor (USM). It demonstrates its validation on two industrial applications, Electro Discharge Machine (EDM) and Electro Discharge Texturing (EDT). This servo control feed drive introduces a new generation for EDM servo control system which extends the system capacities to include a fast dynamic response, a stable machining process, a more accurate machining, reduced arcing-short circuiting process, and improved surface profiles.

The major aim of this investigation was to develop an advanced servo control feed drive using piezoelectric USM technology. The objectives were to (1) develop a piezoelectric USM, (2) design and build a piezoelectric drive for the USM, (3) develop a control unit using piezoelectric USM technology for EDM applications, so as to enhance the inter-electrode gap control, (4) conduct an experimental test for the servo control system in both EDM and EDT, and (6) investigate the influence of the piezoelectric USMs systems technology in a servo control drive in comparison to current servo drive systems.

The developed servo control feed drive system composed of a number of components include, hardware design, a computer aided design (CAD) solid modelling system, finite element analysis, digital analogue design, power electronics, computer simulation and modelling using various packages including ANSYS, ALGOR, VIEWLOGIC and VHDL.

The development process for this servo control system passed through four major stages: Firstly, a linear piezoelectric USM using a single flexural vibrating bar was developed. A methodology for modelling and analysis using finite element analysis was

established and this was used successfully in the design process. A series of experimental test and analysis for the developed prototype was carried out. Secondly, a piezoelectric electronic drive for the USM was developed. The procedure for the design, structure, principle of operation, design and analysis of the main units of the drive was discussed. Thirdly, a servo control unit using piezoelectric USM technology was designed and built. The intention was to add new features to improve the EDM system capability for monitoring, controlling the machining process and inter-electrode gap at high level of precision. Finally, a further development to the developed servo control feed drive was carried out.

The developed servo control system was examined and evaluated using two industrial applications, EDM and EDT. The initial results showed improvements compared to other existing control systems. There was a notable improvement in the dynamic response, stability of the machining, surface finish of products, observable reduction in arcing-short circuiting process and a reduction in the processing time. This demonstrates the influence of piezoelectric USM technology in this field of EDM machining. A resolution of 50 micrometers and response time on the order of 100 microseconds were reached. A significant reduction in the size of the system was also successfully obtained.

ACKNOWLEDGEMENTS

It is my pleasure to have this opportunity to present my deepest thanks and my sincere appreciation to my supervisor Professor Jeffery A G Knight, Dean of the Faculty of Applied Sciences for giving me the opportunity to conduct research in such interesting area and for his professional supervision, constructive discussions and guidance throughout the progress of this research work.

My sincere appreciation goes to Professor Hassan S H Abdalla, Head of Department of Design & Management and Communications and leader of the Global Concurrent Engineering Research Group who guided and supports me throughout the progress of this research work.

All my thanks go to Professor R Bansevicius for his guidance, support, help and constructive discussion throughout this research work. All my thanks also go to Professor M S Ahmed, Chief Executive of Smart Technology Ltd, for his valuable ideas, guidance and help.

I would like particularly to thank Professor Philip Moore, Dr. R J Nash and Dr Sarah V. Hainsworth for their valuable support, constructive discussions and encouragement throughout preparing the material of this thesis.

I would like to express particular thanks for Miss YuFang Cheng, Mr. Alexander Smith, Mr. Colin Taylor, Dr. A M Ahmed, Dr. Esam Shehab, Mr. M. Khalifa, Dr. Neil Anderson, Mr. W El-Ganzoury, Mr. Kevin, Mr. Robert Burdett, Mr. John Maginty, Mr. Paul Dean, Mr. Keith Nocton, Mr. Keith Harrop, Mr. Paul Sasoo, Mr. Trevor Woolfoll, Mr. Mark Davies, Mr. Calvin English, Mr. Rod Copell and Mr. Tim O'mara for their help during the time of my research.

Finally, I would like to present particular wishes and sincere appreciation for my parents, Professor. Mohammed Shafik, Eng. Osama Shafik, Dr. S. Fekkai and all my family.

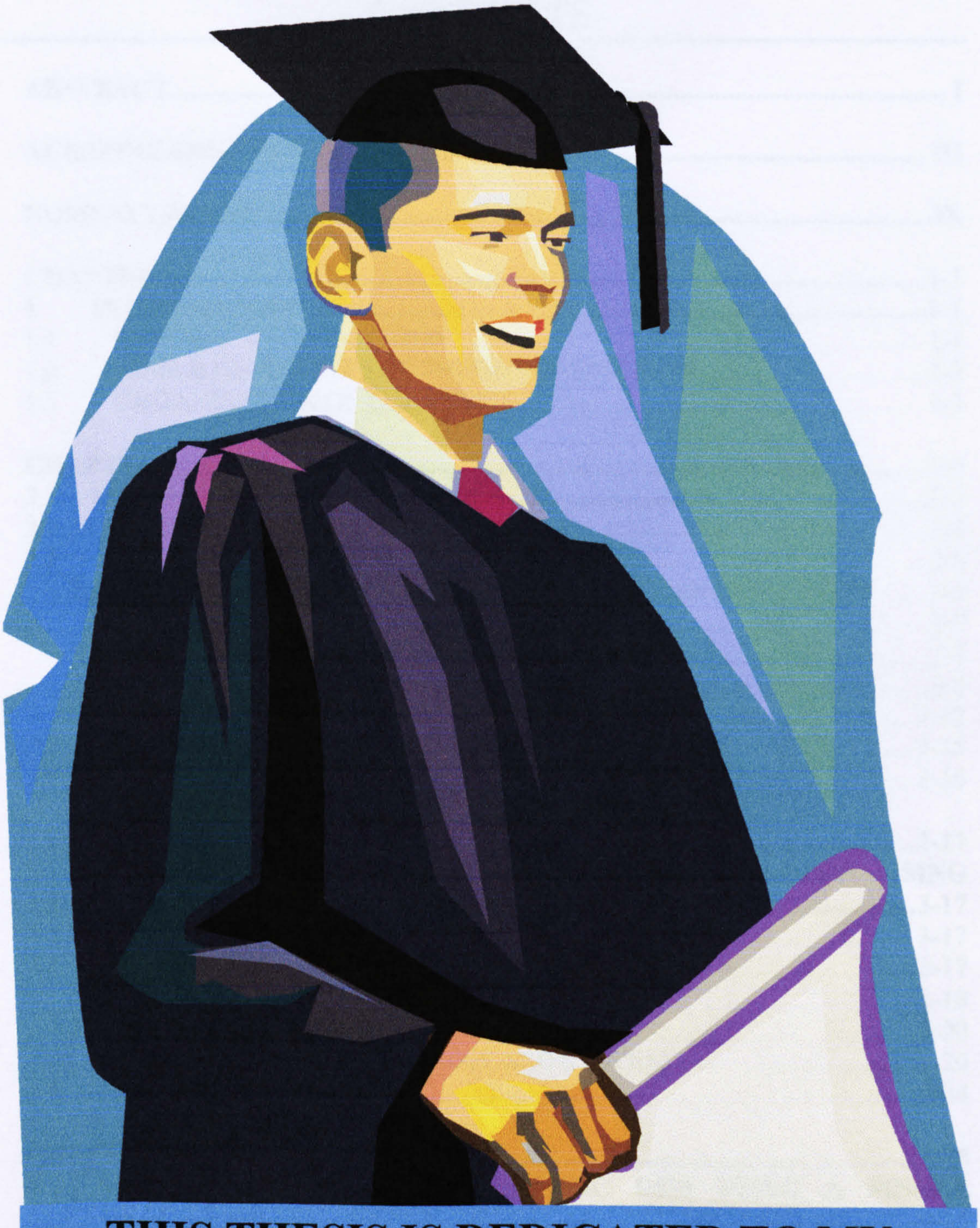

THIS THESIS IS DEDICATED TO MY PARENTS WHOM TAUGHT ME HOW TO BE OBJECTIVE, MOTIVATED AND RESPECTABLE

CONTENTS

NOMENCLATURE

Acronyms

A/D	**Analogue/Digital**
ANSYS	**FEA simulation package**
ASEN	**Antisensitivity**
BF, BFE, BFUNIF-ANSYS	**Commands for converting nodal load to element load**
CAD	**Computer Aided Design**
Ch1	**Channel one**
Ch2	**Channel two**
CONTAC49	**ANSYS Finite Element**
CTS	**Certain piezo-ceramic material**
D, F=ANSYS	**Commands for determination of nodal DOF**
D/A	**Digital/Analogue**
DC	**Direct Current**
DENS	**Density**
DOF	**Degree of freedom**
EDM	**Electro Discharge Machine**
EDT	**Electro Discharge Texturing**
EMM	**Electromagnetic Motor**
Ex	**Young's Modulus**
FEA	**Finite Element Analysis**
FNNC	**Fuzzy Neural Network Controller**
FNNI	**Fuzzy Neural Network Identifier**
FNN's	**Fuzzy Neural Network**
Fp	**Flushing pressure**
Ig	**Gap current**
KEYOPT	**Key option of ANSYS finite element**
KHz	**Kilo Hertz**
KN	**ANSYS contact stiffness**
LCC	**Inductance-Two capacitance**
LLCC	**Two inductance-Two capacitance**
LZT	**Lead-Zirconate-Titanate**

M.R.R	**Material removal rate**
NN	**Neural Network**
PC	**Personal Computer**
PERX, PERY, PERZ	**Arguments of MP command**
Pol	**Polarity**
PZT	**Piezoceramic transducer**
r.p.m	**Revolution per minute**
RF	**Radio Signal**
RNN	**Recurrent Neural Network**
S	**Switch**
SCU	**Servo Control Unit**
Sec	**Second**
SEN	**Sensitivity**
SF, SFE-ANSYS	**Commands for determination of surface loads**
SOILD72	**ANSYS Finite Element**
SOILD98	**ANSYS Finite Element**
Tb	**Prepulse current**
TTL	**Transistor-Transistor-Logic**
TW	**Sparking time**
U(t)	**Electric signal**
USM	**Ultrasonic Motor**
Vg	**Gap voltage**
Vol. Wear	**Volumetric wear**
Vp-p	**Voltage amplitude peak to peak**

Symbols

d_{31}-Transverse piezoelectric module

d_{33}-Longitudinal piezoelectric module

E-Electric field strength

f-Frequency

V-Volt

I- Current

k-Coupling coefficient

x, y, z-Axis label

t_1 and t_2 are Formation of discharge channel

t_3-Period duration which the discharge channel is in existence

t_4- Implosion of the discharge channel

t_5- De ionisation of the discharge channel

t_d-Initial delay until the resistance of the dielectric fluid is overcome

t_e- Period of discharge

$t_{0\min}$-Minimum pulse interval that allows sufficient de-ionisation to prevent arcing

t_i-Duration of energy pulse

$t_{p\min}$-Minimum cycle pulse (pulse time plus de ionisation)

τ-pulse ratio

$\bar{f}$-Resisting force

V_a-Average voltage

V_n-Open circuit voltage

f_s-Switching frequency

f_0-Resonant frequency

T_0- Maximum torque

V_T-Maximum voltage

$\bar{\tau}$-Instantanous torque

f_c-Pre-load pressing force

A_r -Torque factor

ϕ_c -Duration of contact

F_{real} -Real amplitude

F_{imag} -Imaginary amplitude

θ -Phase angle

F_e -Maximum amplitude of the exciting force

Ωm -Ohm meter

F -Force

T -Total torque

μ -Friction coefficient

d -Diameter of the shaft

R_a -Roughness

μ_s -Static Friction coefficent

μ_k -Kinetic Friction Coefficient

α - Angular acceleration in $rad/\sec^2$

Ω_v -Vibrational velocity of the stator

Ω_R -Angular velocity of the stator

C_d -Damped capacitance

R_d -Dielectric loss

L -Inductance

R -Resistance

C -Capacitance

P -Power

A_i -Current amplification factor

A_V -Voltage amplification factor

CHAPTER 1

1 INTRODUCTION

1.1 GENERAL INTRODUCTION

Servo control feed drives using DC servomotors have been known for more than a hundred years and have many applications in the areas of process and machine control. Machining and process control can be classified according to the level of precision and dynamic response as normal machining, precision machining, high precision machining and ultrahigh precision machining. It is understood that higher accuracy, finer resolution and fast dynamic response are essential for high precision manufacturing processes.

In the mid 1940s servo control feed drives using DC servomotor technology were implemented in Electro Discharge Machining (EDM) applications. EDM applications are classified as high precision machining. The main principle of operation of EDM is based mainly on a spark discharge between two conducting surfaces separated by a dielectric medium. The generated spark duration is on the order of microseconds and the inter-electrode gap size is of 10 to 100 micrometers. EDM is widely used in various applications including creating different complex and intricate shapes, slots, drilling holes, and cutting. It has also been implemented in surface texturing for more than twenty-five years [Shafik, M. and Knight, J. A. G., 2002, Shafik, M. et al., 2001, Simao, J., et al., 2001, Ahmed, M. S. and Knight, J. A. G., 1988]. Texturing is creating irregularities with regular or irregular spacing that tend to form patterns or texture on the surface. Texture contains roughness and waviness that can assist in providing the inherent quality of any subsequent paint finish, appearance and lifetime. Since the requirements of high precision and accurate machining of EDM applications never stops rising, much of the research has been concerned with the servo control feed drive level of precision and dynamic response. Certain authors have identified these problems [Behrens, et al., 2001, Jacob, T., 1999, Ro, and Hubbel, 1992]. Success in presenting a realistic solution to these problems has been limited. Thus there was a need to develop a new servo control feed drive using innovative technology that could provide high precision, fast dynamic response and robust stability.

Piezoelectric ultrasonic motor (USM) technology offers many opportunities in the field of high precision servo positioning control [Lin, F. J., et al., 2001, Izuno, Y., et al., 1998, Izuno, Y. and Nakaoka, M., 1996]. It has been used widely in both instrumentation and machine tool applications such as, EDM [Shafik, M. and Knight, J. A. G., 2002], EDT [Shafik, M., et al., 2001], micro-machining [Masuzawa, T., 2001], artificial prostheses [Ise, et al., 1991], auto focusing drives for single-lens reflex cameras [Hosoe, 1989], rotary supports for video cameras [Ise, 1989] and artificial heart actuators [Fukunaga, et al., 1989]. These applications show that piezoelectric USM servo control systems can be more effective than DC servomotor drives whenever high and ultrahigh precision level of control is required [Lin, F. J., et al., 2000, Izuno, and Nakaoka, 1990, Sashida, T. and Kenjo, T., 1993]. This is due to their high resolution, high stiffness, large output force, compactness and quick dynamic response despite their limited positioning ranges [Masuzawa, T., 2001, Lin, F. J., et al., 2000, Hoshi, and Kawamura, 1994, Ise, et al., 1991]. These distinctive features presented a challenge to design a new servo control feed drive using piezoelectric USMs technology to improve EDM servo control system degree of precision, dynamic response, performance and extend its capabilities to include more accurate machining.

1.2 AIMS & OBJECTIVES OF THIS INVESTIGATION

The main aim of this research work was to investigate and develop a new servo control feed drive using piezoelectric USM technology for use in the EDM system industrial applications. The objectives were to:

- Design and build a linear piezoelectric USM for the servo control feed drive.
- Design and build a piezoelectric drive to drive the motor.
- Design and build an advanced control unit for EDM applications using piezoelectric USM technology.
- Conduct a series of experimental test for the developed control system in both of EDM and EDT applications.
- Investigate the dynamic response and the stability of piezoelectric USM servo control system when compared with the existing EDM systems that use DC servomotors.

1.3 ORGANISATION OF THE THESIS

The reminder of this thesis is divided into eight chapters (see Figure 1-1).

Chapter 2 presents a critical literature survey of key publications, technical reports, and case studies, in related areas to the current research work.

Chapter 3 introduces the steps have been undertaken to fulfil the main aims and objectives of this research. It sets out the tools used in the system development.

Chapter 4 provides the development of a piezoelectric USM using a single flexural vibrating bar. The design procedure for this type of motor is discussed. A methodology for modelling and analysis is established. This was followed by series of experimental investigations into the developed prototype.

Chapter 5 sets out the development, of a piezoelectric drive for the USM. The intention was to design and build a piezoelectric drive that is able to provide the motor with the required operating paramters in a wide band of amplitude and frequency.

Chapter 6 describes the integration of the developed servo control system into an EDM system. The essential units required and modifications needed to conduct this integration are presented in this chapter. This concludes with an experimental examination of the system and main features can be obtained.

Chapter 7 demonstrates a series of experimental examination and evaluation of the developed servo control feed drive system in two industrial applications, EDM and EDT. This was included an investigation into dynamic response, stability of the control system, the capability to control and an investigation into surface profiles of the machined products. This was carried out using various electro-machining parameters, including level of the current, on-off time and duty cycle of the spark.

Chapter 8 sets out the general conclusions and discussions for this research work. It also gives the major contributions and limitations of the developed control system using piezoelectric ultrasonic motor.

Chapter 9 presents recommendations and future work. This is followed by a list of references of the current research work.

Appendix (A) provides short review covering properties of piezoelectric material, the key points considered in the established methodology of modelling and analysis, specifications of the finite element used in modelling and analysis of the proposed motor.

Appendix (B) provides the modified piezoelectric electronic drive using power MOSFETs and some of the essential electronic circuits that have been design and used during the examination and validation of the developed control system.

Appendix (C) gives an introduction to EDM industrial applications, EDM servo control system, main machining processes, the mechanical system dynamic response time and machining parameters

Appendix (D) illustrates some of the installation process of the developed system in both EDM and EDT system. Some photos illustrate the various conditions of machining for both systems are also presented. It also shows samples of the investigation carried out into the traditional drives using DC servomotor.

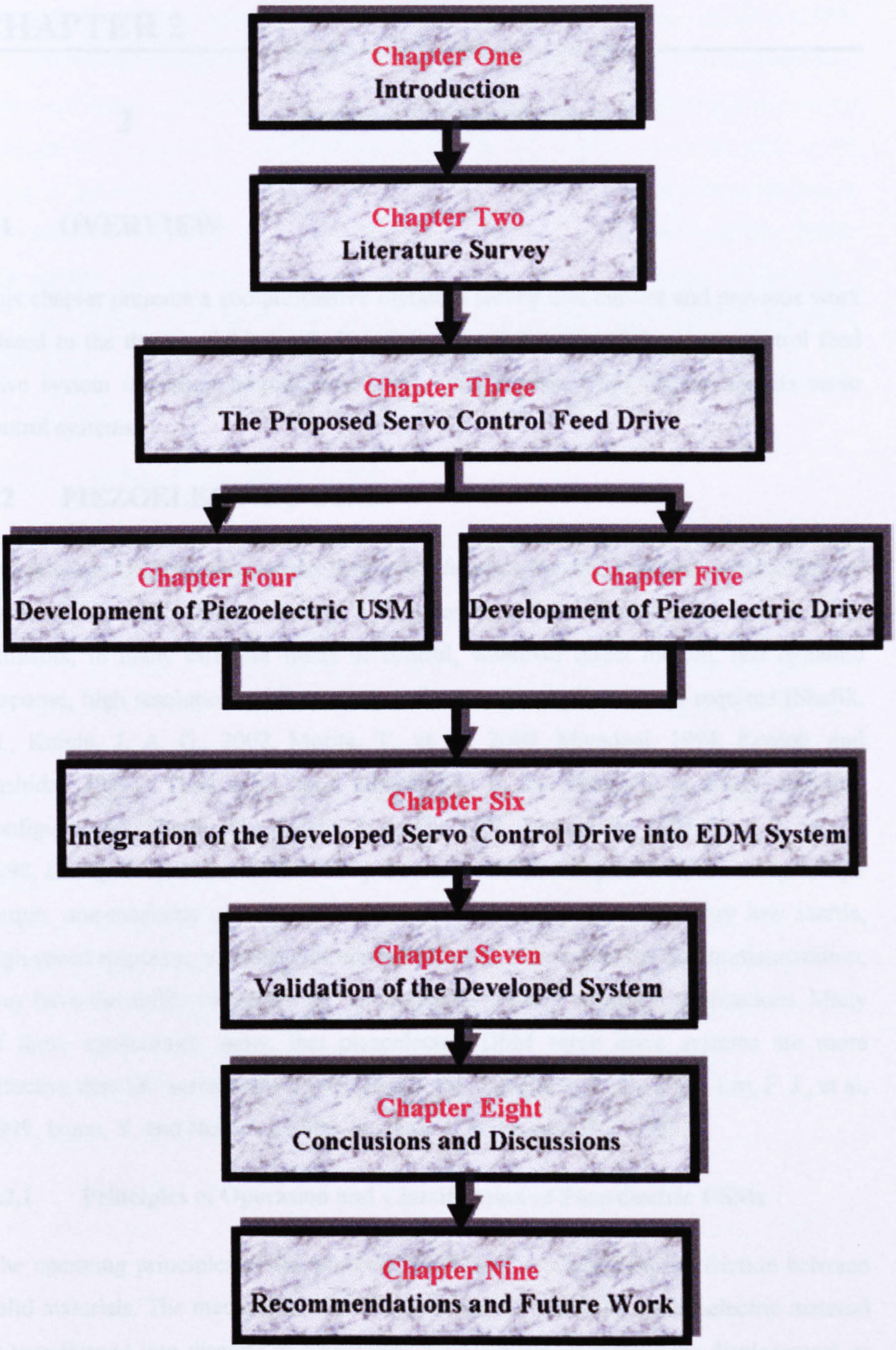

Figure 1-1 Structure and organisation of this thesis

CHAPTER 2

2 LITERATURE SURVEY

2.1 OVERVIEW

This chapter presents a comprehensive literature survey into current and previous work related to the theme of this work. It covers the components of the servo control feed drive system including piezoelectric USM, piezoelectric USM drivers and its servo control systems.

2.2 PIEZOELECTRIC USMs

Piezoelectric USMs present many distinctive features for direct motion control that are not available with other technology. This gives them the potential to be used as servo actuators, in many different fields of control, wherever direct motion, fast dynamic response, high resolution, stiffness, output force and compactness are required [Shafik, M., Knight, J. A. G., 2002, Morita, T., et al., 2000, Miyadani, 1994, Kenjoh, and Sashida, 1991]. They also have adaptability to be obtained in many different configurations [Shafik, M., Knight, J. A. G., 2001, Muralt, P., 1999, Koc, B., et al., 1998, Zhang, B. and Zhenqi, Z., 1997]. Because of their compact size, low weight, high torque, non-magnetic operation, freedom for constructional design, very low inertia, high-speed response, possibility of electromagnetic noise reduction and miniaturization, they have the ability to replace DC servomotors in many industrial applications. Many of these applications show, that piezoelectric USM servo drive systems are more effective than DC servomotor drives [Shafik, M., Knight, J. A. G., 2002, Lin, F. J., et al, 1999, Izuno, Y. and Nakaoka, 1996, Sashida, T. and Kenjo, T., 1993].

2.2.1 Principles of Operation and Classification of Piezoelectric USMs

The operating principles of the piezoelectric USMs are based on the friction between solid materials. The mechanical vibration generated by exciting a piezoelectric material is transformed into discrete or continuous displacement or force. This displacement or force is used to create motion in different forms, rotational, or linear or complex motion based on the friction between the piezoelectric material and material used for fabricate

the motor parts. Many different rules have been used to classify the piezoelectric USMs. They are typically classified according to the principles of operation, motor construction and motor functions [Uefa, S. and Tomikawa, Y., 1993]. The classification based on the principle of operation is interrelated to the method of exciting the active parts of the motor to generate the driving force. A further classification, according to construction, is based on the motor design. For example, there are piezoelectric USMs using a disk or ring vibrator, piezoelectric USMs using a rod vibrator and piezoelectric USMs using a thin plate rectangular vibrator. The motor function classification is related to the motor characteristics and the type of motion. According to this classification, there are two main types of piezoelectric USMs, namely rotary and linear motors.

2.2.1.1 Rotary Piezoelectric USMs

Rotary motors take many different forms continuous motors, stepping motors, and motors rotating in one direction. For instance travelling wave piezoelectric USM may be used as a rotary or linear motor. Its principle of operation is based on mechanical vibration generated by a piezoelectric vibrator and its effect is brought by the means of frictional forces. These frictional forces allow vibration to be converted into rotational motion. These principles of operation are complicated and have non-linear characteristics. In addition, it has non-stationary time variations due to the frictional driving mechanism between the stator and rotor under static pressure. The criteria for these types of motors are high torque at low speed operation, high holding torque due to frictional force without the input of power, flexible design, compactness, low electromagnetic noise, reversible controllability, low cost and low torque ripple. These criteria are often modified according to application. The serious problem with this type of motor is high efficiencies are difficult to achieve because of the power consumption of the vibration system. Also the excitation frequency is limited to the model response frequencies. Therefore, it cannot be fully adjusted for speed. Travelling wave piezoelectric USMs are used in many applications [Shafik, M. and Knight, J. A. G., 2002, Shafik, M., et al., 2001, Ise, et al., 1991, Hosoe, 1989, Fukunaga, et al., 1989].

2.2.1.2 Linear Piezoelectric USMs

The classification of linear piezoelectric USMs is usually based on their operating principles and total number of the piezoelectric element (actuators) used [Zhenqi, Z.,

1995]. The classification can also be based on applications, such as in instruments, manufacturing processes and machine tools. Each application has its own significant needs, configuration and design. For instance, the travelling wave and hybrid transducer piezoelectric USM has been used as a linear motor. The hybrid transducer piezoelectric USM has been introduced by [Newton, D., et al., 1997]. The motor has two ways for controlling velocity. The first one is to vary the step size per cycle by adjusting the voltage between the longitudinal piezoelectric vibrators. The other varies the step per second by adjusting the frequency of operation. The ideal method for controlling the velocity of this type of motor is to vary the voltage amplitude while setting the frequency to resonant. The motor is typical of other linear motors, the velocity decreases with increasing the load. It also has the capability for low speed control when operating at a very low frequency.

2.2.2 Configuration of Piezoelectric USMs

Many different configurations of piezoelectric USMs have been developed [Shafik, M., et al., 2001, Hu, J., et al., 2001, Dong, S., et al., 2000, Dong, S., et al., 1999]. This review covered some of these configurations and the main principles of operation, methodology of design, methodology of modelling and analysis, manufacturing process, parts design, material selection, weaknesses and major characteristics for these configurations.

A novel standing wave-type noncontact linear USM has been introduced by [Hu, J., et al., 2001]. In this work the motor design and analysis were presented. The authors introduced a prototype using a wedge-shaped aluminium stator that was placed horizontally and driven by a multilayer lead zirconate titanate (PZT) vibrator. This linear USM used a properly controlled ultrasonic standing wave to levitate and drive a slider. The levitation and motion of the slider were examined. A theoretical model was developed assuming that the driving force was generated by the turbulent acoustic streaming in the boundary air layer next to the bottom surface of the slider. They presented an experimental methodology to increase the displacement and speed of the slider. They found that increasing stator vibrational displacement or decreasing the gradient of the stator vibration velocity and the weight per unit area of the slider led to an increase of the slider displacement. They also found, that increasing the amplitude

and gradient of the stator vibration velocity or decreasing the weight per unit area of the slider and the driving frequency, gave rise to an increase in slider speed. The authors succeeded in calculating the characteristics of the motor and this agreed well with their experimental results.

Dong, S., et al., (2000) developed a miniature piezoelectric USM based on circular bending vibration mode in the area of precise positioning. They showed their prototype had improved construction based on a free-free bending vibration mode. They presented the methodology for design, construction, and the operation principle for the motor. Finite-element analysis was used in the modelling and the modes of vibration and driving mechanism were modelled. The characteristics of the prototype were investigated experimentally. The developed prototypes showed some advantages such as low speed (70 r.p.m), large torque (0.855 Nm), very high resolution (0.01 degrees) and good speed stability over 10 hours. The miniature motor was successfully applied to a laser resonant cavity as a precision driving element.

Dong, S., et al., (1999) investigated a rod-type piezoelectric USM using the base bending vibration mode of small size (15 mm in diameter and 25 mm in length). They showed that the developed construction giving fine positional accuracy with two directions driven directly by two piezoelectric USMs. A prototype with a resolution of 12 nm was successfully developed and applied to precision regulating mechanism for a laser resonant cavity. The developed motor could be controlled using a microprocessor. It had the facility to provide the positional movements in stepping mode responding to a pulse signal. This showed that it was possible to use the characteristics of piezoelectric USMs with large torque at low speed and high angle resolution to develop high displacement resolution and large driving force.

Aoyagi, M. and Tomikawa, Y., (1999) developed a new USM using a combination of longitudinal and torsional vibrators. These studies were aimed at improving the performance of this type of motors. The authors demonstrated that the motor was innovative and of improved design. They were concerned with the longitudinal vibration mode and the output method for its mechanical power. The longitudinal vibration mode with one node on each of the longitudinal and torsional vibrators was applied to control the frictional force on the contact surface. This mode strongly caused a repulsive

collision of both vibrators. Consequently, the maximum torque and the maximum efficiency of the improved motor increased markedly when compared to conventional performance. Moreover the input electric power for the longitudinal vibrator was considerably reduced.

Morita, T., et al., (1999) presented a new USM to be used as a micro actuator. This had high torque, low speed and simple construction. A discussion of this type of micro USM that made up of bulk PZT, was presented in this study. The stator transducer was 2.4 mm in diameter and 10 mm in length. The maximum revolution speed was 650 r.p.m and the maximum output torque was $0.22x10^{-3}$ Nm. The driving frequency was 85 KHz. The bulk PZT motor was applied as an actuator in a robot hand.

Koc, B., et al., (1998) developed a USM using a metal-ceramic composite actuator generating torsional displacement. The motor comprised of three components, a stator, a rotor and a ball bearing. The stator was made of an active piezoelectric ring, poled in the thickness direction and bonded with two windmill-like slotted metal endcaps. The stator was excited through its two electrodes, generating ultrasonic vibration in the radial direction at a radial mode resonant frequency. The two identical metal endcaps on both sides of the ring, bonded after being displaced 45 degrees to each other, transfers radial vibration into longitudinal and tangential vibrations. The combination of these vibrations generates rotation due to frictional interaction between the centre part of the top endcap and the periphery of the rotor. The study discussed a prototype for a diameter of 11.0 mm. The motor transient characteristics were measured and presented in this work. The maximum torque of $1.36x10^{-3}$ Nm at a speed of 480 r.p.m was obtained.

Kusakabe, C., et al., (1998) introduced the effect of the pressing force applied to a rotor on a disk-type USM driven by self-oscillation. The authors showed the relationship between the pre-load pressing forces applied to the rotor and the rotation characteristic of an USM driven by self-oscillation. The motor used here was an in-phase drive-type USM using two degenerate bending vibration modes of a disk. The picked-up electrical signal caused by self-oscillation was positively fed back into the piezoelectric ceramics for driving an operational amplifier and a step-up transformer. The pressing force

applied to the rotor was measured using a force gauge coupled to the shaft of the USM. The result of these considerations showed that the selection of the picking-up position for the feedback signal was important for stable starting and running of the disk-type USM driven by self-oscillation.

Xu, W. and King, T. G., (1996) presented a new configuration for piezoelectric USMs using a roller clutch mechanism. In this investigation the authors described the construction, the operational principle and characteristics of this configuration. They used three waveforms to investigate the electrical and mechanical characteristics of the motor. The main results of this investigation showed that:

- The new configuration of these motors would be operated with variable speed by changing the excitation frequency of the piezoelectric stacks.
- The performance of the motor differed for three waveforms used.
- The input frequency affected the motor performance especially at resonant frequency.
- The excitation wave shape affected the slope of the speed and frequency curve.
- The main advantages of this configuration were, single phase drive, wide speed range, and simple instruction.
- The main disadvantages were: the stepped backlash during the motor rotation and the rotation was possible only in one direction.

Saigoh, H., et al., (1995) presented a multiplayer piezoelectric USM using the first longitudinal and the second bending vibrations. The motor was a linear USM type. The authors introduced the construction of the vibrator motion, characteristics of a sample vibrator, an analytical and experimental study. They showed the results relative to two main parameters. The first depended on the thickness of elastic material, and the second on the pre-load pressing force applied to the vibrator. The results of this work showed that:

- Much lower driving voltage than the motor using a single plate vibrator would operate the motor.
- The driving voltage range and driving current rang of the first longitudinal and the second bending vibrators could be selected by adjusting the Multilayer structure.

- The main disadvantage of this motor was, the leftward travelling speed was faster than that in rightward direction. Because, the disposition of frictional material on the vibrators on the two edges were not symmetrical.

2.2.3 Piezoelectric USMs Servo Control Drives

Many different rules and methodologies have been used to develop piezoelectric USM servo control drives, such as Fuzzy Logic (FL), Neural Network (NN), Fuzzy Logic and Neural Network (FLNN) [Lin, F. J., et al., 2000, Kobayashi, Y., et al., 1999, Lin, F. J., et al., 1999]. Each methodology has its own principles of operation, construction and functions according to the needs of the application. However, it has proved difficult to predict the behavior of an USM because of the certain non-linear properties. To avoid these problems created by the non-linear properties few designers focused on using neural network controllers [Lin, F. J., et al., 2000, Lin, F. J., et al., 1999]. A review that covers various methodologies used in USM servo control is presented in this section. This was aimed at investigating the state-of-the-art of USM controllers and to give the information that can be used to optimise current system tools.

Lin, F. J., et al., (2000) introduced a Recurrent Neural Network (RNN) control for a one inductance and two capacitances (LCC)-resonant USM drive. The newly designed driving circuit was developed for the travelling wave-type USM. It consisted of a push-pull DC-DC power converter and a two-phase voltage source inverter using one inductance and two-capacitance resonant technique. Because the dynamic characteristics of the USM were difficult to obtain and the motor parameters varied with time, a RNN controller was proposed to control the USM drive system. In the proposed controller, a dynamic back propagation algorithm was adopted to train the RNN on-line using a proposed delta adaptation law. However, because of the convergence of the tracking error, analytical methods based on a discrete-type Lyapunov function were proposed to determine the varied learning rates for the training of the RNN.

Lin, F. J., et al., (1999) introduced fuzzy neural networks for control USM drives with two inductances and two capacitors (LLCC) resonant technique. In this work the authors demonstrated the application of Fuzzy Neural Networks (FNN's) in the identification and control of an USM, Firstly, the USM was derived using a newly designed high-

frequency two-phase voltage-source inverter using the LLCC resonant technique. Then, two FNN's with varied learning rates were proposed to control the rotor position. The USM drive system was identified using a fuzzy neural network identifier (FNNI) to provide the sensitivity information for the drive system to a fuzzy neural network controller (FNNC). A back propagation algorithm was used to train both the FNNI and FNNC on-line. Moreover, to guarantee the convergence of identification and tracking errors, analytical methods based on a discrete-type Lyapunov function were proposed to determine the varied learning rates of the FNN's. This showed that an accurate tracking response can be obtained due to the powerful on-line learning capability of the FNN's, Furthermore, the influence of parameter variations and external disturbances on the USM drive system were reduced effectively.

Lin, F. J., et al., (1999) presented a Fuzzy neural network position controller for a USM drive using push-pull DC-DC converter. The FNN controller was trained on-line using a proposed delta adaptation law. The authors introduced a new driving circuit for the travelling-wave type USM that was a push-pull DC-DC power converter and a two-phase series-resonant inverter combination. The network structure, the on-line learning algorithm and the proof of convergence of the learning algorithm of the FNN were described. The operating principles of the proposed driving circuit for the USM were described in detail. Then, the FNN position controller was implemented to control the USM drive to reduce the influence of parameter uncertainties and external disturbances. The performance of the proposed driving circuit and FNN controller also was demonstrated.

Lin, F. J., et al., (1999) introduced an USM drive using a current-source parallel-resonant inverter with energy feedback. The authors presented USM drive using a two-phase current-source parallel-resonant inverter. They described a single-phase equivalent model of the USM. Then detailed theory for the newly designed driving circuit for the USM, in which the inherent parasitic capacitances formed by the polarized piezoelectric ceramic of the USM were parts of the two parallel-resonant tanks, was introduced. Since the dynamic characteristics of the USM were greatly influenced by the variation in the quality factors of the parallel-resonant tanks, two transformers were added to feed the stored energy in the resonant tanks back to the DC source to reduce the quality factors.

Lin, F. J., et al., (1998) presented a fuzzy neural network controller for parallel-resonant USM drive. In these studies the authors presented a newly designed driving circuit for the travelling-wave-type USM that consisted of a push-pull DC-DC power converter and a current-source two-phase parallel-resonant inverter. Moreover, since the dynamic characteristics of the USM were difficult to obtain and the motor parameters were time varying, a fuzzy neural network (NN) controller was developed to control the USM drive system. In this proposed controller, a fuzzy model-following controller was implemented to control the rotor position, and an on-line trained NN with variable learning rates was implemented to tune the output-scaling factor of the fuzzy controller. Analytical methods based on a discrete-type Lyapunov function were used to guarantee the convergence of tracking error and to determine the desired variable learning rates. The experimental results showed that an accurate tracking response would be obtained using the proposed controller. This showed also that the influences of parameter variations and external disturbances on the USM drive also would be reduced effectively.

Izuno, Y. and Nakaoka, M., (1998) introduced a speed tracking servo control system with speed ripple reduction scheme for travelling-wave-type USM. The authors showed the necessity to consider the effect of the load torque and the control characteristics of the speed tracking for speed tracking servo control system. It was clear that these parameters were only partly reported and were insufficient for practical applications. In addition the fluctuation of the speed, or the speed ripple, caused by the manufacturing process of the USM has not been studied carefully. The authors presented a new speed servo control system in which speed ripple reduction, load torque characteristics, and speed tracking were taken into consideration. The developed system used two control loops. A speed control loop using a variable gain was constructed in the driving frequency control section. Further, only the speed ripple was extracted from the revolving speed detection signal and used for feedback compensation to the constant voltage control loop in the applied voltage control section.

Izuno, Y., et al., (1998) presented a speed tracking servo control system incorporating a travelling-wave-type USM and evaluations of its feasibility. This was aimed at solving the main problems associated with piezoelectric USM applications especially in servo

motion control systems. These problems are the inherent speed ripple characteristics, the speed regulation characteristics under the condition of applied load torque and the speed tracking. To solve these problems the authors presented and discussed theoretically some control schemes for ultrasonic-actuated motor systems that included fuzzy reasoning control, adaptive control, repetitive learning control and neural-network-based learning control. They also presented a newly proposed precise speed tracking servo control system using the compact travelling-wave-type USM. The developed control scheme comprised of both the driving frequency control loop with the variable-gain strategy and the applied voltage control loop with the speed ripple reduction strategy of the USM. The results of this study showed a significant improvement in the speed characteristics of the motor

2.3 DC MOTORS AND PIEZOELECTRIC USMs

There are many criteria that can be used to differentiate between two control systems using DC servomotor or piezoelectric USM. These criteria include dynamic response, accuracy, degree of resolution, methodology used to create the motion, output force, compactness, power and control. The investigation into the available DC servomotor and USM control systems showed that:

- **Micrometer Positioning Application**

DC servomotors have significant problems when it comes to demanding positioning control to high level of accuracy in the micrometer range [Jacob, T. 1999, Ro and Hubbel, 1992]. There is instability through shaft that was developed when the servo amplifier gain exceeds a certain threshold. Gain is usually set high to obtain the best possible system accuracy and repeatability. But beyond certain point the servomotor oscillates, taking away any further improvements.

- **Response Time**

DC motors have a significant delay compared the piezoelectric USMs. This is due to their typically high moments of inertia of the rotor that can cause significant delays in the response time of the motor. The piezoelectric USM delay is result of its principle of operation.

- **Resolution**

Piezoelectric USMs involve a reaction between solid-state parts hence, the resolution is generally better than the DC motors.

- **Compactness**

The size of DC servomotor in general is larger than the Piezoelectric USM. Piezoelectric USMs have adaptability to be obtained in different configurations with a compact size.

2.4 CONCLUSION

A critical investigation into state-of-the-art for the existing EDM and recent developed piezoelectric USMs servo control systems was conducted. An investigation into EDM control system shows that there is a great concern about the existing servo control system level of precision and dynamic response [Behrens, et al., 2001, Jacob, T., 1999, Ro, and Hubbel, 1992]. An investigation into piezoelectric USMs shows that [Hu, J., et al., 2001, Muralt, P., 1999, Zhang, B. and Zhenqi, Z., 1997, Lin, F. J., et al., 2001, Nakaoka, M., 1996]: The piezoelectric USM can produce extremely fine position changes down to sub-nano-meter range. The smallest changes in operating voltage were converted into smooth movements. Piezoelectric USMs offered a position within a range of 100 μm with sub nano-meter resolution. Piezoelectric USMs offered the fastest dynamic response available. The piezo effect directly converts electrical energy into motion only absorbing electrical energy during movements. Static operation, even holding heavy loads, does not consume power. These characteristics presented a challenge to develop a servo control system using this technology which could enable to improve existing system level of precision, dynamic response, performance and extend its capabilities to include more accurate machining.

CHAPTER 3

3 THE PROPOSED SERVO CONTROL FEED DRIVE USING PIEZOELECTRIC USM

3.1 INTRODUCTION

This chapter presents steps undertaken to develop a servo control feed drive using piezoelectric USM technology. This is including the basic configuration of the proposed system, the architecture of the system and engineering tools that can be used to build up the system. It also introduces the framework considered to develop the proposed system. It ends with a summary covering the main outcomes of the proposed control system using piezoelectric USM technology.

3.2 THE PROPOSED SERVO CONTROL FEED DRIVE

Development of a piezoelectric USM presents a real opportunity to use this technology to improve existing servo control feed drive system parameters such as, dynamic response, accuracy, resolution, precision in machining process and reduce size at high performance. Three technical issues have to be addressed. Firstly the characteristics of the piezoelectric USM servo control system had to compare with the current systems in use. Research by [Hu, J., et al., 2001, Lin, F. J., et al., 2001, Izuno, Y., 1998] stated that servo control systems using piezoelectric USMs as actuator have the following features:

- The motor speed regulation characteristics were stable regardless of step load torque disturbance.
- The speed servo tracking characteristics were acceptable on a practical basis.
- High-precision positioning control and zero stationary deviation irrespective of target position or load could be attained.

The second issue is the load capacity of the motor. This has to be considered. The principles of operation of an EDM system are based on spark discharge process. This means that the EDM system main processes place a little real load on the driving motor that presents a real opportunity to exploit piezoelectric USMs technologies.

The third issue is the effect of the sparking temperature on the ultrasonic motor performance. This potential problem was overcome with the reduction in the servo control drive size. Reduction in the drive size gives possibility to emerge the system into oil, which improves cooling rate and safety aspect of the system.

3.2.1 The Architecture of the Proposed System

An approach was developed to encompass the use of different engineering design tools. It is an integration of different disciplines of sciences, which were servomechanisms, USM technology, analogue digital design, circuit protection design and analysis, advanced control, control unit design and analysis, programming, computer simulation and modelling. From the concept to realisation the development of the units of the approach passed through many different stages. In each case the required specifications for each unit were considered and these identified the layout for unit and the required components. Figure 3-1 shows the methodology used in the development process of each unit of the proposed approach.

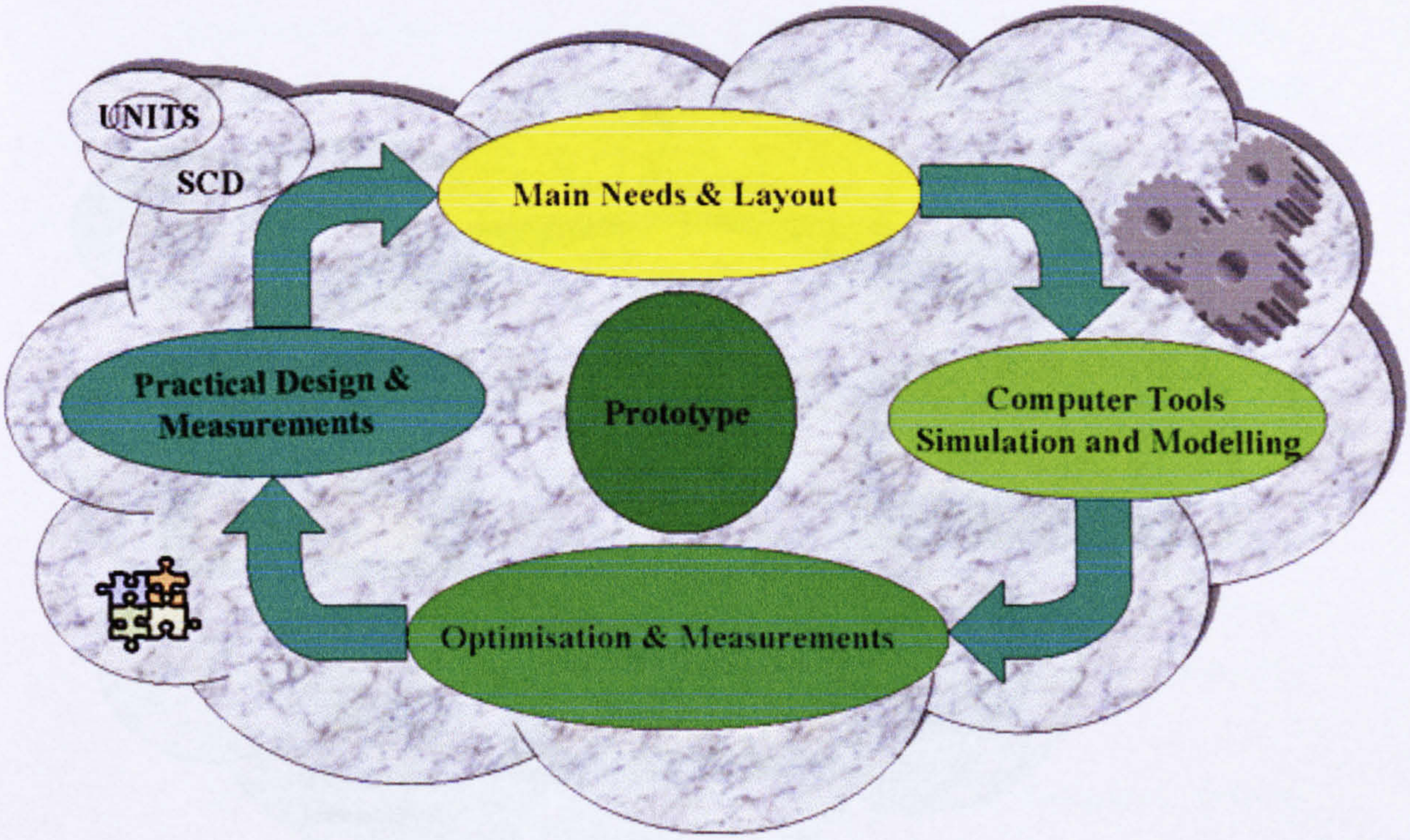

Figure 3-1 Methodology for design used in developing the main units of the proposed approach for control

Computer tools were used for optimising the design of each unit. This was carried out using various software packages. Finite element analysis were used for piezoelectric USM modelling and analysis. A methodology for modelling and analysis using finite element analysis was established and used successfully in the design process. VIEWLOGIC, EDWIN, P-SPICE, and EASY PC were used for electronic circuits modelling and analysis and VHDL for the servo control unit. Then a prototype for each unit was built. Here a particular attention was given to major needs and characteristics for the proposed approach.

This methodology was also used successfully to develop a prototype for the proposed approach. This was carried out, by integrating the main units, into the mainframe of the system and this was consisted of a new servo control feed drive using a linear piezoelectric USM, a new linear piezoelectric USM using a single flexural vibrating bar, an advanced piezoelectric drive, a new texturing control unit and a new control unit for EDM based on ultrasonic motors technologies. The principles used to measure and optimise the proposed approach performance compared with the existing one are shown in Figure 3-2.

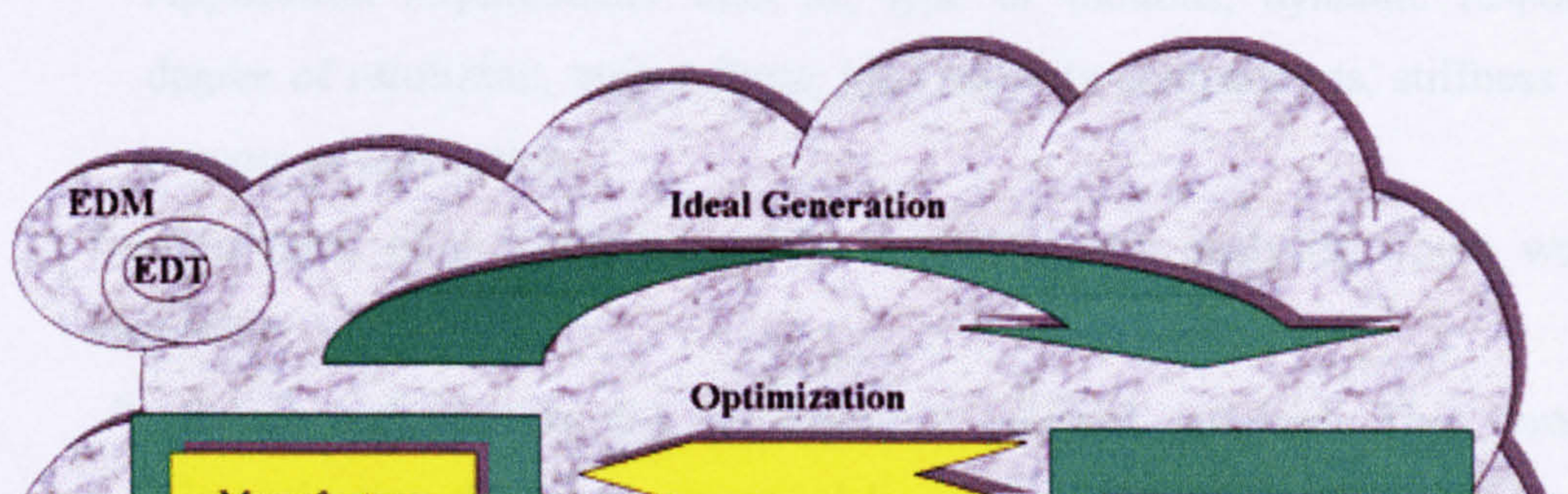

Figure 3-2 Main principles of optimisation used in the proposed servo control system design process

3.2.2 Design Specifications

- ° The proposed control feed drive to be able to provide a dynamic response time and resolution on the order of microns.
- ° The proposed system to be compact and easy to maintain.
- ° The system to be able to be installed in application where linear motion and limited load capacity is required.
- ° Figure 3-3 shows block diagram illustrates the integration of the proposed servo control feed drive into EDM system and necessary modification carried out into the system.

3.3 FRAMEWORK FOR THE PROPOSED SYSTEM

The remainder of the developments process of the proposed system are as follows:

1. Design and build a new linear ultrasonic motor using a single flexural vibrating bar to meet EDM application needs. This was included:

- Establishment of a new procedure for design, to consider:
  - ° Application requirements such as, type of motions, dynamic response, degree of resolution, output force, load capacity compactness, stiffness and process of fabrication.
- Establishment of a methodology for modelling and analysis, which would enable to:
  - ° Select and identify the piezoelectric material required. This through investigating the micro structural level of different materials and how it reacts to the applied load.
  - ° Investigate material deformation. Mishandling of material deformation may produce jerking phenomenon. The jerking phenomenon affects and reduces the motor degree of resolution, accuracy and consequently industrial applications.
  - ° Investigate the modes of vibration, the modes of vibrations used to determine and develop the motor principles of motion and degrees of freedom.
  - ° Optimise the motor signal response parameters, signal response parameters are used to design piezoelectric drive of the motor.

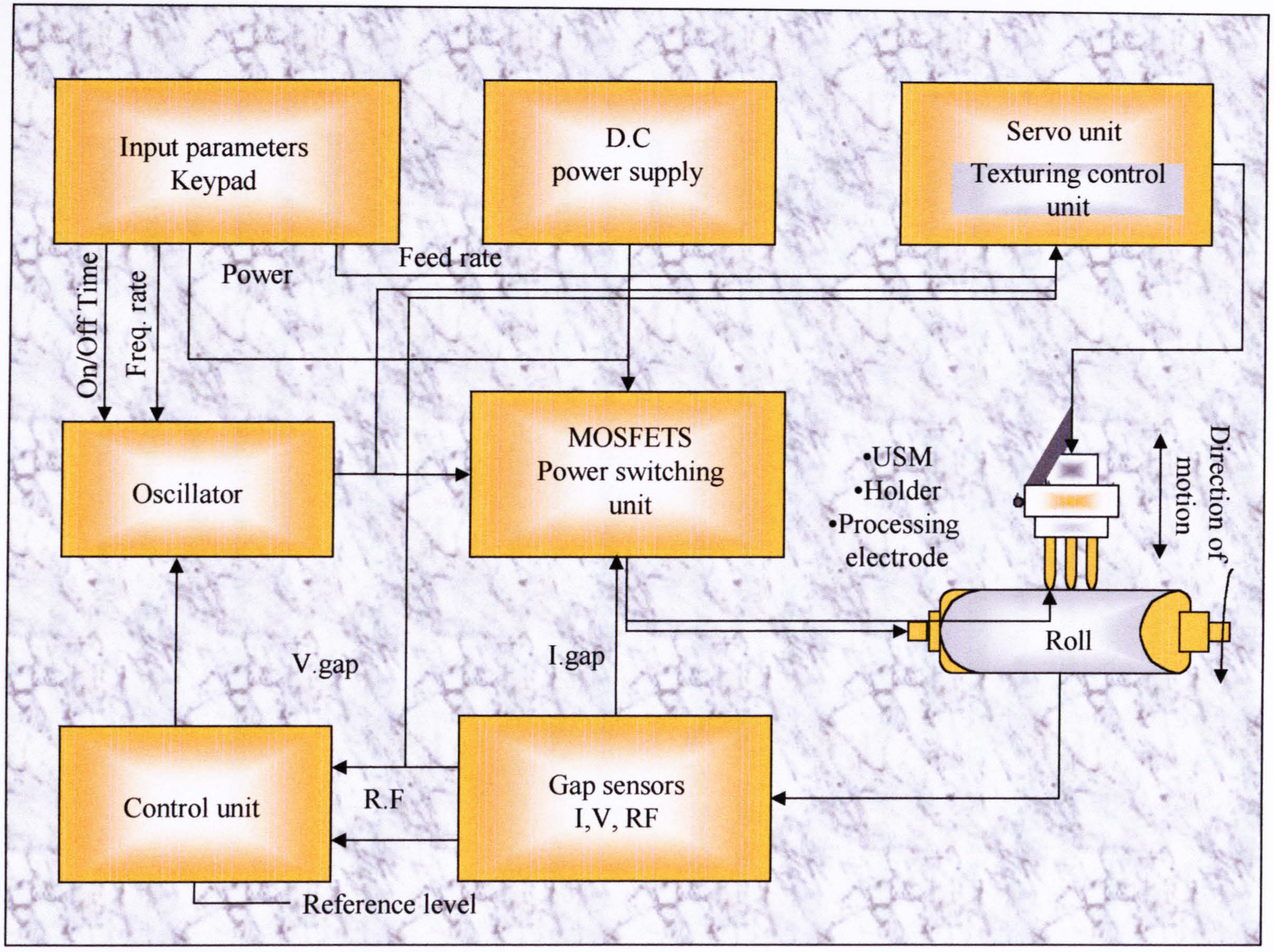

Figure 3-3 Electro Discharge Machining system block diagram for the proposed approach using piezoelectric USM

- Investigate the interaction between the motor parts, investigate and examine the amplitude response variation against different applied loads.
- Optimise the resolution of the motor. Here a new methodology is to be established. This is to investigate the minimum amplitude response at lower operating conditions against exciting load. As well as the optimised diameter ratio between the driving wheel and the shaft.
- Optimise the dimensions of the motor parts to meet the planned characteristics such as, resolution, dynamic response and compactness.

• Create a critical study for various engineering analysis tools which uses finite element analysis principles such as ANSYS and ALGOR packages.
• Draw out the proposed piezoelectric USM principles of motion.
• Optimise the motor practical operating parameters (frequency, amplitude and phase).
• Design and build the parts for the motor to cover:

- Design of a flexural vibrating electrode, pulley and shaft, shaft carrying bearing, axial electrode, axial electrode carrying bearing, pre-load spring and frame for the motor.

• Create an experimental treatment for the motor parts to cover:

- Determine the major characteristics for the motor, such as resolution, output force load capacity, stiffness, power transmission and efficiency.

2. Design and build an advanced piezoelectric drive to include:

• Optimise the operating parameters of the ultrasonic motor.
• Draw up the layout of the motor drive based on the optimised operating parameters. This step was included:

- Design and analysis of the drive input circuits,
- Design and analysis of the multistage cascade voltage amplifier,
- Design and analysis of a power amplifier,
- Design and analysis of a sharp band passes filter,
- Design and analysis of a piezoelectric oscillator.

• Create a computer simulation for all these units of the drive using VIEWLOGIC software, to ensure of the drive capability to control.
• Create required improvements into the developed drive to meet EDM system requirements.

- Investigate the use of power MOSFETs in advance and design innovative power switching firing circuits.

3. Integrate the drive with the ultrasonic motor and examine the main characteristics of the drive such as:
    - Variations of the motor input current against input voltage.
    - Variations of the motor's properties with the current applications such as: Variations of the motor travelling speed against exciting frequency, voltage and load.
    - Measure the maximum load, resolution and load capacity.
4. Consider improvements to the motor major characteristic to include the motor travelling speed and torque.
5. Design and build a servo control unit for the EDM-system using an ultrasonic motor. This was intended to:
    - Design a layout for the EDM-servo control unit and its main parts followed by:
    - Design and build an analogue to digital converter for the EDM-servo control unit.
        - ° Design a potential divider, a voltage comparator, and a shaping circuit.
        - ° Design and model of the servo control unit digital circuit.
        - ° Design and build the digital to analogue converter,
    - Create computer simulation for the developed servo control unit using VIEWLOGIC and VHDL software.
    - Create computer simulation for a case study for the real system using VHDL software.
6. Integrate the developed servo control drive main units into the system mainframe and carry out a comprehensive study to cover major characteristics of the needs for the current application.
    - Examine the limitations of the developed drive and create the necessary modification to overcome it.
7. Examine and evaluate the developed system characteristics and compare it to the existing system using DC servomotor to cover:
    - An investigation into the stability of the machining system.

- An investigation into the surface profiles of the product machined using both systems for control.
- An investigation into the system material removal rate, degree of roughness and capability for control.

3.4 SUMMARY

The current research sets out the steps undertaken to develop an advanced servo control feed drive using piezoelectric USMs technology to improve the existing servo control feed drive level of precision, dynamic response, stability of machining and degree of resolution. It presents a new control system using piezoelectric USM technology. This system should be able to be implemented in various applications.

The main architecture and developments processes for the proposed control system were discussed. This included, engineering design tools used in the development process, the methodology used to design main units and framework were undertaken to develop the system.

CHAPTER 4

4 A NOVEL LINEAR PIEZOELECTRIC USM USING A SINGLE FLEXURAL VIBRATING BAR

4.1 OVERVIEW

This chapter provides the development process of a linear piezoelectric USM using a single flexural vibrating bar. It presents design methodology, conceptual design, basic configuration, modelling and analysis, principle of operation, motor structure, experimental examination and evaluation of the main characteristics of the motor. The chapter ends with improvements into the characteristics of the developed prototype.

4.2 INTRODUCTION

In order to design a system that uses a motor for feed control it is essential to have an understanding of the strengths and the weaknesses of several types of motor that are available. Then it should be possible to choose the most suitable for the application in question and commence design. There are several features a designer should appreciate. These features include dynamic response time, resolution, load capacity, output force, total torque, size, power, phasing, commutation, position feedback and the type of control, i.e. open loop or close loop control. However, these features vary according to the type of the motor and application requirements. Most modern piezoelectric USMs offer flexibility of design, compact size, low weight, slow speed, high torque, non-magnetic operation, freedom of constructional design, very low inertia, lightweight mechanisms with fast dynamic responses, direct drive, fine positioning resolution, high stiffness, the possibility of electromagnetic noise reduction and miniaturization [Hu, J., et al., 2001, Dong, S., et al., 2000, Morita, T.. et al., 2000]. Thus they have the potential to replace DC servomotors in many applications such as in feed/position control.

The design of a piezoelectric USM is a complicated and involved the needs to:

- Understanding the needs of the application such as, type of motions, dynamic response time, resolution, positioning, load capacity, configuration, output force, size, speed, torque and type of control.
- Being aware of the fundamental of design of piezoelectric ultrasonic motors and various configurations can be obtained.
- Realizing piezoelectric material properties and the technical methodology that can be used to convert the material properties into motion.
- Investigating modes of vibration of the chosen piezoelectric material that are used to determine and create the principle of motion.
- Considering deformation properties of the chosen piezoelectric material that help to prevent the potential for jerking effect.
- Looking at the microstructure level of the piezoelectric material and its reaction for various types of applied load such as electric load.

This research work proposed a piezoelectric USM for linear industrial applications. This motor should be able to provide linear motion, fast dynamic response, micro resolution, acceptable power, load capacity and output force. The proposed motor principle of operation is based on converting the continuous flexure and linear force, generated externally through the flexural vibrating bar, into rotary and linear motion through friction between bar and the rotor. Gromakovskii, V. A. and Sashida, T., 1978 produced one of the first rotary prototypes of this type of motor with one direction of motion. The proposed motor consisted of four main parts, the stator, the rotor, sliding element and frame. The stator is a single vibrating bar, made from piezo-ceramic material that has the ability to transform the applied electrical load into mechanical vibration. The stator and the rotor form the rotary structure and the three parts jointly with the frame of the motor form the linear structure. It was recognised that this type of motor needed to be mechanically supported at its vibration nodes to prevent disturbance of the vibration mode. It was also found, that its characteristics, were influenced considerably by the friction between the rotor and the stator, properties of the active element, pre-load pressing forces, dimensions of the driving wheel and the shaft. Therefore, these parameters were carefully considered to avoid errors of previous design of this type of motor. Especial attention was given to pre-load pressing force. Increasing the pressing

force disturbed the vibration mode and suppressed the vibrator displacement and linear motion deteriorated.

4.3 DESIGN PROCEDURE

The design of a linear piezoelectric USM capable of providing a micrometer resolution, high stiffness, high output force and compactness is serious challenge and not an easy task. However, in order to develop this type of motor it is necessary to set out a design strategy to avoid the weakness of previous designs.

To achieve micro-resolution requires a positioning system free from mechanical backlash and stick-slip. Mechanical backlash and stick-slip can lead to large errors and should not be used in micrometer positioning control especially when high stiffness and a large output force are required.

Mishandling of the deformation of the piezoelectric material can cause a jerking effect. Jerking effect reduce the resolution of motor. Therefore, it must be carefully considered in the design process for this type of motor. It can be avoided by preventing undesired deformation of the piezoelectric material to be transmitted into motion and therefore only to use axial deformation. Investigating the deformation of the chosen material and choosing a suitable method for housing the piezoelectric electrode can help prevent such undesired deformation.

Many parameters have also to be considered for high resolution including the ratio between the diameters of the driving wheel and the shaft, moment of inertia of the rotor, and material used to produce the parts of the motor.

Stiffness is a very important issue for a compliant mechanism. The stiffness of piezoelectric USM is dependent on the type of contact between the motor parts, types of materials, and pre-load pressing force between two surfaces in contact.

For many applications a compact piezoelectric USM is more desirable. However, in some cases where the specifications are high it is very difficult to achieve compactness. Compactness means that multifunctions have to be designed into a limited number of

components. This has been considered in the proposed motor design process. Therefore the rotor of the proposed motor has been designed composed of driving wheel and the shaft. The frame of the motor was also designed with many functions to give the flexibility to achieve the required characteristics including:

- A frame which is easy to integrate the parts of the motor as a linear piezoelectric USM,
- A mechanical system featuring few component for compactness,
- A mechanical system having only surface type contact for high stiffness,
- A structure having no mechanical joint suffering external loads,
- A linear mechanism with an unlimited travel range,
- A mechanical transmission free from backlash and stick-slip,
- A structure housing for preventing piezoelectric stacks from shear stress, and a structure for isolating the undesired piezoelectric deformations causing jerking effect.

Followed these points there are a need to:

° Specify the limit of the maximum torque T_0 and speed required,

° For this type of motor the total torque can be calculated as a time average of the instantaneous torque [Uefa, S. and Tomikawa, Y., 1993].

$$T_0 = \bar{\tau} \qquad 4\text{-}1$$

° Then the maximum torque can be given by:

$$T_0 \leq \mu f_c r_c$$

assuming the input voltage is large. This means that the frictional force always limits the torque.

μ is the friction coefficient between the stator and the rotor, f_c is the pre-load pressing force and r_c is the contact radius.

° Modelling of the motor and optimisation of the maximum and minimum displacement of the piezoelectric element.

° Specify the torque-voltage relation T_0/V_T,

° Determining the pre-load pressing force f_c from the torque relation [Uefa, S. and Tomikawa, Y., 1993]:

°

$$T_0 \leq \mu f_c r_c \qquad 4\text{-}2$$

Here the friction coefficient is dependent on the material selected and the contact radius is known from the radius of the motor.

° The duration of the contact is determined from the pre-load pressing force, the characteristics of the vibration system and input signal.

° Calculating the required torque factor A_r by substituting the T_0/V_T into torque relation [Uefa, S. and Tomikawa, Y. 1993].

$$T_0 = \bar{\tau} = \frac{A_r V_T}{\pi} \sin\frac{\phi_c}{2} \qquad 4\text{-}3$$

Where, V_T are the total applied voltage and ϕ_c the duration of the contact. The specification for the vibration system can be calculated from the torque factor.

° Determination of the various dimensions of the parts of the motor including diameters of the rotor and the shaft.

4.4 CONCEPTUAL DESIGN

Conceptual design of this type of piezoelectric USM mainly depends on the method adopted to produce the driving force or displacement. On the proposed motor the concept is based on superposition of longitudinal and bending vibration modes of a piezoelectric ceramic plate. However, to create a strong second bending vibration mode, the polarisation direction of the piezoelectric vibrator perpendicular to the electrodes, the piezoelectric ceramic vibrator was arranged as shown in figures 4-1 and 4-2. The longitudinal and bending vibration modes are coupled by asymmetry of the piezoelectric ceramic vibrator. Driving the electrode A and C by a single phase AC signal with a frequency closer to the resonant frequency of the vibrator provide one direction of motion and switching to electrode B and C change the bending vibration mode by a phase shaft of 180 degree which leads to reverse the direction of the elliptical motion generated at the edge of the vibrator. The rotational motion is converted into linear motion using the friction between the shaft and the sliding element of the motor.

4.5 BASIC CONFIGURATION

Figure 4-1 shows proposed configuration and main parts of the motor. This considers application needs such as type of motion, degree of resolution, speed, output force required, load capacity, torque, compactness, integration of the parts into the frame of the motor, production of the parts, maintenance, and errors of previous design of such type of motor.

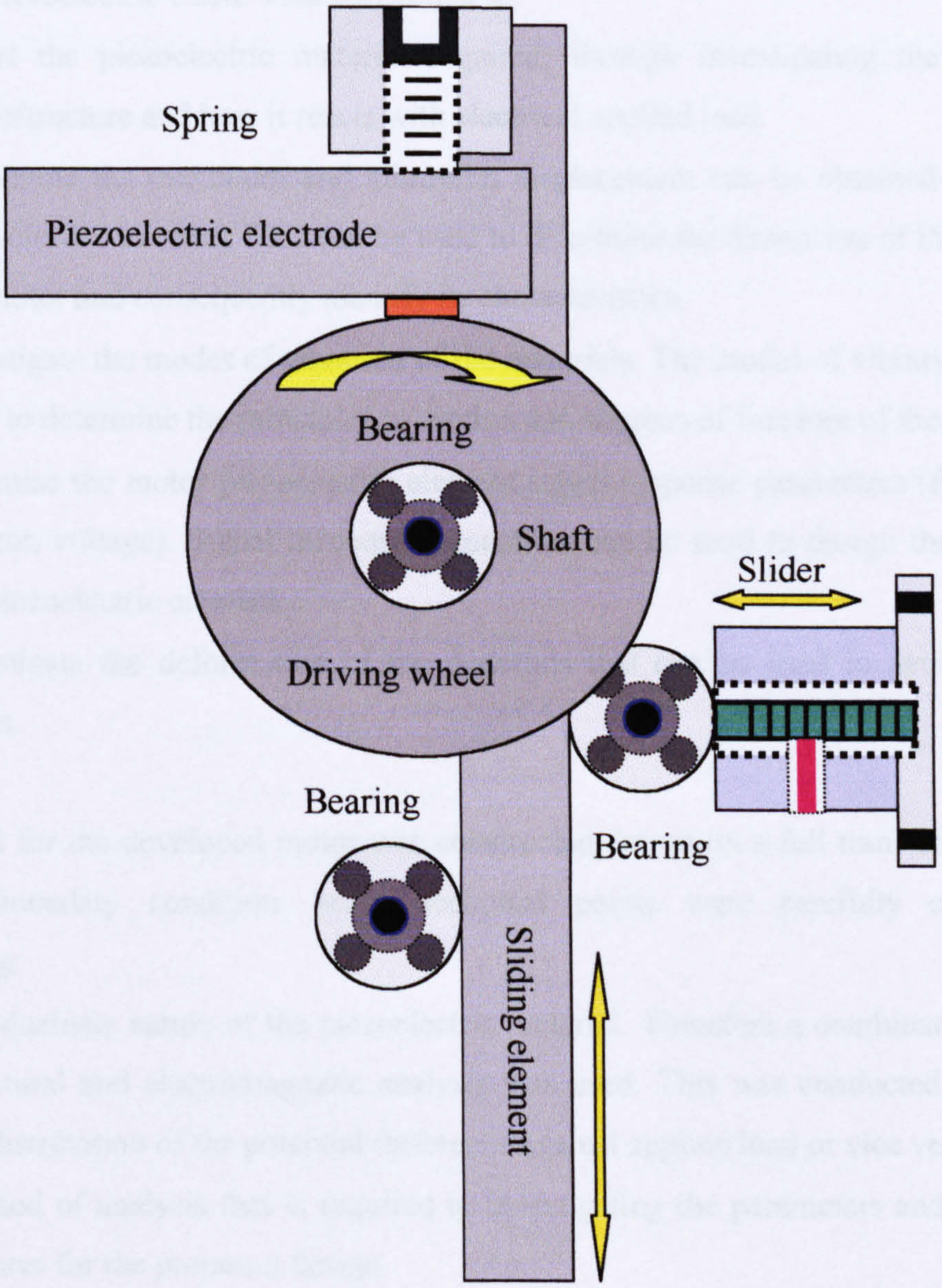

Figure 4-1 Basic configuration of the proposed linear piezoelectric USM using a single flexural vibrating bar

4.6 MODELLING USING FINITE ELEMENT ANALYSIS

Piezoelectric USMs have many complex non-linear characteristics. Normally two methods of analysis can be used to simulate and model piezoelectric USMs. These are the analytical analysis and finite element analysis (FEA). FEA has been used successfully in many industrial applications as an engineering tool [Vadim, D., et al., 1997, Newton, D., et al., 1997, Lin, M. W., 1994, Woo, S., Hyun, C. P., et al., 1993]. Here it has been used for setting out the methodology of modelling and analysis for the proposed piezoelectric USM. This was aimed to:

- Select the piezoelectric material required, through investigating the material microstructure and how it reacts with electrical applied load.
- Determine the maximum and minimum displacement can be obtained from the piezoelectric element. This can be used to determine the dimension of the parts of the motor and consequently identify its characteristics.
- Investigate the modes of vibration of the materials. The modes of vibration can be used to determine the principles of motion and degrees of freedom of the motor.
- Optimise the motor piezoelectric element signal response parameters (frequency, current, voltage). Signal response parameters can be used to design the drive of the piezoelectric element.
- Investigate the deformation of the materials that can be used to avoid jerking effect.

A model for the developed motor was constructed, based on a full translation of the motor boundary condition. Many technical points were carefully considered including:

- The dualistic nature of the piezoelectric material. Therefore a combination of the structural and electromagnetic analysis was used. This was conducted to obtain the distribution of the potential difference against applied load or vice versa.
- Method of analysis that is required to investigating the parameters and technical features for the proposed design.
- Justification between practical construction and practical boundary conditions. Therefore the polarization vectors for each element and gravity that complete the model boundary condition were carefully considered.

4.6.1 Principles of FEA

FEA is the one of the most successful engineering tools used in analysis piezoelectric ultrasonic motors. Its accuracy is mainly dependent on the description of the boundary conditions of the system. It evaluates and determines required parameters by performing an algebraic solution to a set of equations that describe an ideal model structure with a finite number of variables [ANSYS 5.7-5.3 Manual, 2000, 1996]. The solution of a set of equations allows determination of the displacement, stress, voltage and strain for each point on a piezoelectric element at any time. Therefore, it is possible to optimise different operating conditions and determine a steady state of the motor against a range of input loads.

The methodology of analysis is quite different from one model to another. An outline of the main modelling sequences, used in the proposed piezoelectric USM model, is as follows:

- Entering ANSYS (xansys53-xansys57)
- Preparing the ANSYS medium for the proposed model (preferences-structural and electromagnetic analysis, h-method)
- Model creation (pre-processor)
    - Define element/Key-options,
    - Define real constant,
    - Define material properties,
    - Create geometrical model,
    - Boolean operation,
    - Meshing.
- Loads
    - Loads/type of analysis,
    - Loads/Complete description of the environment (gravity...),
    - Loads/Piezoelectric electrode outer surface.
- Solution
    - Solution/Options,
    - Solution/Solve current LS.
- Results

- Results/Graph (Histpostprocessor),
- Results/Nodal (DOF)(General postprocessor),
- Results/Nodal (TOTAL STRAIN) (General postprocessor).

➢ Exit ANSYS

4.6.2 Description of the Physical Problem

The translation of the physical problem into boundary condition is the most important step in finite element analysis. This is concerned with how accurate the physical properties and parameters of the material used can be translated into FEA boundary conditions. In the proposed motor, the flexural vibrating electrode is made from a piezoceramic material. This type of material has a dualistic nature (see Appendix A). It is able to transform electrical energy into mechanical vibration with two modes of vibration, based on the method of excitation. In the proposed motor the modelled configuration is shown in Figure 4-2. The piezoelectric electrode (stator) was defined to be the active element and the driving wheel (rotor) was defined to be the passive element.

4.6.3 Preparation of the ANSYS Medium

As stated earlier the piezoelectric electric material has a dualistic nature. It handles the interaction between structural and electromagnetic analysis fields. Therefore in the model of the proposed motor the coupled field finite element (see Appendix A) was used to describe the piezoelectric material physical properties into boundary conditions. Coupled field analysis is one of the finite elements that consider the interaction between two or more fields of engineering. It allows for non-linearity and solves the voltage distribution due to applied displacement, or vice-versa. Then ANSYS medium was prepared to conduct such model by setting these conditions, preferences: structural and electromagnetic analysis, h-method.

Two methods can be used to define coupled field analysis. These two methods are, direct and indirect analysis. In this model the direct method is used to identify the coupled field analysis [ANSYS manual version 5.3, 1996].

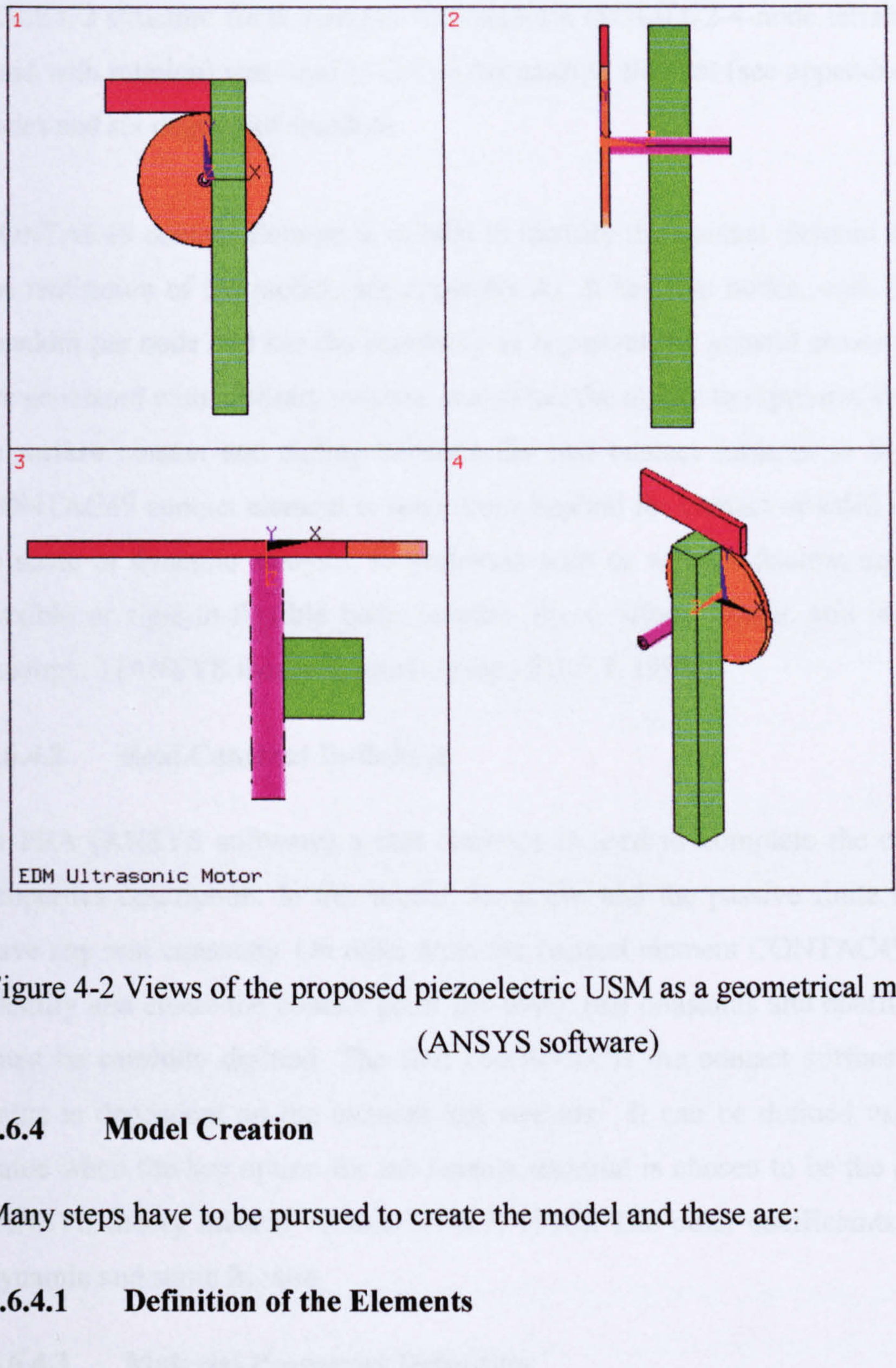

Figure 4-2 Views of the proposed piezoelectric USM as a geometrical model using FEA (ANSYS software)

4.6.4 Model Creation

Many steps have to be pursued to create the model and these are:

4.6.4.1 Definition of the Elements

ANSYS software offers more than a hundred different types of finite elements. Each element can define a set of materials according to their physical characteristics. In this model SCALAR98 TET (tetrahedral couple field solid element) coupled field finite element was used to define the piezoceramic material (see appendix A). It has ten nodes with row degree of freedom per node and suitable for different loads. The solutions for this element are obtained in two ways, Nodal DOF which includes all nodal solutions, and additional output element parameters.

SOLID72 structure finite element with rotation (SOLID72-4-node tetrahedral structural solid with rotation) was used to define the passive element (see appendix A). It has four nodes and six degrees of freedom.

CONTAC49 contact element is chosen to identify the contact element and to complete the realisation of the model (see appendix A). It has five nodes, with three degrees of freedom per node and has the capability to represent the general contact of models that are generated with arbitrary meshes. It also has the ability to represent and identify point to surface contact and sliding between the two contact surfaces in three dimensions. CONTAC49 contact element is sometimes applied for contact of solid bodies or shells, to static or dynamic analysis, to problems with or without friction and to flexible-to-flexible or rigid-to-flexible body contact. So, it allows elastic and inflexible friction (keyopt...) [ANSYS theory manual version 5.3-5.7, 1996].

4.6.4.2 Real Constant Definition

In FEA (ANSYS software) a real constant is used to complete the element physical properties description. In this model the active and the passive finite elements do not have any real constants. On other hand the contact element CONTAC49 that is used to identify and create the contact point has many real constants and coefficients and these must be carefully defined. The first coefficient is the contact stiffness parameter. Its value is dependent on the element key options. It can be defined using a maximum value when the key option for the contact material is chosen to be the penalty function [ANSYS theory manual version 5.3-5.7, 1996]. The other coefficients defined are the dynamic and static friction.

4.6.4.3 Material Properties Definition

In this model the parameters used to define an active element (piezo-ceramic material) are elastic stiffness, density, Poisson's ratio, electric permittivity and friction coefficients. However, the parameters used to define the passive element (silver steel) are elastic stiffness and density.

4.6.4.4 Generation of the Geometrical Model

The results of the mathematical model of the piezoelectric elements, is mainly dependent on the relation between the shape and size. In creating this model various dimensions of a rectangular piezoelectric bar were used. This was aimed to optimise the dimension of vibrating bar and the maximum displacement can be obtained. Tables 4-1, 4-2 and 4-3 show the dimensions of various parts (stator, rotor and sliding element) used in this modelling. One of the most important points to be considered in building any model for FEA is the justification between the position of the actual parts of the motor and modelled boundary condition. So the active and the passive elements have to be oriented and in contact as in the actual structure.

Table 4-1 Dimensions of the stator (piezo-ceramic vibrating bar) in mm

Length	Width	Thickness
40 mm	**10 mm**	**2 mm**

Table 4-2 Dimension of the rotor (driving wheel) in mm

Diameter of the driving wheel	Diameter of the shaft	Length of the shaft
40 mm	**2 mm**	**30 mm**

Table 4-3 Dimension of the sliding element in mm

Outer radius	Inner radius	Length
10 mm	**9 mm**	**150 mm**

4.6.4.5 Meshing

To complete the model definition, meshing by attributes has been used to assign the material for each part of the motor. After that, the smart and size step process is used to choose the size of the element followed by free meshing of the entire created model (creation of the particles).

4.6.4.6 Piezoelectric Orientation

The most important factor, when dealing with the piezoelectric material is the correct orientation of the piezoelectric polarization vector. It is the main concept used to create the motor principle of motion. Therefore, it was necessary to define the polarisation

vector for each element. In this model the entire element was selected and rotated around z-axis by an angle of 90^0 degrees in order to build a full description of the polarisation vector for each element of the piezoelectric vibrating bar.

4.6.4.7 Generation of the Contact Point to the Surface

Many steps in the FEA are needed to generate the contact point between two surfaces in contact (the active and the passive element). In this model the following steps were used:

- Defining the target surface and the contact surface,
- Generating the contact elements by attributes and then generates the contact points to the surface.

These steps give the ANSYS package the ability to generate the contact point automatically. Contact occurs when the contact surface (Nodes) penetrate the target surface (Base) [ANSYS manual 2000].

4.6.4.8 Definition of the Real Environment

In order to create a full translation of the physical construction of the motor into boundary condition, it was necessary to define gravity. This step completes the identification of the model boundary conditions.

4.6.5 Model Analysis

In current model two types of finite elements analysis have been used, model analysis and harmonic analysis. These were used to determine and investigate the major technical parameters required from modelling the motor. These offer two types of loads, the nodal and the pertaining to element. In the nodal case the loads were applied to nodes of the element that do not have direct links with element properties. It is often considered with the nodal degree of freedom (DOF) and can be brought in by the F commands (i.e. nodal displacements or forces, etc). Element loads include surface loads, body loads and inertial loads (see appendix A).

4.6.6 Modal Analysis

Modal analysis is used to determine the natural frequencies and mode shapes of the material structure. The natural frequencies and mode shapes are important parameters in

the design of a structure under dynamic loading conditions. They are also required if spectral analysis or mode superposition harmonic analysis or transient analysis are needed. Modal analysis is linear analysis and non-linearity will be ignored even if defined. Therefore, only the linear element behaviour is valid in modal analysis. However, if the contact elements are included in the model, the stiffness is calculated based on the initial status and is never changed. Both Young's modules (EX) and density (DENS) must be defined for modal analysis. Material properties may be linear, isotropic or orthotropic, constant or temperature dependent. Non-linear properties, if any, are ignored. The only loads valid in a typical modal analysis are displacement constraints. Other loads may be specified, but will be ignored for the mode extraction. The program will calculate a load vector and write it to the mode shape file (job name mode), so that it can be used in a subsequent mode-superposition harmonic or transient analysis.

4.6.7 Harmonic Response Analysis

Harmonic analysis has been used to optimise the steady state response of the linear structure to the loads that vary sinusoidally against time. This idea is based on calculating the structure response at several frequencies and obtaining a graph of some response quantity (displacement) versus frequency. The peak response occurs at forcing frequencies that are matched with the natural frequencies of current model. Harmonic response analysis is linear analysis, any non-linearity will be ignored even if defined. Therefore, only linear element behaviour is valid in a harmonic analysis. Non-linear elements, if any, are treated as linear. However, if the contact element is included in the model, the stiffness is calculated based on the initial status and never changed.

Three methods are available to create harmonic response analysis: the full, reduced and the superposition method. In this model the full method has been used. This method is the easiest one of these three methods to use. It uses full system matrices (i.e. no matrix reduction) to calculate the harmonic response analysis. The main advantages of using the full method are:

- It is easy to use, because it is not necessary to choose the master degrees of freedom mode shape.
- It is uses full matrices. Therefore, no matrix approximation is involved.

- It allows unsymmetrical matrices that are typical of such applications.
- It calculates all displacement and stresses in a single pass.
- It accepts all types of loads, nodal forces, imposed (non-zero) displacement, and element loads (pressure and temperatures).
- It allows the effective use of solid model loads.

The main disadvantage of the full method is, that it is usually more expensive than the other methods. Therefore, if the system matrixes are symmetric, which is the case of the most structural analysis, the reduced method or the superposition method should be first considered. But in this case the system matrix is unsymmetrical, so the full method is preferred. Another disadvantage is that pre-stressed option is not available. In other words, the reduced method can be used but the master degree of the freedom has to be defined where the displacement will be calculated only at the master DOF. Superposition cannot be used because the imposed displacement cannot be applied. For all three methods of harmonic analysis, there are many restrictions that must be considered. All loads must be sinusoidal, varying all time, have the same frequency, non-linearity is not permitted; transient effects are not calculated. In other words, these restrictions can be overcome by performing transient dynamic analysis, with harmonic loads expressed as a time history loading function. To specify the loads under the harmonic analysis the following options are available. Dynamic options include the forcing frequency range and different forms of damping. General options include the number of harmonic solutions and stepped or ramped loads. The load may be stepped or ramped. The ramped load means that the load amplitude is gradually increased with each sub-step but with stepping loads, the same load amplitude will be maintained for all sub-steps in the frequency range. The stepped option is used in this model.

Results from harmonic analysis are written to the structural results file (job name. RST).

The data stored in these files are

- Primary data:
- Nodal displacement (ux, uy, uz, rotx, roty, rotz)
- Derived data:
    - Nodal and element stresses
    - Nodal and element strains

- -Element forces
- -Nodal reaction forces

Etc.

4.6.8 Loads

Three pieces of information are essential for harmonic analysis. These are amplitude, phase and the forcing frequency range. This information is provided as a database in a real and imaginary form as illustrated in table 4-4.

Table 4-4 Samples of the input signals used in proposed linear piezoelectric USM signal response optimisation

Applied signal Volt	Real part Volt	Imaginary part Volt
40, 0.0	**40**	**0.0**
-40, 0.0	**-40**	**-4.84×10^{-14}**
50, 0.0	**50**	**0.0**
-50, 0.0	**-50**	**-6.05×10^{-14}**
60, 0.0	**-60**	**0.0**
-60, 0.0	**-60**	**-7.26×10^{-14}**

Equations 4-4 and 4-5 have been used to calculate the real and the imaginary part of the input exciting force. Equation 4-6 provides the amplitude of the exciting force and equation 4-7 the force phase angle θ. In this model, the phase has been used because multiple loads out of phase were used in model optimisation.

$$F_{real} = F_e \cos\theta \qquad 4\text{-}4$$

$$F_{imag} = F_e \sin\theta \qquad 4\text{-}5$$

$$F_e = \sqrt{(F_{real})^2 + (F_{imag})^2} \qquad 4\text{-}6$$

$$\theta = \tan^{-1}(\frac{F_{imag}}{F_{real}}) \qquad 4\text{-}7$$

F_e is the amplitude of the exciting force, F_{real} is the amplitude of the real part and F_{imag} is the amplitude of the imaginary part.

4.6.9 Solutions

The solution is the last step of the modelling and the step for signal evaluation. One of the main advantages of the FEA package (ANSYS software) is the boundary condition screen that provides the whole database for the model. It also provides the facility to choose the path of the outputs for future use.

4.6.10 Evaluations of the Results

Two steps, using the ANSYS package, can be used to evaluate the results from the modelling. These two steps are the POST26 and POST1. POST26 allows selection the forcing frequency for the highest displacement. POST1 is used to process the entire model at these critical frequencies. These steps give the facility to optimise the optimum signal parameters (amplitude, frequency and phase) under the modal and harmonic analysis.

4.6.11 Input Data

The input data used in the motor optimisation are given in tables 4-5, 4-6 and 4-7.

4.6.12 Frequency Optimisation

The piezoelectric vibrating bar is arranged as shown in Figure 4-3. The first surface is segmented into four sub-surfaces, which were arranged electrically to provide two sub-electrodes namely A and B. The second surface is connected to the earth and is labelled as electrode C. Then a single-phase signal with a wide frequency band is used to investigate their natural frequencies.

Figures 4-4, 4-5, 4-6 and 4-7 show the variation of the amplitude (displacement), phase, real and imaginary part against input frequency for the rotary structure of the proposed motor [Input signal was a positive signal on the order of 50volts].

Figures 4-11, 4-12, 4-13 and 4-14 show the variation of the amplitude (displacement), phase, real and imaginary part against exciting frequency for the rotary structure of the proposed motor [Input signal was a negative signal on the order of 50volts].

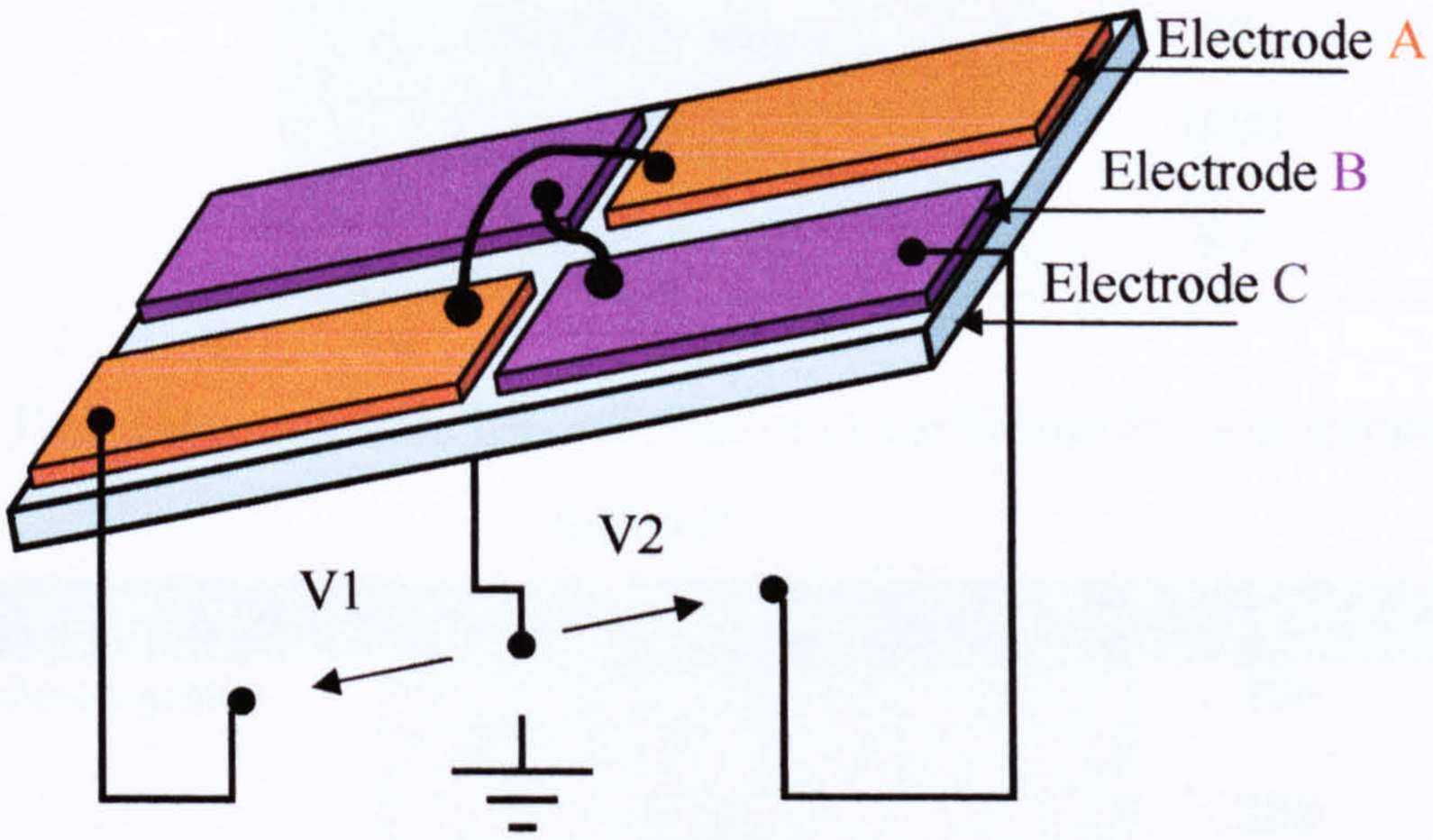

Figure 4-3 Basic configuration of the vibrating bar in a piezo-ceramic material and method used to generate motion

Table 4-5 Properties of Lead Zirconate Titanate-PC4D piezoceramics material used in modelling the proposed piezoelectric USM

Material	Coefficient	Coefficient Value
LZT PC4D	**Relative permittivity (Ωm)**	**1325**
	Dielectric loss (Ωm)	**0.002**
	Resistively (Ωm) x 10^{12}	**10**
	Quality factor	**1600**
	Density (kg/m^3)	**7550**
	Poisson's ratio	**0.3**
	Coupling factor	**0.7**

Table 4-6 Properties of Russian piezo-ceramic (CTS-19) material used in modelling the proposed piezoelectric USM

Material	Coefficient	Coefficient Value
CTS-19	**Elastic stiffness (N/m^2)**	**5.5-8.5 x10^9**
	Electric permittivity	**1500+/-300**
	Coupling Coefficient	**0.4**
	Quality factor	**50**
	Density (kg/m^3)	**7000**
	Poisson's ratio	**0.3**

Table 4-7 Transformation from E-coefficient to D-coefficient for piezoceramics material

Material	Coefficient	Value
Piezo-ceramics	d_{13} **x** 10^{-12}	**100**
	d_{33} **x** 10^{-12}	**200**

From Figures 4-4 and 4-11 it can be seen that the amplitude (displacement) changes sharply for the piezo-ceramic vibrating bar at a resonant frequency that is around 42.2 kHz. This initially shows the operating frequency and the response time of the proposed piezoelectric USM motor. The response time can be calculated roughly as Q times the vibration period. Q is the quality factor of the motor and can be determined using relation [Yaakov, S., et al., 1999]:

$$Q = \frac{R_m}{\sqrt{\frac{L}{C_\Sigma}}} \qquad 4\text{-}8$$

Where R_m is the equivalent resistor of the vibrating bar at a fixed operating frequency, L is the inductance of the LC-driving circuit and C_Σ is the total capacitance which is not constant and it is depend on the vibrating bar internal capacitance, cable internal capacitance and LC-driving circuit capacitance.

The resolution of the proposed motor can also be determined, from this analysis using the expansion obtained from the material deformation. For instance the minimum extension obtained using FE analysis was found to be 10.1125 μm (see Figure 4-4 for the rotary structure of the motor). This can be used to determine the angular displacement θ. Angular displacement can be determined using dynamic model shown in Figure 4-40 (a) and relation: $\theta = \frac{s}{R}$. s is the arc length and R is the radius of the driving wheel of the motor. Using θ it will be possible to determine average angular velocity $\bar{\omega}$ using the relation: $\bar{\omega} = \frac{\Delta\theta}{\Delta t}$. $\bar{\omega}$ can be used to determine the average angular acceleration $\bar{\alpha}$ of the system using the relation: $\bar{\alpha} = \frac{\Delta\omega}{\Delta t}$. Where $\Delta\omega$ is the change on the angular velocity for a specified period of time Δt. Consequently it will be possible to determine the minimum rate of the motion.

Figures 4-6, 4-7, 4-13 and 4-14 show the influence of the real part and imaginary part of the input signal. This shows that the real part is of the order of 10^{-5} meters and the imaginary part is of the order of 10^{-20} meters. This is showed clearly that the real part of the applied signal has the major influence on the vibrating bar when compared to the imaginary part of the input signal on the case of positive half cycle of the input signal and vice versa for the other half.

Figures 4-18, 4-19, 4-20 and 4-21 show the variation of the amplitude (displacement), phase, real and imaginary part against input frequency for the linear structure of the proposed motor [Input signal was a positive signal on the order of 50volts].

Figures 4-28, 4-29, 4-30 and 4-31 show the variation of the amplitude(displacement), phase, real and imaginary part against input frequency for the linear structure of the proposed motor Input signal was a negative signal on the order of 50volts].

Here it can be seen the influence of the sliding element, as a real load. It affects the amplitude (displacement) variation against the input frequency as shown in Figures 4-18

and 4-28. These also show the influences of the load on the extension and contraction steps of the piezoelectric element of the motor.

Figures 4-5, 4-12, 4-19 and 4-29 show the variation of the phase against exciting frequency within the same input frequency range for both structures of the motor. These variations can be used to select and identify the shape of the input signal required to drive the proposed motor.

4.6.13 Amplitude Optimisation

An optimisation of the signal response parameters of the proposed model has been carried out. This optimisation was theoretically interrelated to the expansion and deformation of the LZT material. However, the experimental results show that many technical points have to also be considered during this optimisation such as the temperature of the piezoelectric LZT bar, operating conditions of the motor and its application. Samples of the input signal that have been used in the model signal response optimisation process, are illustrated in table 4-4. The model deformed shape for different input signal in x, y and z direction are determined.

Figures 4-8, 4-9, and 4-10 show the deformation mode (1) in x, y, and z direction at the optimised operating frequency and with real part of the input signal for the rotary structure of the motor [Input signal was a positive signal on the order of 50volts].

Figures 4-15, 4-16, and 4-17 show the deformation mode (2) in x, y, and z direction at the optimised operating frequency and with real part of the input signal for the rotary structure of the motor [Input signal was a negative signal on the order of 50volts].

Figures 4-22, 4-23, and 4-24 show the deformation mode (1) in x, y, and z direction at the optimised operating frequency and with real part of the input signal for the linear structure of the motor [Input signal was a positive signal on the order of 50volts].

Figures 4-32, 4-33, and 4-34 show the deformation mode (2) in x, y, and z direction at the optimised operating frequency and with real part of the input signal for the linear structure of the motor [Input signal was a negative signal on the order of 50volts].

It can be seen from these Figures the two modes of vibration of the piezoceramic vibrating bar for both rotary and the linear structure of proposed model. These two modes of vibration can be used to determine the principle of operation of the motor. Controlling the phase between these two modes of vibration controlled the direction of propagation of the piezoelectric material and consequently the direction of motion of the motor.

Figures 4-25, 4-26, 4-27, 4-35, 4-36 and 4-37 show the actuator-total strain mode (1) and mode (2) in x, y and z direction at the optimised operating frequency for the linear construction of the motor at various input signals. This also shows clearly the distribution of the influence of the input signal on the piezoelectric vibrating bar. It is allow investigating the deformation of this type of material. The investigation of the material deformation can be used in preventing the 'jerking' effect that occurs as a results of mishandling of the bar deformation.

Various materials have been used in this analysis and the aim of this was to select the required piezo-ceramic material that would meet the design need. This was carried out using the properties and various input signal. Based on material deformations and modes of vibrations, LZT-PC4D piezo-ceramic material, has been selected and has been used successfully in the developed prototype. These analyses also show that the real part of the input signal has a major influence on the vibrating bar compared to the imaginary part of the input signal as shown in Figure 4-6, 4-7, 4-13 and 4-14 respectively.

This established methodology of analysis using FEA for the proposed model enables to select the piezoelectric material required, and optimise the driving parameters. It also used in proposing an innovative technique to control the direction of motion by controlling the phase between the two modes of vibration. It illustrates the piezoelectric element maximum and minimum displacement, which is mainly dependent on the properties of the material and input signal parameters. This can be used in determining the resolution of the motor.

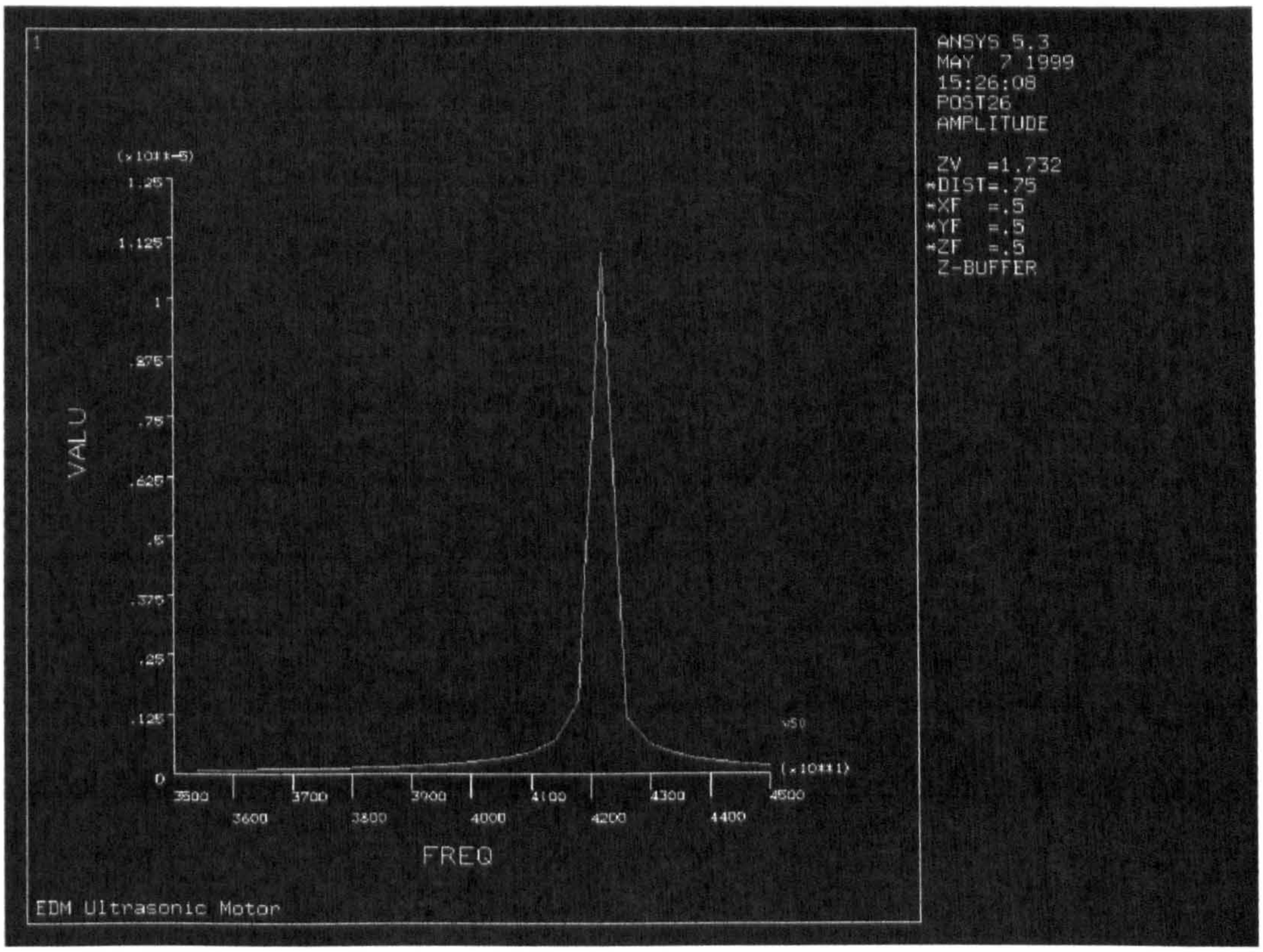

Figure 4-4. The amplitude (displacement) variation against exciting frequency for the proposed piezoelectric USM 'rotary structure' (AC 50V)

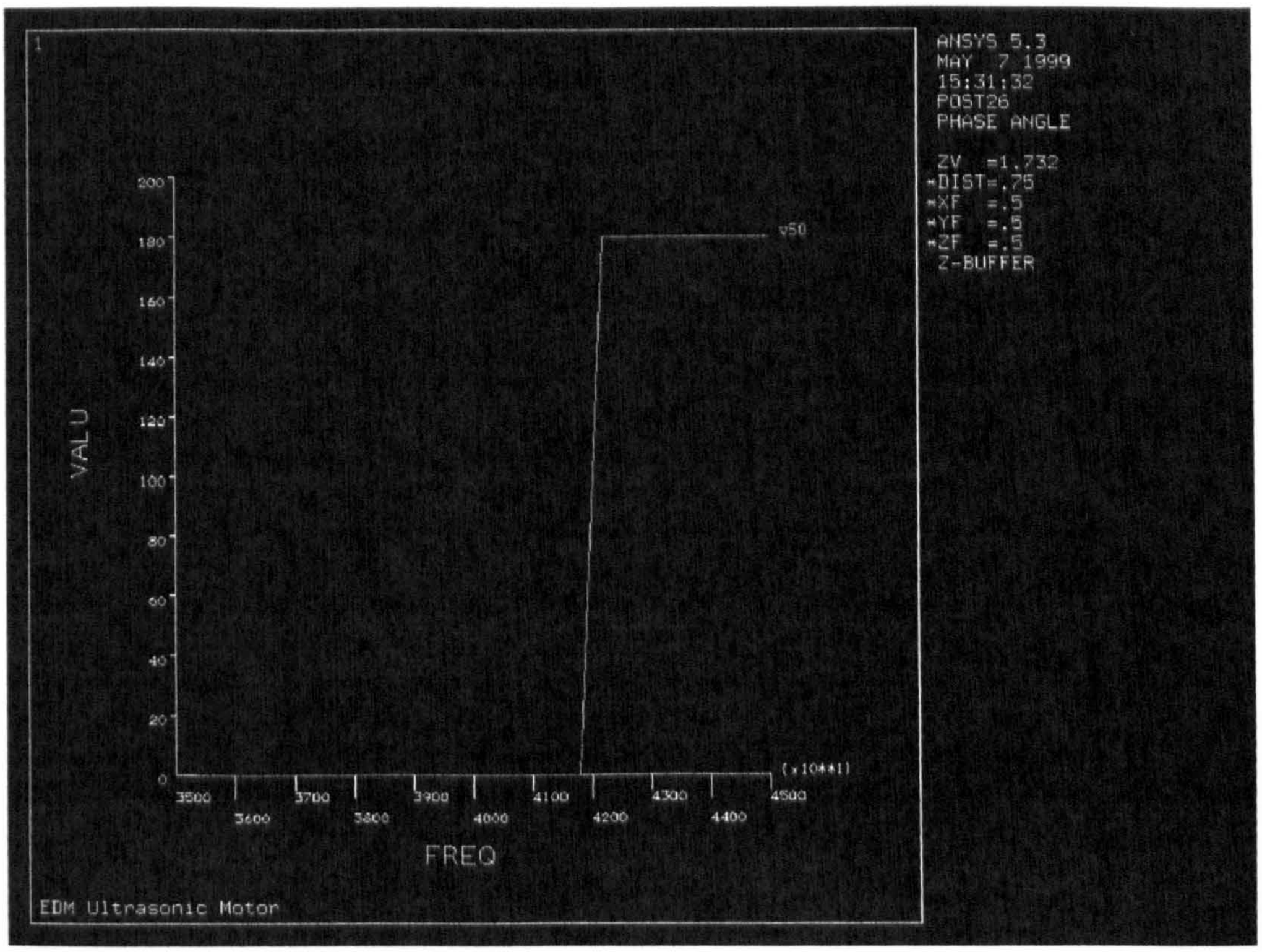

Figure 4-5. The phase variation against exciting frequency for the proposed piezoelectric USM 'rotary structure' (AC 50V)

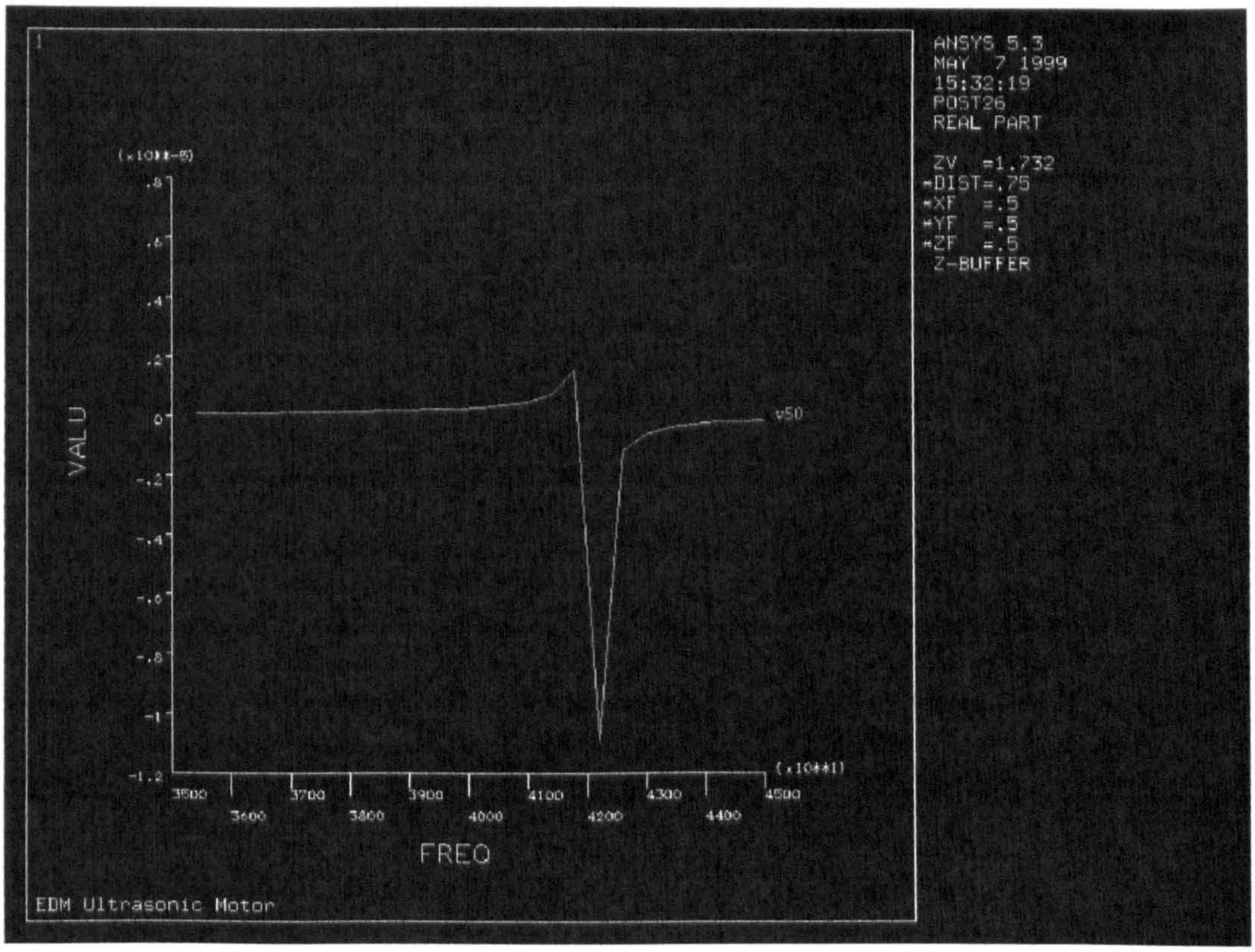

Figure 4-6. The real part amplitude (displacement) variation against exciting frequency for the proposed piezoelectric USM 'rotary structure' (AC 50V)

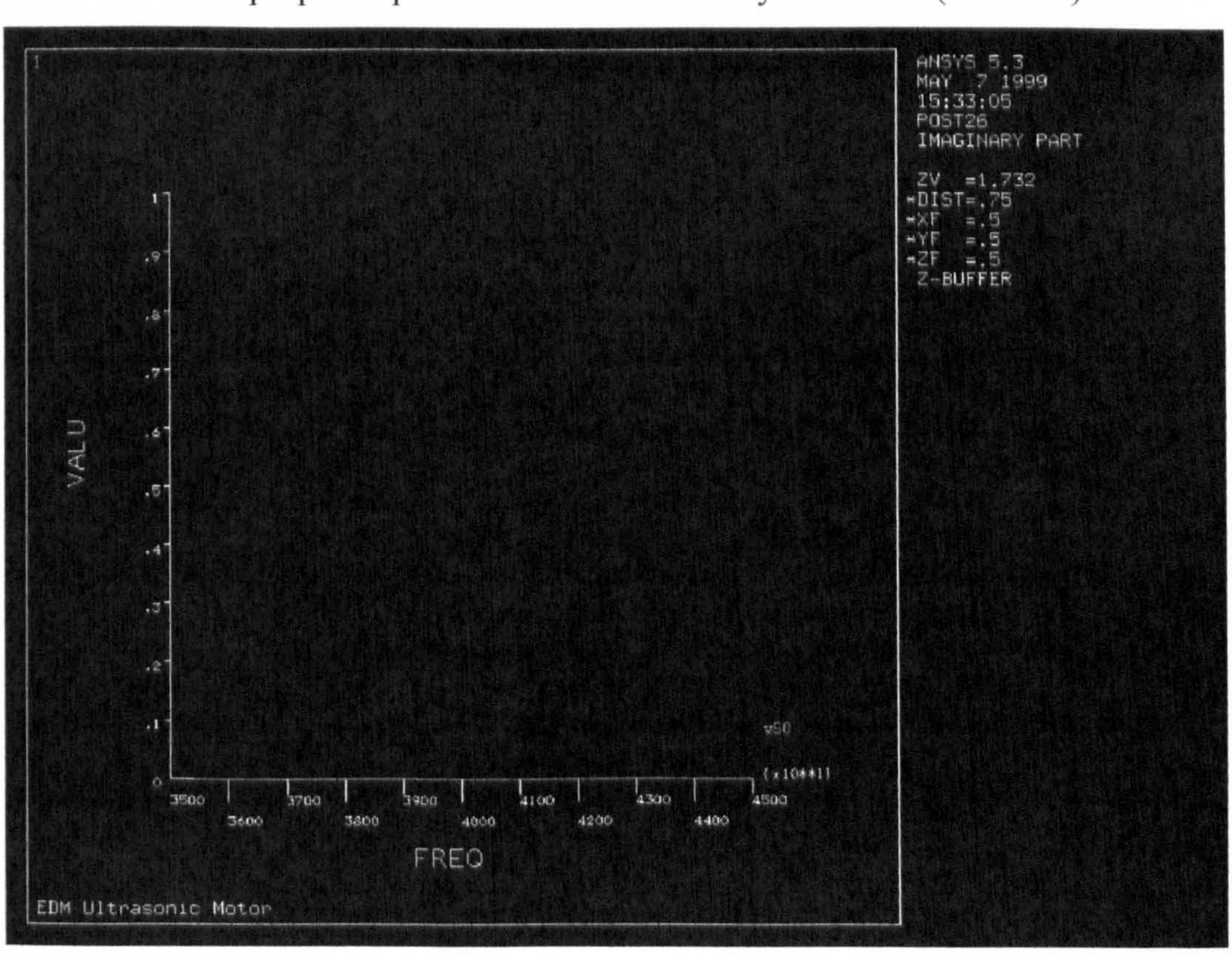

Figure 4-7. The imaginary part amplitude (displacement) variation against exciting frequency for the proposed piezoelectric USM 'rotary structure' (AC 50V)

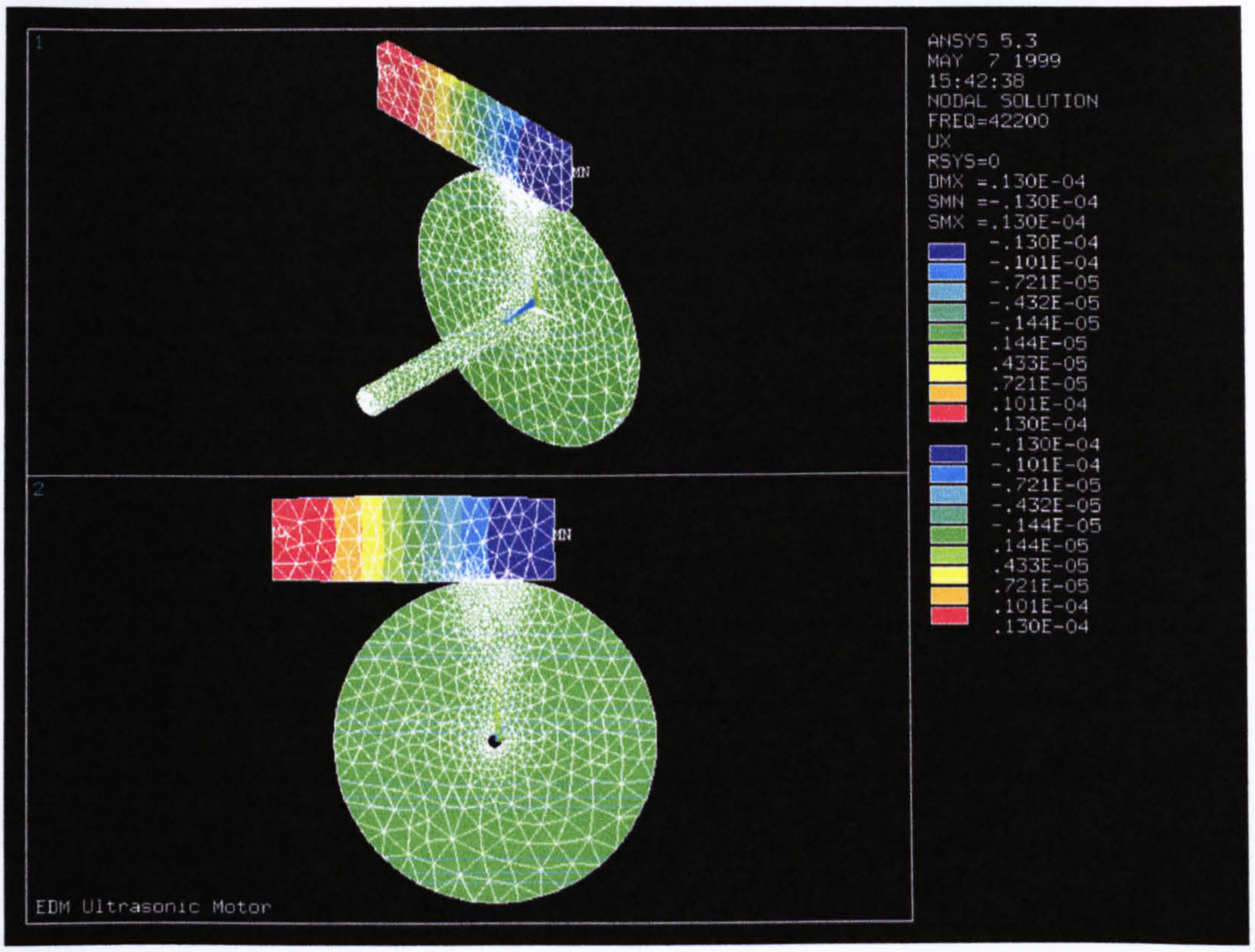

Figure 4-8. Deformed shape for the real part of the input signal for the motor at the optimised operating frequency 'Mode (1)-rotary structure' (x-direction) (50Volt)

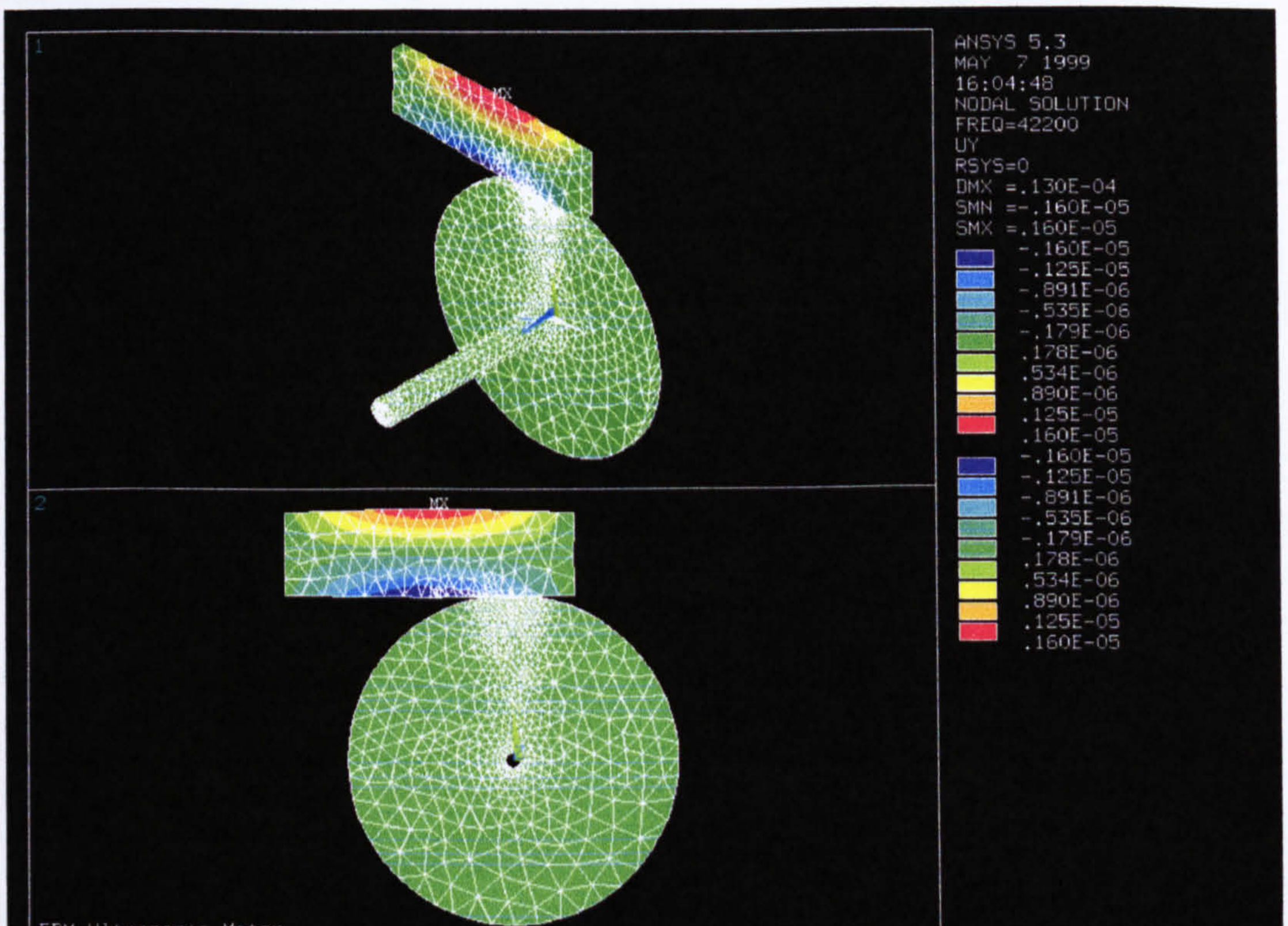

Figure 4-9. Deformed shape for the real part of the input signal for the motor at the optimised operating frequency 'Mode (1)-rotary structure' (y-direction) (50Volt)

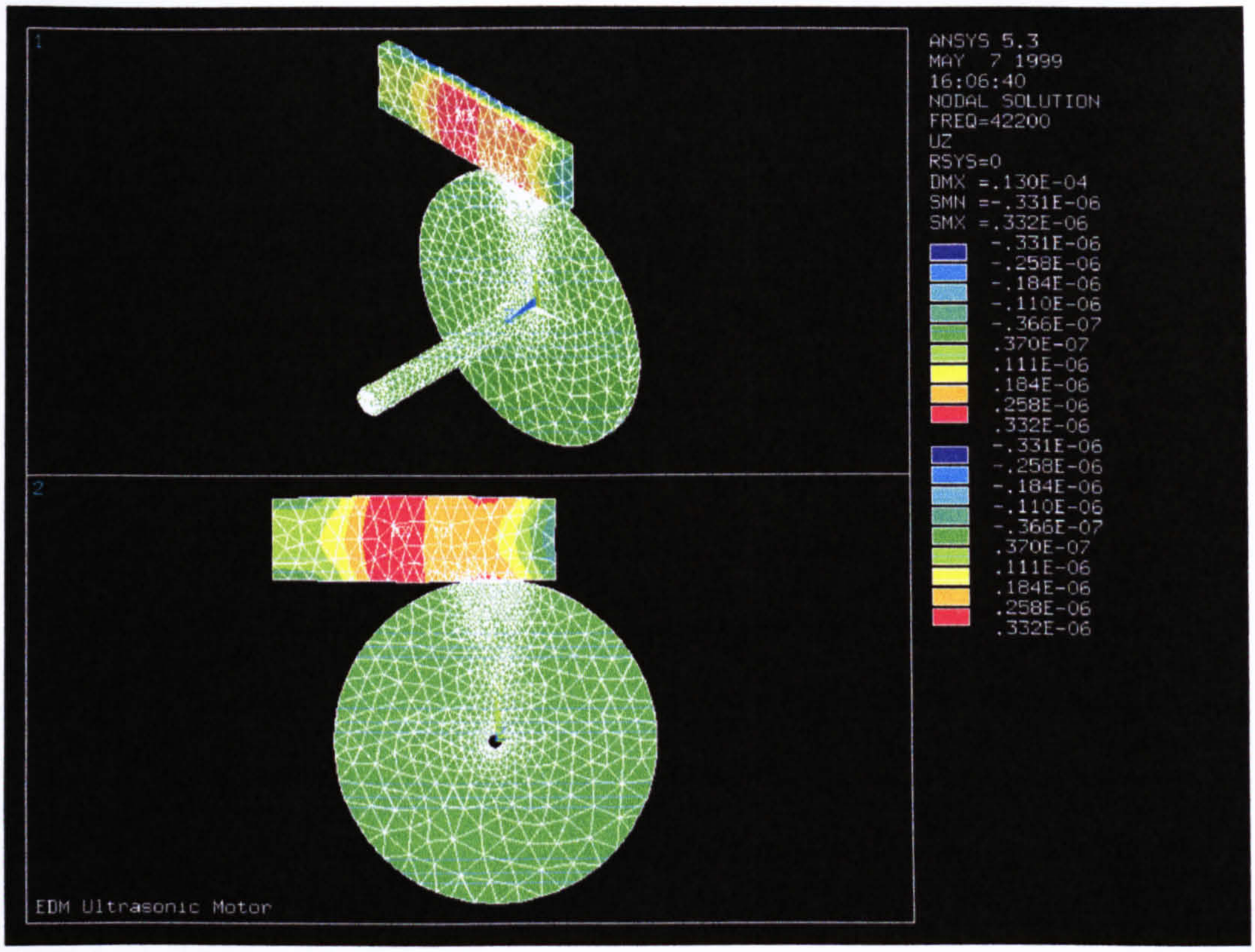

Figure 4-10. Deformed shape for the real part of the input signal for the motor at the optimised operating frequency 'Mode (1) -rotary structure' (z-direction) (50Volt)

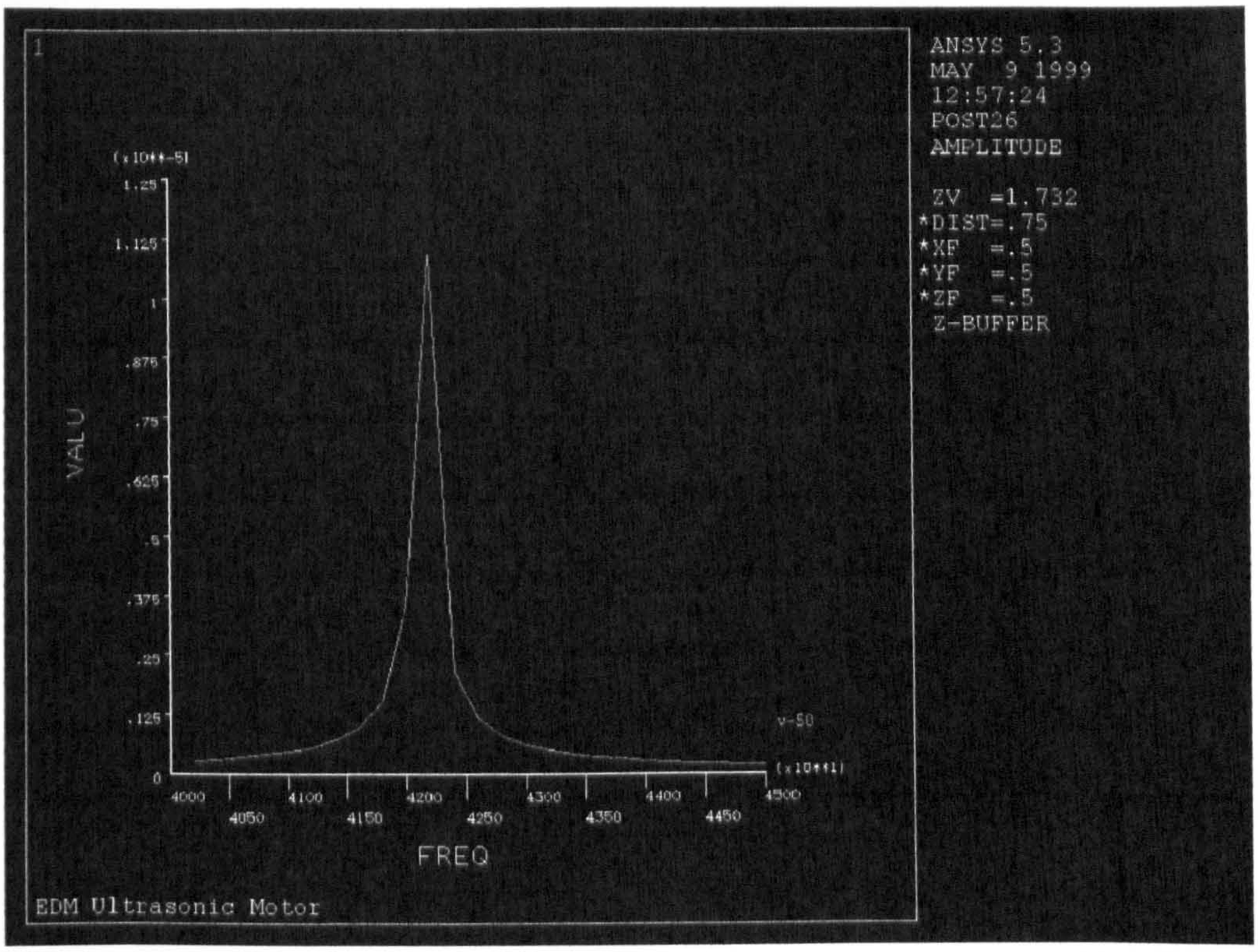

Figure 4-11. The amplitude (displacement) variation against exciting frequency for the proposed piezoelectric USM 'rotary structure' (-50Volt)

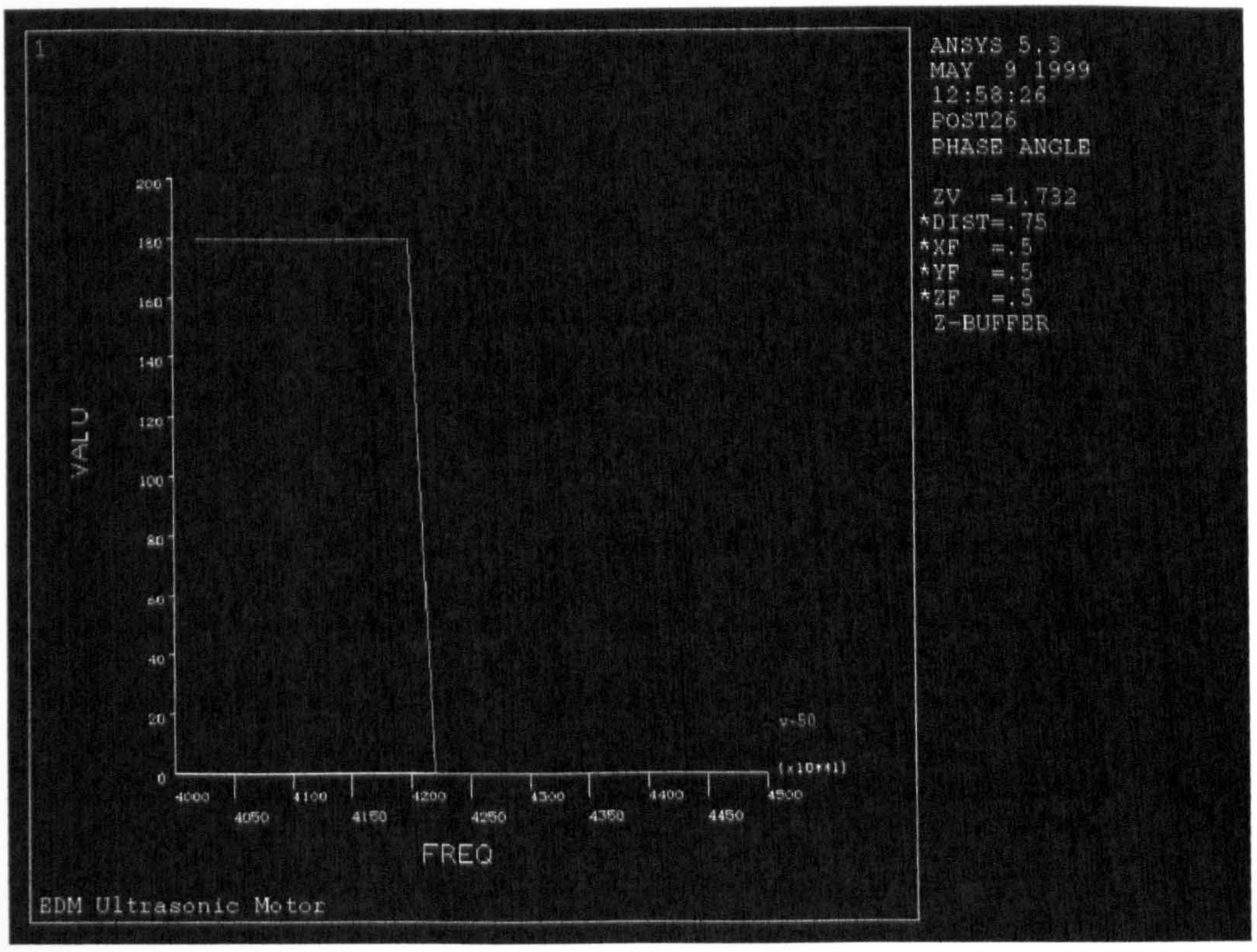

Figure 4-12. The phase variation against exciting frequency for the proposed piezoelectric USM 'rotary structure' (-50Volt)

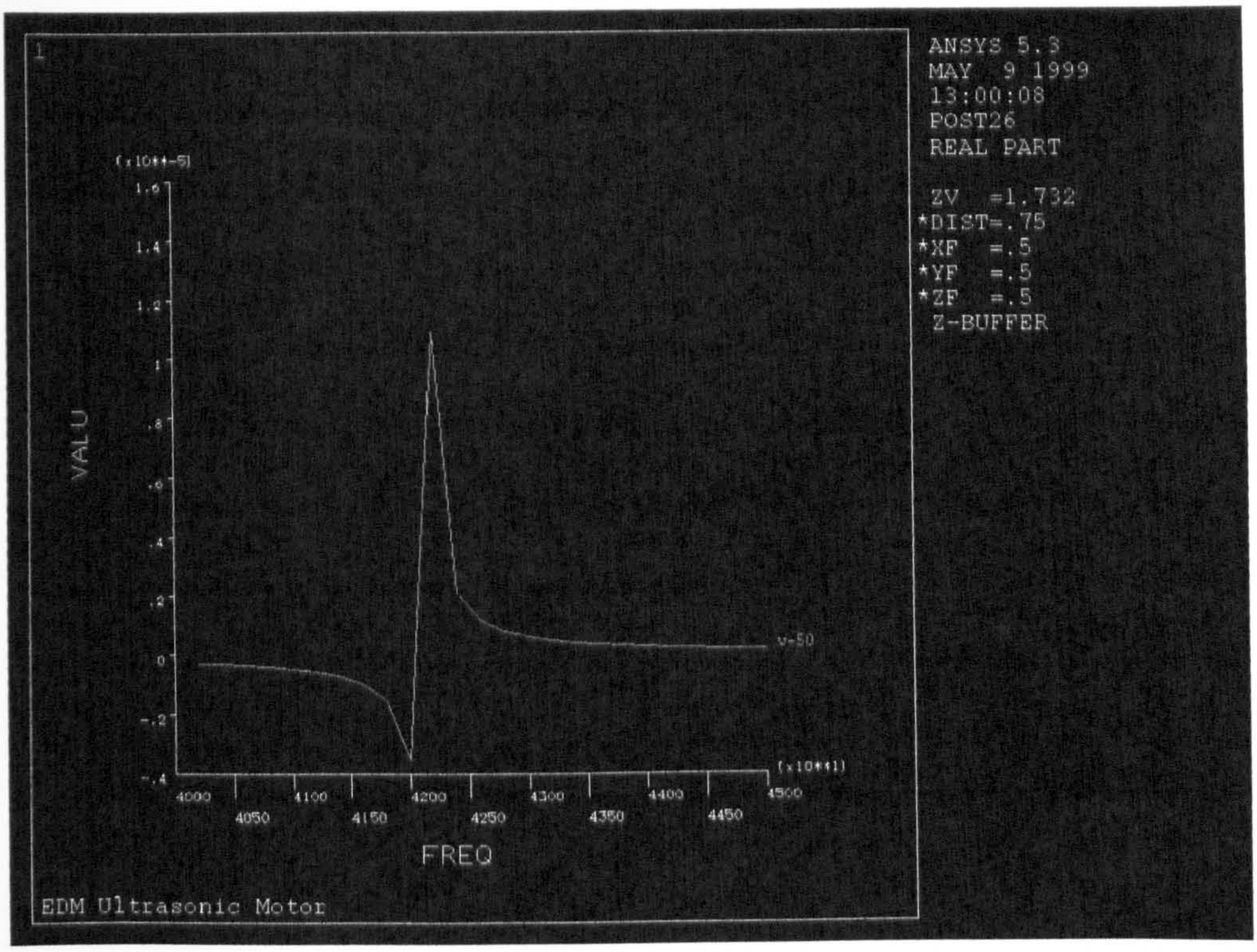

Figure 4-13. The real part amplitude (displacement) variation against exciting frequency for the proposed piezoelectric USM 'rotary structure' (-50Volt)

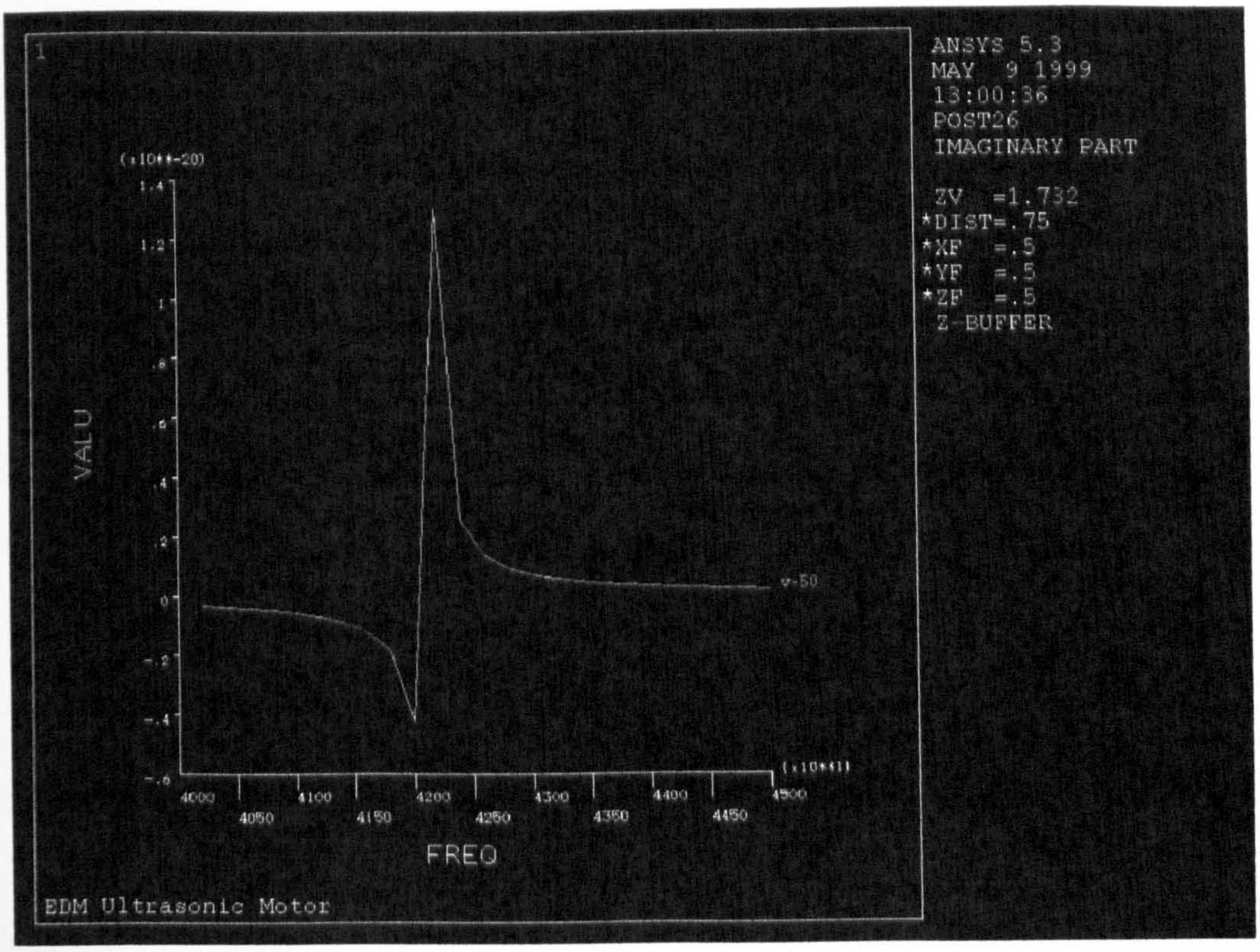

Figure 4-14. The imaginary part amplitude (displacement) variation against exciting frequency for the proposed piezoelectric USM 'rotary structure' (-50Volt)

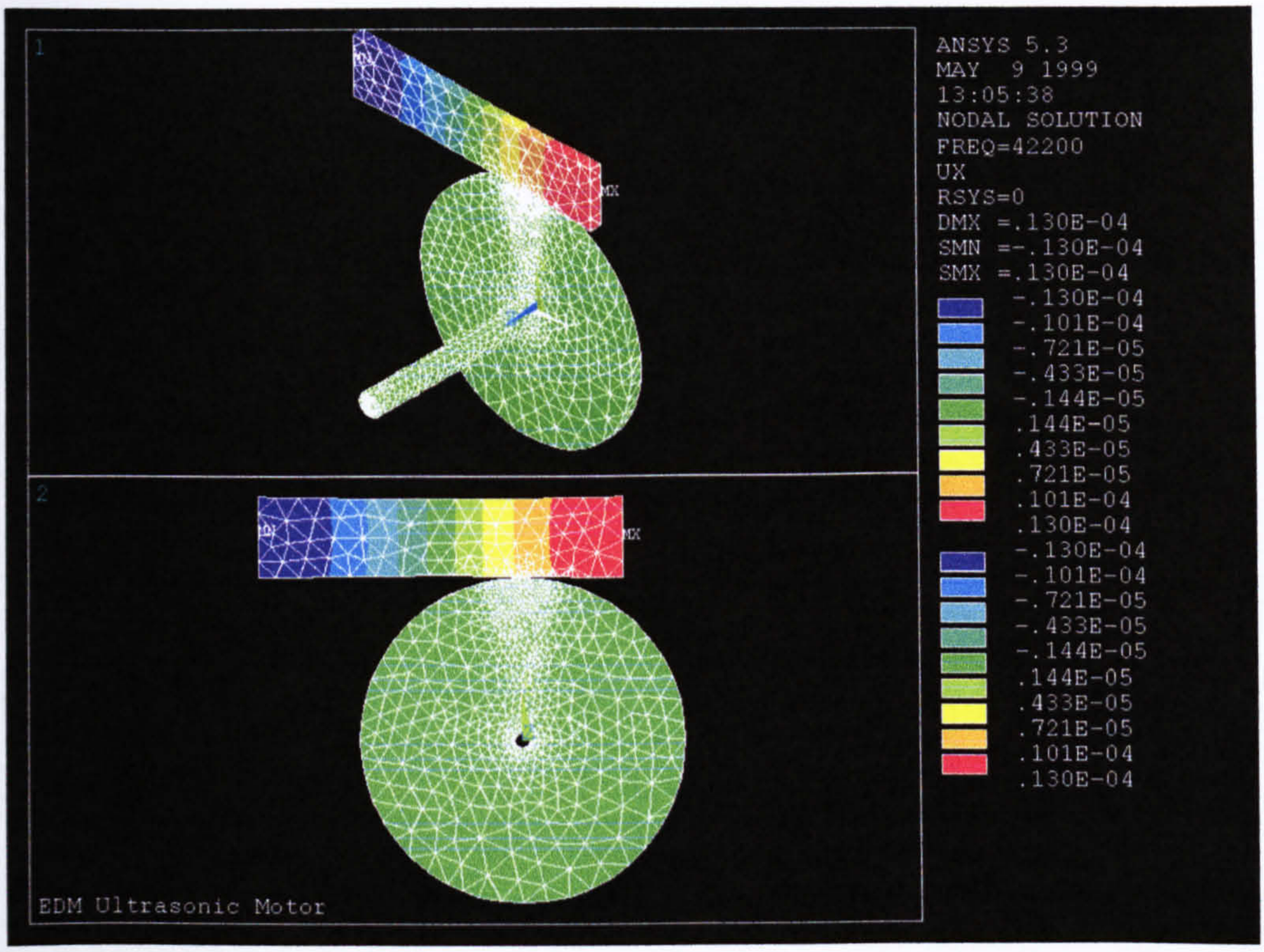

Figure 4-15. Deformed shape for the real part of the input for the motor at the optimised operating frequency 'Mode (2) -rotary structure' (x-direction) (-50Volt)

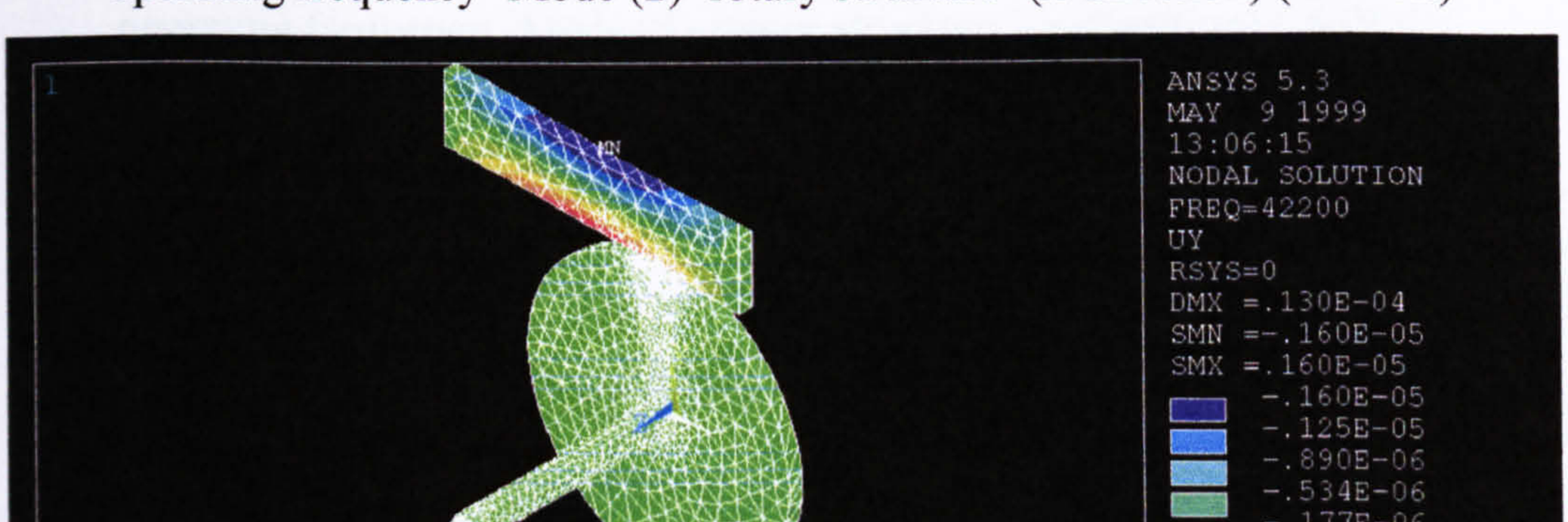

Figure 4-16. Deformed shape for the real part of the input for the motor at the optimised operating frequency 'Mode (2) -rotary structure' (y-direction) (-50Volt)

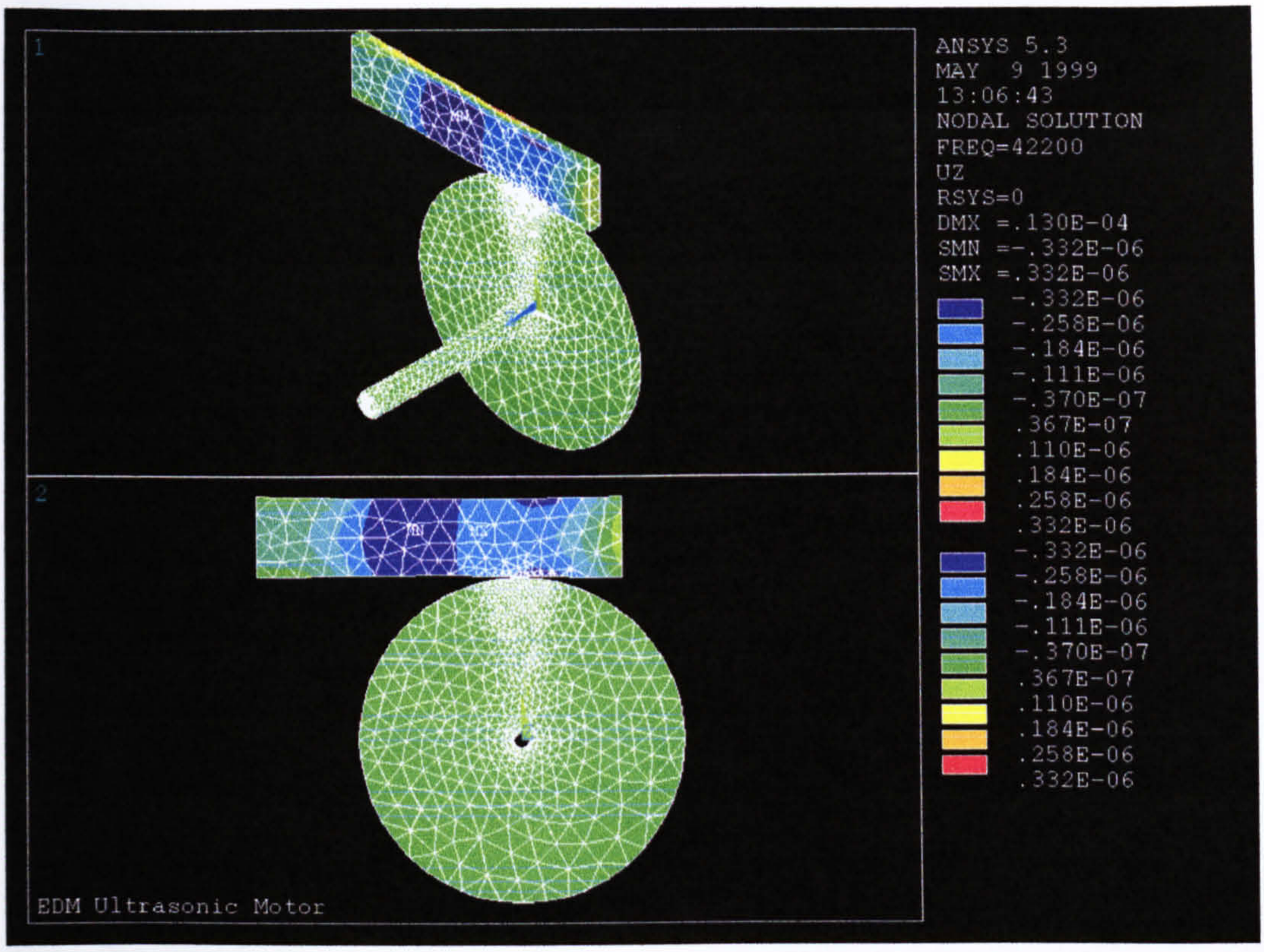

Figure 4-17. Deformed shape for the real part of the input for the motor at the optimised operating frequency 'Mode (2)-rotary structure' (z-direction) (-50Volt)

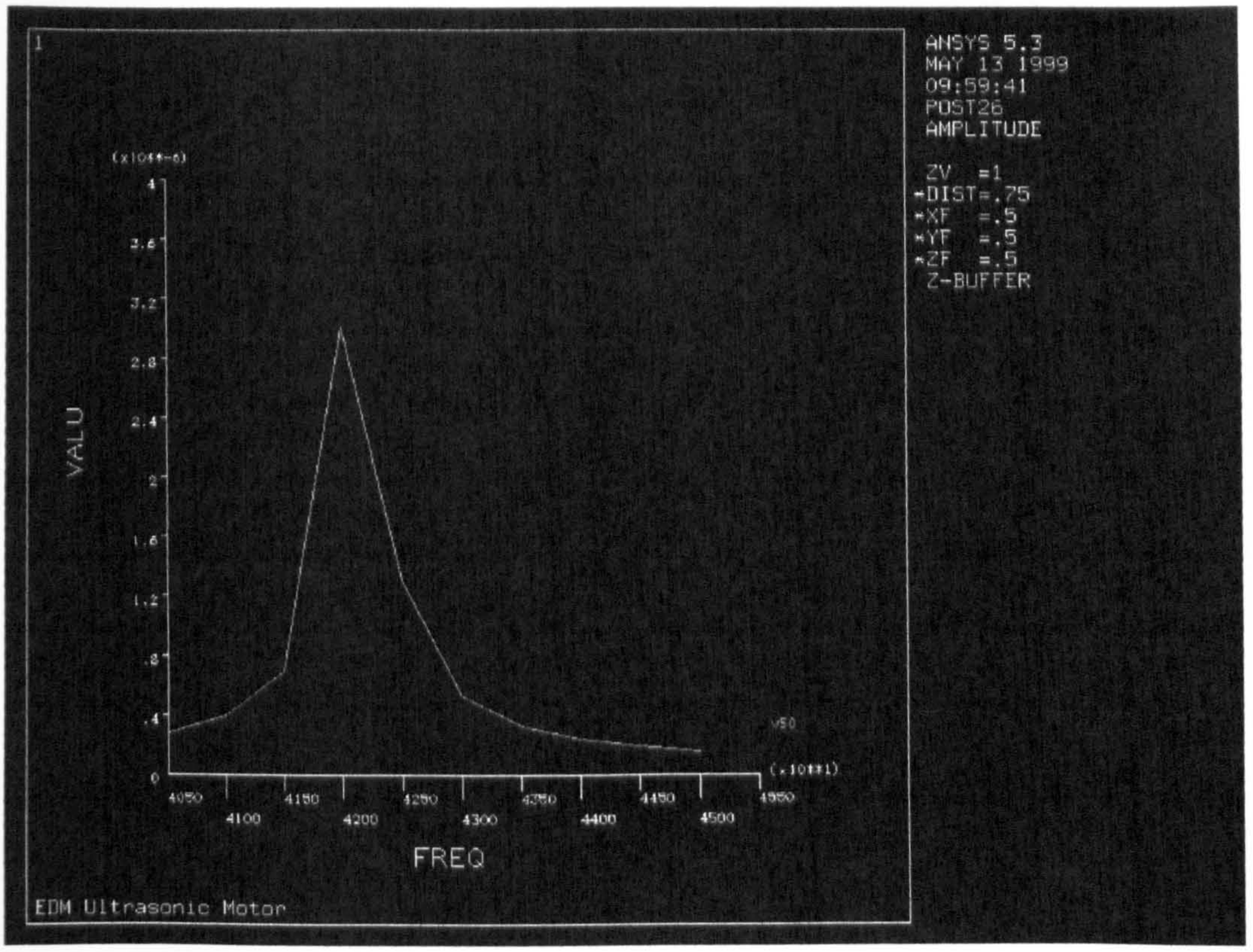

Figure 4-18. The amplitude (displacement) variation against exciting frequency for the proposed piezoelectric USM 'linear structure' (50Volt)

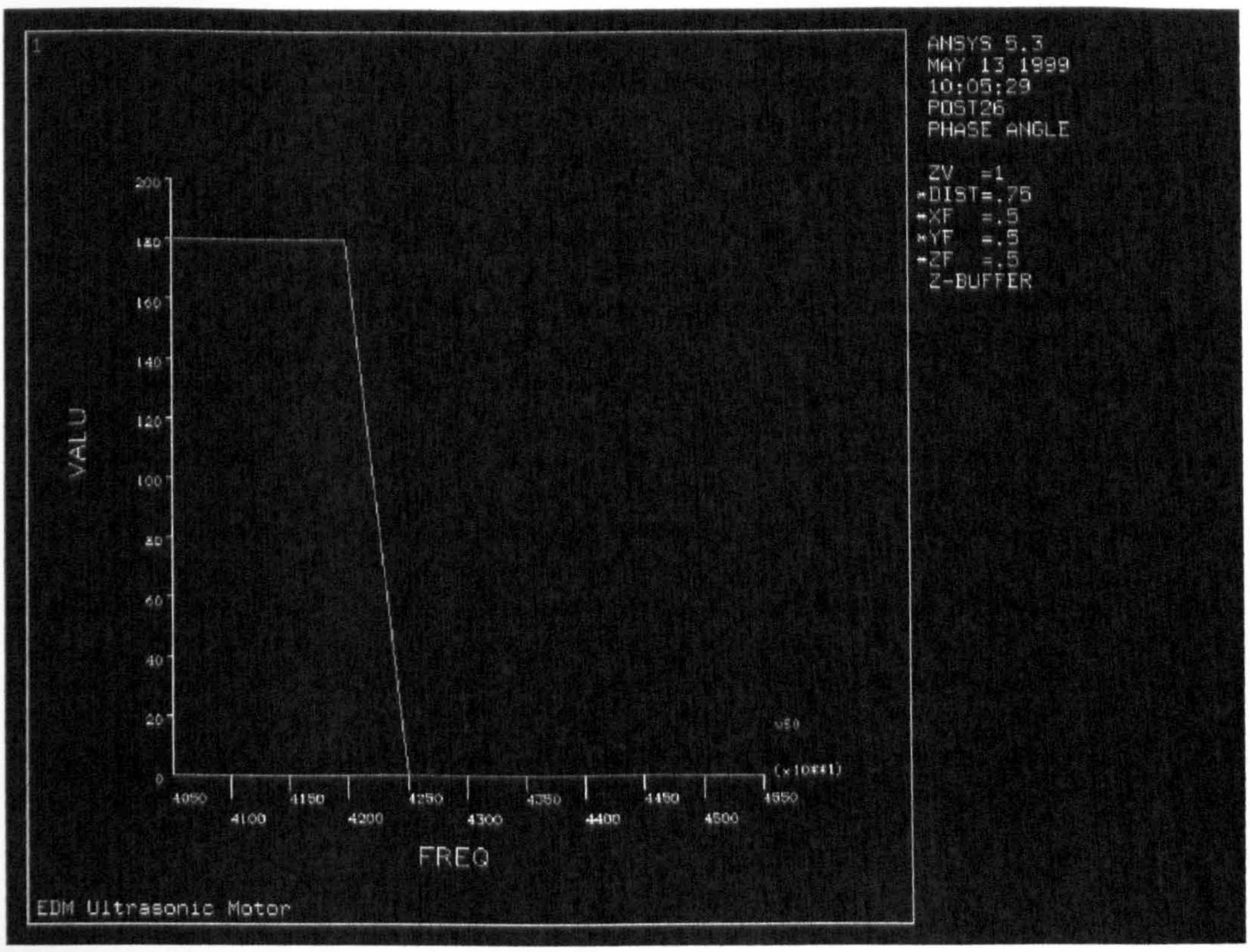

Figure 4-19. The phase variation against exciting frequency for the proposed piezoelectric USM 'linear structure' (50Volt)

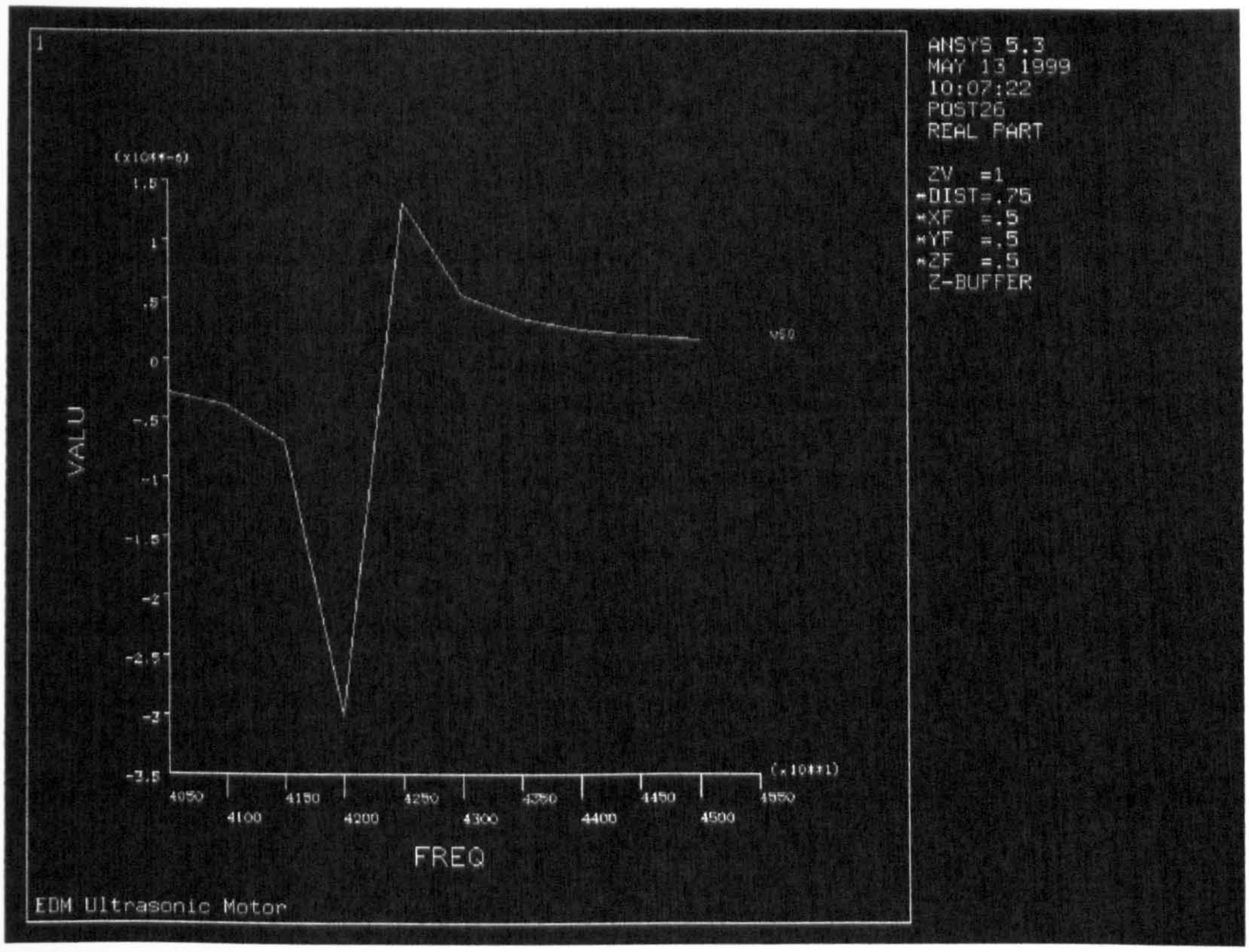

Figure 4-20. The real part amplitude (displacement) variation against exciting frequency for the proposed piezoelectric USM 'linear structure' (50Volt)

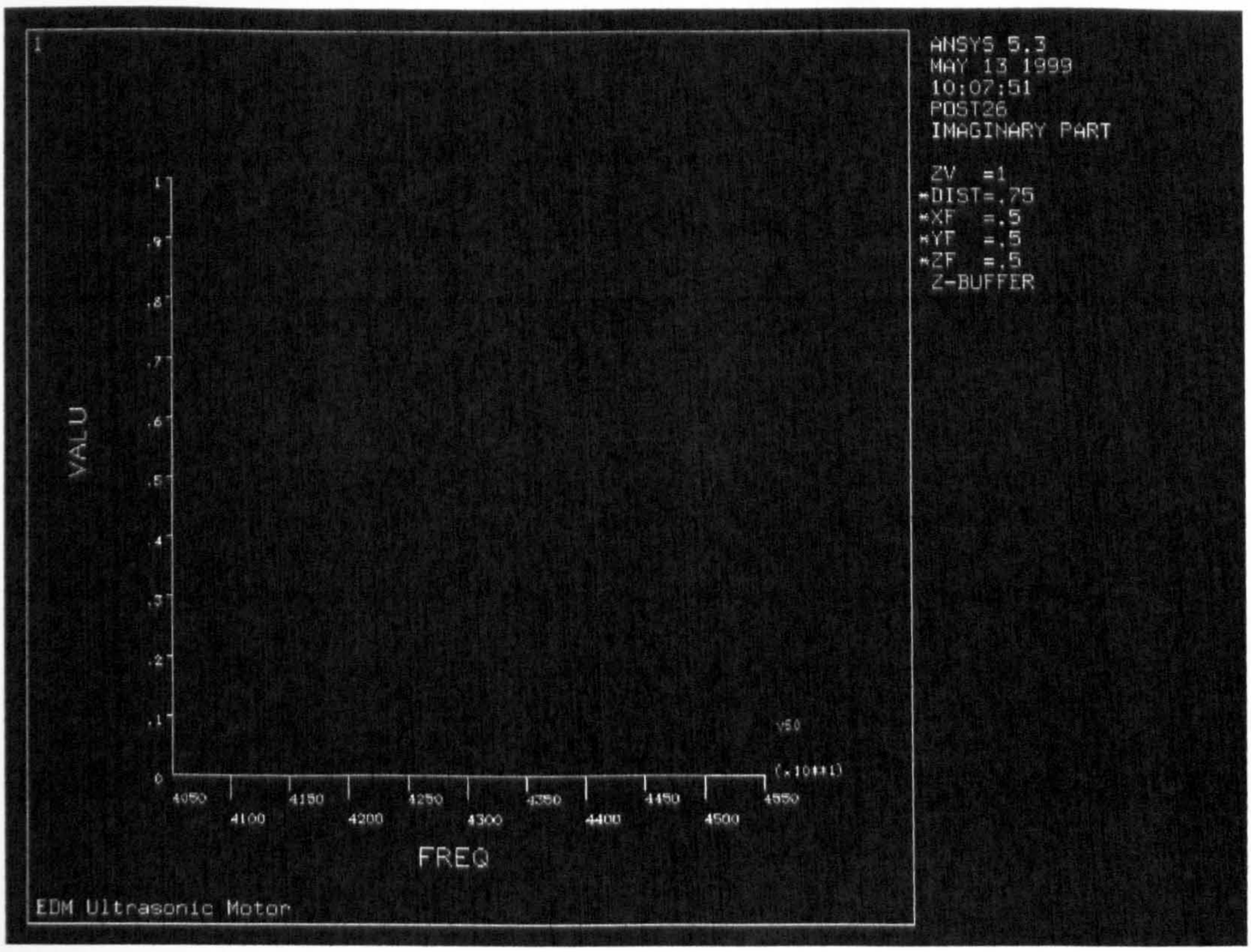

Figure 4-21. The imaginary part amplitude (displacement) variation against exciting frequency for the proposed piezoelectric USM 'linear structure' (50Volt)

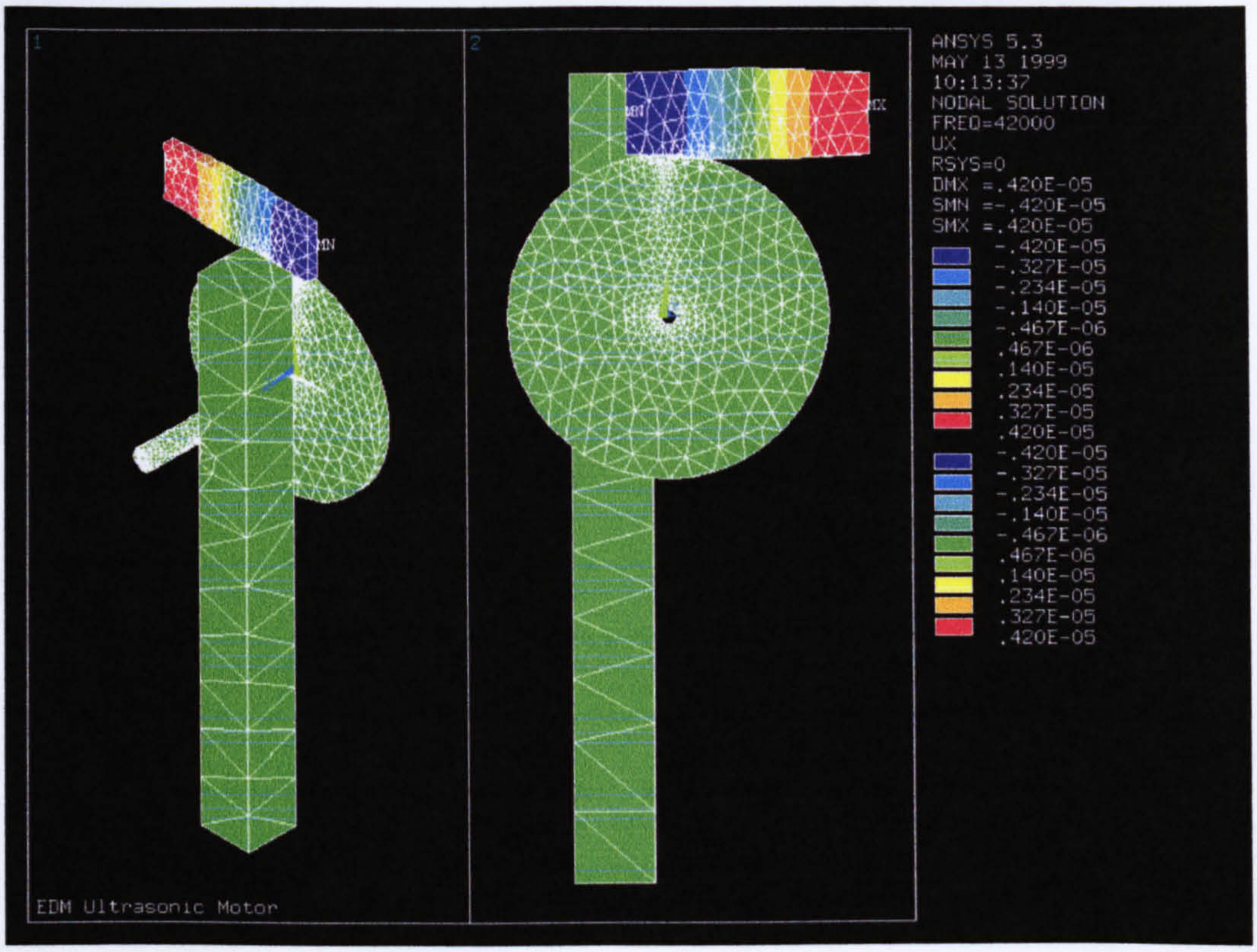

Figure 4-22. Deformed shape for the real part of the input for the motor at the optimised operating frequency 'Mode (1)-linear structure' (x-direction) (50Volt)

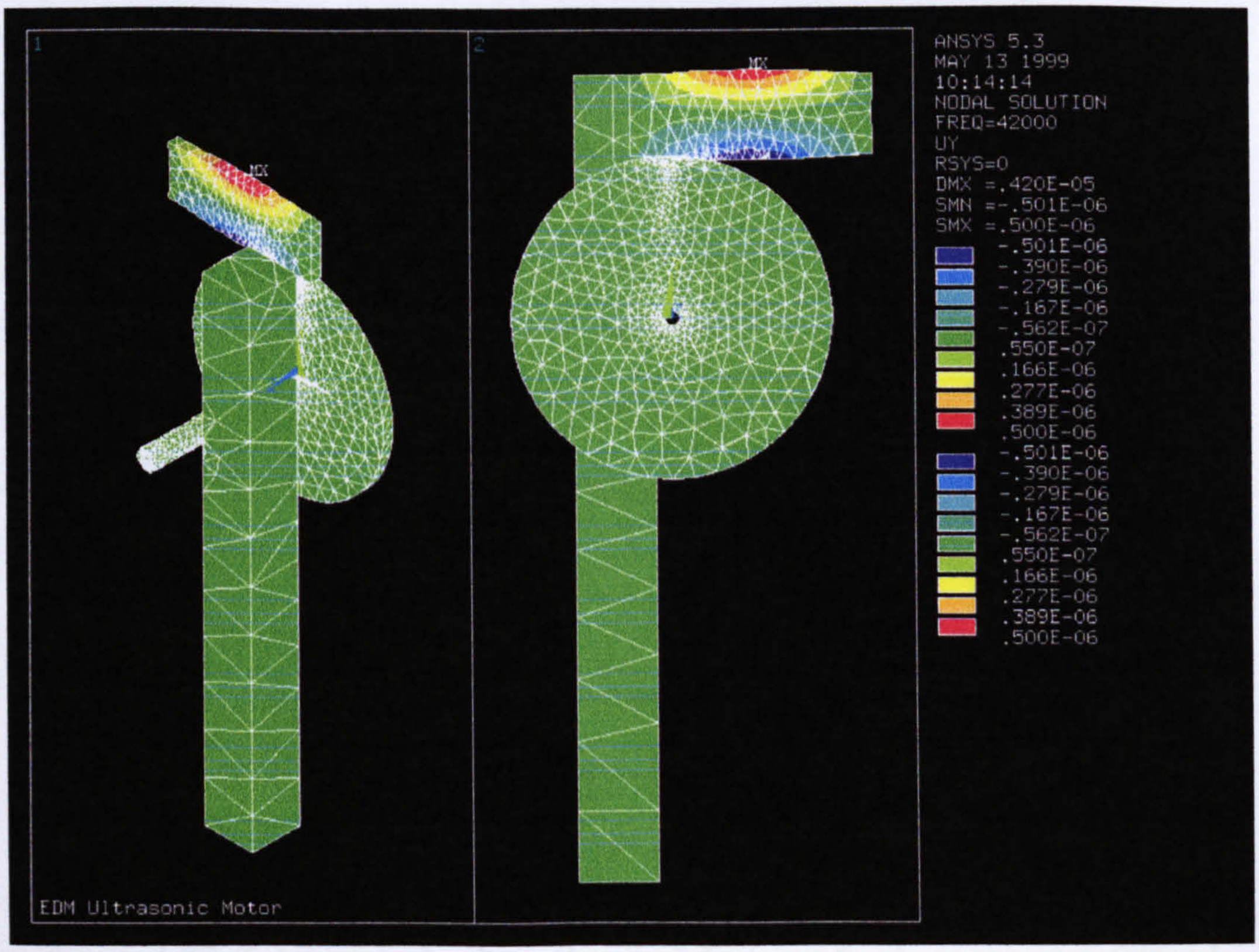

Figure 4-23. Deformed shape for the real part of the input for the motor at the optimised operating frequency 'Mode (1)-linear structure' (y-direction) (50Volt)

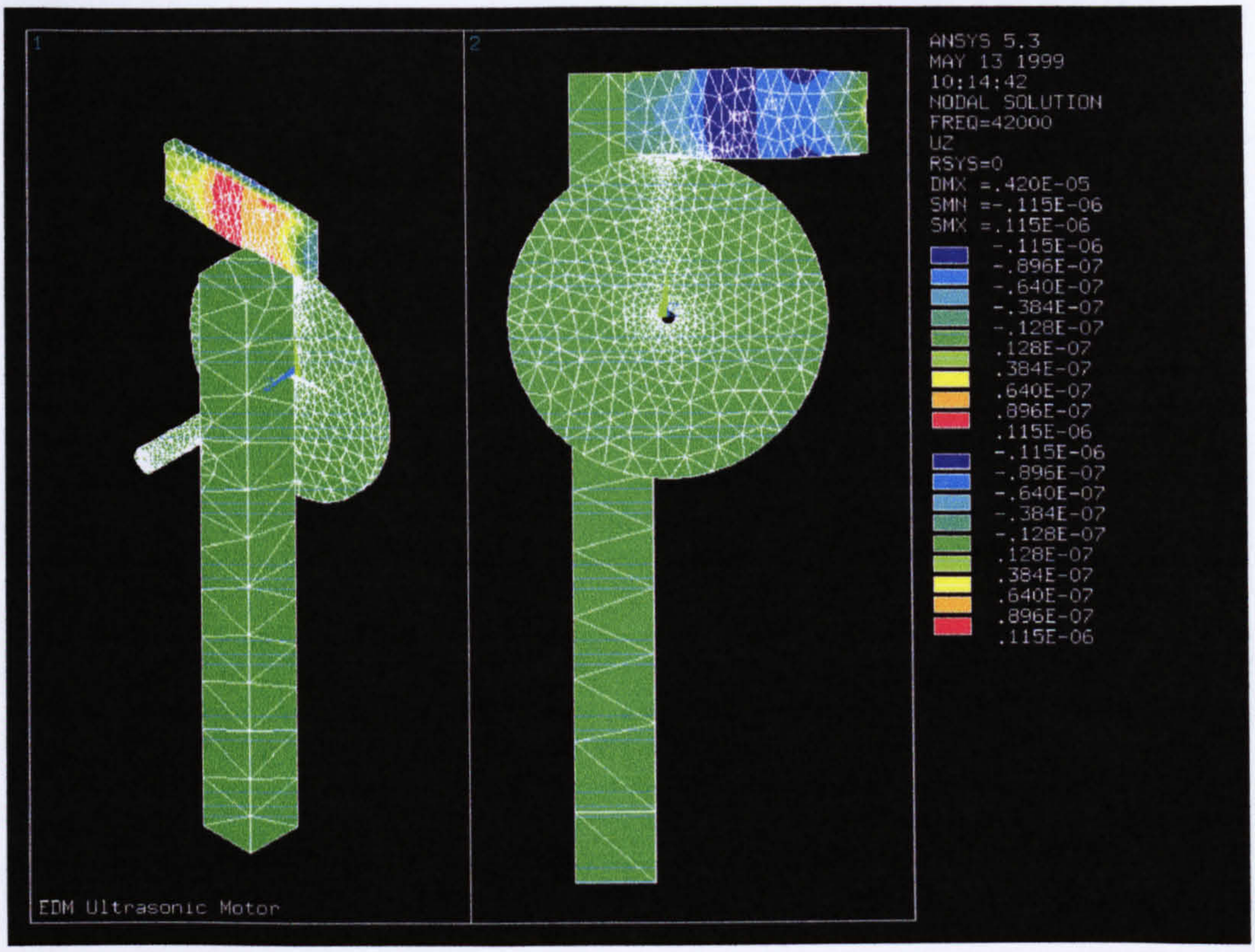

Figure 4-24. Deformed shape for the real part of the input for the motor at the optimised operating frequency 'Mode (1)-linear structure' (z-direction) (50Volt)

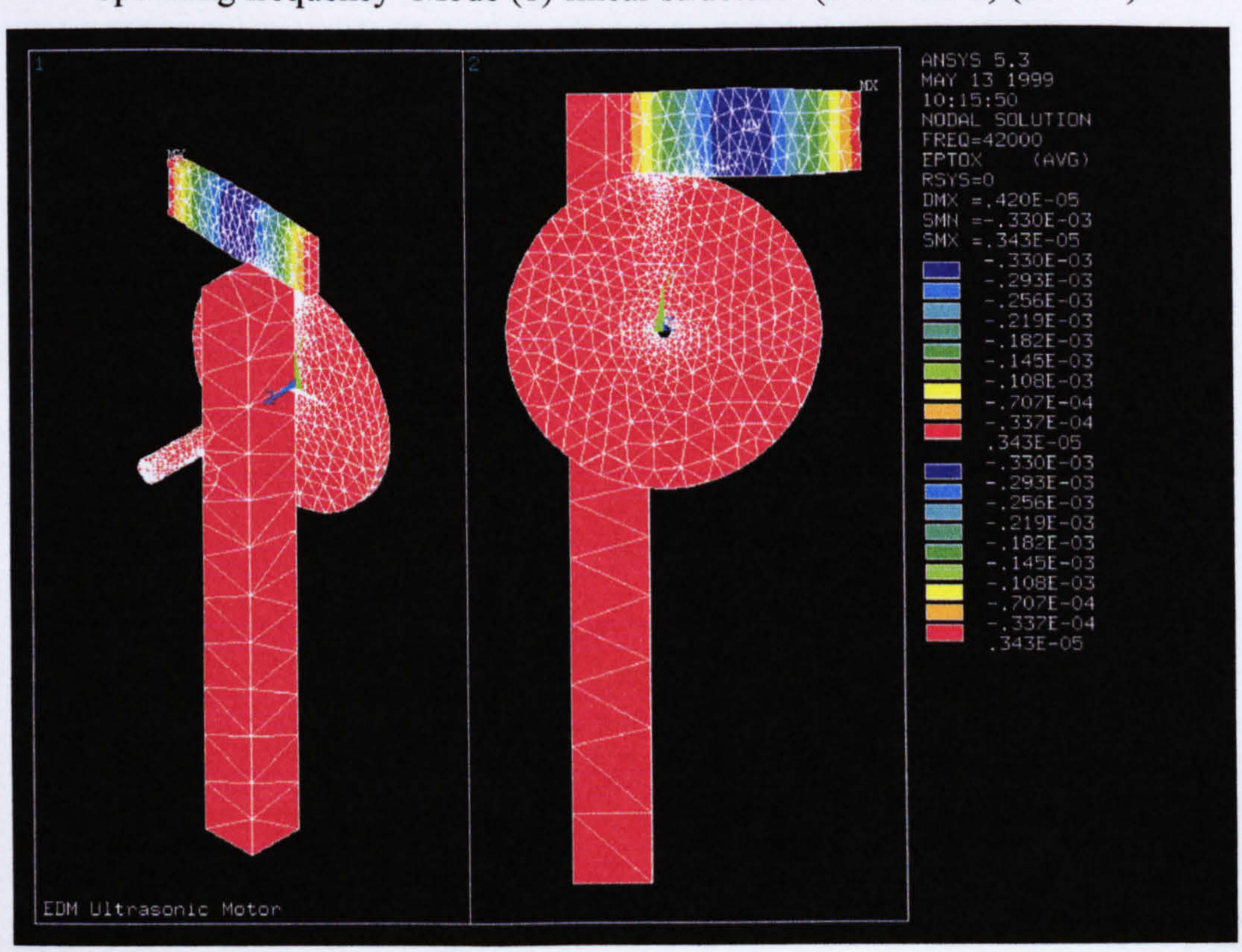

Figure 4-25. Total strain for the real part of the input for the motor at optimised operating frequency 'Mode (1)-linear structure' (x-direction) (50Volt)

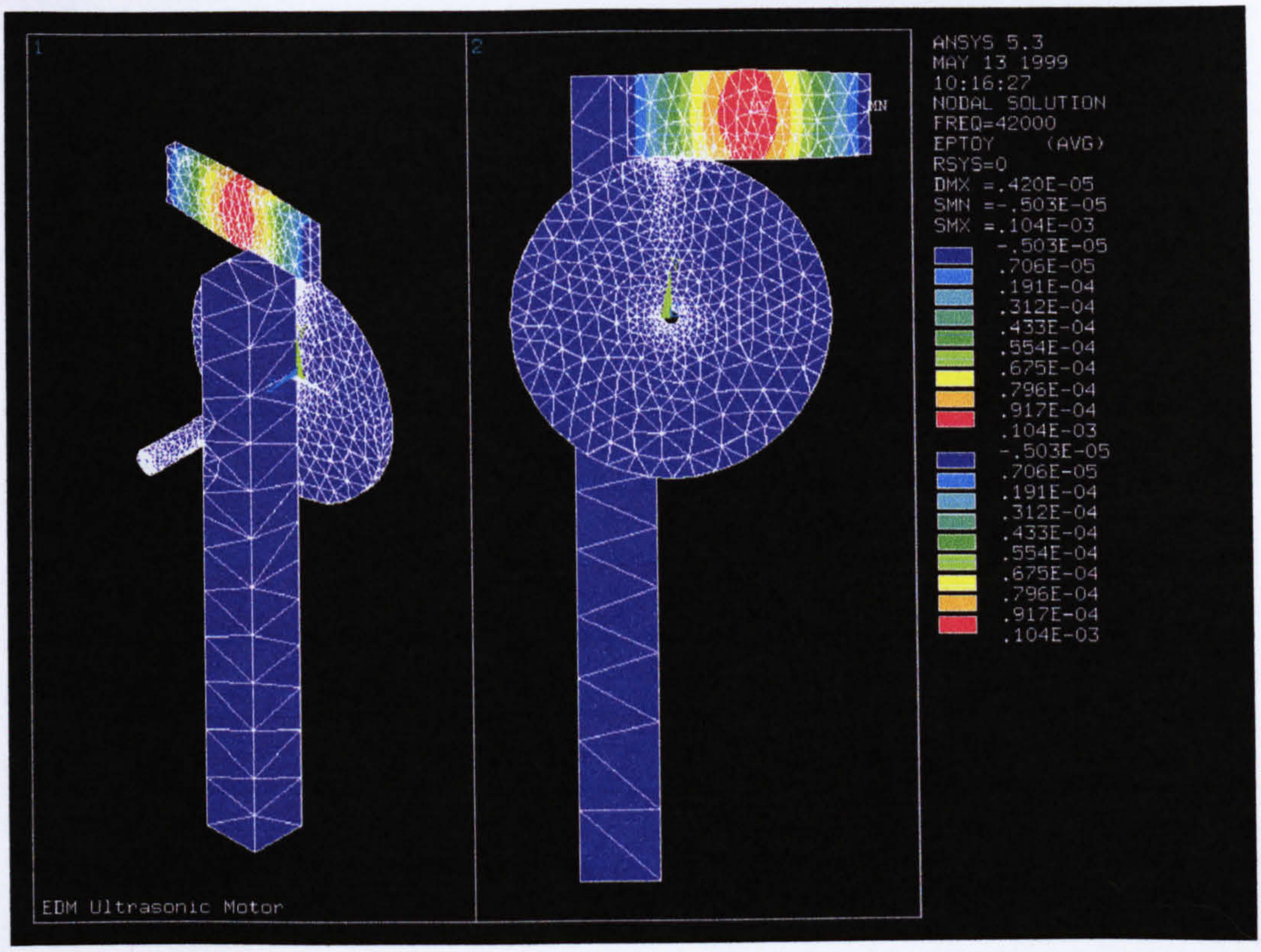

Figure 4-26. Total strain for the real part of the input for the motor at optimised operating frequency 'Mode (1)-linear structure' (y-direction) (50Volt)

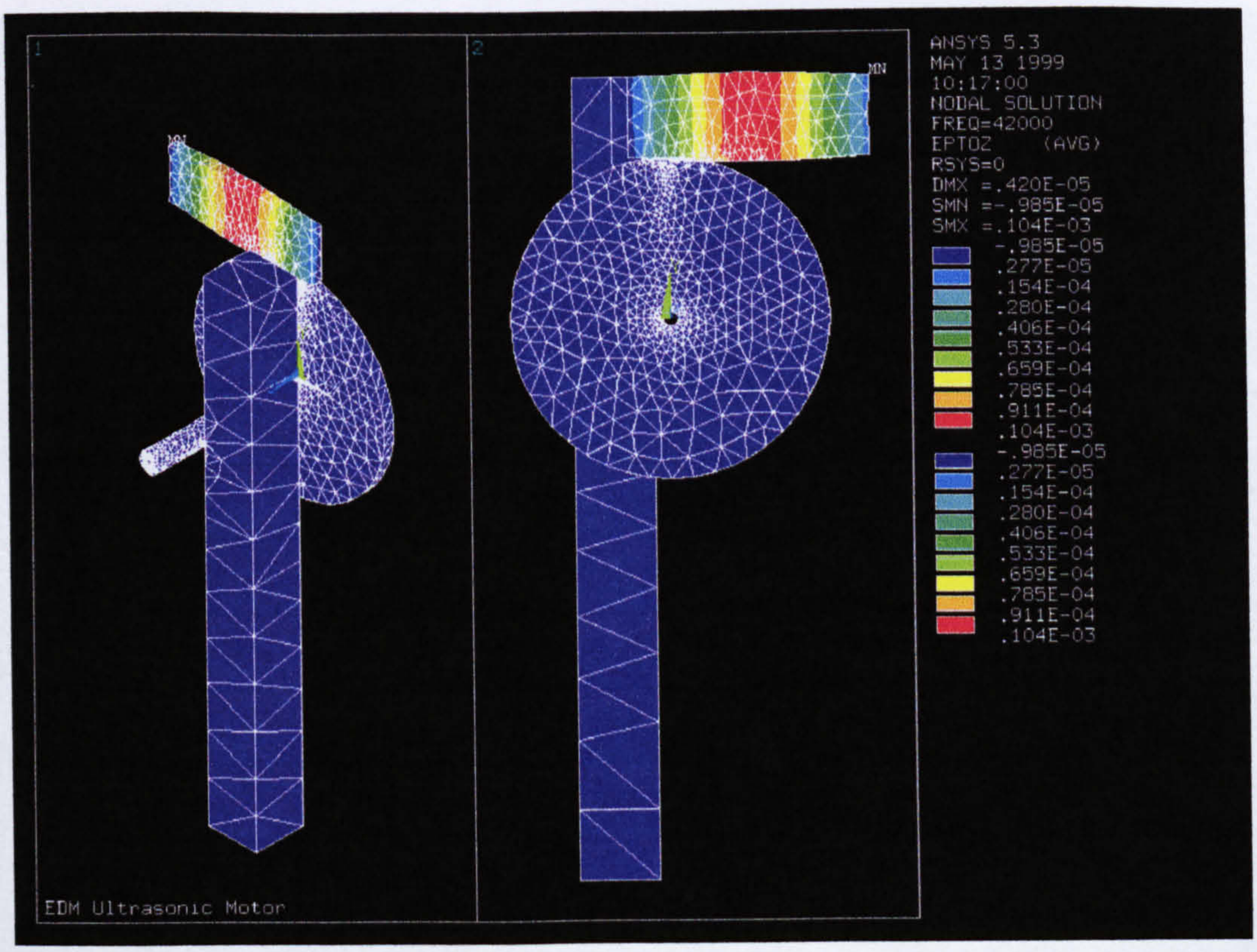

Figure 4-27. Total strain for the real part of the input for the motor at optimised operating frequency 'Mode (1)-linear structure' (z-direction) (50Volt)

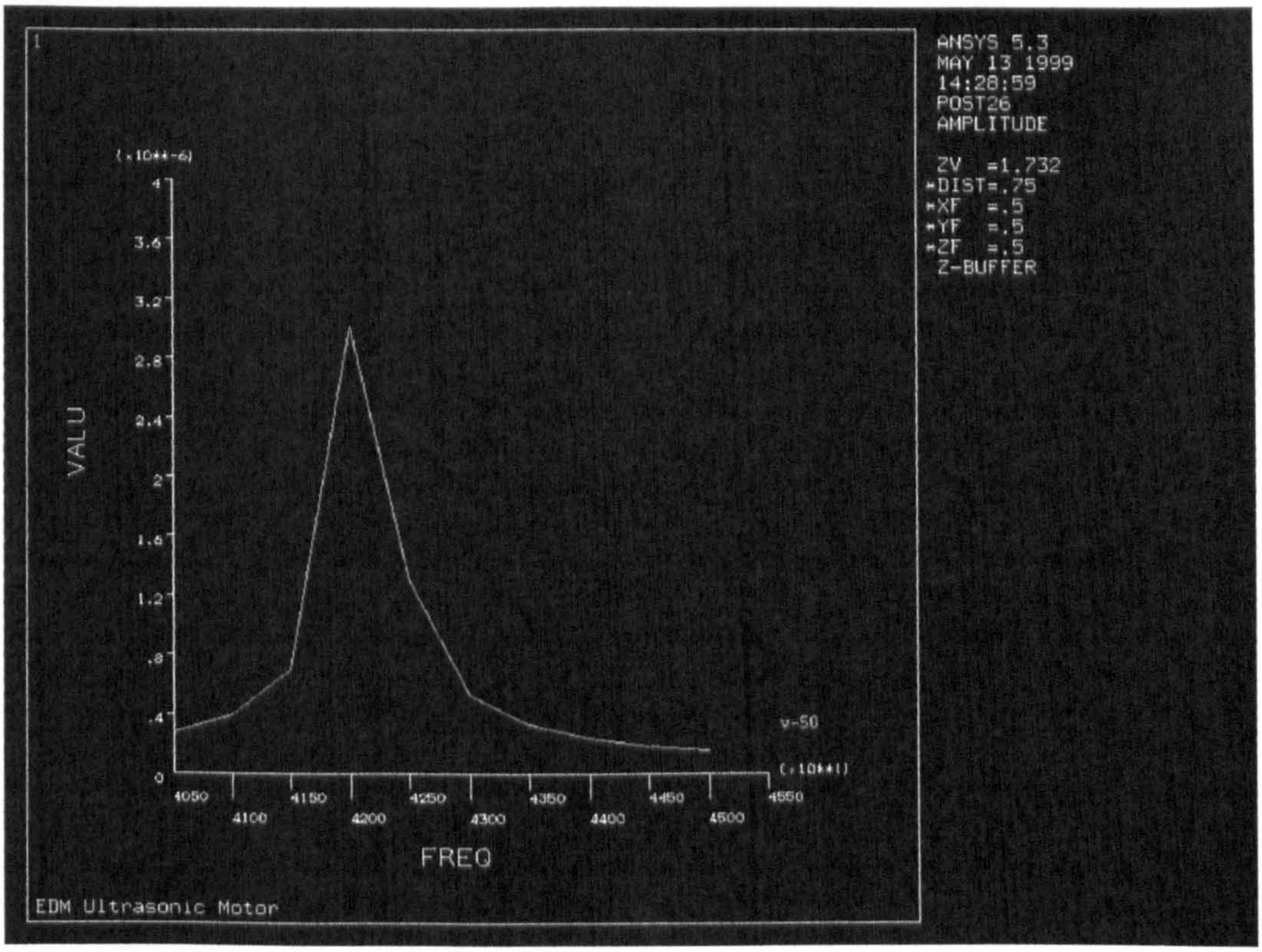

Figure 4-28. The amplitude (displacement) variation against exciting frequency for the proposed piezoelectric USM 'linear structure' (-50Volt)

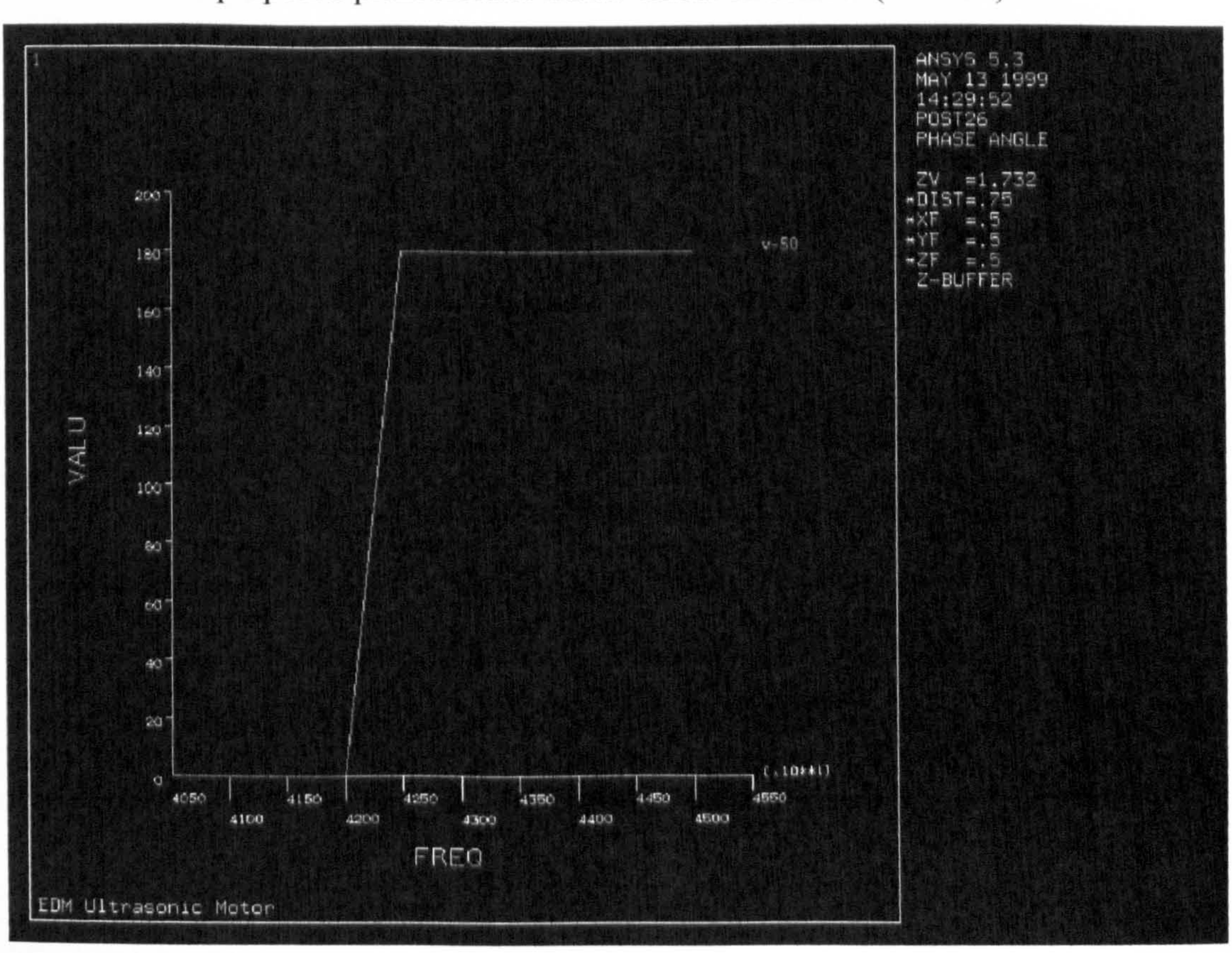

Figure 4-29. The phase variation against exciting frequency for the proposed piezoelectric USM 'linear structure' (-50Volt)

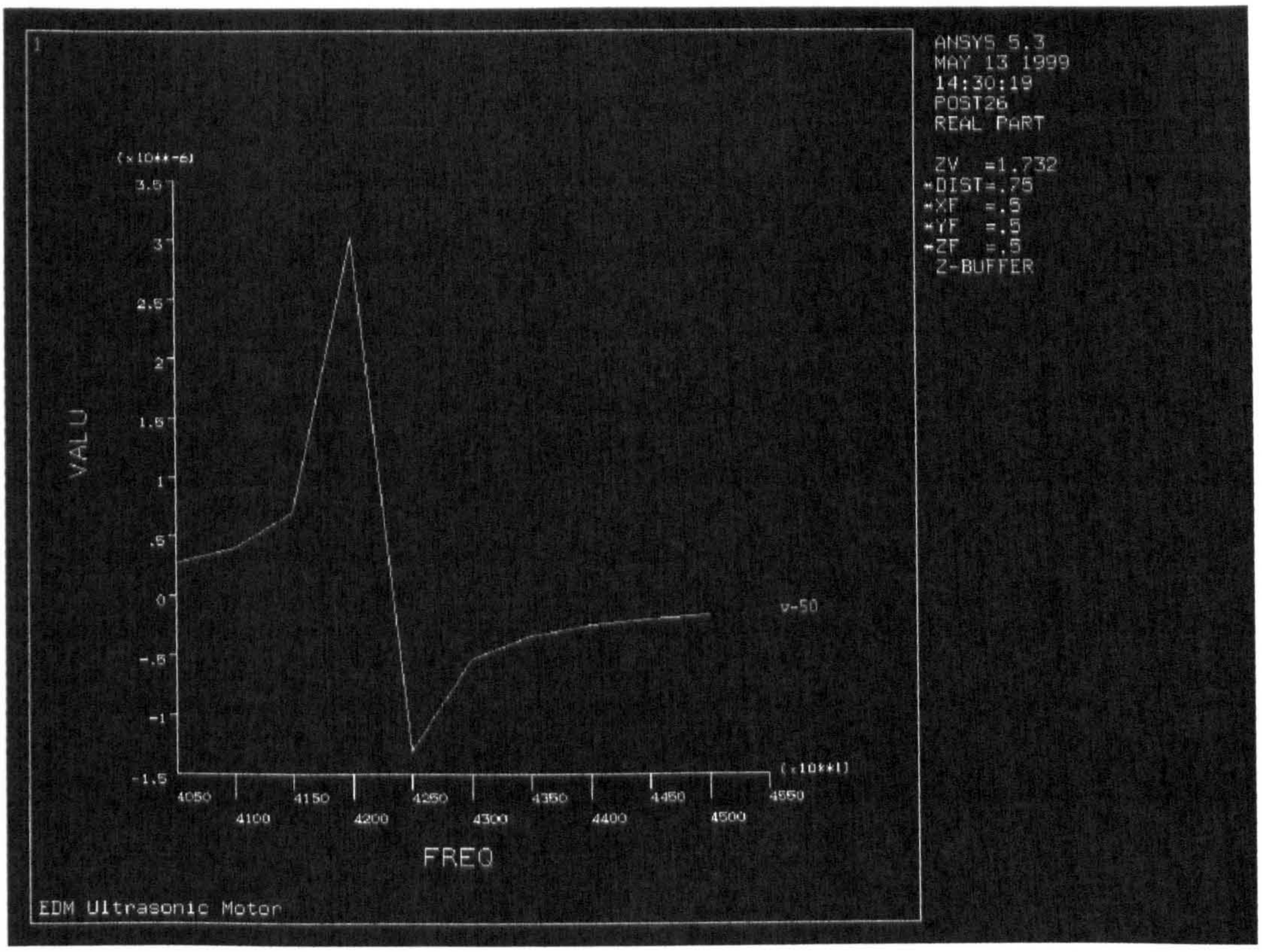

Figure 4-30. The real part amplitude (displacement) variation against exciting frequency for the proposed piezoelectric USM 'linear structure' (-50Volt)

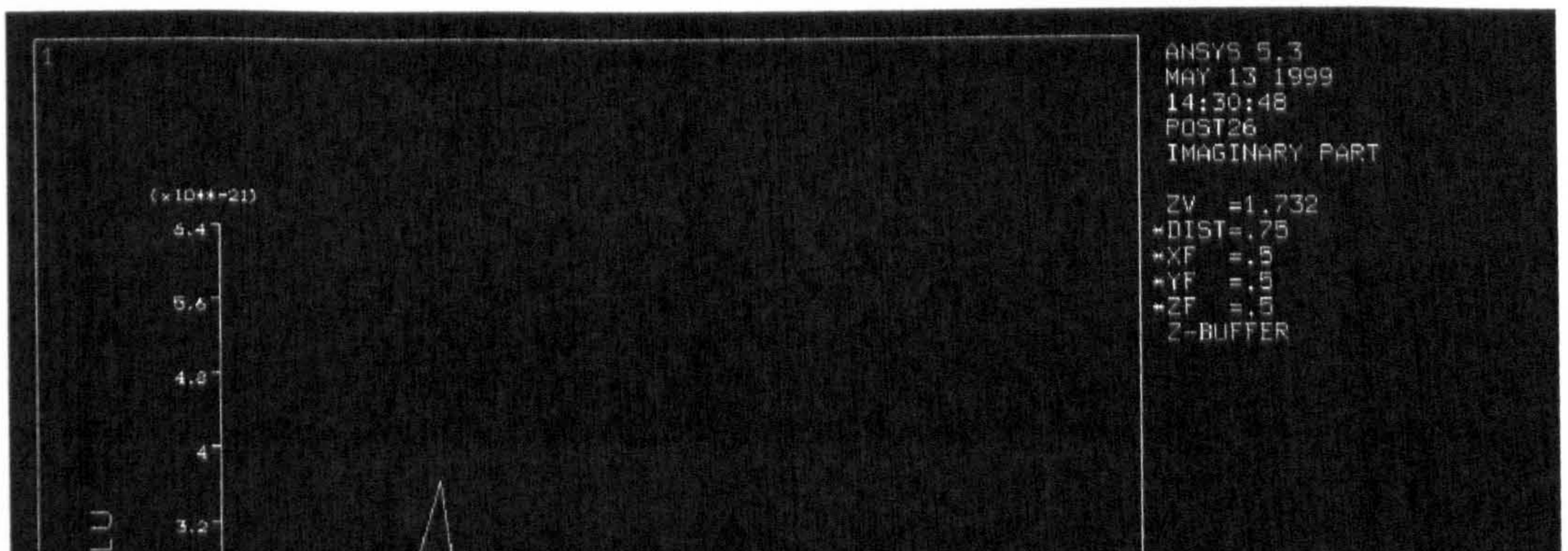

Figure 4-31. The imaginary part amplitude (displacement) variation against exciting frequency for the proposed piezoelectric USM 'linear structure' (-50Volt)

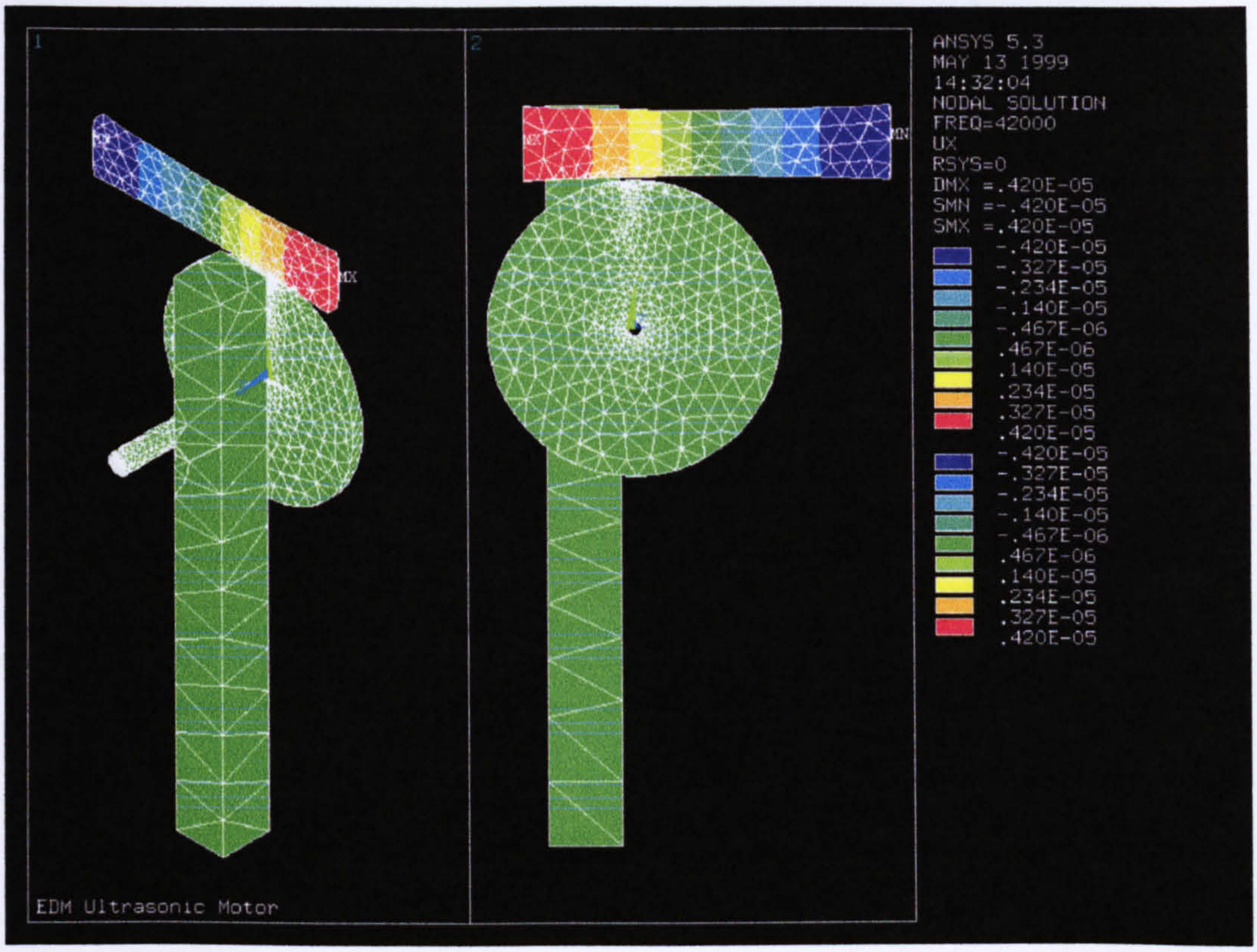

Figure 4-32. Deformed shape of the real part of the input for the motor at the optimised operating frequency 'Mode (2)-linear structure' (x-direction) (-50Volt)

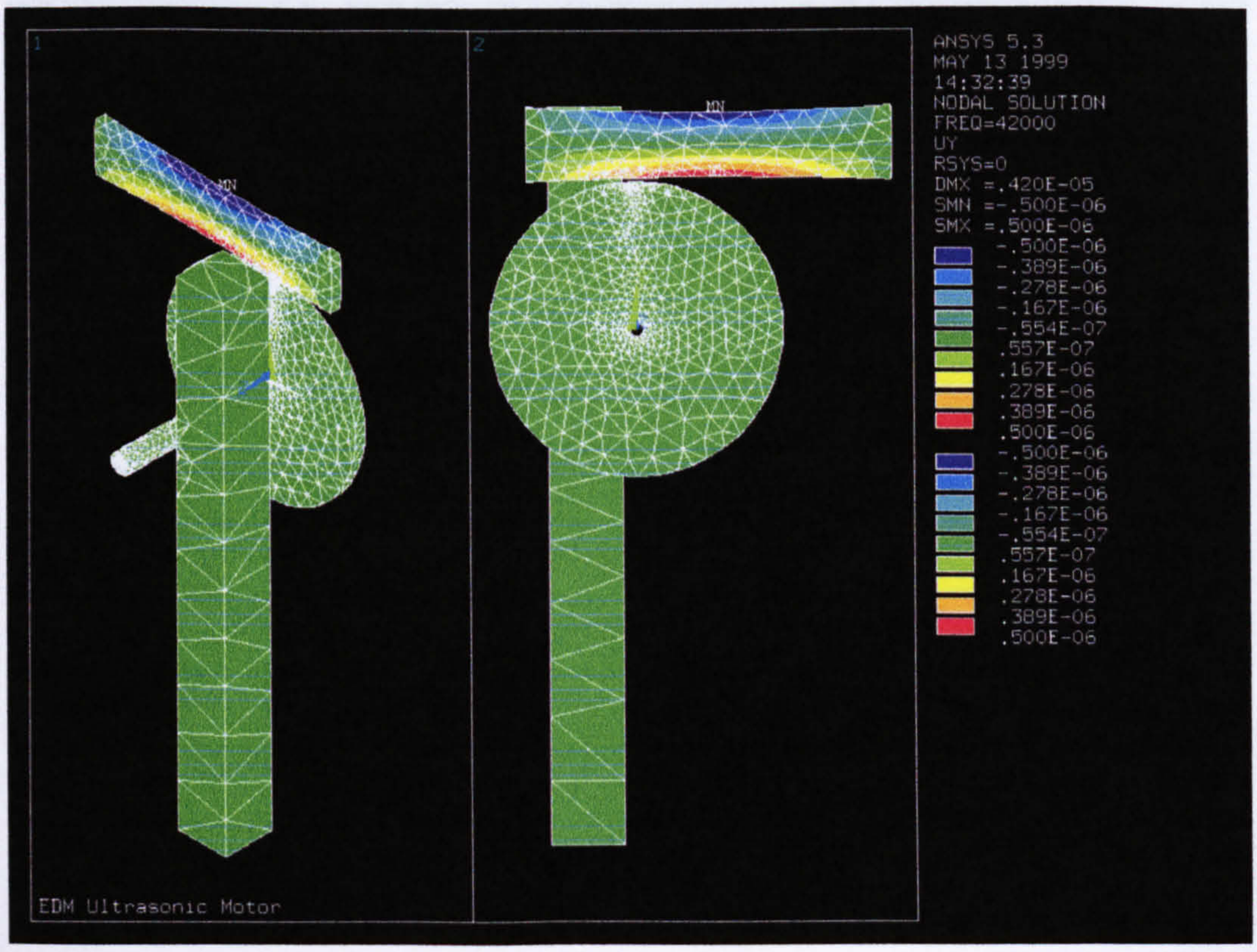

Figure 4-33. Deformed shape of the real part of the input for the motor at the optimised operating frequency 'Mode (2)-linear structure' (y-direction) (-50Volt)

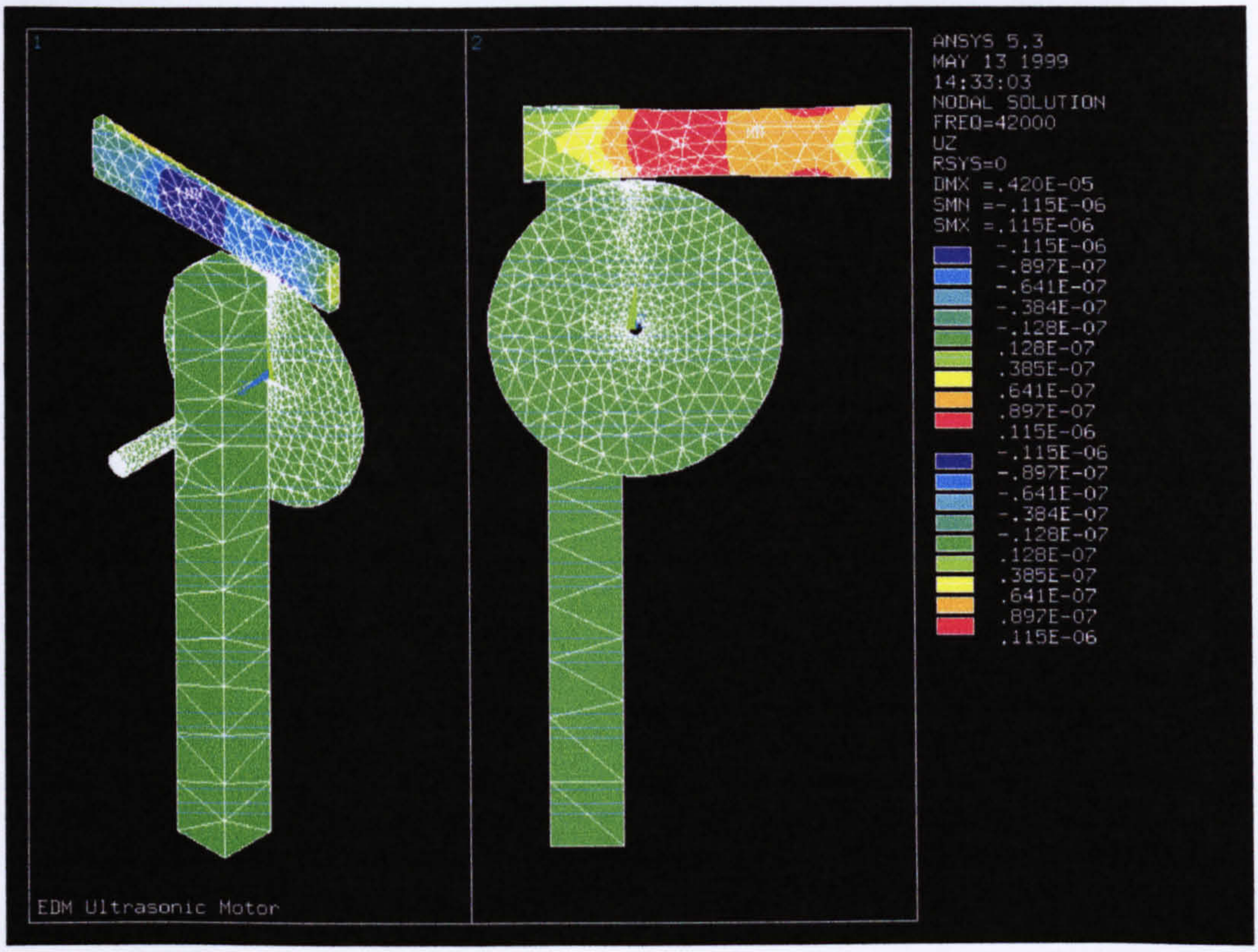

Figure 4-34. Deformed shape of the real part of the input for the motor at the optimised operating frequency 'Mode (2)-linear structure' (z-direction) (-50Volt)

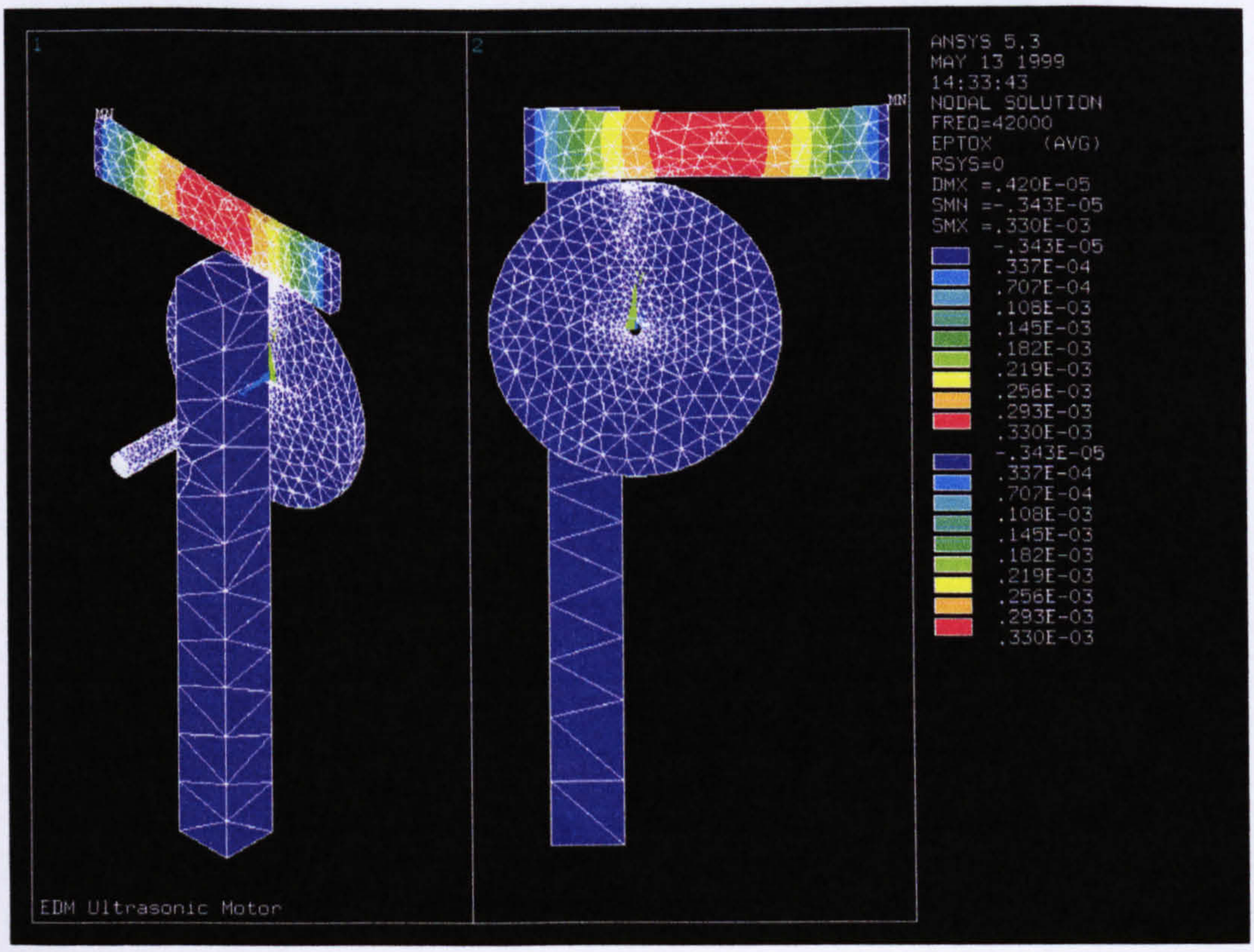

Figure 4-35. Total strain for the real part of the input for the motor at optimised operating frequency 'Mode (2)-linear structure' (x-direction) (50Volt)

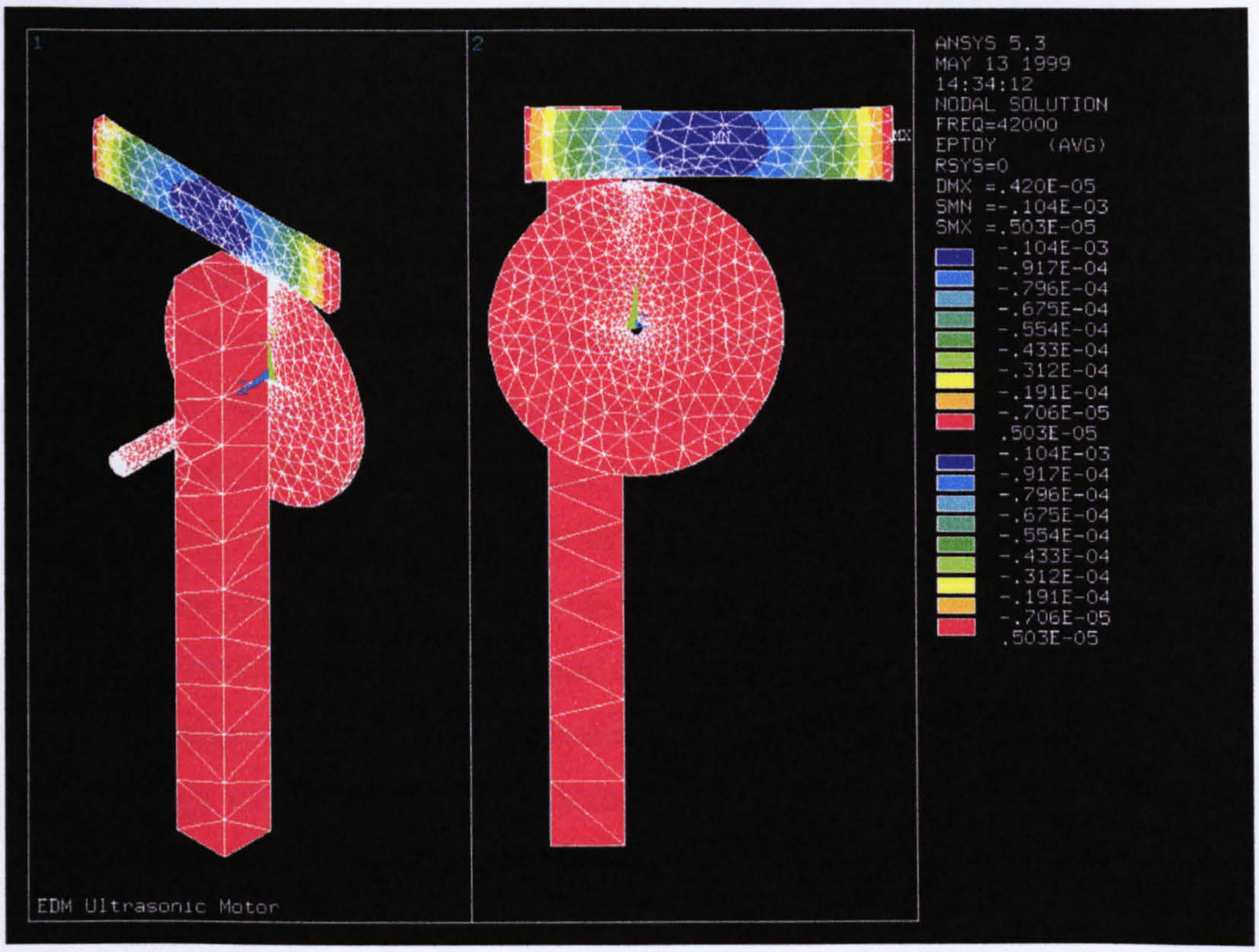

Figure 4-36. Total strain for the real part of the input for the motor at optimised operating frequency 'Mode (2)-linear structure' (y-direction) (50Volt)

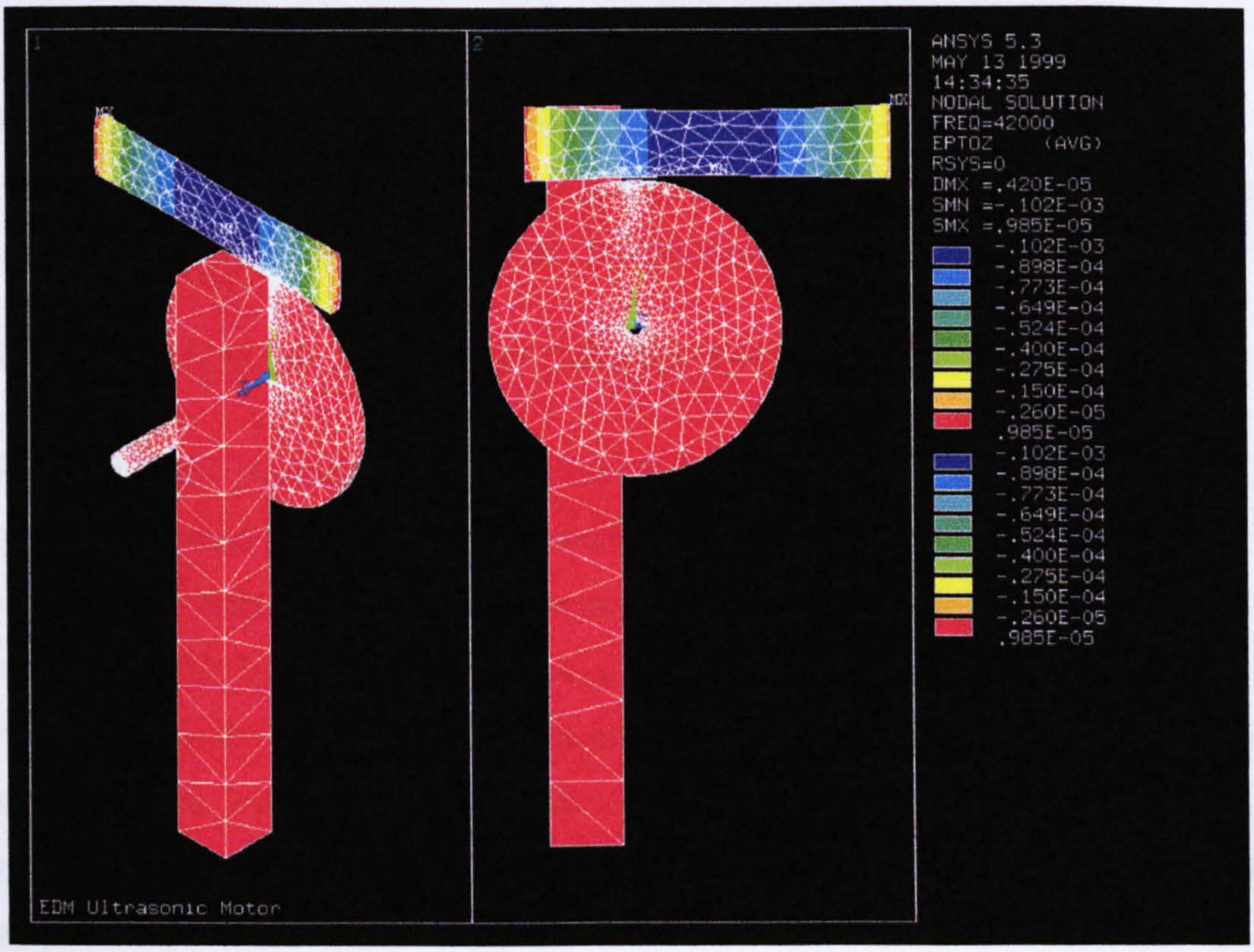

Figure 4-37. Total strain for the real part of the input for the motor at optimised operating frequency 'Mode (2)-linear structure' (z-direction) (50Volt)

4.7 PRINCIPLE OF OPERATION

The principle of operation of the proposed motor is based on using standing wave vibrations, which has a fixed wave length. The concept is to utilise two oscillation modes to obtain desired motion of the piezoelectric element longitudinal and transverse (bending) vibrations, one vibration produces a normal force while the other vibration generates thrust force, which is perpendicular to the normal force, resulting in an elliptical trajectory of the element edge, by attaching the piezoelectric ceramic plate edge to a driving wheel using a coil spring. The elliptical trajectory is converted into a rotary motion as shown in figures 4-38 (a), (b), (c) and (d). As the combination of two modes of vibrations create a friction based driving force between the stator and the rotor at the contact edge, a movement in forward or backward direction created depending on the methodology used to exciting the piezoelectric ceramic plate to generate two modes of vibrations. The linear motion was developed using the friction based driving force between the shaft and the sliding element.

4.8 MOTOR STRUCTURE

A single vibrating bar with three driving terminals was used. Two terminals were used to create two directions of motion. When one terminal was activated for driving in the forwards direction or backwards direction the second was left open or used as a short circuit terminal to the common terminal. The third terminal was connected to earth.

4.9 DESIGN OF THE MOTOR COMPONENTS

The design of the piezoelectric USM is mainly based on the vibrating bar specifications that are determined from the required characteristics of the motor including, speed and torque. Here a single piezo-ceramic flexural vibrating bar made up of either a piezo-ceramic PZT-PC4D or CTS19 was used to generate mechanical motion. Figures 4-39 (a) and (b) show the construction and the actual component of the bar used in the motor. The dimensions and material properties of the bar define its resonant frequency. Samples of the vibrator with different degrees of surface finish and friction coefficient were produced.

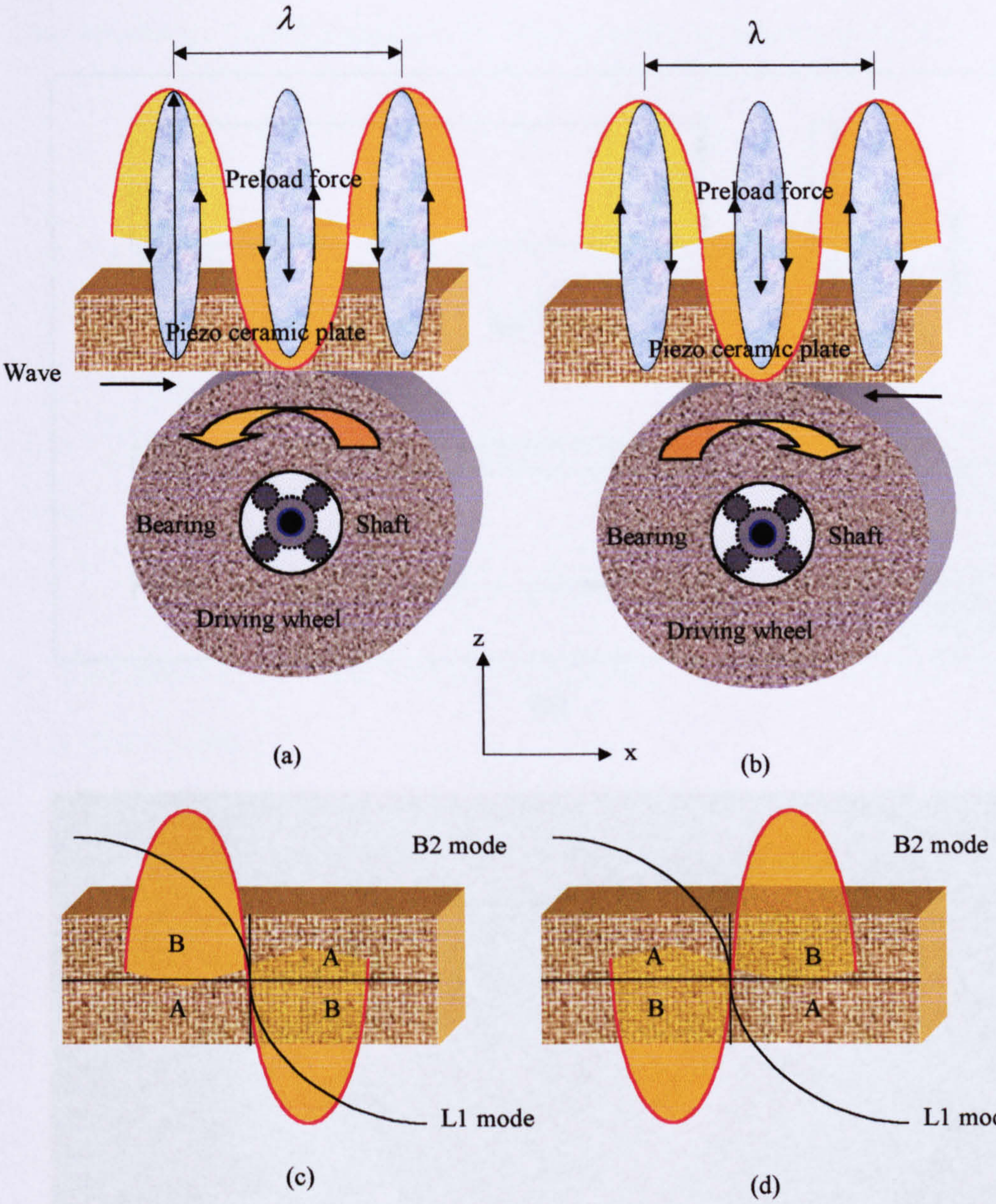

Figure 4-38. Principles of creating and reverse direction of motion for the proposed motor (a) the forward direction (b) the backward direction (c) and (d) bending vibration modes excited at frequency closed to longitudinal vibration mode

The diameter of the motor and the torque factor was determined using the design specifications including speed, torque and degree of resolution. Assume the speed of the motor is known and it is given in revolution per minute. Then it will be possible to calculate the angular acceleration $\omega = 2\pi f$ and the average angular acceleration $\bar{\alpha} = \Delta\omega / \Delta t$ of the proposed motor. Where $\Delta\omega$ is the change on the angular velocity, for a specified period of time, Δt and f is the velocity in revolution per second.

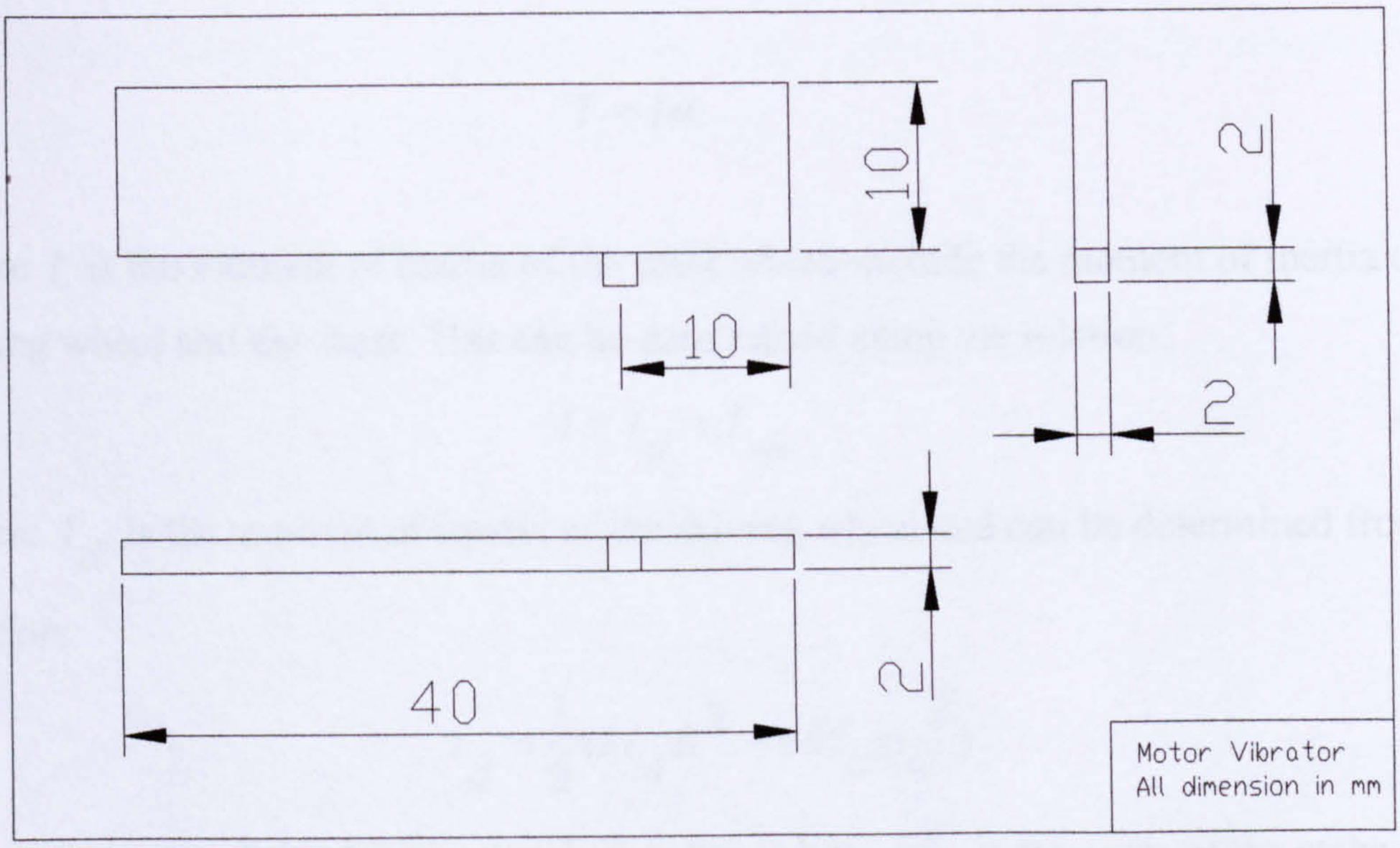

(a)

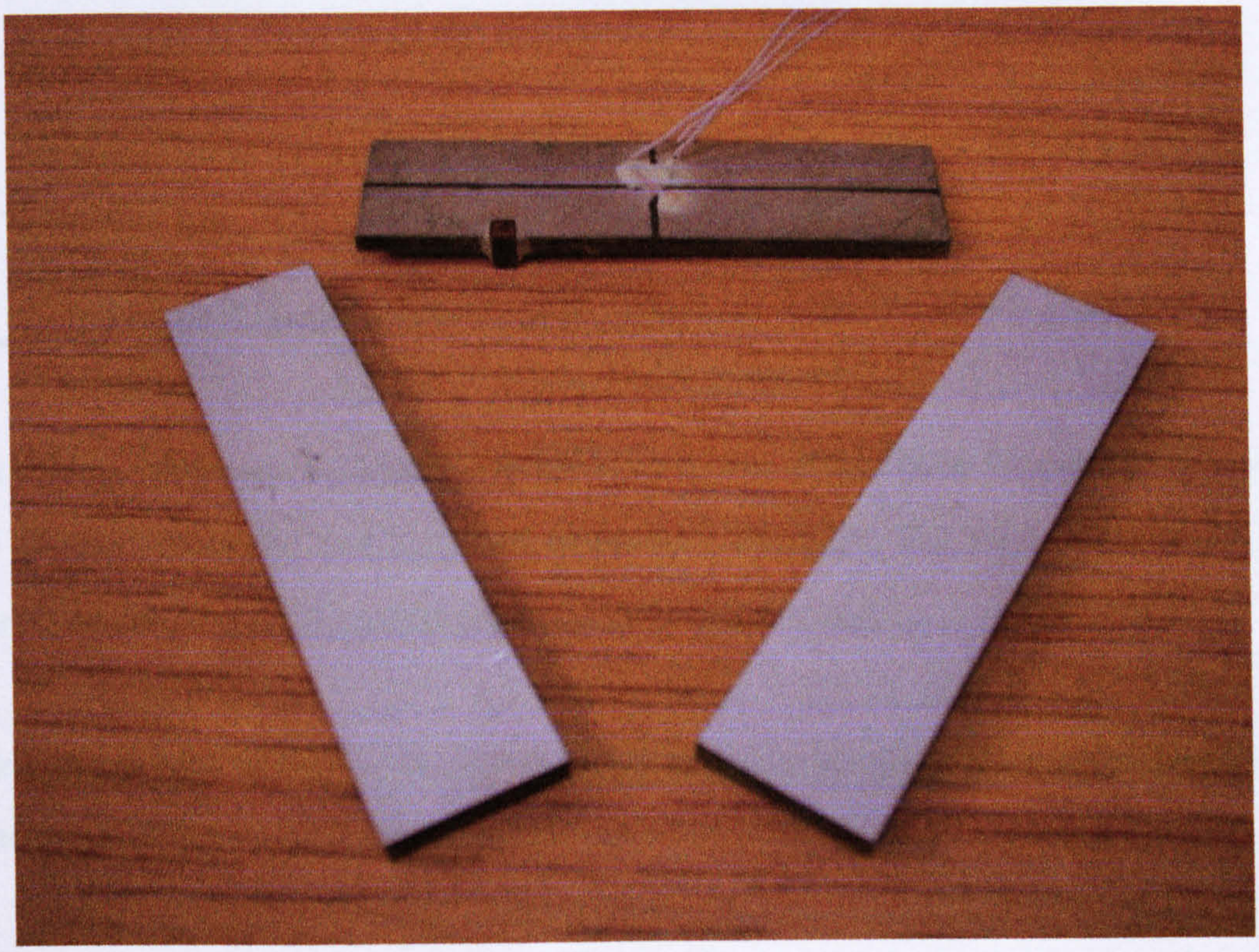

(b)

Figure 4-39 The construction of the single piezo-ceramic flexural vibrating bar used in the developed prototype

Using Newton's 2nd law for rotation, the torque can be determined using the relation:

$$T = I\alpha \qquad 4\text{-}9$$

where I is the moment of inertia of the rotor which include the moment of inertia of the driving wheel and the shaft. This can be determined using the relation:

$$I = I_d + I_{sh} \qquad 4\text{-}10$$

Where I_d is the moment of inertia of the driving wheel and can be determined from the relation:

$$I_d = \frac{1}{2}(M_d R^2 - 6M_{ic} r_{ic}^{\ 2})$$

M_d is the mass of the driving wheel, R is the radius, M_{ic} is the mass of the etched hole and r_{ic} is the radius.

I_{sh} is the moment of inertia of the shaft and can be determined from the relation:

$$I_{sh} = \frac{1}{2} M_{sh} r_{sh}^{\ 2}$$

M_{sh} is the mass of the shaft, and r_{sh} is the radius.

The driving wheel and the shaft were made up as one piece. Therefore using the volume and the density of the material used to produce the rotor, the mass of the shaft M_{sh}, driving wheel M_d and etched holes M_{ic} can be determined.

Using the model shown in Figure 4-40 (a) and the relation between the torque and various acting forces on the rotor components this gives:

$$T = F_R \frac{D}{2} = F_r \frac{d}{2} \qquad 4\text{-}11$$

Where F_R is the elliptical force, produced using piezoelectric vibrating bar, F_r is the driving force transferred to the shaft using torque factor A_r, D is the diameter of the driving wheel, and d is the diameter of the shaft.

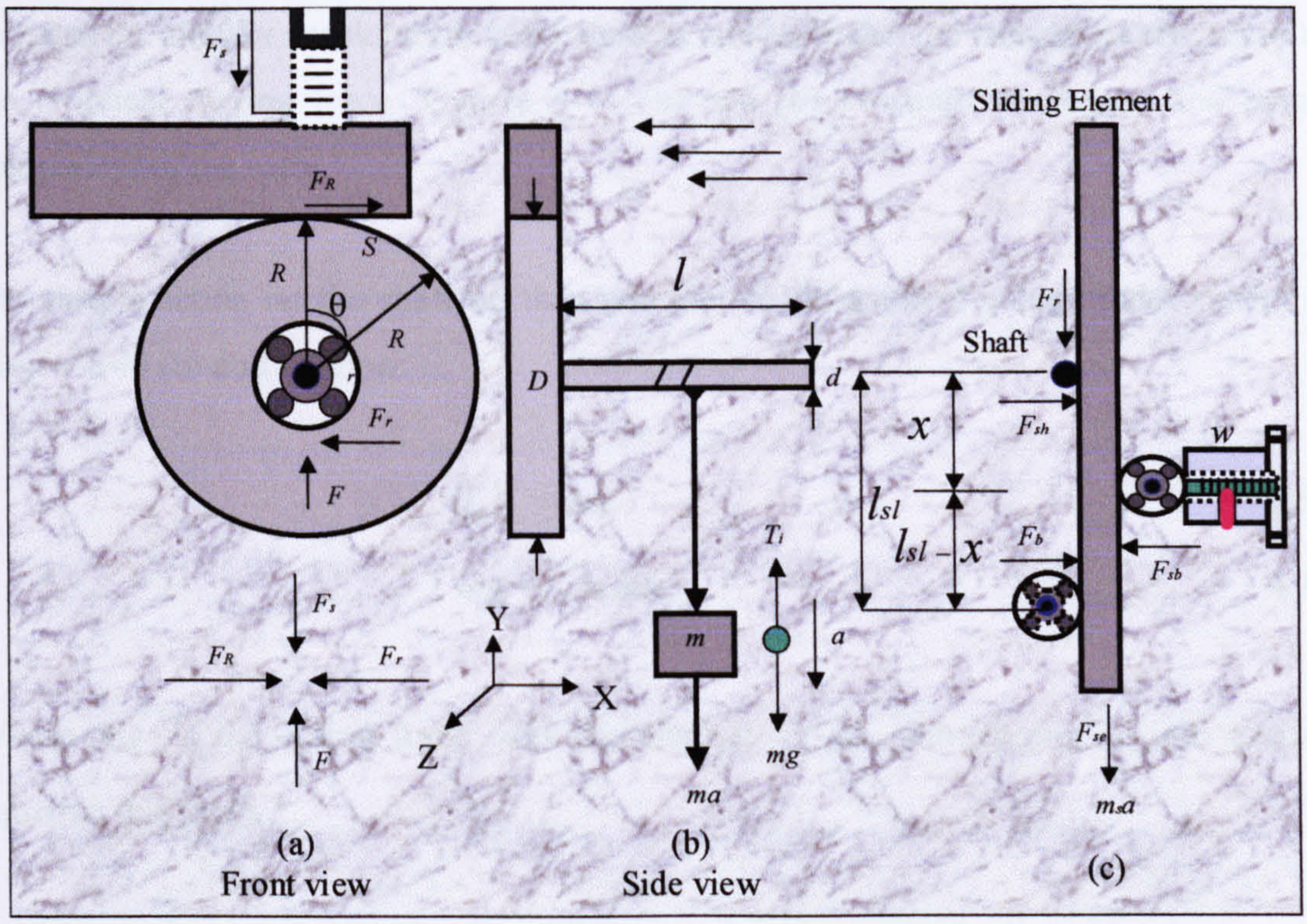

Figure 4-40. Dynamic models used in the determination of the dimension of the various parts of the proposed motor

Using these relations the torque factor of the motor and the diameter of the component of the rotor including driving wheel and the shaft can be obtained. The transferred force to the shaft also can be determined using the torque factor relation:

$$F_r = F_R \frac{D}{d} \qquad 4\text{-}12$$

This relation also shows that the torque factor $A_r = \frac{D}{d}$ is a very important factor has to be carefully considered during the design process of the motor. It is influenced the efficiency of the elliptical driving force produced by the piezoelectric vibrating bar, the resolution of the motor and maximum travelling speed.

The length of the shaft l was determined according to the allowable ratio for l/d and to meet the methodology of design of the proposed structure. This was considered the properties of the material used to produce the shaft and the moment of inertia of the rotor. The moment of inertia of the rotor was considered to be small as possible to increase the angular acceleration of the system and to obtain the maximum efficiency of the elliptical driving force. Figures 4-41 (a) and (b) illustrate the layout and actual component of the rotor.

The torque acting on the shaft on this case can be determined using model shown in Figure 4-40 (b) and relation:

$$\sum F_y = ma \qquad 4\text{-}13$$

$$mg - T_t = ma \qquad 4\text{-}14$$

Where mg is the acting force over the shaft, $a = r_{sh}\alpha$, substituting a into tension equation this gives

$$T_t = m(g - \alpha r_{sh}) \qquad 4\text{-}15$$

The torque acting on the shaft is given by:

$$\tau = r_{sh} T_t \qquad 4\text{-}16$$

Using the torque relation and tension obtained from the model, the torque acting in the shaft can be determined using:

$$\tau = r_{sh} m(g - \alpha r_{sh}) \qquad 4\text{-}17$$

Four bearings were used in the motor design. Two were used as shaft carry bearings built into the motor frame, and two were used to guide the motor sliding element. One bearing was designed to give the motor the facility to control the pre-load pressing force between the shaft and the sliding element and this is shown in Figure 4-42. The second one was used to keep the sliding element close to the shaft.

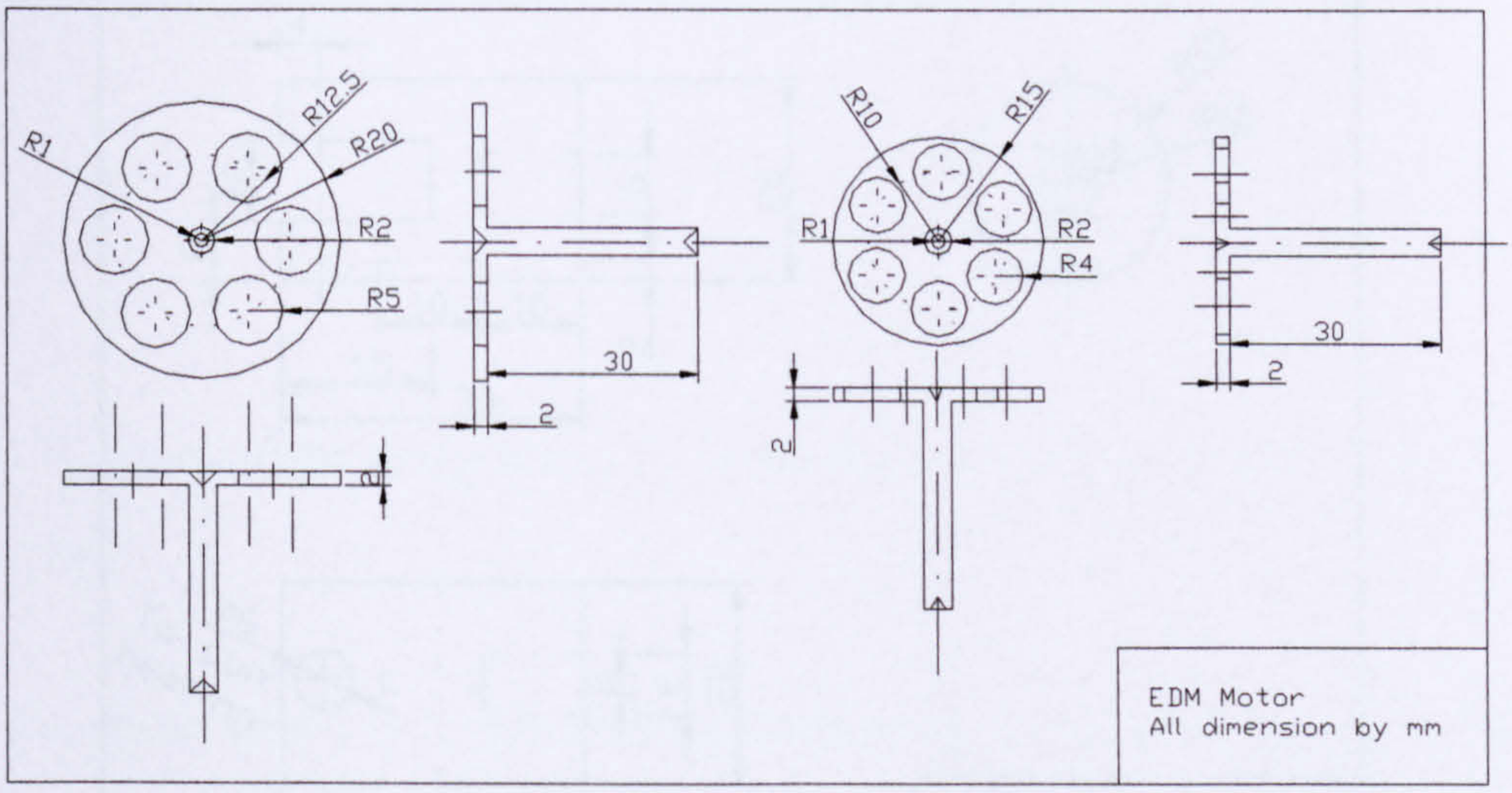

(a)

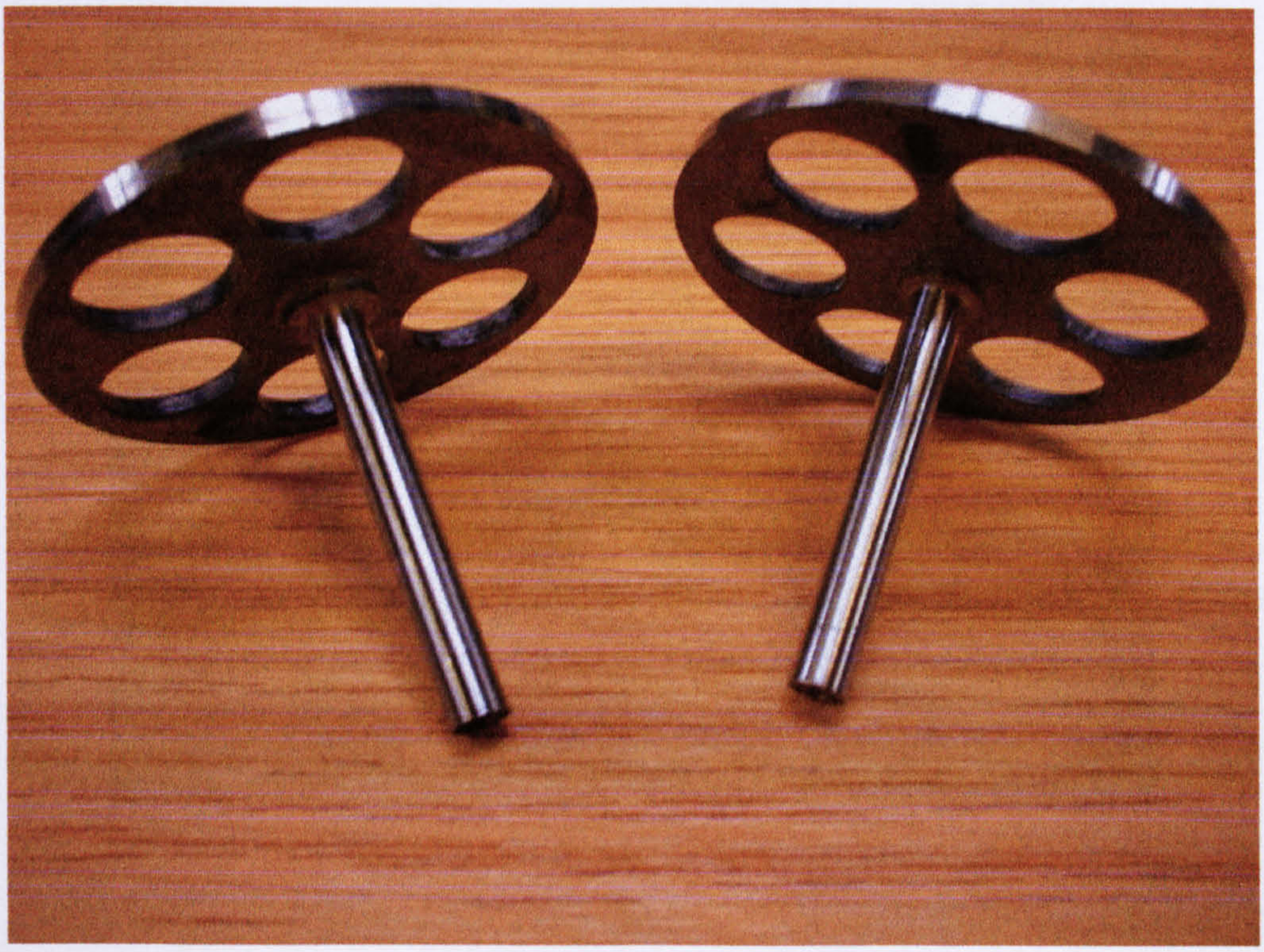

(b)

Figure 4-41 (a) The rotor layout and dimensions in mm, (b) is a photograph of the produced rotor.

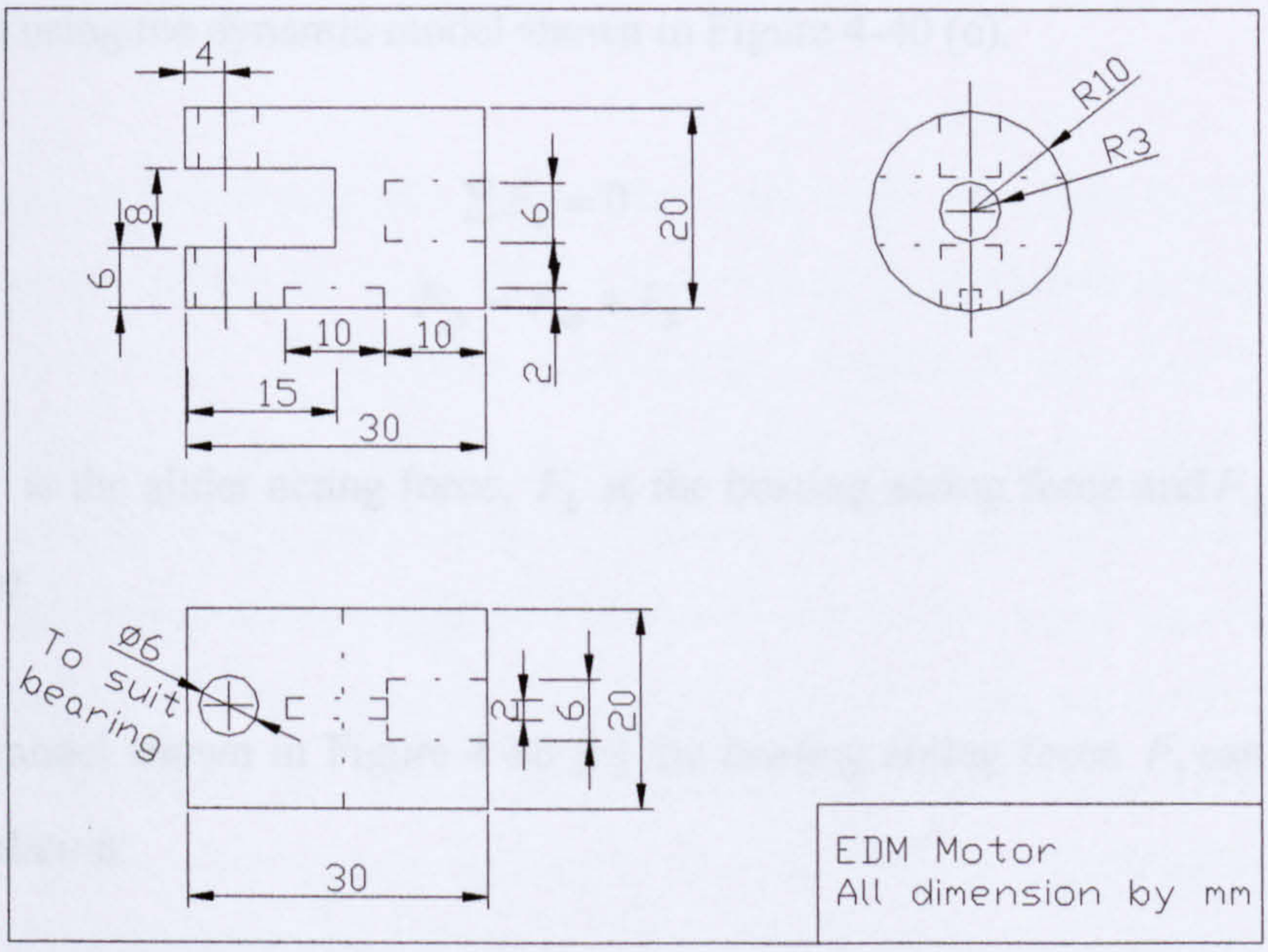

(a)

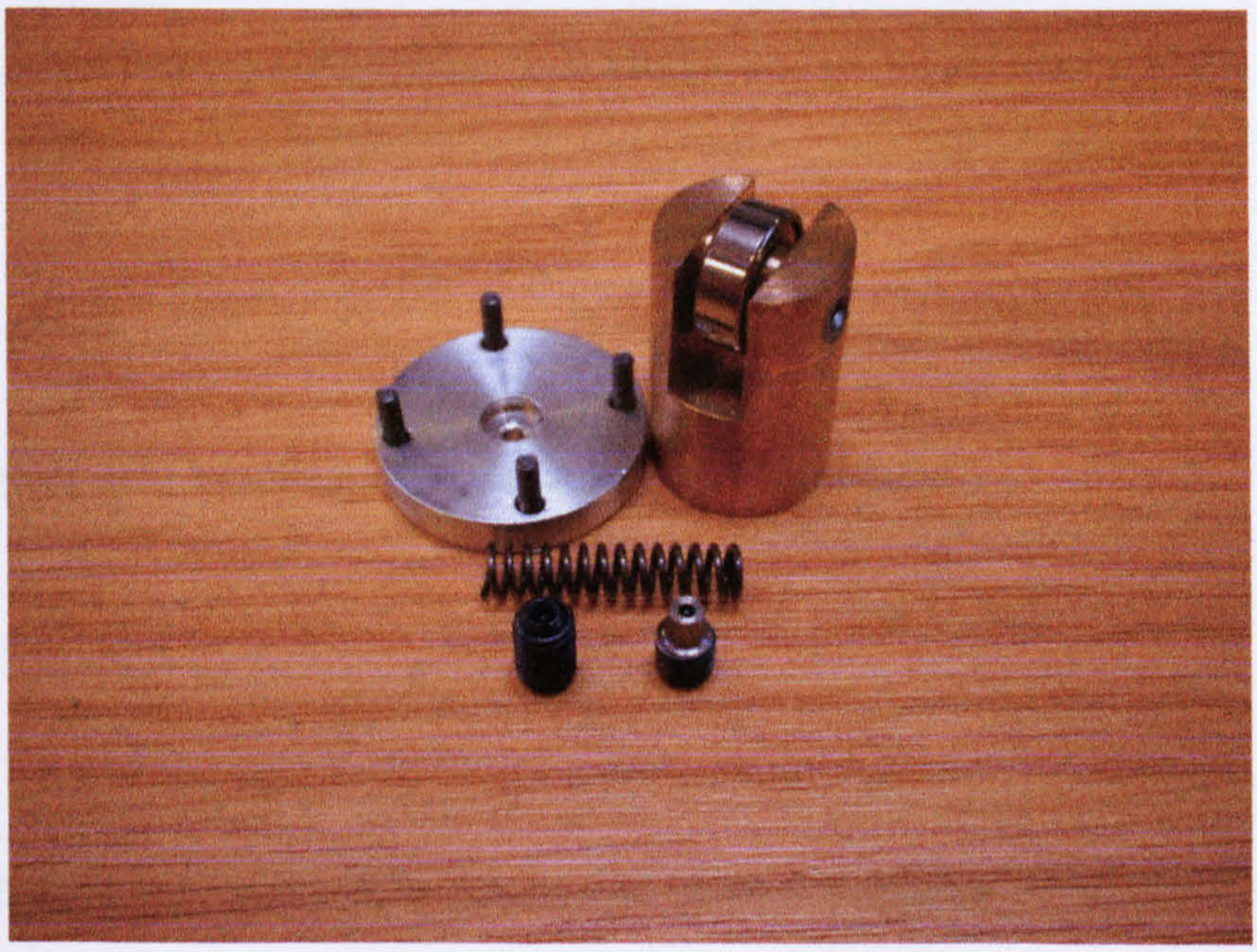

(b)

Figure 4-42 Sliding element bearings (a) layout (b) a photograph of the developed sample

The load force acting in the shaft and locations of bearings of the sliding element can be determined using the dynamic model shown in Figure 4-40 (c).

$$\sum F_x = 0 \qquad 4\text{-}18$$

$$F_{sb} = F_{sh} + F_b \qquad 4\text{-}19$$

Where F_{sb} is the slider acting force, F_b is the bearing acting force and F_{sh} is the shaft acting force.

From the model shown in Figure 4-40 (c) the bearing acting force F_b can be obtained from the relation:

$$F_{sb}X = F_b l_{sl} \qquad 4\text{-}20$$

consequently the bearing acting force found to be:

$$F_b = F_{sb}\frac{X}{l_{sl}} \qquad 4\text{-}21$$

Substituting F_b into slider acting force this gives the relation:

$$F_{sb} = F_{sb}\frac{X}{l_{sl}} + F_{sh} \qquad 4\text{-}22$$

Then the shaft acting force can be determined using the relation:

$$F_{sh} = F_{sb}(1-\frac{X}{l_{sl}}) \qquad 4\text{-}23$$

On the current motor design the slider element was located on the middle to keep the acting force on the shaft small as possible. The acting force on the shaft on this case was found to be half the slider acting force. This shows that it is very important to consider

the locations of the guiding bearings and monitoring its acting force on the system active elements.

Four pins and an interchangeable spring were used to fix the vibrating bar. The spring has been used to support the vibrating bar at the vibration node and to keep the stator in contact with the rotor. Its optimum pre-load pressing force was used to control the motor resolution, stiffness and torque. It was also used to keep stator and rotor in contact, and this gave the piezo-ceramic vibrating bar the ability to transfer the elliptical force into rotational motion using the friction between the stator and the rotor. The optimum pre-load pressing force was developed based on observing the motor travelling speed variation against the various pressing forces, at the optimum operating voltage and frequency. The four pins were used to prevent vibrating bar interference and stop extension. They also give the vibrating bar the ability to transfer the vibrational force into rotating motion based on frictional between the stator and the rotor.

Two guides were also designed and fixed to the top and bottom of the motor fame, to prevent the sliding element plane motion.

The frame of the motor was a part of the concept and has been designed with a layout to ensure compactness of the design and easy to integrate the parts of the motor. The motor components were integrated successfully into the frame of the motor. Figures 4-43 and 4-44 illustrate the components and the final assembled configuration of the motor.

The motor was tested and initial results showed that there were some teething problems. These included irregular angular and travelling speed. These problems arise from inaccuracies in the manufacture of the parts for the motor. The irregular angular speed was due to the deviations on the roundness of the driving wheel and the irregular travelling speed was from the deviations in roundness of the shaft. The roundness of the driving wheel and the shaft were measured. Figures 4-45, 4-46, 4-47 and 4-48 show the measured roundness of the driving wheel and the shaft of the motor, as it measured using roundness testing machine. It is clear from these measurements that there was a major deviation in driving wheel roundness that was of the order of 2 to 4 micrometers. This is shown in Figures 4-45 (a) and 4-46 (a). The shaft roundness deviation was of the order of the order of 5.0 to 7.0 micrometers as shown in Figure 4-47.

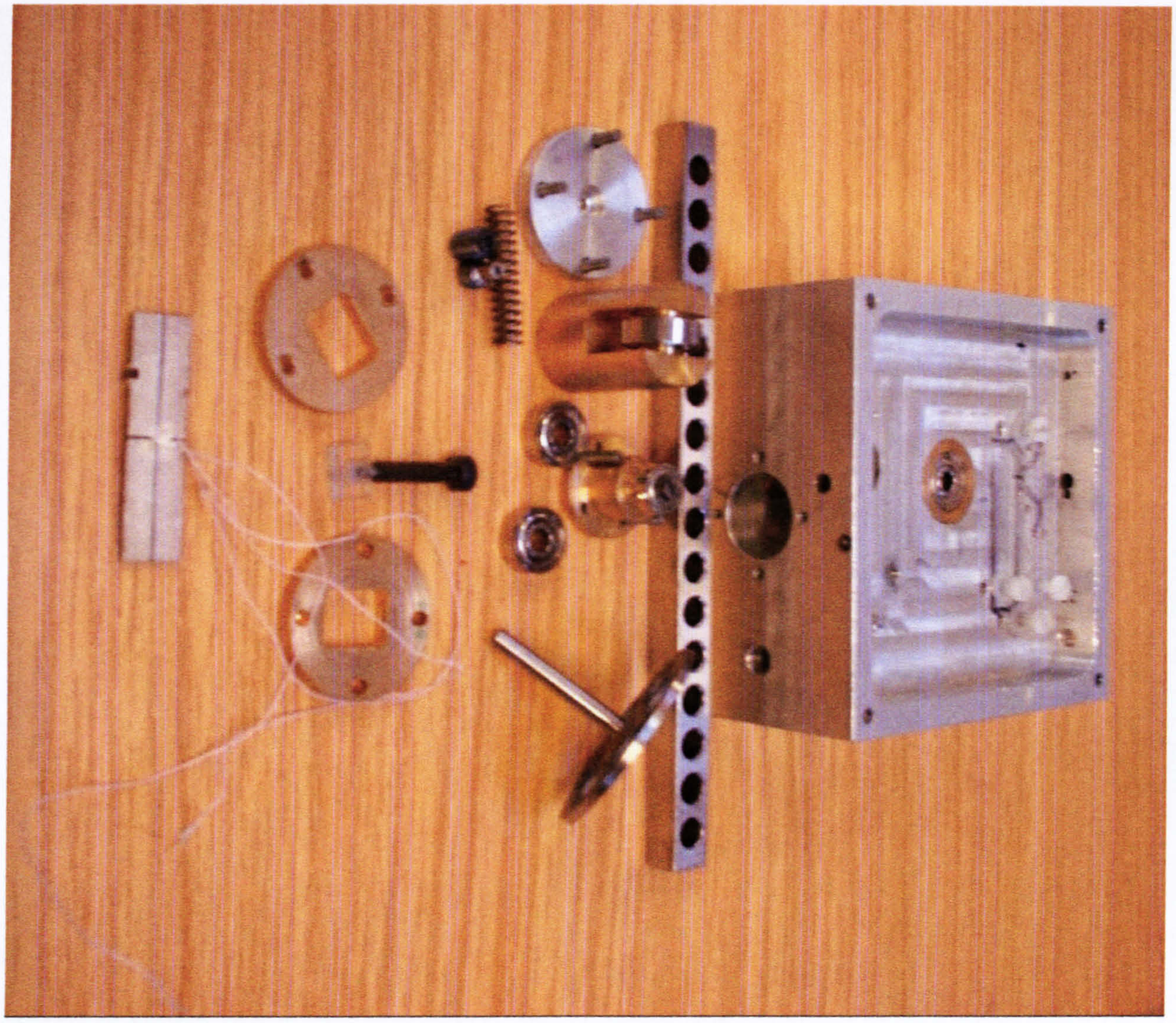

Figure 4-43 Assembled and practical configuration of the developed linear piezoelectric USM using a single flexural vibrating bar

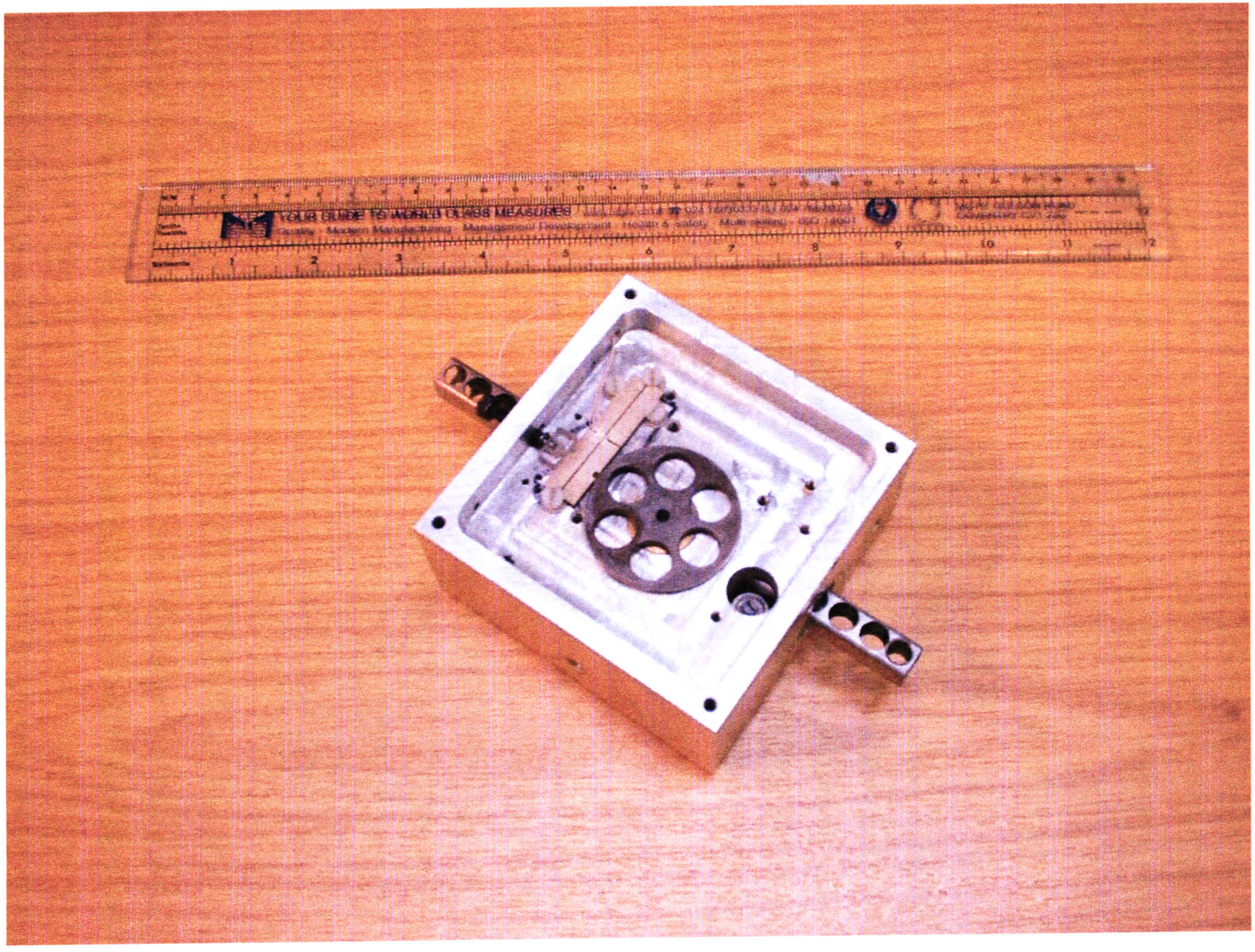

Figure 4-44 The main parts of the developed linear USM using a single piezo-ceramic flexural vibrating bar

The shaft and the driving wheel were re-machined to correct the errors. The same test was carried out again for the re-machined parts to measure the roundness. It was found that there was an improvement and the deviation was reduced to 1 to 1.5 micrometers as shown in Figures 4-45 (b), 4-46 (b) and 4-48. The concentricity of the produced parts such as the rotor was also tested and this shows no error. The parts were then reintegrated into the frame of the motor and a series of experimental test was conducted to measure characteristics of the motor.

4.10 EXPERIMENTAL RESULTS AND DISCUSSION

Different systems were built to measure characteristics of the developed prototype. These included optimisation of prototype operating parameters, resolution, response time, efficiency, travelling speed, load capacity and the capability for control using either the amplitude or frequency of the input signal. Figures 4-49 and 4-50 show two systems used in these experimental measurements. A full description of the apparatus used in these experiments is given below:

A piezoelectric driver was used to provide the piezo-ceramic vibrating bar with the alternative driving voltage. A function generator was used to provide various shapes of signal including sinusoidal, saw tooth and square wave. A display unit, which consists of a digital oscilloscope and PC computer, was used to trace the signal and optimise the motor operating parameters. A speedometer was used to measure the travelling speed of the motor. An electro microscope was used to measure the fine resolution of the motor. A stopwatch was used to calculate the running time and the time response of the motor. A programmable switching unit interfaced with a PC computer was used to control the motor directions of motion and to analyse the measured characteristics of the motor.

4.10.1 Optimisation of the Operating Parameters of the Motor

An optimisation for the developed prototype operating parameters (frequency, voltage, current) has been carried out using the same arrangement used in the modelling of the motor as shown in Figure 4-3. Figures 4-49 and 4-50 show these systems used in this optimisation. The electrode A and B is connected to a single phase AC power source with a wide range of amplitude and frequency. Two switches S1 and S2 have been used to regulate the AC input power for these two electrodes.

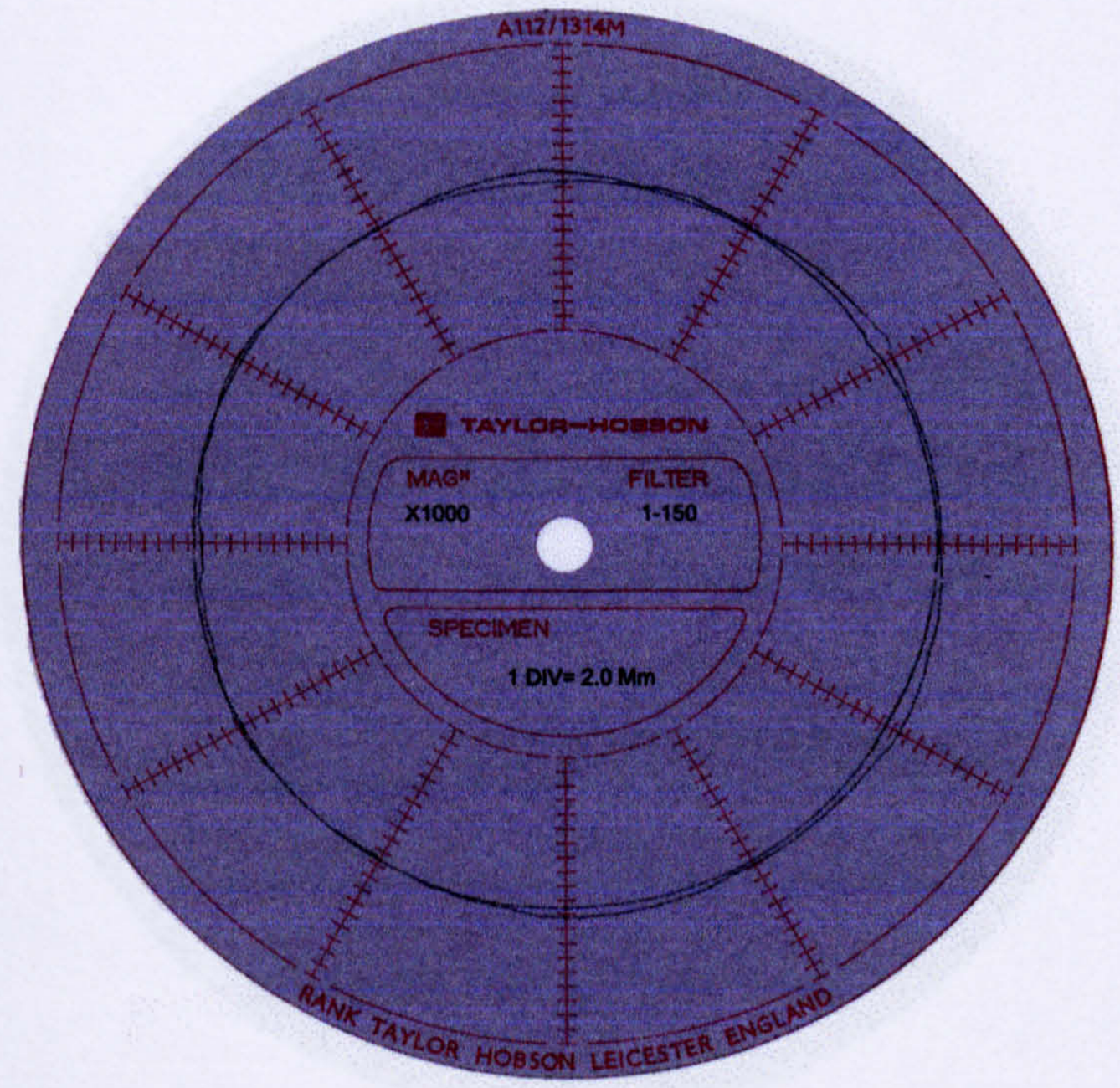

(a)

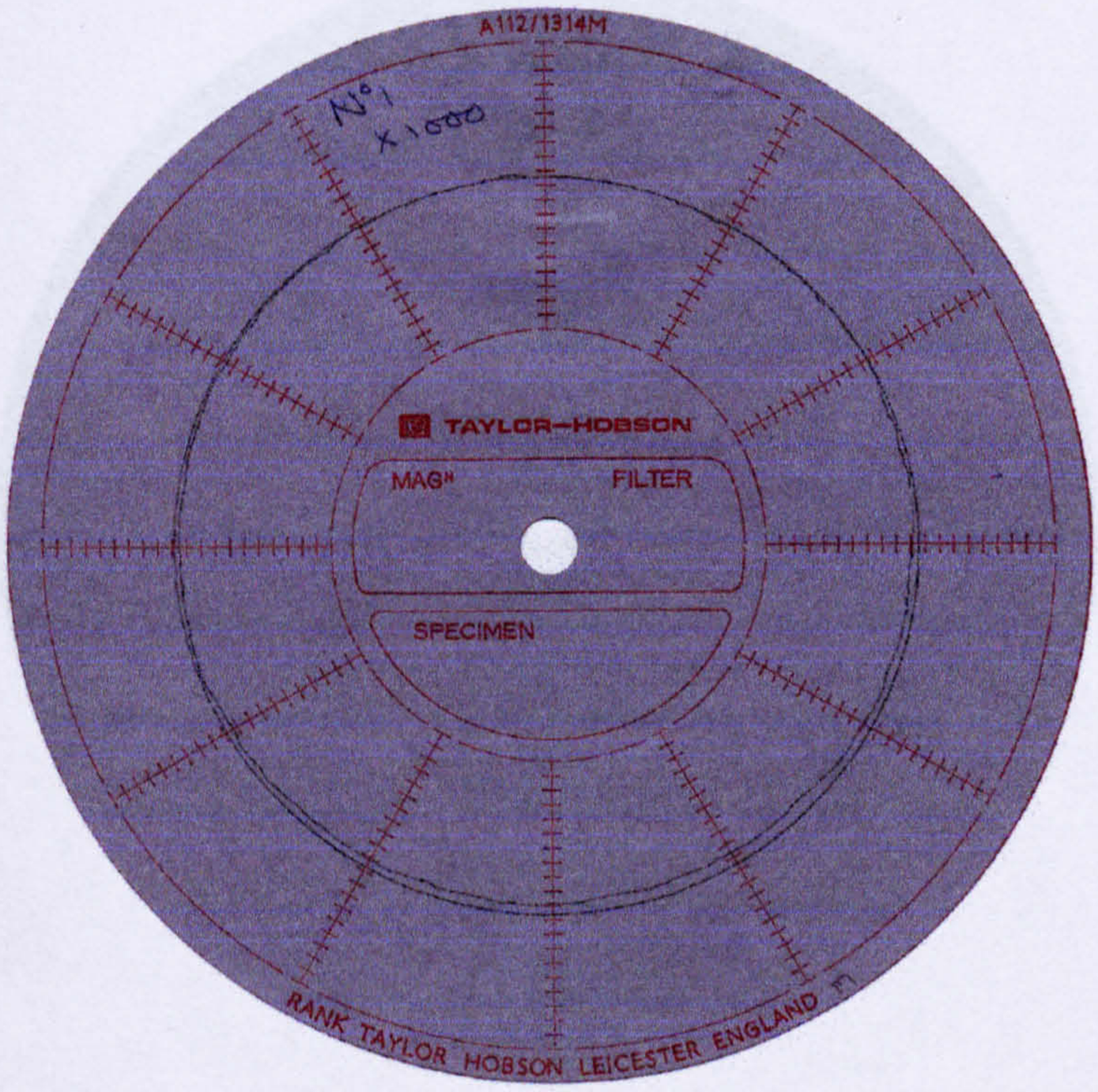

(b)

Figure 4-45 Behaviour of the driving wheel roundness (a)- before and (b)- after roundness treatment (No. 1 diameter 40 mm) Magnification [1:1000]

(a)

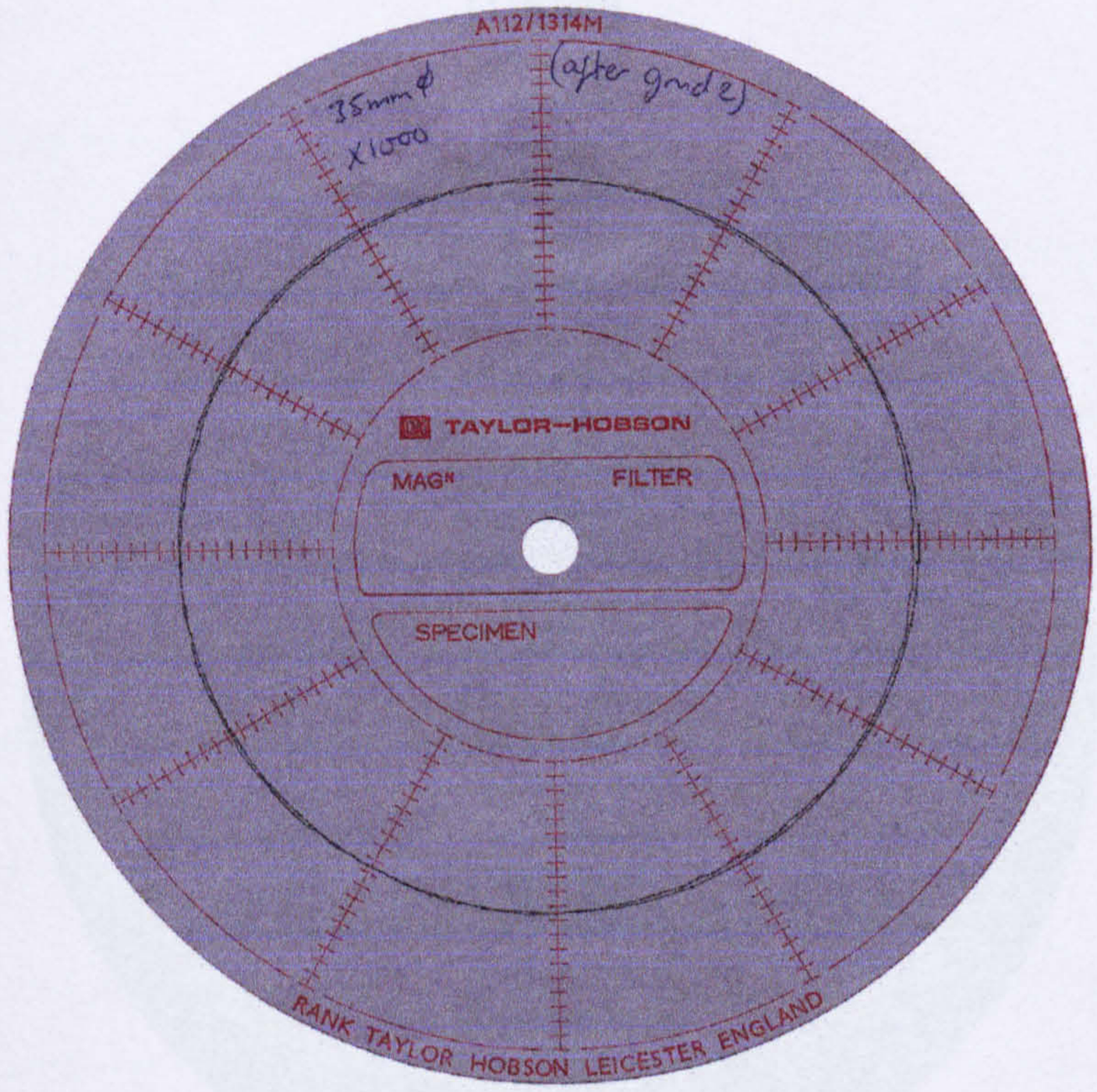

(b)

Figure 4-46 Behaviour of the driving wheel roundness (a) before and (b) after roundness treatment for the current piezoelectric USM (diameter 40 mm) Magnification [1:2000]

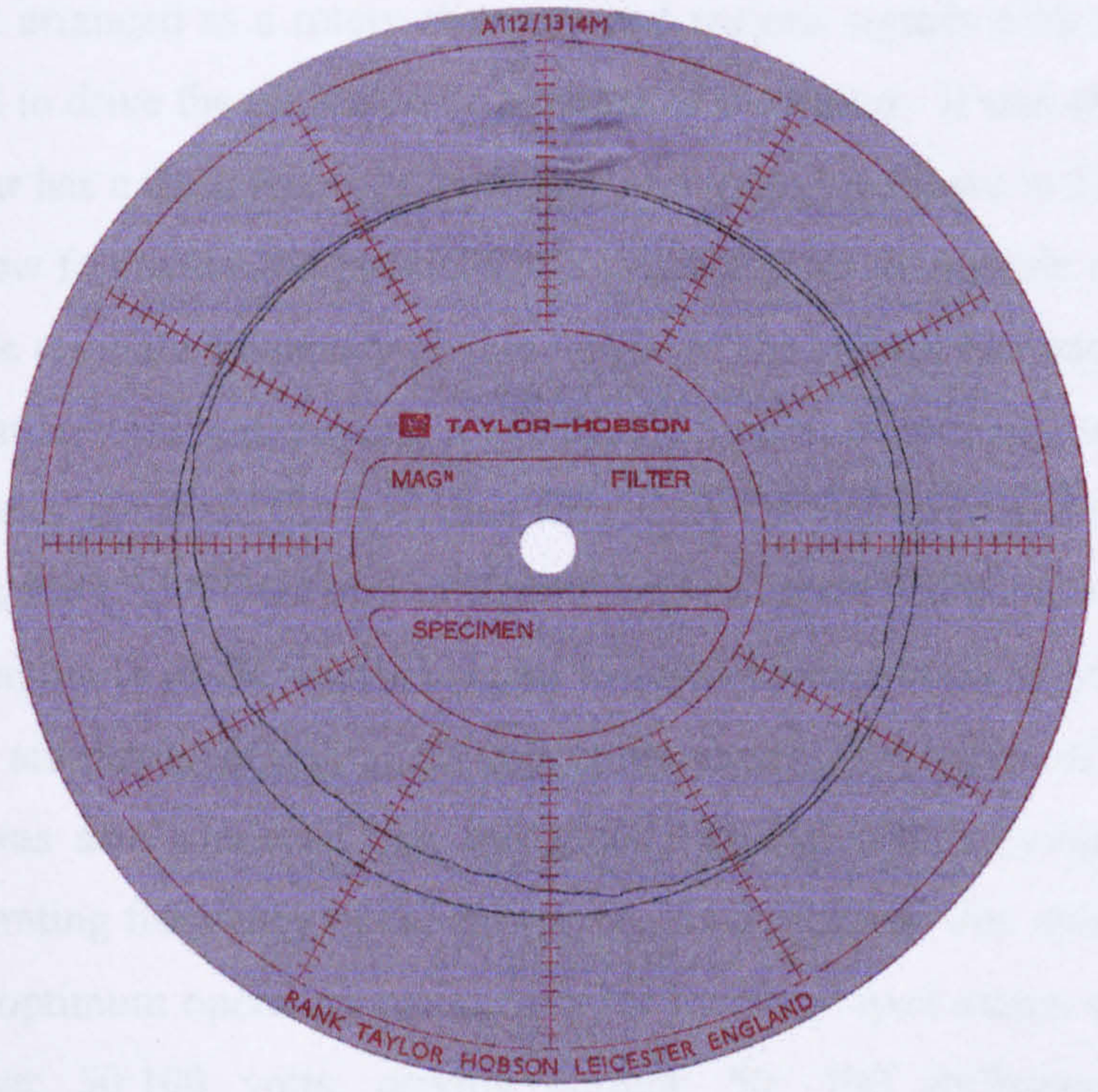

Figure 4-47 Behaviour of the shaft roundness (No.1 diameter 40 mm) Magnification [1:1000]

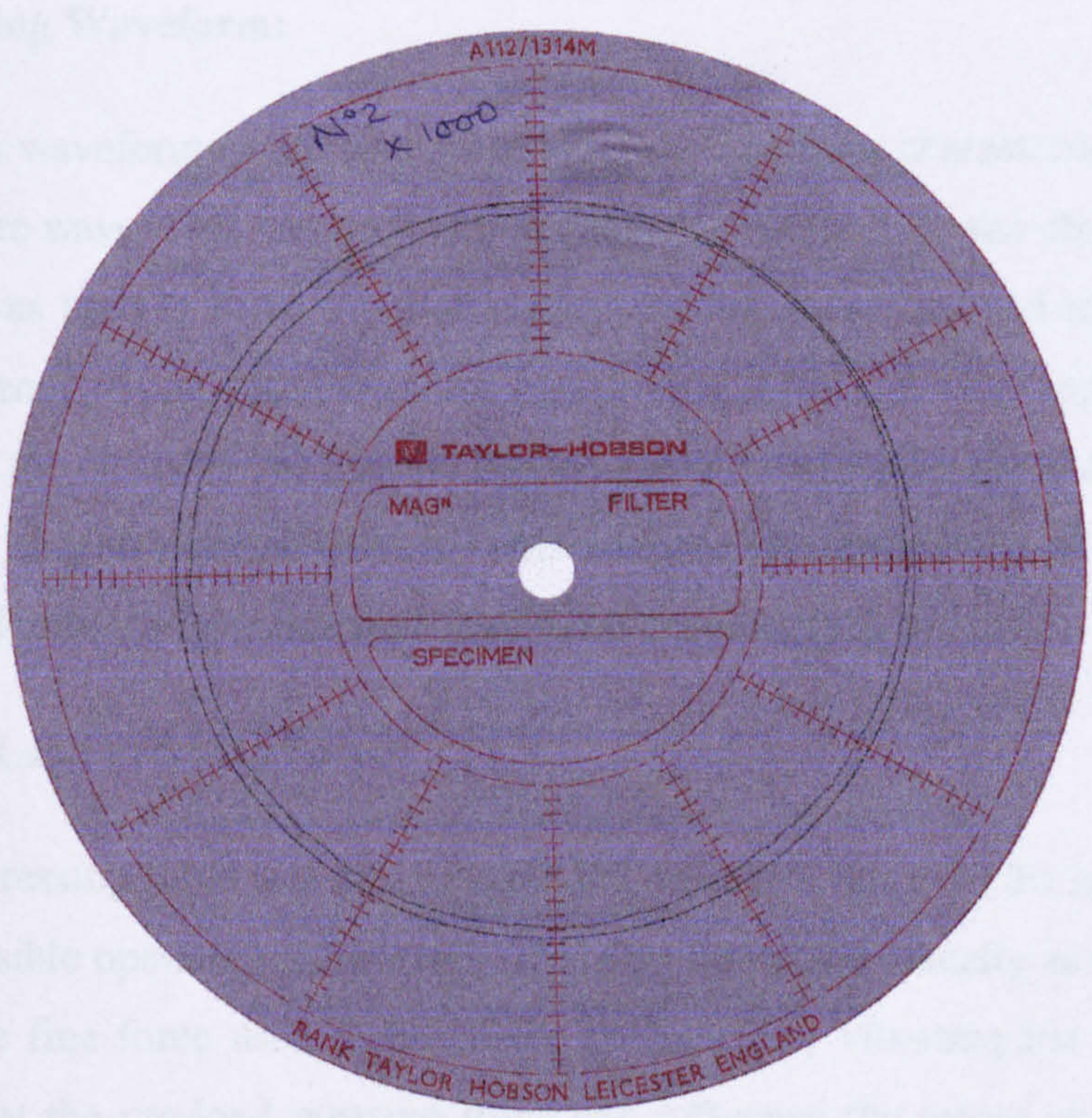

Figure 4-48 Behaviour of the shaft roundness for the piezoelectric USM after treatments (No. 2 diameter 40 mm) Magnification [1:1000]

The motor first arranged as a rotary structure and various signals with wide frequency band were used to drive the piezoelectric element of the motor. It was observed that the piezoelectric bar has a three resonant frequency and these are shown in Figures 4-51 and 4-52. At the low frequency the piezoelectric element gives an audible signal that is an indication of the resonant frequency on this range. At the highest resonant frequency the piezoelectric bar start vibrate creating a vibrational motion on standing wave form. This resonant frequency is named the operating frequency for the motor and this is shown in Figure 4-51 (d) for PZT PC4D and in Figure 4-52 (d) for CTS-19. It was noticed that increase the amplitude of the applied signal to some levels at this operating frequency increasing the amplitude of vibration and consequently the speed of the developed prototype. It was also observed that the speed reduced with varying the frequency around the operating frequency of the prototype. As a result of this optimisation it was found that the optimum operating parameters for the developed motor were as fellows: Driving voltage: 50:100 volts, driving current: 50: 100 milliamperes, operating frequency equal 41.5 kHz for PZT-piezoceramic and 37.5 kHz for the CTS19 piezoceramic.

4.10.2 Driving Waveform:

Three different waveforms were used to investigate the motor characteristics, sine, saw tooth and square wave. This can be found in detail in chapter 5. It was observed that if a square wave was used to drive the motor the operating frequency had to be below the resonant frequency, to prevent the motor overdriving. Motor overdriving increases the temperature of the piezoelectric bar and consequently transfers the piezoelectric element into different band of characteristics. This reduces the efficiency of the operating parameters and restricts the performance of the piezoelectric drive.

4.10.3 Pre-Load Pressing Force:

The pre-load pressing force was optimised based on the variation of the travelling speed at the best possible operating parameters. This was optimised visually as it was difficult to measure the fine force used to thrust the piezoelectric vibrating bar into the rotor. This shows that the pre-load pressing force can influence the motor characteristics. It can also have an effect on the electrode wear rate which in turn could affect the motor lifetime.

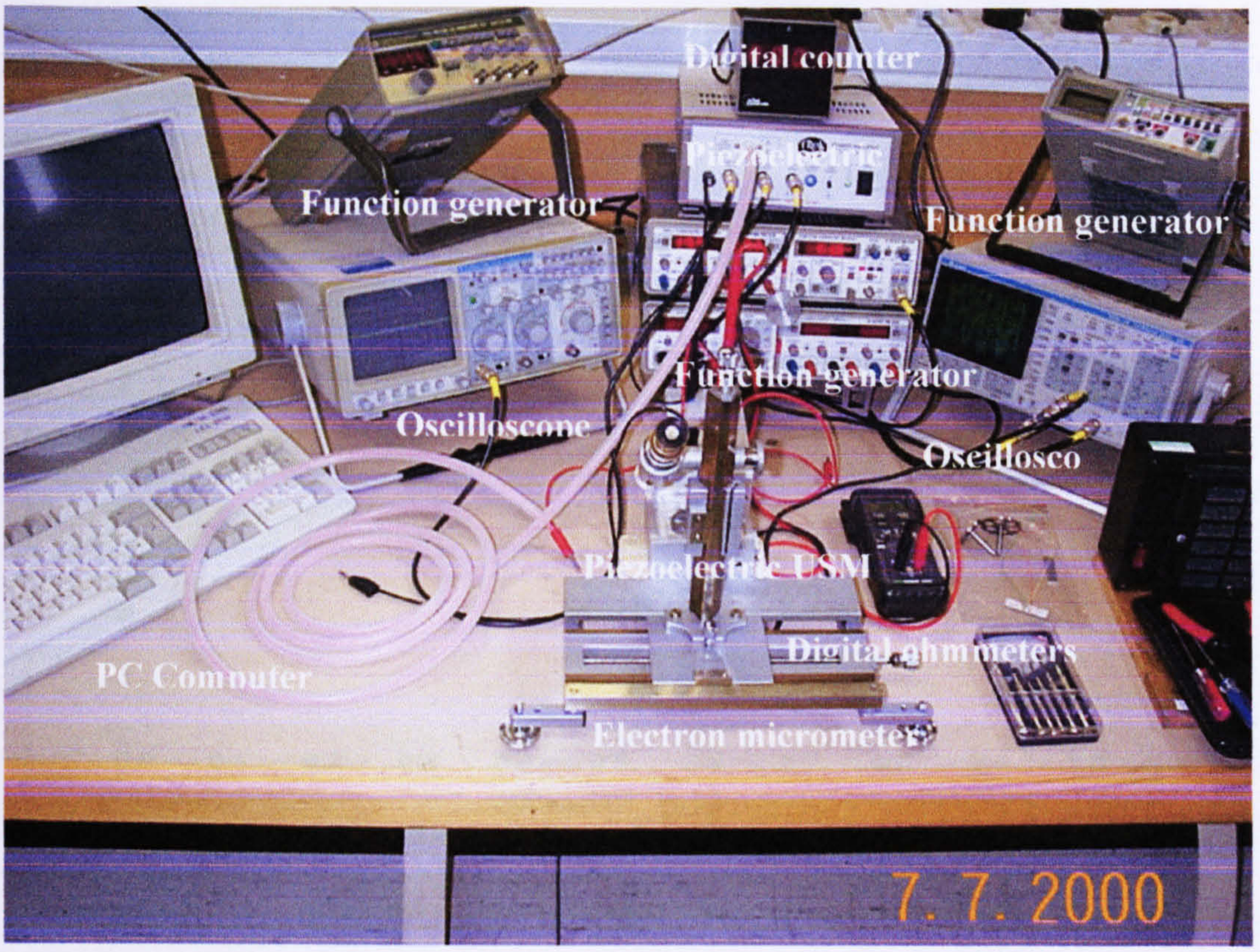

Figure 4-49 Experiment system used to measure the motor characteristics and to optimise its operating parameters

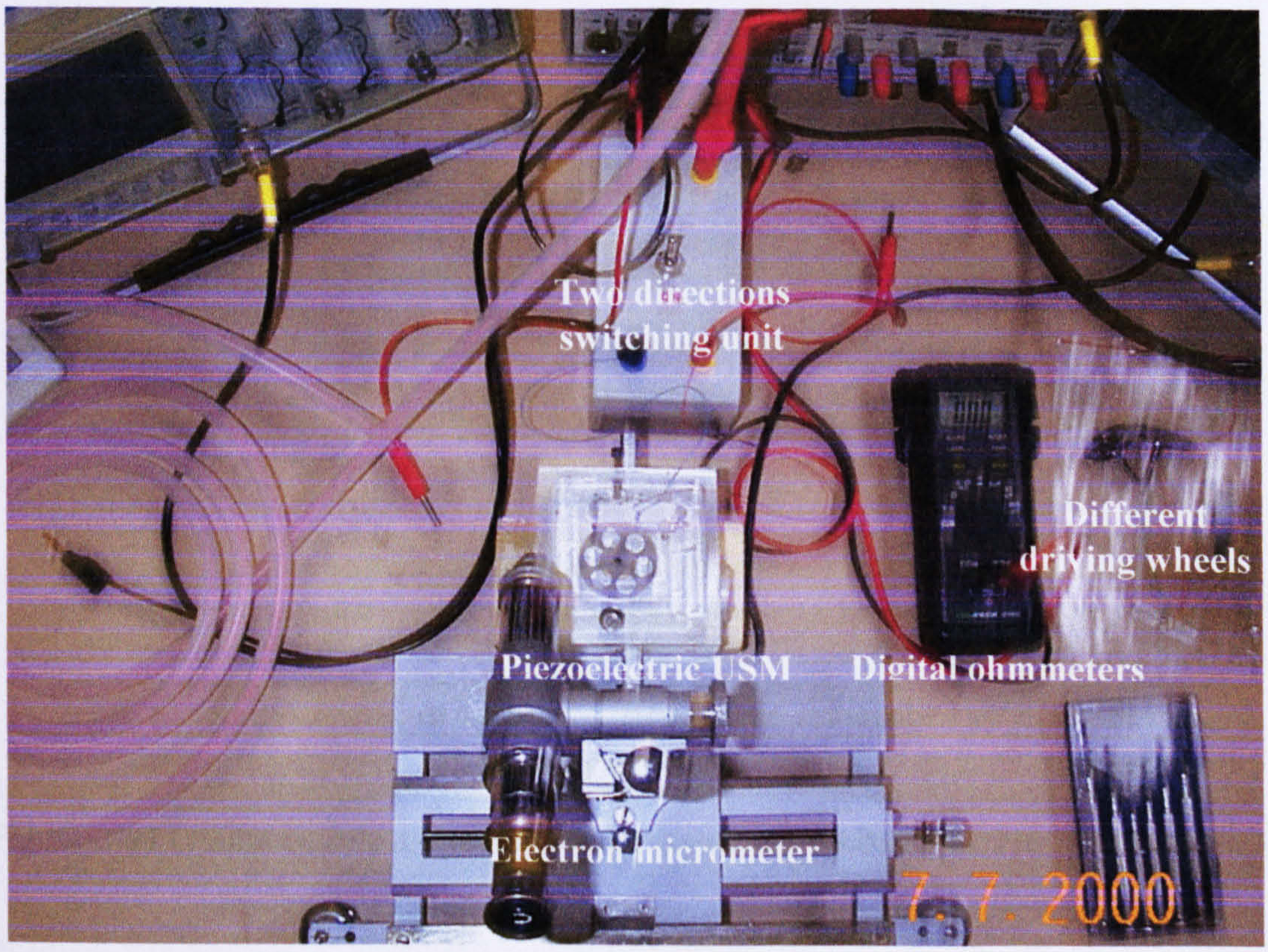

Figure 4-50 Experiment system used to measure the resolution of the developed motor using basic principles of measurements and a high-resolution microscope

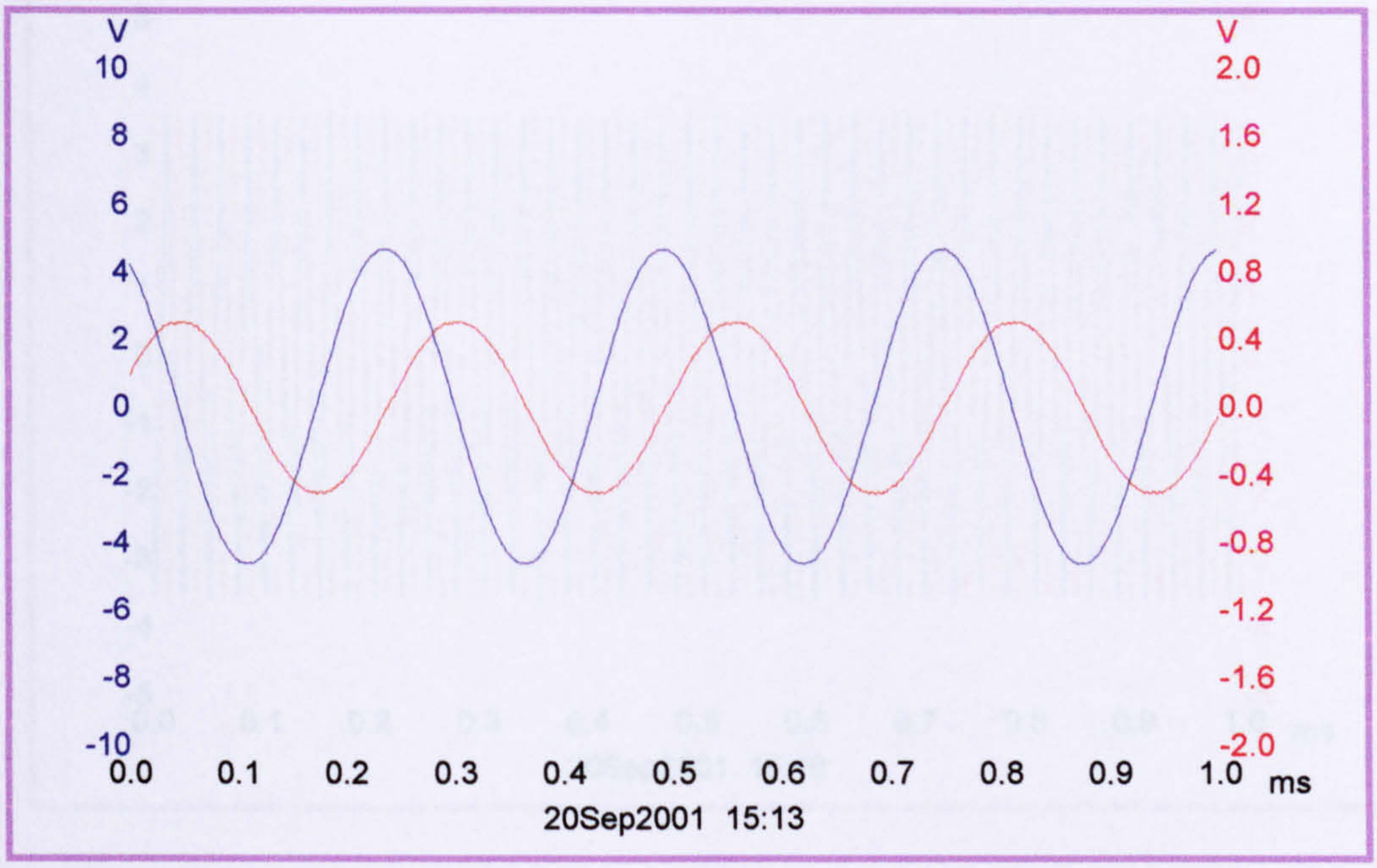

(a)

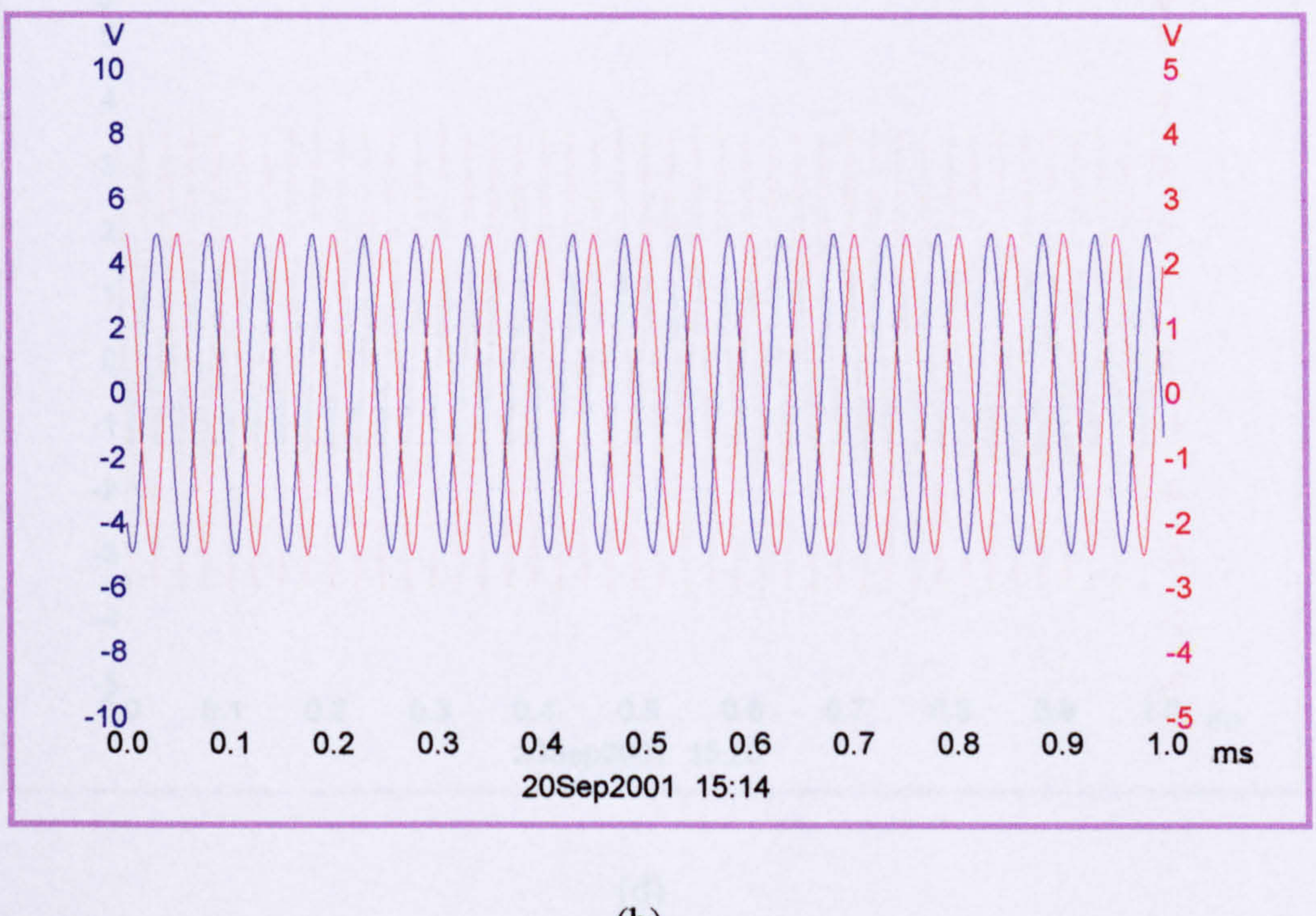

(b)

Figure 4-51 Optimisations of the operating parameters (voltage, current and frequency) for the developed prototype (Piezo-ceramic PZT-PC4D)
[Ch1-blue-voltage and Ch2-red-current, scale 1-10]

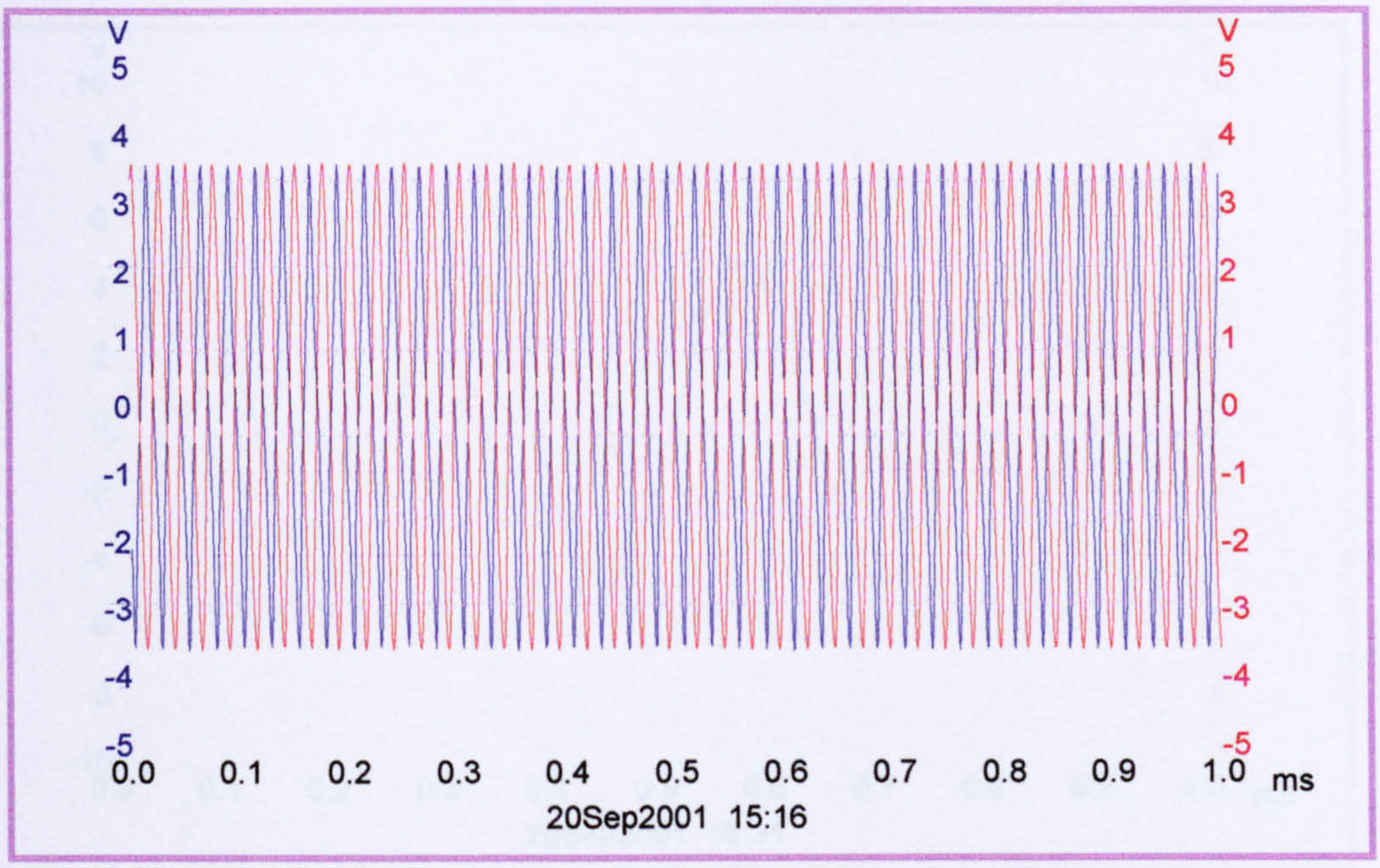

(c)

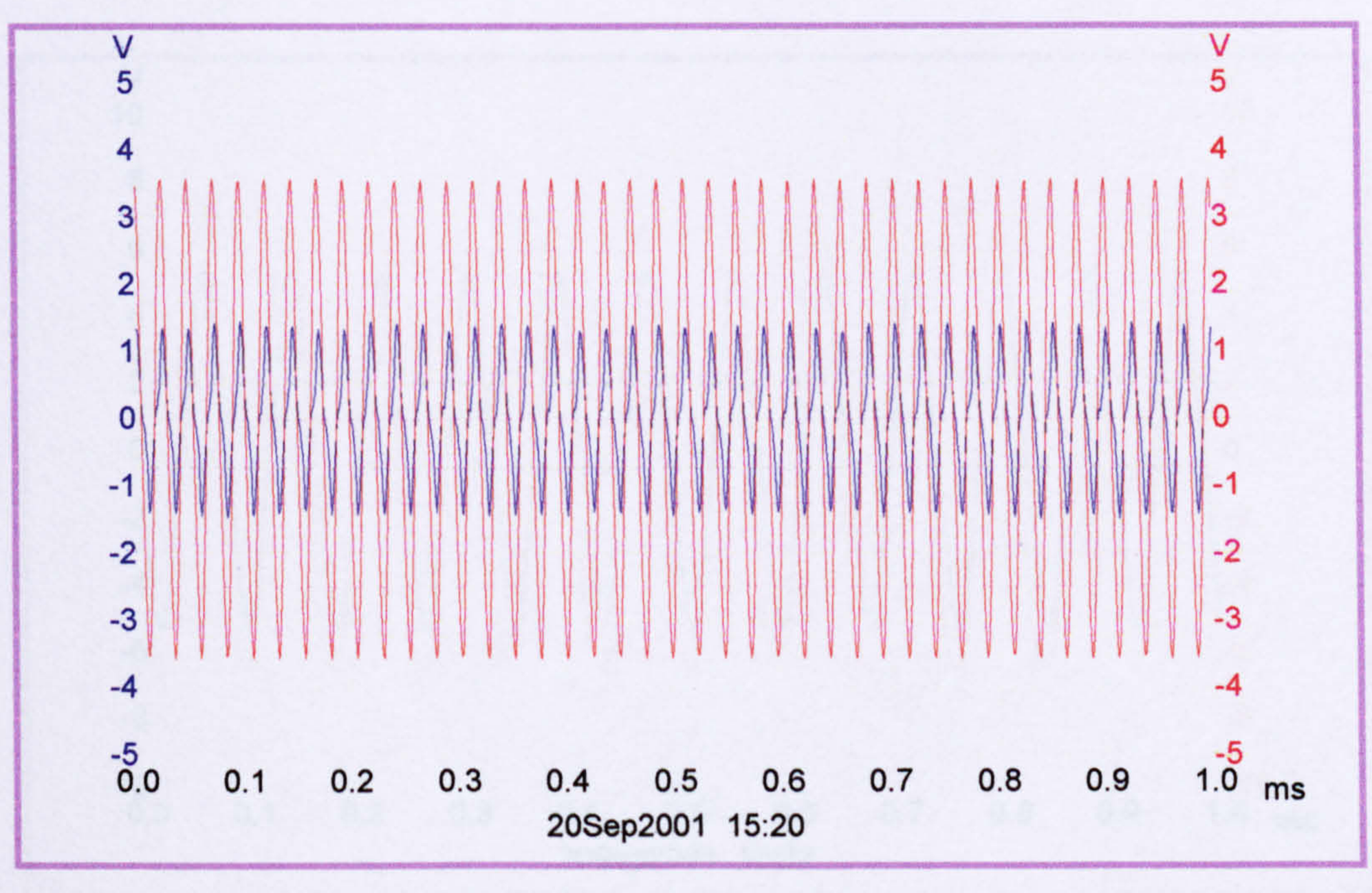

(d)

Figure 4-51 Optimisations of operating parameters (voltage, current and frequency) for the developed prototype (Piezo-ceramic PZT-PC4D)
[Ch1-blue-voltage and Ch2-red-current, scale 1-10]

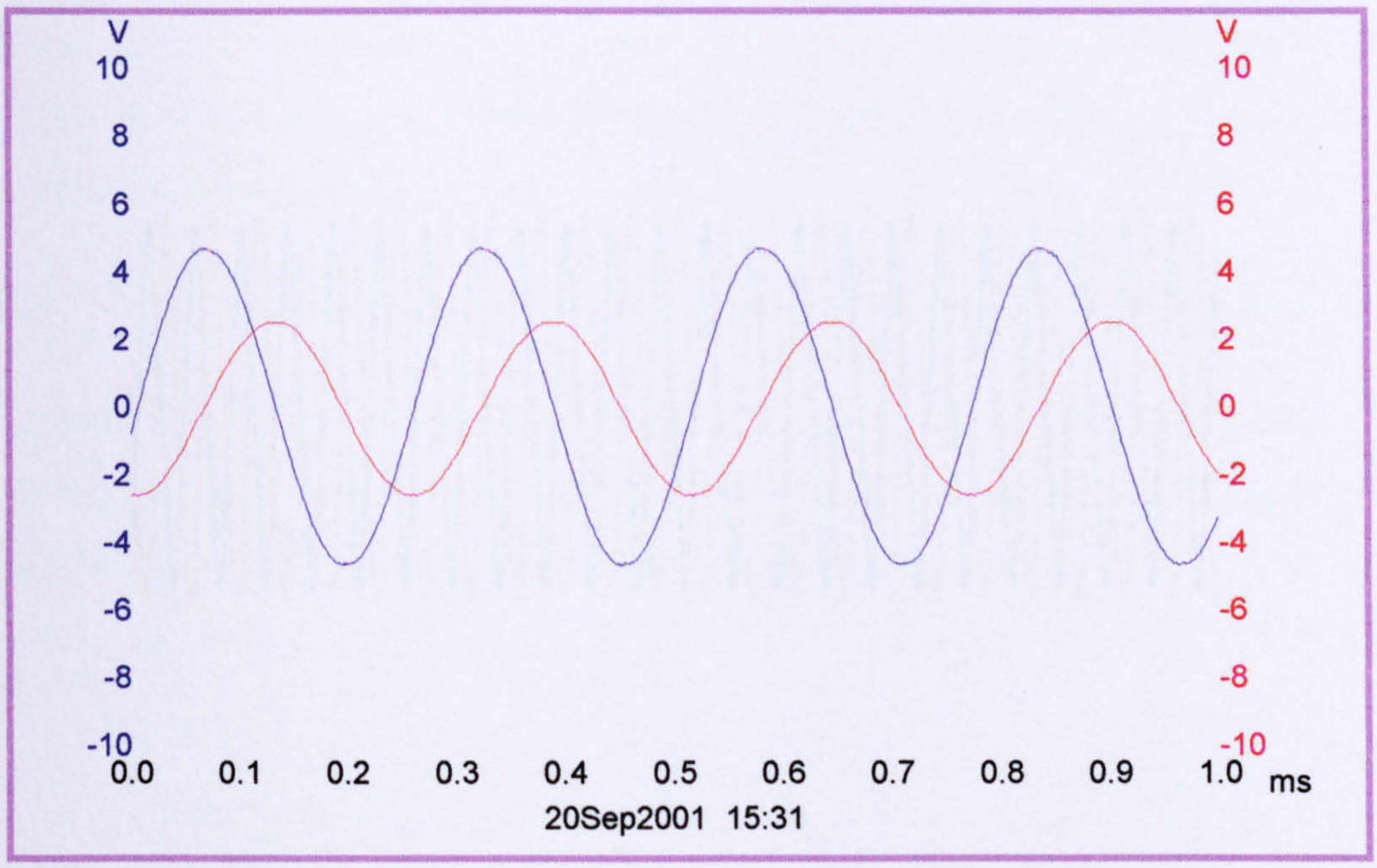

(a)

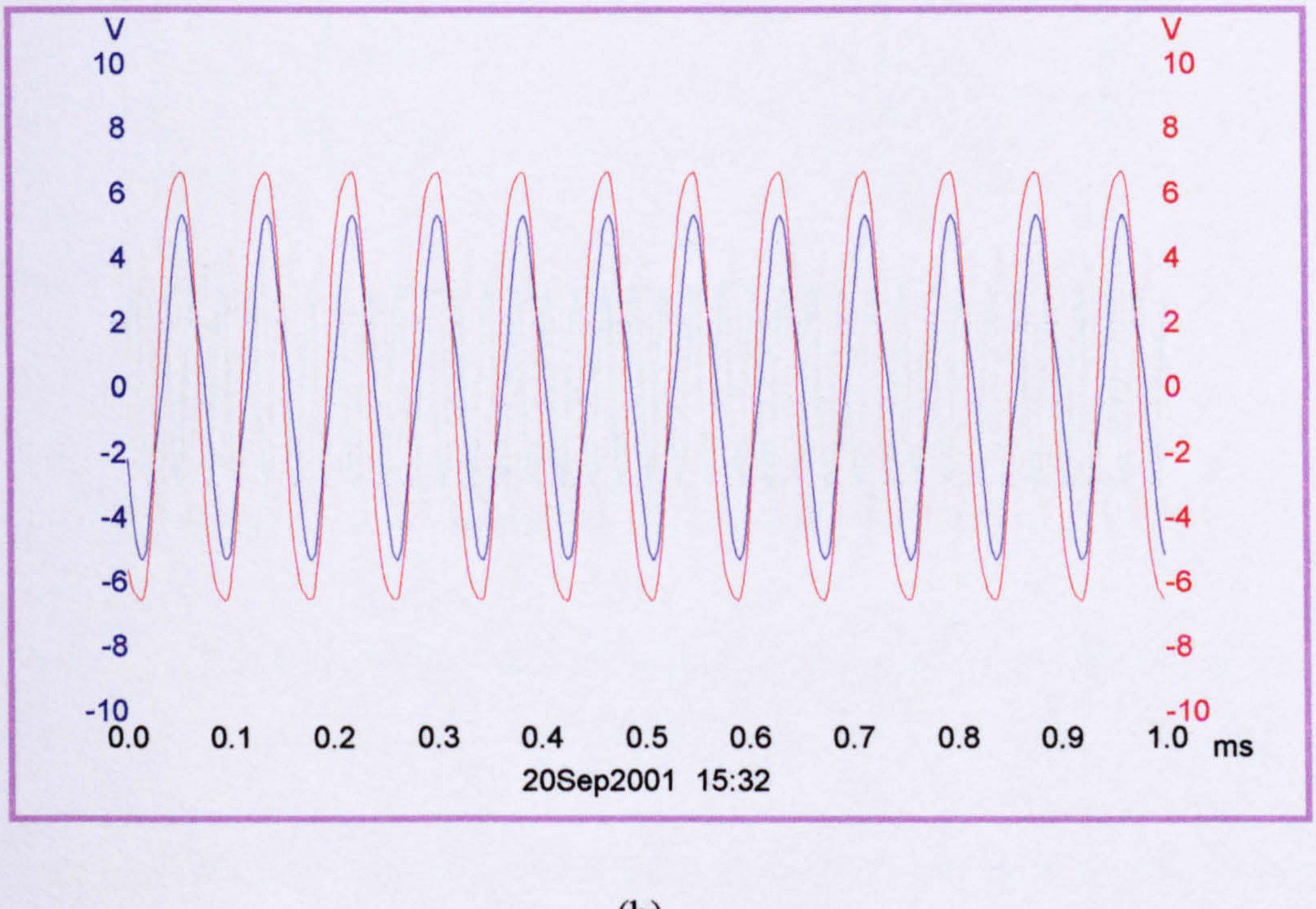

(b)

Figure 4-52 Optimisation of operating parameters (voltage, current and frequency) for the developed prototype (Piezo-ceramic PZT-PC4D)
[Ch1-blue-voltage and Ch2-red-current, scale 1-10]

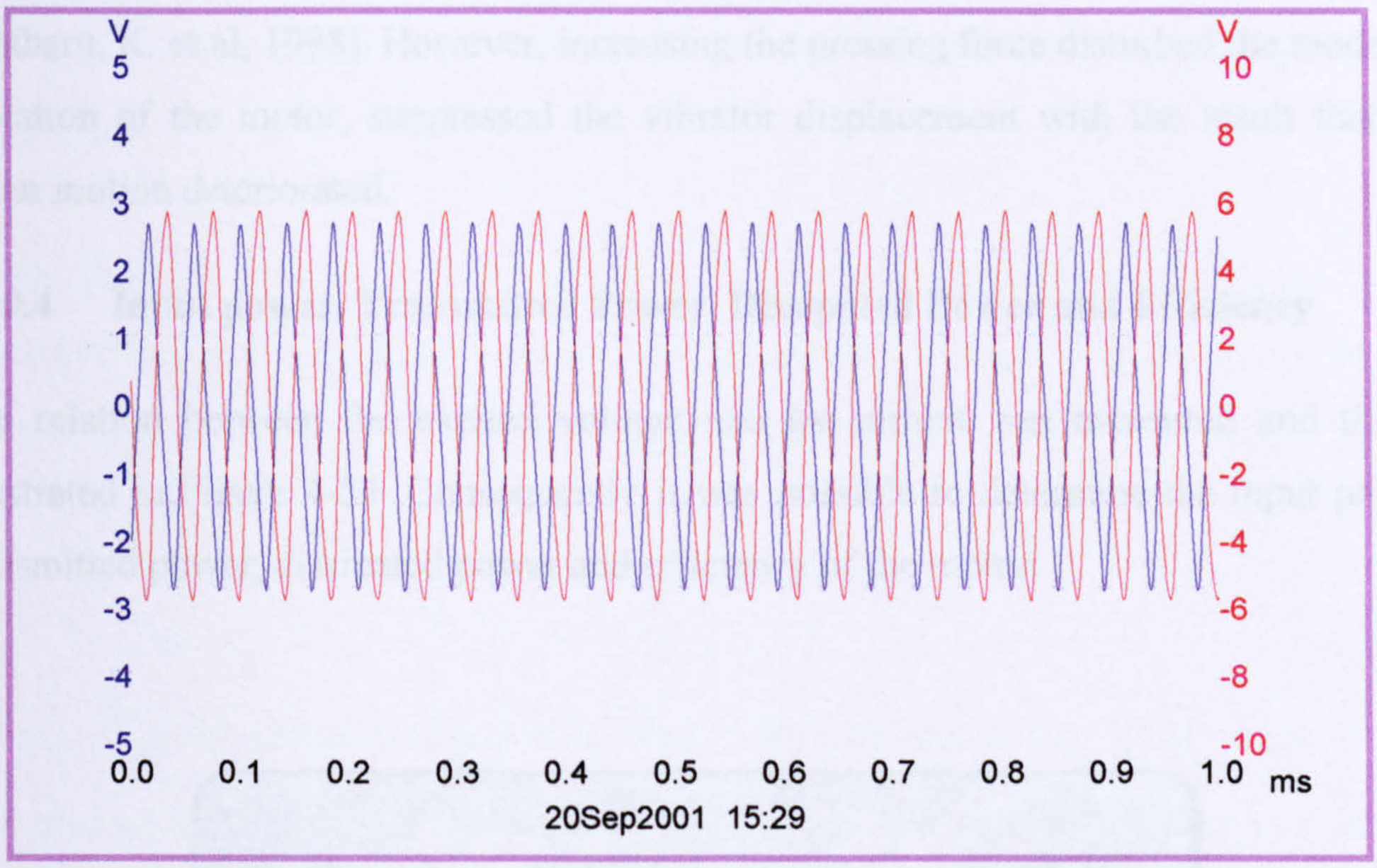

(c)

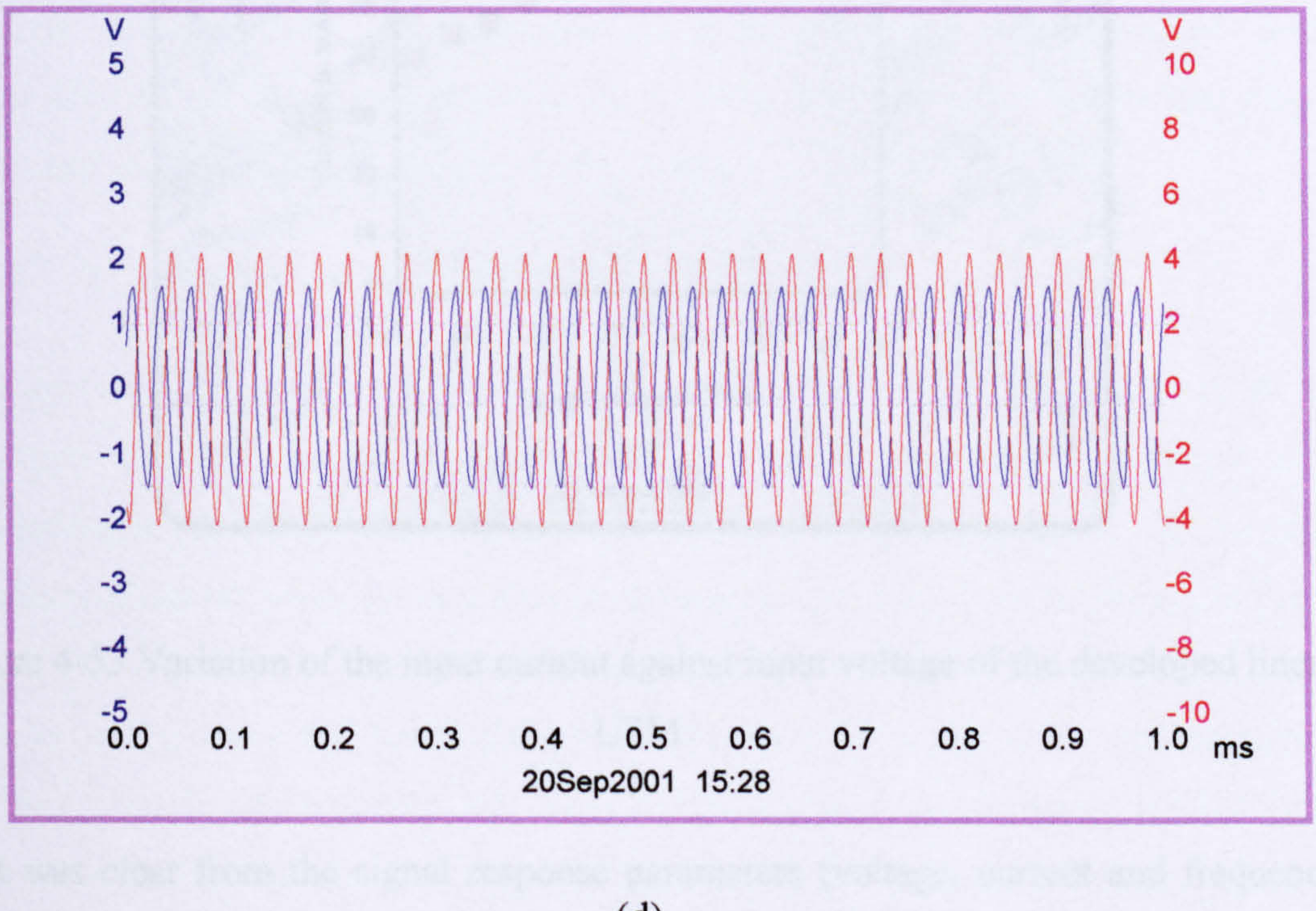

(d)

Figure 4-52 Optimisations of operating parameters (voltage, current and frequency) for the developed prototype (Piezo-ceramic PZT-PC4D)

[Ch1-blue-voltage and Ch2-red-current, scale 1-10]

This result shows a close agreement with the previous results conducted in this point [Chiharu, K. et al, 1998]. However, increasing the pressing force disturbed the modes of vibration of the motor, suppressed the vibrator displacement with the result that the linear motion deteriorated.

4.10.4 Input power, Transmitted Power, Dissipated Power and Efficiency

The relation between the excited voltage and its current was measured and this is illustrated in Figure 4-53. Consequently it was possible to determine the input power, transmitted power, dissipated power and efficiency of the motor.

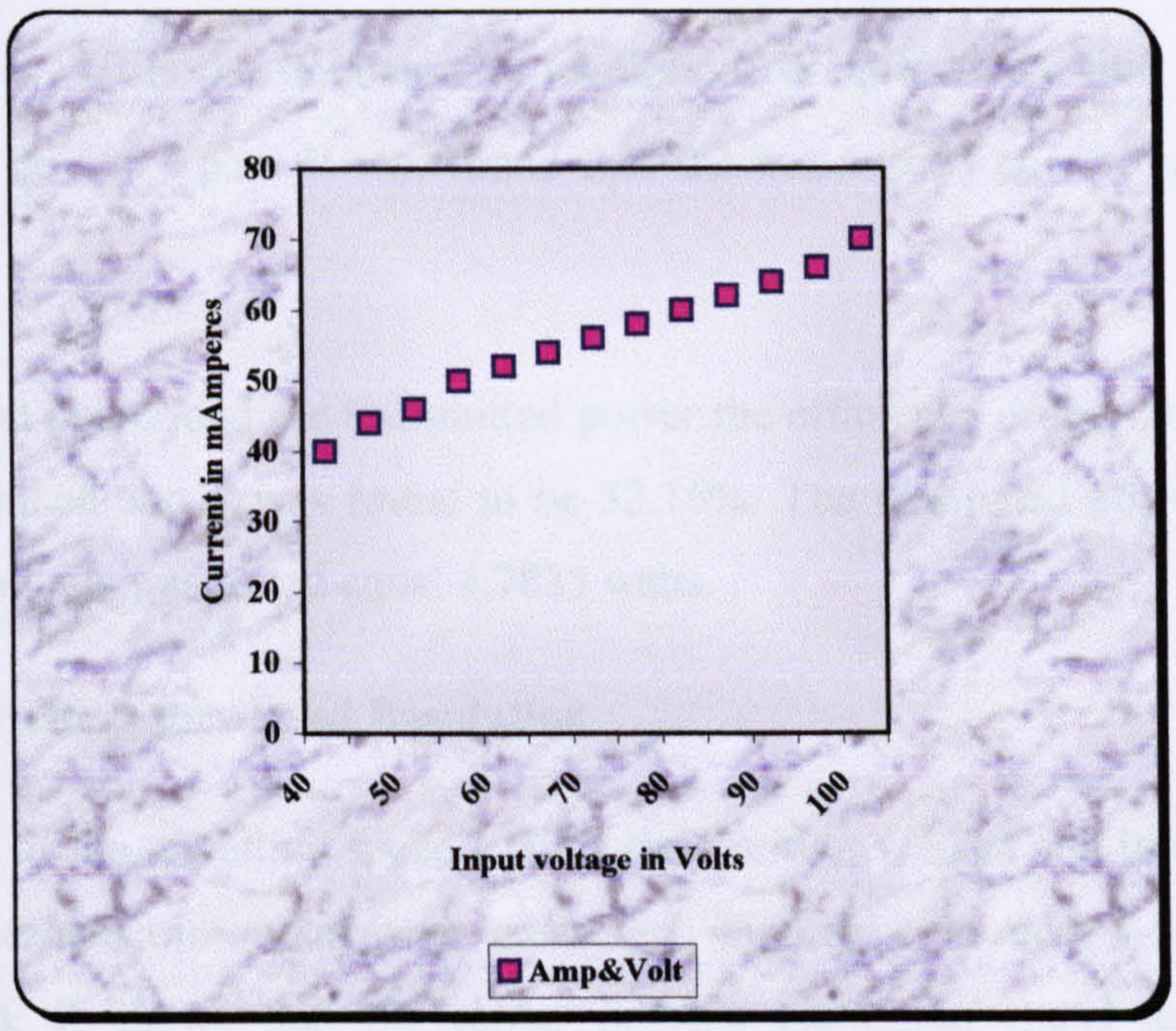

Figure 4-53 Variation of the input current against input voltage of the developed linear USM

As it was clear from the signal response parameters (voltage, current and frequency) optimisation that, the voltage was found to be 50 to 100 Volts, and current found equal 50 to 100 milliamperes. Using the input power relation:

$$P_{i/p} = I_{i/p} V_{i/p}$$

where, $I_{i/p}$ is the input current and $V_{i/p}$ is the input voltage. The input power found to be 10 watts.

In this case the vibrational force of the active piezoelectric electrode is translated into motion based on the frictional between the piezoelectric vibrator and the rotor disk. The transmitted power can be determined using the relation:

$$P_t = T\omega$$

Where, P_t is the transmitted power in Watt, T is the torque and $\omega = 2\pi f$ is the angular velocity $rad/\sec$. f is the frequency in revolution per minute and this was measured and found to be 120 r.p.m. It was found that the transmitted power equal to 5.2165 watts.

Using the input power and the transmitted power the efficiency of the developed motor can be determined and it was found to be 52.16%. The dissipated power also can be determined and this was found equal 4.7835 watts.

4.10.5 Travelling speed and Resolution

The variation of the travelling speed against the exciting voltage and frequency for the developed piezoelectric motor was measured. Figures 4-54 and 4-55 show these measurements. It shows that the motor provide maximum speed at the resonant frequency of the vibrating bar and then decay around this frequency as shown in Figure 4-54. It also clarifies the capability of using the amplitude of the input signal to control the speed of the motor and this is illustrated in Figure 4-55. However, it was noticed that at certain voltage, which is over 100 volts, the piezoelectric bar became very hot which lead to overdriving and notable change in the piezoelectric characteristics takes place.

The resolution was measured. The system used to measure the resolution is shown in Figure 4-50. It is the same system used on optimising the operating parameters. The system was arranged to drive the motor using the lowest operating parameters including frequency and voltage. Then a portable electron microscope was used to measure the

minimum rate the system will provide. This test was carried out many times. It was found that the minimum degree of motion the motor can provide at operating parameters 40 volts, 42.5 KHz was on the order of 50 micrometers. This in fact shows a close agreement to the calculated value using maximum and minimum displacement obtained from finite element analysis.

4.10.6 Capability of the Motor for Control

Figures 4-54 and 4-55 show the motor capability to be controlled using either the frequency or amplitude of the input signal. The experimental test showed that the best driving condition is to set the piezoelectric element into the resonant frequency and use the amplitude of the input signal to control the speed of the motor on the recommended range. This is provided the ability to use self-excitation method that enables to work out the non-linear characteristics of the piezoelectric vibrating bar, and consequently maximum performance can be obtained.

4.10.7 Load Capacity

The variation of the travelling speed against applied load was measured using the proposed systems Figures 4-49 and 4-50. Then the motor was arranged as it will be used in the application developed for and then different loads were applied. This was carried out many times on the forward and backwards direction of motion. Figure 4-56 shows the results of these measurements. It shows the capability of the motor to react with the application under load. It was also noticed as shown in this Figure that the motor like any other linear motor the speed slow down with increasing the applied load [Hu, J. et al, 2001, Newton, D. et al, 1997, Shafik, M. et al, 2001]. It was found that the motor was able to carry a load of approximately 0.833 Newton's. This is mainly dependent on the friction coefficient between the parts of the motor. As it was observed that at certain point when the load exceed the frictional force between the shaft and the sliding element the travelling speed of the sliding element increases as shown in Figure 4-56. These showed that the friction force between the piezoelectric electrode and the driving wheel was higher than between the shaft and sliding element.

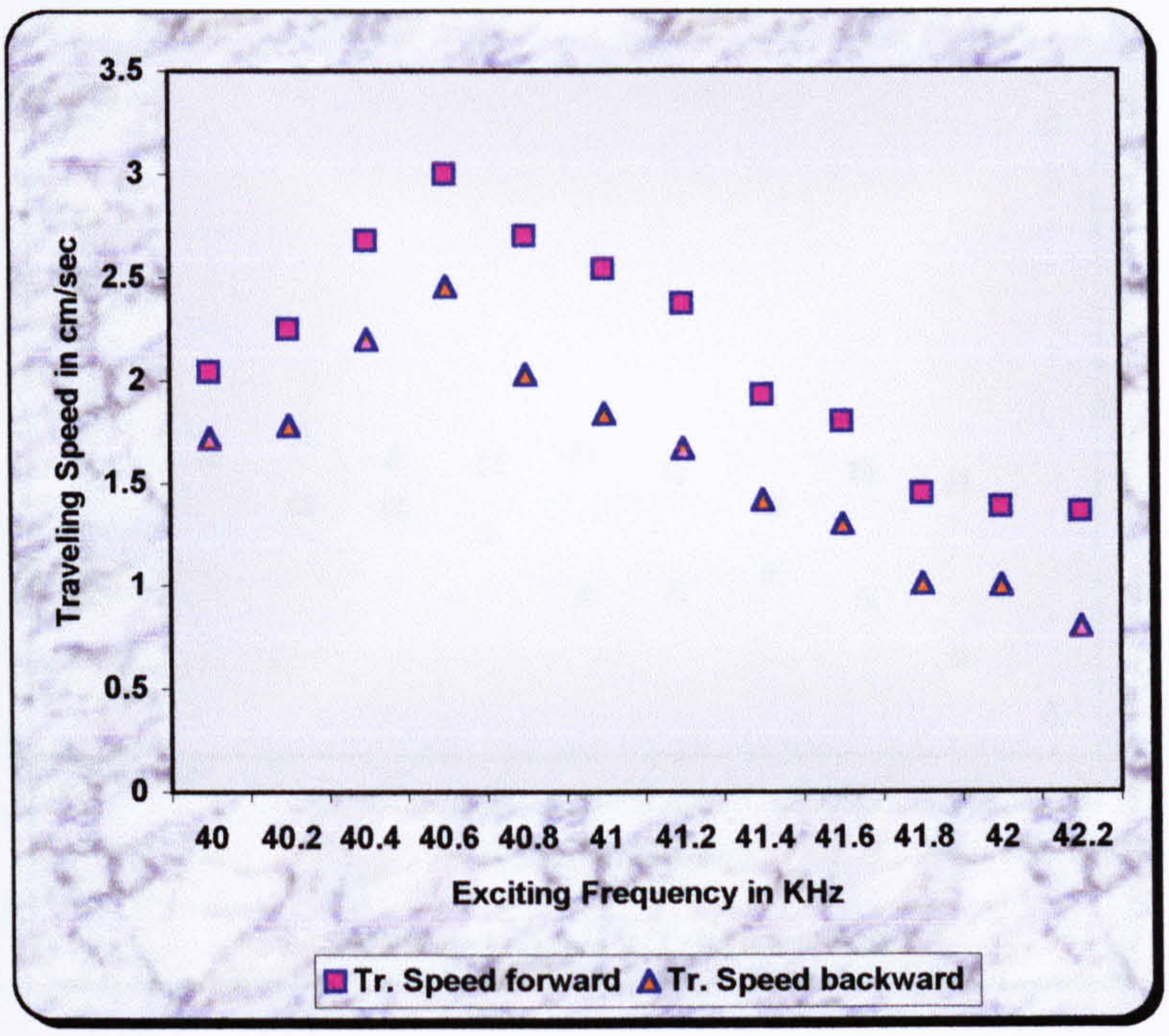

Figure 4-54 Travelling speed variation against the input frequency for the developed USM

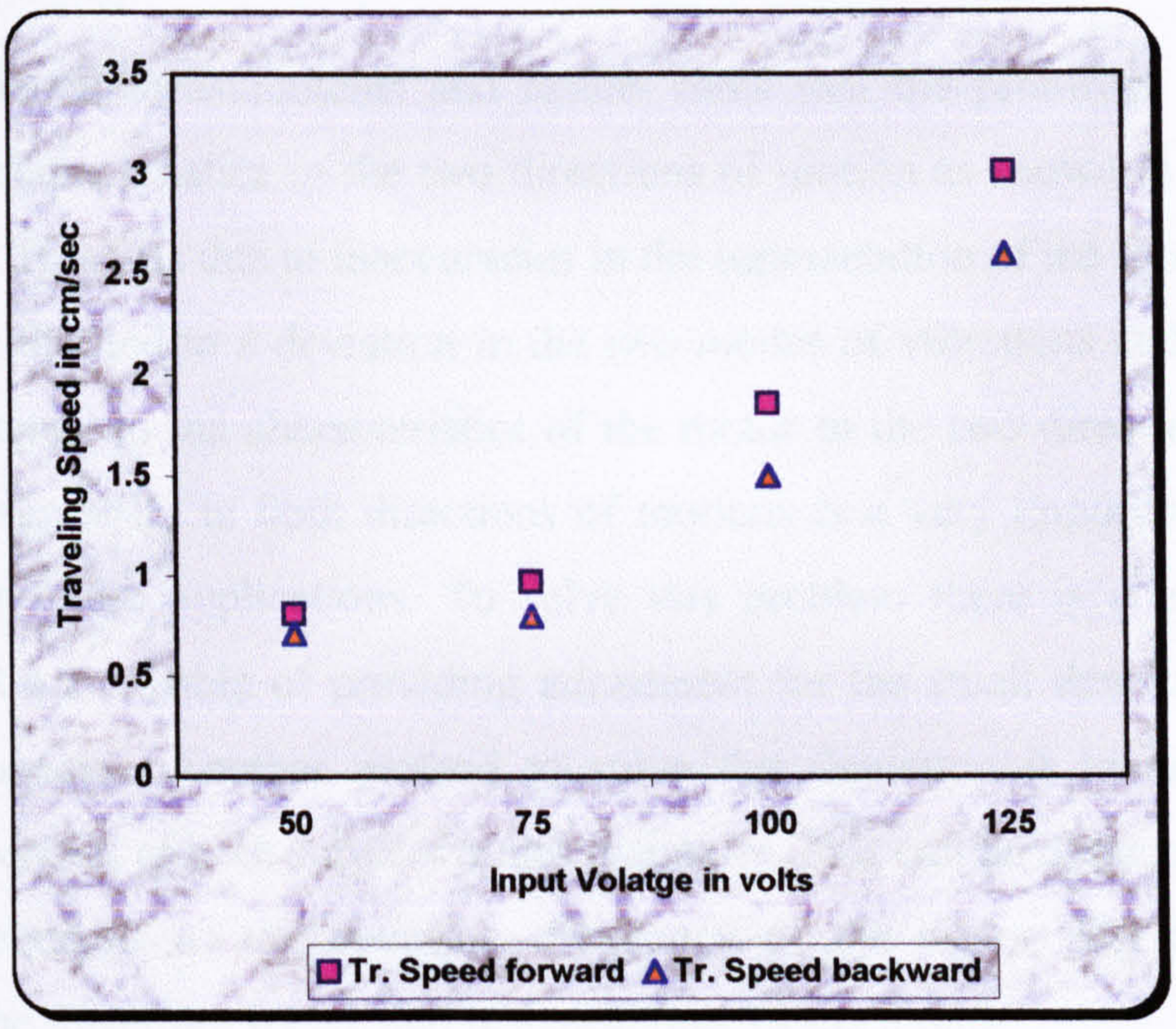

Figure 4-55 Travelling speed variation against the input voltage for the developed linear USM

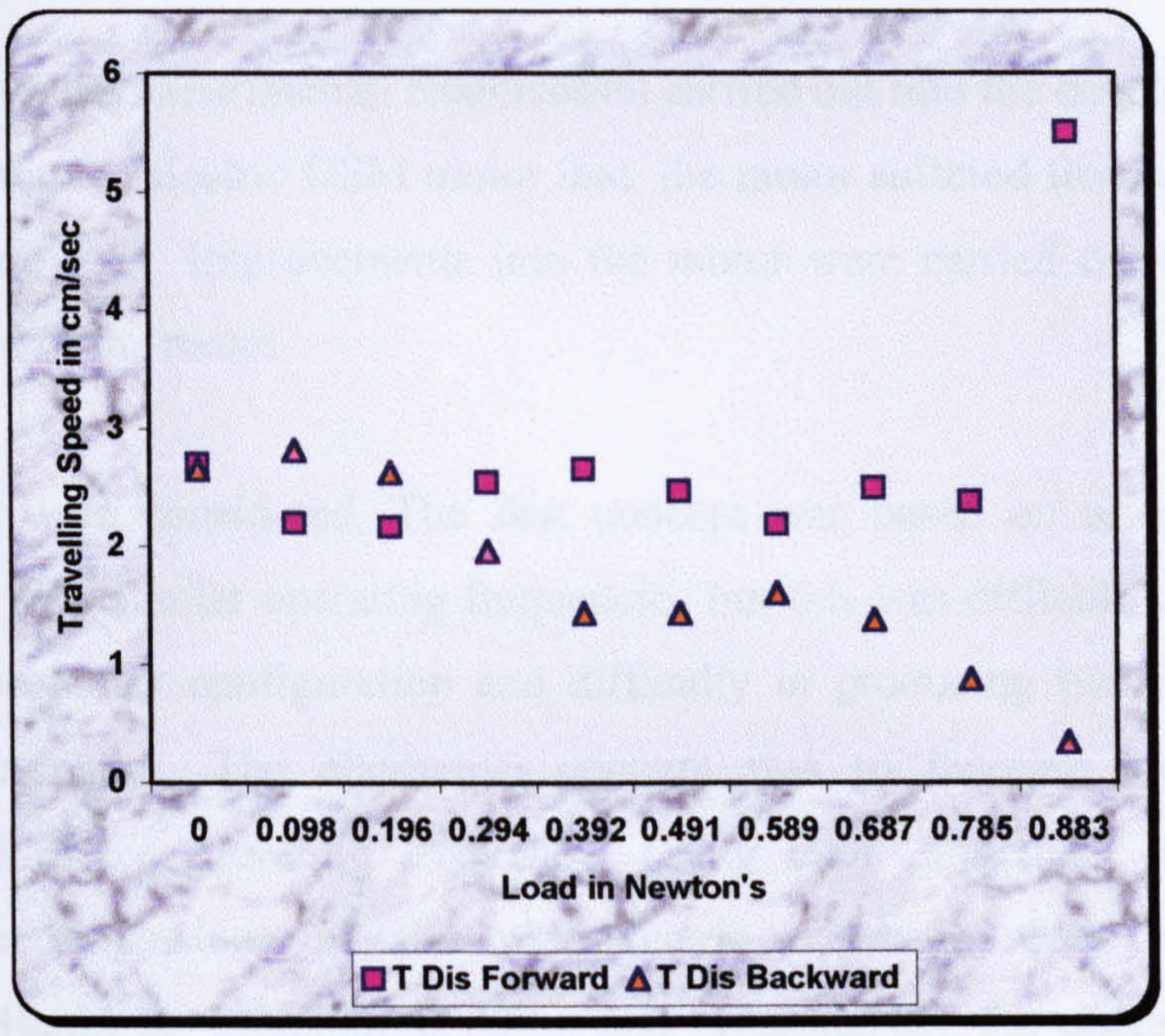

Figure 4-56 Travelling speed against load for the forward and backward direction of motion for the current configuration

4.10.8 Limitations of the Developed Prototype

These experimental measurements and results show that the prototype produced has asymmetrical characteristics in the two directions of motion as shown in Figures 4-54, 4-55 and 4-56. This was due to inaccuracies in the segmentation of the flexural vibrating bar subsurface that led to a deviation in the two modes of vibrations and consequently lack of consistency in the characteristics of the motor in the two directions of motion. The need for similarity in both directions of motions is a very important factor to be considered for future applications. To solve this problem there is a need to design resonators that are capable of providing adjustment for the small deviation in the two resonant frequencies. Another method to solve this deviation is to match the two-resonant frequencies of both sub-electrodes manually. This can be obtained by choosing the lowest frequency as the operating frequency of the motor. But this shows an influence on the travelling speed, and response time of the motor.

4.11 IMPROVEMENTS TO THE DEVELOPED MOTOR

It was clear from the experimental examination carried out into the developed prototype of the proposed piezoelectric USM motor that, the motor suffered from slow motion as shown in Figure 4-54. Improvements into the motor were carried out to increase the travelling speed of the motor.

Two concepts were considered. The first concept was based on using two flexural vibrating bars with similar operating frequencies but this was difficult to achieve. This was due to the motor configuration and difficulty in producing two electrodes with similar characteristics. The alternative concept was to increase motor speed by increasing the motor operating frequency. Using main principles of piezoelectric materials, the dimensions of the piezoelectric electrode were modified from 2mmx10mmx40mm to 4mmx8mmx30mm and consequently the operating frequency was increased from 41.5 KHz to 53.5 KHz. The dimensions of the new electrode and principles concerning piezoelectric material are given on appendix (A).

The electrode was re-integrated into the motor frame and a series of experimental test was conducted. Then measurements of the main characteristics for the motor were taken and these are shown in Figures 4-58, 4-59 and 4-60. These show clearly the motor travelling speed was increased from 28 mm/sec to 37 mm/sec. This proves that the speed of this type of motor were dependent considerably on the operating frequency of the piezoelectric vibrating bar, ratio between the moment of inertia of the parts (stator & rotor) of the motor and the material used to produce these parts. The resolution measured in this case was found to be 70 micrometers. The response time was also improved from order of 80 microseconds.

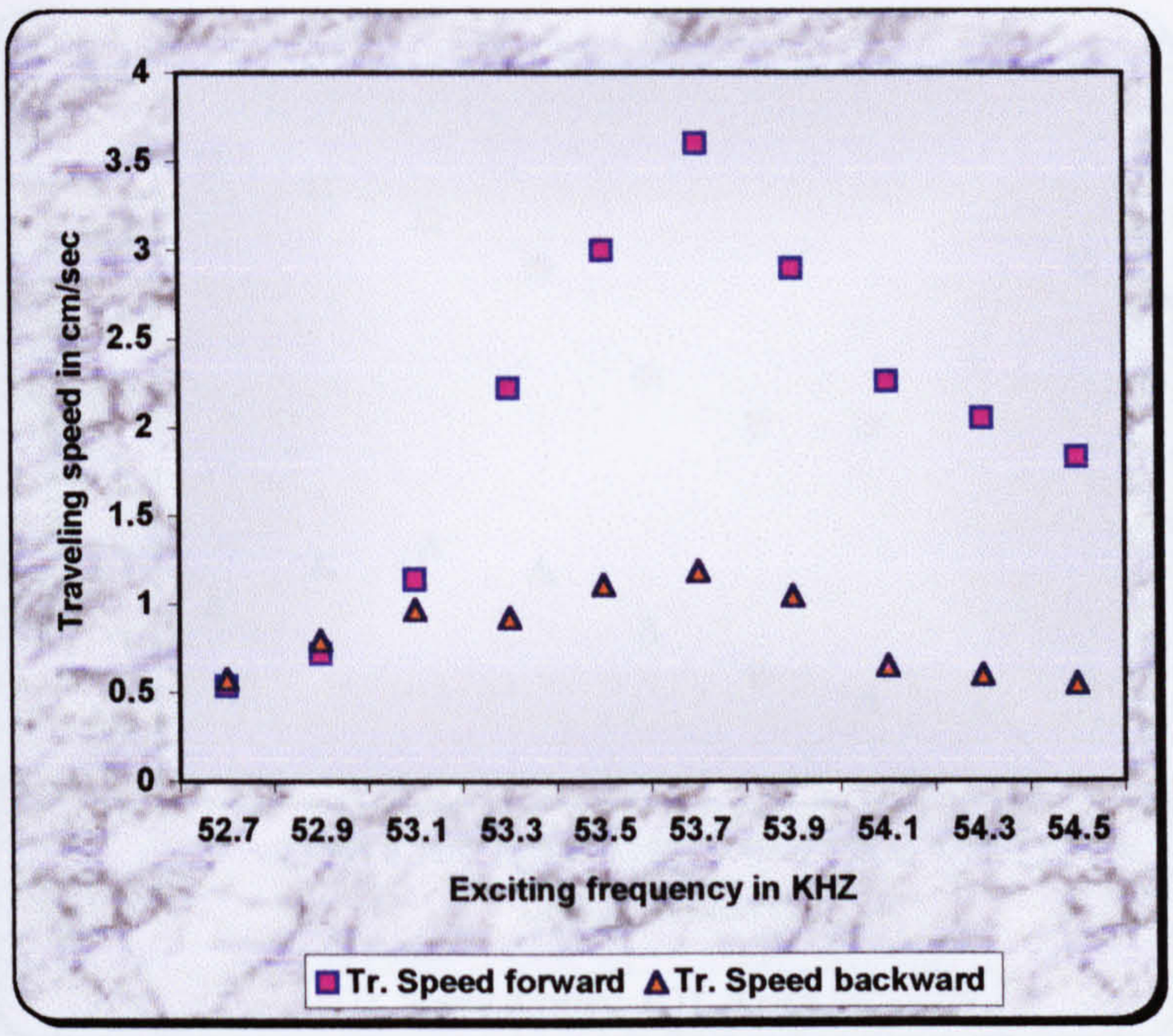

Figure 4-58 Travelling speed against input frequency for the forwards and backwards directions of motion for the modified motor

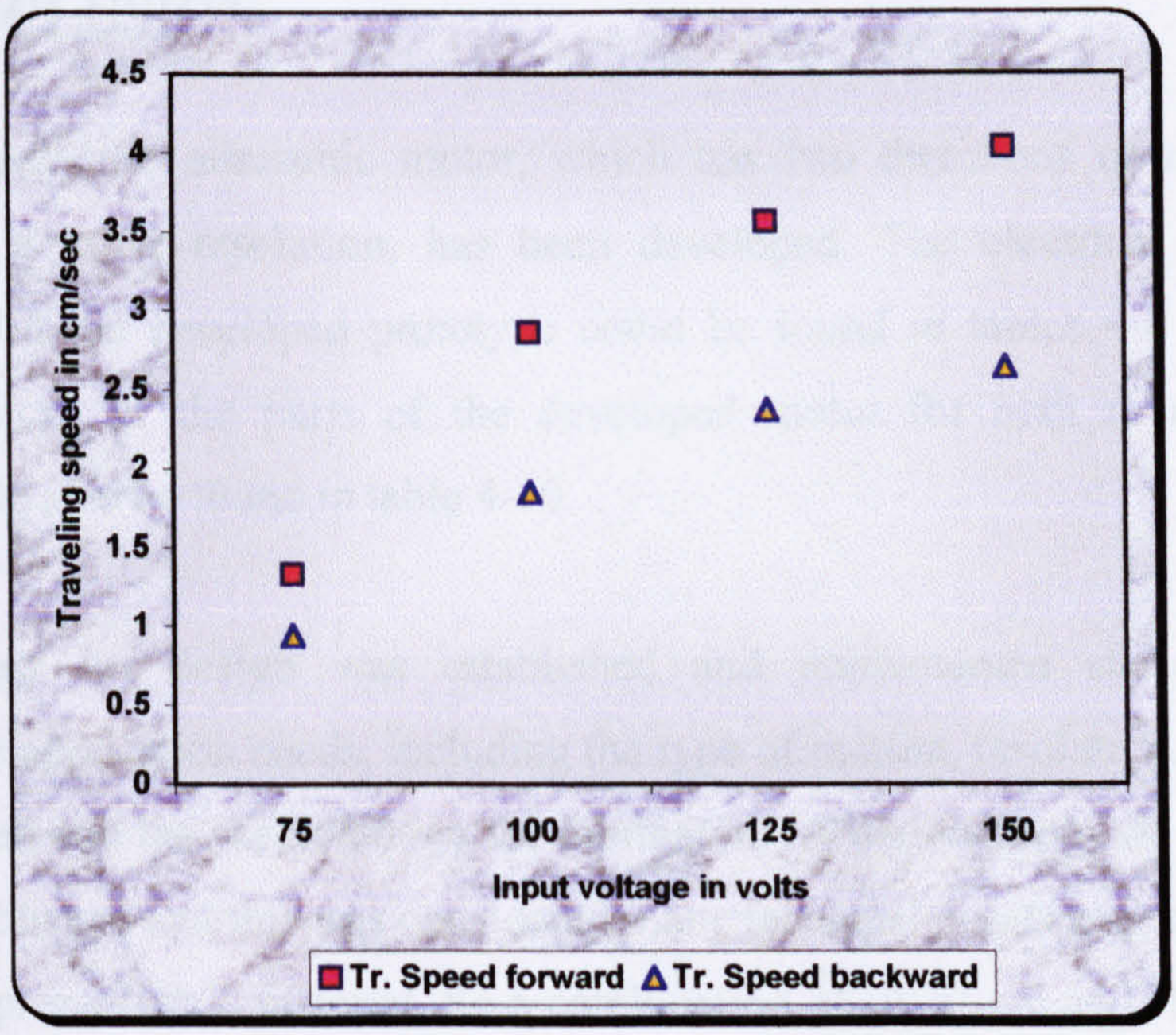

Figure 4-59 Travelling speed against input voltage for the forwards and backwards direction of motion for the modified motor

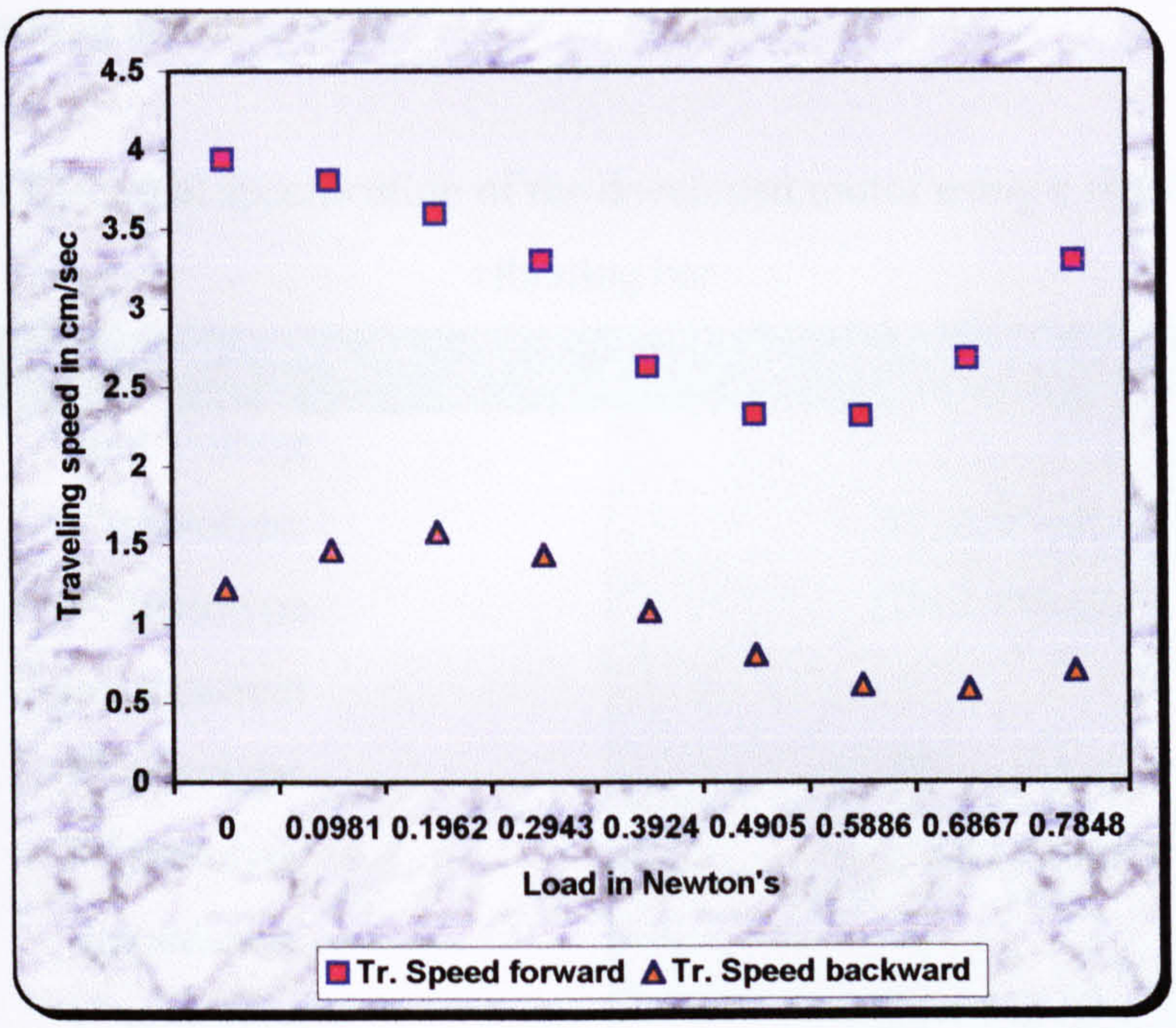

Figure 4-60 Travelling speed against load for forward and backward directions of motion for the modified motor

4.12 CONCLUSION

A linear piezoelectric ultrasonic motor, which has two directions of motion, a fast response and a micro-resolution, has been developed. The electrical and dynamic specifications of the developed prototype could be found in tables 4-8 and 4-9. The actual dimensions of the parts of the developed motor for both rotary and linear structures could also be found in table 4-10.

A methodology for design was established and implemented successfully. This considered the application needs, including the type of motion, resolution, compactness, travelling speed and the methodology for fabrication. A methodology of analysis using FEA was established and this was considered many technical points such as the dualistic nature of the piezoelectric material. So a combination of structural and electromagnetic analysis was used. The orientation of the material polarisation vector was also considered. Two methods of FEA were used to, optimise signal response parameters, and investigate the material deformation and modes of vibration. Material deformation

and the modes of vibration were used to determine the principles of motion of the motor and prevent jerking effect.

Table 4-8 Electrical specification of the developed motor using a single flexural vibrating bar

Power	**10 watt**
Input Voltage	
1st prototype	**50-100 volts**
2nd prototype	**100-150 volts**
Input current	
1st prototype	**50-100 m Ampere**
2nd prototype	**80-150 m Ampere**
Impedance	
1st prototype	**1000-1050 Ohms**
2nd prototype	**1000-1150 Ohms**
Output power	
1st prototype	**5.2165 watts**
2nd prototype	**6.2165 watts**
Efficiency	
1st prototype	**52.6 %**
2nd prototype	**51.8 %**
Frequency range	
1st prototype	**9.38-43.5 kHz**
2nd prototype	**10.38-53.5 kHz**
Operating frequency	
1st prototype	**40.9-43.5 kHz**
2nd prototype	**52.7-55.7 kHz**
Resonant frequency	
1st prototype	**41.5 kHz**
2nd prototype	**53.5 kHz**

Table 4-9 Dynamic specifications of the developed motor using a single flexural vibrating bar

Maximum load	
1st prototype	**0.833 Newton**
2nd prototype	**0.833 Newton**
Maximum speed	
1st prototype	**100-120 r.p.m**
2nd prototype	**160-180 r.p.m**
Angular velocity (ω)	
1st prototype	**12.57** *rad* / sec
2nd prototype	**20.94** *rad* / sec
Angular acceleration	
1st prototype	**6.285** *rad* / sec^2
2nd prototype	**10.47** *rad* / sec^2
Travelling speed:	
1st prototype	**28 mm/second**
2nd prototype	**37 mm/second**

Measurements of the major characteristics of the motor were carried out. This included:

- Signal response parameters (frequency, current and voltage),
- Input voltage variation against current,
- Travelling speed variation against Input voltage and frequency,
- Travelling speed variation against load,
- Resolution, load capacity, and response time.

Theses measurements showed the ability to control speed of the motor using either amplitude or frequency of the input signal.

Theoretical and experimental treatments of the current motor component elements were carried out. This involved:

- Consideration of the developed motor operating parameters motor. This was necessary to determine the major parameters that affected the motor performance including torque and travelling speed. This consideration showed that two main

parameters could be used to control the motor performance, the friction coefficient between the parts of the motor and the operating frequency of the piezoelectric electrode.

Table 4-10 Actual dimensions of the parts of the developed motor using a single flexural vibrating bar

Name of the part	Dimension in mm
Motor (Linear construction)	**90mmx90mm, sliding element 150 mm length**
Motor without sliding element (Rotary construction)	**90mmx90mm**
Piezo-ceramic electrode (1^{st} prototype)	**2mmx10mmx40mm**
Piezo-ceramic electrode (2^{nd} prototype)	**4mmx8mmx30mm**
Driving wheel and shaft	**4mmx40mm**
Shaft	**4mmx30 mm**
Driving wheel	**2mmx40mm**
Sliding element	**10mm outer diameter-8mm inner diameter x150mm**
Eroded electrode	**6mmx50mm**
Original eroded electrode	**10mmx200mm**
Adaptor	**20mmx20mm**

Improvements into characteristics of the developed motor were achieved. These were carried out successfully using results obtained from theoretical and experimental

considerations. This was based on using two major parameters, the friction coefficient between the parts of the motor and the operating frequency of the piezoelectric vibrating bar. Measurements of the main characteristics for the improved prototype were conducted. These measurements showed improvements in the characteristics of the motor. The motor travelling speed was increased from 28 mm/sec to 37 mm/sec. The resolution was changed from 50 to 70 micrometers. The response time was improved from 100 to 80 microseconds. This showed the resolution of the motor decreased and showed the difficulty in having compact size, high processing speed and high resolution at the same time.

CHAPTER 5

5 AN ADVANCED PIEZOELECTRIC USM DRIVE

5.1 OVERVIEW

This chapter describes the development process of a piezoelectric USM drive. The methodology of design, the structure, and the principle of operation of the drive is presented. Experimental examinations of the major characteristics of the drive were carried out. An introduction covers procedure of design used in previous applications is presented in section 5-2. Section 5-3 describes the procedure of design used in the development process. The structure of the proposed drive is discussed in section 5-4. Section 5-5 presents the design of the main units of the proposed drive and section 5-6 introduces the principles of operation of the drive. Section 5-7 gives the experimental examination of the drive and its limitations. A modification to the developed prototype using operational amplifier is discussed. This chapter concludes with a short conclusion covering major characteristic of the drive and its capability for control using either frequency or the amplitude of the signal.

5.2 PIEZOELECTRIC USM DRIVE

Generally the motor industrial applications, type, operating parameters (current, voltage and frequency), power, phasing and optimum operating conditions are the main parameters used to identify the structure and complexity of the drive of a motor. In the case of the piezoelectric USMs, the driving principles are mainly based on high frequency, voltage, phase, current and shape of the driving waveform.

Piezoelectric USM characteristics are complicated and non-linear [Lin, F. J., et al., 2000, Kobayashi, Y., et al., 1999, Lin, F. J., et al., 1999]. This is due to increases in the temperature and changes in the motor operating conditions. Temperature also can create overdriving for the motor that may lead to unstable system. These technical issues must be carefully handled in the design process to avoid motor overdriving which could influence the characteristics of the system.

5.3 DESIGN PROCEDURE

The methodology used in the current piezoelectric USM drive design was as follows:

- Optimise the motor major characteristics. The developed motor characteristics were:
- 1st prototype:
    - Operating frequency 41.5 KHz for PZT 4PCD piezoelectric material,
    - Operating frequency 37.4 KHz for CTS19 piezoelectric material,
    - Driving voltage 50-100 Volts peak to peak,
    - Current 50-100 m Amperes,
    - Angular speed 120 revolution per minute,
    - Travelling speed 28 mm/second,
    - Power 10 Watts.

- 2nd prototype:
    - Operating frequency 53.5 KHz for CTS19 piezoelectric material,
    - Driving voltage 100-150 Volts peak to peak,
    - Current 80-150 m Amperes,
    - Angular speed 160 revolution per minute,
    - Travelling speed 37 mm/second,
    - Power 22.5 Watts.

- Identify the method that can be used to control the direction of motion of the motor.
- Define and select parameters that can be used to control the speed of the motor.
- Identify the type of control that will be used in the application.
- Optimise the drive design based on capability to generate the required driving parameters (voltage, current, and frequency), waveform shape, and performance.
- Select and identify electronic components that will be used to build the prototype. Here the safety aspects must be considered in choosing these components.
- Integrate the drive with the developed piezoelectric USM and create a comprehensive study to examine the capability of the drive to:
    - Generate the driving parameters (voltage, current and frequency) of the motor,

- Control the speed of the motor using either the frequency or the amplitude of the driving signal.

5.4 Structure of the Drive

Figure 5-1 shows the block diagram of the proposed piezoelectric USM drive. It shows the main units of the drive. This shows that the drive consists of a power MOSFETs switching unit, AC power unit and a feed back unit. The switching unit is built up using power MOSFETs and this was used as an interface unit. The AC power unit is composed of a cascade voltage amplifier and a push pull power amplifier. The feedback circuit is composed of a crystal oscillator and a sharp band pass filter. The sharp band pass filter consists of an internal parasitic capacitance of the piezoelectric electrode and the determined inductance. The internal parasitic capacitance can be determined from known standard equations of the piezoelectric material and the inductance can be calculated from the principles of design of the filter.

An array of power MOSFETs switches also was designed and used as a digital analogue interface unit. This introduces a fast interface unit that can match the developed system response time. Figure 5-2 shows the developed electronic circuit and main units of the drive build using recommended electronic components.

5.5 DESIGN OF THE DRIVE MAIN UNITS

This step covers the design of the main units of the drive including the cascade voltage amplifier, the push pull class B power amplifier and the sharp band pass filter. Voltage amplifier design is mainly based on the relationship between the emitter resistance and the potential divider resistance. This relation is shown in equation 5-1 [Savant, C. J., et al., 1987].

$$R_B \leq 0.1 \bar{\beta} R_E \qquad 5\text{-}1$$

$\bar{\beta}$ is the transistor amplification factor, R_B is the potential divider resistance and R_E is the emitter resistance. The potential divider R_B is usually used to reduce the number of line sources and simplify the design of such amplifier. It can be determined using relation 5-2 assuming that the emitter resistance is known:

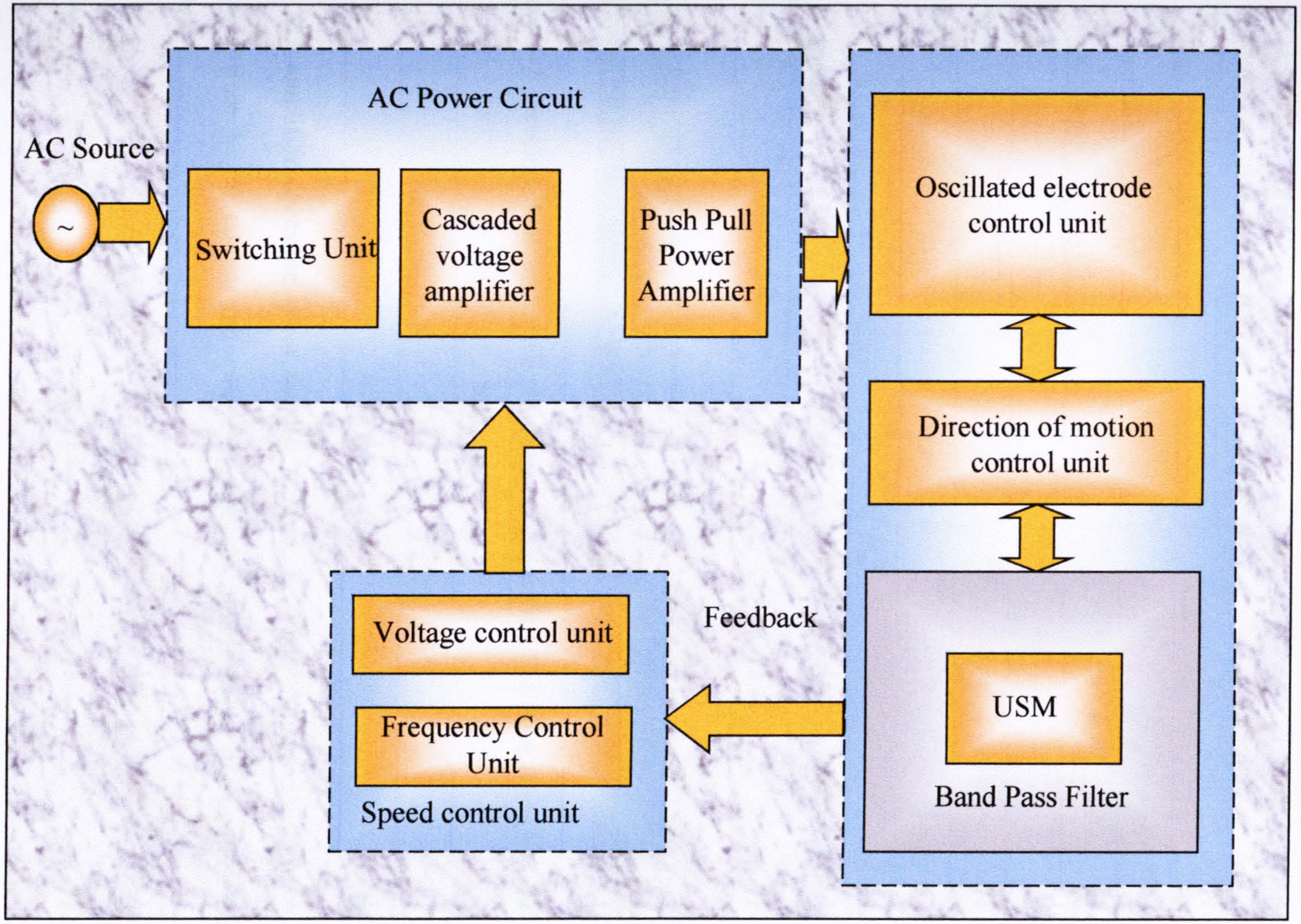

Figure 5-1 Block diagram and main units of the proposed self-oscillation piezoelectric USM drive

Figure 5-2 Developed circuit for the proposed piezoelectric USM drive using bipolar transistor

$$R_B = 0.1\bar{\beta}\ \ R_E \qquad 5\text{-}2$$

Then the amplifier operating point for the current I_{CQ_1} and voltage V_{CQ_1} can be calculated from the DC current and voltage relation, and this is shown in equations 5-3 and 5-4:

$$I_{CQ_1} = \frac{V_{cc}}{R_{ac} + R_{dc}} \qquad 5\text{-}3$$

$$V_{CQ_1} = \frac{V_{cc}^{'}}{2} \qquad 5\text{-}4$$

I_{CQ_1} is the operating current, V_{cc} and $V_{cc}^{'}$ are the load line sources of the amplifier, R_{ac} is the AC voltage resistance, R_{dc} is the DC voltage resistance, and V_{CQ_1} is the operating

voltage of the first stage of the amplifier. I_{CQ_1} and V_{CQ_1} together are indicate the amplifier operating point.

R_{ac} resistance can be calculated using relation 5-5.

$$R_{ac} = \frac{R_{L1}R_{C1}}{R_{L1} + R_{C1}} + R_{E1} \qquad 5\text{-}5$$

R_{L1} is the load resistances, R_{C1} is the collector resistance and R_{E1} is the emitter resistance of the first stage of the amplifier respectively.

The DC voltage resistance R_{dc} can be calculated using equation 5-6

$$R_{dc} = R_{E1} + R_{C1} \qquad 5\text{-}6$$

and V'_{cc} can be determined from relation 5-7. Assuming that, the transistor was working in the middle area of its operating characteristics.

$$V'_{cc} = 2I_{CQ_1}R_{ac} \qquad 5\text{-}7$$

The next stage of the design of the voltage amplifier is to determine the values of the divider resistance R_1 and R_2 of the first stage (see Figure 5-2). These two resistances can be determined using relations 5-8 and 5-9

$$R_1 = \frac{R_{B1}}{(1 - \frac{V_{BB_1}}{V_{CC}})} \qquad 5\text{-}8$$

$$R_2 = R_{B1}(\frac{V_{cc}}{V_{BB1}}) \qquad 5\text{-}9$$

V_{BB1} is the base bias voltage provided by the line source through the potential divider resistances R_1 and R_2. R_{B1} is the total resistance of the potential divider for the first stage of the amplifier. This base bias voltage can be calculated using relation 5-10.

$$V_{BB1} = V_{BE} + I_{CQ_1}[\frac{R_{B1}}{\beta} + R_{E1}] \qquad 5\text{-}10$$

V_{BE} is the base emitter bias voltage.

Then the maximum output voltage can be calculated, and this can be used to drive the next stage of the amplifier.

In the design process to justify the deviation between the practical side and the theoretical one, the second step of the amplifier is provided with a variable resistance embedding in series with the resistance R_4. Then the load power can be determined using relation 5-11.

$$P_{Load} = \frac{1}{8} I^2_{CQ_1} R_{L1} \qquad 5\text{-}11$$

R_{L1} is the load resistance of the first stage and is the input resistance of the next stage of the amplifier.

The dissipated power can be calculated using equation 5-12.

$$P_{diss} = V_{CQ_1} I_{CQ_1} \qquad 5\text{-}12$$

The dissipated power is a very important parameter must be carefully considered in the design process as it is used to select the suitable electronic component for the proposed design. For safety reasons the components of the drive were chosen with a power ratio that is higher than the calculated power.

The design process of the next stage of such cascade voltage amplifier followed similar steps to the first stage. Only the load resistance and the input resistance for various stages of the drive must be carefully considered. Mishandling of the impedance between two stages may create many technical problems that could affect the electronic circuit performance and may burn the circuit.

Equation 5-13 shows the relationship used to determine the potential divider resistance for the second stage of the amplifier.

$$R_{B2} = \frac{R_3 R_4}{R_3 + R_4} \qquad 5\text{-}13$$

R_3 and R_4 are the potential divider resistances of the second stage of the amplifier.

Equation 5-14 was used to determine the potential divider bias voltage V_{BB2}.

$$V_{BB_2} = V_{cc}[\frac{R_3}{R_3 + R_4}] \qquad 5\text{-}14$$

The current at the operating point of the cascade voltage amplifier for the second stage can be determined using relation 5-15.

$$I_{CQ2} = \frac{V_{BB2} - V_{BE2}}{R_{B2} / \bar{\beta} + R_{E2}} \qquad 5\text{-}15$$

V_{BE_2} is the base emitter bias voltage for the second stag, R_{B2} is the total resistance of potential divider for the second stage and R_{E2} is the emitter resistance.

The input resistance R_{in2} of the second stage can be determined using relation 5-16

$$R_{in2} = \frac{R_{B2} h_{ie2}}{R_{B2} + h_{ie2}} \qquad 5\text{-}16$$

where, h_{ie2} is the internal resistance of the transistor and V_{BE2} =0.7 volt.

Following the design process of the amplifier, the analysis step is one of the very important steps. It is aimed at determining the required current and voltage amplification factors for the proposed cascade voltage amplifier.

The current amplification A_i can be determined using equation 5-17.

$$A_i = \frac{i_{o/p}}{i_{i/p}} \qquad 5\text{-}17$$

where $i_{o/p}$ *and* $i_{i/p}$ are the input and the output current of the amplifier. The voltage amplification factor A_v can be calculated using relation 5-18.

$$A_v = A_i \frac{R_L}{R_{in}} \qquad 5\text{-}18$$

The input resistance in this case is the input resistance of the first stage and it can be determined using the relation:

$$R_{in1} = \frac{(R_{B1}\,\bar{\beta})(h_{ib1} + R_{E1})}{R_{B1} + \bar{\beta}(h_{ib1} + R_{E1})}$$

where h_i is the internal amplification factor of the transistor.

In this case the load resistance R_L is the input resistance of the class B power amplifier and this can be determined using equation 5-22.

The main purpose of the power amplifier used in the design was to deliver the maximum undistorted symmetrical output voltage swing to a low load resistance. This undistorted signal was used to drive the motor with appropriate power in full period. The power amplifier, as shown in Figure 5-2, consisted of two complementary transistors Q_3 and Q_4, where Q_3 is an n-p-n and Q_4 is a p-n-p bipolar transistor. When Q_3 is turning "on" operation, Q_4 must be turn to "off" operation and vice versa.

To determine the component of the power amplifier, equation 5-19 can be used to determine the base current i_{b_p} of the amplifier.

$$i_{bp} = \frac{i_{cp}}{\bar{\beta}} \qquad 5\text{-}19$$

i_{cp} is the maximum collector current and can be calculated from equation 5-20.

$$I_{c_{Max}} = i_{cp} = \frac{V}{R_L} \qquad 5\text{-}20$$

$I_{c_{Max}}$ is the DC collector current, V is the required output voltage and R_L is the load resistance.

In this case the load resistance was found to be around 1000 ohms. The required output voltage was found to be 50-100 volts AC sinusoidal.

The potential divider resistance R_5 of the power amplifier can be determined using equation 5-21.

$$R_s = \frac{(V_{cc}/2) - V_{BE} - V_{LP}'}{i_{bp}} \qquad 5\text{-}21$$

V'_{LP} is the load voltage of the power amplifier. Then the input resistance for the power amplifier R_{in}, can determined using relation 5-22 (see Figure 5-2):

$$R_{in} = \frac{(R_f + R_s)(R_f + \frac{R_s \bar{\beta} R_L}{(R_s + \bar{\beta} R_L)})}{(R_f + R_s) + (R_f + \frac{R_s \bar{\beta} R_L}{(R_s + \bar{\beta} R_L)})} \qquad 5\text{-}22$$

R_L is the resistance of the load (piezoelectric USM) and R_f is the forward resistance of the diode.

The power supply P_{sup} of the power amplifier can be determined using relation 5-23:

$$P_{sup} = \frac{V_{cc} I_{c_{Max}}}{\pi} + \frac{V^2_{cc}}{2R_f + 2R_s} \qquad 5\text{-}23$$

and the output power P_o can be determined using equation 5-24.

$$P_o = \frac{1}{2} i^2_{c_{Max}} R_L \qquad 5\text{-}24$$

The power rating for each transistor P_{Trans} can be calculated using relation shown in equation 5-25.

$$P_{Trans} = \frac{V^2_{cc}}{4\pi^2 R_L} \qquad 5\text{-}25$$

For safety reasons the transistor power ratio was often chosen higher than the determined power.

Then the gain of the class B push pull power amplifier can be determined based on the relationship between the input current, the bias resistance and the output current. The relationship used to determine the gain is shown in equation 5-26.

$$A_i = \bar{\beta} \frac{i_o}{i_{in}} \qquad 5\text{-}26$$

where i_0 *and* i_{in} are the input and the output current of the class B power amplifier. The voltage gain can be determined using equation 5-18.

In this proposed power amplifier, capacitor C_3 was used to reduce the number of voltage line sources and to provide the required bias for both transistors Q_3 and Q_4. A variable resistance also was used in series with the potential divider R_5, to control the voltage amplification factor of the second stage and prevent signal distortion.

The main reasons for using a class B power amplifier were: The collector current does not zero during the input voltage period. This means, that there was no dissipated power in the quiescent condition for both transistors.

One point had to be carefully considered when designing a class B push pull power amplifier. This point is the non-linear cut-off region that was included in the operating range. This would produce distortion near the Q-operating point. This was overcome on the proposed design using two transistors that had very close characteristics and two diodes in forward bias in series with a small variable resistance.

In current power amplifier three technical points were also considered on the design process:

The first was the distortion that was resolved using a small variable resistance in series with the two diodes to make I_{CQ} for Q_3 and Q_4 be slightly above zero. This also caused both amplifiers amplify the AC input signal simultaneously, in the cut-off region, thus compensating for the lower individual amplification in that region. The second point was that thermal run away which would be caused by two complementary transistors, because of the asymmetrical characteristics or uncompensated V_{BE} being reduced by high temperatures. This would lead to a higher collector current, resulting in additional dissipated power and heating. Using a small variable resistance in series with the emitter to increase the bias level reduced this problem. The third point was the two diodes have to be forward biased to avoid output distortion. This bias must be at a level to keep the diode current large enough to be in the linear region of their forward bias for all applied inputs. Therefore, the maximum negative peak current of the diodes had to be less than

the direct current bias. This meant that the DC component of the current had to be larger than the AC component, so when it is added to the DC component, the resultant current did not become negative. The current relation restriction for this case is given by equation 5-27.

$$I_D \rangle \left| i_{d_p} \right| \qquad 5\text{-}27$$

I_D and i_{d_p} is the DC amplitude of the diode current component and the amplitude of the AC component.

A sharp band pass filter was designed and implemented in the developed drive. This was to allow the feedback unit to acquire the piezoelectric vibrating bar resonant frequency. The filter parameters were determined based on a biquadratic transfer function, as in equation 5-28 [Savant, C. J., et al., 1987]. Using equation 5-28 and assuming that poles $P_0 = P_2 = 0.0$, the filter components can be determined. Where P_0, P_1 and P_2 are the poles of the filter.

$P_0 = P_2 = 0.0$ so the first pole can be determined from equation 5-29.

$$G(s) = \frac{P_1 s}{s^2 + \frac{\omega_0}{Q} s + {\omega_0}^2} \qquad 5\text{-}28$$

$$P_1 = \frac{1}{CR} \qquad 5\text{-}29$$

Assuming the resonant frequency of the piezoelectric electrode is equal to the resonant frequency of the filter. Then, using equation 5-30 the components of the band pass filter can be determined.

$$\omega_0 = \frac{1}{\sqrt{LC}} \qquad 5\text{-}30$$

where R, L and C are the main component of the band pass filter. The internal parasitic capacitance of the piezoelectric component was determined using standard equation of the piezoelectric material. Then it was used in equation 3-30 to determine the inductance of the filter. The filter quality can be also determined using equation 5-31.

$$Q = R\sqrt{C/L} \qquad 5\text{-}31$$

One of the most important properties of the piezoelectric crystal is, when it is compressed, expanded or twisted, it generates a low output voltage [see appendix (A)]. The reverse action can be obtained if there is enough voltage to excite it. This applied voltage distorts the crystal mechanically. Then it vibrates at a specific resonant frequency which is stand on the dimension of the crystal. In this case enough voltage was used to excite the crystal. The frequency of vibration was filtered and feedback using a sharp band pass filter. The main advantage of using this technique was to adopt characteristics change as this change in the piezoelectric vibrating bar with temperature could influence its operating parameters.

5.6 PRINCIPLE OF OPERATION OF THE DRIVE

The principles of operation of the drive are based on input voltage variation. When the input voltage is zero the base current of the transistor is also zero and the collector current became very small, consequently the transistor is on the condition "off". In this case the dissipated power P_d of the transistor can be given by:

$$P_d = I_c V_R \qquad 5\text{-}32$$

where I_c is the collector current and V_R is the voltage load. When the input voltage is increased the collector current increases and is limited by the relationship shown in equation 5-33.

$$V_{cc} = I_c R_L \qquad 5\text{-}33$$

When the transistor is turned "on", the dissipated power can be determined from the relationship shown in equation 5-34.

$$P_d = I_c V_{ce} \qquad 5\text{-}34$$

V_{ce} is equal 0.2 volt at saturation. This principle of operation is similar for all various stages of the proposed drive.

The first part of the cascade voltage amplifier was to provide by phase shift of 180 degrees and a small amplification factor. The second part was to provide by the whole amplification factor of the whole stage. The output of the cascade voltage amplifier was transferred to a class B push pull power amplifier. The two resistances R_s were used as a potential divider to avoid the distortion of the power amplifier and control the base bias voltage for both transistors. The motor was connected in series with the output voltage. A two half-phase power MOSFETs switching unit was used to control the motor directions of motion. The motor active element was set at the resonant frequency, using a feedback signal picked up using band pass filter and feedback damping potential divider. Then the amplitude of the output voltage of the developed drive was used to control the speed of the motor.

5.7 EXPERIMENTAL RESULTS

The piezoelectric USM drive was built, tested and integrated successfully with the developed piezoelectric USM. A series of experimental tests and measurements of the capability of the drive for control were carried out.

Figure 5-3 shows the experimental system used to measure and examine the drive characteristics. This system shows various equipments used in the system including:

- Piezoelectric USM drive which provide by the required high frequency AC power to drive the piezoelectric electrode of the piezoelectric USM motor,
- Function generation which used to provide the input signal required to drive the piezoelectric USM driver,
- Display unit which composed of two oscilloscopes to display and monitor the relation between the input and the output signal for different stages of the drive
- An analogue-switching unit that used to control the direction of motion of the motor.

Three different waveforms were used, sinusoidal, square and saw tooth and two types of piezoelectric materials.

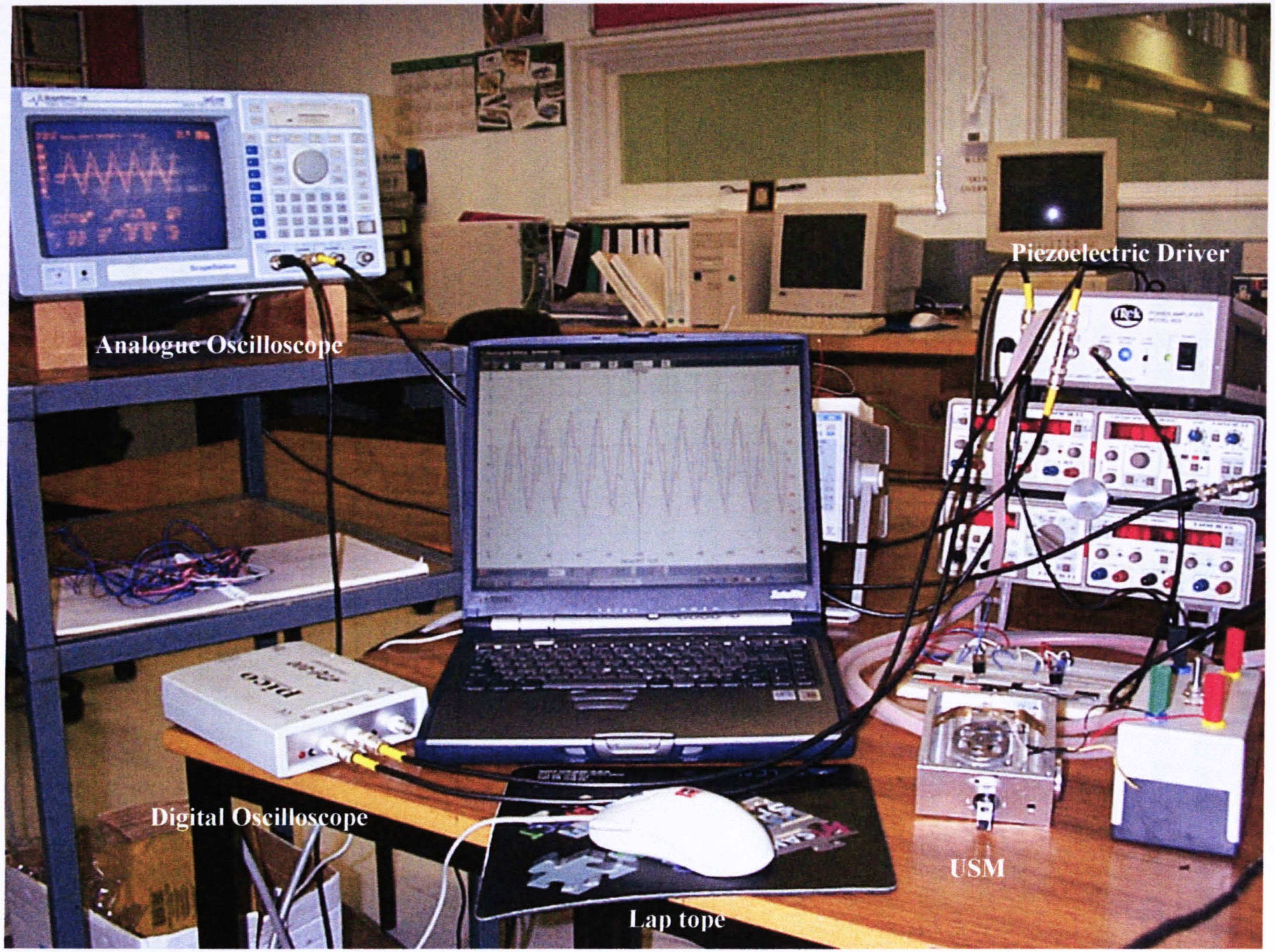

Figure. 5-3 Equipment used to examine the developed self-oscillation drive using an operational amplifier and bipolar

Figures 5-4, 5-6 and 5-8 show the variation of the input signal against output signal of the developed drive using bipolar transistor at different input voltage and resonant frequencies 3.52 KHz, 12.14 KHz and 41.5 KHz for PZT 4PCD, respectively. This shows the drive capability to generate a driving waveform, required operating parameters for the motor and facility to use the amplitude to control the speed of the motor.

Figures 5-5, 5-7 and 5-9 show the variation of the current against load voltage across the motor at different input voltage and resonant frequencies 3.52 KHz, 12.14 KHz and 41.5 KHz for PZT 4PCD, respectively. These Figures show the distortion occurred for the driving signal waveform at different operating frequencies and voltage. These distortions affect the motor performance and the speed of the motor. This shows that the drive was unable to generate the required operating parameters for the motor in wide band. Figure 5-10 shows the variation of the input signal against output signal of the developed drive using a bipolar transistor at an operating frequency 41.5 KHz for PZT 4PCD. Figure 5-11 shows the variation of the load current against load voltage across the motor in the case of square waveform driving signal.

Figure 5-12 shows the variation of the input signal against output signal of the developed drive using a bipolar transistor at operating frequency 41.5 KHz (1) for PZT 4PCD and Figure 5-13 shows the variation of the load current against load voltage across the motor in the case of saw tooth wave driving signal. This showed the capability of the drive to drive the motor using different waveforms. This helped to investigate the behaviour of this type of motor with different driving waveforms.

Figure 5-14 shows the variation of the input signal against output signal of the developed drive using bipolar transistor at different input voltage and operating frequency 37.4KHz (1) for CTS19 material. Figure 5-15 shows the variation of the load current against load voltage across the motor. Figure 5-16 shows the variation of the input signal against output signal of the developed drive using bipolar transistor at operating frequency 37.4KHz for CTS19 and Figure 5-17 shows the variation of the load current against load voltage across the motor in the case of square wave driving signal.

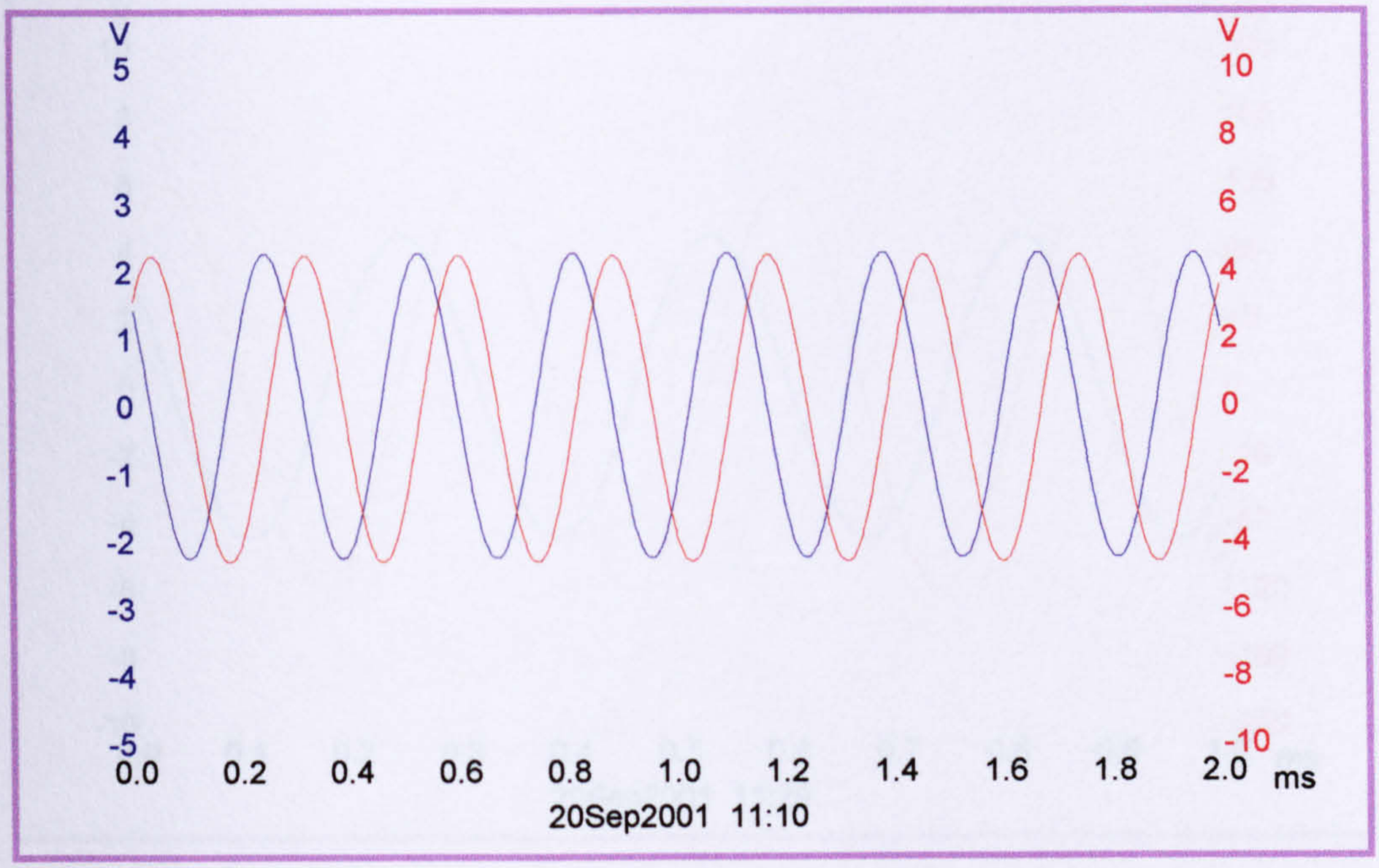

(a)

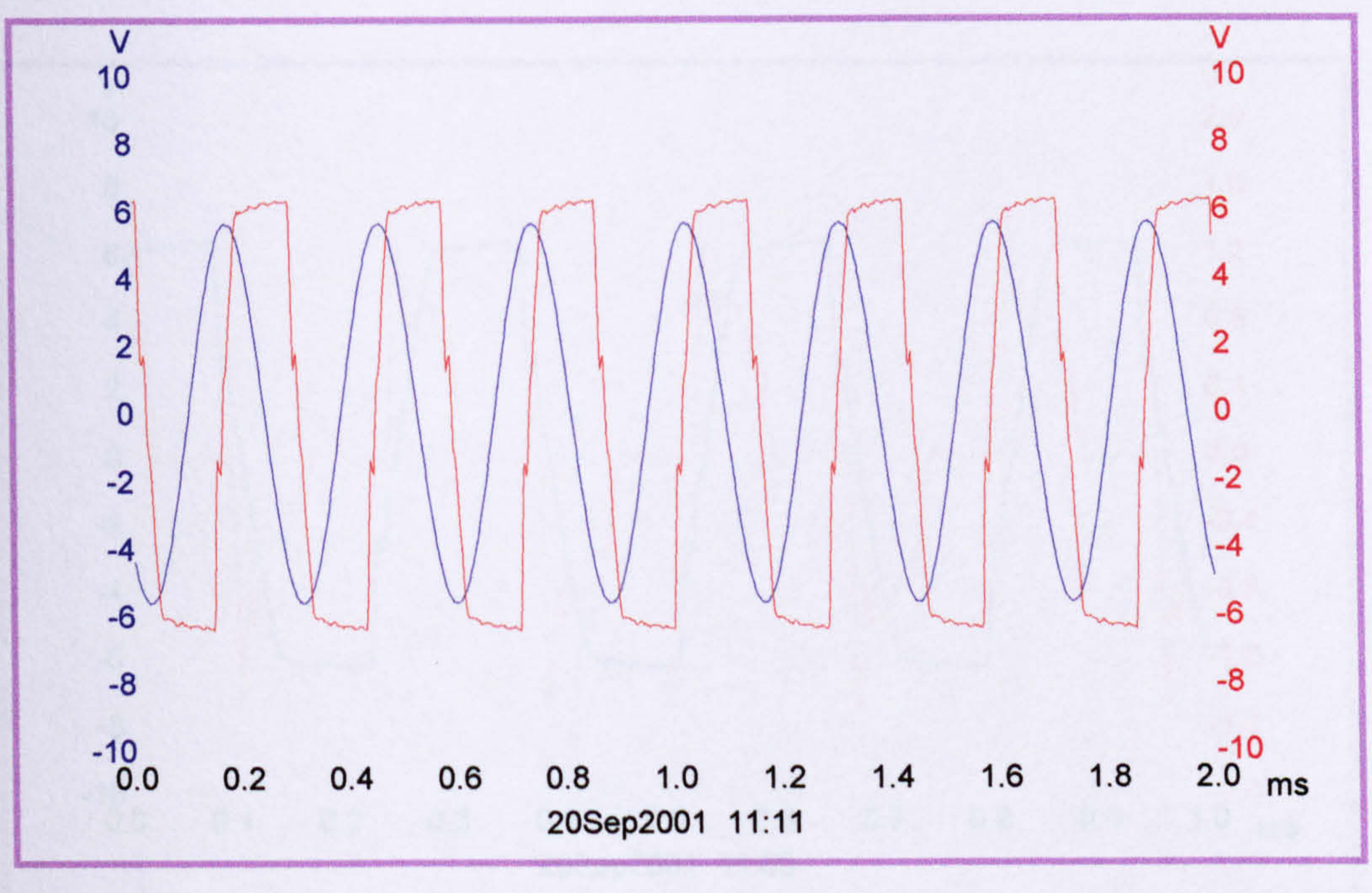

(b)

Figure 5-4 Waveform variation of the input signal (ch1-blue) and output signal (ch2-red) [Scale 1: 10] of the developed piezoelectric drive for different amplification factor at resonant frequency 3.52 KHz (2) for PZT 4PCD

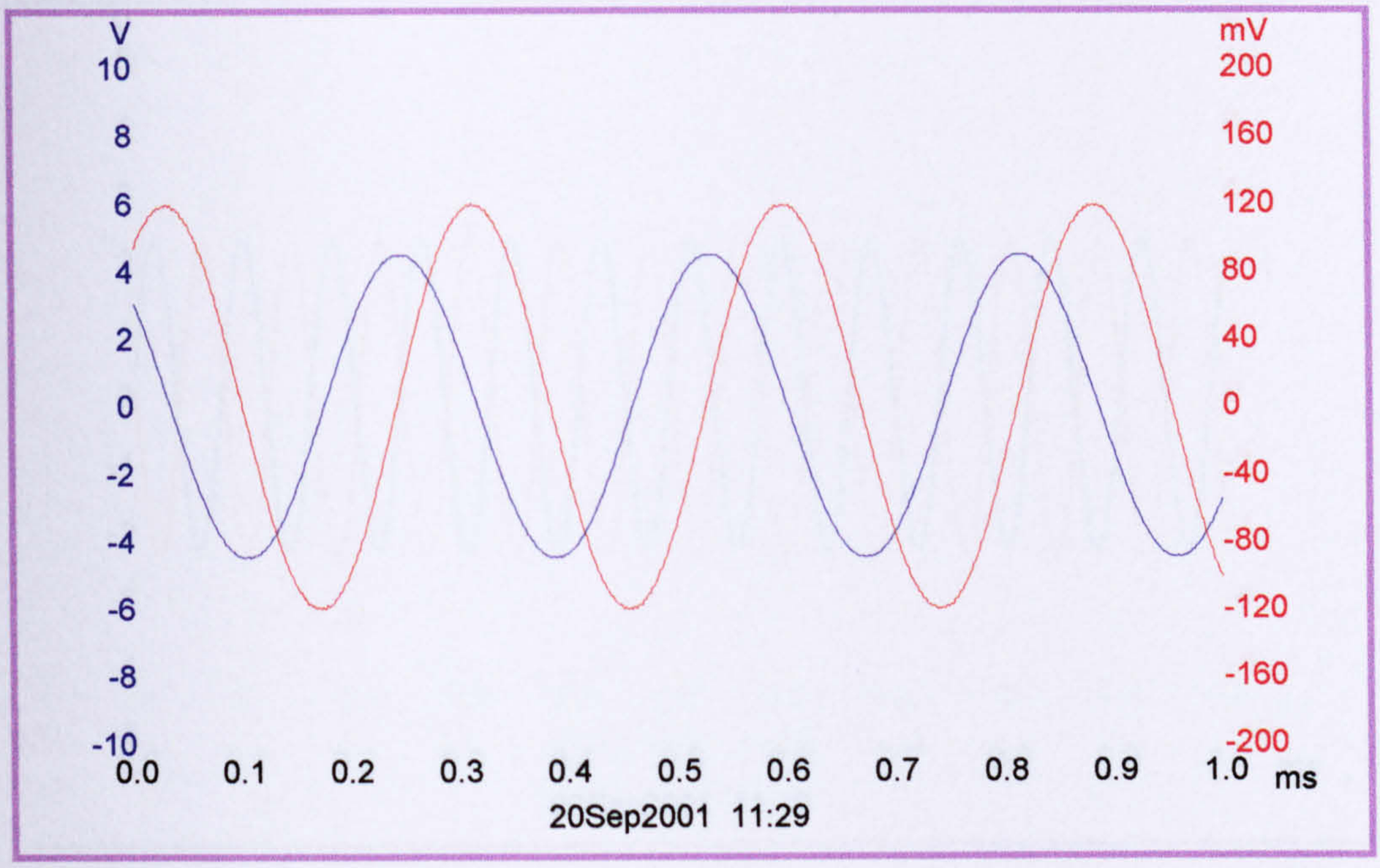

(a)

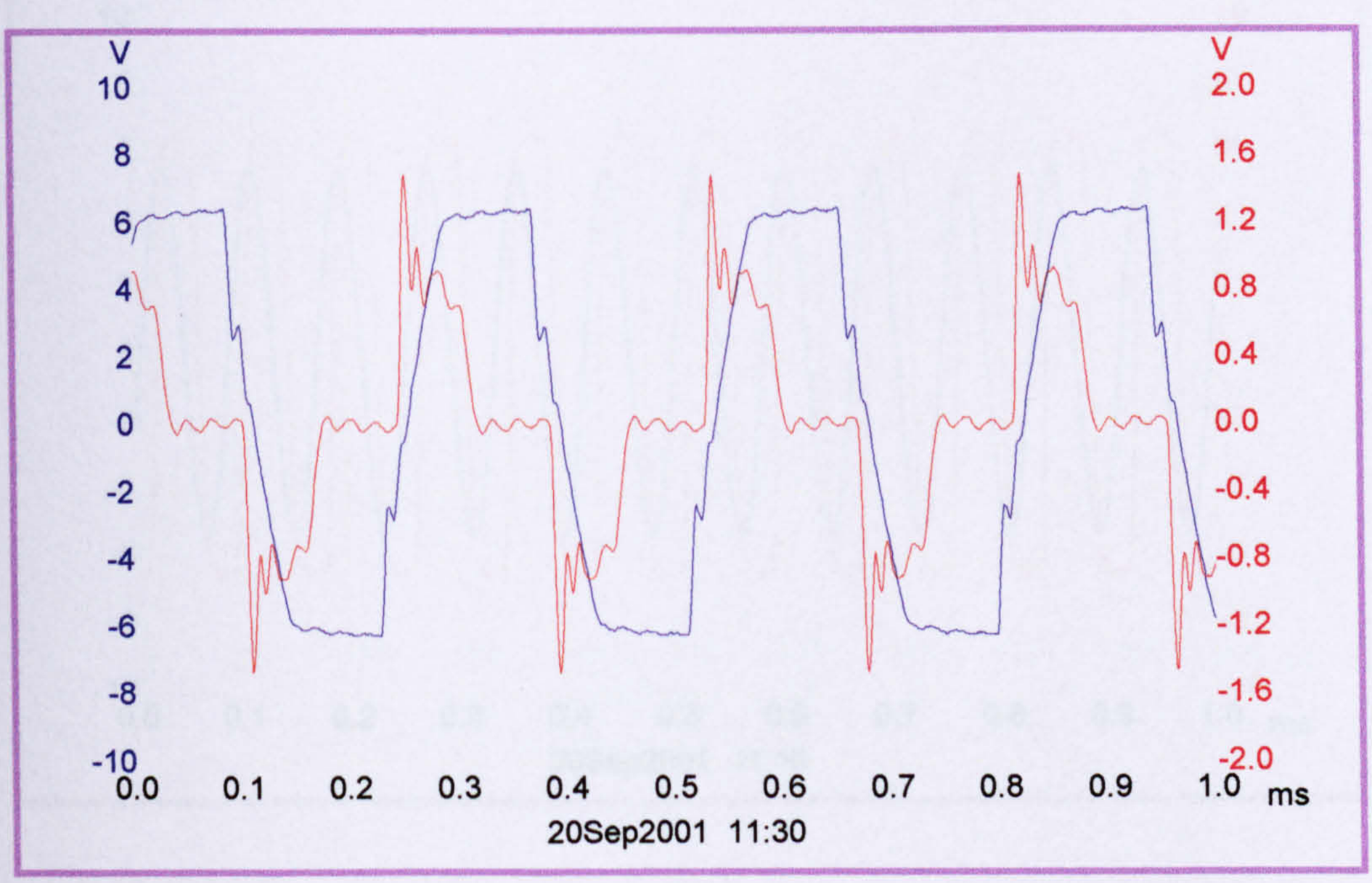

(b)

Figure 5-5 Waveform variation of the load current (ch2-red) and load voltage across the motor (ch1-blue) using self-oscillation a bipolar drive different amplification factor at resonant frequency 3.52KHz (2) for PZT 4PCD [Scale 1 : 10]

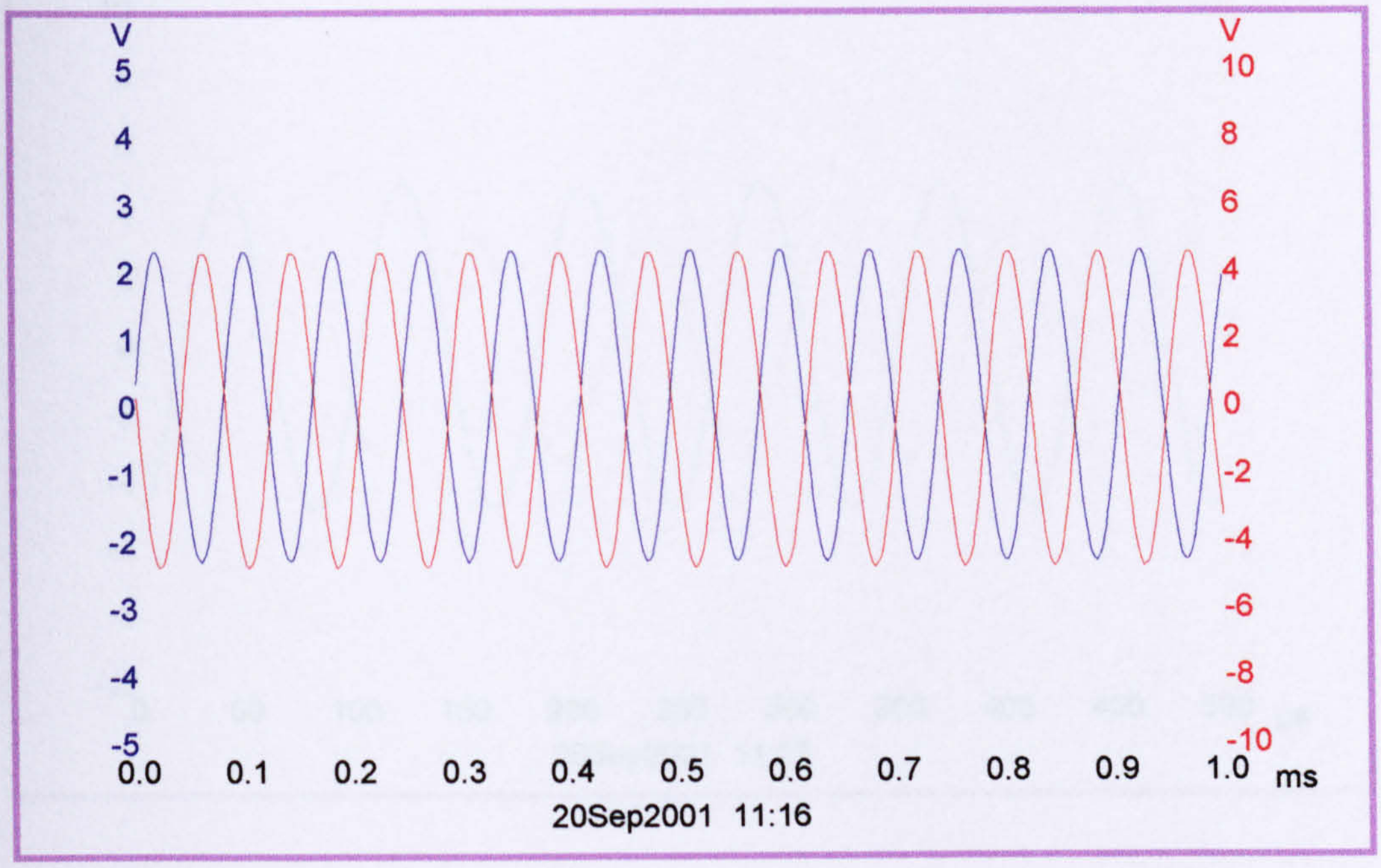

(a)

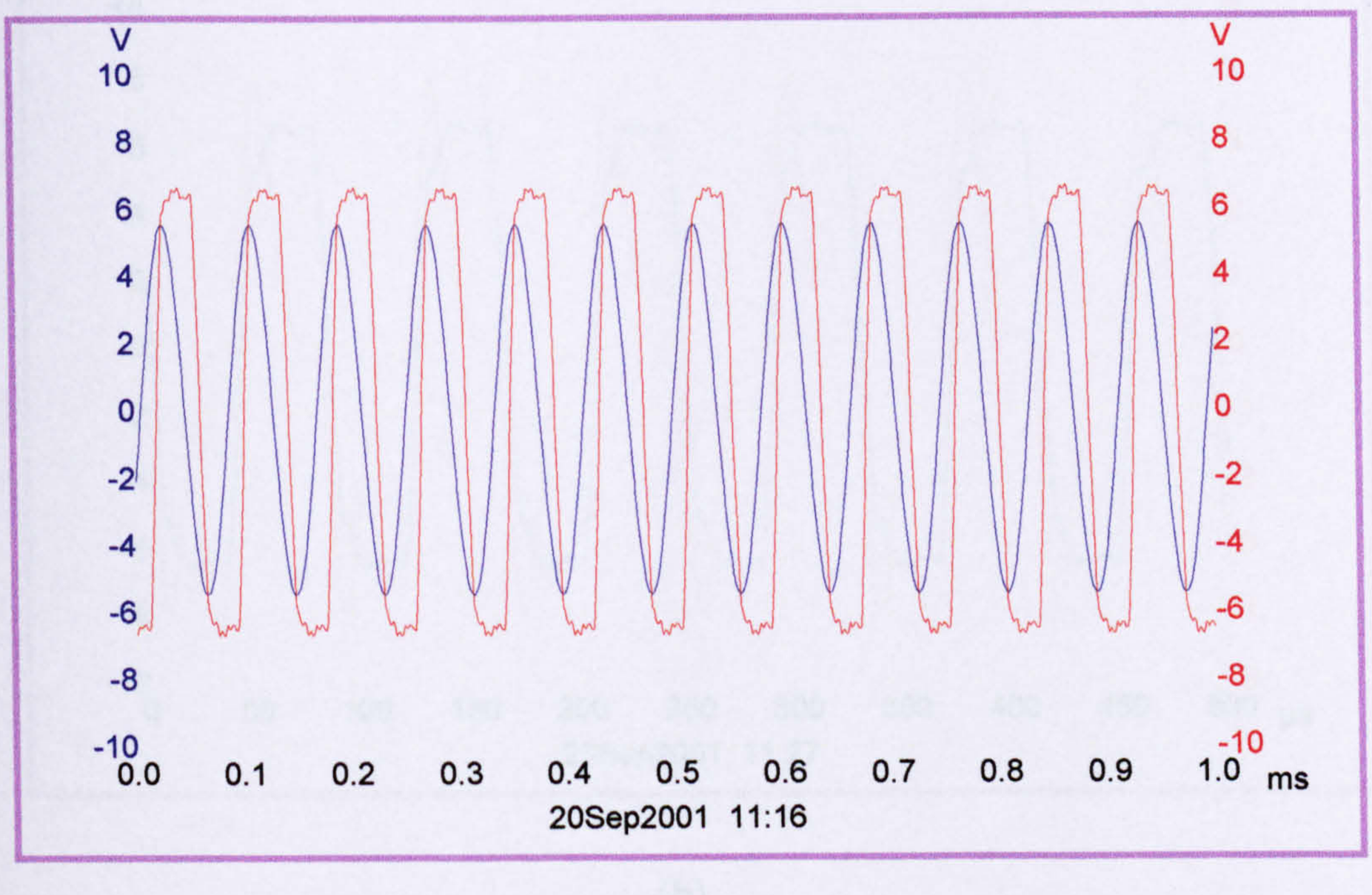

(b)

Figure 5-6 Waveform variation of the input signal (ch1-blue) and output signal (ch2-red) [Scale 1: 10] of the developed piezoelectric drive for different amplification factor at resonant frequency 12.14 KHz (2) for PZT 4PCD

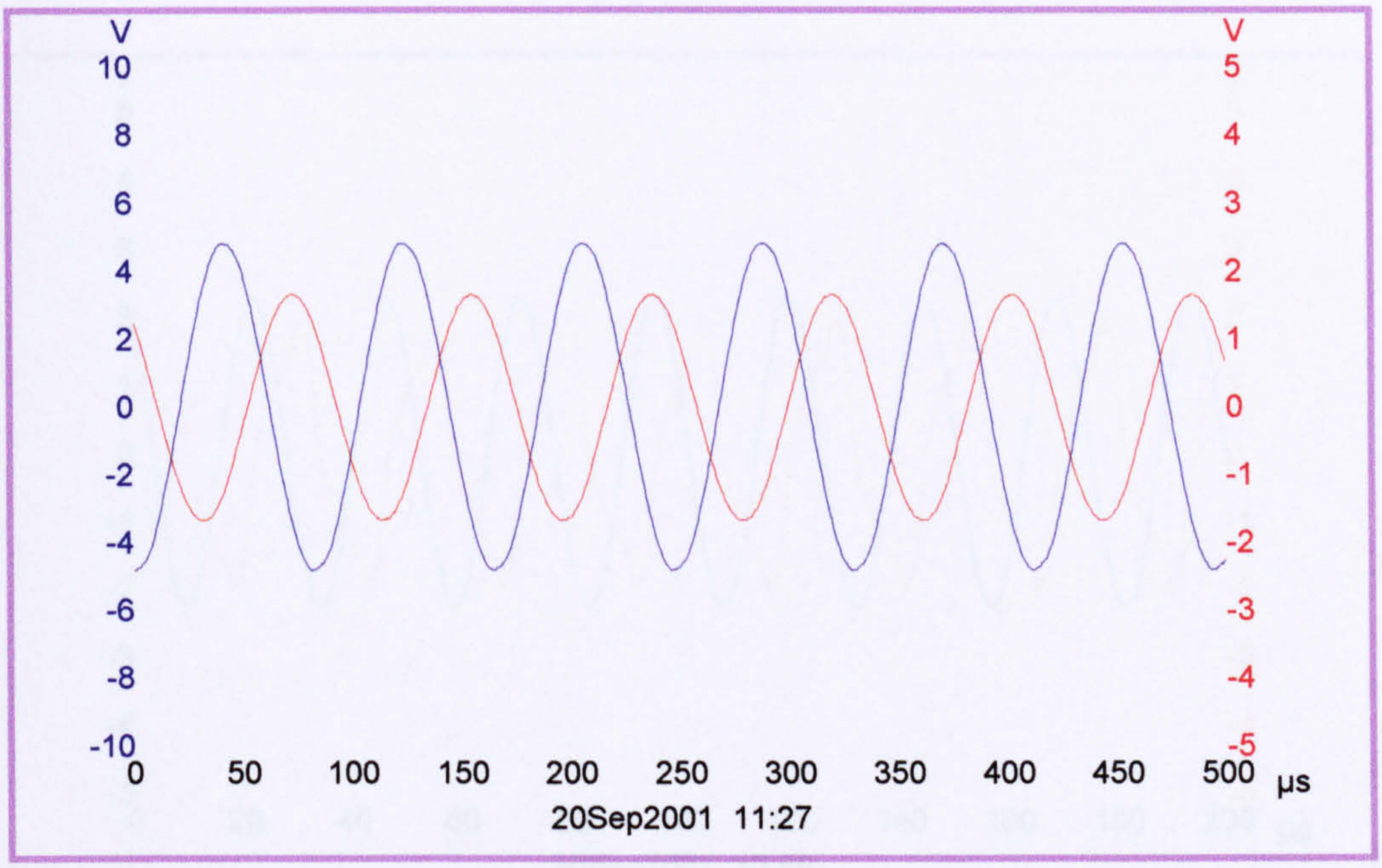

(a)

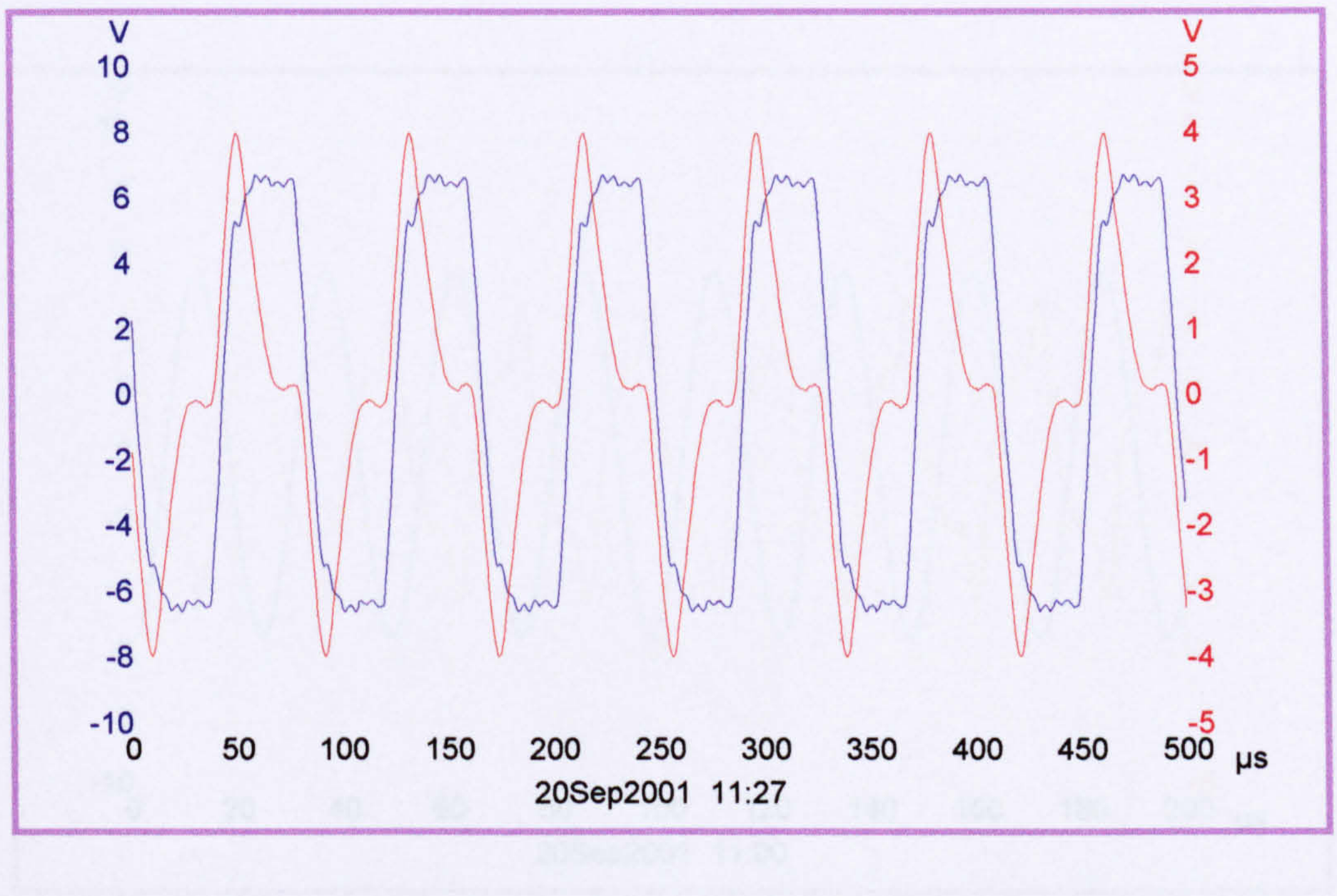

(b)

Figure 5-7 Waveform variation of the load current (ch2-red) and load voltage across the motor (ch1-blue) using self-oscillation a bipolar drive different amplification factor at resonant frequency 12.14 KHz (2) for PZT 4PCD [Scale 1 : 10]

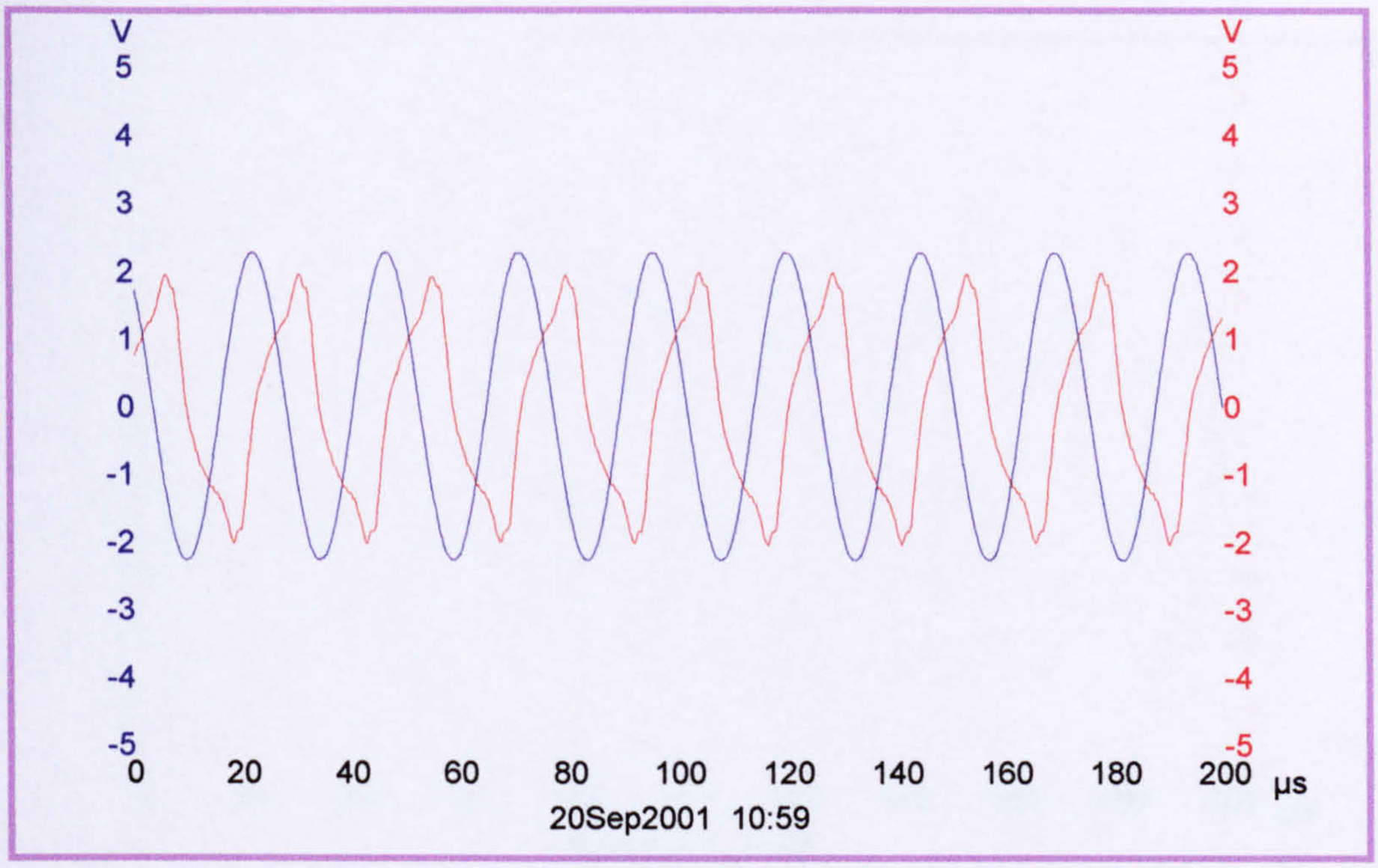

(a)

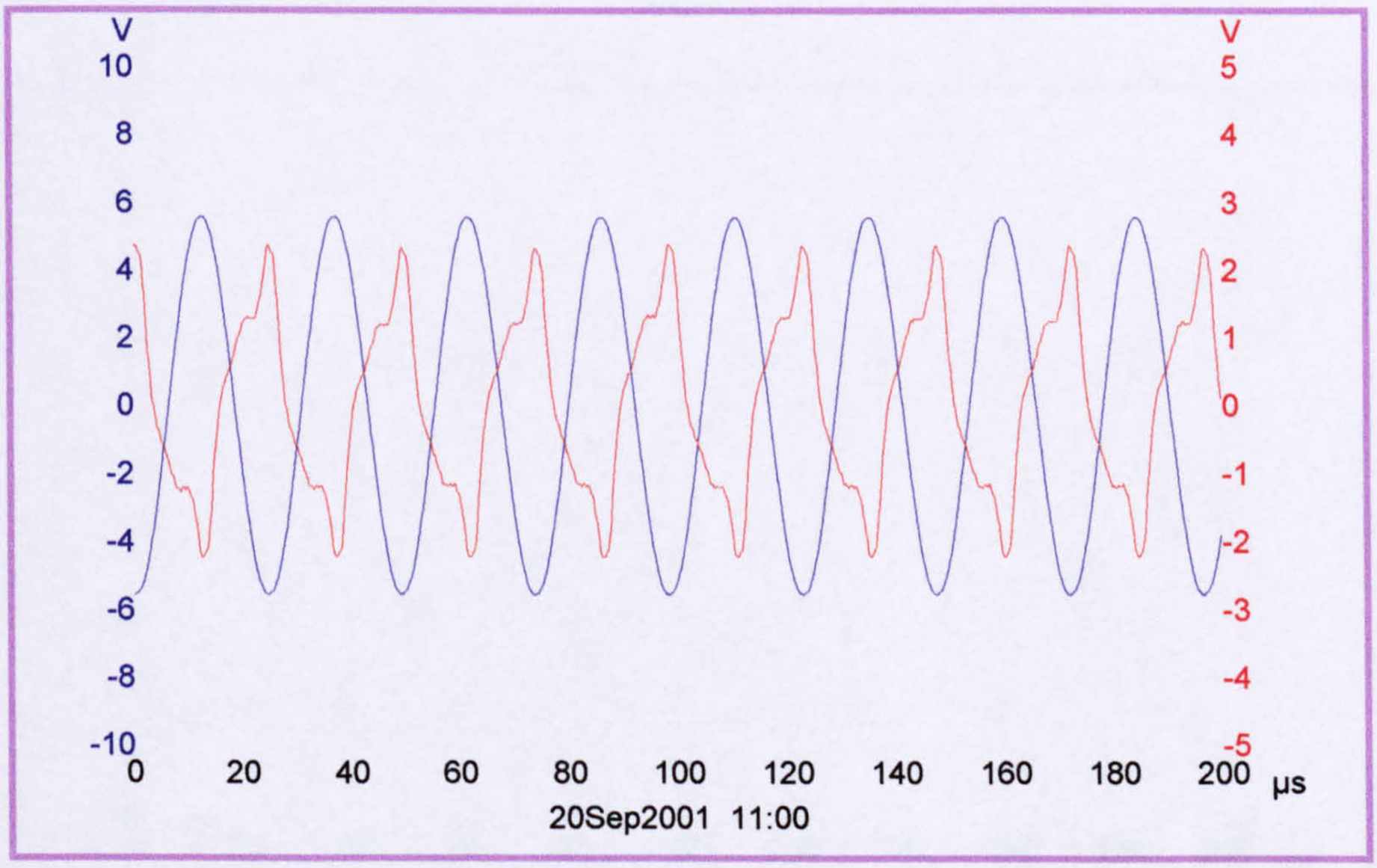

(b)

Figure 5-8 Waveform variation of the input signal (ch1-blue) and output signal (ch2-red) [Scale 1: 10] of the developed piezoelectric drive for different amplification factor at resonant frequency 41.5 KHz for PZT 4PCD

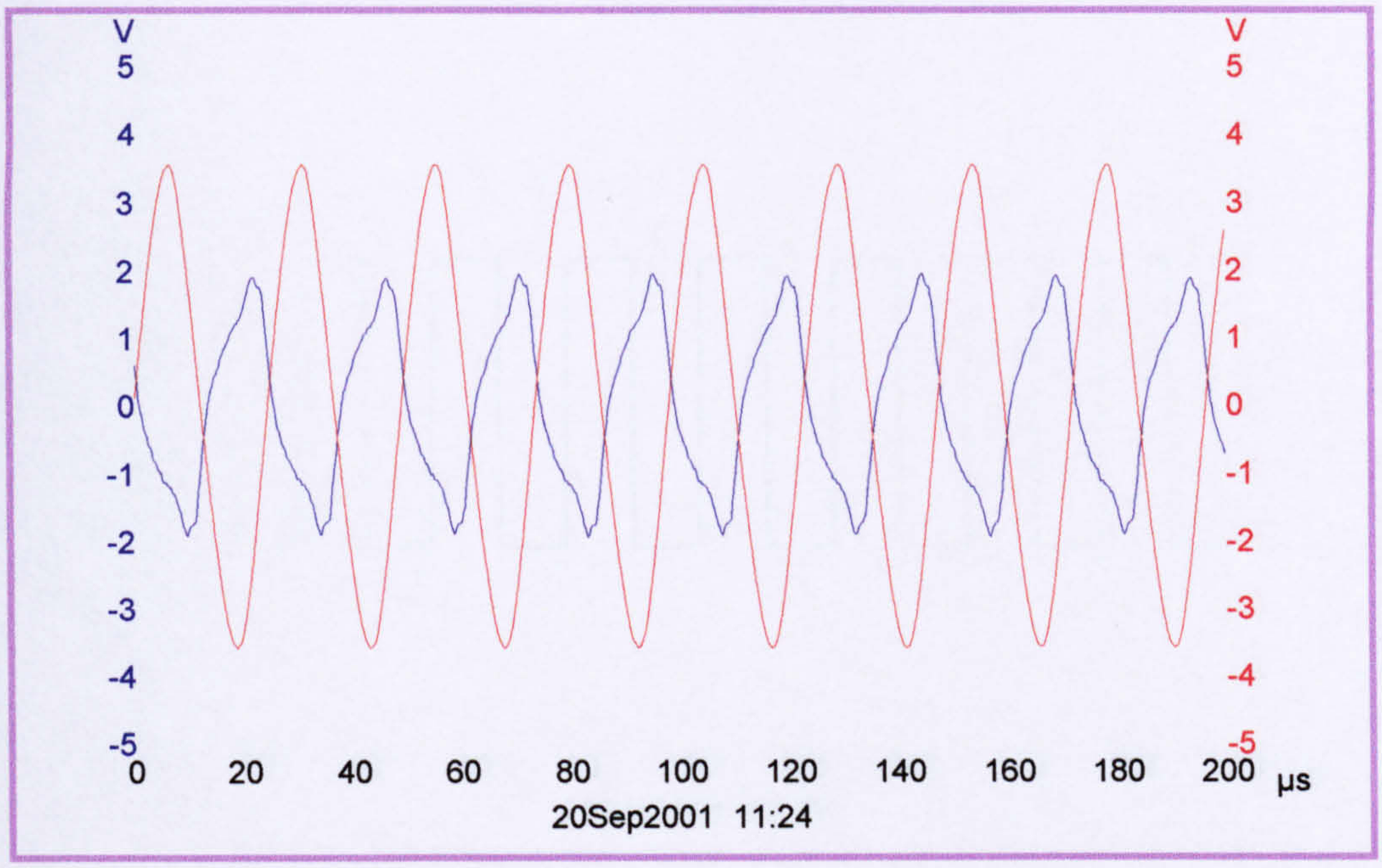

(a)

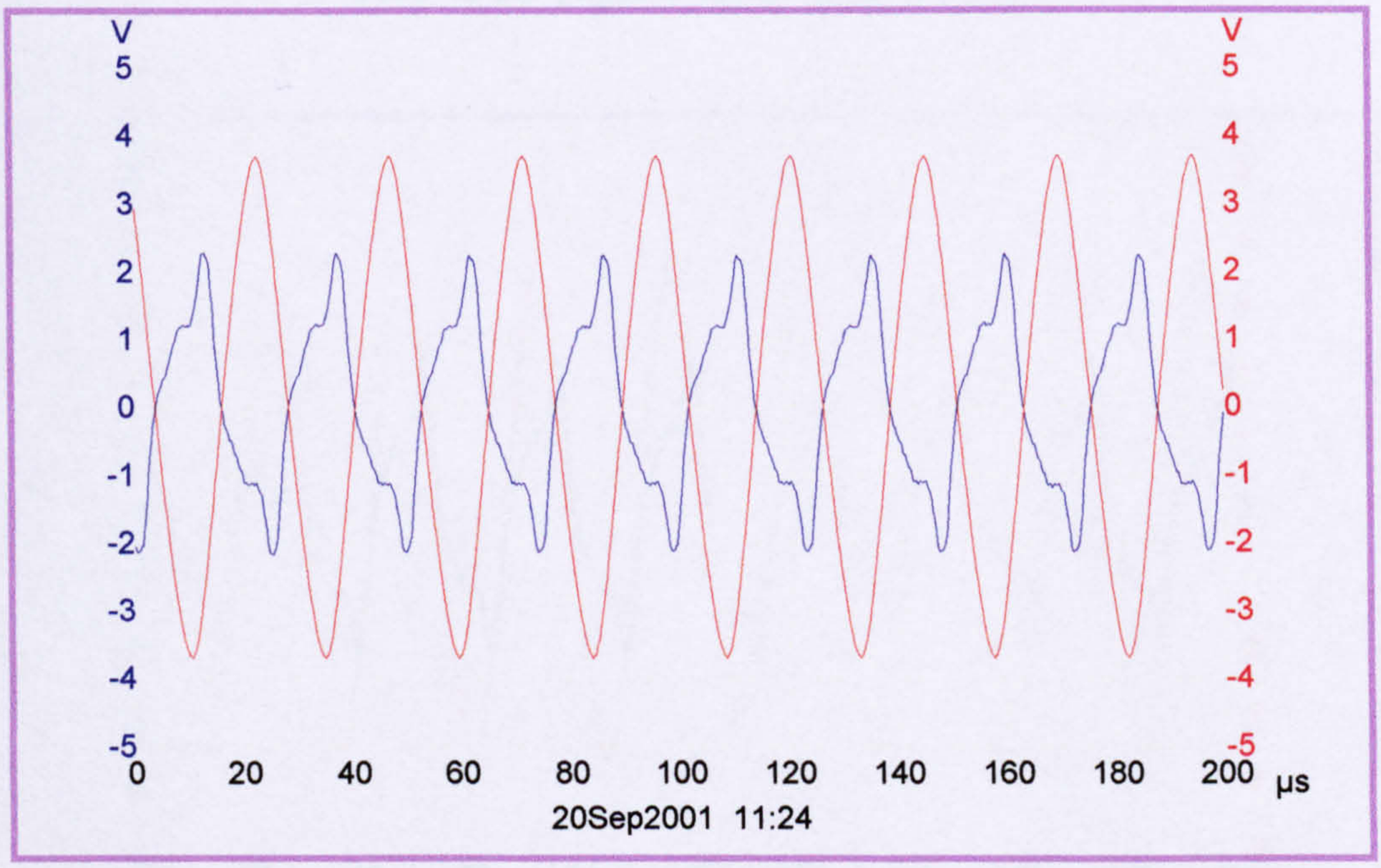

(b)

Figure 5-9 Waveform variation of the load current (ch2-red) and load voltage across the motor (ch1-blue) using self-oscillation a bipolar drive different amplification factor at resonant frequency 41.5 KHz (2) for PZT 4PCD [Scale 1 : 10]

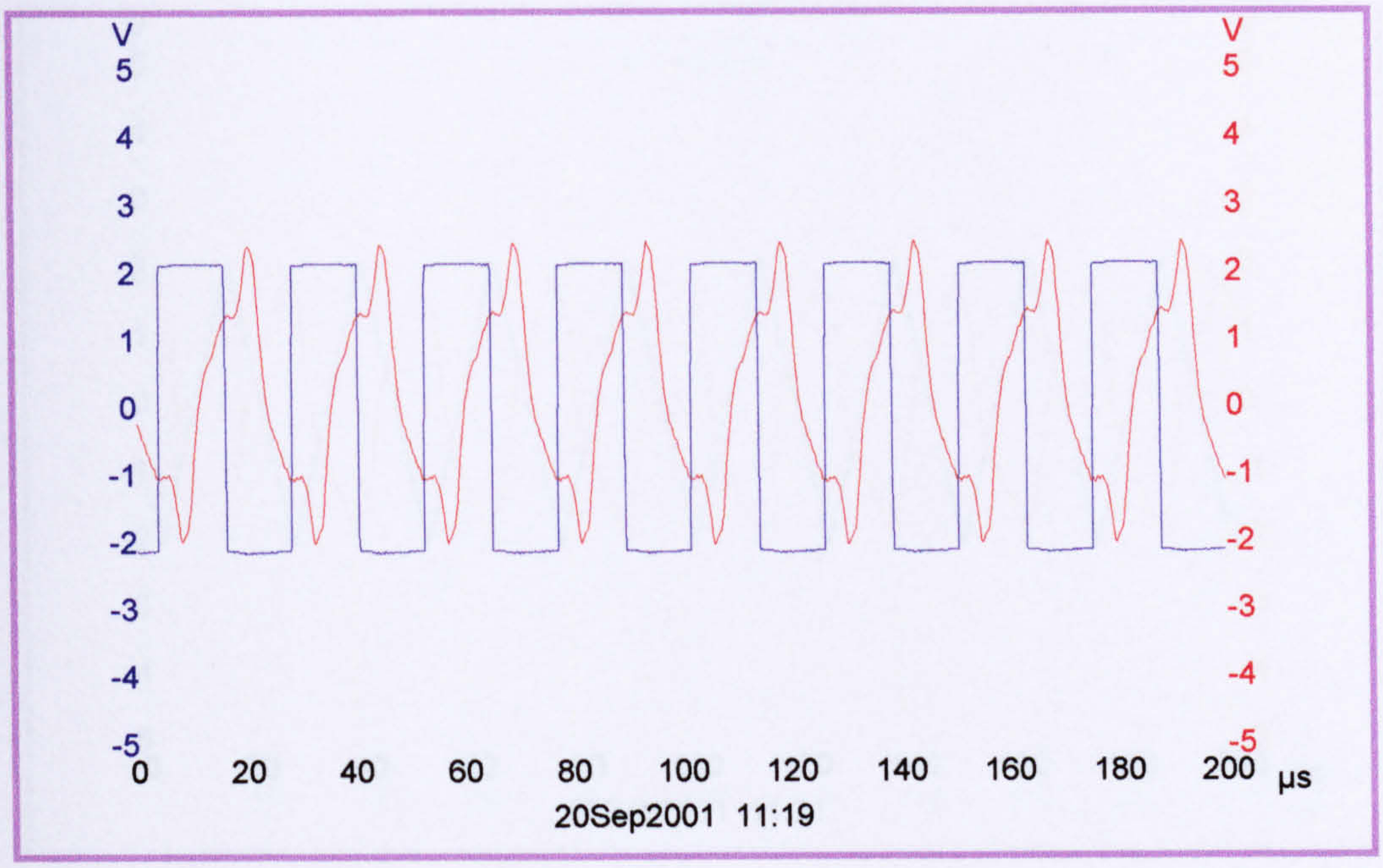

Figure 5-10 Waveform variation of the input signal (ch1-blue) and output signal (ch2-red) of the developed piezoelectric USM drive at resonant frequency 41.5 KHz (1) for PZT 4PCD [square wave- Scale 1 : 10]

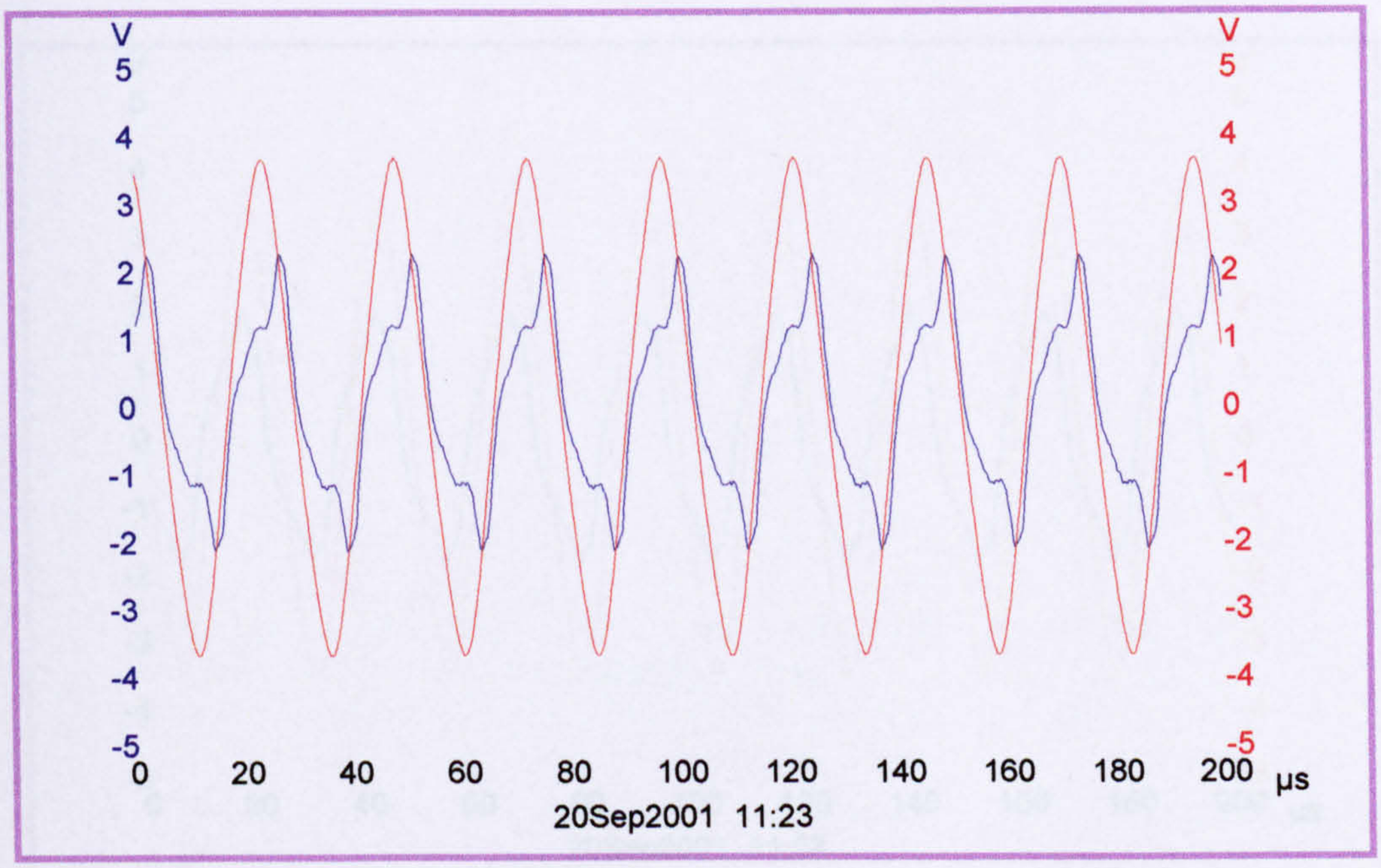

Figure 5-11 Waveform variation of the load current (ch2-red) and load voltage across the motor (ch1-blue) using self-oscillation a bipolar drive at resonant frequency 41.5 KHz (3) for PZT 4PCD [square wave- Scale 1 : 10]

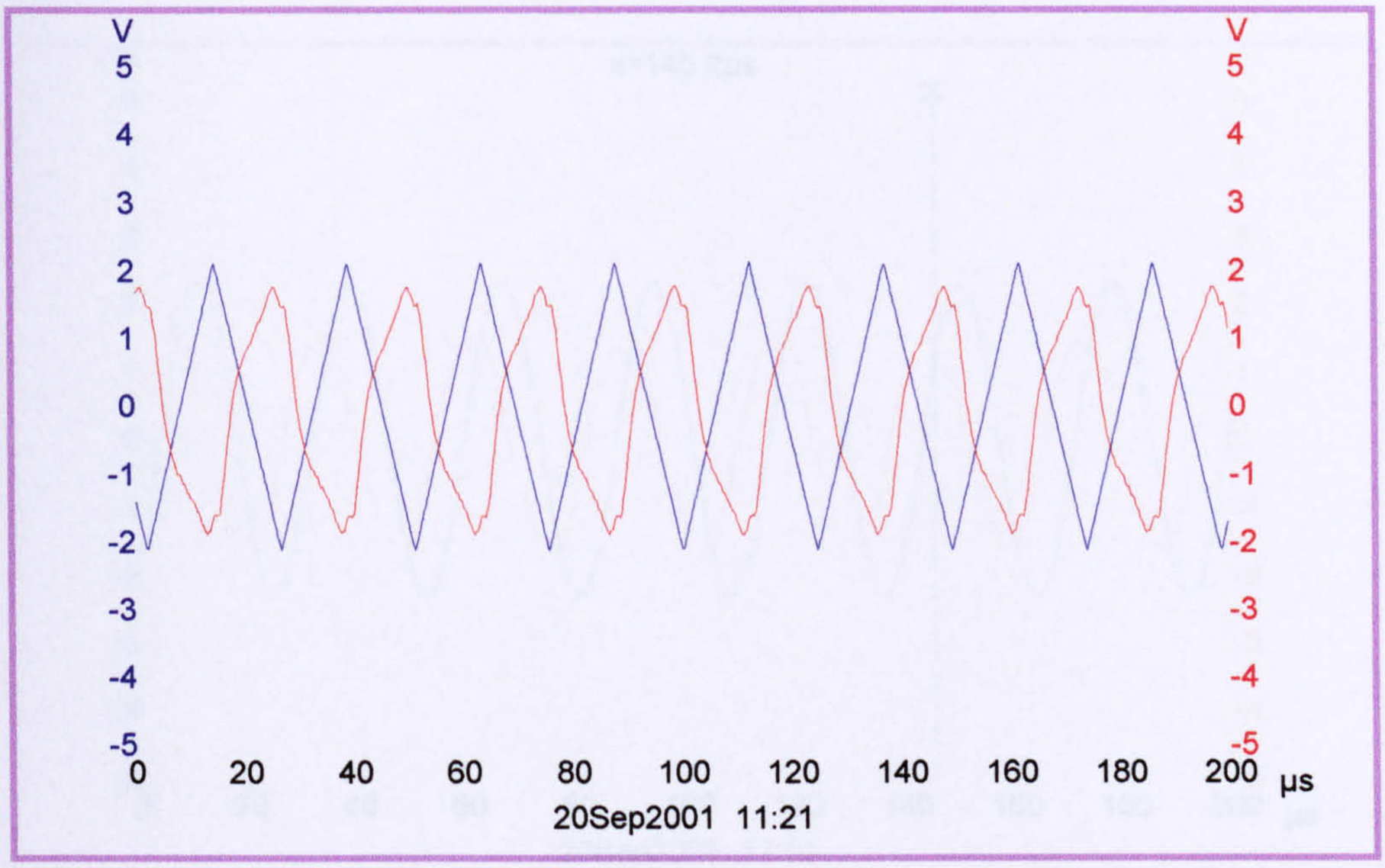

Figure 5-12 waveform variation of the input signal (ch1-blue) and output signal (ch2-red) of the developed piezoelectric USM drive at resonant frequency 41.5 KHz (1) for PZT 4PCD [saw tooth wave- Scale 1 : 10]

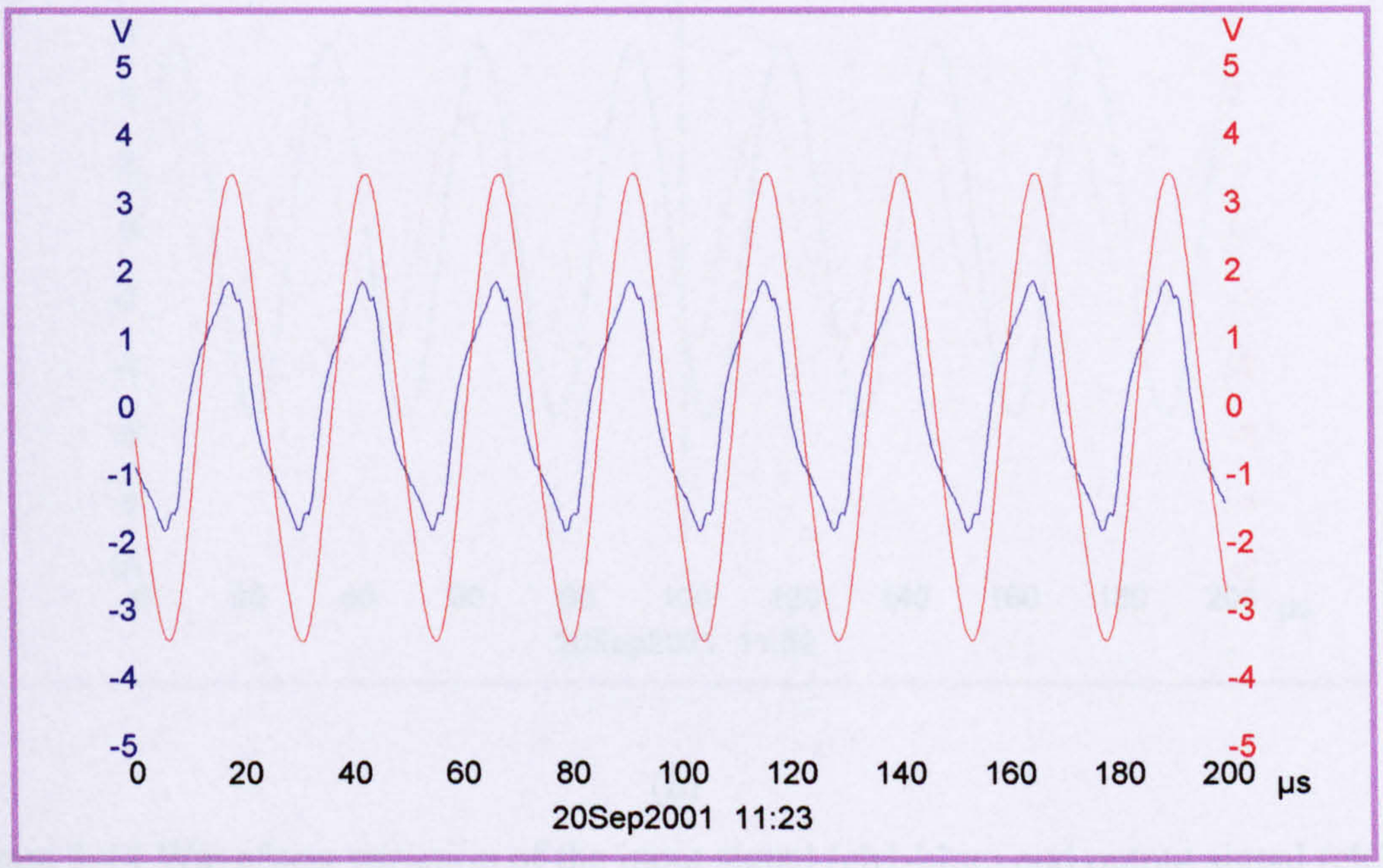

Figure 5-13 Waveform variation of the load current (ch2-red) and load voltage across the motor (ch1-blue) using self-oscillation a bipolar drive at resonant frequency 41.5 KHz (3) for PZT 4PCD [saw tooth wave- Scale 1 : 10]

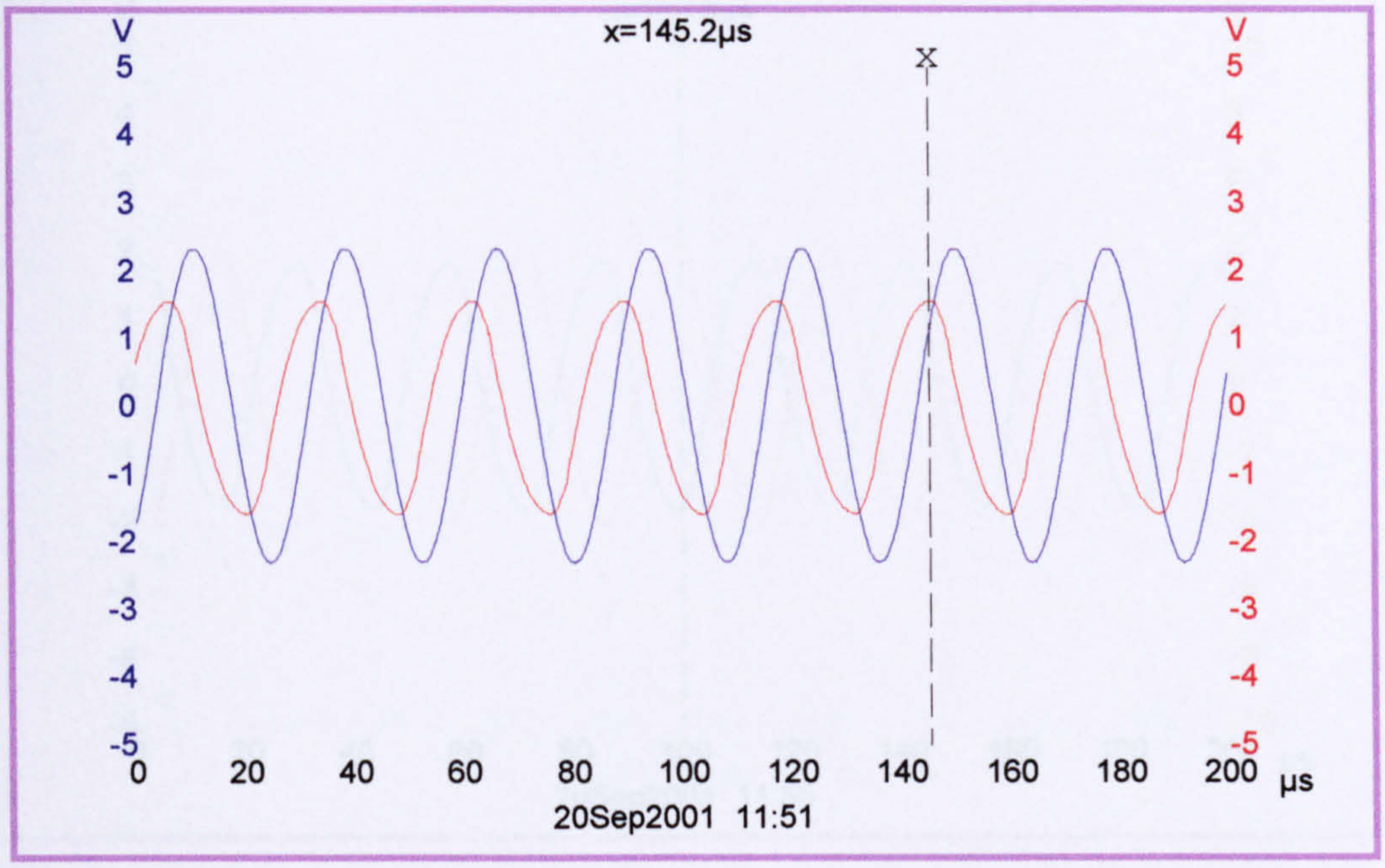

(a)

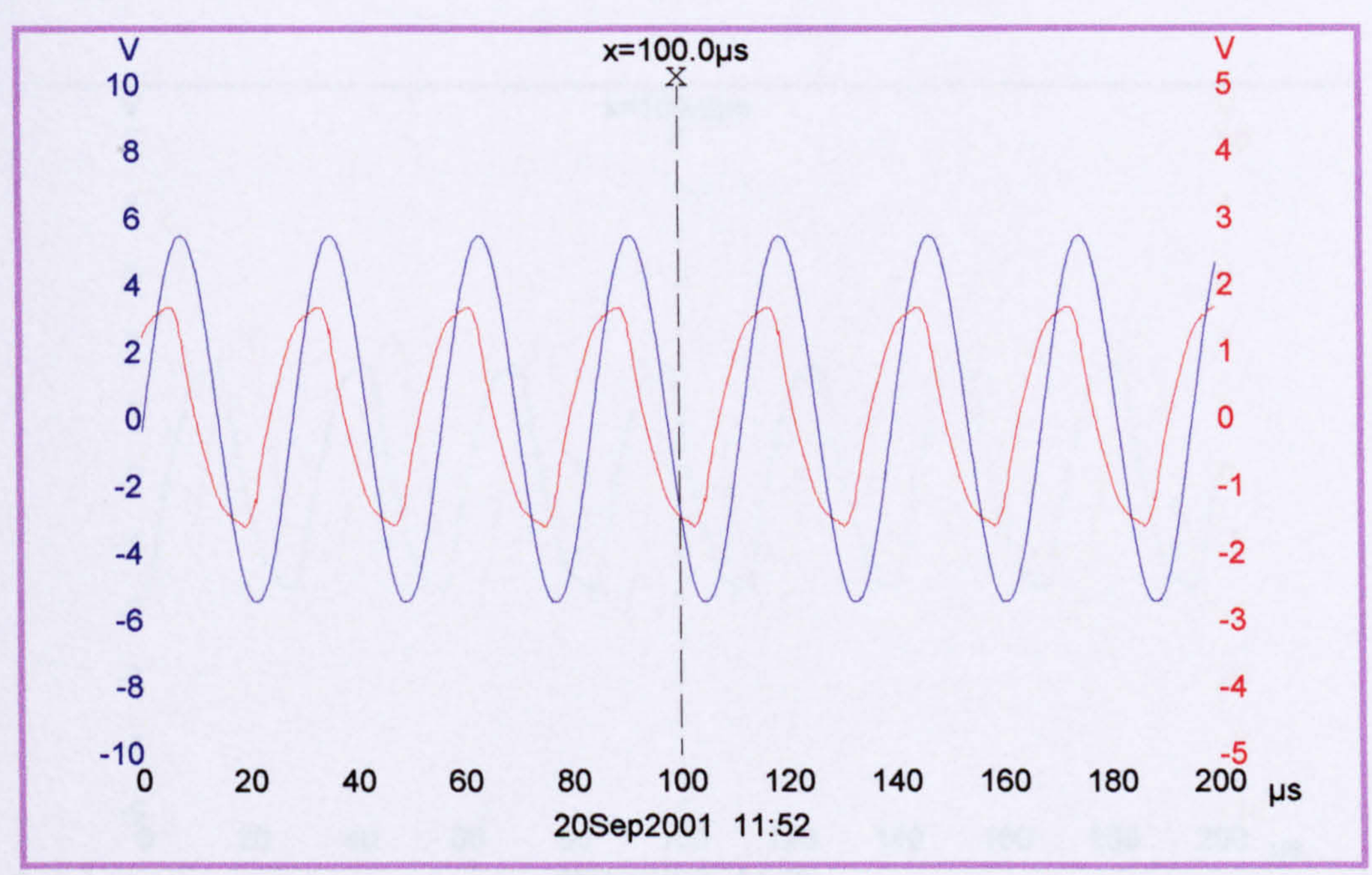

(b)

Figure 5-14 Waveform variation of the input signal (ch1-blue) and output signal (ch2-red) [Scale 1: 10] of the developed piezoelectric USM drive for different amplification factor at resonant frequency 37.4 KHz for CTS19

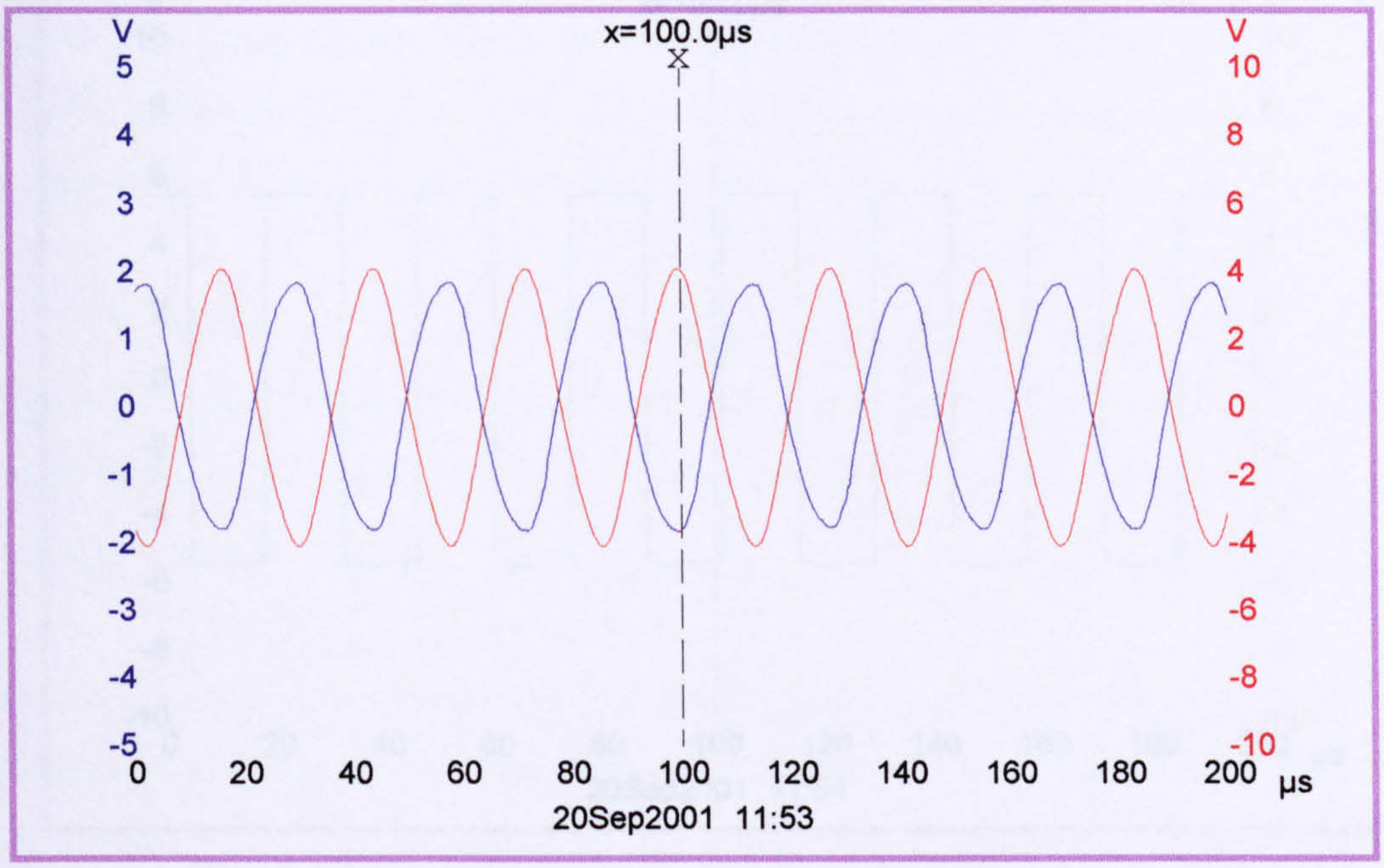

(a)

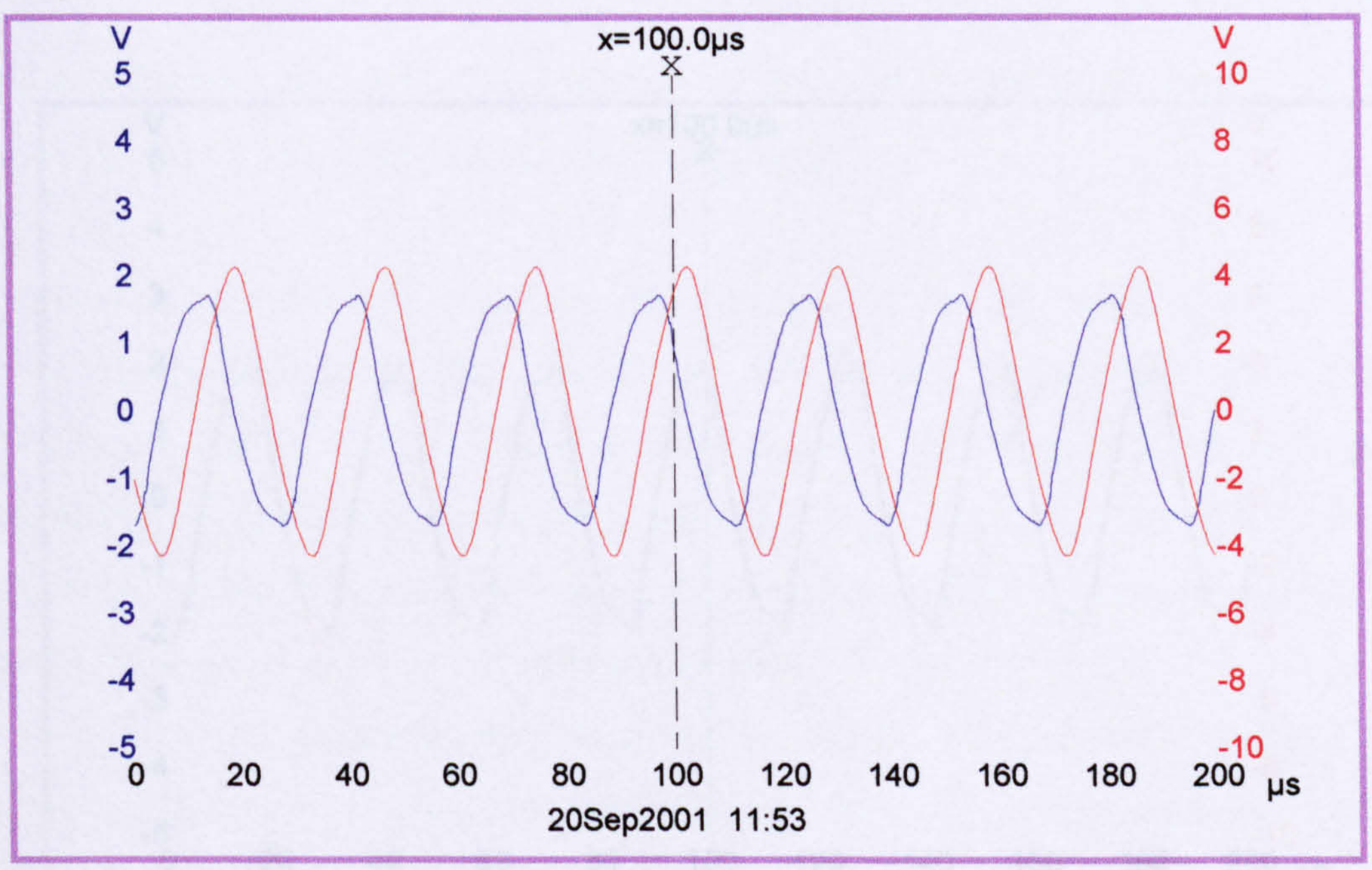

(b)

Figure 5-15 Waveform variation of the load current (ch2-red) and load voltage across the motor (ch1-blue) using self-oscillation a bipolar drive for different amplification factor at resonant frequency 37.4 KHz for CTS19 [Scale 1 : 10]

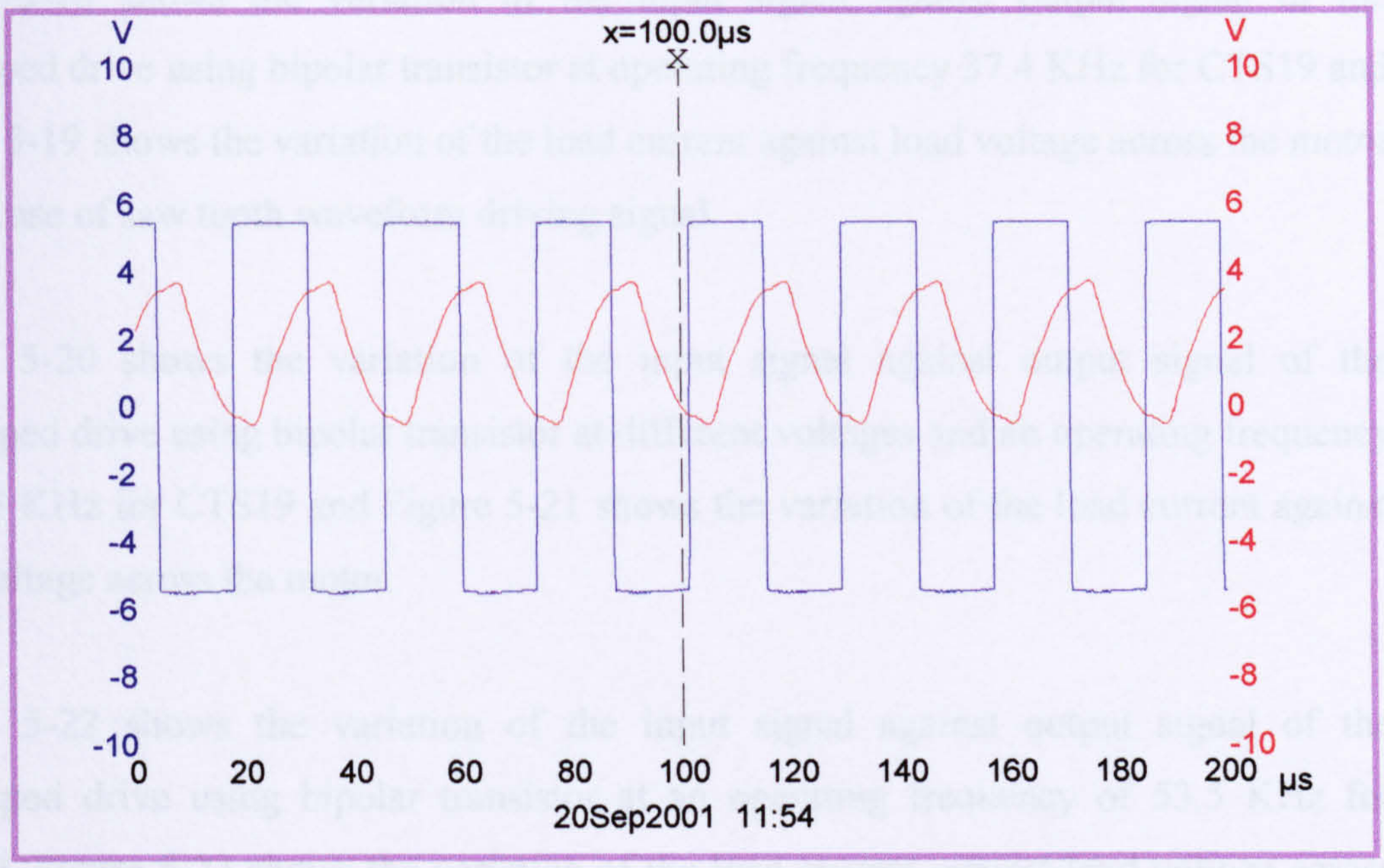

Figure 5-16. Waveform variation of the input signal (ch1-blue) and output signal (ch2-red) [Scale 1: 10] of the developed piezoelectric USM drive at resonant frequency 37.4 KHz (1) for CTS19 [square wave]

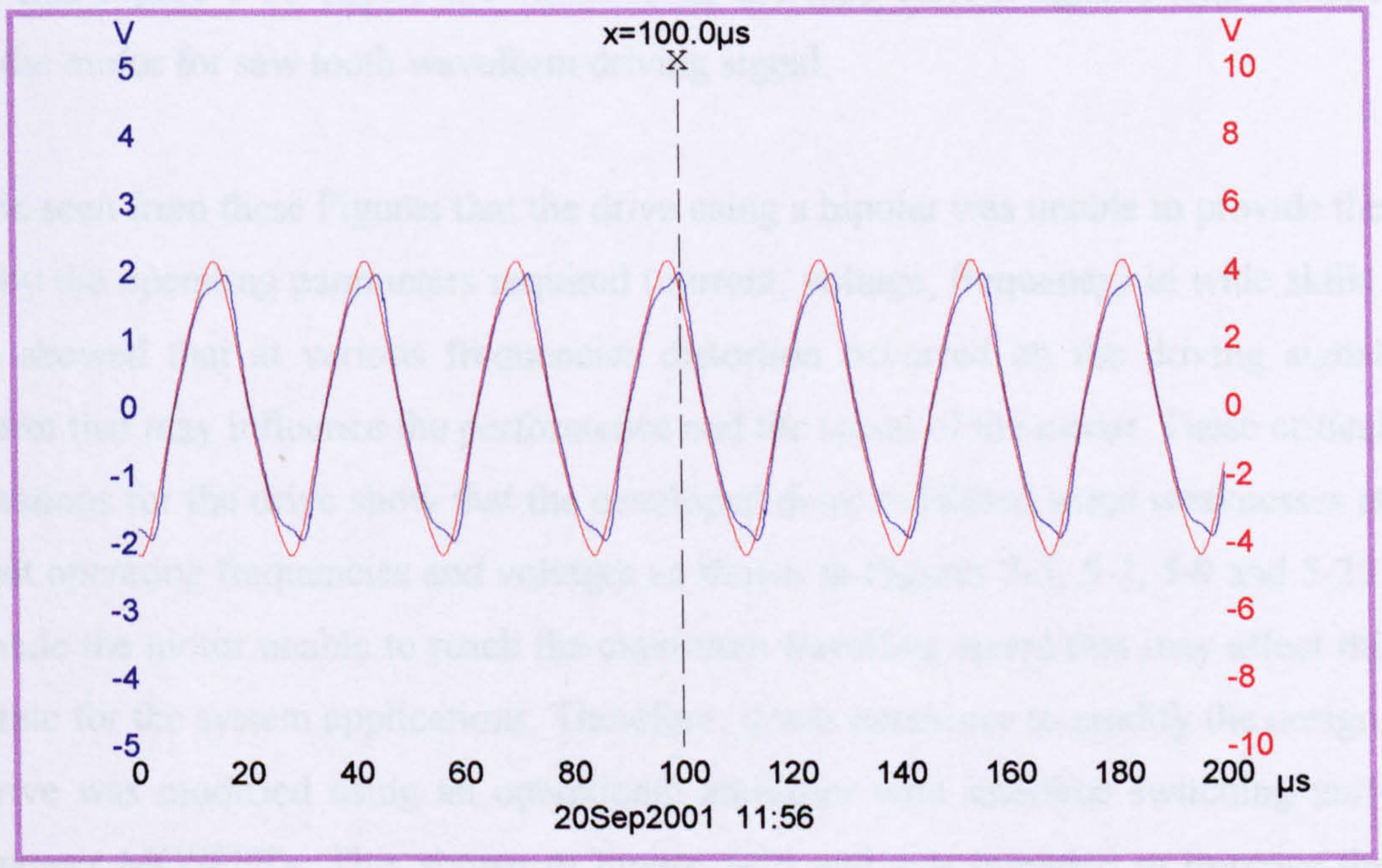

Figure 5-17 Waveform variation of the load current (ch2-red) and load voltage across the motor (ch1-blue) using self-oscillation a bipolar drive at resonant frequency 37.4 KHz for CTS19 [square wave- Scale 1 : 10]

Figure 5-18 shows the variation of the input signal against output signal of the developed drive using bipolar transistor at operating frequency 37.4 KHz for CTS19 and Figure 5-19 shows the variation of the load current against load voltage across the motor in the case of saw tooth waveform driving signal.

Figure 5-20 shows the variation of the input signal against output signal of the developed drive using bipolar transistor at different voltages and an operating frequency of 53.5 KHz for CTS19 and Figure 5-21 shows the variation of the load current against load voltage across the motor.

Figure 5-22 shows the variation of the input signal against output signal of the developed drive using bipolar transistor at an operating frequency of 53.5 KHz for CTS19. Figure 5-23 shows the variation of the load current against load voltage across the motor for the square waveform-driving signal.

Figure 5-24 shows the variation of the input signal against output signal of the developed drive using bipolar transistor at an operating frequency of 53.5 KHz for CTS19 and Figure 5-25 shows the variation of the load current against load voltage across the motor for saw tooth waveform driving signal.

It can be seen from these Figures that the drive using a bipolar was unable to provide the motor by the operating parameters required (current, voltage, frequency) in wide skills. It also showed that at various frequencies distortion occurred on the driving signal waveform that may influence the performance and the speed of the motor. These critical examinations for the drive show that the developed drive exhibited some weaknesses at different operating frequencies and voltages as shown in Figures 5-5, 5-7, 5-9 and 5-20. This made the motor unable to reach the maximum travelling speed that may affect the speed rate for the system applications. Therefore, it was necessary to modify the design. The drive was modified using an operational amplifier with interface switching unit-using power MOSFETs. This shown in Figure 5-26 and was intended to improve the drive capability for control.

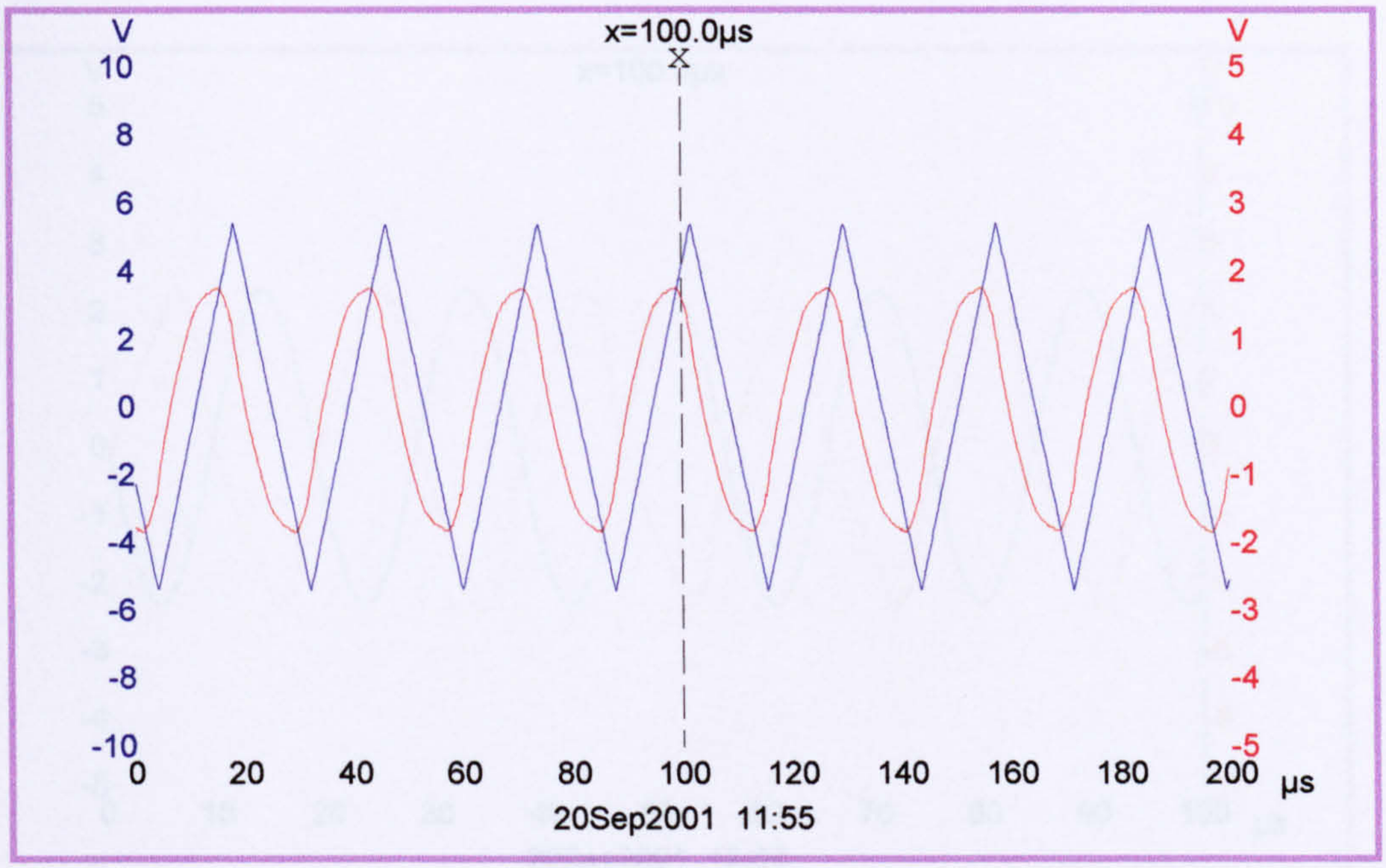

Figure 5-18 Waveform variation of the input signal (ch1-blue) and output signal (ch2-red) [Scale 1: 10] of the developed piezoelectric USM drive at resonant frequency 37.4 KHz (1) for CTS19 [saw tooth wave]

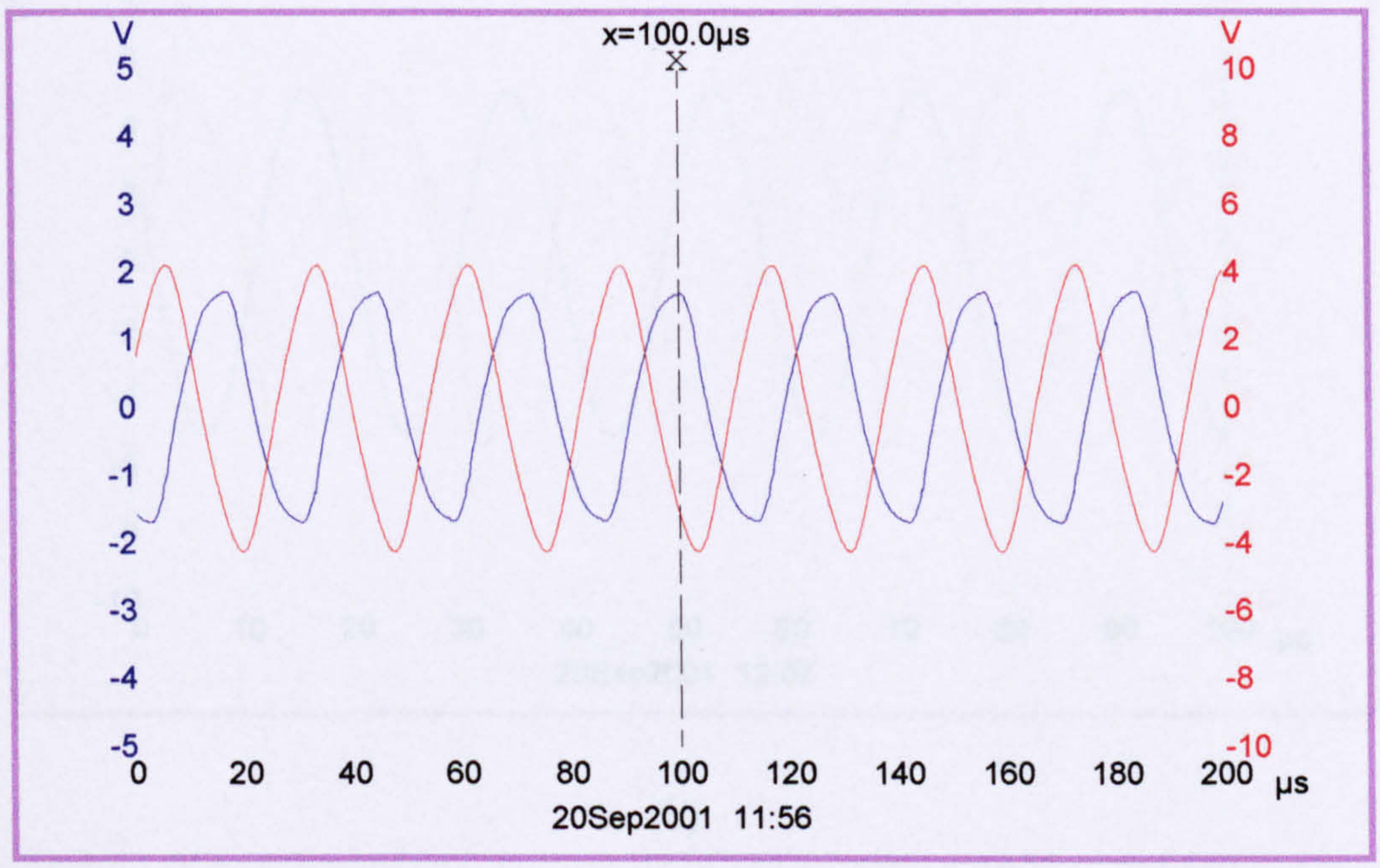

Figure 5-19 Waveform variation of the load current (ch2-red) and load voltage across the motor (ch1-blue) using self-oscillation a bipolar drive at resonant frequency 37.4KHz (3) for CTS19 [saw tooth wave- Scale 1 : 10]

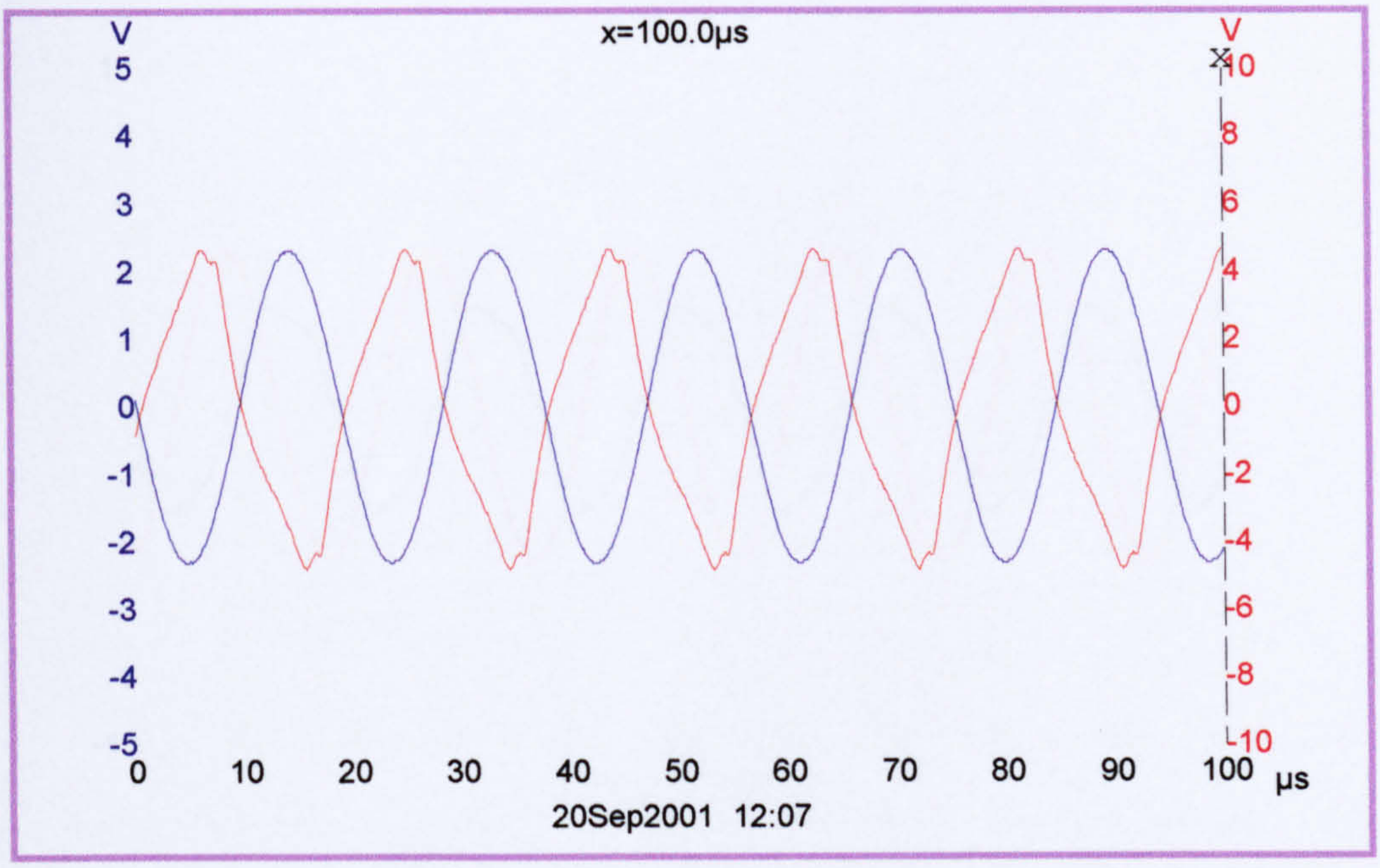

(a)

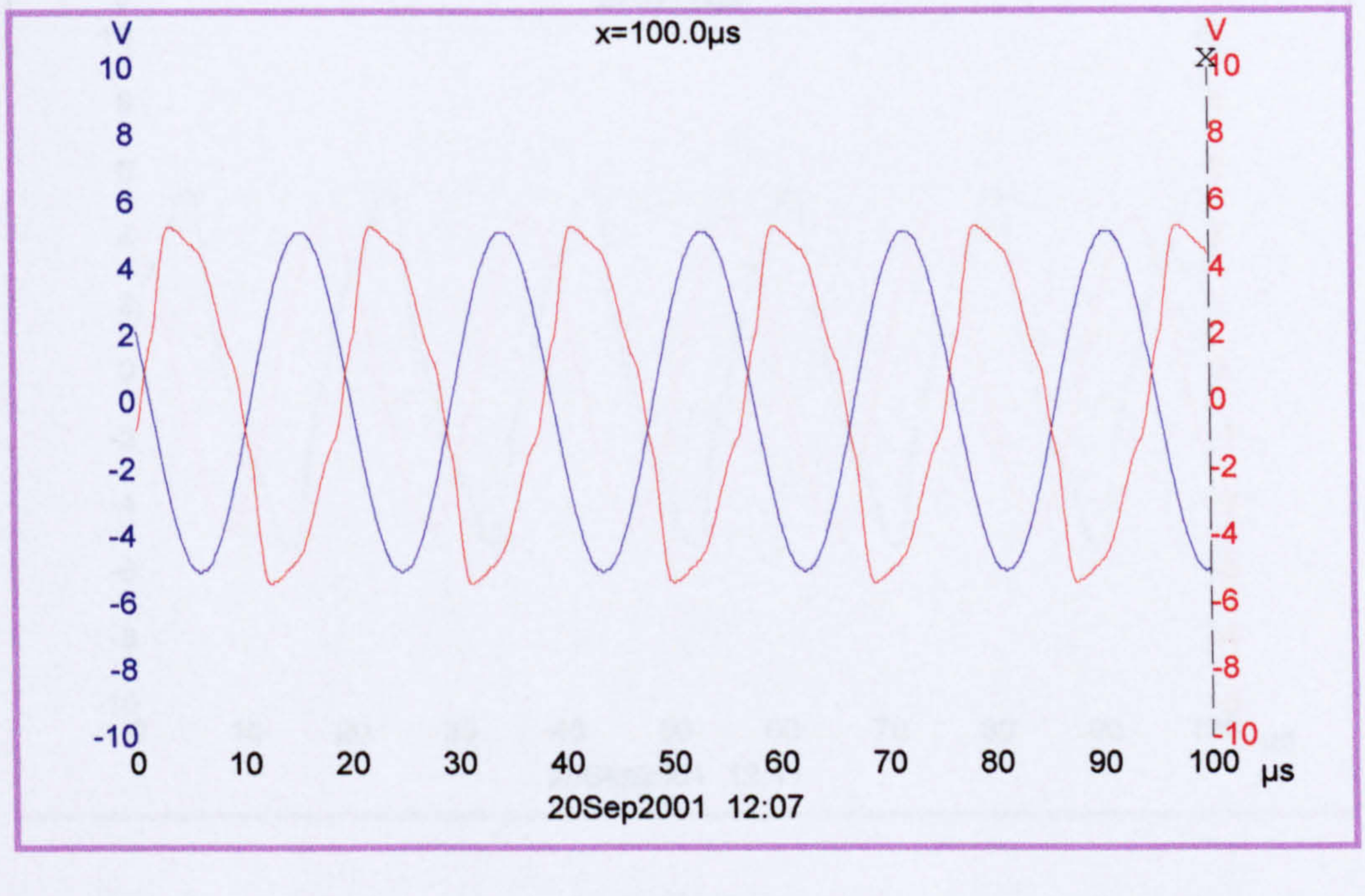

(b)

Figure 5-20 Waveform variation of the input signal (ch1-blue) and output signal (ch2-red) [Scale 1: 10] of the developed piezoelectric USM drive for different amplification factor at resonant frequency 53.5 KHz for CTS19

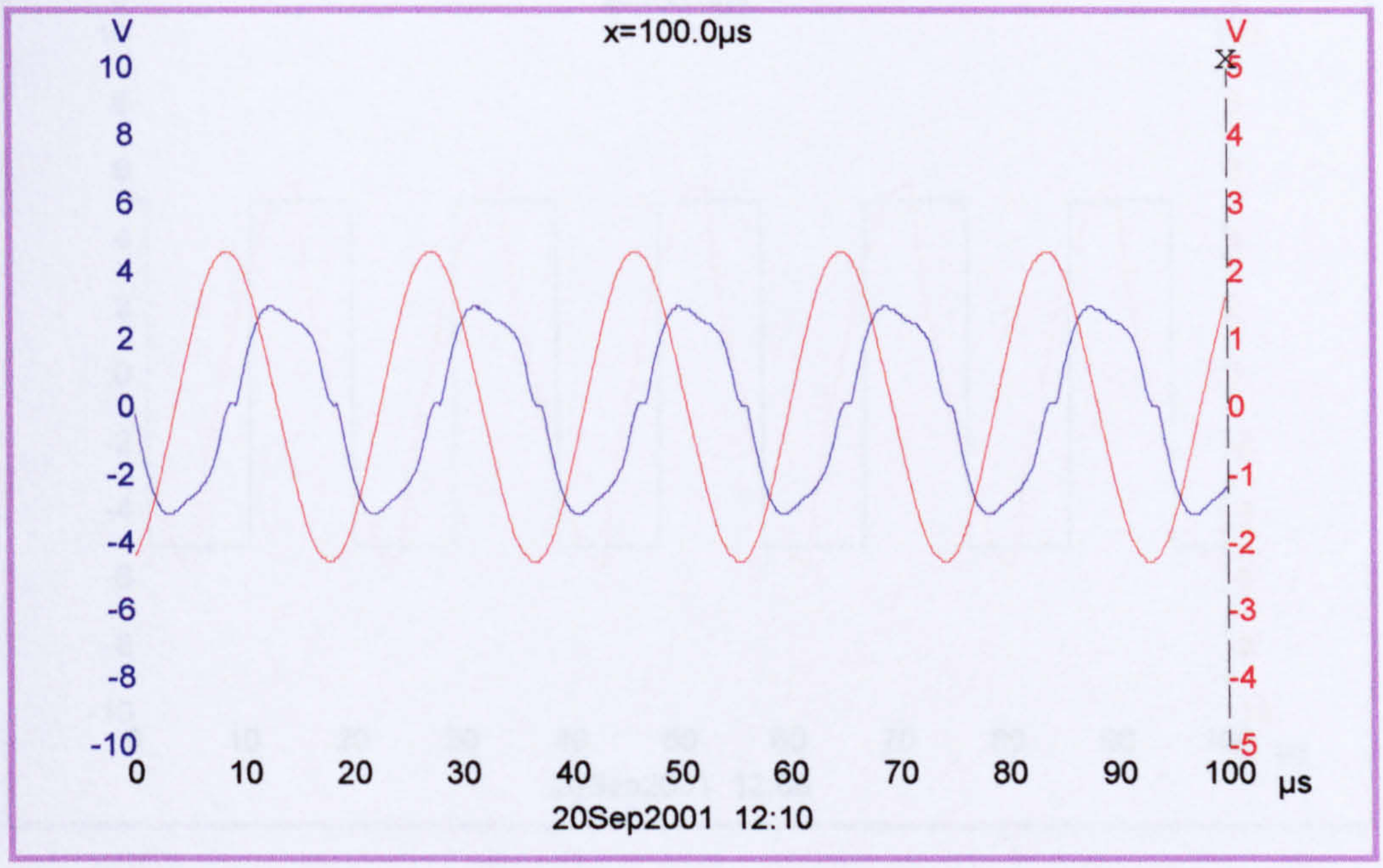

(a)

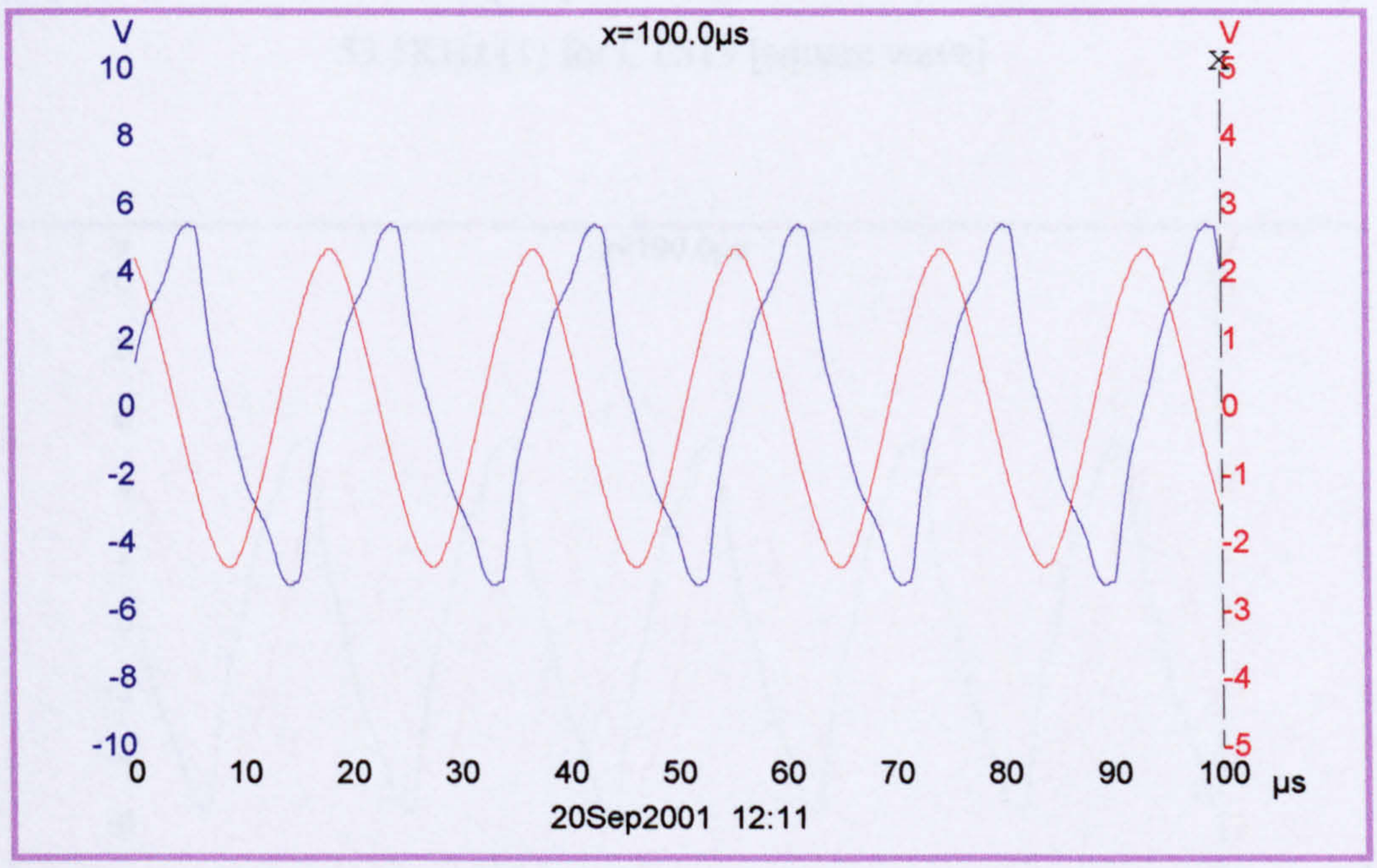

(b)

Figure 5-21 Waveform variation of the load current (ch2-red) and load voltage across the motor (ch1-blue) using self-oscillation a bipolar drive for different amplification factor at resonant frequency 53.5KHz for CTS19 [Scale 1 : 10]

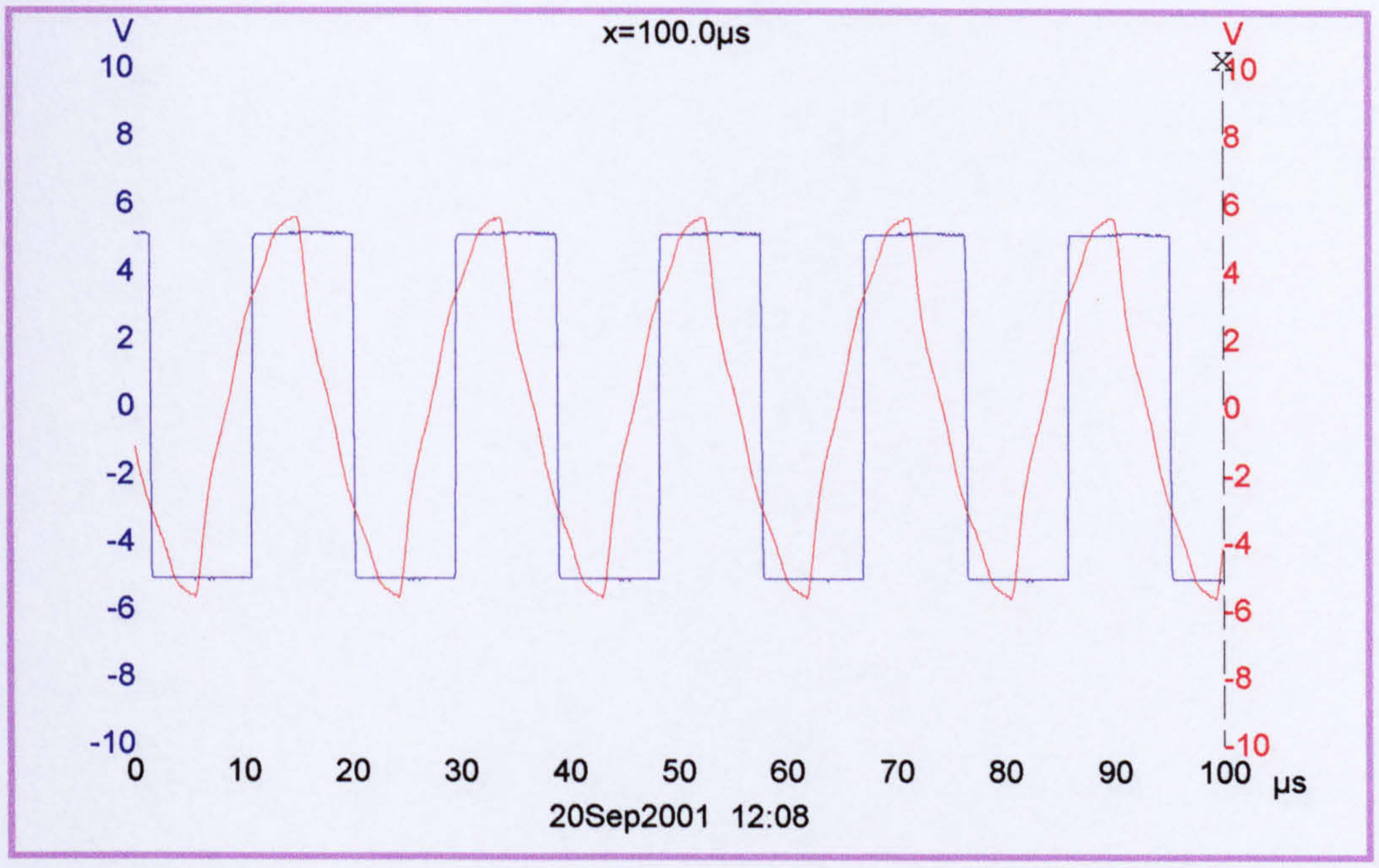

Figure 5-22 Waveform variation of the input signal (ch1-blue) and output signal (ch2-red) [Scale 1: 10] of the developed piezoelectric USM drive at resonant frequency 53.5KHz (1) for CTS19 [square wave]

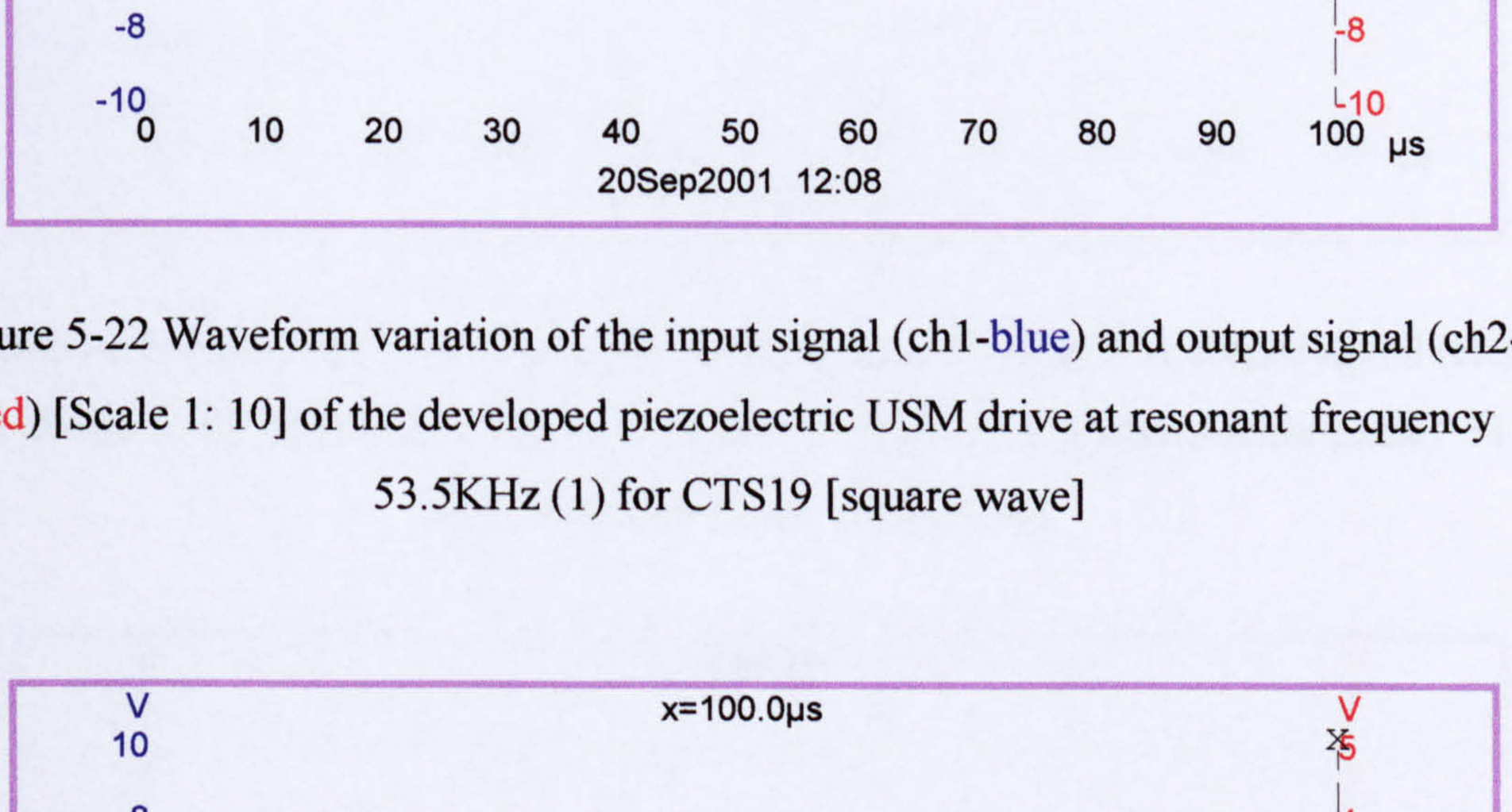

Figure 5-23 Waveform variation of the load current (ch2-red) and load voltage across the motor (ch1-blue) using self-oscillation a bipolar drive at resonant frequency 53.5KHz (1) for CTS19 [square wave- Scale 1 : 10]

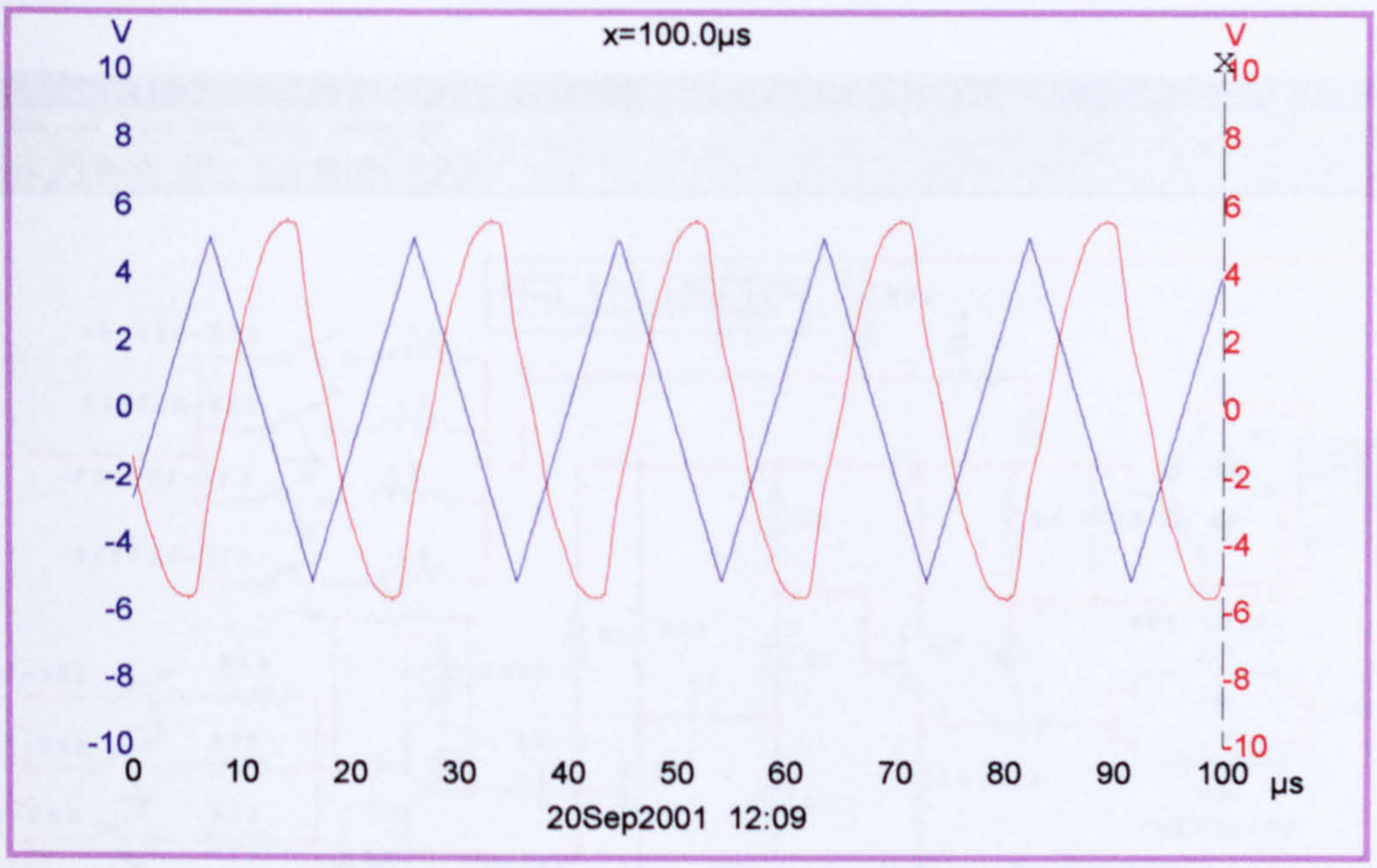

Figure 5-24 Waveform variation of the input signal (ch1-blue) and output signal (ch2-red) [Scale 1: 10] of the developed piezoelectric USM drive at resonant frequency 53.5 KHz for CTS19 [saw tooth wave]

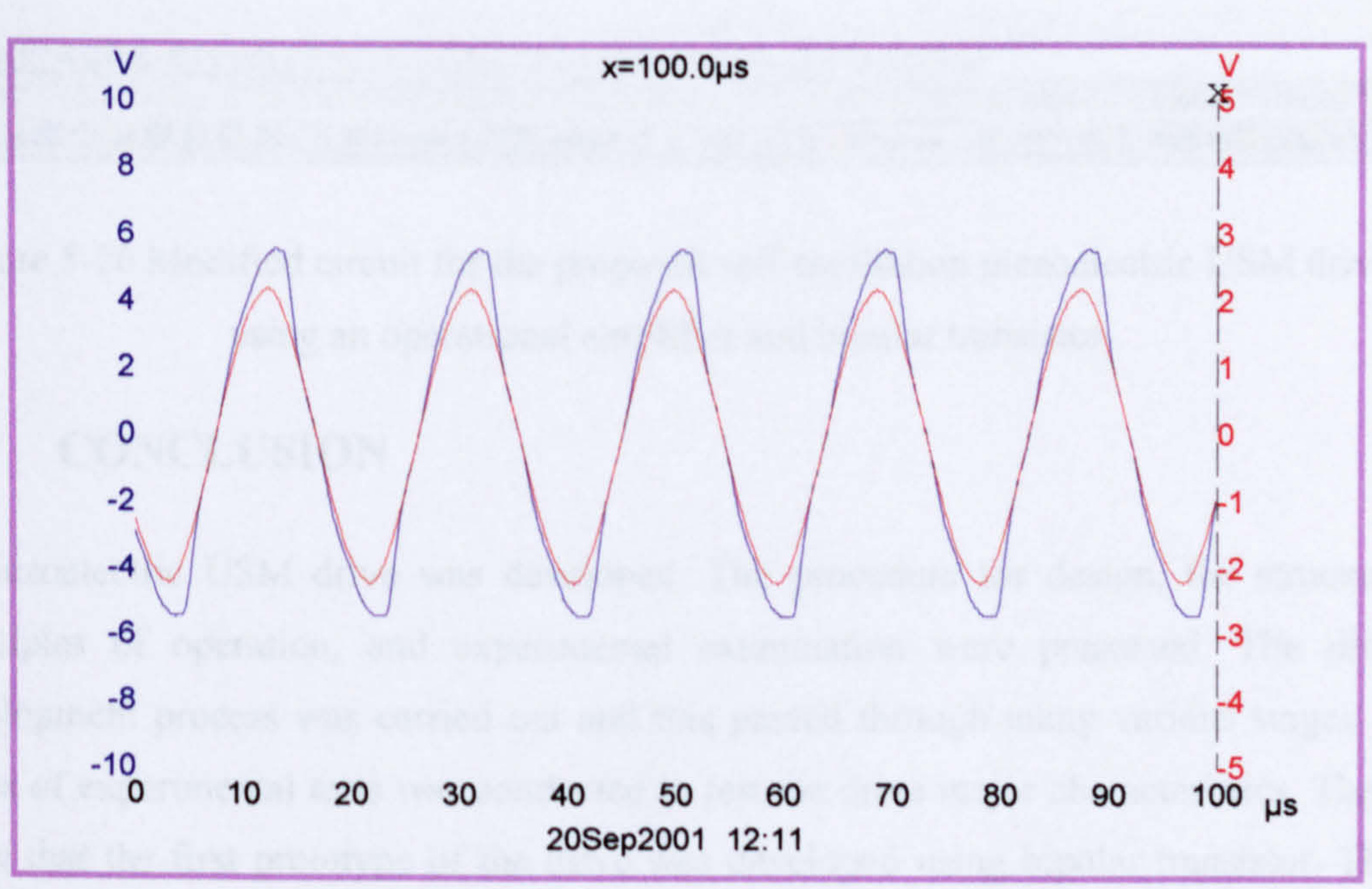

Figure 5-25 Waveform variation of the load current (ch2-red) and load voltage across the motor (ch1-blue) using self-oscillation a bipolar drive at resonant frequency 53.5 KHz (1) for CTS19 [saw tooth wave-Scale 1 : 10]

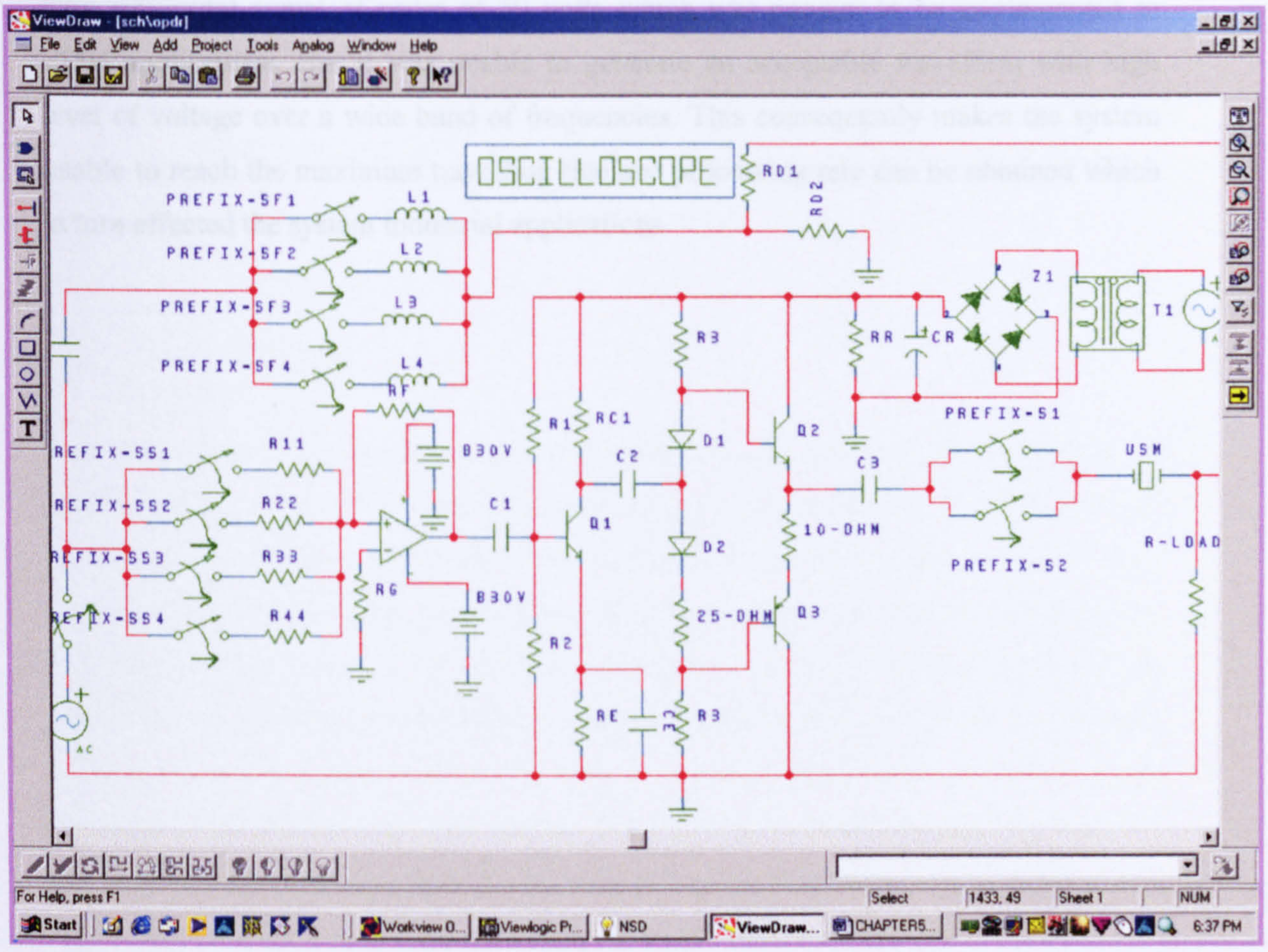

Figure 5-26 Modified circuit for the proposed self-oscillation piezoelectric USM drive using an operational amplifier and bipolar transistor

5.8 CONCLUSION

A piezoelectric USM drive was developed. The procedure for design, the structure, principles of operation, and experimental examination were presented. The drive development process was carried out and this passed through many various stages. A series of experimental tests was conducted to test the drive major characteristics. These show that the first prototype of the drive was developed using bipolar transistor. This suffered from waveform shape distortion and un-ability to generate the required operating parameters of the motor over wide ranges. The drive was modified using an operational amplifier and a power MOSFETs (see appendix B). This was aimed at improving the drive capability and driving signal waveform. A critical examination and

evaluation of the drive was carried out. This showed that the drive was able to provide a pure sinusoidal signal of order of 50 volts which was enough to be implemented in EDM applications. But it was unable to generate an acceptable waveform with high level of voltage over a wide band of frequencies. This consequently makes the system unable to reach the maximum travelling rate and processing rate can be obtained which in turn affected the system industrial applications.

CHAPTER 6

6 INTEGRATION OF THE DEVELOPED PIEZOELECTRIC FEED DRIVE INTO AN EDM SYSTEM

6.1 OVERVIEW

The developed piezoelectric ultrasonic system has the potential to be utilised in application that require micro dynamic response and micro resolution. A whole series of machining process each based upon the electro-discharge phenomena and EDT have evolved since 1940s to date. These electro discharge systems are described in appendix (C). One common feature of an electro discharge system is to move the cutting (eroding) tool (usually described as an electrode) towards and away from the material being machined in a short time period. This is to reduce open circuit and short circuit operation of the electro discharge system. The traditional manner to effect the required rapid movement of the electrode has been by use a DC servomotor which drives a ball screw arrangement that allow the conversion of the rotary motion into linear motion. The nut in the ballscrew arrangement usually fastened to a slide that is guided by a slideway thus linear motion can be affected. In the recent past some electro discharge systems have used AC servomotors because of their better performance but essentially the same kinematical arrangement of rotary motor/ballscrew/ slide/ slideway is in place.

The particular EDM process known as EDT generally has a multi rotary motor/ballscrew/slide/slideway arrangement in a small volume. The function being to focus as many electrodes on to a given area as is possible given the limitations of the design constraints that is dominated by the physical size and volume of DC or AC servomotors and the other kinematic element required to effect rotary to linear motion.

One of the potential advantage of the developed feed drive using piezoelectric USM is its compact size in comparison to a DC or AC servo motor thus allowing the possibility of bringing to fruition a design for an EDM and EDT servo head (i.e. a multi rotary

motor/ballscrew/slide/slideway arrangement) that has the ability to effect many electrodes, each separately servo controllable, on to a given area. The piezoelectric USM has the same kinematic capability as a rotary motor/ballscrew/slide/slideway arrangement, is controllable within the limits that DC/AC servos operate and EDM systems requirements. The EDT process was therefore chosen as one of an appropriate test bed application for the developed ultrasonic drive. Consequently the required unit and modification needed to conduct this examination is presented in this chapter. This concludes with an experimental examination of the developed system and main features can be obtained.

6.2 CONFIGURATION OF EDM SYSTEM USING PIEZOELECTRIC USM DRIVE

The arrangement of the units of the EDM system using the developed piezoelectric USM drive and modification to be carried out is shown in Figure 6-1. This was included the servo control drive, servo control unit, feedback unit and input unit.

6.2.1 System Composition

- Normal EDM machine with DC servo control drive,
- Input keypad, Programmable power unit, Servo control system,
- EDM control unit, Programmable oscillators unit, Power switching unit, Sensors unit, and Dielectric system.

6.2.2 Piezoelectric USM Drive:

- Normally the number of motors used in such application is considerably dependent upon the size of the roll and the eroded electrode cross-sectional area.
- Each motor to have one driving sliding element,
- Each sliding element to be driven with an individual actuator,
- The sliding element to be made from appropriate material.
- Each eroded electrode to be moved towards and away from the roll, so as to achieve inter-electrode gap.
- Each sliding element to be provided with one adapter.

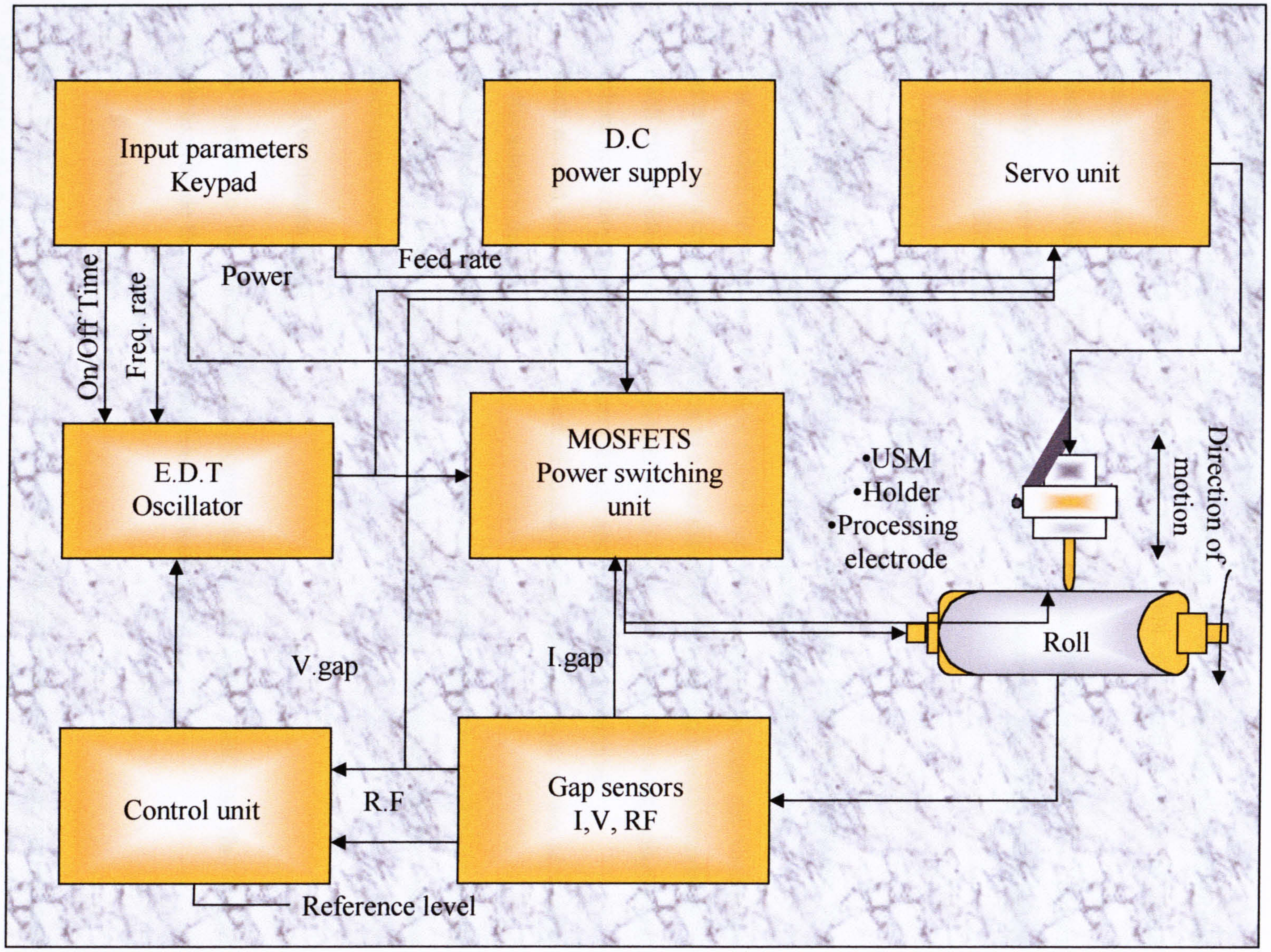

Figure 6-1 Electro Discharge Machining system block diagram for the proposed approach using linear piezoelectric USM

- The adapter to be made from appropriate insulating materials. Its design could be varied according to number of eroded electrodes and system applications.
- Each adapter to have the ability to carry at least three eroded electrodes arranged in particular configuration to covered assigned area.
- Each eroded electrode, in the proposed system, to have an individual electrical source, to provide a suitable voltage and current for each process of main machining processes.
- Each servo-control drive to have a single piezoelectric amplifier (AC power supply) to drive piezoelectric USM with the required operating parameters (frequency, voltage and current).

6.2.3 Eroded Electrode (Machining Tool):

- Each eroded electrode to be moved towards and away from the workpiece in a perpendicular direction, so as to achieve the required inter-electrode gap.
- The eroded electrode to be made from a suitable material to suit the workpiece material. This could be according to a manufacturer advice and known standards.
- Each eroded electrode to be provided by an open circuit voltage with polarity and values according to a manufacturer advice and machining conditions.
- Each eroded electrode to be attached to the adaptor using a right screw according to the adaptor design.
- Each eroded electrode to be moved towards or away from the workpiece by its associated piezoelectric USM and servo drive unit according to the electro discharge system process.

6.2.4 Oscillators Unit:

EDM-system to be provided with programmable oscillators unit and this would enable to provide the required on-off time and test signal.

6.2.5 Feedback Unit:

This is to be a gap sensor unit to determine the spark parameters (voltage, current and RF emission) in the gap between the two electrodes (eroded electrode and workpiece).

6.2.6 DC power Supply and Switching Unit:

The programmable DC power supply and the MOSFETs switching units to be able to provide the system with the requested power for each machining process according to method of control.

6.2.7 Dielectric Oil System

- To provide the system with insulation, cooling and restriction of the spark area.
- To cover the workpiece or roll and eroded electrode most of the time of processing (appendix (C)).

6.2.8 Roll

- To be mounted in the EDM machine.
- To be able to rotate in two directions, clock wise and anti-clock wise.
- To be able to control the speed of rotation.
- The roll material used to determine the material of the eroded electrode and open circuit machining voltage.

6.3 EDM- SERVO CONTROL UNIT

A servo control system is needed for an EDM-system to ensure that the eroded electrode moves at the proper rate for each machining cycle, to maintain the correct inter-electrode spark gap and to retract the eroded electrode if the gap is bridged by particles from the eroded material. Therefore the servo control system has to be highly responsive to ensure high efficiency of machining. In this application the major duty of the servo control system is to command the gap voltage sensor system in the power supply and control the infeed rate of the eroded electrode to the workpiece in order to match the predetermined rate of material removal. When the sensor system determines that the inter-electrode gap has been bridged the servo control system must also react by reversing the direction of motion of the drive until the gap is cleared.

In most of EDM-applications the variation in the gap parameters (voltage, current and radio frequency signal) are the major boundaries used to monitor and control the machining process. These are used to ensure the correct movement of the eroded

electrode, to maintain the correct spark gap and to avoid arcing and short-circuiting processes.

The proposed servo control unit offers:

- Similar functions to that were provided by the old system with a compact size, fast response and high level of precision.
- A novel servo control feed drive using piezoelectric ultrasonic motor.
- A tolerance, protection, audible and visible units were developed for high level of accuracy and also to increase the safety of machining of the system.

6.3.1 Design Procedure for the proposed Unit

The methodology for design of a servo control system varies from one application to another. The steps taken to develop the current unit were:

- Identify the main machining processes in the application and method used to monitor these processes.
- Identify the type of control that will be used to control the applications main machining process.
- Select and define main control parameters such as: voltage, current and radio frequency (RF) signal.
- Select and define main machining parameters such as sparking pulse, feeding rate range, removal rate, discharging power and degree of surface finish.
- Produce the layout of the unit of control.
- Create comprehensive analysis for the unit main parts and optimise the unit design, such as interface units (analogue digital unit, digital analogue unit), processing unit, programmable unit…etc.
- Create a computer simulation and modelling to examine capability of the unit to monitor and control the main machining processes for this application.
- Select and identify the electronic components that will be used to build the practical prototype, i.e. solid-state analogue to digital devices, programmable devices, interface unit and etc.
- Integrate and examine the developed unit with the main system and create case study included the main machining process and applications needs.
- Design an audible, visible and protection unit for the whole system of control.

6.3.2 Structure of the Unit

The structure of the EDM-servo control unit, using gap voltage variation is proposed and is shown in Figures 6-2 and 6-3. Figure 6-2 shows the structure of the analogue to digital unit (interface unit) and this consists of a voltage divider unit, comparator unit, shaping unit and hex Schmitt unit. Voltage divider is used to monitor the gap voltage to the level that can be easy to process through various stages of the processing unit. Comparator unit is used to identify the process running by comparing the detected voltage with a reference voltage previously identified. Shaping unit and hex Schmitt unit is used to interface between analogue unit and the digital unit.

Figure 6-3 illustrates the structure of the processing unit and digital to analogue unit (interface unit). The processing unit is design to process the detected signal and produce the required orders to control feed rate, direction of motion of the drive, oscillator unit, power unit, circuit protection unit, audible and visible unit. The digital to analogue unit is used to interface between the produced order from the processing unit and different units of the system. The proposed unit is also included a tolerance unit which gives the design its own accuracy. Its also extends the proposed unit facility for control and monitoring of main machining process.

A circuit protection was considered during the design process. It provides a protection to stop the system and give the operator visible and audible alarm if the system is in short circuit condition.

The EDM-system has four main machining processes namely:

- Open circuit process,
- Sparking process,
- Arcing process, and
- Short circuit process.

On the most of the sophisticated EDM machine the spark parameters (voltage, current, RF signal) used to control these four processes. In this work, the inter-electrode gap voltage variation is discussed.

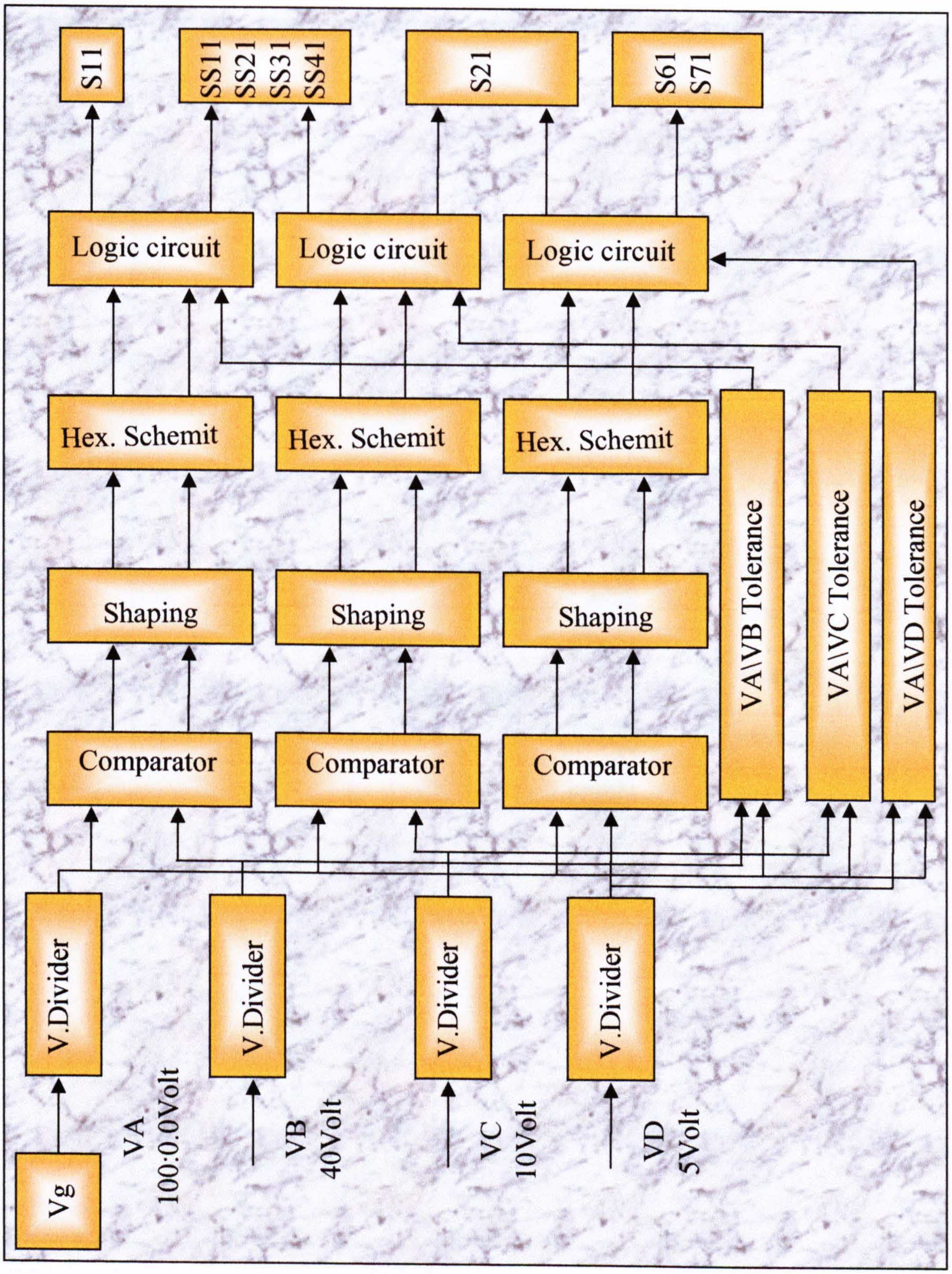

Figure 6-2 Analogue to digital unit for the proposed Electro Discharge Machining servo control unit

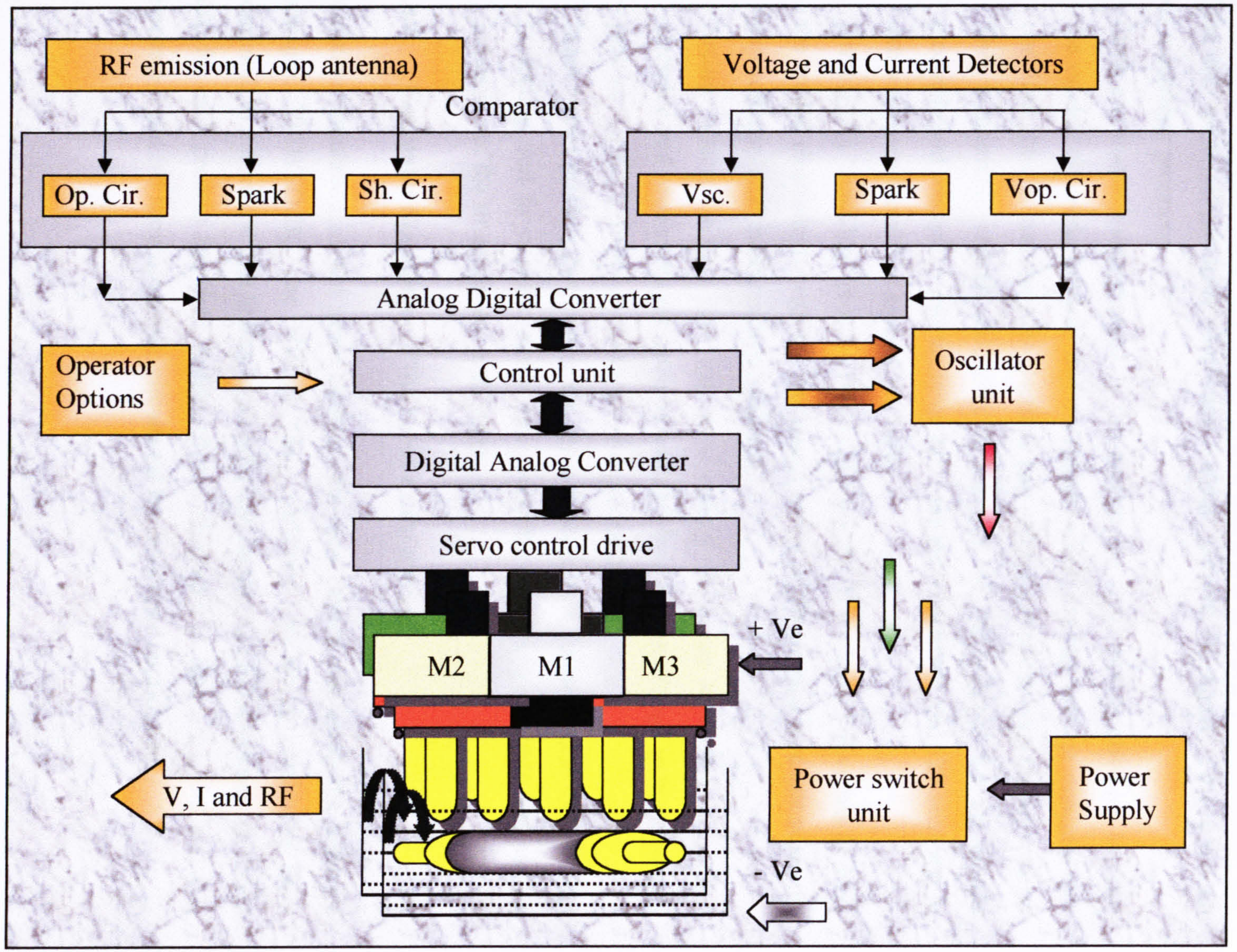

Figure 6-3 Digital to analogue unit for the proposed Electro Discharge Machining servo control unit

6.3.3 Principles of Operation of the Unit

The principles of operation of the EDM-servo control system are based on the variation of the inter-electrode gap spark parameters (voltage, current, RF signal). There are main four machining processes.

- Open circuit-machining process. In this process the servo control drive has to drive the eroded electrode towards the workpiece, when the gap voltage indicates this condition. In this case the inter-electrode gap voltage called the open circuit voltage. This is normally chosen according to the type of the material for the eroded electrode and workpiece. Normally its value ranges between 40 and 120 volts and in extreme cases it could be around 300 volts.
- Discharging "sparking" process. In this process the servo control drive has to drive the eroded electrode towards the workpiece with a predetermined feed rate when the gap voltage signal indicates, this condition.
- Arcing process. In this case the servo control drive has to retract the eroded electrode and reverse the direction of motion when the gap voltage indicates arcing process. This is followed by new cycle for processing.
- Short circuit process. In this case the servo control drive has to initiate the essential protecting unit to stop the motor and gives the operator an audible and visible indication of the situation (alarm & light).

6.3.4 Computer Simulation of the Servo Control Unit

Computer simulation of the servo control unit was carried out using the software packages, VIEWLOGIC and VHDL. Many different machining conditions were examined, to ensure the unit ability to monitor and control the EDM-system. The truth table for each process has been developed and illustrated in tables 6-1, 6-2 and 6-3. Figures 6-4 and 6-5 show electronic circuits for the developed control unit.

Table 6-1 Truth table for the open circuit machining process of the EDM-system computer simulation

Inputs	Case1	Case2	Case3	Case4	Outputs
A1	**0**	**0**	**0**	**0**	**S1**
A2	**0**	**1**	**1**	**0**	**SS1~SS3**
A3	**0**	**0**	**0**	**0**	**SS1~SS3**
A4	**0**	**0**	**0**	**0**	**S2**
A5	**0**	**0**	**0**	**0**	**S2**
A6	**0**	**0**	**0**	**0**	**S6/S7**

Table 6-2 Truth table for the discharging machining process of the EDM-system computer simulation

Inputs	Case1	Case2	Case3	Case4	Outputs
A1	**0**	**1**	**1**	**0**	**S1**
A2	**0**	**1**	**1**	**0**	**SS1~SS3**
A3	**0**	**0**	**0**	**0**	**SS1~SS3**
A4	**0**	**1**	**1**	**0**	**S2**
A5	**0**	**0**	**0**	**0**	**S2**
A6	**0**	**0**	**0**	**0**	**S6/S7**

Table 6-3 Truth table for the short circuit machining process of the EDM-system computer simulation

Inputs	Case1	Case2	Case3	Case4	Outputs
A1	**0**	**0**	**0**	**0**	**S1**
A2	**0**	**0**	**0**	**0**	**SS1~SS3**
A3	**0**	**0**	**0**	**0**	**SS1~SS3**
A4	**0**	**0**	**0**	**0**	**S2**
A5	**0**	**1**	**1**	**0**	**S2**
A6	**0**	**1**	**1**	**0**	**S6/S7**

Figure 6-4 shows the analogue to digital circuit and Figure 6-5 shows the digital to analogue circuit. Where, A1, A2, A3, A4, A5 and A6 are the output conditions obtained form the analogue to digital converter of the servo control system. Case (1), case (2), case (3) and case (4) are the conditions for machining. S1, ss1~ss3, ss1~ss3, s2, s6/s7 are the power MOSFET switching unit which is used as an interface unit between the control unit, power supply, piezoelectric USM drive, protection, audible and visible unit of the system.

Figures 6-6 (a), (b) and (c) show the initial results from the analogue unit simulation for different machining processes. Three voltage were used as a reference voltage for the four processes of the EDM system which were V_{r_1}, V_{r_2} and V_{r_3}. According to the voltage in the inter-electrode gap V_g the servo control system generates the processing parameters that commanded power supply and the drive to move with the appropriate feed rate and direction of motion.

In the case of $V_{r_1} > V_g > V_{r_2}$, as shown in Figure 6-6 (a), the condition is an open circuit. The motor is activated in a forward direction and drives the eroded electrode into the workpiece with a maximum feeding rate.

In the case of $V_{r_2} > V_g > V_{r_3}$, as shown in Figure 6-6 (b), the condition is a discharging process. The servo control system activates the servo control unit commands power supply and the drive to move with the appropriate feed rate and direction of motion.

In the case of $V_{r3} > V_g$, as shown in Figure 6-6 (c), the condition is either the arcing or short-circuiting process.

In the case of arcing process the servo control system activates the backward direction of motion, and retracts the eroded electrode to the starting position for a new cycle of processing. In the case of short circuit the servo control system, stops the power and activates the protection, audible and visible units.

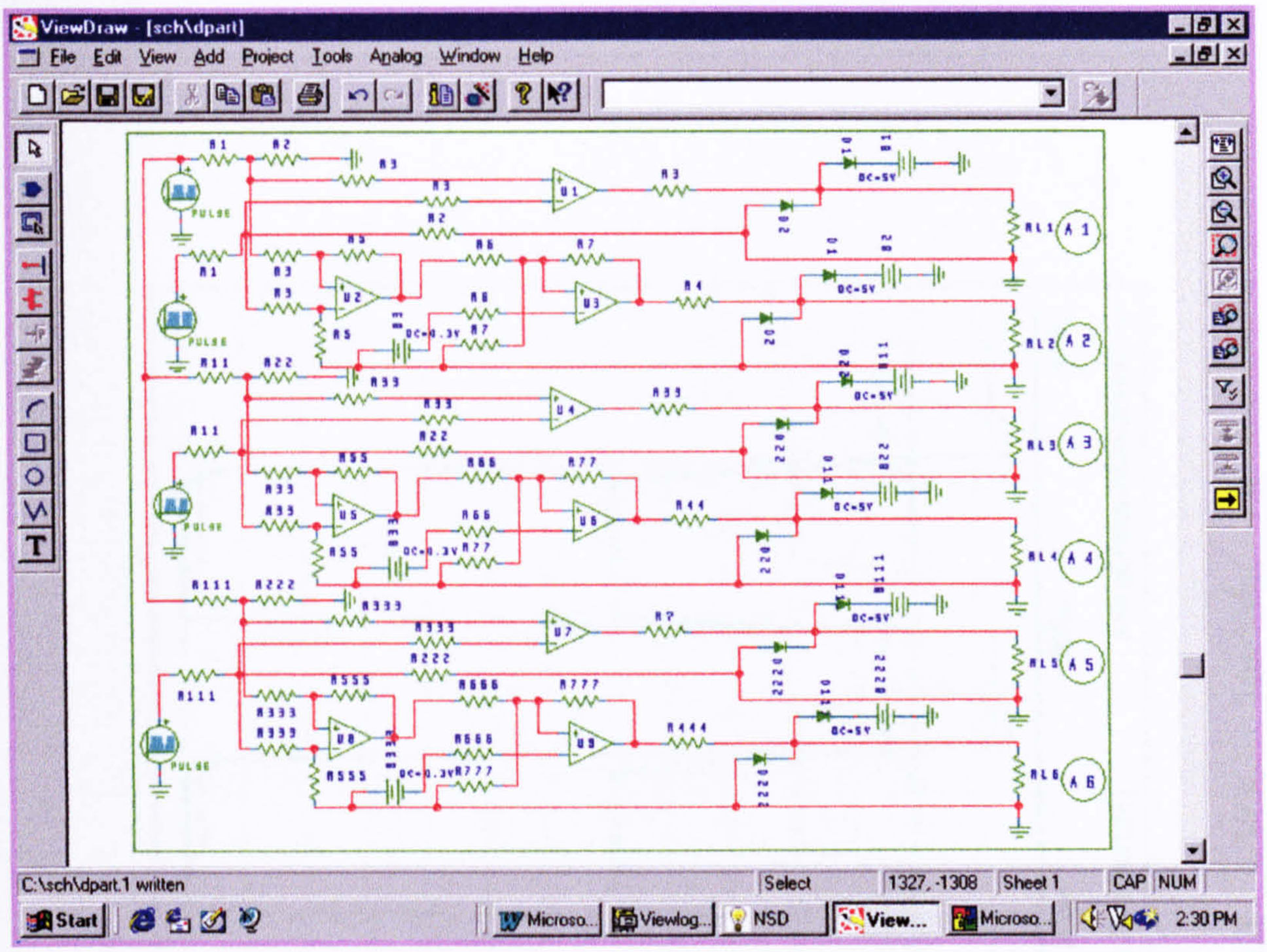

Figure 6-4 Developed circuit for the A/D of an EDM servo control system

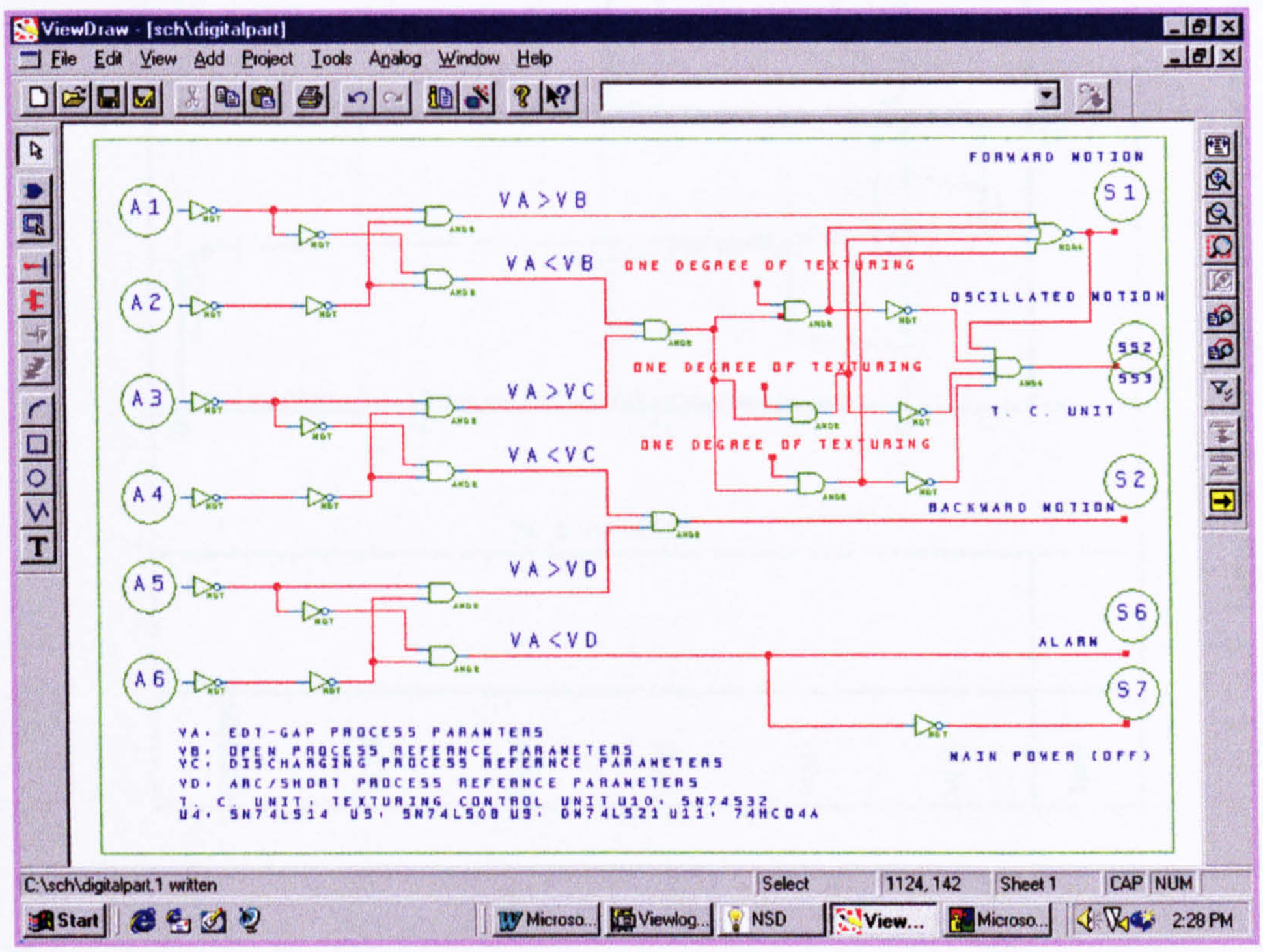

Figure 6-5 Developed circuit for the processing unit and D/A unit of the EDM servo control system

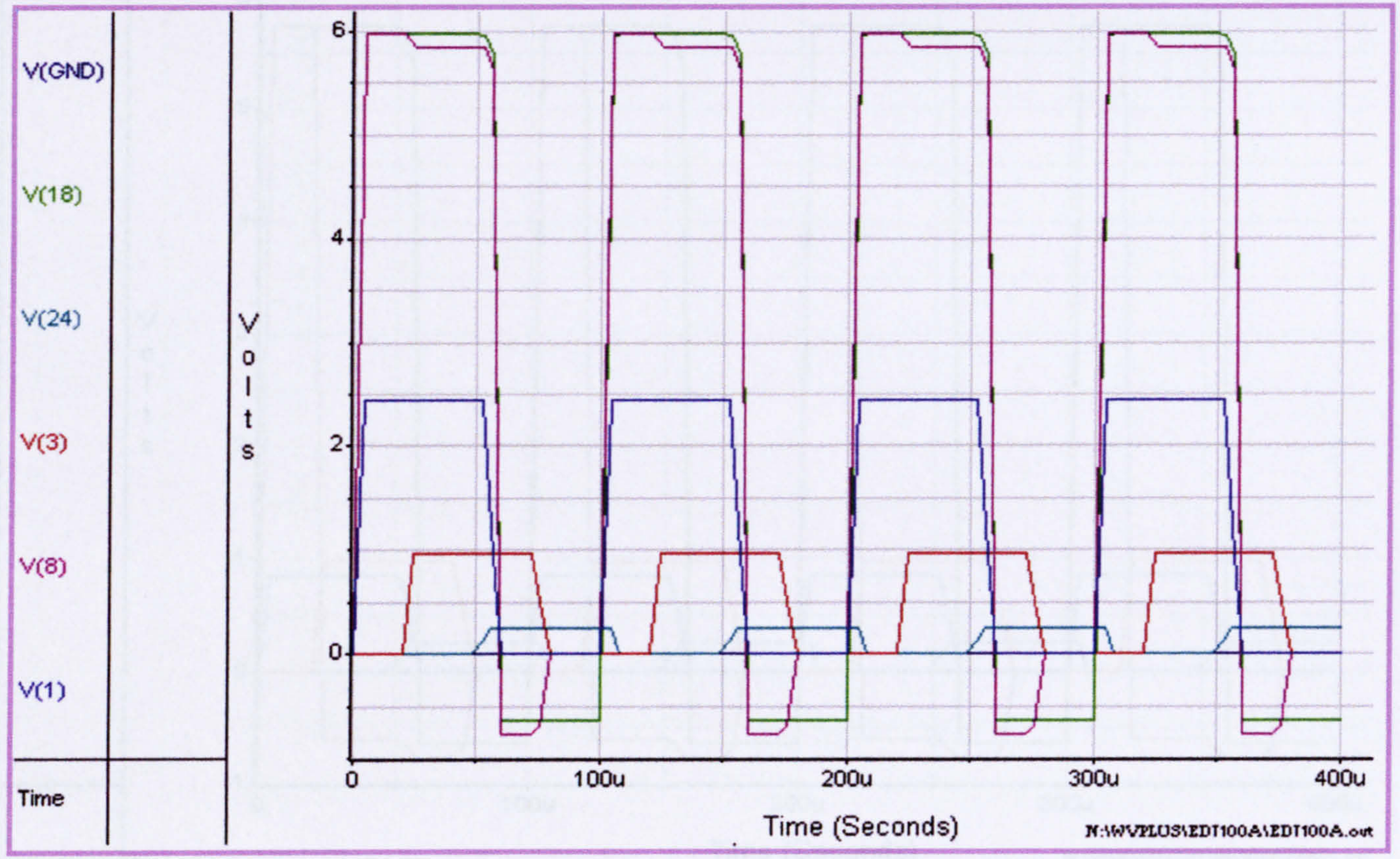

Figure 6-6. (a) Open circuit process, [Vr1(__), Vr2(__), Vr3(___) and Vg(___)]

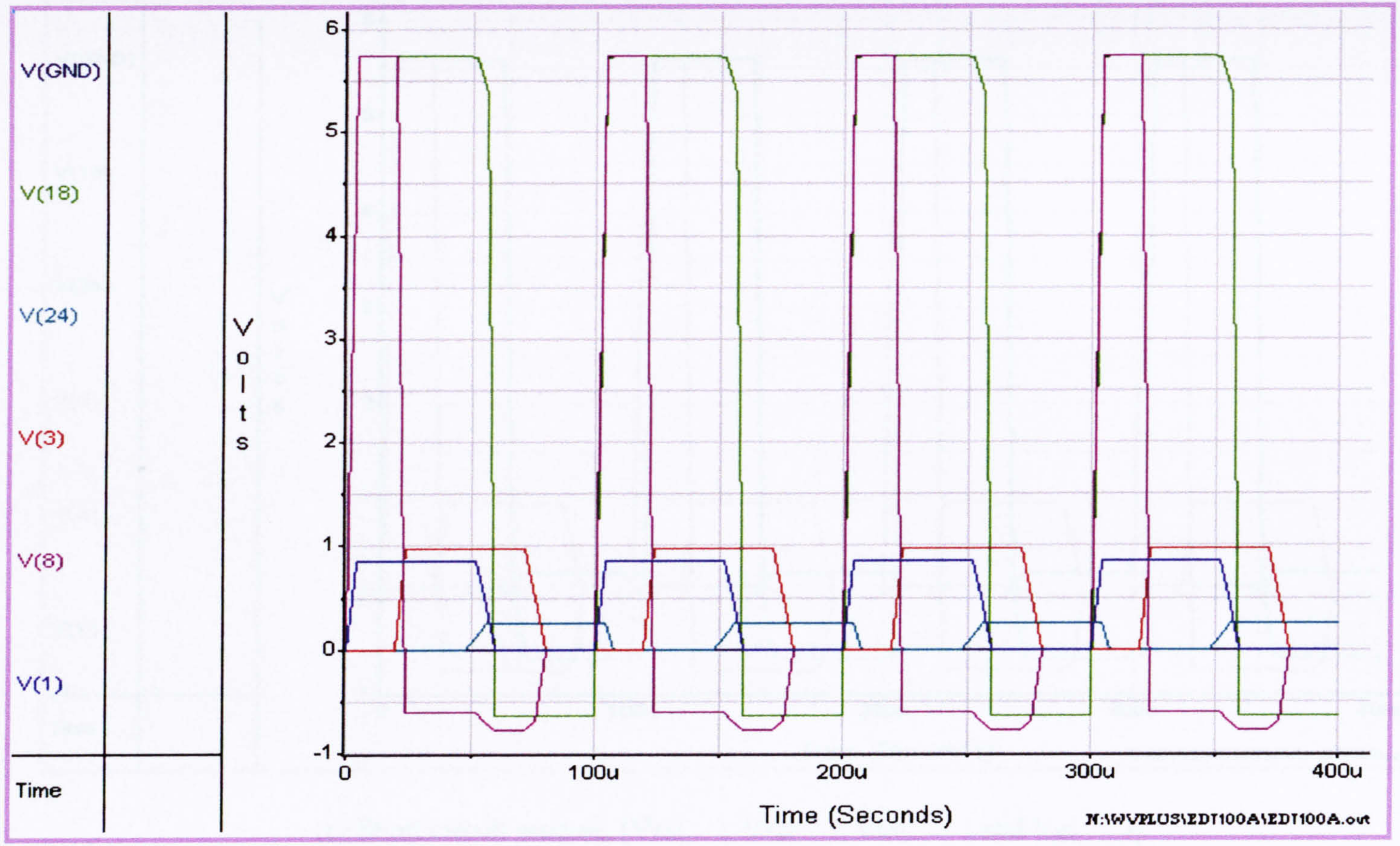

Figure 6-6. (b) Discharging process, [Vr1(__), Vr2(__), Vr3(___) and Vg(___)]

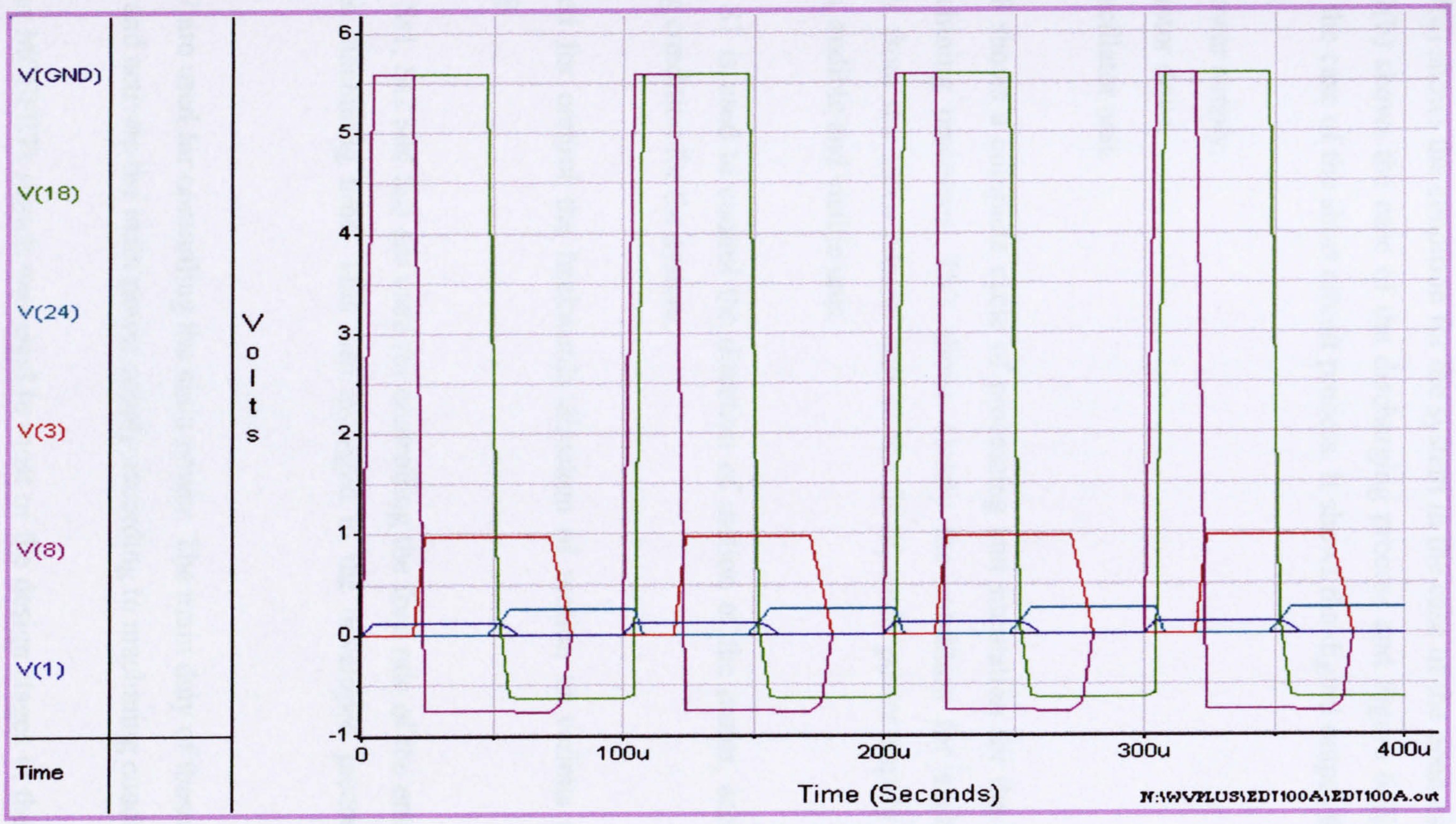

(c) Short circuit process, [Vr1(__), Vr2(__), Vr3(__) and Vg(__)]

Figure 6-6. Computer simulation for the analogue part of EDT servo control unit (a) sensor output volt <=100 (b) sensor output volt <=40% (c) sensor output volt <=10% of

Figures 6-7 (a), (b) and (c) show the initial results from the digital unit simulation for the EDM-system main machining process.

Figure 6-7(a) shows the condition for the system in the case of the open circuit process. Figure 6-7(b) shows the case of the discharging process and Figure 6-7(c) shows the system in the case of the short circuit process. It shows the digital output that is used to command:

- The power supply,
- The motor drive,
- The oscillator unit.

Figure 6-8 shows a complete cycle of processing and simulation for the EDM-system main machining processes. This shows clearly the condition for each switch and commands from the servo control unit to the drive, main power supply control unit, protection, audible and visible unit.

Switches S1 is used to control the direction of motion of the motor, according to the machining condition for the system.

Ss is used for control the backwards direction of motion in various conditions of machining.

Switches Ss1, Ss2 and Ss3 are used for controlling the feed rate of the eroded electrode during the machining time. This was arranged in the developed piezoelectric USM drive.

S6 and S7 are used for controlling the main power. The main duty of these two switches is to stop and activate the main power supply according to machining conditions.

The power MOSFETs switch was used in most of the design stages in the system as an interface unit. This shows close agreement with the developed system using piezoelectric USM response time.

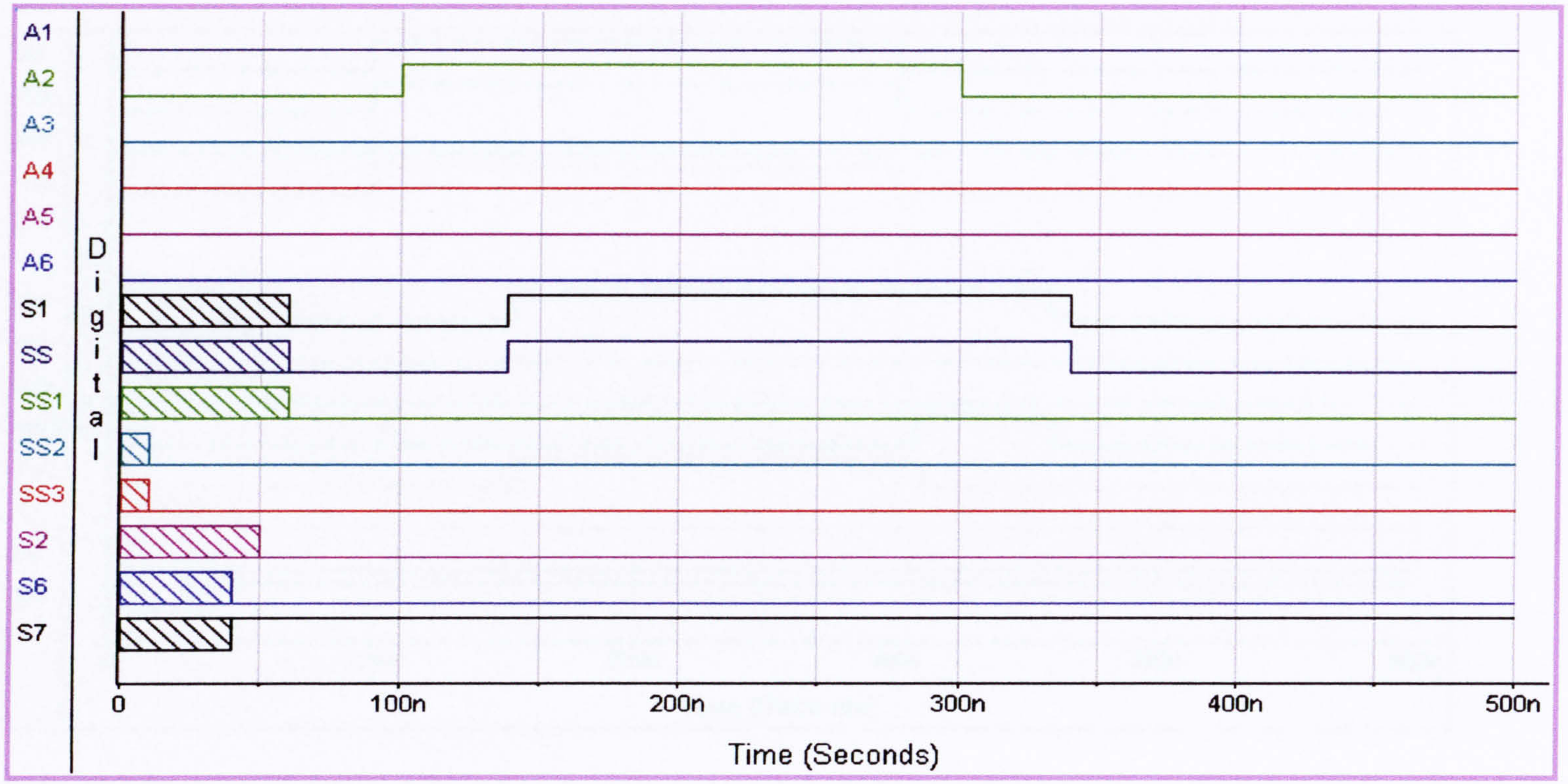

Figure 6-7 (a). Open circuit process

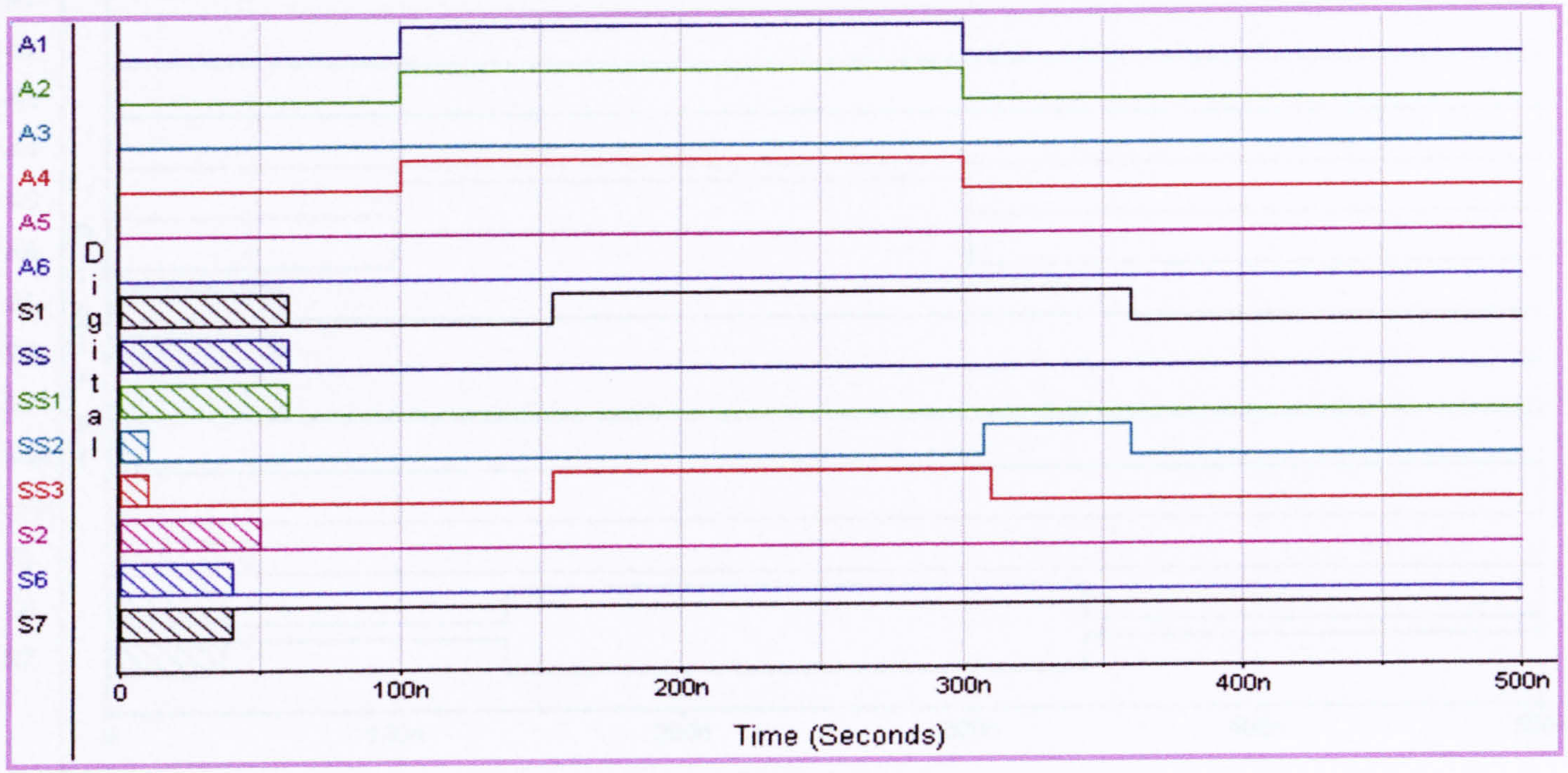

Figure 6-7 (b). Discharging process

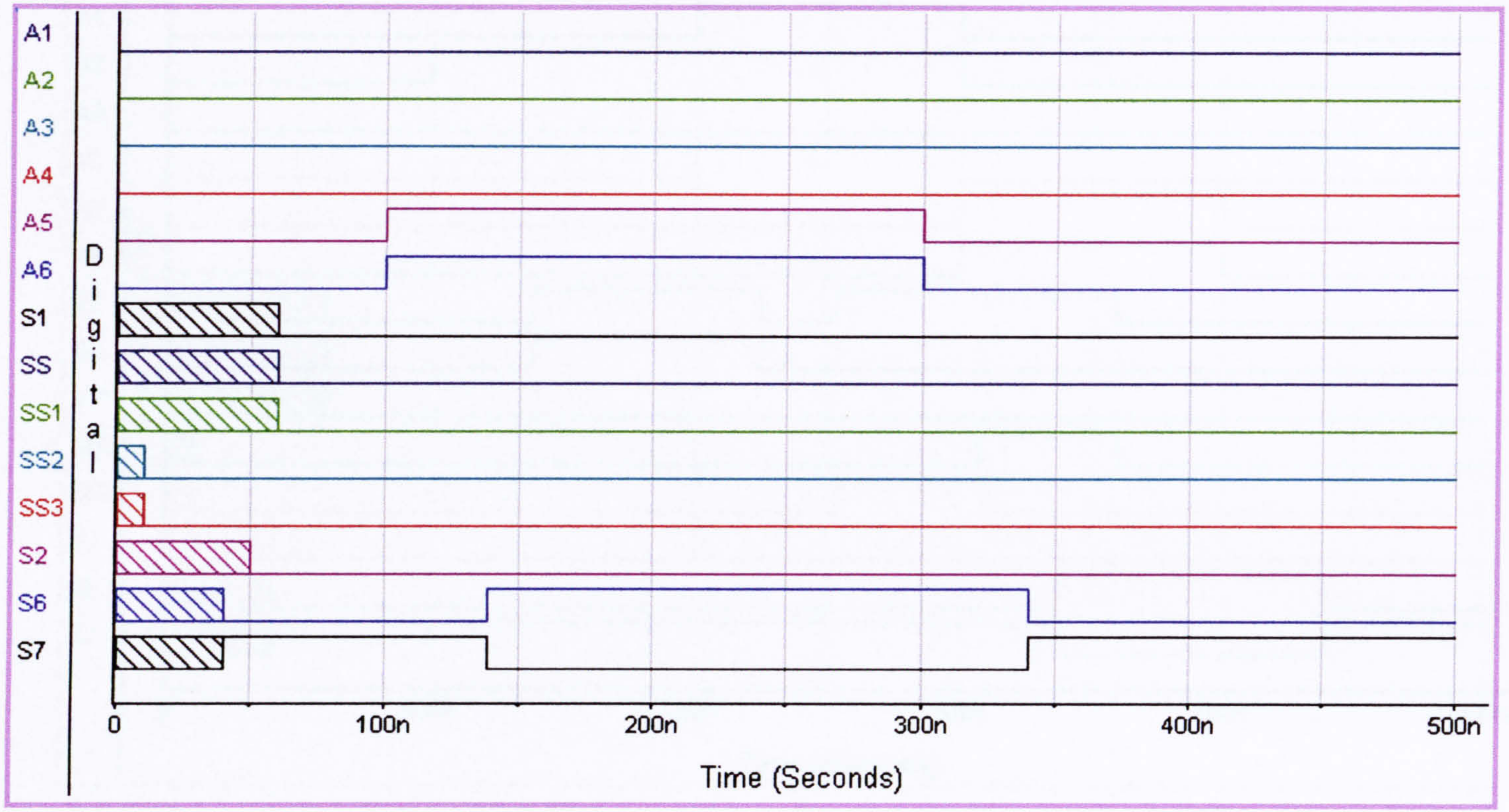

(c). Short circuit process

Figure 6-7 Computer simulation results for digital unit of EDT-Industrial application servo control unit (a) is the open circuit (b) is the texturing (c) is the short circuit situation

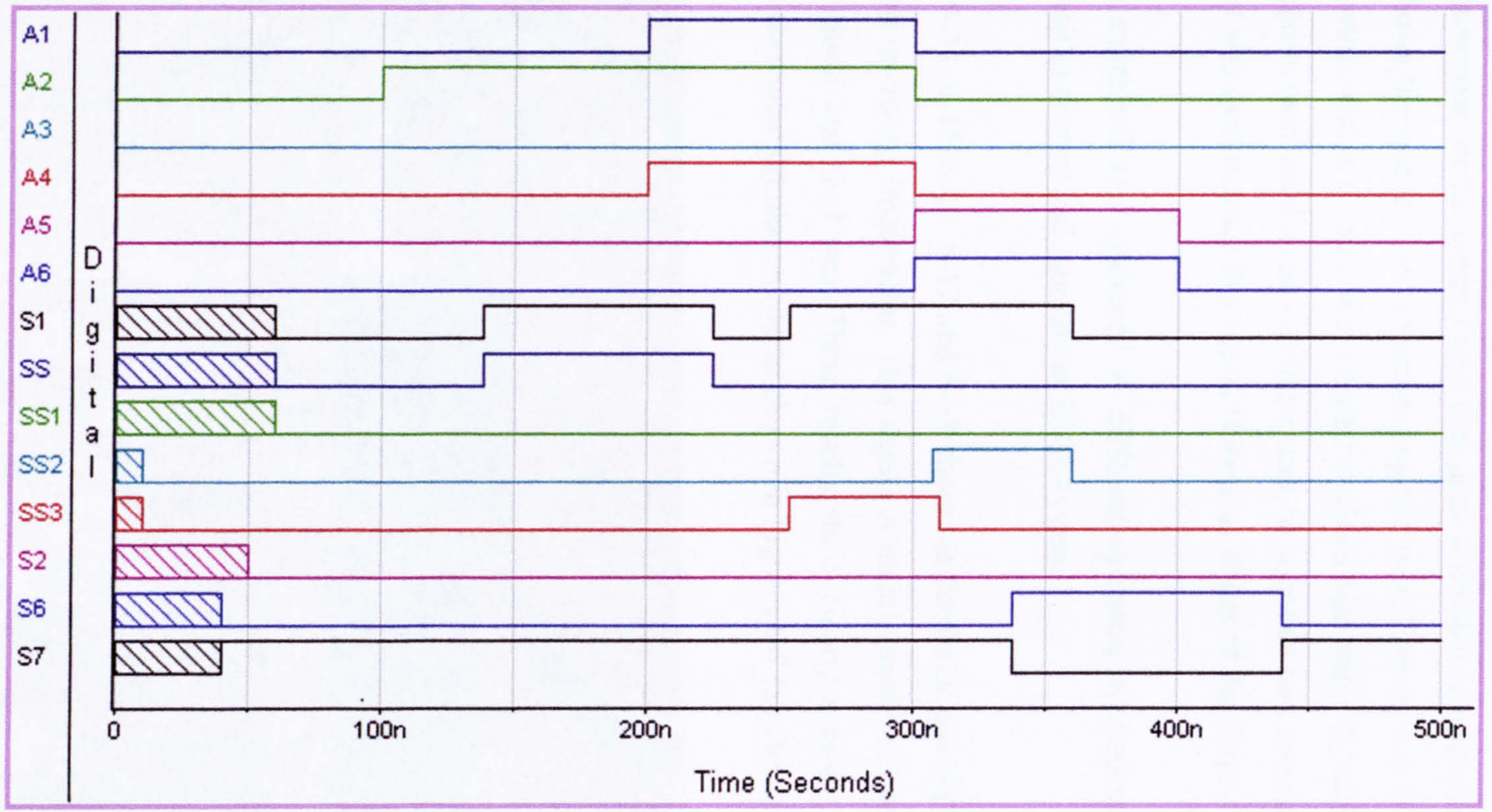

Figure. 6-8 Computer simulation for digital unit of EDT- application servo control unit for a complete cycle of operation

6.4 EXAMINATION OF DEVELOPED UNIT

The developed control unit was examined for various conditions of machining. Figure 6-9 shows a prototype for the control unit that uses solid-state electronic components. Figure 6-10 shows the system used in examining the unit. This system consists of two function generators and a display unit (digital oscilloscope and PC computer). Two function generators were used as an oscillator unit, to generate two testing signal. Then the display unit was used to trace this signal at various stages of the control unit.

The unit was examined and evaluated at different operating frequencies to test the ability of the unit to control and monitor an EDM-system.

Figures 6-13, 6-14, 6-15, 6-16, 6-17 and 6-18 show the feedback control signal for the unit at different operating frequencies. This signal is mainly used to control the motor direction of motion and feed rate. These results show clearly a close agreement in comparison to computer simulation results shown in Figures 6-7 (a), (b), (c) and 6-8.

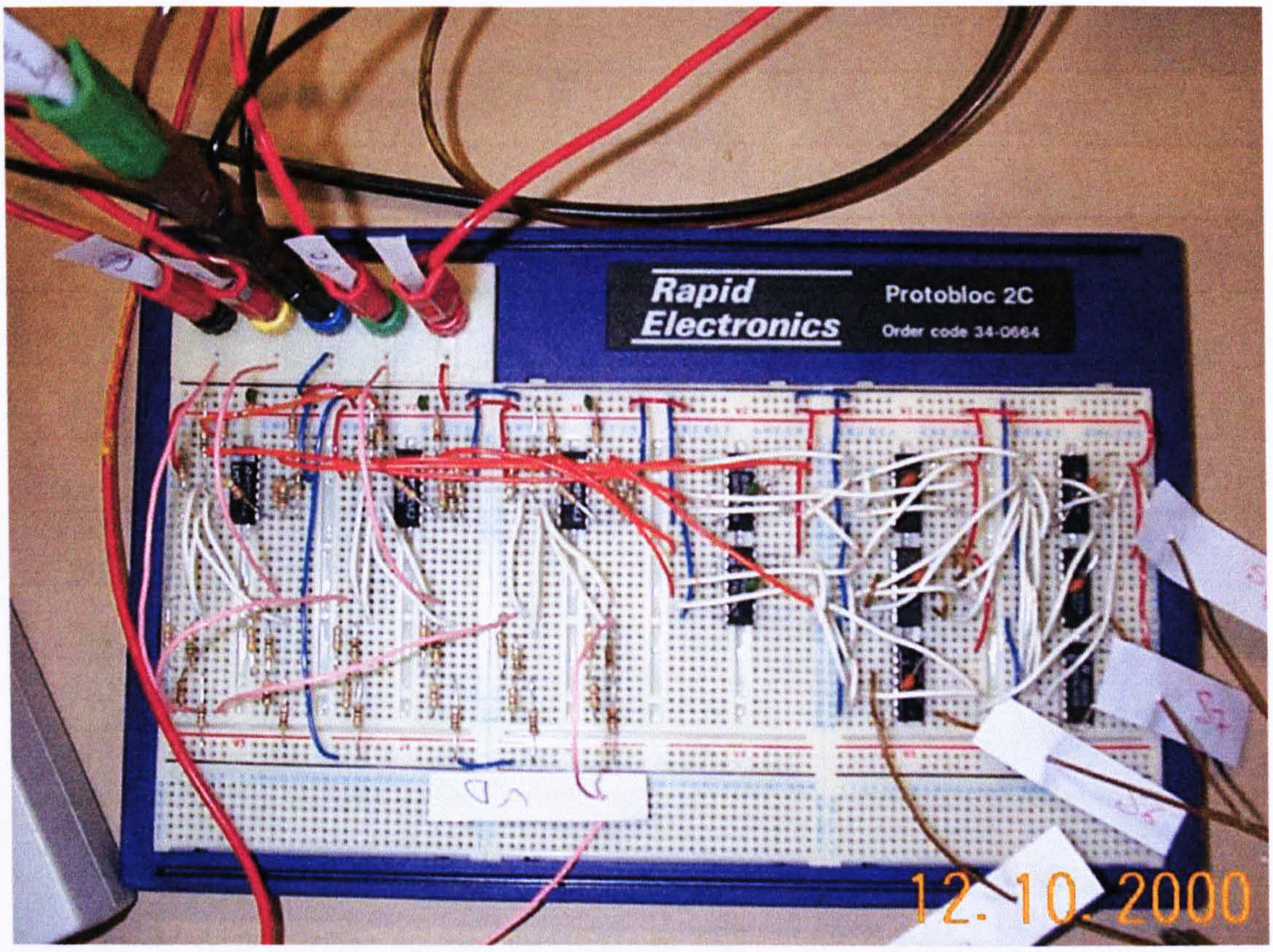

Figure 6-9 Prototype for the developed EDM servo control unit using piezoelectric USM for the gap voltage

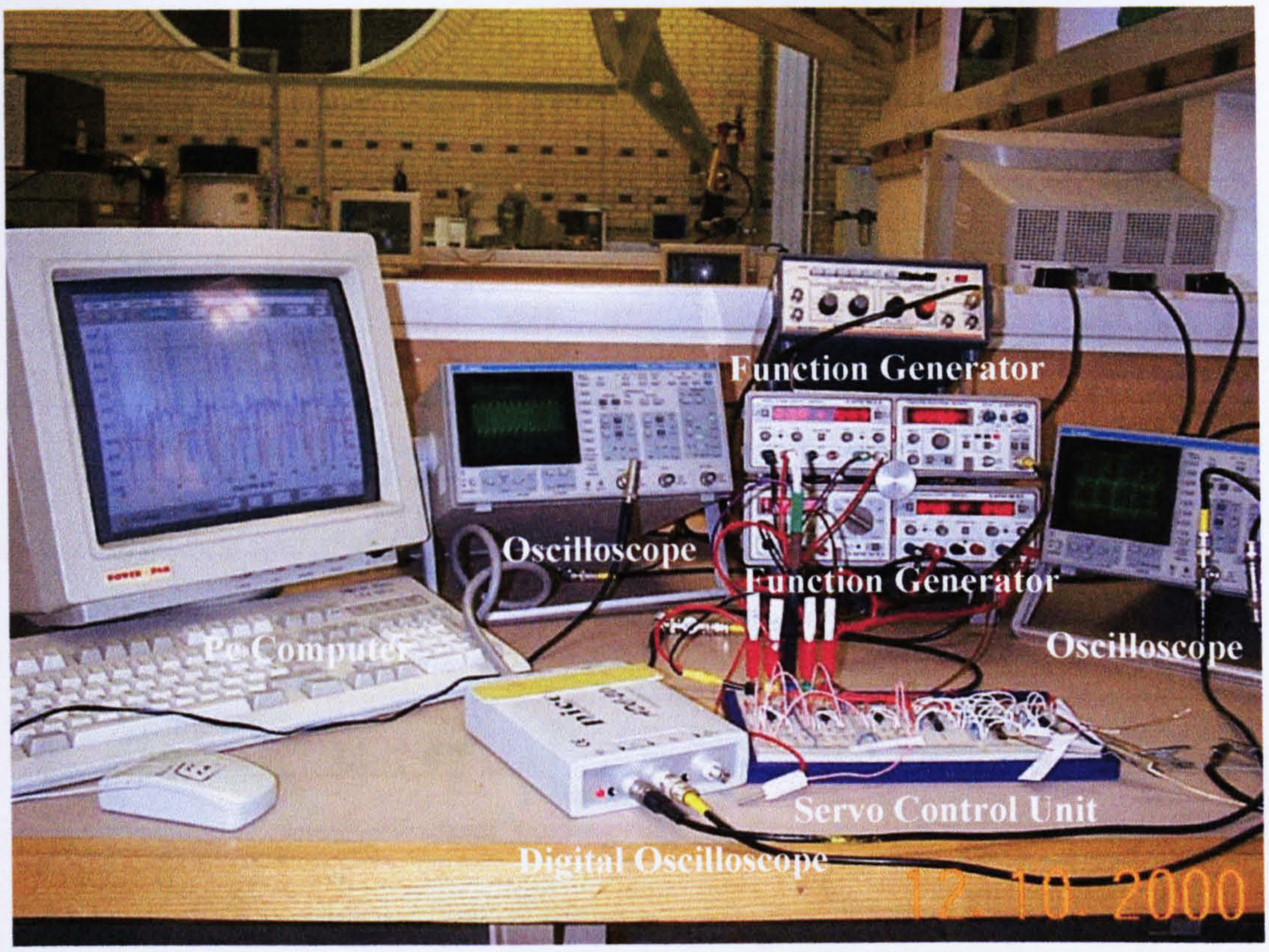

Figure 6-10 Main equipment used to examine the developed EDM servo control unit

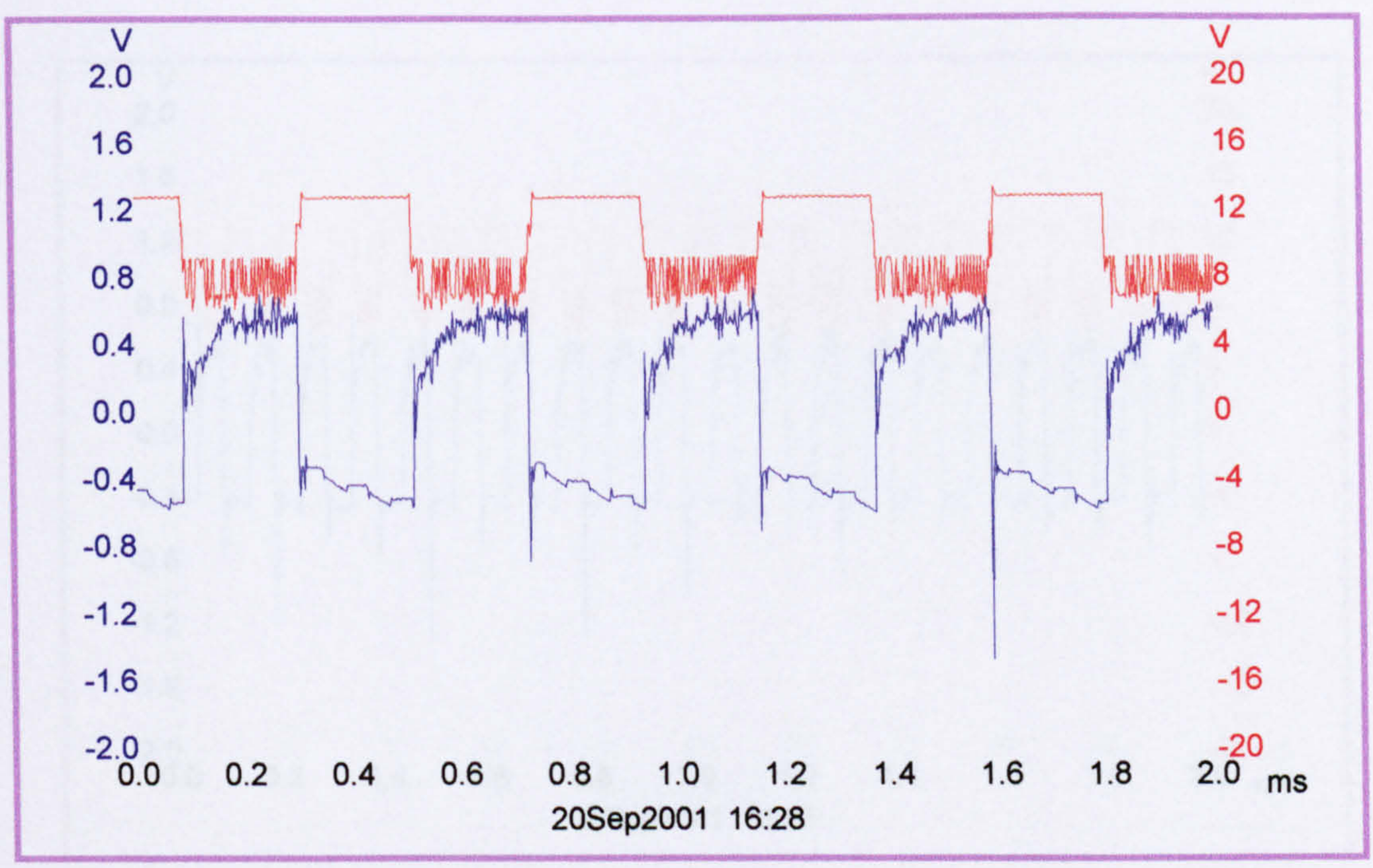

Figure 6-11 The output signal of the servo unit used to control the forwards and backwards motion of the system for different manufacturing process [frequency 2.34 kHz]

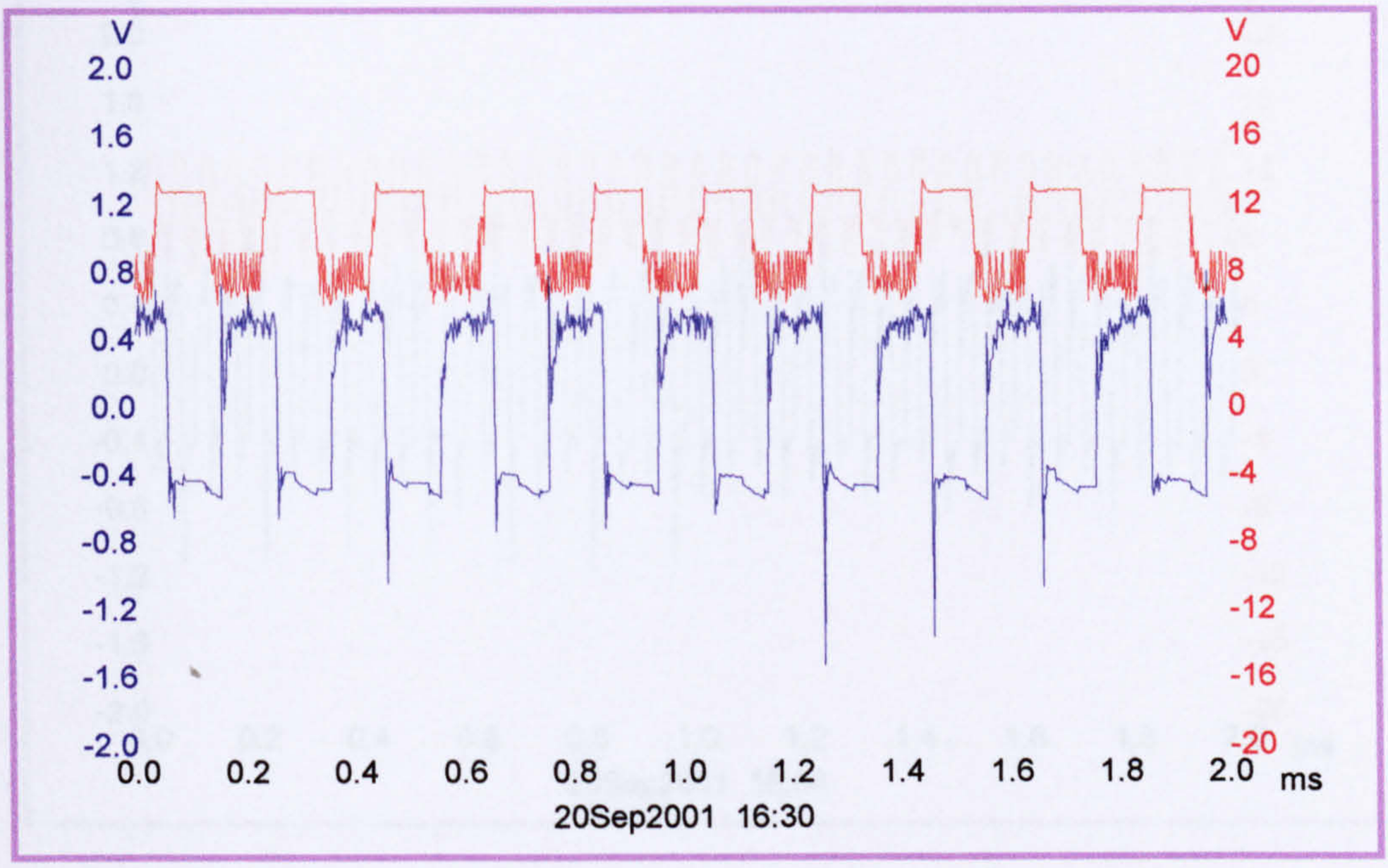

Figure 6-12 The output signal of the servo unit used to control the forwards and backwards motion of the system for different manufacturing processes [frequency 5 kHz]

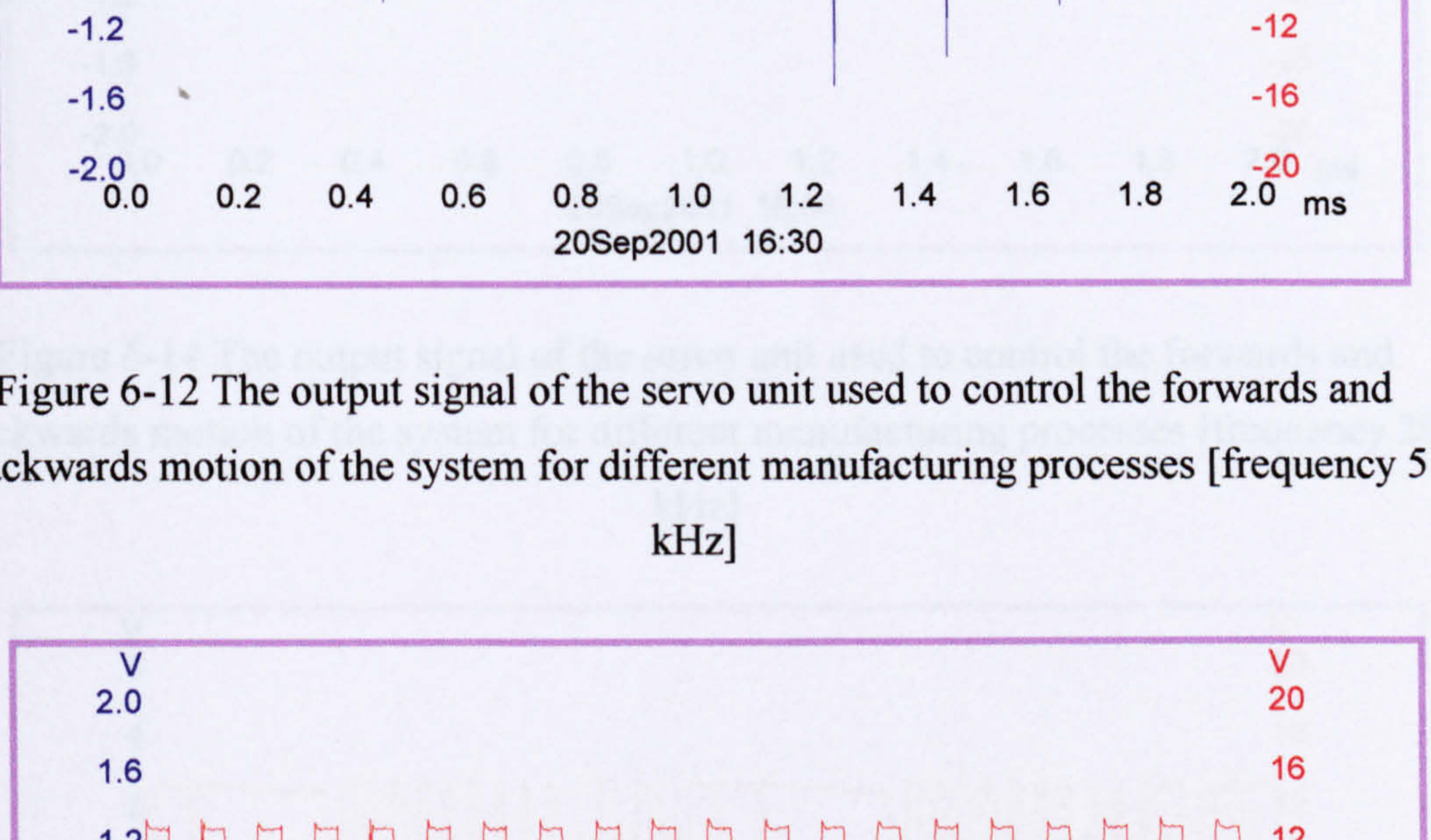

Figure 6-13 The output signal of the servo unit used to control the forwards and backwards motion of the system for different manufacturing processes [frequency 10 kHz]

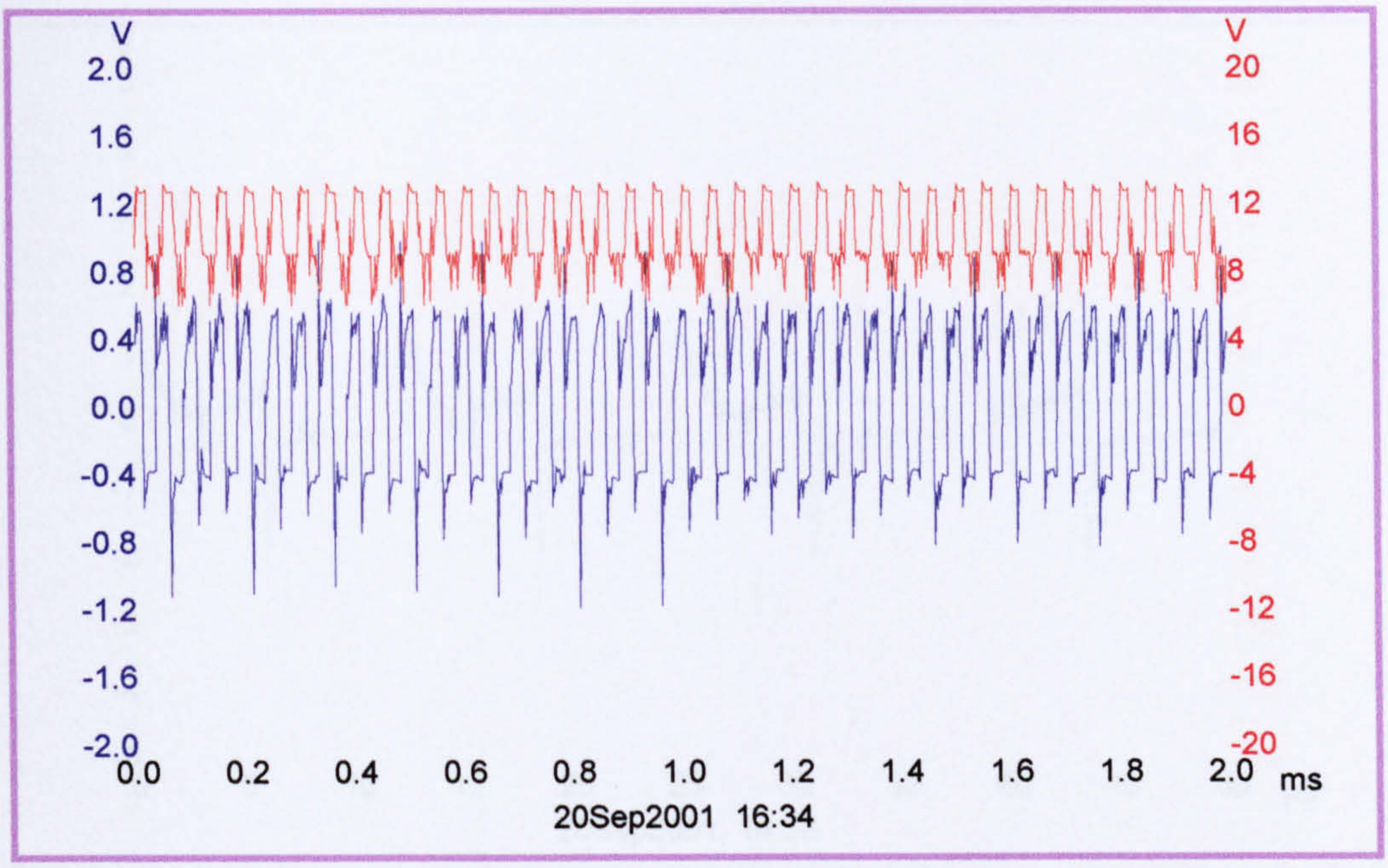

Figure 6-14 The output signal of the servo unit used to control the forwards and backwards motion of the system for different manufacturing processes [frequency 20 kHz]

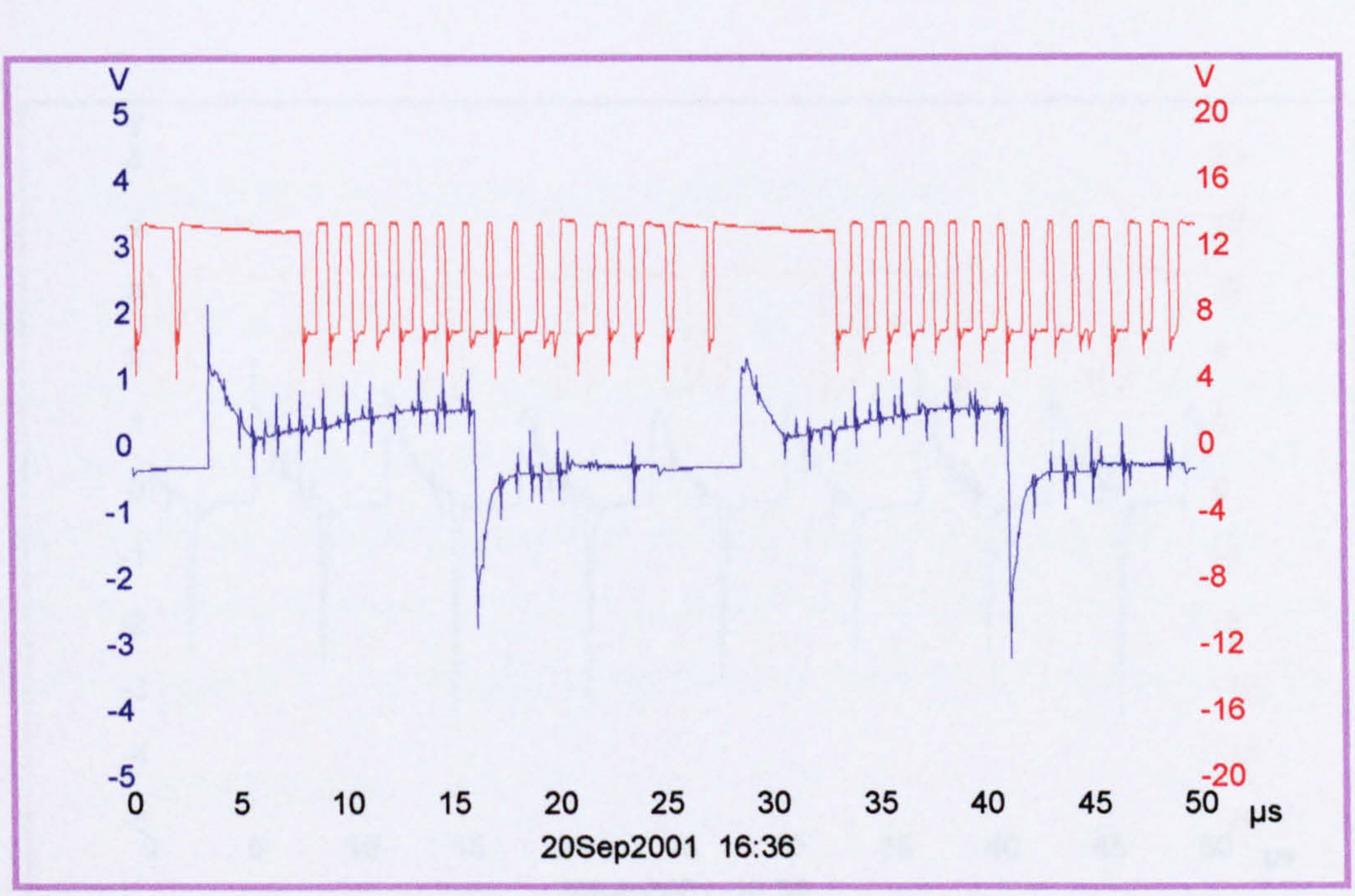

Figure 6-15 The output signal of the servo unit used to control the forwards and backwards motion of the system for different manufacturing processes [frequency 40 kHz]

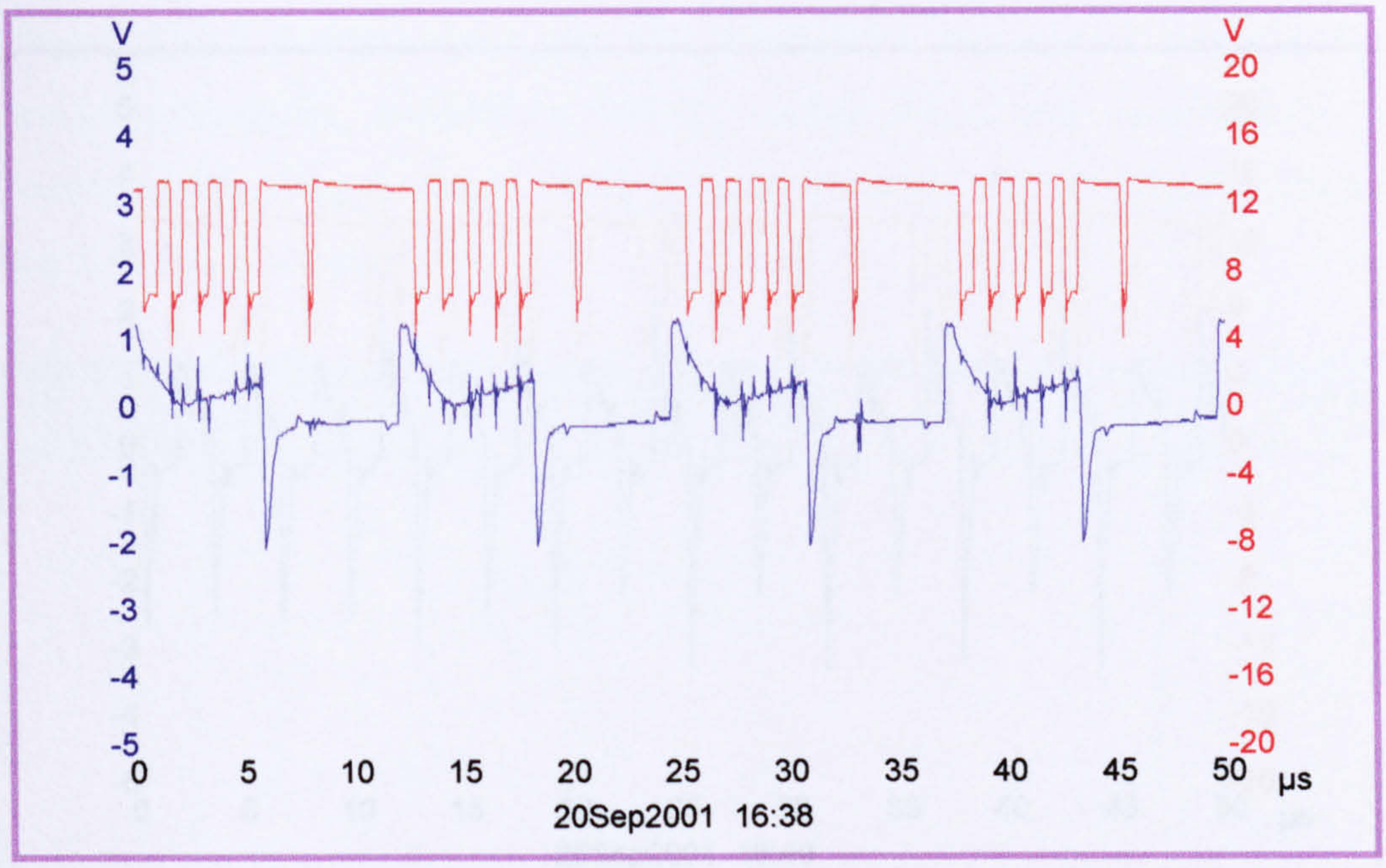

Figure 6-16 The output signal of the servo unit used to control the forwards and backwards motion of the system for different manufacturing processes [frequency 80 kHz]

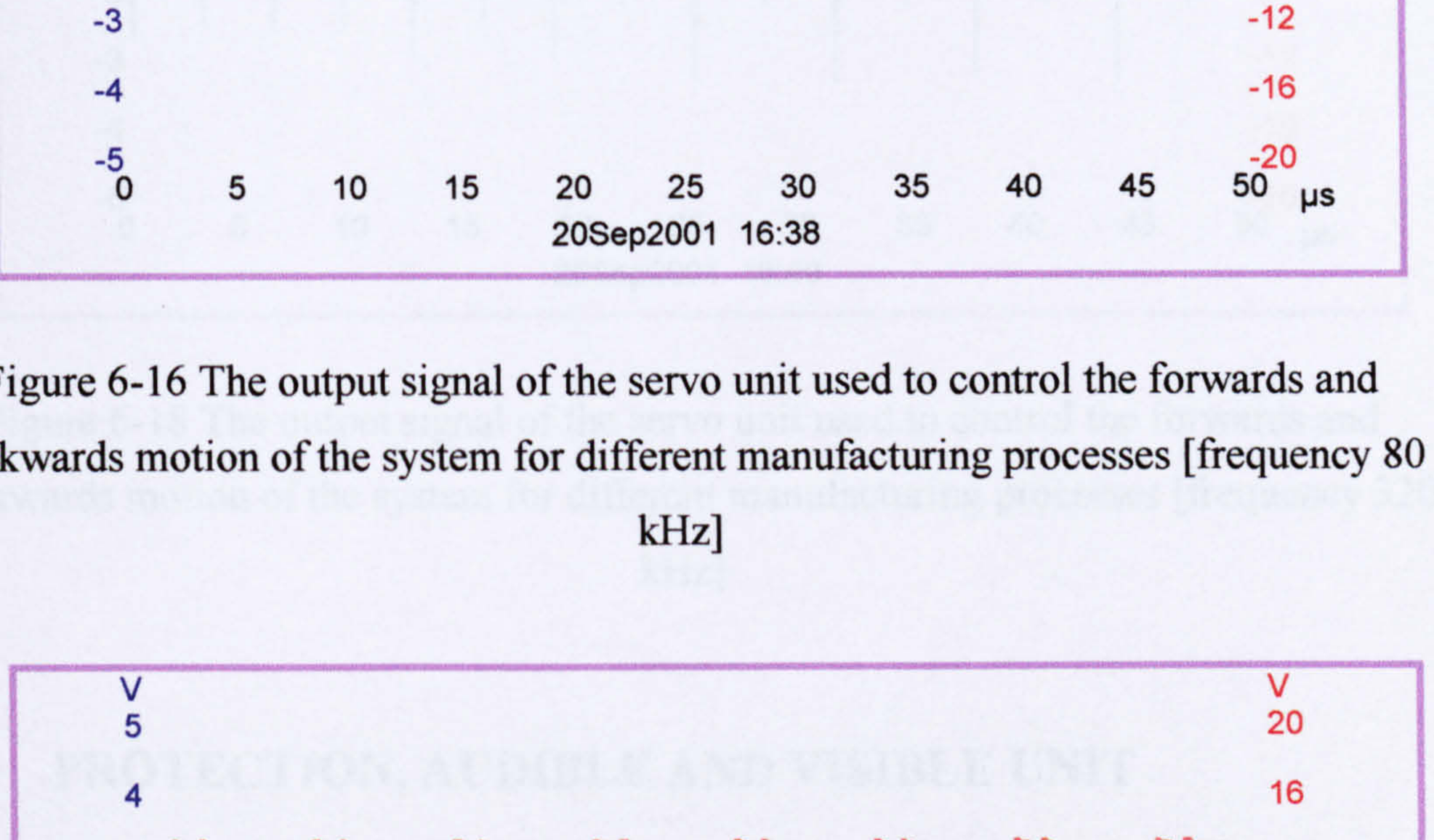

Figure 6-17 The output signal of the servo unit used to control the forwards and backwards motion of the system for different manufacturing processes [frequency 160 kHz]

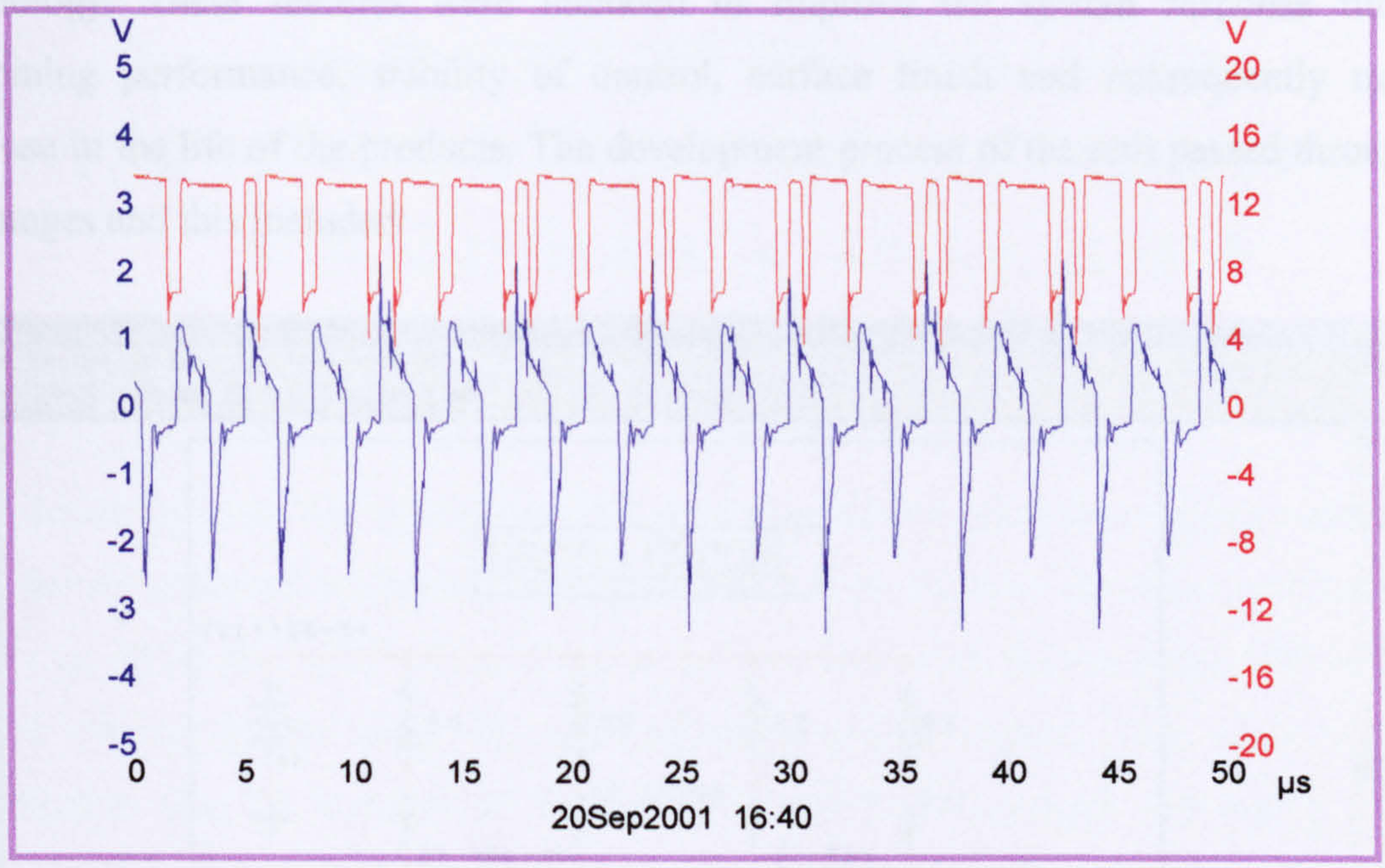

Figure 6-18 The output signal of the servo unit used to control the forwards and backwards motion of the system for different manufacturing processes [frequency 320 kHz]

6.5 PROTECTION, AUDIBLE AND VISIBLE UNIT

Finally a protection, audible and visible unit was developed and integrated into the system. The developed unit electronic circuit is shown in Figure 6-19. The circuit is a part of the servo control unit. It is designed to provide a visible light with different colours to show the processing conditions running. For the arcing and the short circuit processes circuit was designed to provide an audible and visible alarm and to protect the whole system against fire by stopping the system and restarting a new processing cycle.

6.6 CONCLUSION

An integration of the developed servo control feed drive system into the EDM system has been carried out. The required modification to integrate and examine the developed drive using piezoelectric USM in EDM system is carried out and presented in this chapter. This was included the control unit, the feedback unit, the tolerance unit, the circuit protection unit, audible and visible unit. The developed unit offers features that

were not possible to obtain using current control system using DC servomotor technology. These features were intended to improve the system response time, machining performance, stability of control, surface finish and consequently may increase in the life of the products. The development process of the unit passed through few stages and this included:

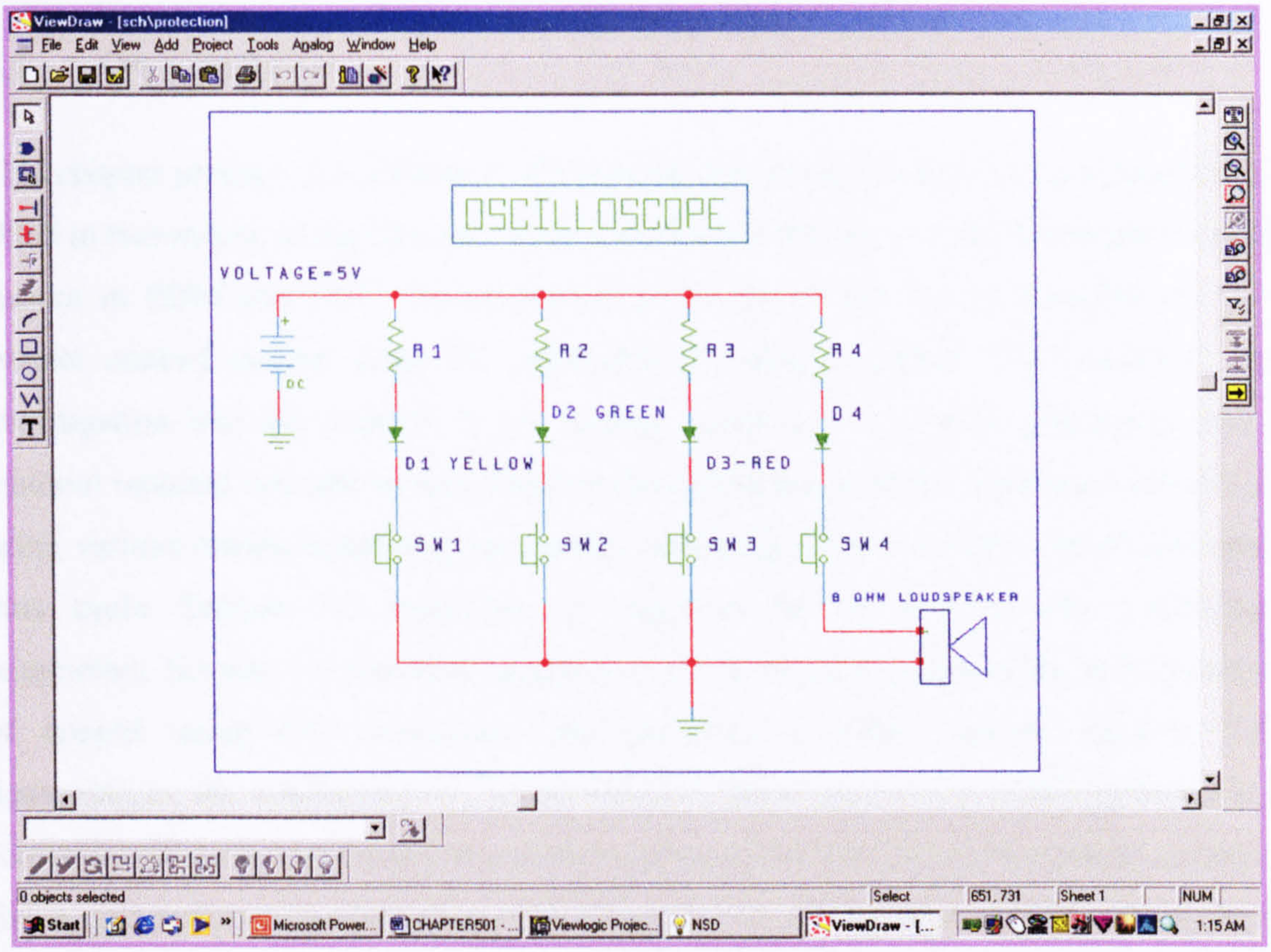

Figure 6-19 The protection, audible and visible circuit used for the developed EDT-system

- Computer simulation of the developed unit was carried out using VIEWLOGIC and VHDL software. The inter-electrode gap voltage variation was used and discussed in this simulation. The initial results showed the ability of the developed system to control the EDM-system main machining process.
- Developments of a tolerance unit that also provided the developed servo control system with the required degree of accuracy and safety.
- Development of a protection, audible and visible unit.

CHAPTER 7

7 VALIDATION OF THE DEVELOPED PIEZOELECTRIC SERVO CONTROL FEED DRIVE IN EDM-INDUSTRIAL APPLICATIONS

7.1 OVERVIEW

This chapter presents the validation of the developed control system using piezoelectric USM in two industrial applications. It presents a demonstration of the developed control system in EDM and EDT. An evaluation of the developed system compared to the current control system using DC servomotor is also presented. This included, an investigation into the stability of the system, capability of control, processing time, material removal rate and surface finish of the machined products. This was carried out using various electro-machining parameters, including level of current, on/off time and duty cycle. Section 7-2 introduces an overview for the EDM-system machining parameters. Section 7-3 provides equipment used in this investigation for both systems of control using DC servomotor and piezoelectric USM system. Section 7-4 demonstrates the application of the developed control system on EDM applications. Experimental examination and discussions included the stability of the system, surface finish, and material removal rate is presented. Section 7-5 demonstrates the application of the developed control system in EDT applications. Experimental examination and discussions included the stability of the system, surface finish, and processing time is presented. This chapter concludes with an overview for the features obtained using developed piezoelectric servo feed drive system.

7.2 EDM MACHINING PARAMETERS

In EDM machining, dynamic response, the level of precision of the servo drive and the selection of machining parameters of the system are the most important parameters used to control machining conditions, accuracy, material removal rate, machining time and surface finish of machined products.

The previous research [Shafik, M., et al., 2001, Simao, J., et al., 1996, McGeough, J. and Rasmussen, H., 1992, El-Menshawy, F. and Ahmed, M. S., 1985] carried out in studying this technique of machining show, that the parameters of machining for this system were classified as follows, four of them were named as a 'planning parameters' and are dependent on the kind of machining operation. These parameters are polarity, open-circuit or no load voltage, discharge current and pulse duration.

The remainder of these machining parameters are called 'the adjusted parameters' which are used to give the best operating conditions. These parameters include material of the tool electrode, pulse interval, inter-electrode gap and circulation rates. The pulse interval, gap control and circulation are normally called 'operating parameters' which in modern machine are automatically monitored and corrected.

Previous work [McGeough, J. and Rasmussen, H., 1992, El-Menshawy F. and Ahmed, M. S., 1985] showed that the level of the current, on-off time and frequency of the spark were the major factors influence the material removal rate of the machining system and surface finish of machined products [appendix (C)]. In this investigation these electro-machining parameters were used to evaluate the developed control system using piezoelectric USM when compared to the current system using DC servomotor. The others parameters which named adjusted parameters were elected as follows:

- Machining conditions selected as a copper to steel,
- Pulse interval of the order of 12 μsec,
- Gap voltage of the order of 38 volt, and
- Gap current of the order of 5 amperes.

7.3 EQUIPMENT USED

The installation of the developed control system using piezoelectric USM passed through many stages. The system was integrated and tested statically as discussed in chapter 6. Then a modification to some of the system units was carried out. Then the developed system was re-integrated and installed successfully in the EDM-Machine as shown in Figures 7-1 and 7-2. Figure 7-1 shows the system arranged for EDM normal machining. Figure 7-2 shows the system arranged for EDT machining.

A list of the equipment used in this investigation using both systems for control was as follows:

- A Normal EDM-machine arranged for EDM and EDT machining as shown in Figures 7-1 and 7-2,
- DC servomotor as shown in Figure 7-3,
- DC motor drive,
- Linear piezoelectric USM as shown in Figure 7-3,
- Piezoelectric motor drive,
- Function generator,
- Directional control unit,
- Programmable power supply,
- Dielectric oil system,
- EDT-system as shown in Figure 7-2,
- Roll mounted into the EDM machine as shown in Figure 7-2,
- Ultrasonic drive of five heads as shown in figiure 7-2,
- Roll drivers,
- Two DC motors,
- Fire extinguisher,
- Digital oscilliscope,
- Laptop,
- Stop watch,
- Micrometer,
- Digital balance,
- Tool electrode made from copper,
- Workpiece made from an alloy steel,
- Roll made from an alloy steel,
- Roll used was of the order of 100mm diameter and 480mm length,

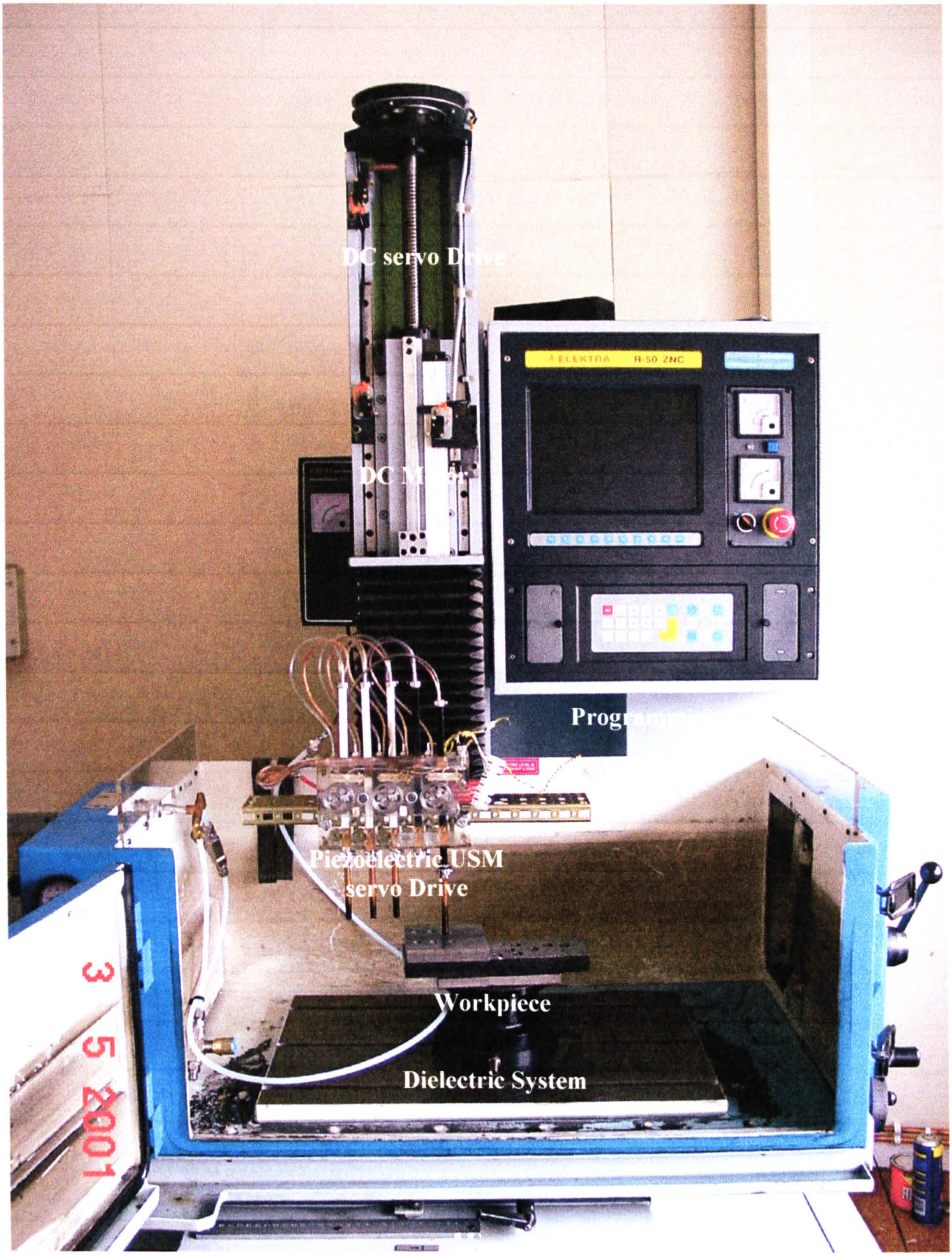

Figure 7-1 Installation of the developed drive using piezoelectric USM in the EDM-machine

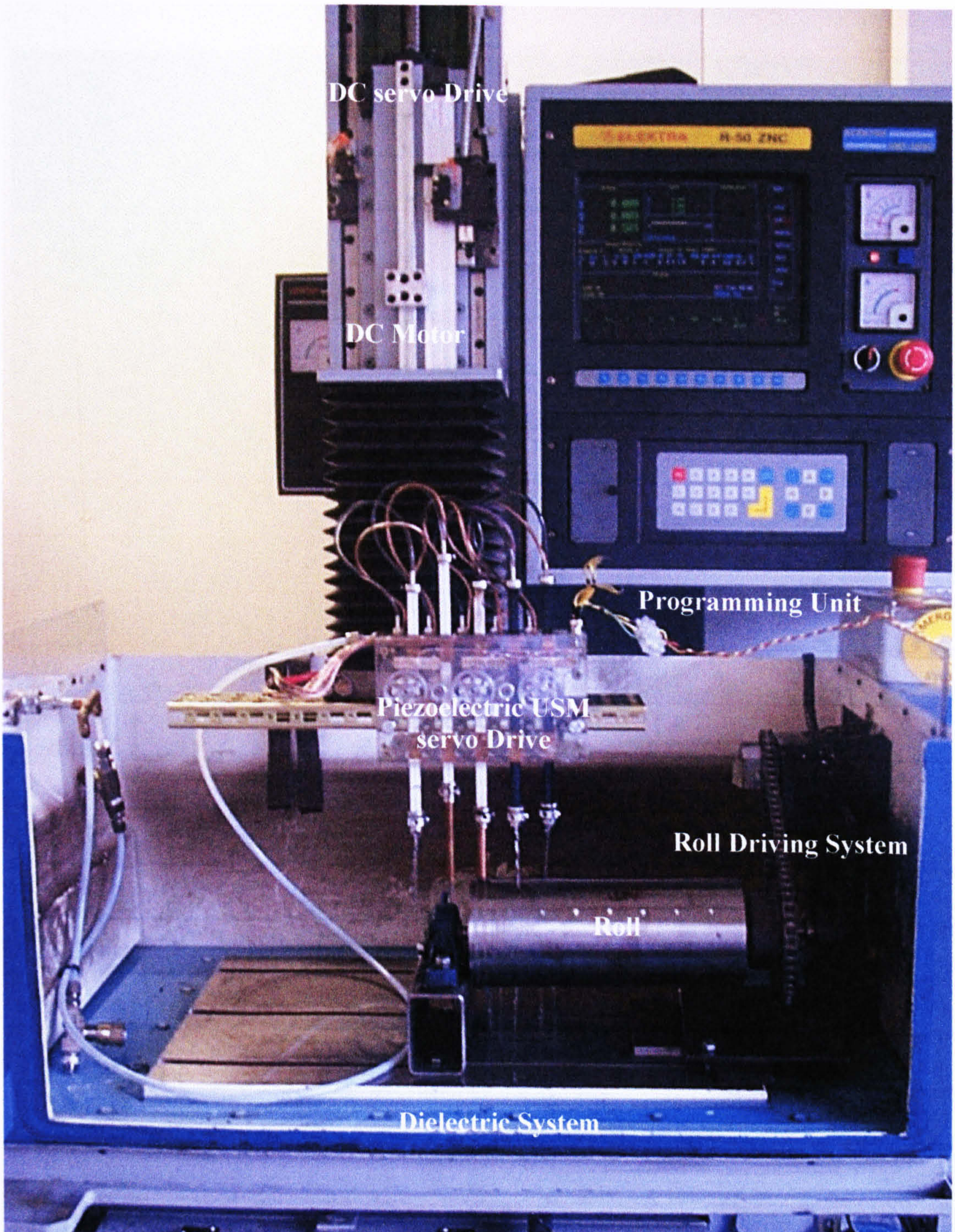

Figure 7-2 Installation of the developed drive using piezoelectric USM in a five head arrangement in the EDT-machine

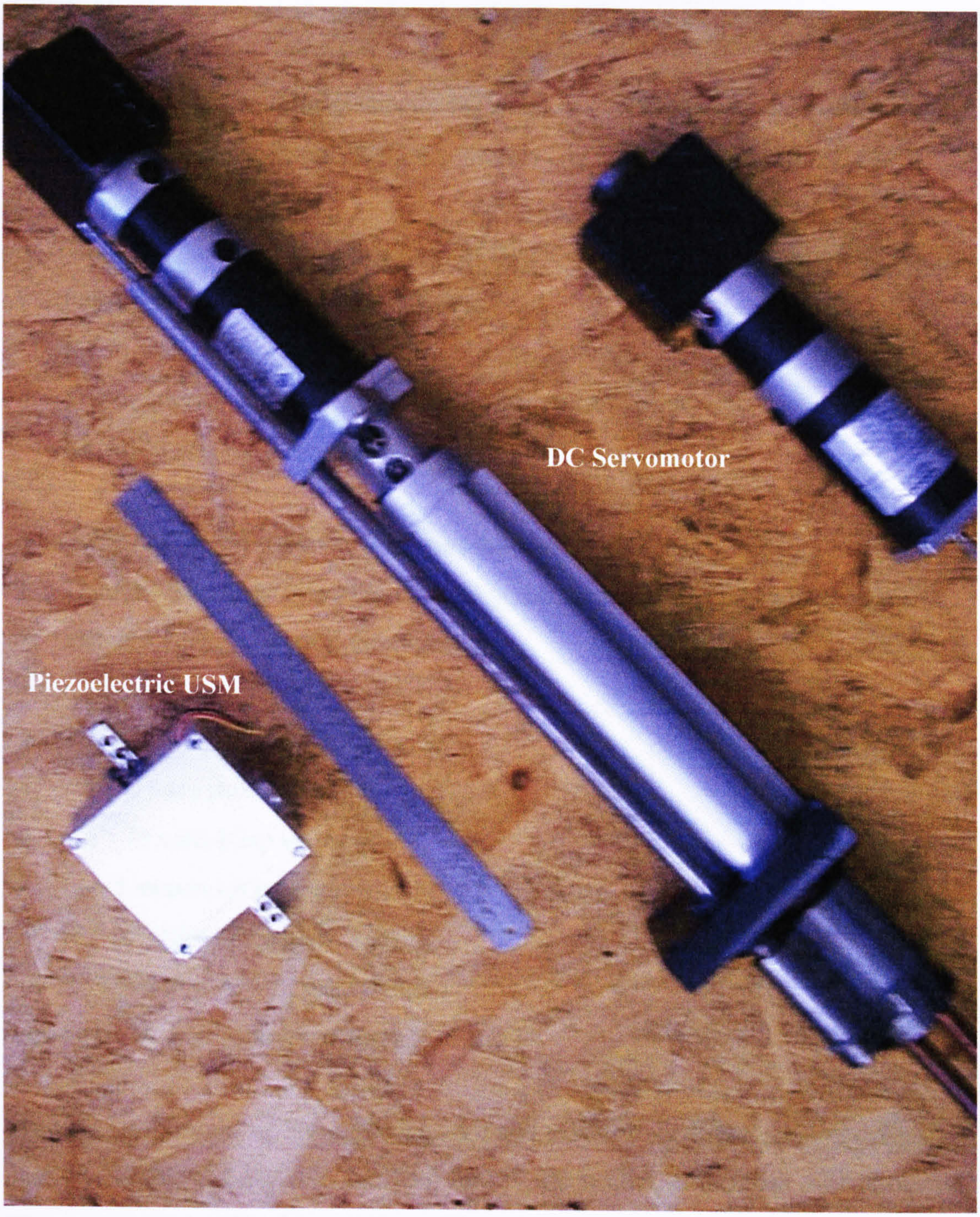

Figure 7-3 DC motor (bottom) and developed drive using piezoelectric USM (top left)

7.4 EDM- APPLICATION

In the case of EDM application the current system using DC servo control drive was used for machining different holes using various electro-machining parameters. This included the level of current, on-off time and duty cycle.

- The level of current used was on the order of 2 amperes up to 20-amperes, 'on' time of 50 μsec and duty cycle of 12 μsec.

- The on/off time was used at a level of 20 μsec up to 750 μsec, level of current was 8 amperes and duty cycle was 12 μsec.

- The duty cycle was used at level of 2 μsec up to 12 μsec, 'on' time of 50 μsec and level of current of 8 amperes.

The other machining parameters were as follow:

- The feed rate of the system in the case of auto-position was 0.656 mm/sec,
- SEN = 5 [Sensitivity of Z-axis speed],
- ASEN = 5 [Antiarc sensitivity],
- TW =1.0 μsec [Sparking time],
- T = 0.5 μsec [Lifetime],
- Vg = 38 volts [Gap voltage],
- Ig = 5 amperes [Gap current],
- Ib = 0. 0 [Prepulse spark current],
- POL=-ve [Polarity of machining],
- Fp=0.2 bar [Flushing pressure].

Then the DC servomotor drive disconnected and the developed servo control drive using piezoelectric USM activated. The feed rate of the system in the case of auto-position was measured to be 5.1 mm/sec. The same machining conditions were used. Investigations into the stability of the two control systems, processing time, surface finish, and material removal rate were carried out. This was necessary to investigate the

capability of the developed drive to control inter-electrode gap safely and investigate its influence on the surface finish of the machined products.

7.4.1 Experimental Work and Results

Two expermintal arrangements were used. The first was carried out using DC servomotor using standard programming provided with the EDM machine. The faciliy to change machining parameters during machining process was used to control machining conditions of the system. The second test was carried out using developed servo control system which used piezoelectric USM. As shown in Figure 7-1, the system was arranged for machining using both control systems using a solid state dual switch. The electro machining parameters used in this investigation are given in tables 7-1, 7-2 and 7-3. The investigation was included, the stability of the system, surface finish, surface roughness, Pc peak/cm, processing time and material removal rate.

7.4.1.1 Stability of the System

Normally the stability of such technique of machining is measured through the stability of the current and voltage in the inter-electrode machining gap. The feedback control signal could be used also as a measure of the stability, time of machining and capability to control. In this investigation the inter-electrode gap voltage and feedback control signal were used to measure and evaluate the stability of both systems for control using DC servomotor and piezoelectric USM.

Figures 7-4 to 7-17 show the variation in the inter-electrode gap voltage, and feedback control signal, for various machining parameters for both systems. Channel 1 (red signal) shows the variation in the feedback control signal and channel 2 (blue signal) shows the variations in the inter-electrode gap voltage.

Figures 7-4, 7-6, 7-8, 7-10, 7-12, and 7-14 show the variation in the EDM machining conditions using piezoelectric ultrasonic control system.

Figures 7-5, 7-7, 7-9, 7-11, 7-13, 7-15, 7-16 and 7-17 show the variation in the EDM machining conditions using DC servo control system.

As shown in Figures 7-7, 7-9, 7-11 and 7-13 the system, using DC servomotor system, is unstable, the servo drive spent most of the time retracting the eroded tool electrode to avoid the arcing and short-circuiting. Arcing and short circuiting process can produce an over heating which may produce unacceptable surface profiles and result in some cracks. It can be also seen from Figures 7-15, 7-16 and 7-17 that the inter-electrode gap voltage is shorted with increase in the level of machining parameters. However, it can be seen here from Figures 7-4, 7-6, 7-8, 7-10, 7-12 and 7-14 that the developed control system using piezoelectric USM provides a good stability for machining in comparison to the system using DC servomotor at various levels of machining conditions. A reduction in the arcing and short circuiting process was also possible to be obtained which let to improve in the surface of the machined products and reduce in the processing time for machining.

Table 7-1 Electro-machining parameters used in the investigation on the effect of the level of current in the surface finish of the machined product using both systems of control using piezoelectric USM and motor

Test No	Sparking Current (Ampere)	On-Time (μSec)	Gap Voltage (Volt)	Gap current (Ampere)	Duty cycle (μSec)
1	**2**	**50**	**38**	**5**	**12**
2	**4**	**50**	**38**	**5**	**12**
3	**6**	**50**	**38**	**5**	**12**
4	**8**	**50**	**38**	**5**	**12**
5	**10**	**50**	**38**	**5**	**12**
6	**12**	**50**	**38**	**5**	**12**
7	**14**	**50**	**38**	**5**	**12**
8	**16**	**50**	**38**	**5**	**12**
9	**18**	**50**	**38**	**5**	**12**
10	**20**	**50**	**38**	**5**	**12**

Table 7-2 Electro-machining parameters used in the investigation of the effect of on/off time in the surface finish of the machined product using both systems for control (piezoelectric USM and DC motor)

Test No	Sparking Current (Ampere)	On-Time (μSec)	Gap Voltage (Volt)	Gap current (Ampere)	Duty cycle (μSec)
1	**8**	**30**	**38**	**5**	**12**
2	**8**	**50**	**38**	**5**	**12**
3	**8**	**75**	**38**	**5**	**12**
4	**8**	**100**	**38**	**5**	**12**
5	**8**	**150**	**38**	**5**	**12**
6	**8**	**200**	**38**	**5**	**12**
7	**8**	**300**	**38**	**5**	**12**
8	**8**	**400**	**38**	**5**	**12**
9	**8**	**500**	**38**	**5**	**12**
10	**8**	**750**	**38**	**5**	**12**

Table 7-3 Electro-machining parameters used in the investigation of the effect of duty cycle in the surface finish of the machined product using both systems for control (piezoelectric USM and DC motor)

Test No	Sparking Current (Ampere)	On-Time (μSec)	Gap Voltage (Volt)	Gap current (Ampere)	Duty cycle (μSec)
1	**8**	**50**	**38**	**5**	**2**
2	**8**	**50**	**38**	**5**	**4**
3	**8**	**50**	**38**	**5**	**6**
4	**8**	**50**	**38**	**5**	**8**
5	**8**	**50**	**38**	**5**	**10**
6	**8**	**50**	**38**	**5**	**12**

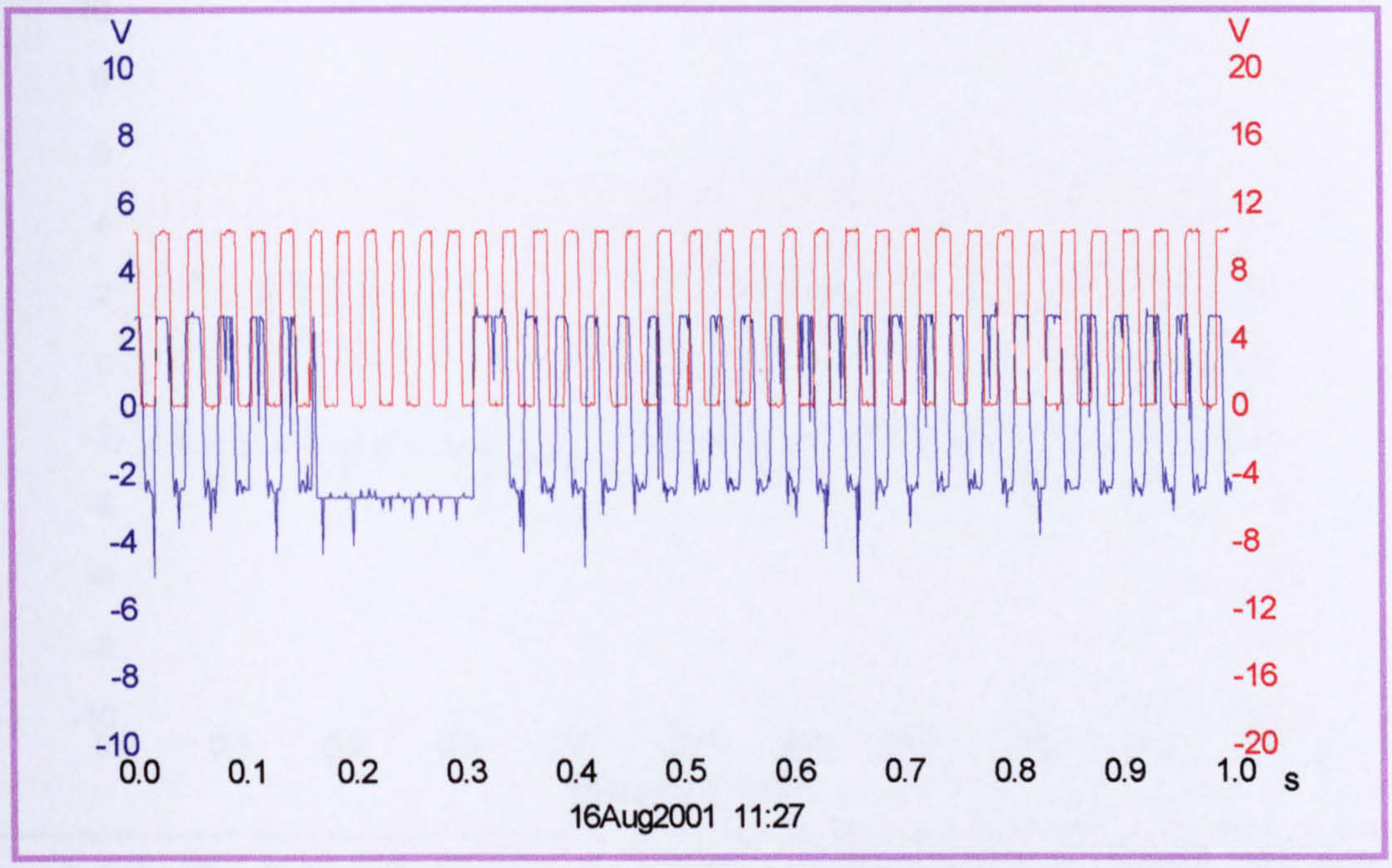

Figure 7-4 Feedback control signal (red) and inter-electrode gap voltage (blue) variation for EDM machining using the developed piezoelectric USM control system [gap current 5A, gap voltage of 38 volts & duty cycle 2 μsec]

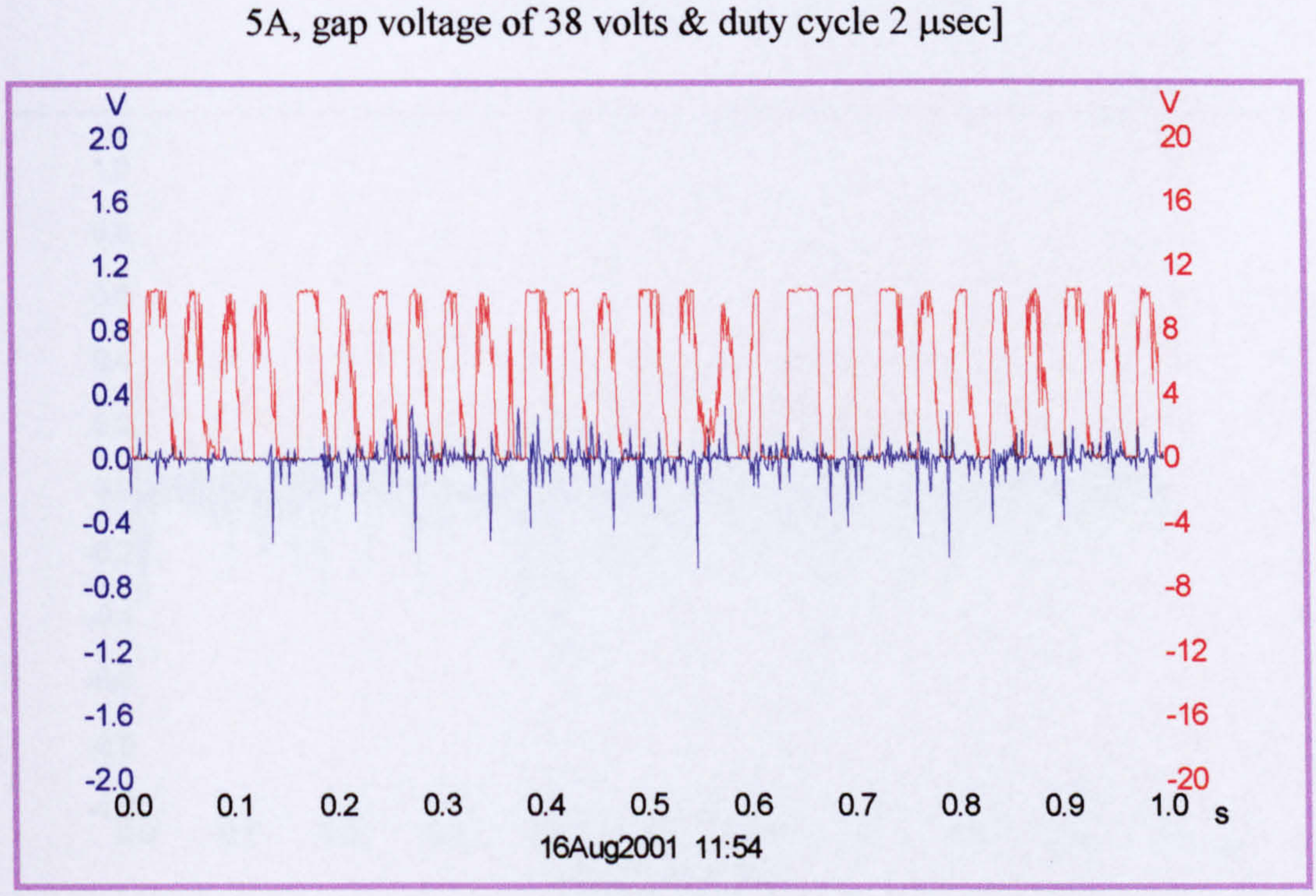

Figure 7-5 Feedback control signal (red) and inter-electrode gap voltage (blue) variation for EDM machining using the current DC servo control system [gap current 5A, gap voltage of 38 volts & duty cycle 2μsec]

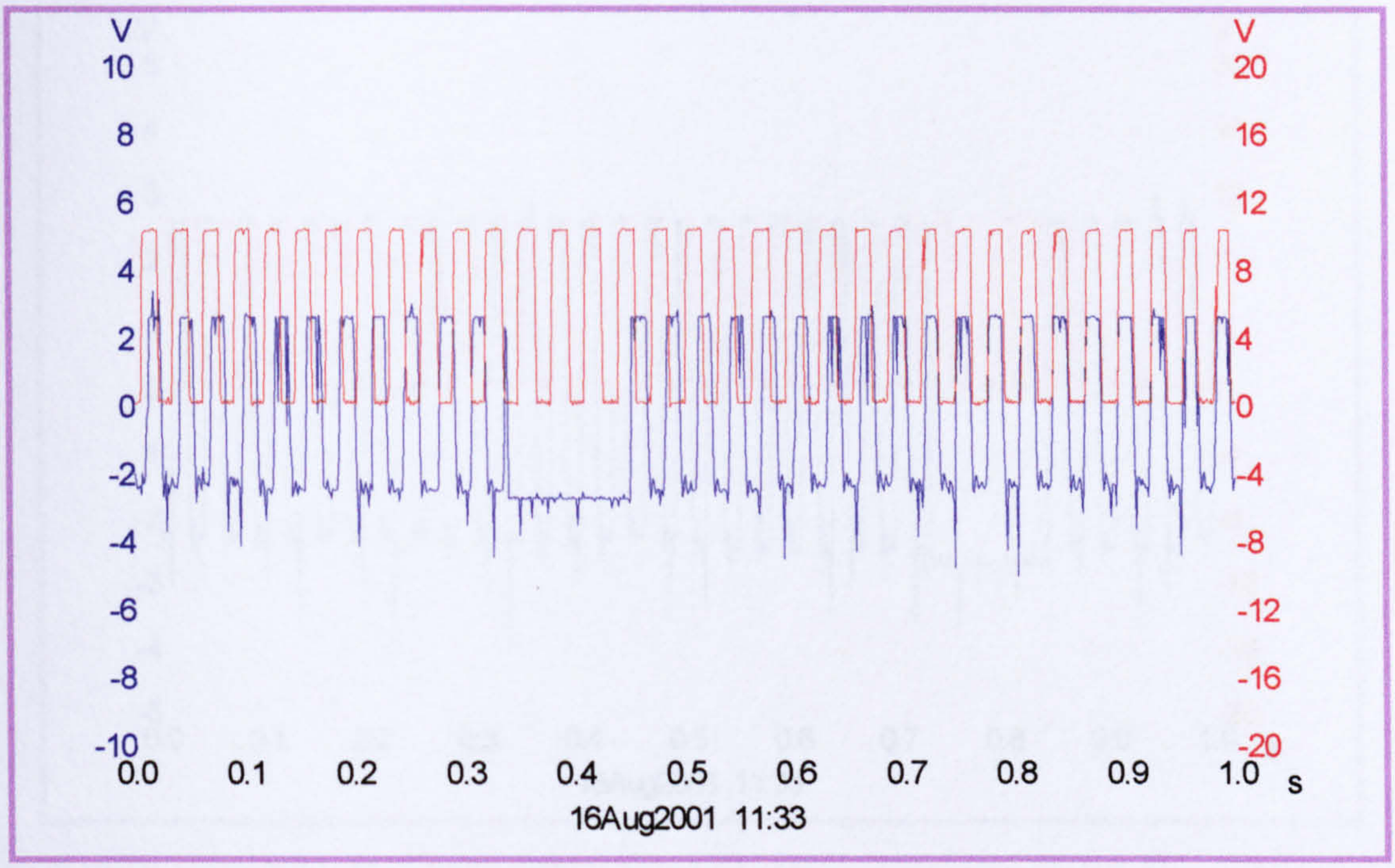

Figure 7-6 Feedback control signal (red) and inter-electrode gap voltage (blue) for EDM machining using the developed piezoelectric USM control system [gap current 5A, gap voltage of 38 volts & duty cycle 4μsec]

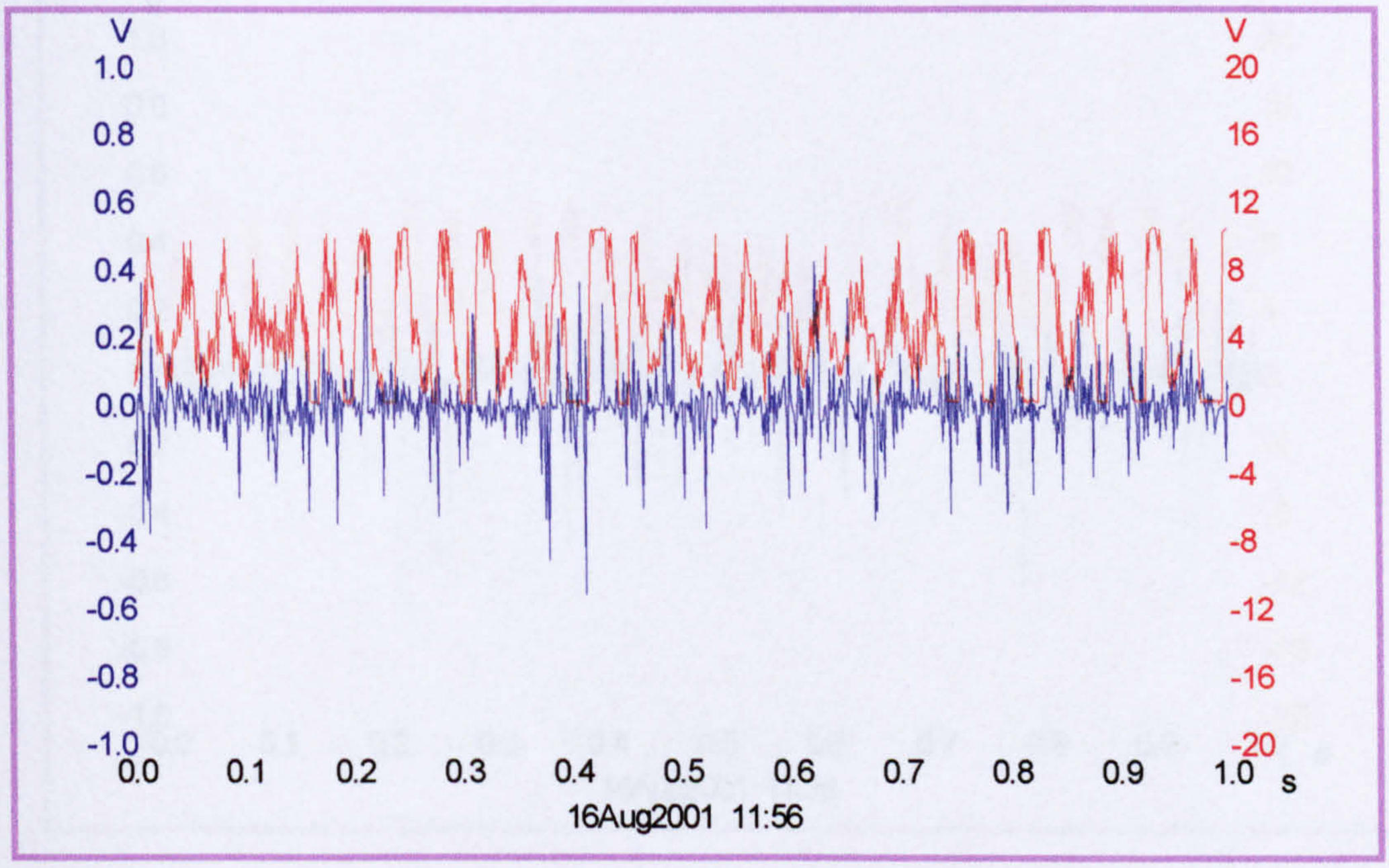

Figure 7-7 Feedback control signal (red) and inter-electrode gap voltage (blue) variation for EDM machining using the current DC servo control system [gap current 5A, gap voltage of 38 volts& duty cycle 4μsec]

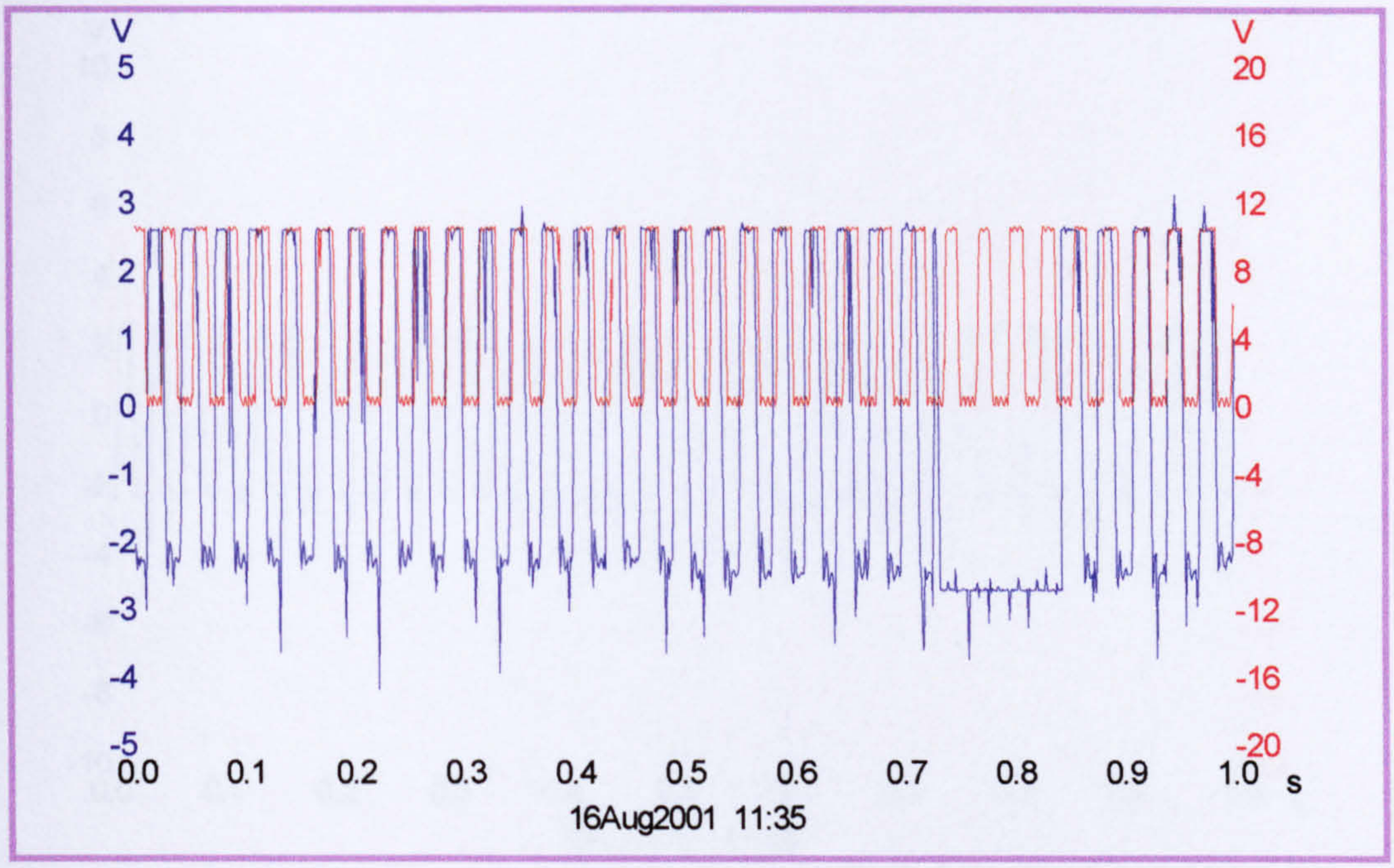

Figure 7-8 Feedback control signal (red) and inter-electrode gap voltage (blue) variation for EDM machining using the developed piezoelectric USM control system [gap current 5A, gap voltage of 38 volts & duty cycle 6μsec]

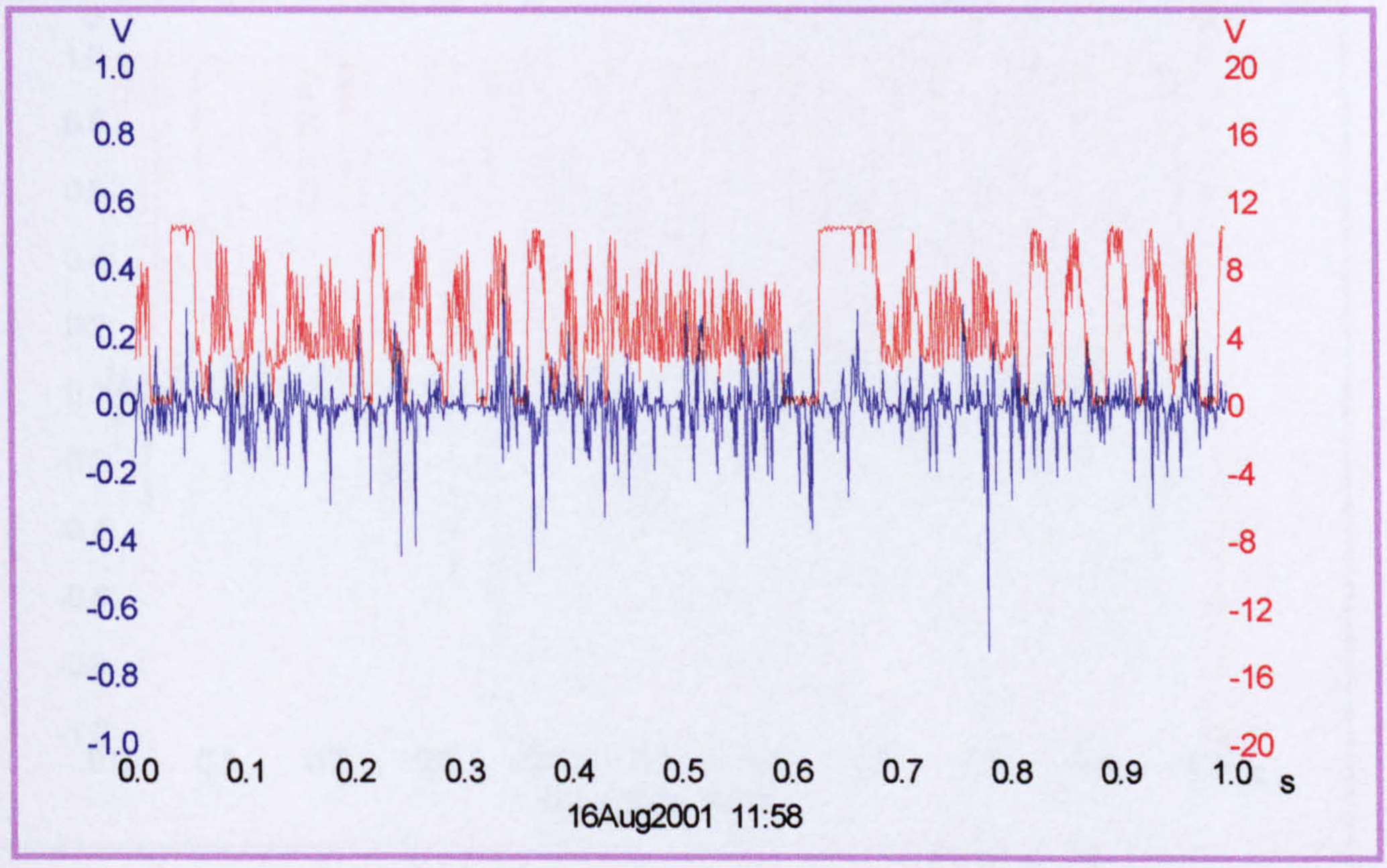

Figure 7-9 Feedback control signal (red) and inter-electrode gap voltage (blue) variation for EDM machining using the current DC servo control system [gap current 5A, gap voltage of 38 volts & duty cycle 6μsec]

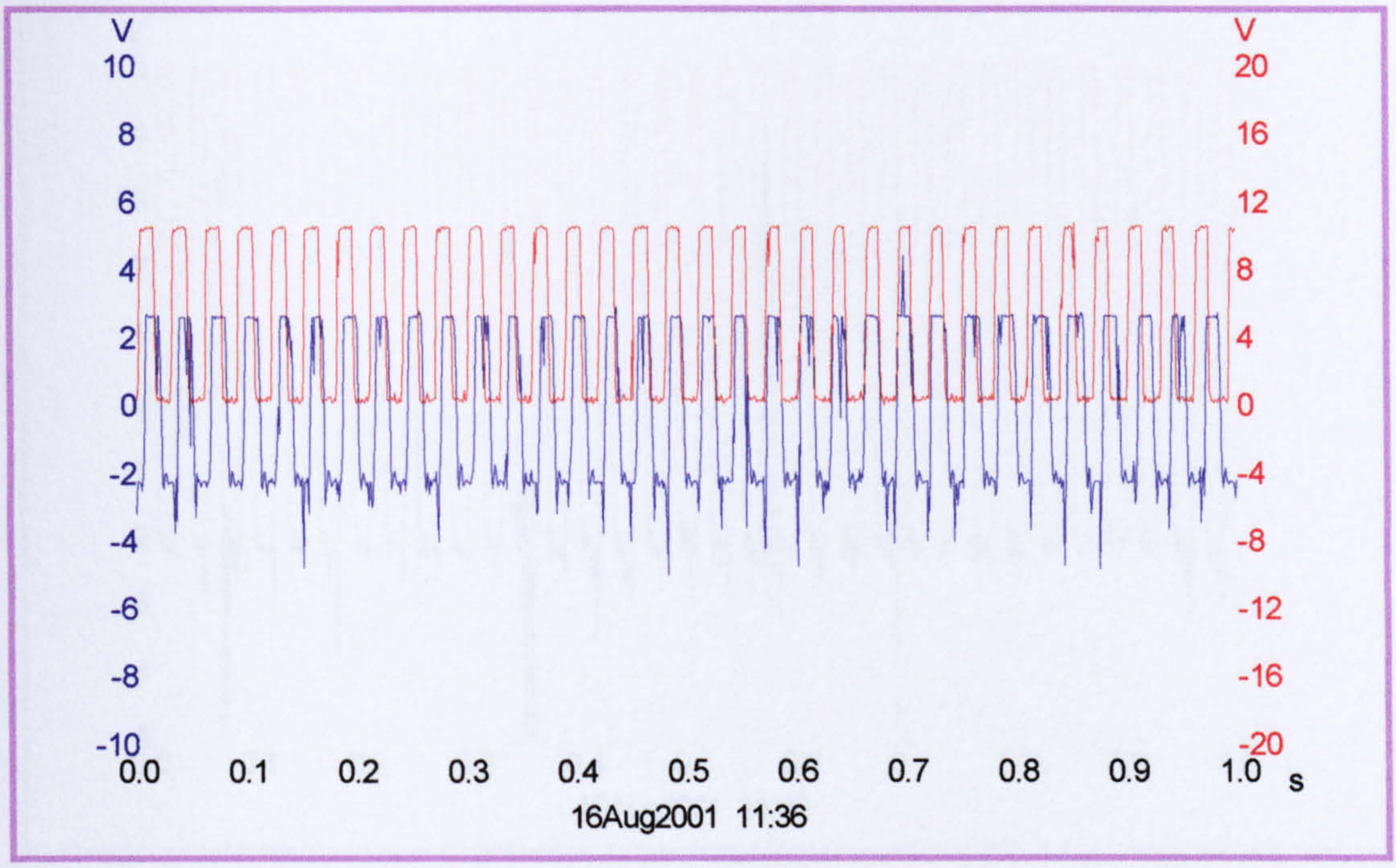

Figure 7-10 Feedback control signal (red) and inter-electrode gap voltage (blue) variation for EDM machining using the developed piezoelectric USM control system [gap current 5A, gap voltage of 38 volts & duty cycle 8μsec]

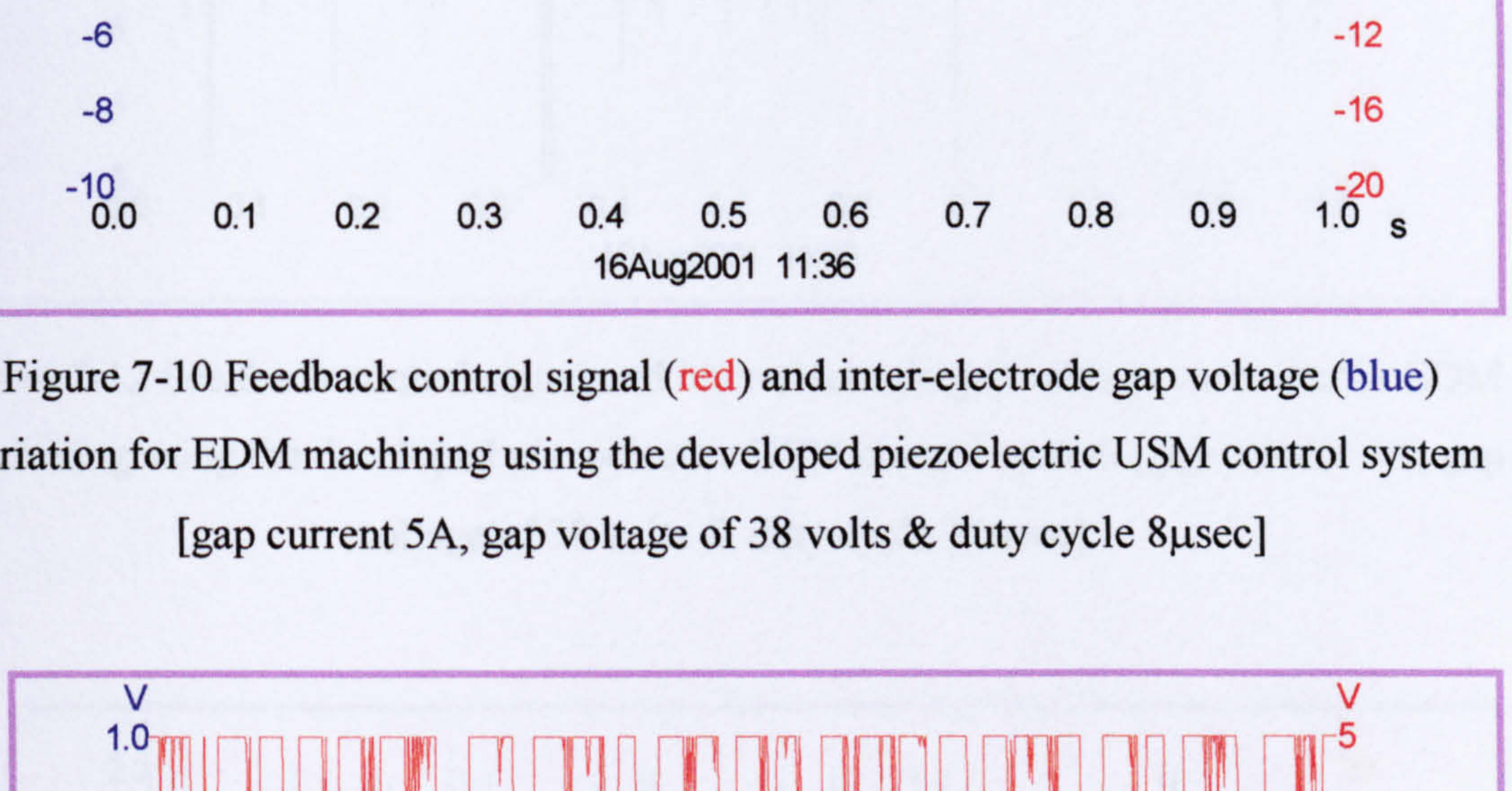

Figure 7-11 Feedback control signal (red) and inter-electrode gap voltage (blue) variation for EDM machining using the current DC servo control system [gap current 5A, gap voltage of 38 volts & duty cycle 8μsec]

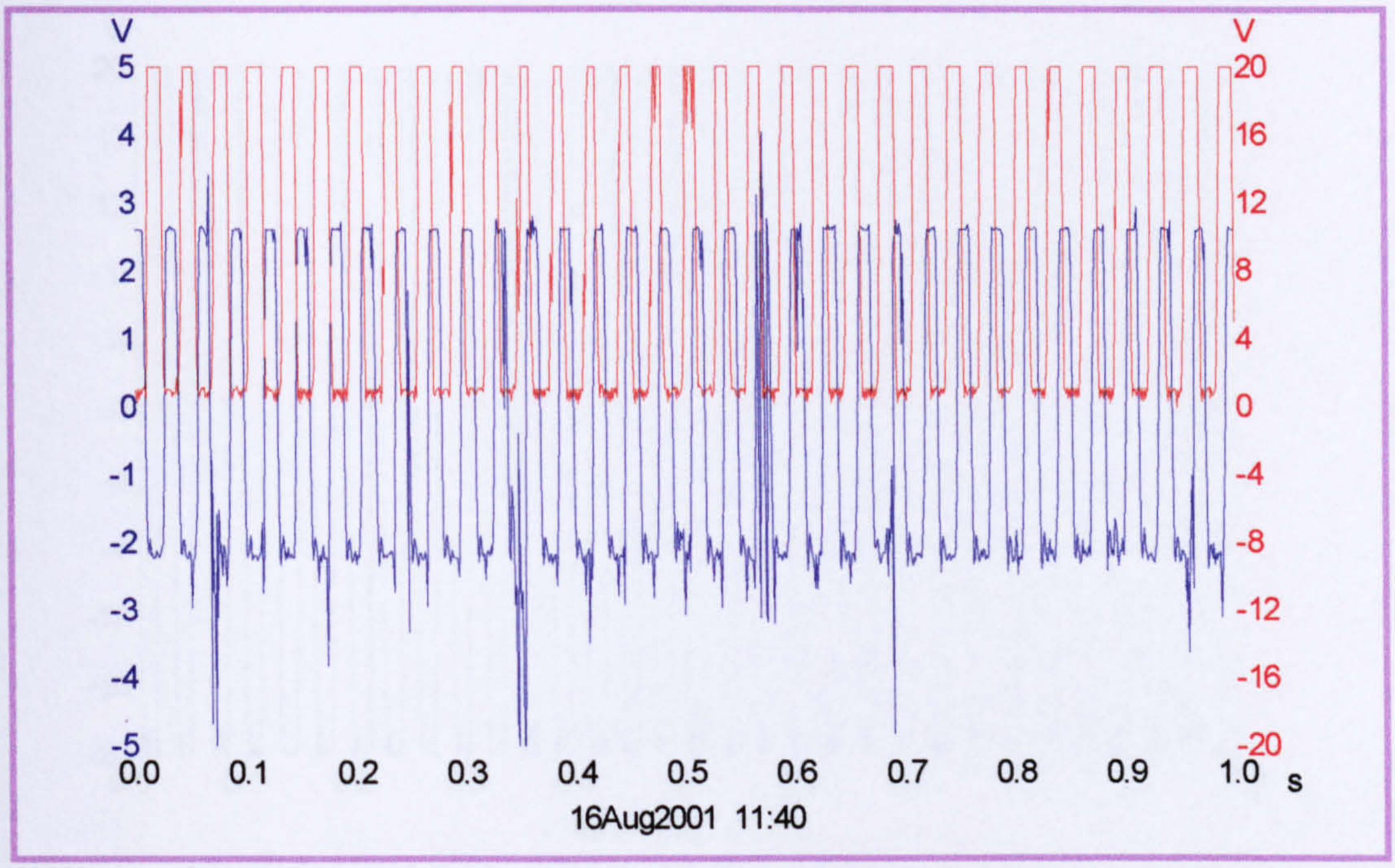

Figure 7-12 Feedback control signal and inter-electrode gap voltage variation for EDM machining using the developed piezoelectric USM control system [gap current 5A, gap voltage of 38 volts & duty cycle 10μsec]

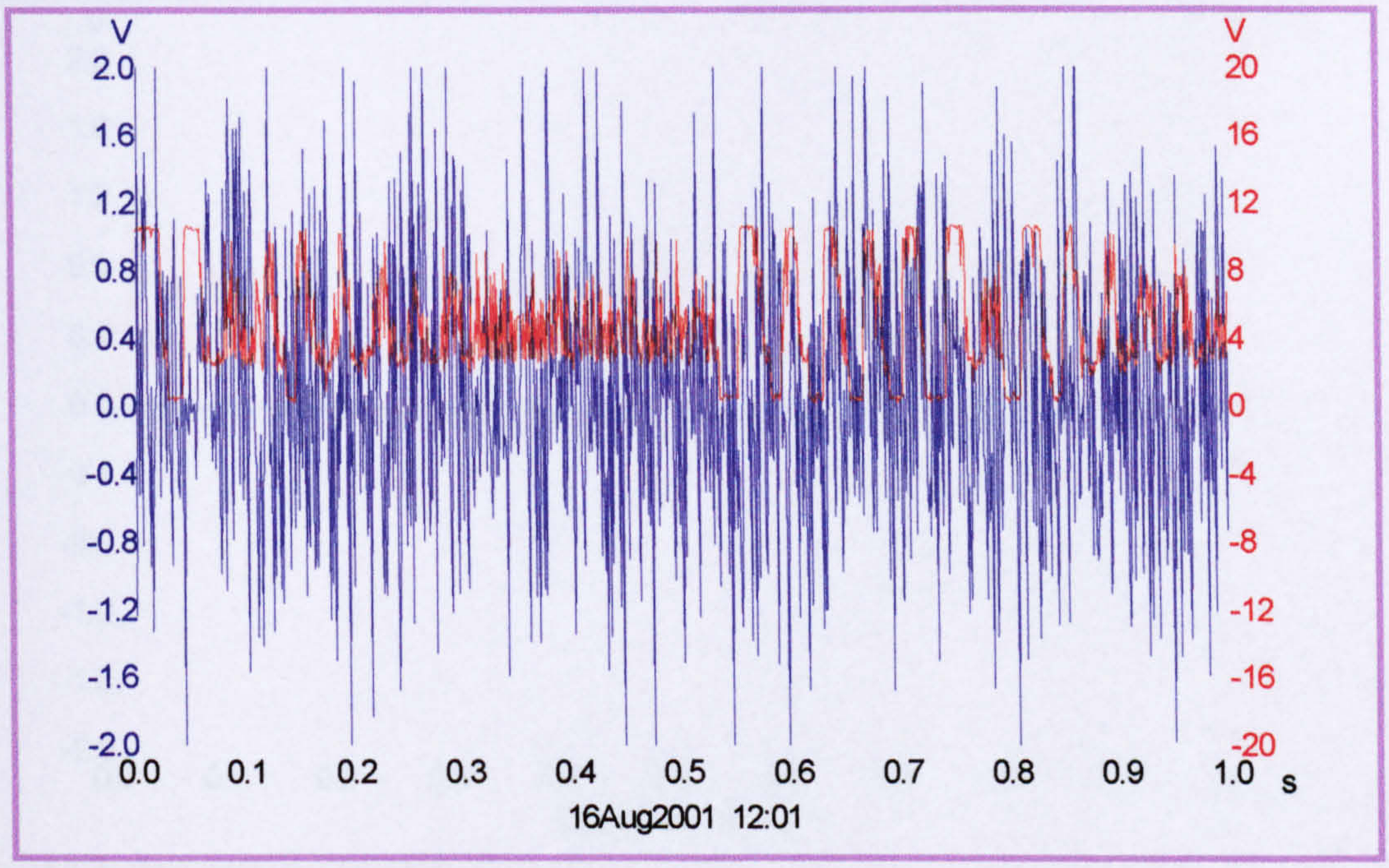

Figure 7-13 Feedback control signal (red) and inter-electrode gap voltage (blue) variation for EDM machining using the current DC servo control system [gap current 5A, gap voltage of 38 volts & duty cycle 10μsec]

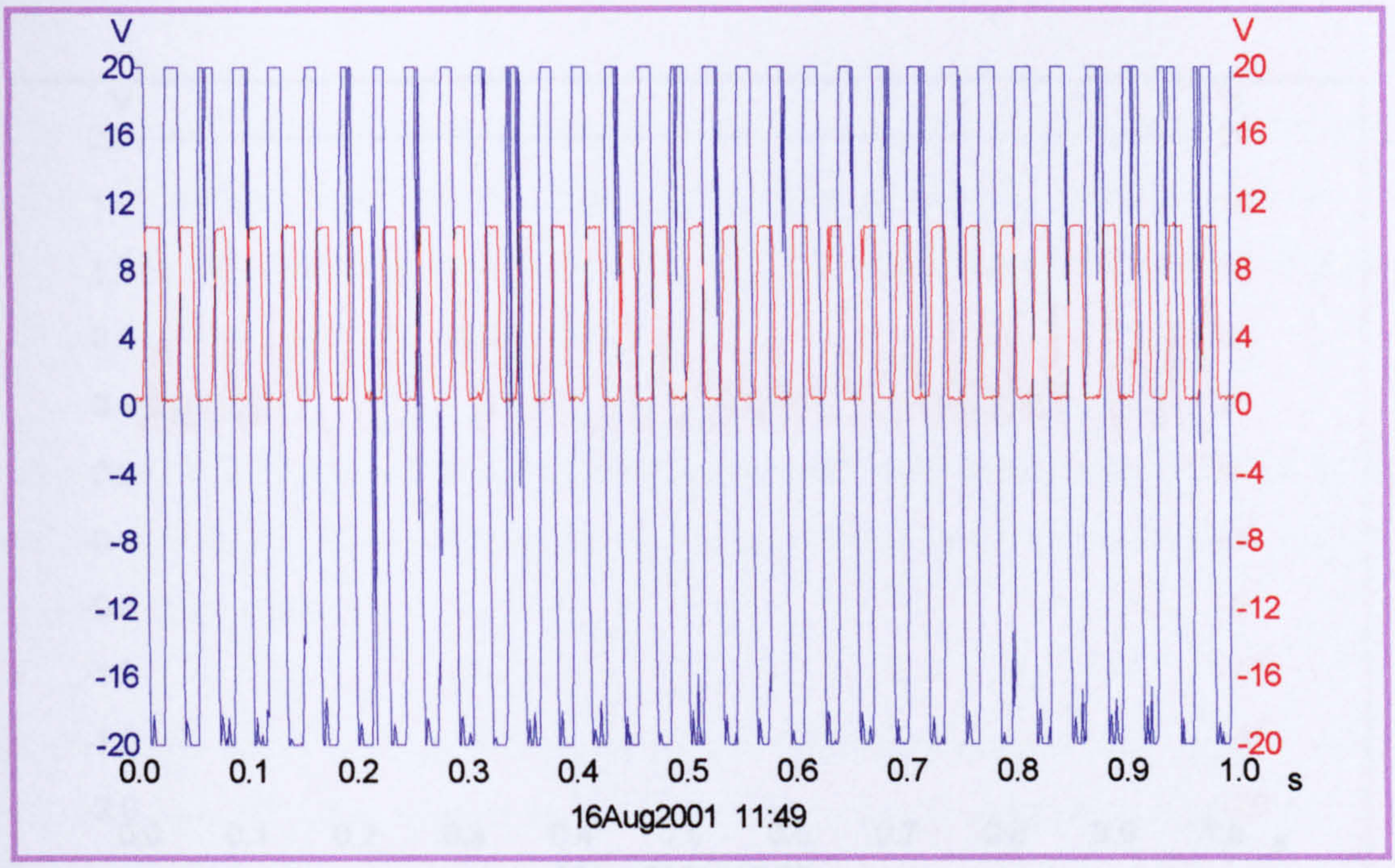

Figure 7-14 Feedback control signal and inter-electrode gap voltage variation for EDM machining using the developed piezoelectric USM control system [gap current 5A, gap voltage of 38 volts & duty cycle 12μsec]

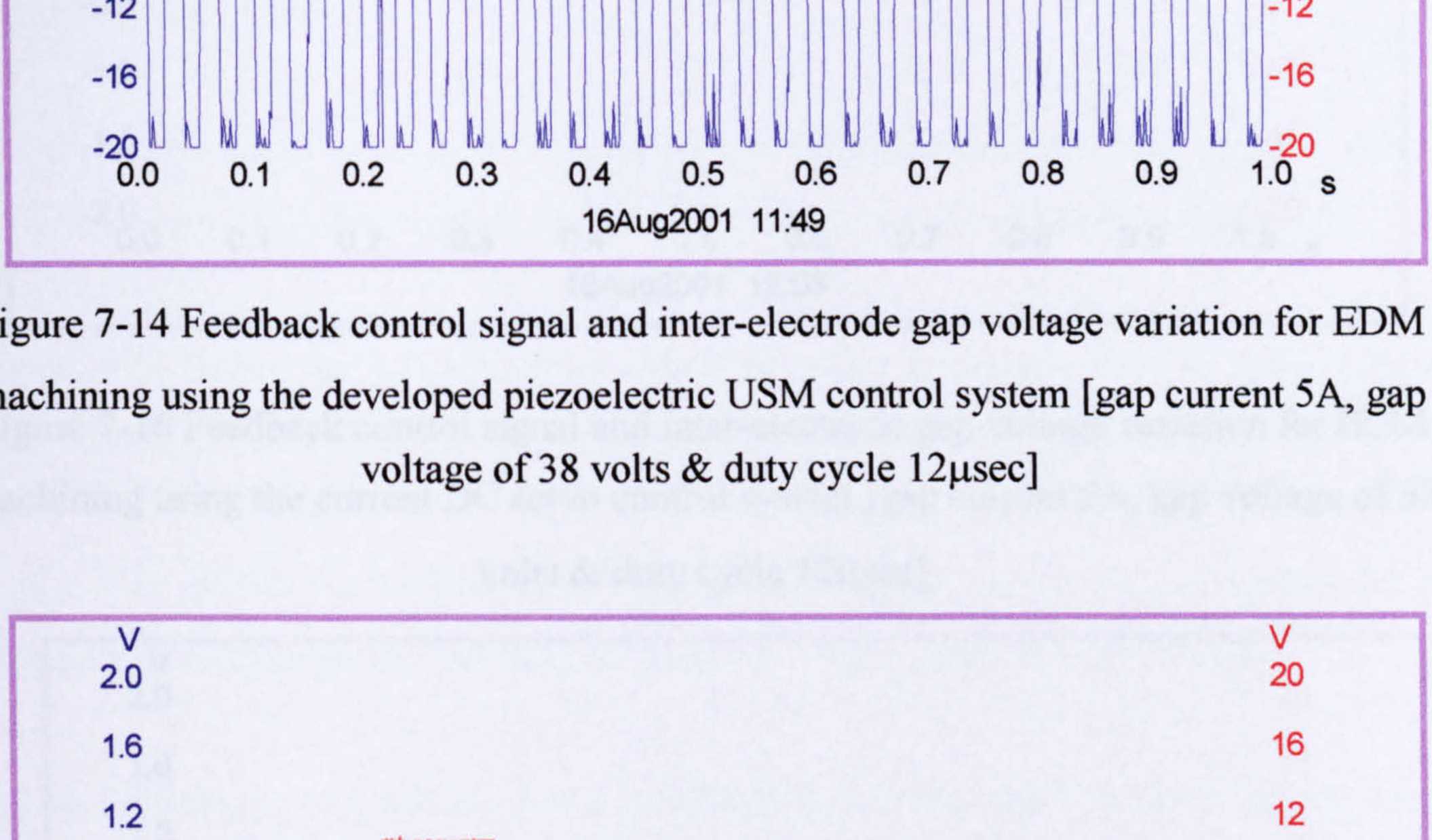

Figure 7-15 Feedback control signal (red) and inter-electrode gap voltage (blue) variation for EDM machining using the current DC servo control system [gap current 5A, gap voltage of 38 volts & duty cycle 12μsec]

7.4.1.2 Surface Finish

Scanning electron microscopic investigations into the machined surface finish for both systems of control using various electro-machining parameters were carried out. A Leica Cambridge Scanning Electron Microscope was used. Figures 7-18 and 7-19 show the arrangements used in this investigation.

Figures 7-20 to 7-27 show the surface finish machined using both systems of control DC servo control system and piezoelectric ultrasonic control system using various electro-machining parameters.

Figures 7-20, 7-22, 7-24 and 7-26 show the microstructure of the surface finish machined using DC servo control system and various electro-machining parameters.

Figure 7-20 shows the surface finish machined using DC servo control system for a peak current of 4 amperes, 'on' time 50 μsec and with a duty cycle of 12 μsec.

Figure 7-22 shows the surface finish machined using DC servo control system for a peak current of 6 amperes, 'on' time 50 μsec and with a duty cycle of 12 μsec.

Figure 7-24 shows the surface finish machined using DC servo control system for a peak current of 8 ampere, 'on' time 50 μsec and with a duty cycle of 12 μsec.

Figure 7-26 shows the surface finish machined using DC servo control system for a peak current of 10 ampere, 'on' time 50 μsec and with a duty cycle of 12 μsec.

Figures 7-21, 7-23, 7-25 and 7-27 show the surface finish machined using an ultrasonic control system and various electro-machining parameters.

Figure 7-21 shows the surface finish machined using piezoelectric ultrasonic control system for a peak current 4 ampere, 'on' time 50 μsec and with a duty cycle of 12 μsec.

Figure 7-23 shows the surface finish machined using piezoelectric ultrasonic control system for a peak current 6 ampere, 'on' time 50 μsec and with a duty cycle of 12 μsec.

Figure 7-25 shows the surface finish machined using piezoelectric ultrasonic control system for a peak current 8 ampere, 'on' time 50 μsec and with a duty cycle of 12 μsec.

Figure 7-27 shows the surface finish machined using piezoelectric ultrasonic control system for a peak current 10 ampere, 'on' time 50 μsec and with a duty cycle of 12 μsec.

Figures 7-28 and 7-29 show the surface finish machined using DC servomotor and piezoelectric ultrasonic control system for a peak current 10 ampere, 'on' time 50 μsec and with a duty cycle of 12 μsec for a cross section area of 20 microns. This shows a close investigation into the surface finish machined using both systems and illustrates the improvement in surface finish due to the stability obtained using piezoelectric ultrasonic control system.

These electron microscopic investigations into the surface finish of the machined products using both systems of control showed that:

- The surface finishes of the machined products using piezoelectric ultrasonic control system were improved. This was due to the stability of machining conditions of the developed control system, which was obtained from the high resolution and fast response of the piezoelectric USM control system. The improvements in the machined products surface finish may lead to extended product lifetime and EDM machine applications.
- The surface finishes of the machined products using piezoelectric ultrasonic system provide a smooth surface finish when compared to the current control system.
- The degree of roughness of the developed surface was slightly high compared to the current system of control using DC servo control system.
- The developed control system showed also a reduction in the arcing and short circuit processes.
- The time of machining was reduced. This was due to the response time of the developed control system that was obtained on the order of microseconds.

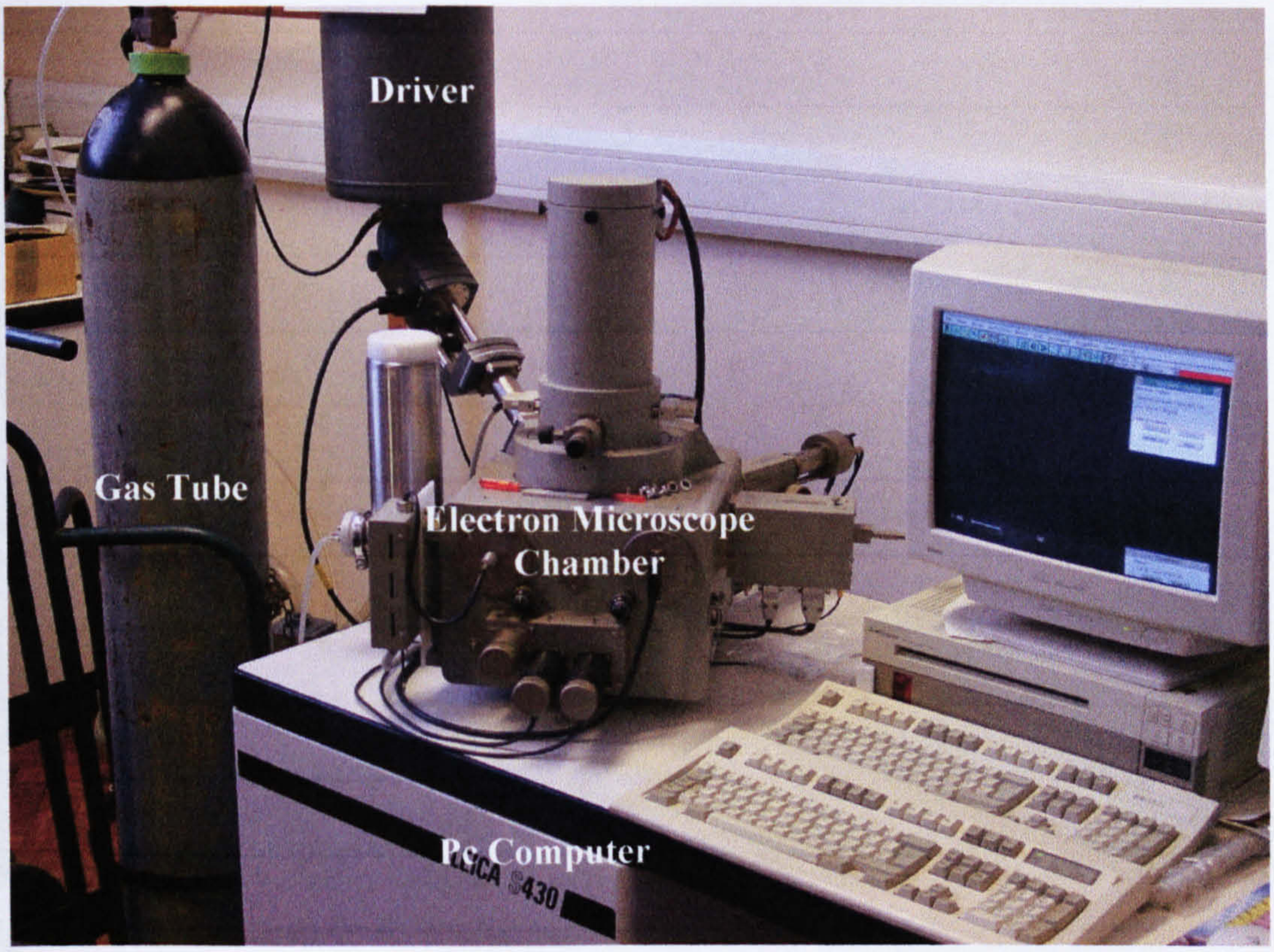

Figure 7-18 Leica Cambridge Electron Microscope used to investigate the microstructure of the machined surface using both systems of control

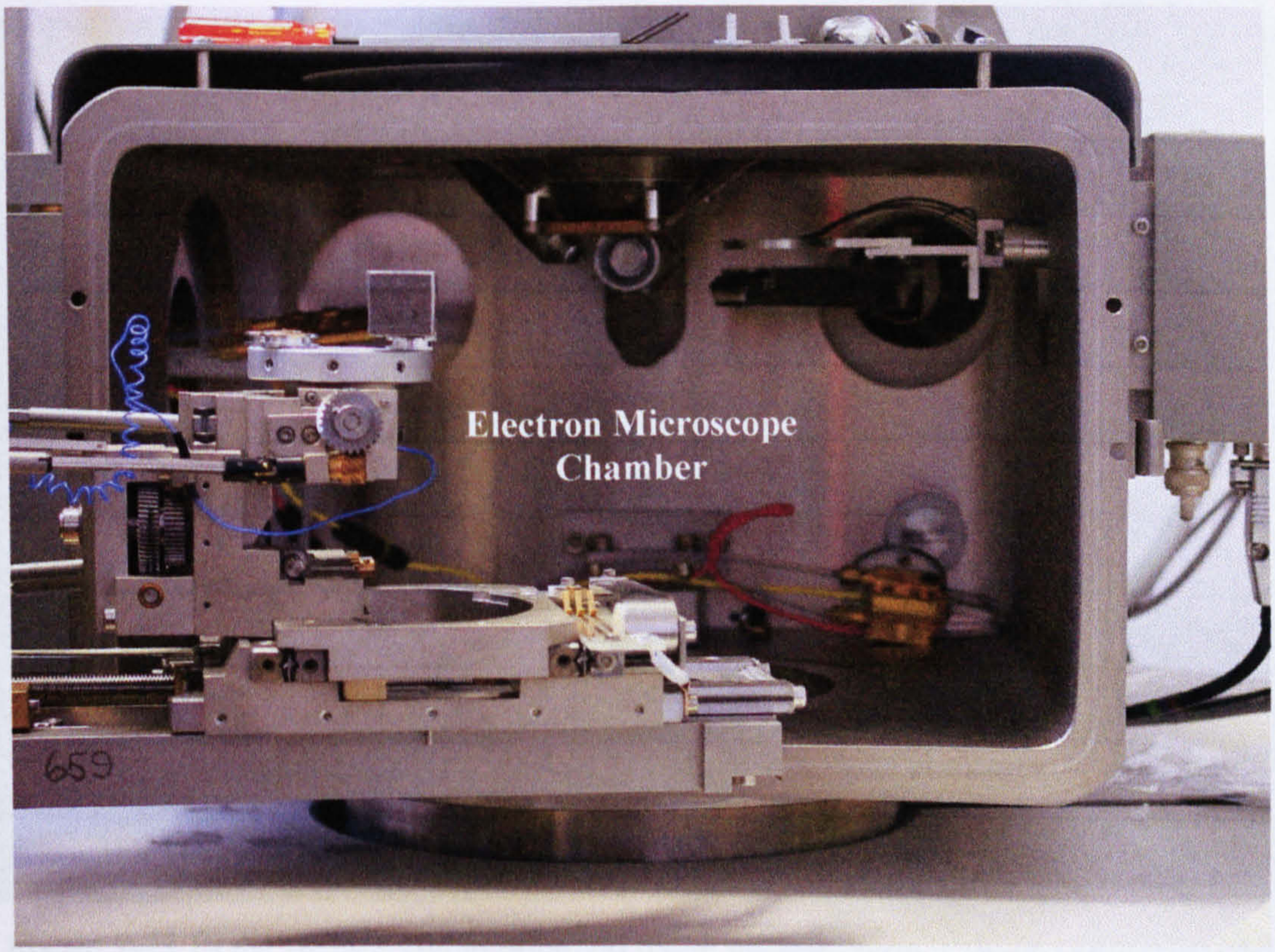

Figure 7-19 Specimen Placement in Electron Microscope used in the surface profile investigations

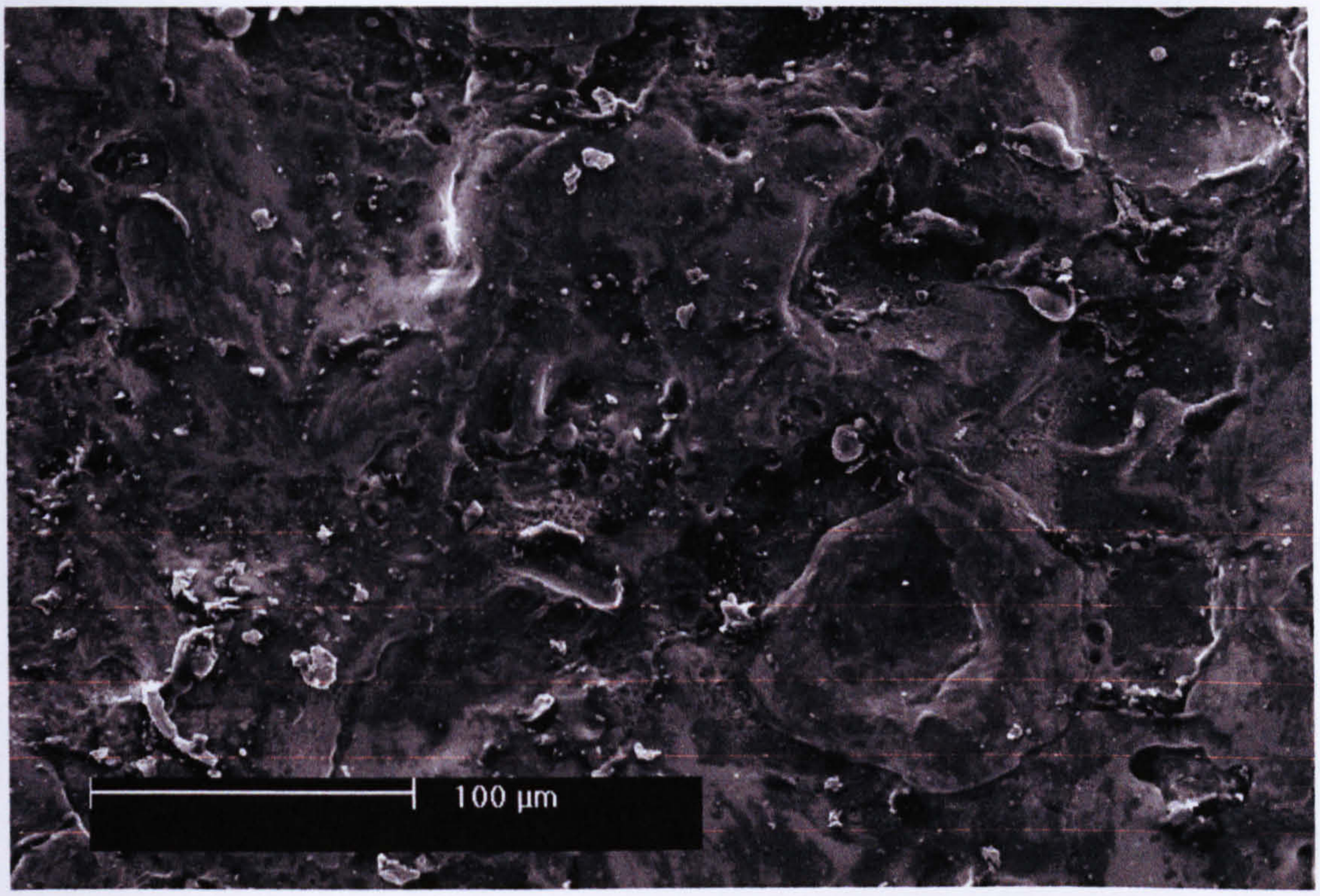

Figure 7-20 EDM surface finish obtained using DC servo control system using current level 4 amperes, 'on' time 50 µsec, duty cycle 12 µsec

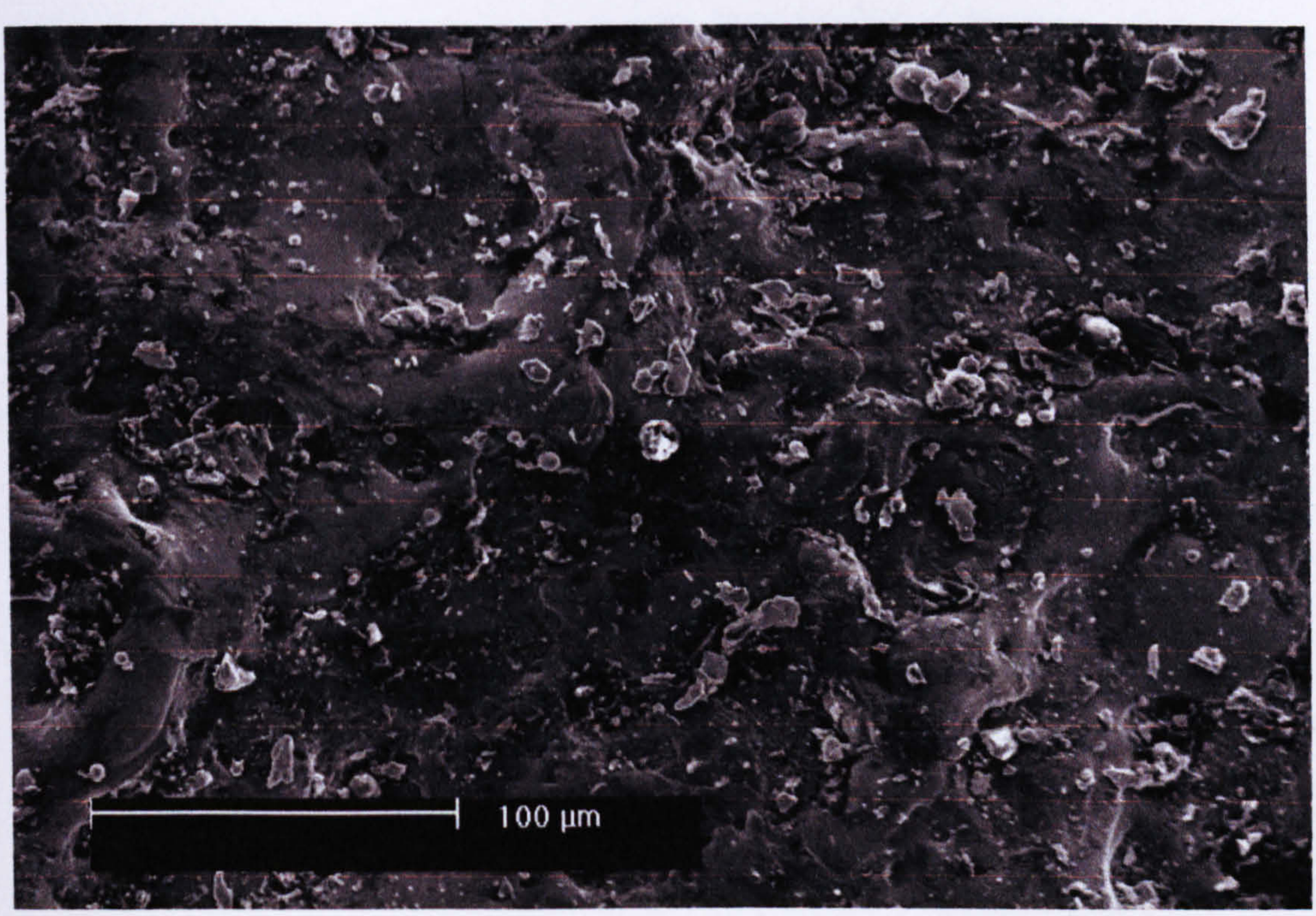

Figure 7-21 EDM surface finish obtained using piezoelectric USM system of control using current level 4 amperes, 'on' time 50 µsec, duty cycle 12 µsec

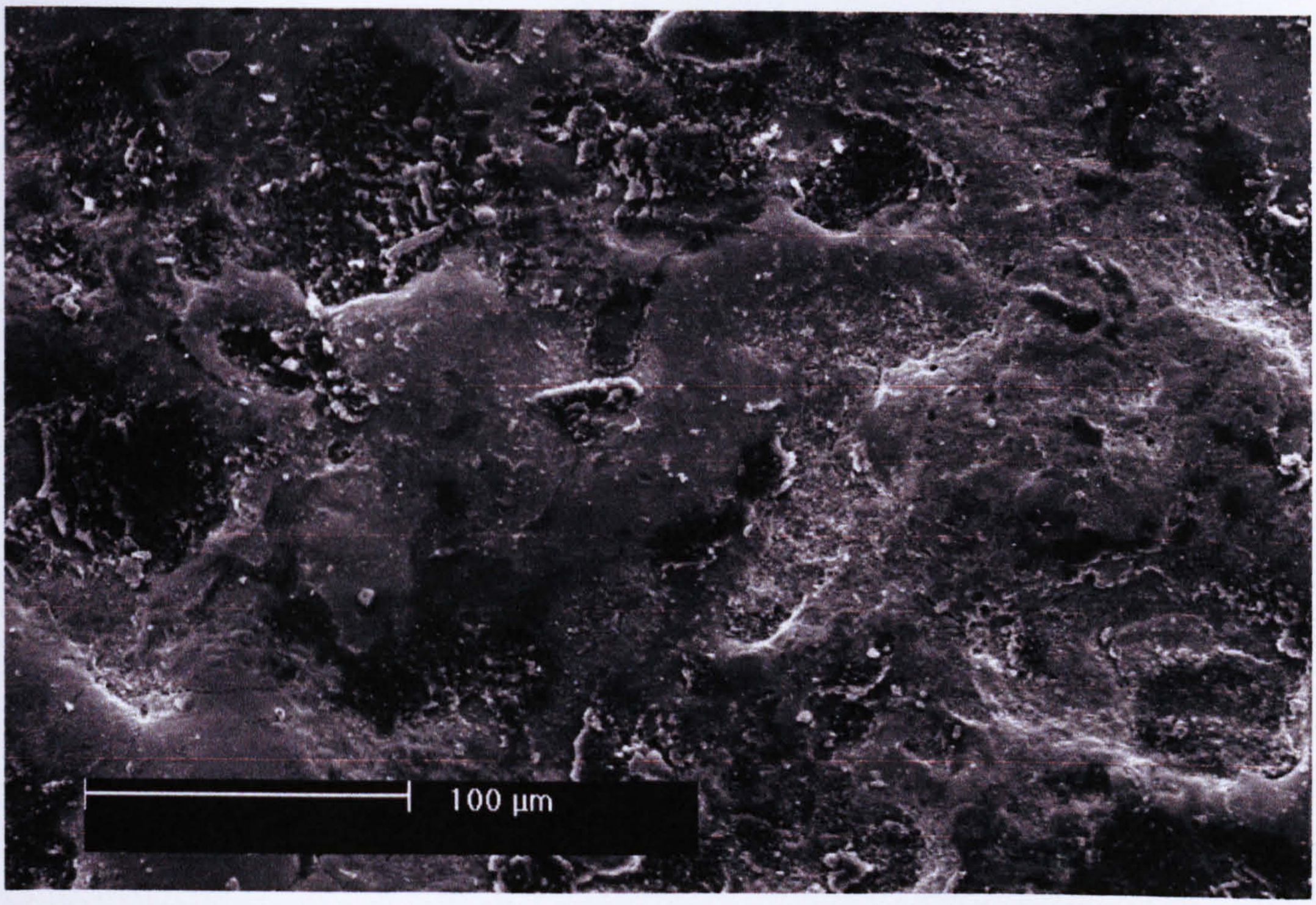

Figure 7-22 EDM surface finish obtained using DC servo control system using current level 6 amperes, 'on' time 50 µsec, duty cycle 12 µsec

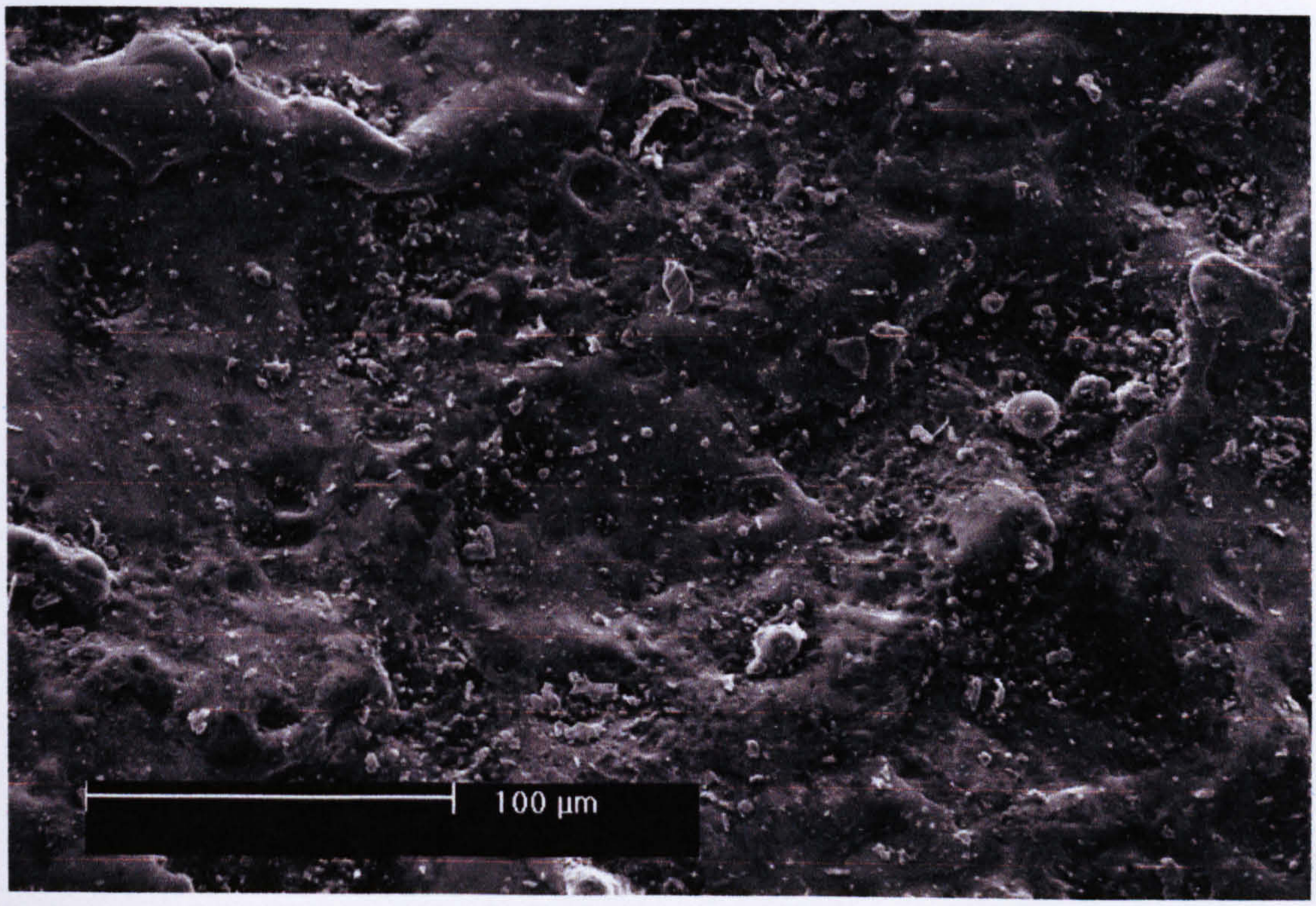

Figure 7-23 EDM surface finish obtained using piezoelectric USM system of control using current level 6 amperes, 'on' time 50 µsec, duty cycle 12 µsec

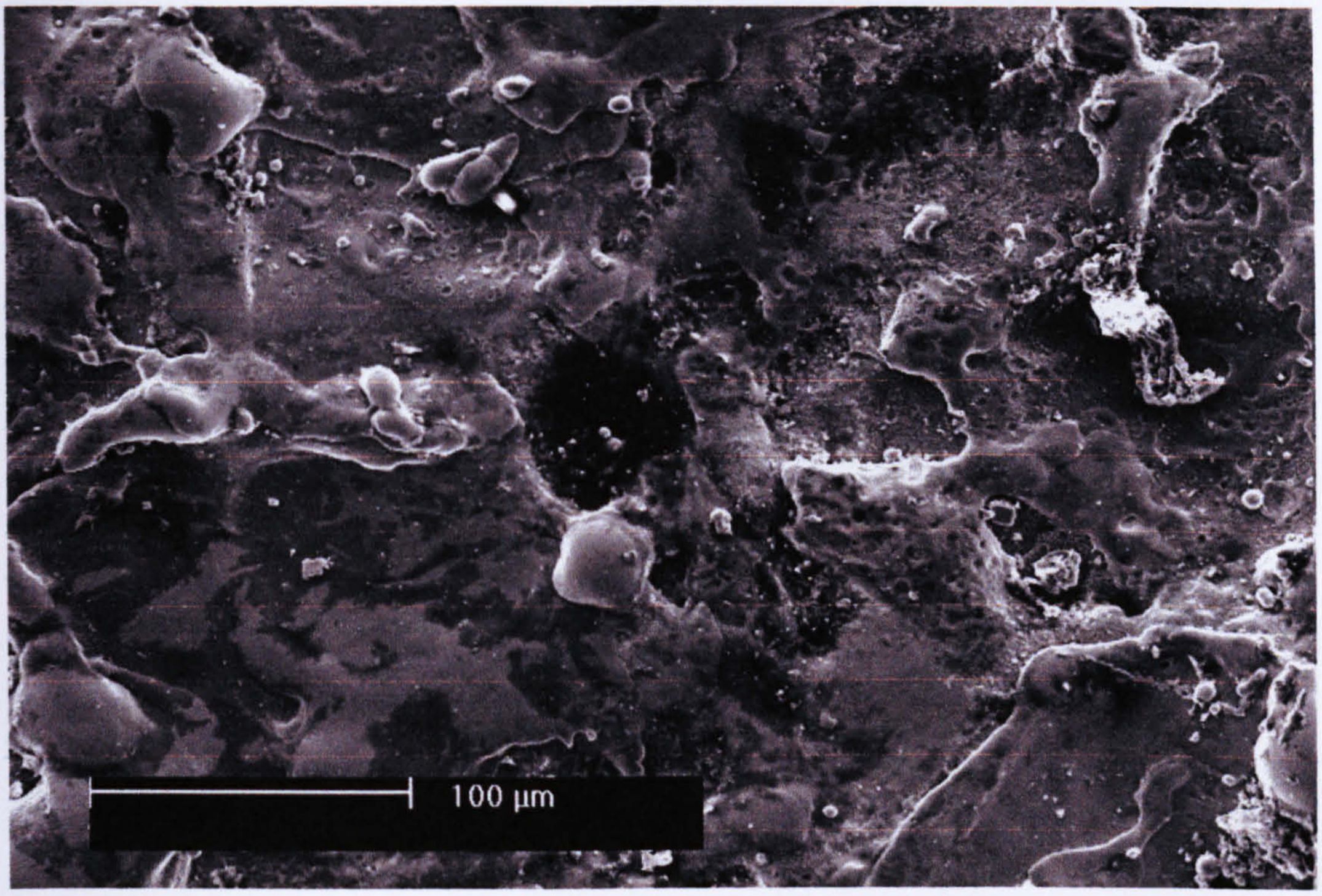

Figure 7-24 EDM surface finish obtained using DC servo control system using current level 8 amperes, 'on' time 50 µsec, duty cycle 12 µsec

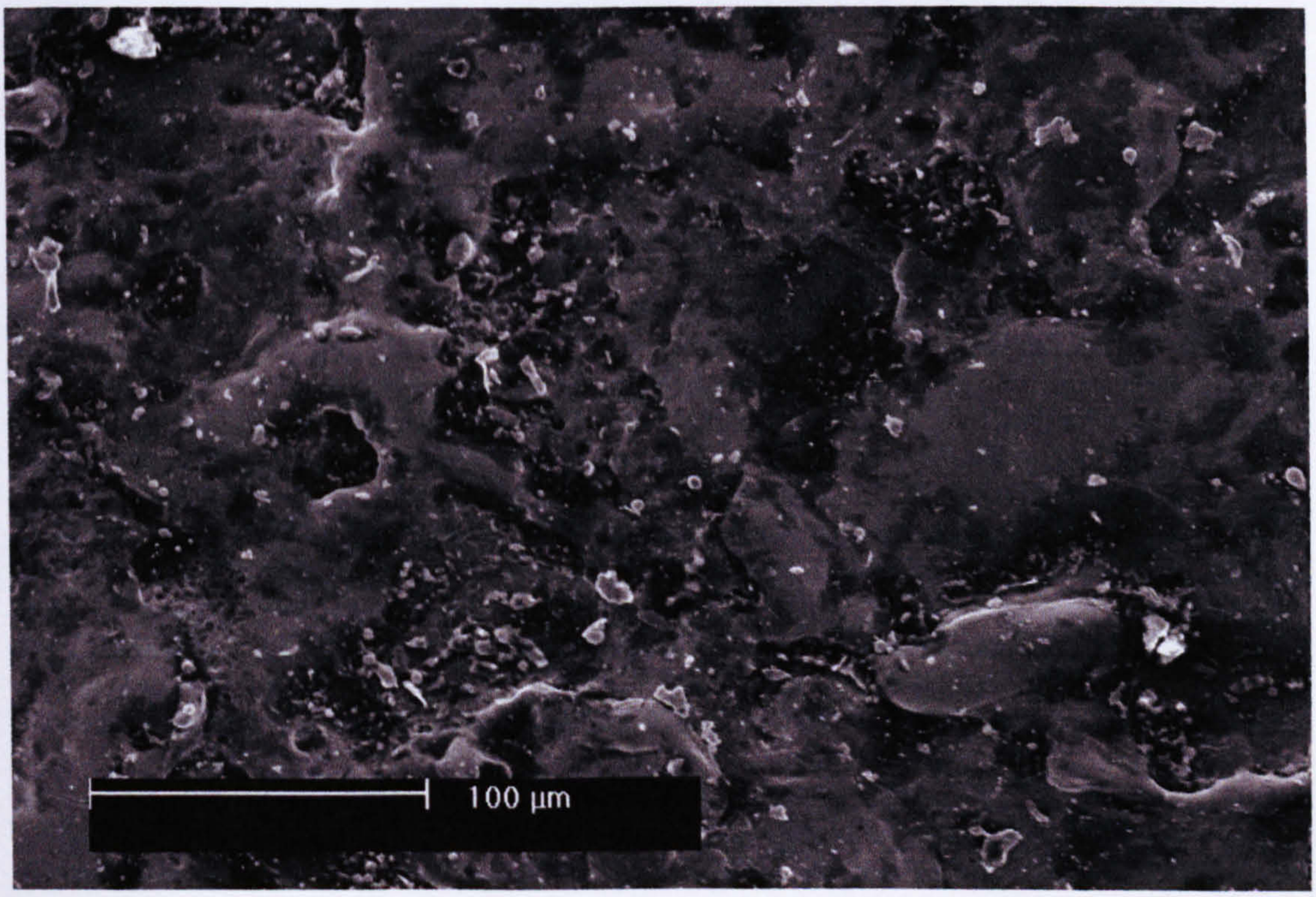

Figure 7-25 EDM surface finish obtained using piezoelectric USM system of control using current level 8 amperes, 'on' time 50 µsec, duty cycle 12 µsec

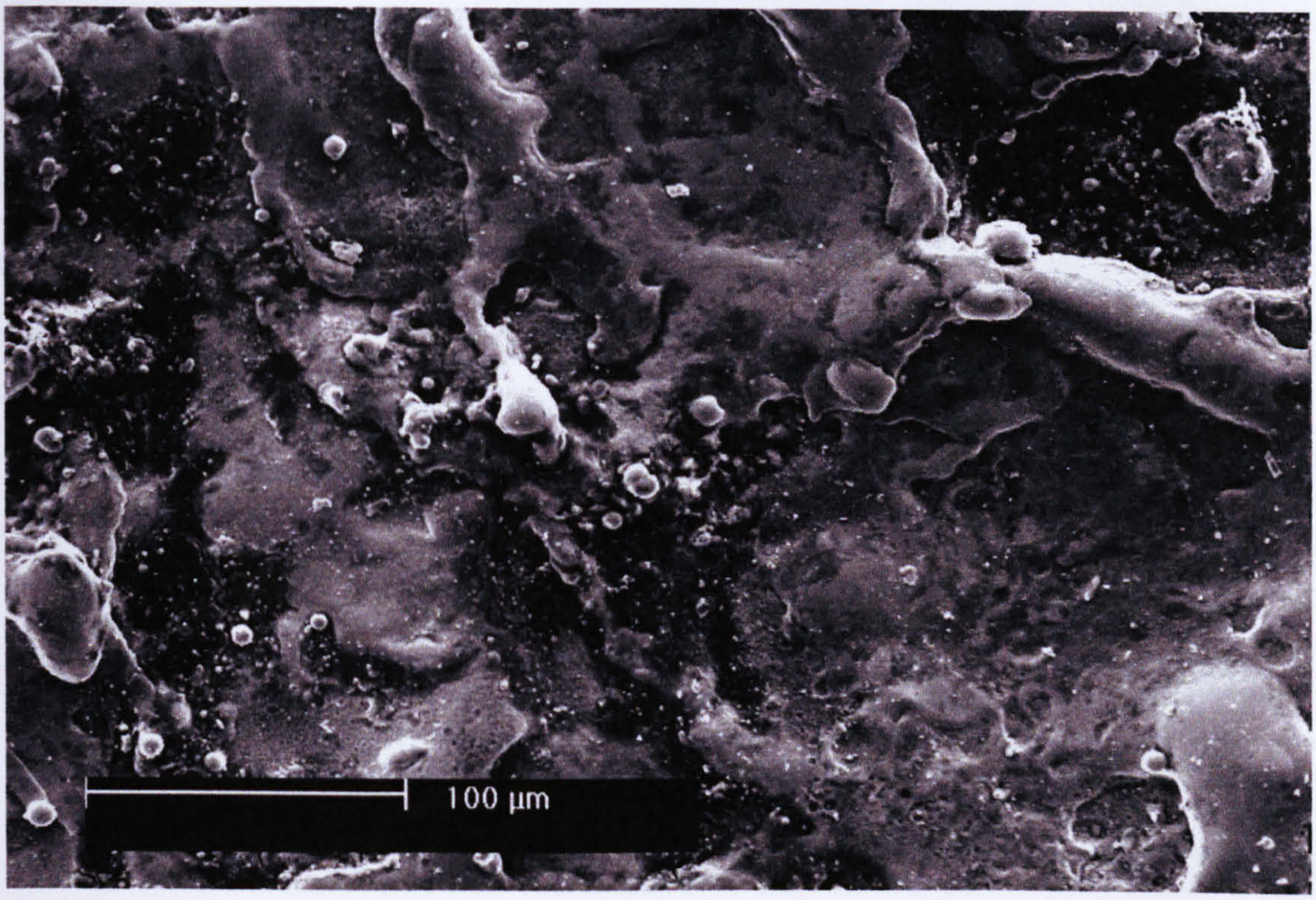

Figure 7-26 EDM surface finish obtained using DC servo control system using current level 10 amperes, 'on' time 50 µsec, duty cycle 12 µsec

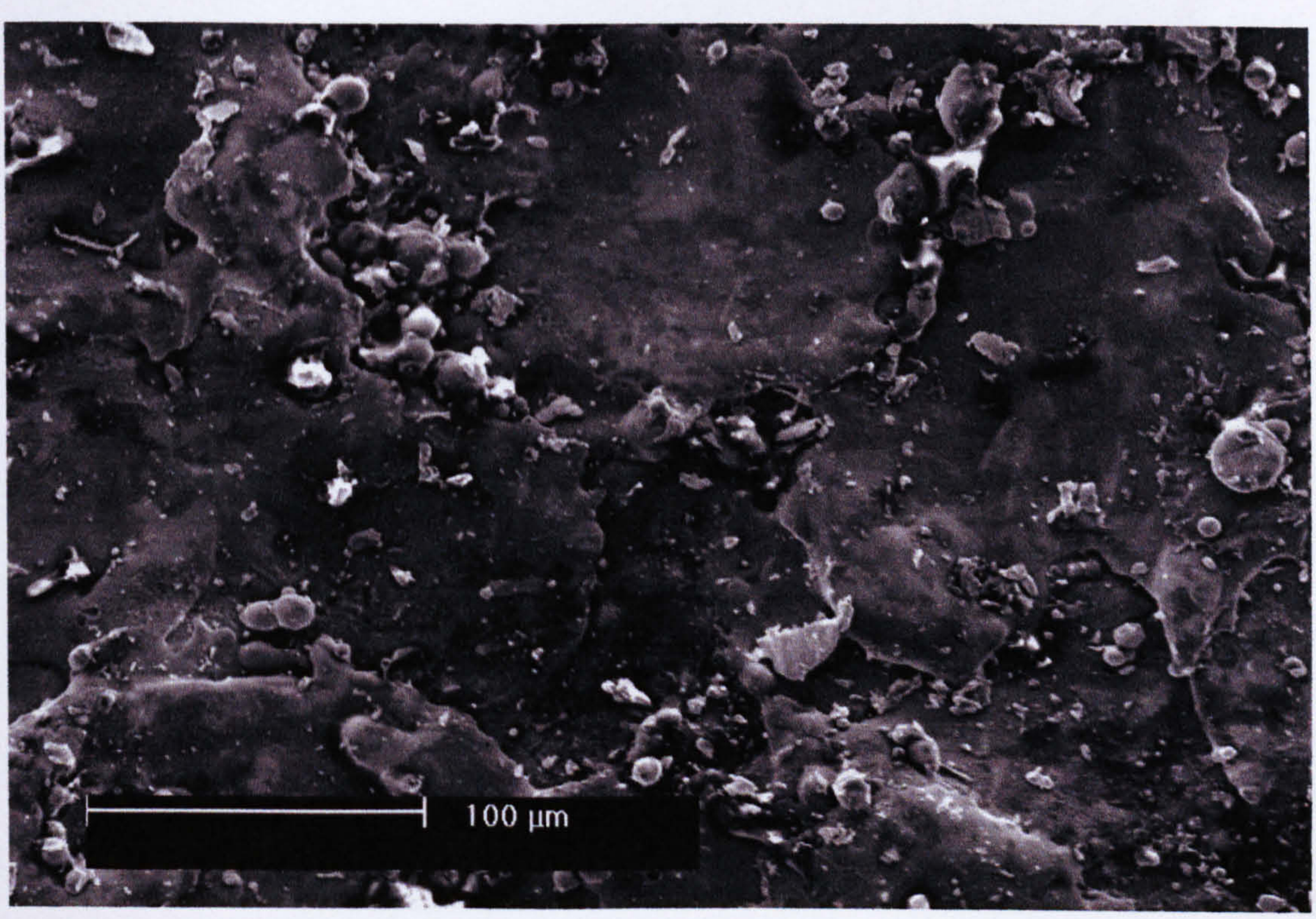

Figure 7-27 EDM surface finish obtained using piezoelectric USM system of control using current level 10 amperes, 'on' time 50 µsec, duty cycle 12 µsec

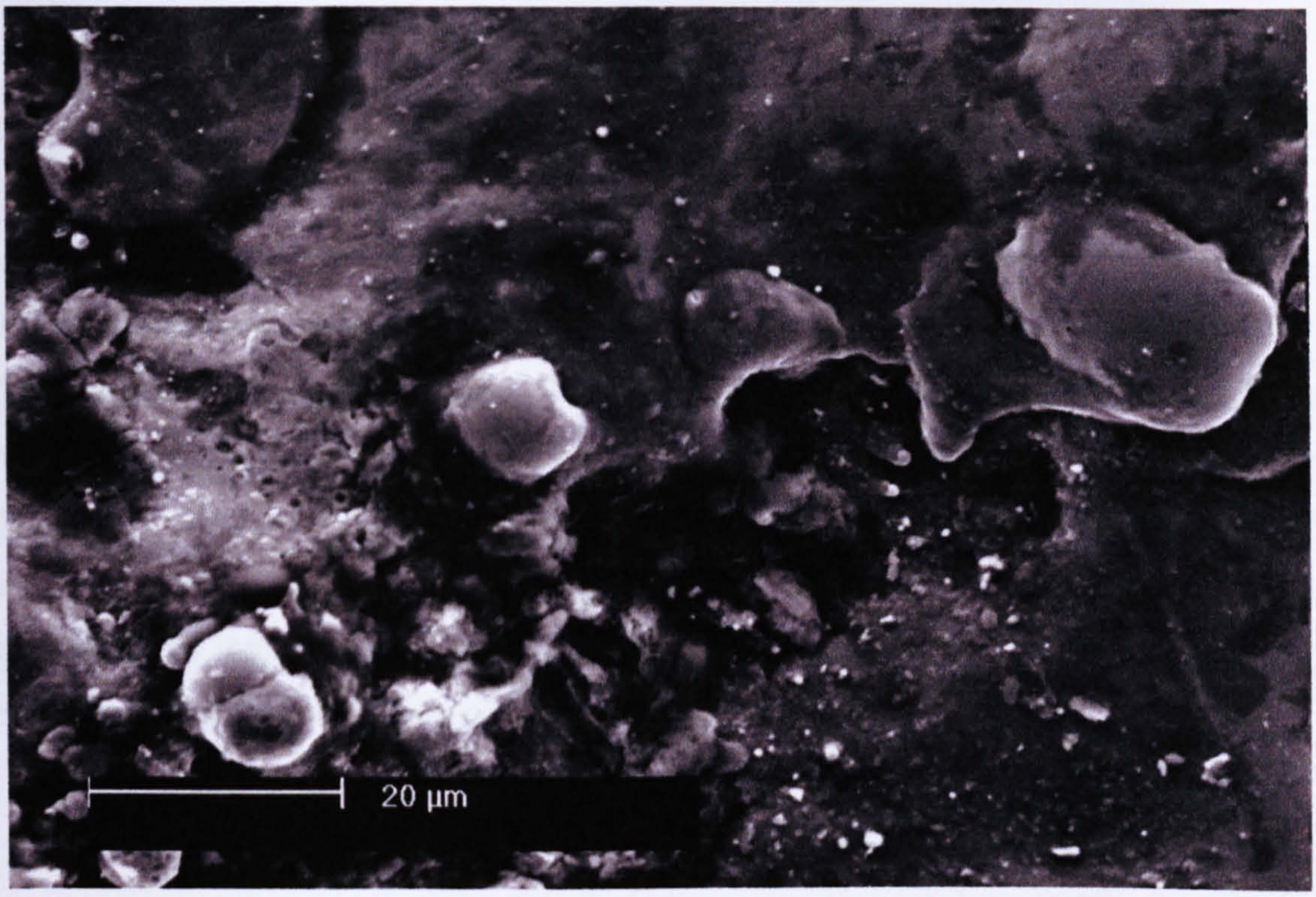

Figure 7-28 EDM surface finish obtained using DC servo control system using current level 10 amperes, 'on' time 50 µsec, duty cycle 12 µsec

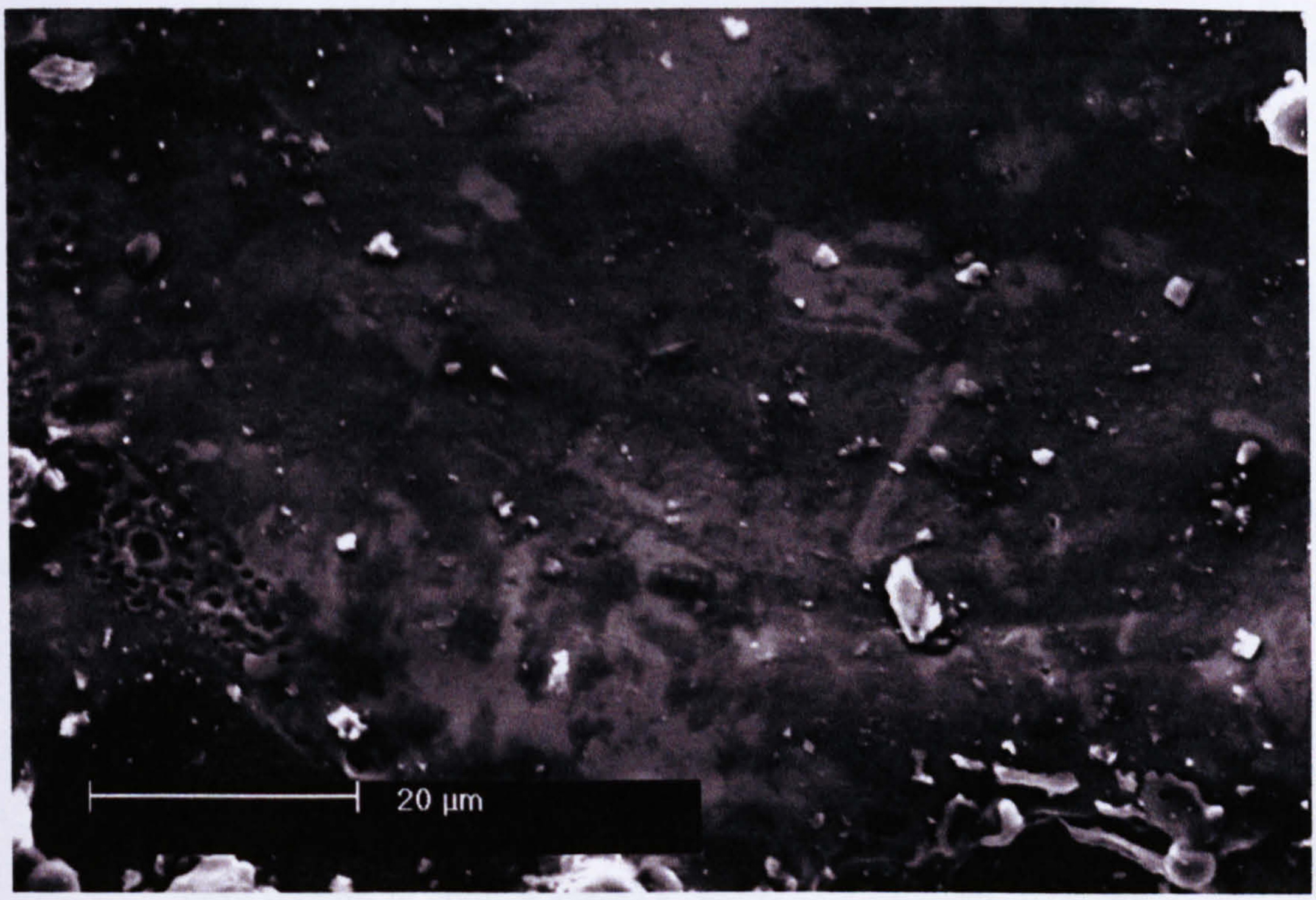

Figure 7-29 EDM surface finish obtained using piezoelectric USM system of control using current level 10 amperes, 'on' time 50 µsec, duty cycle 12 µsec

7.4.1.3 Roughness and Peak Count

The roughness and peak count of different machined holes using various electrical operating parameters were measured. Normally the surface roughness of a machined surface is measured using special equipment. In the case of machining holes it was difficult to achieve the measurements using normal equipment because of the need for a flat surface. Surface roughness in the current case was measured using visual measurements using a comparator chart. The chart was produced on a plate with series of surface finishes. Comparison of the achieved surface with the chart enabled estimation of the degree of surface roughness to be obtained. The relationship between the estimated degree of roughness of the machined products using both systems of control and various machining parameters is shown in Figure 7-30.

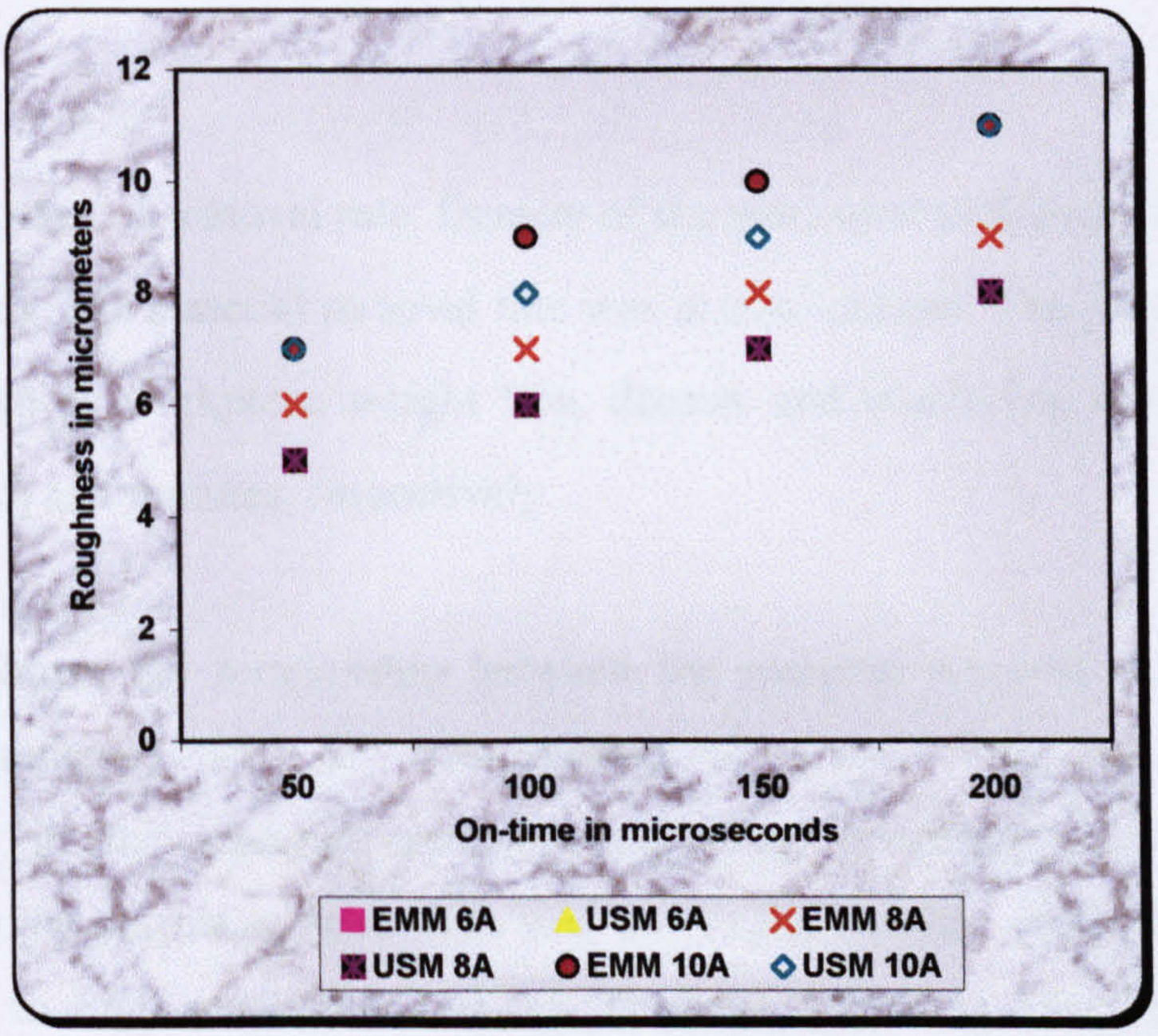

Figure 7-30 Variations of the degree of roughness against machining parameters for both systems of control using DC motor and piezoelectric USM

This investigation shows that the measurements of roughness in the case of the piezoelectric USM control system, gave a close agreement to the current system. This was with improvements in the surface finish of the machined products. The trace of the obtained relation also shows a close agreement with the results reported in this area of research [Appendix (C)].

7.4.1.4 Material Removal Rate

Calculation of the material removal rate was carried out using material removal rate relation equation 7-1. The main parameters of the relation were obtained during machining process for various machining parameters using both systems of control.

$$M.R.R(mm^3/\min) = \frac{[workpiece\ \ weight\ \ loss(gm)x1000]}{[Density(gm/cc)]x[Machining\ \ time(\min)]} \qquad 7\text{-}1$$

$M.R.R$ is the material removal rate. Density of the steel used in this calculation was 7.8 Mg/m^3 (gm/cc). The material removal rate was in mm^3/minute. The parameters used in calculation such as workpiece weight loss, density and machining time were in gm, Mg/m^3 (gm/cc) and minutes, respectively.

Figure 7-31 shows the relationship between the material removal rate and various machining parameters used for both systems of control. This shows clearly the improvements in the material removal rate using developed control system in comparison to the current system. This was due to the stability of machining that was obtained due to high resolution and fast response which in turn lead to a stable machining and shorter processing time.

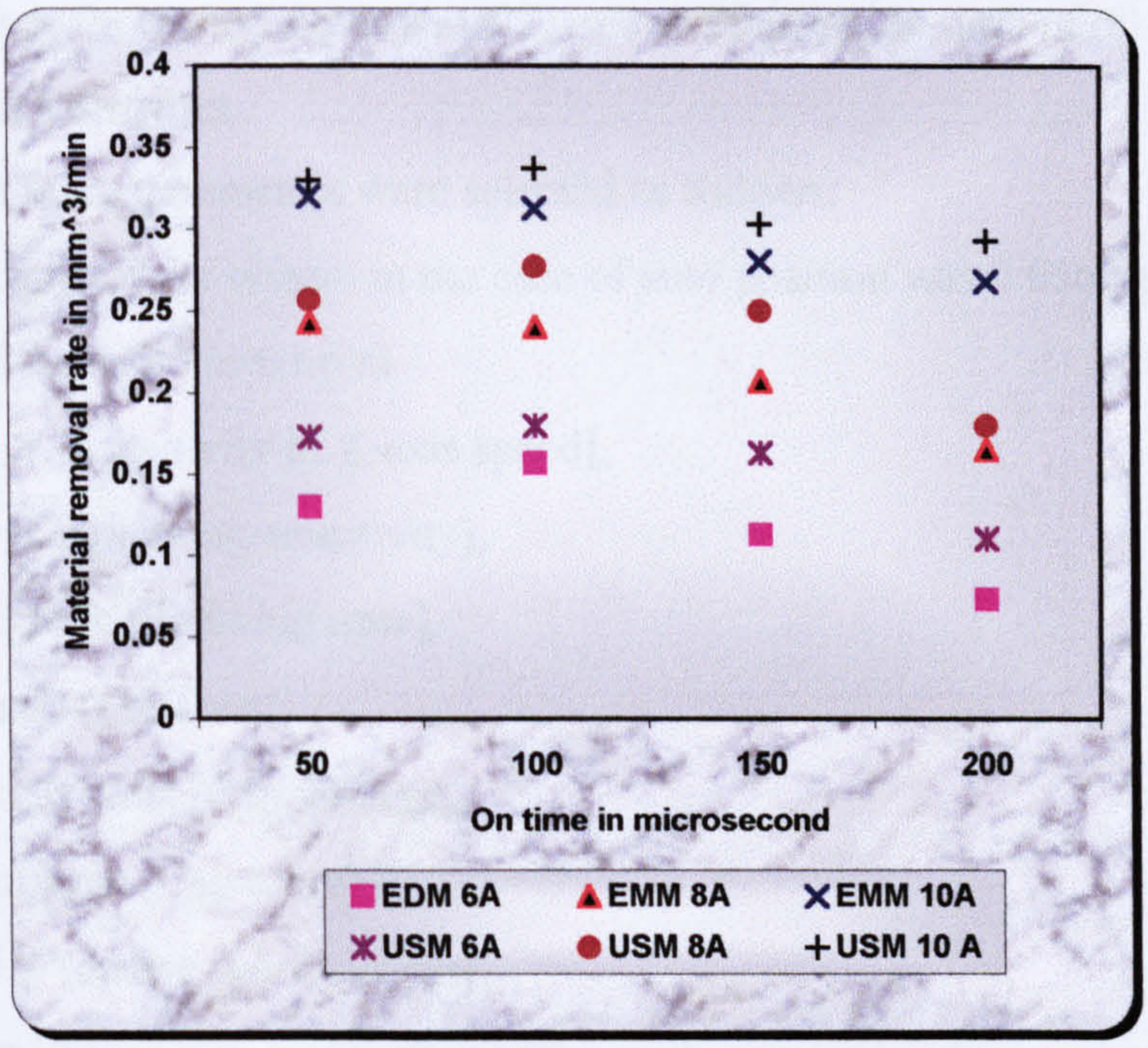

Figure 7-31 Variations of material removal rate for various electro-machining parameters for both systems of control

7.5 EDT- APPLICATION

The EDT-system is a variation on the EDM system. As with ED die sinking, ED wiring, ED sawing and ED grinding, the major difference is only related to change in the configuration of the EDM machine main elements.

In this evaluation the current EDT- control system using DC servo control drive and developed control system using piezoelectric ultrasonic drive, were used for texturing. The levels of current, on/off time and duty cycle were used as main electro-machining parameters. This was aimed at examining and evaluating the developed system stability, capability for control and machining when compared to the current control system.

The electro machining parameters used were as fellows:

- The level of current was on the order of 2 ampere up to 8-amperes, 'on' time of 50 μsec and with a duty cycle of 12 μsec.
- The on-off time was of the order of 10 μsec to 50 μsec, level of current 8 amperes and with a duty cycle of 12 μsec.

- The duty cycle was of the order of 2 μsec to 12 μsec, on time of 50 μsec and level of current 8 amperes.

The other machining parameters were selected as follows:

- The feed rate of the system in the case of auto position was 0.656 mm/sec.
- Speed of the roll was 6 r.p.m
- SEN = 1:3 [Sensitivity of Z-axis speed],
- ASEN = 3-9 [Antiarc sensitivity],
- TW =1.0 μsec [Sparking time],
- T = 0.5μsec [Lifetime],
- Vg = 38: 50 volts [Gap voltage],
- Ig = 5 amperes [Gap current],
- Ib = 0. 0 [Prepulse spark current],
- POL=-ve [Polarity of machining] and
- Fp=0.2 bar [Flushing pressure].

7.5.1 Experimental Work and Results

The current system using DC servo control drive was used for machining different degrees of texturing using various electro-machining parameters. This included the current level, on-off time and duty cycle. Then the developed system using an ultrasonic control system with the same machining conditions and electro-machining parameters was used. Tables 7-4, 7-5, 7-6 and 7-7 show the machining paramteres used in this evaluation.

Table 7-4 Machining parameters used in the investigation of the effect of the level of current on the surface finish of the textured product using both systems of control (piezoelectric USM and DC motor)

Test No	Sparking Current (Ampere)	On-Time (μs)	Gap Voltage (Volt)	Gap current (A)	Duty cycle (μs)
1	**2**	**50**	**38**	**5**	**12**
2	**4**	**50**	**38**	**5**	**12**
3	**6**	**50**	**38**	**5**	**12**
4	**8**	**50**	**38**	**5**	**12**

Table 7-5 Machining parameters used in the investigation of the effect of the on-off time on the surface finish of the textured product using both systems of control (piezoelectric USM and DC motor)

Test No	Sparking Current (Ampere)	On-Time (µSec)	Gap Voltage (Volt)	Gap current (Ampere)	Duty cycle (µSec)
1	**8**	**10**	**38**	**5**	**12**
2	**8**	**20**	**38**	**5**	**12**
3	**8**	**30**	**38**	**5**	**12**
4	**8**	**50**	**38**	**5**	**12**

Table 7-6 Measured parameters results of machining using various levels of current on the surface finish textured using both systems of control (piezoelectric USM and DC motor)

Test No.	Peak current Ip (Ampere)	DC motor Roughness Ra µm	DC motor Peak count Pc/cm	USM Roughness Ra µm	USM Peak count Pc/cm
01	**2**	**1.31**	**130**	**1.795**	**120**
02	**4**	**2.425**	**112**	**3.015**	**96**
03	**6**	**2.61**	**102**	**3.49**	**91**
04	**8**	**3.215**	**86**	**3.65**	**80**

Table 7-7 Measured parameters results of machining using various on/off times on the surface finish textured using both control systems (piezoelectric USM and DC motor)

Test No.	On/off time µSec	DC motor Roughness Ra µm	DC motor Peak count Pc/cm	USM Roughness Ra µm	USM Peak count Pc/cm
01	**10**	**2.27**	**112**	**2.45**	**115**
02	**20**	**2.60**	**103**	**2.95**	**109**
03	**30**	**2.88**	**94**	**3.2**	**99**
04	**50**	**3.17**	**82**	**4.27**	**70**

The feed rate in the case of the ultrasonic system of control was of the order of 5.1 mm/sec. The experimental evaluation of both systems of control in this case included:

- Stability of the system,
- Surface finish (roughness, Pc peak/cm),
- Capability of the system to monitoring and control the inter-electrode gap, and
- Safety of machining process.

7.5.1.1 Stability of the System

The stability of the EDT-system was measured from the stability of the gap voltage and current in addition to the control signal obtained from the control unit. The feedback signal and inter-electrode gap voltage variation were obtained at various operating parameters and machining conditions. This was used in this investigation to determine the stability of the two systems of control.

Figures 7-32 to 7-47 illustrate feedback control signal and inter-electrode gap voltage variations for various electro-machining parameters for both systems for control using DC servomotor and piezoelectric USM.

Figures 7-32, 7-34, 7-36, and 7-38 show the variation in the feedback control signal and gap voltage for different levels of current using piezoelectric ultrasonic control system.

Figures 7-38, 7-40, 7-42, and 7-44 illustrate the variations in the feedback control signal and gap voltage for different on times machining. Figure 7-46 shows the stability of the system for machining period of 10 seconds.

Figures 7-33, 7-35, 7-37, and 7-39 show the variation in feedback control signal and gap voltage for various levels of current using DC servo control system.

Figures 7-39, 7-40, 7-43, and 7-45 illustrate the variation for different on times machining. Figure 7-47 shows the stability of the system for machining period of 10 seconds.

These Figures show the stability of the system using both systems of control at various operating conditions. It clearly shows the improvements in the EDT- system stability using developed control system when compared to the current system which uses DC servomotor. The developed system also shows a reduction in the arcing and short-circuiting processes which in turn may lead to a clear reduction in the machining time and an improvement in the surface finish of the products.

Two factors were also observed to play a significant influence in the stability of the system namely the sensitivity and the antiarcing factor. The facility to changing the operating parameters during machining was used, in this case to provide a stable system. It was clear that mishandling of the sensitivity and antiarcing factor produced jerking effect which leads to unstable machining which in turn increased the arcing and short circuit process. The arcing and short circuit processes produce poor surface finish. This was clear in the case of the DC servo control system rather than the developed control system using piezoelectric USM.

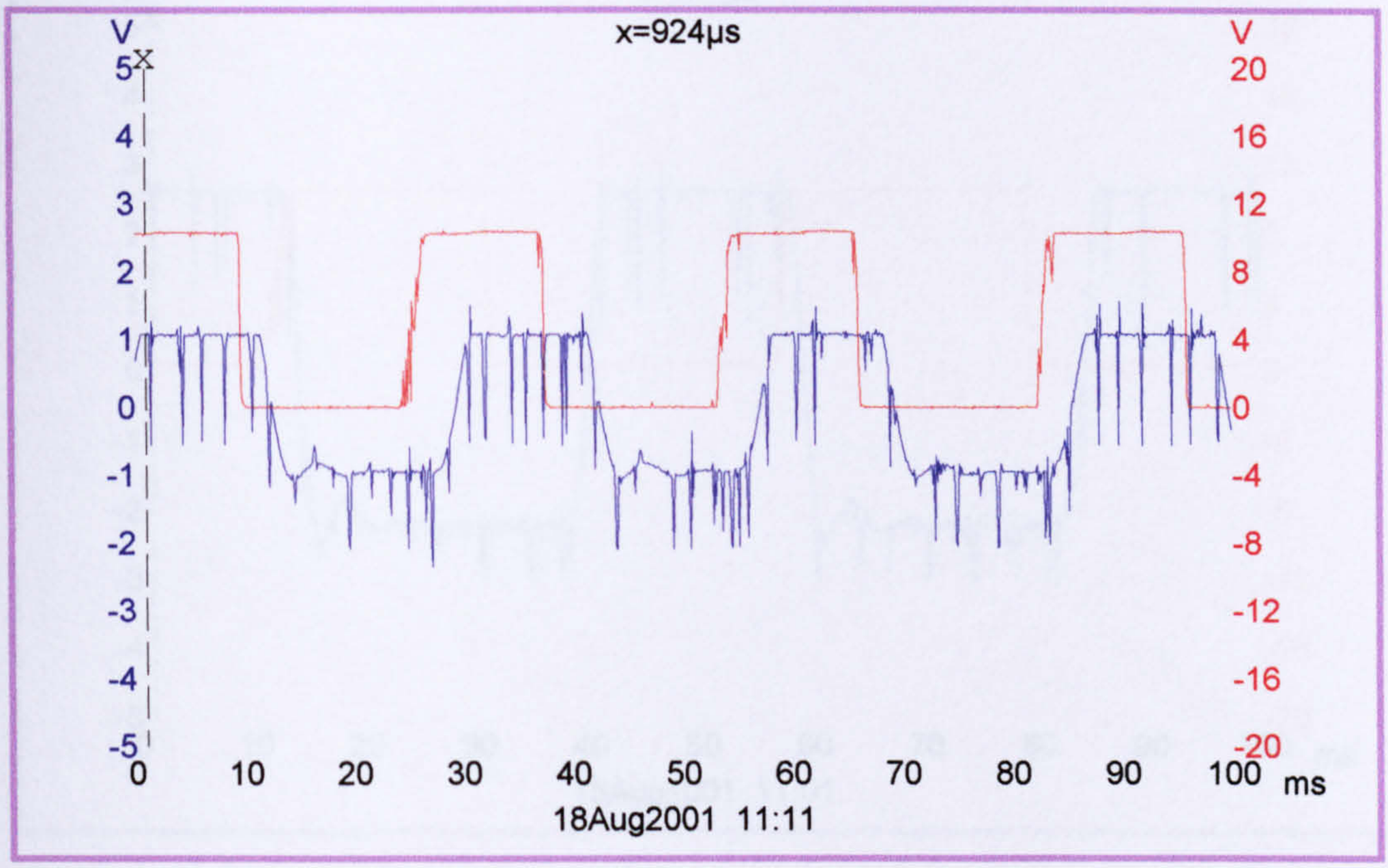

Figure 7-32 Feedback control signal (red) and inter-electrode gap voltage (blue) variation for EDT machining using the developed piezoelectric control system [peak current 2A, duty cycle 12 µsec & 'on' time 50 µsec]

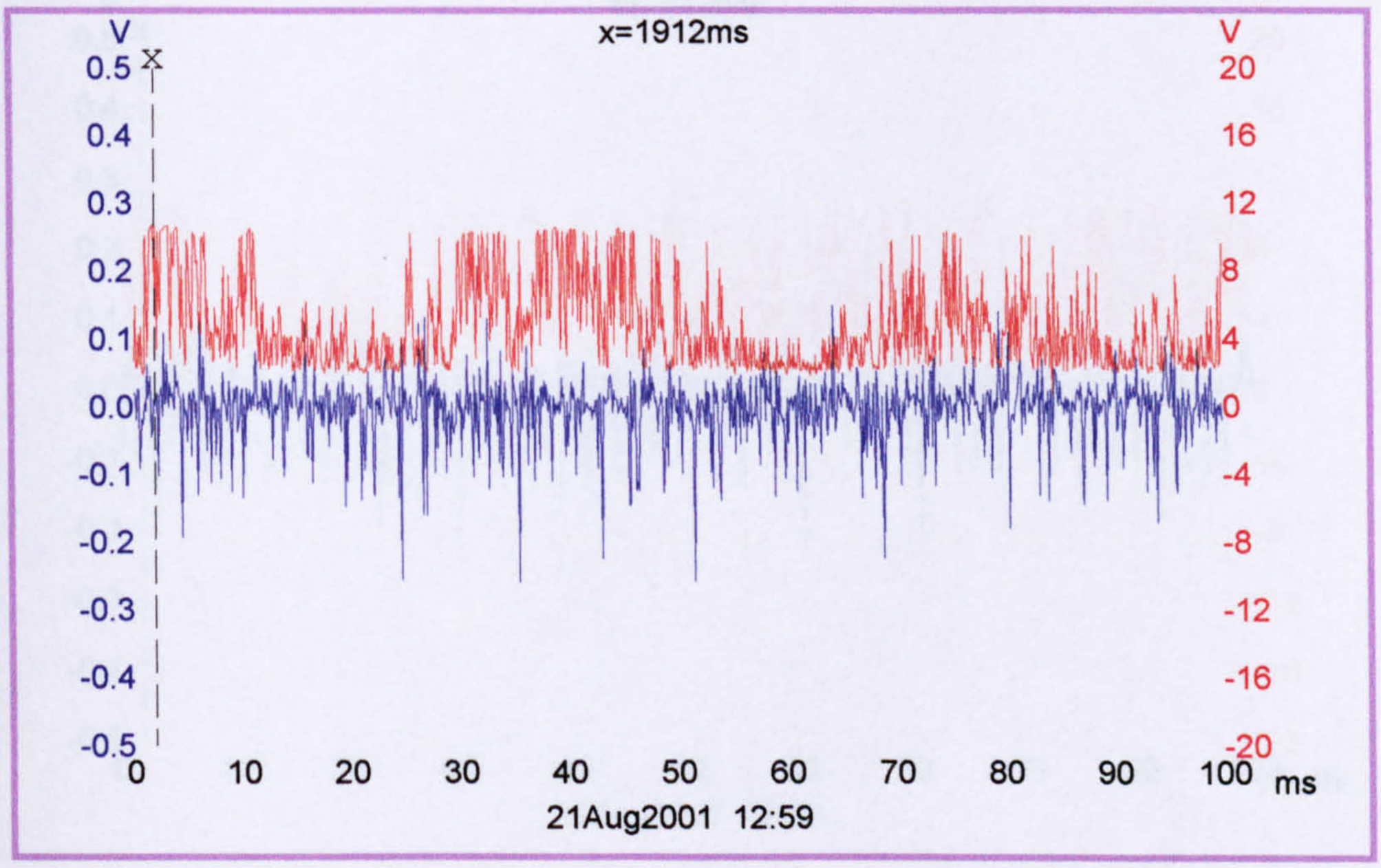

Figure 7-33 Feedback control signal (red) and inter-electrode gap voltage (blue) variation for EDT machining using an existing DC servo control system [peak current 2A, duty cycle 12 µsec & 'on' time 50 µsec]

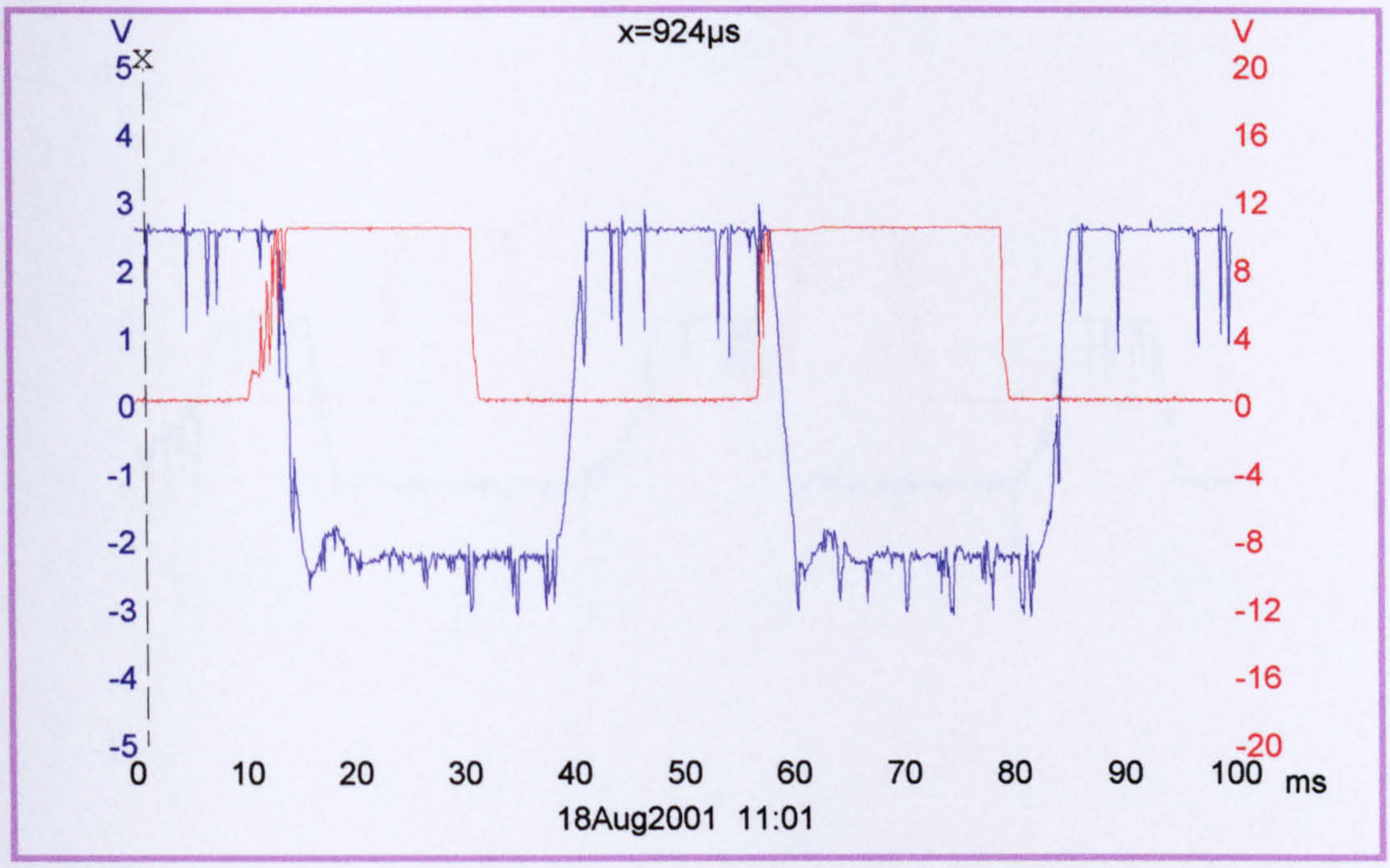

Figure 7-34 Feedback control signal (red) and inter-electrode gap voltage (blue) variation for EDT machining using the developed piezoelectric control system [peak current 4A, duty cycle 12 µsec & 'on' time 50 µsec]

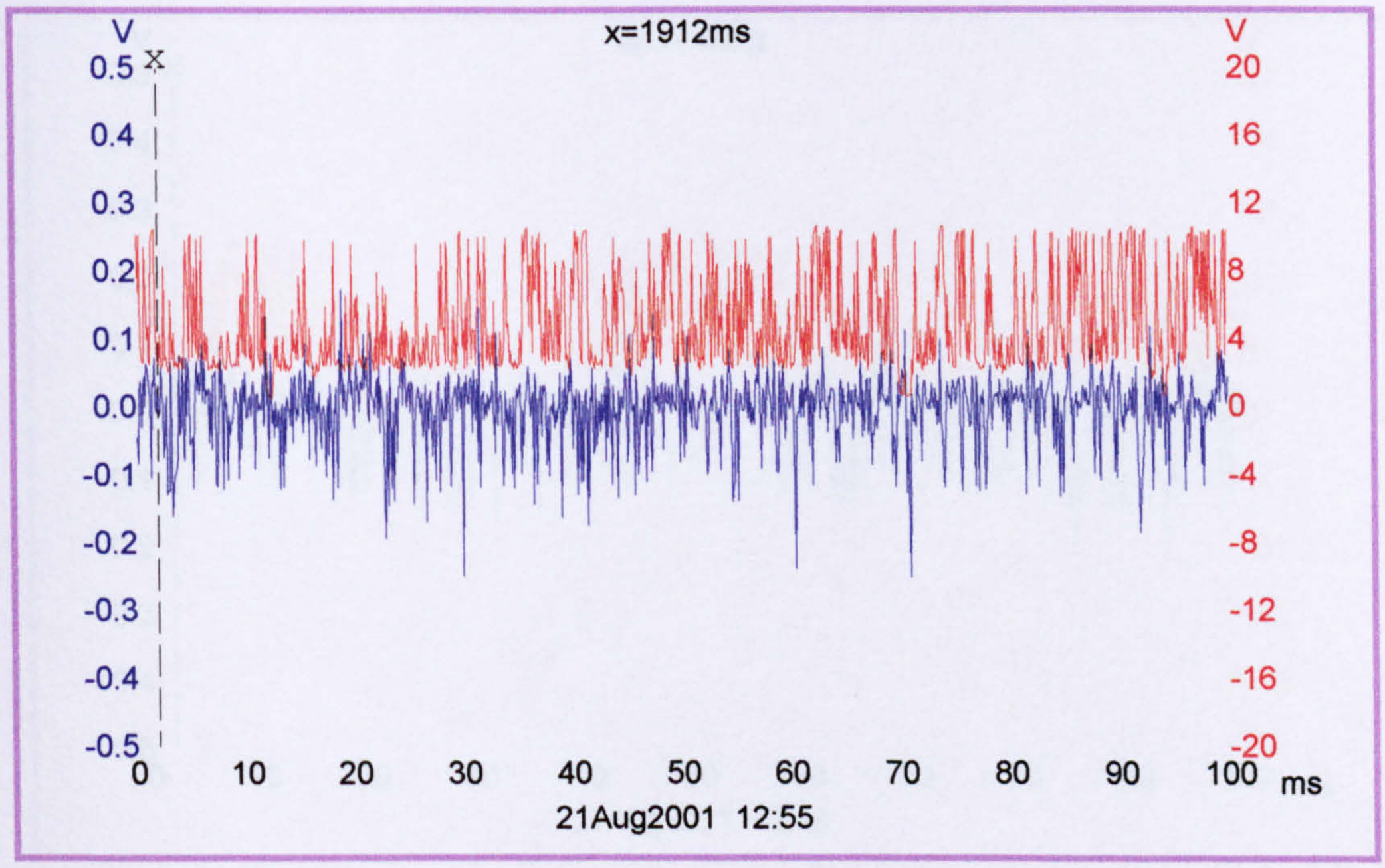

Figure 7-35. Feedback control signal (red) and inter-electrode gap voltage (blue) variation for EDT machining using an existing DC servo control system [peak current 4A, duty cycle 12 µsec & 'on' time 50 µsec]

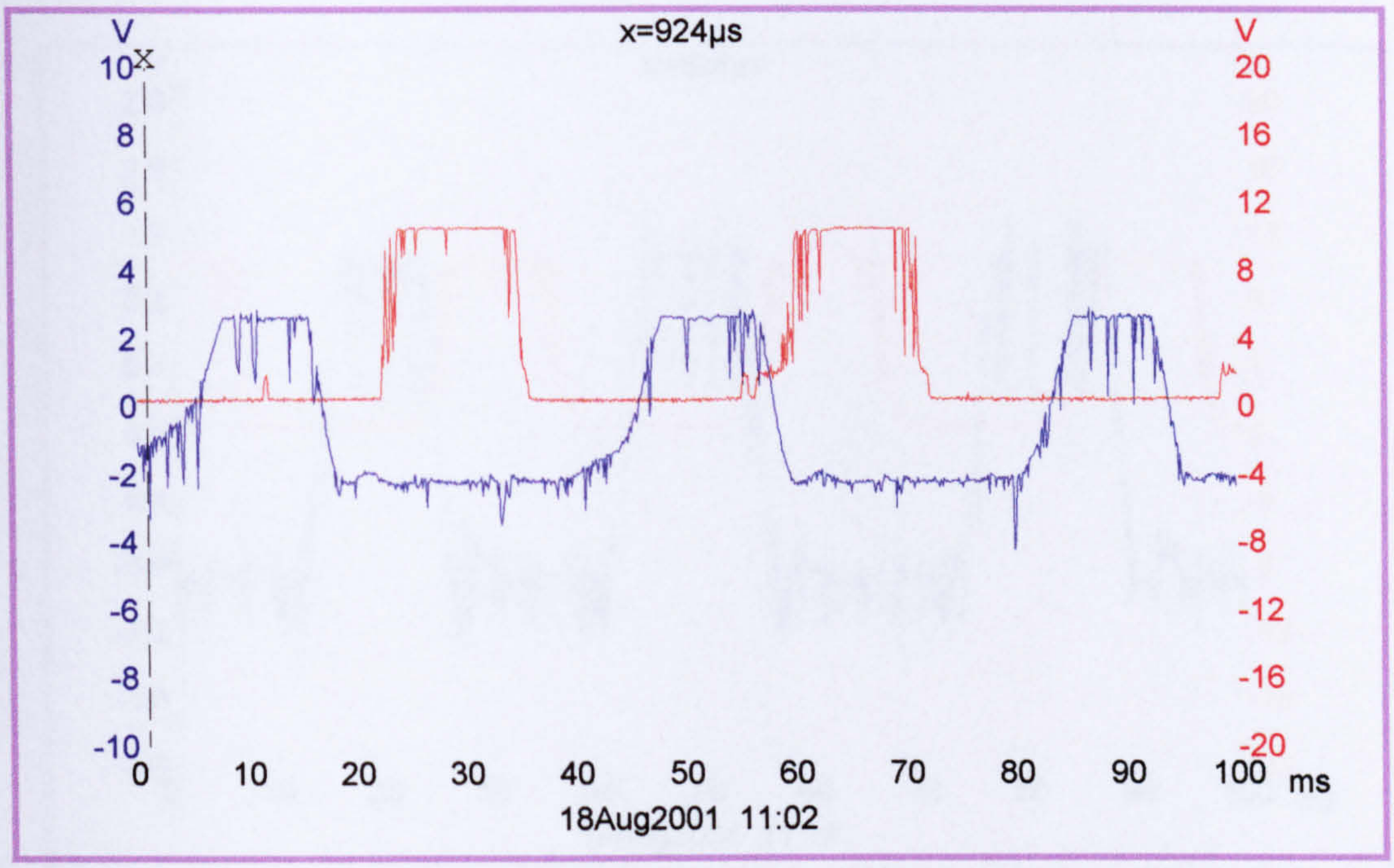

Figure 7-36 Feedback control signal (red) and inter-electrode gap voltage variation (blue) for EDT machining using the developed piezoelectric control system [peak current 6A, duty cycle 12 µsec & 'on' time 50 µsec]

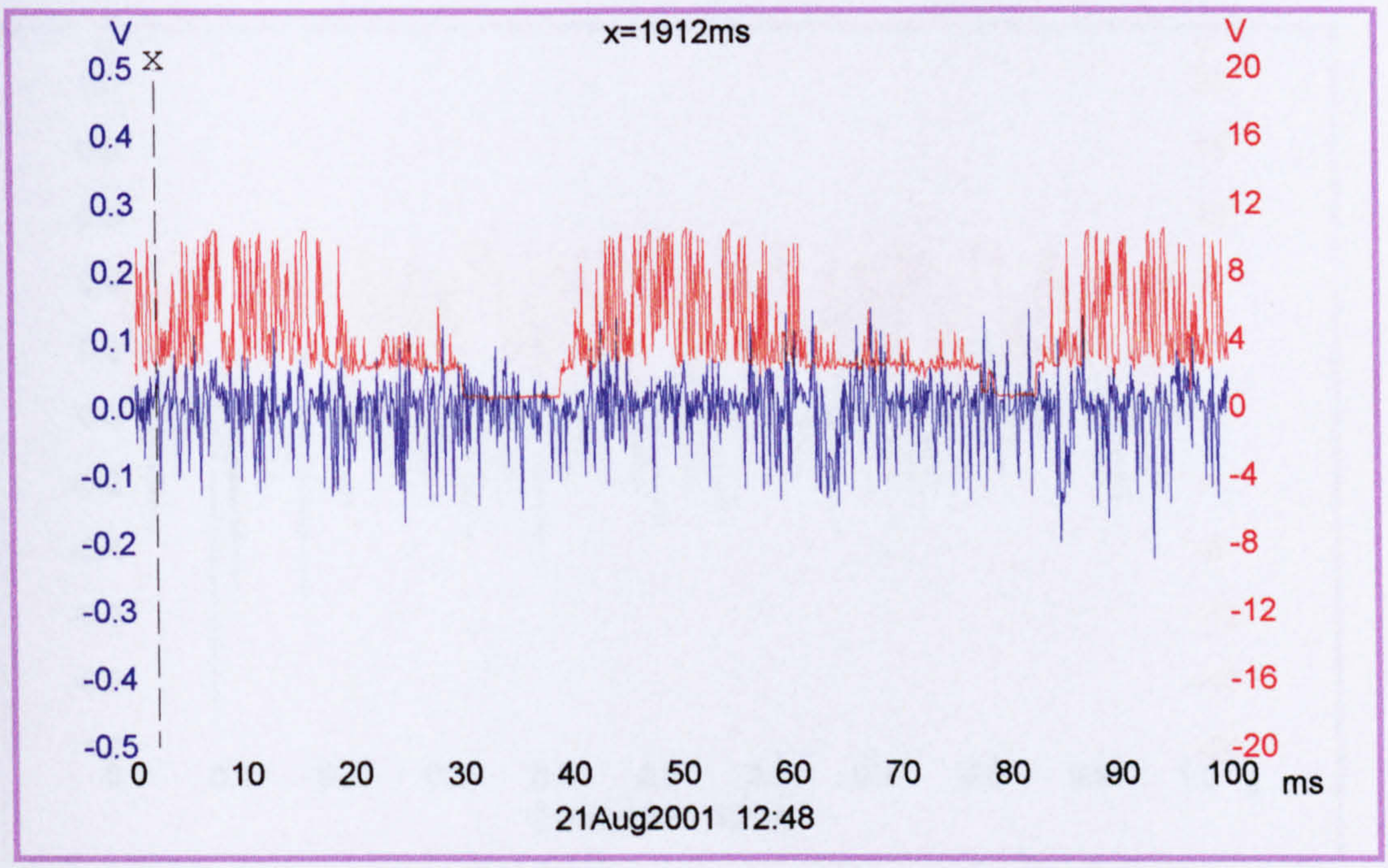

Figure 7-37 Feedback control signal (red) and inter-electrode gap voltage(blue) variation for EDT machining using an existing DC servo control system [peak current 6A, duty cycle 12 µsec & 'on' time 50 µsec]

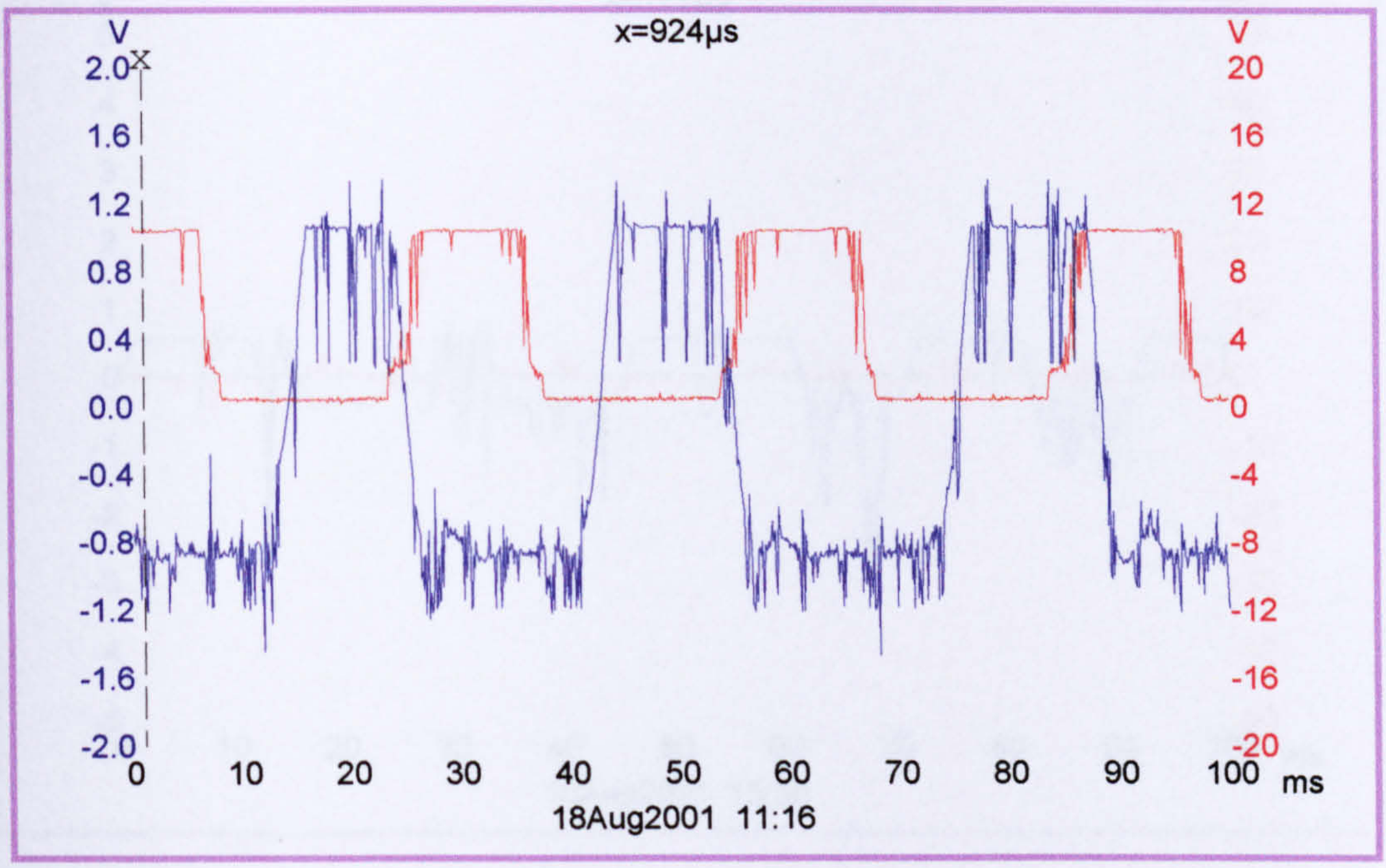

Figure 7-38 Feedback control signal (red) and inter-electrode gap voltage (blue) variation for EDT machining using the developed piezoelectric control system [peak current 8A, duty cycle 12 µsec & 'on' time 50 µsec]

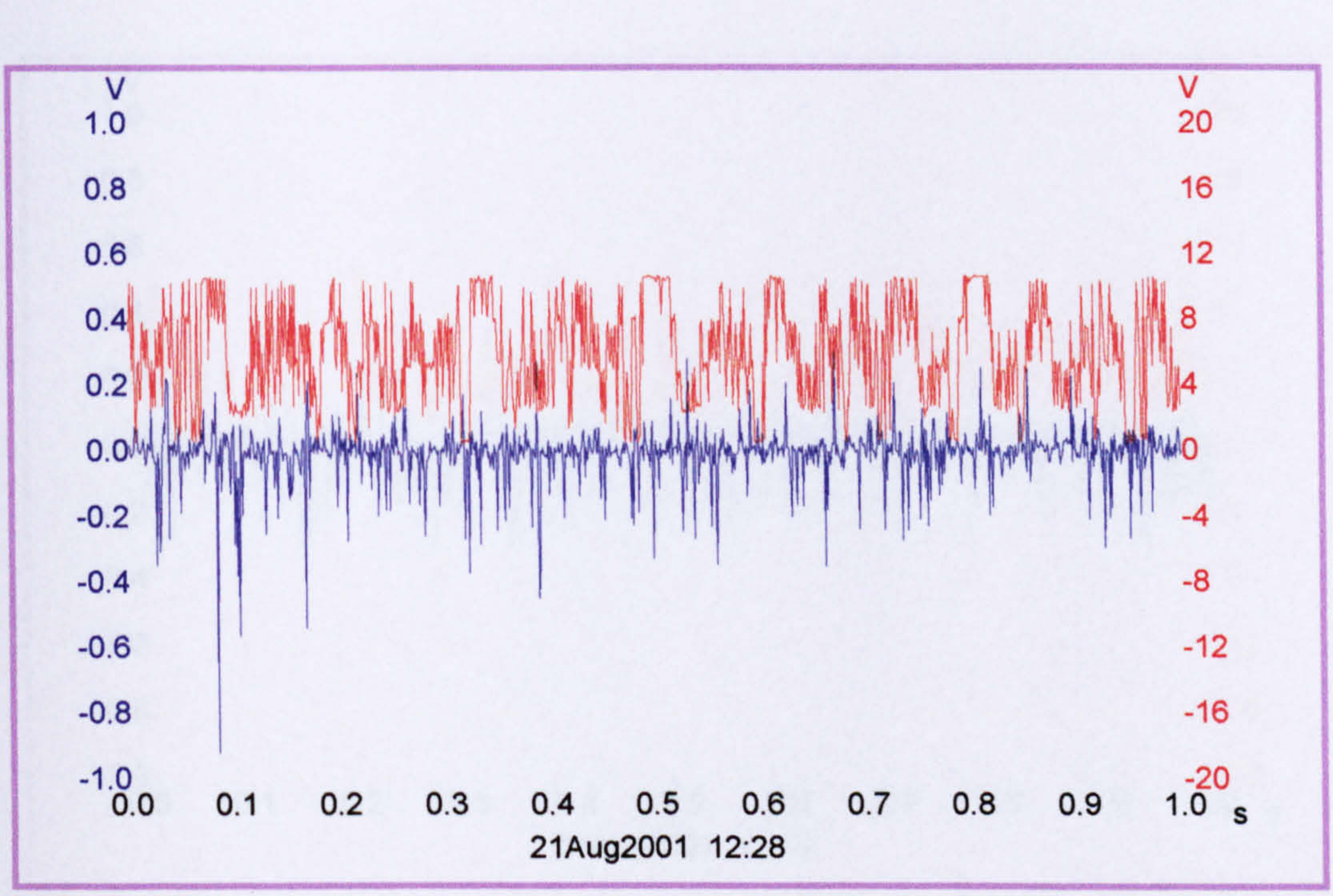

Figure 7-39. Feedback control signal (red) and inter-electrode gap voltage (blue) variation for EDT machining using an existing DC servo control system [peak current 8A, duty cycle 12 µsec & 'on' time 50 µsec]

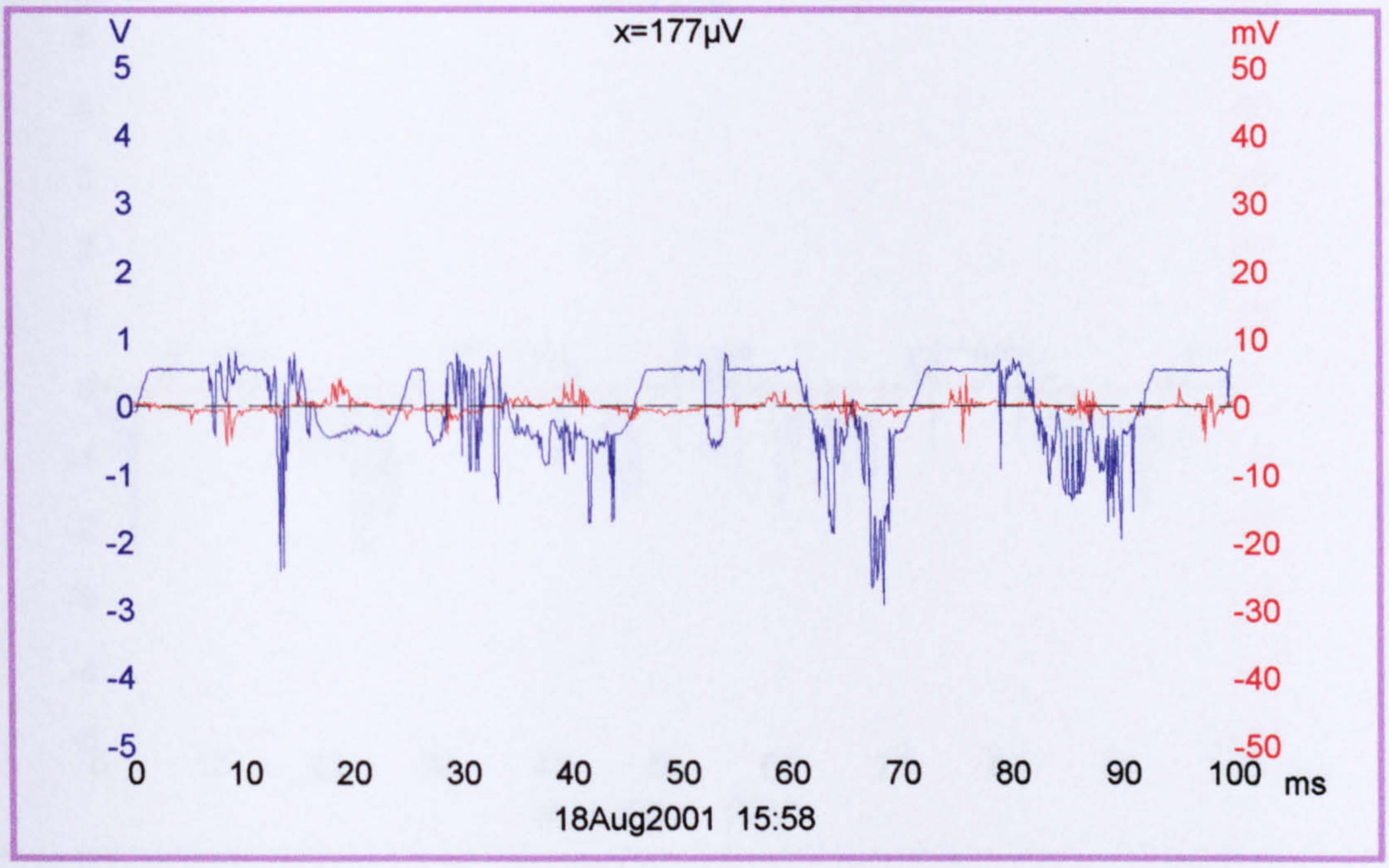

Figure 7-40. Feedback control signal (red) and inter-electrode gap voltage (blue) variation for EDT machining using the developed piezoelectric control system [peak current 8A, duty cycle 12 μsec & 'on' time 30 μsec]

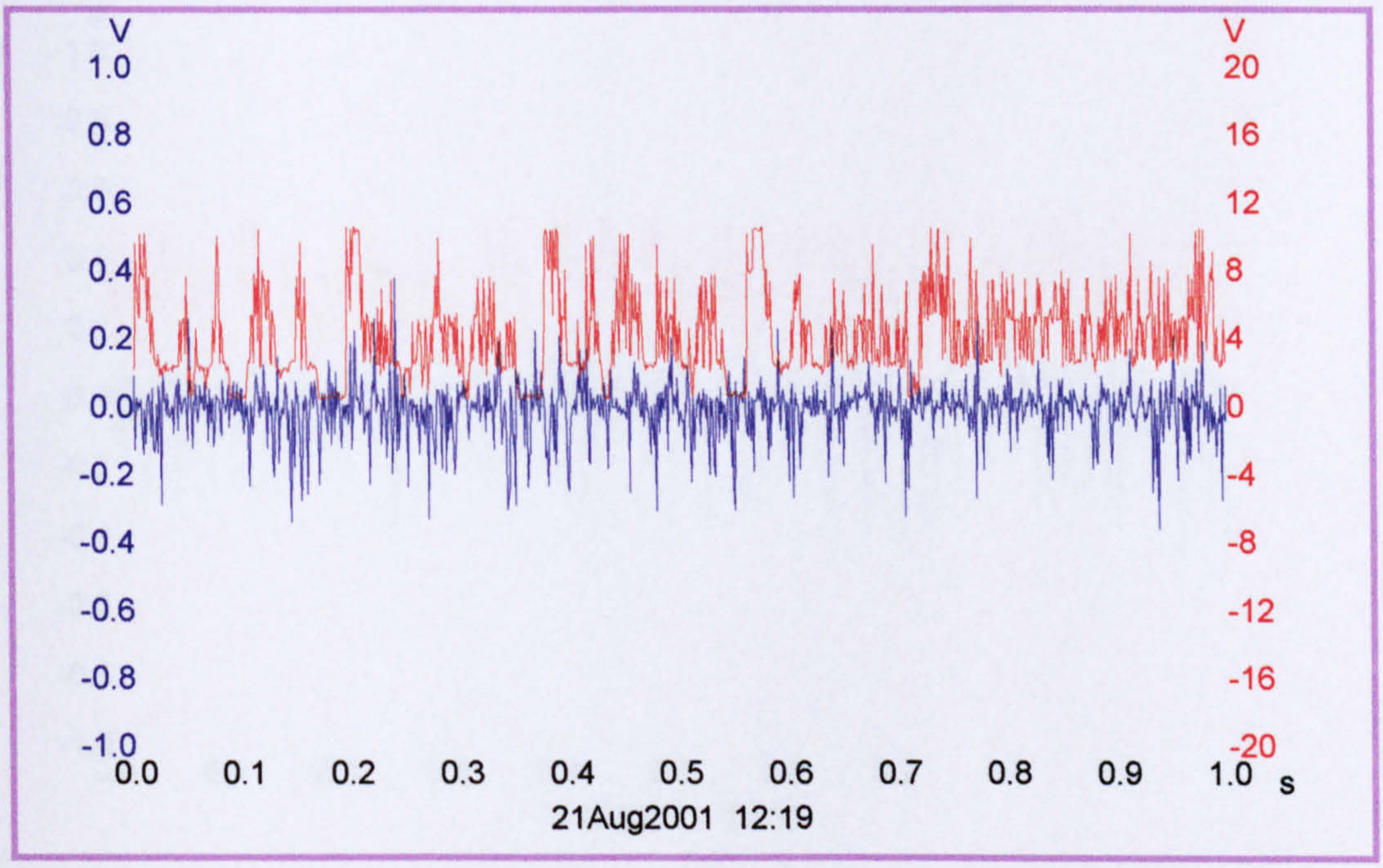

Figure 7-41. Feedback control signal (red) and inter-electrode gap voltage (blue) variation for EDT machining using an existing DC servo control system [peak current 8A, duty cycle 12 μsec & 'on' time 30 μsec]

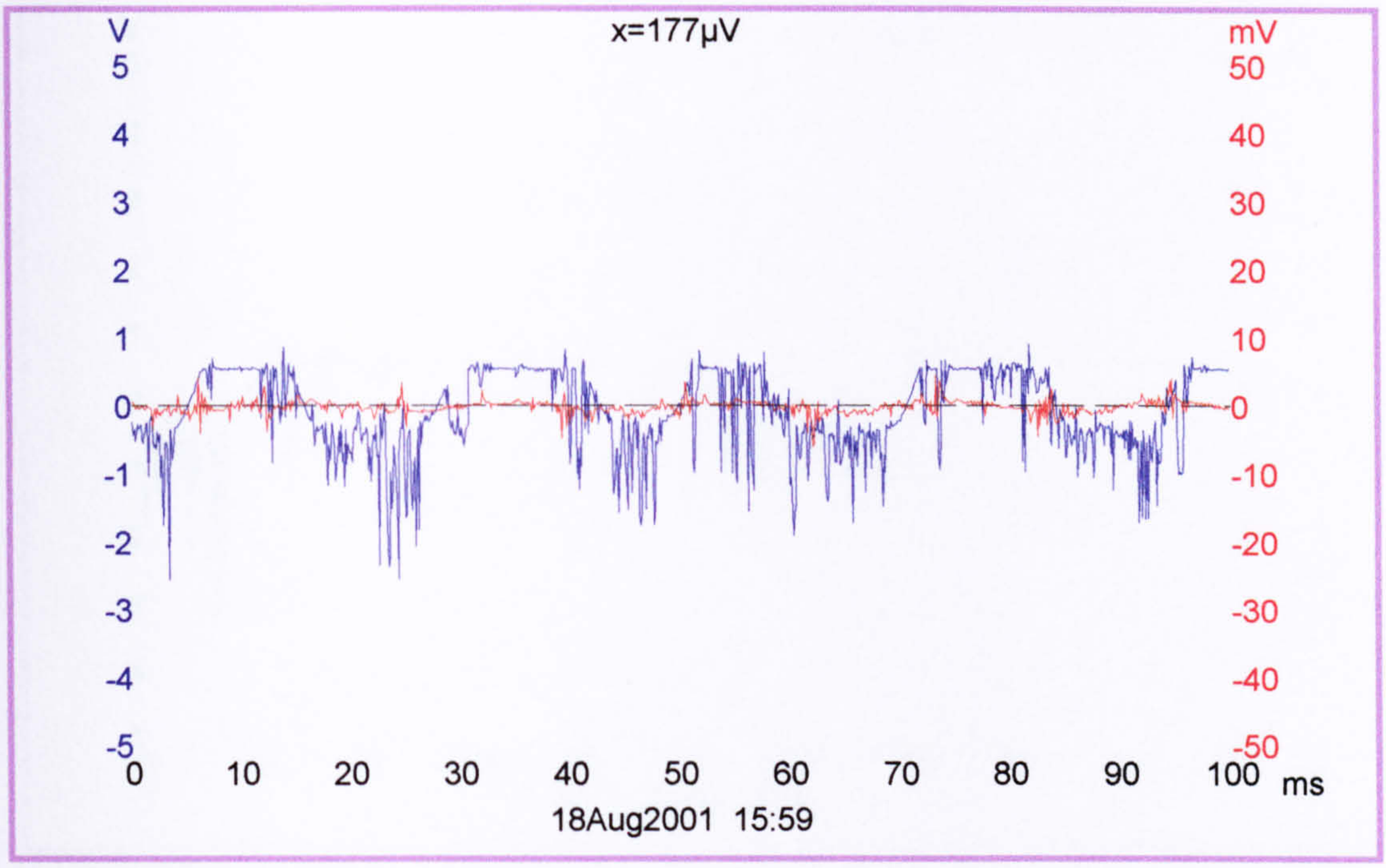

Figure 7-42. Feedback control signal (red) and inter-electrode gap voltage (blue) variation for EDT machining using the developed piezoelectric control system [peak current 8A, duty cycle 12 μsec & 'on' time 20 μsec]

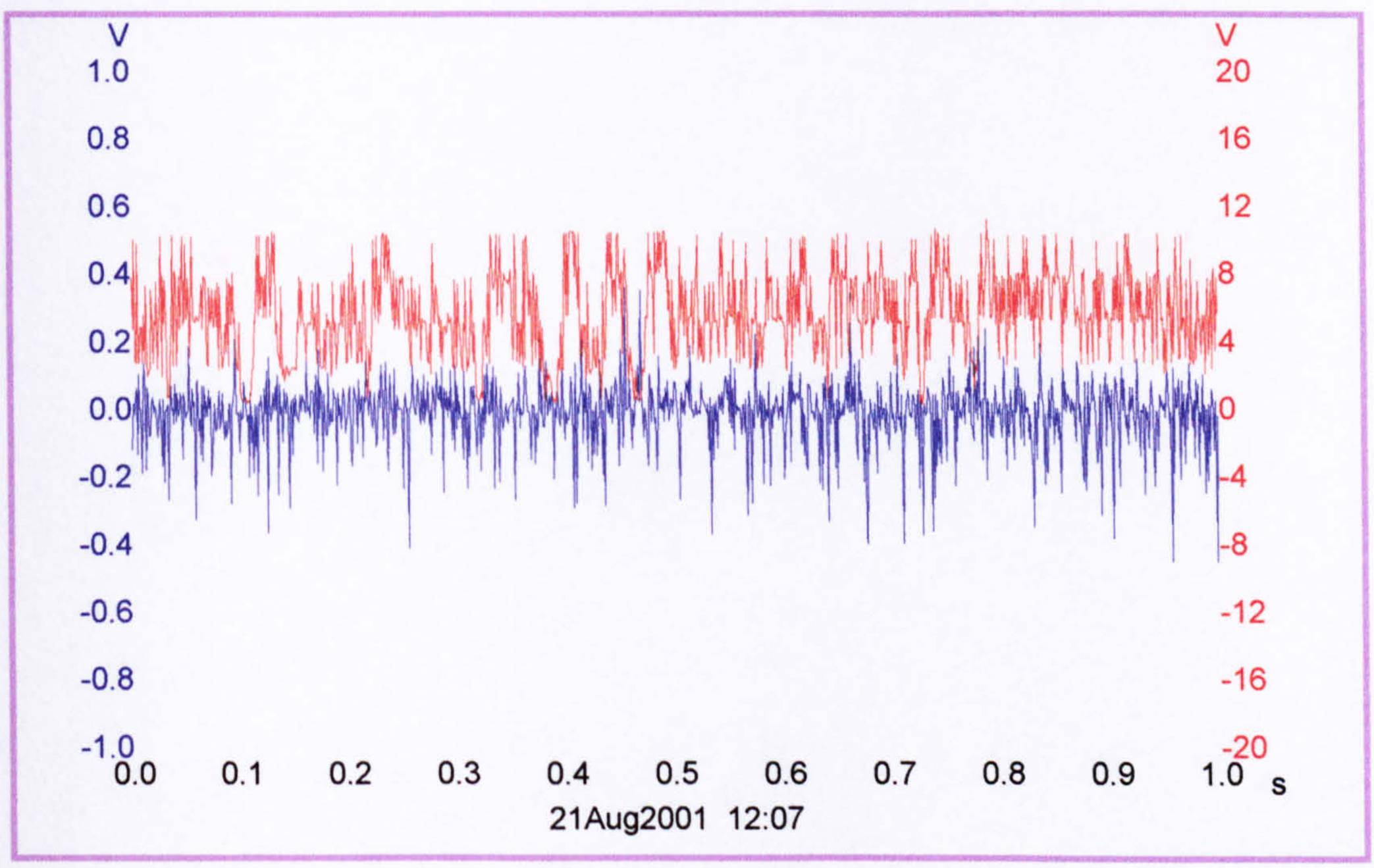

Figure 7-43. Feedback control signal (red) and inter-electrode gap voltage (blue) variation for EDT machining using an existing DC servo control system [peak current 8A, duty cycle 12 μsec & 'on' time 20 μsec]

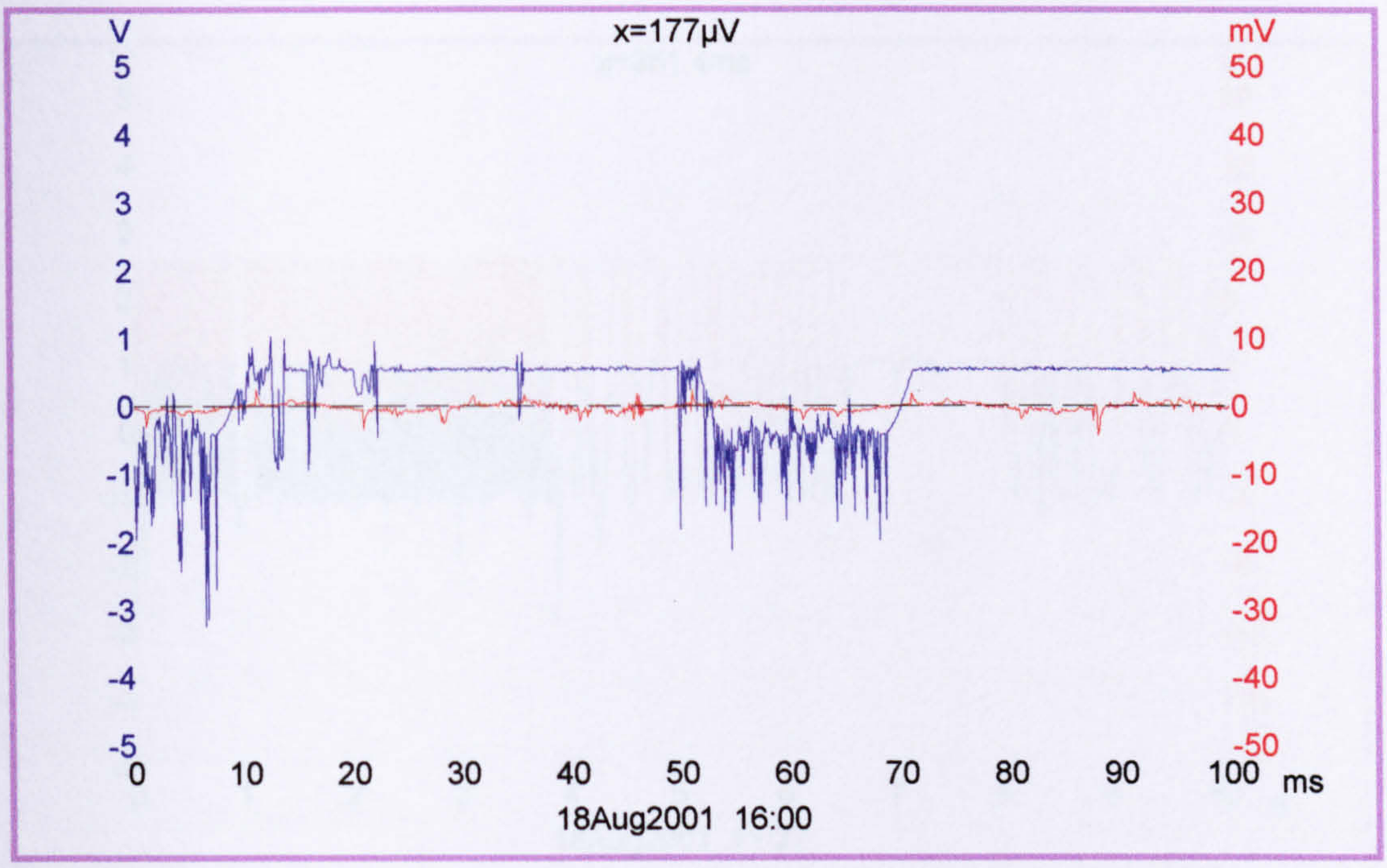

Figure 7-44. Feedback control signal (red) and inter-electrode gap voltage variation (blue) for EDT machining using the developed piezoelectric control system [peak current 8A, duty cycle 12 μsec & 'on' time 10 μsec]

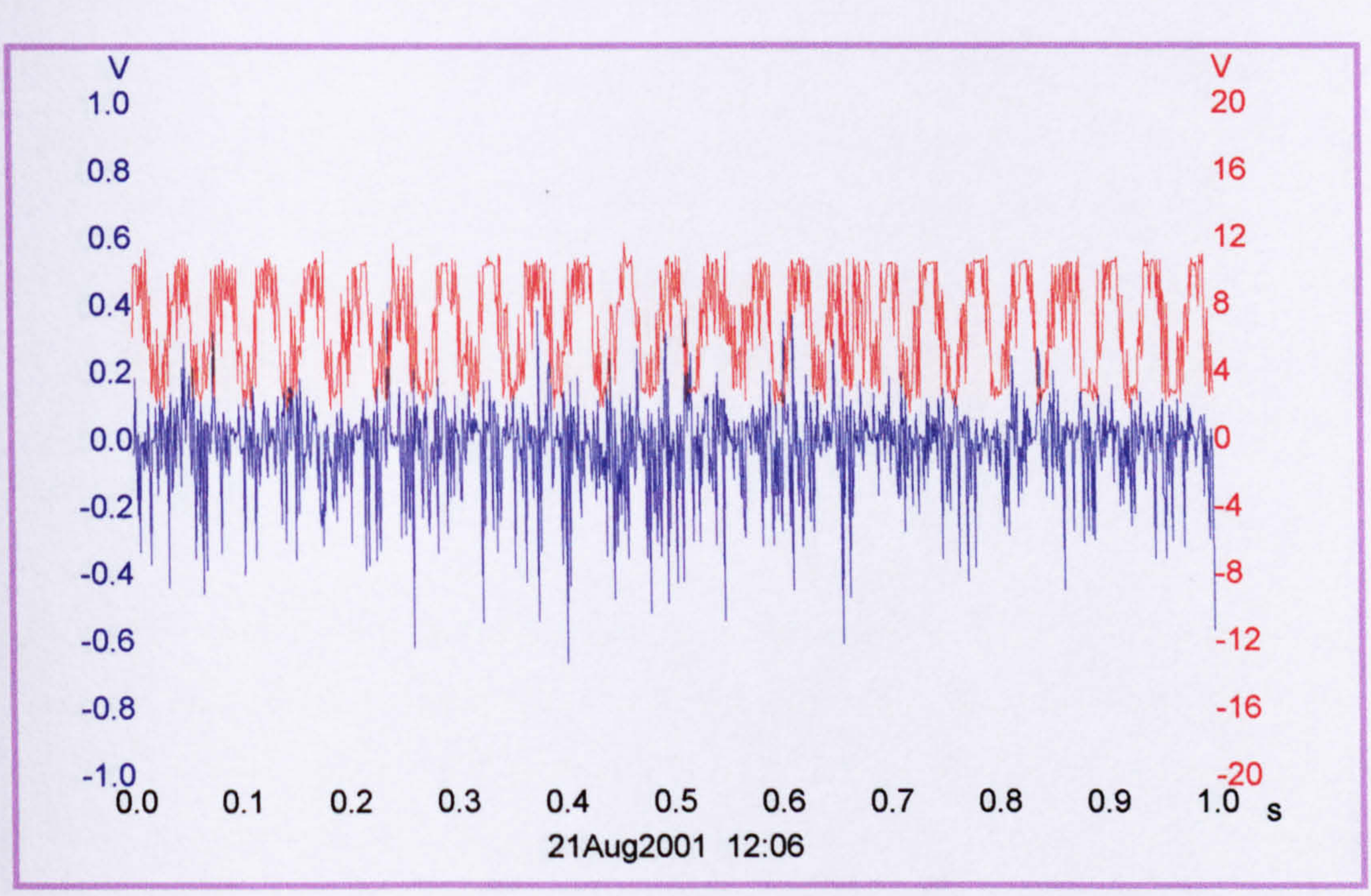

Figure 7-45 Feedback control signal (red) and inter-electrode gap voltage (blue) variation for EDT machining using an existing DC servo control system [peak current 8A, duty cycle 12 μsec & 'on' time 10 μsec]

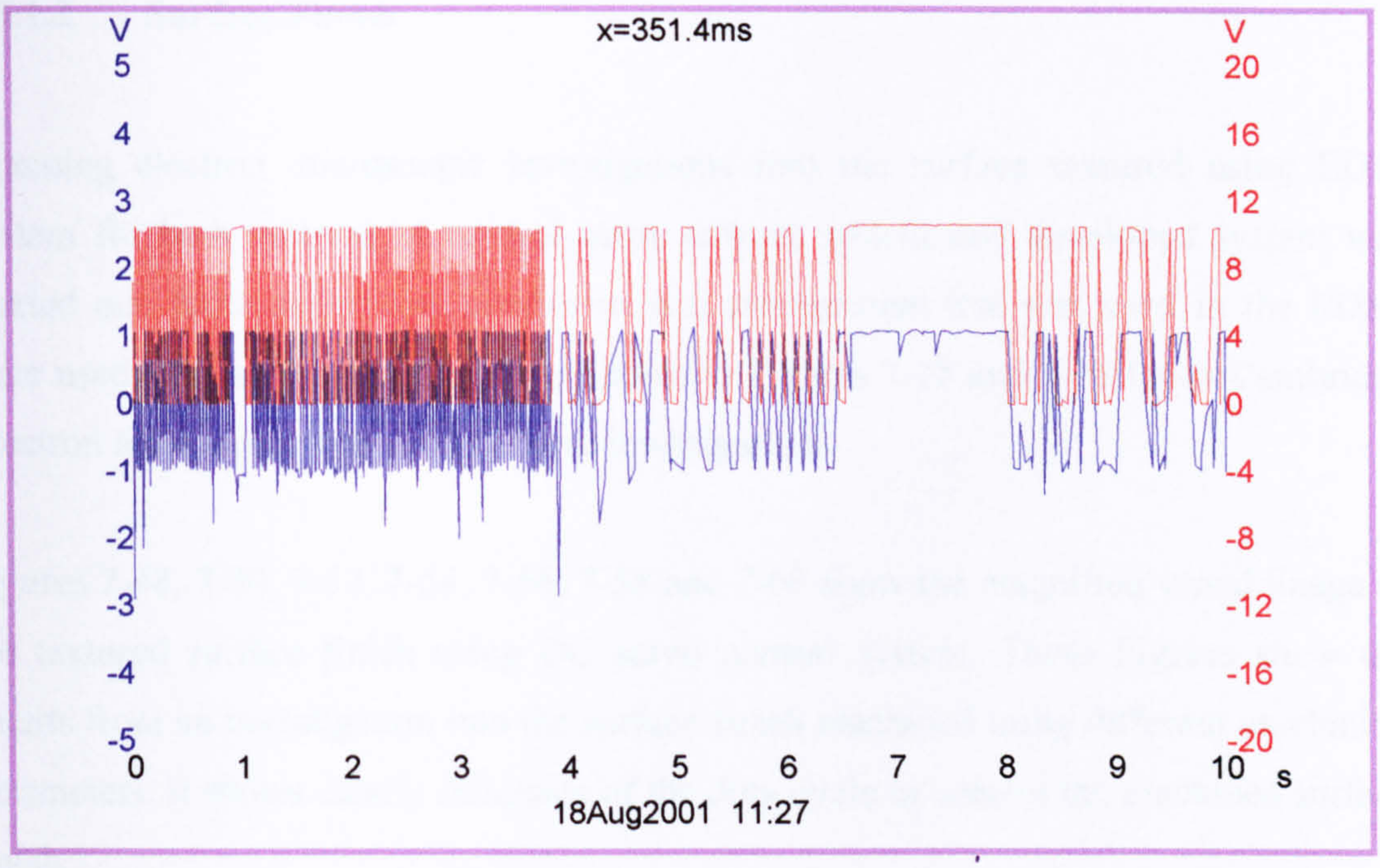

Figure 7-46 Stability of the feedback control signal (red) and inter-electrode gap voltage (blue) of the EDT system using the developed piezoelectric control system for period of 10 sec [peak current 8A, duty cycle 12 μsec & 'on' time 50 μsec]

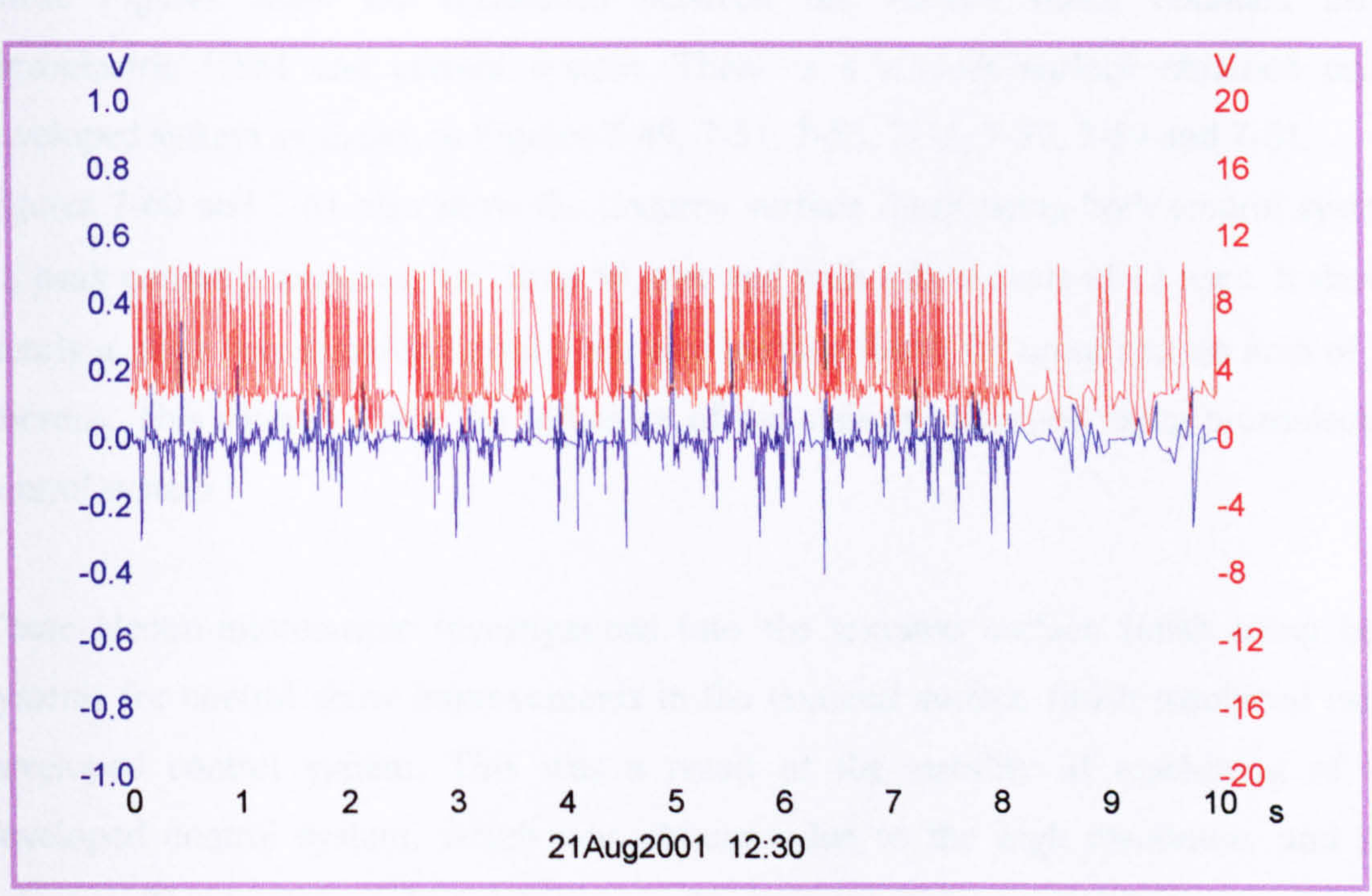

Figure 7-47 Stability of the feedback control signal (red) and inter-electrode gap voltage (blue) of the EDT system using an existing DC servo control system for period of 10 sec [peak current 8A, duty cycle 12 μsec & 'on' time 50 μsec]

7.5.1.2 Surface Finish

Scanning electron microscopic investigations into the surface textured using EDT-system for both systems of control using current system and developed system was carried out. Same machining conditions and arrangement that was used in the EDM, were used in these investigations. As shown in Figures 7-18 and 7-19 Leica Cambridge Electron Microscope was used in these investigations.

Figures 7-48, 7-50, 7-52, 7-54, 7-56, 7-58 and 7-60 show the magnified visual image of the textured surface finish using DC servo control system. These Figures show the results from an investigation into the surface finish machined using different machining parameters. It shows clearly influence of the duty cycle to control the machined surface finish.

Figures 7-49, 7-51, 7-53, 7-55, 7-57, 7-59 and 7-61 show the magnified visual image of the textured surface finish using piezoelectric control system and same machining conditions used in current system.

These Figures show the difference between the surface finish obtained using piezoelectric USM and current system. There is a smooth surface obtained using developed system as shown in Figures 7-49, 7-51, 7-53, 7-55, 7-57, 7-59 and 7-61.

Figures 7-60 and 7-61 also show the textured surface finish using both control system for peak current 6 amperes, 'on' time 50 μsec and with a duty cycle of 12 μsec. It shows clearly a close investigation into the textured surface finish for cross section area of 20 microns. This shows clearly the influence of the stability obtained using piezoelectric control system.

These electro-microscopic investigations into the textured surface finish using both systems for control show improvements in the textured surface finish machined using developed control system. This was a result of the stability of machining of the developed control system, which was obtained due to the high resolution, and fast response. This leads to a clear reduction in the arcing and short-circuiting process which in turn may lead to a smooth surface finish and reduced overall machining time.

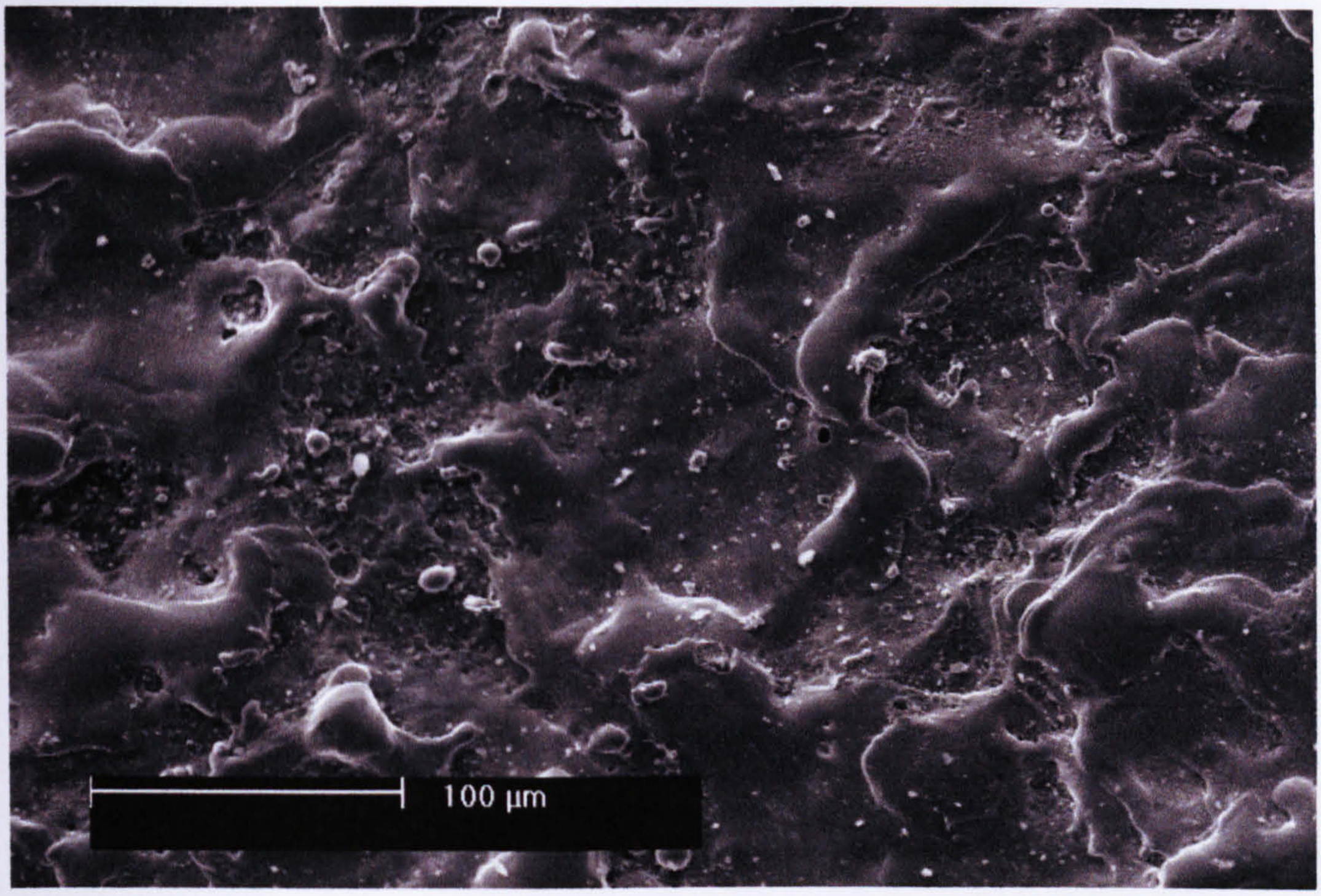

Figure 7-48 EDT surface finish using DC servo control system and operating parameters, current 6 amperes, 'on' time 50 µsec and duty cycle 2 µsec

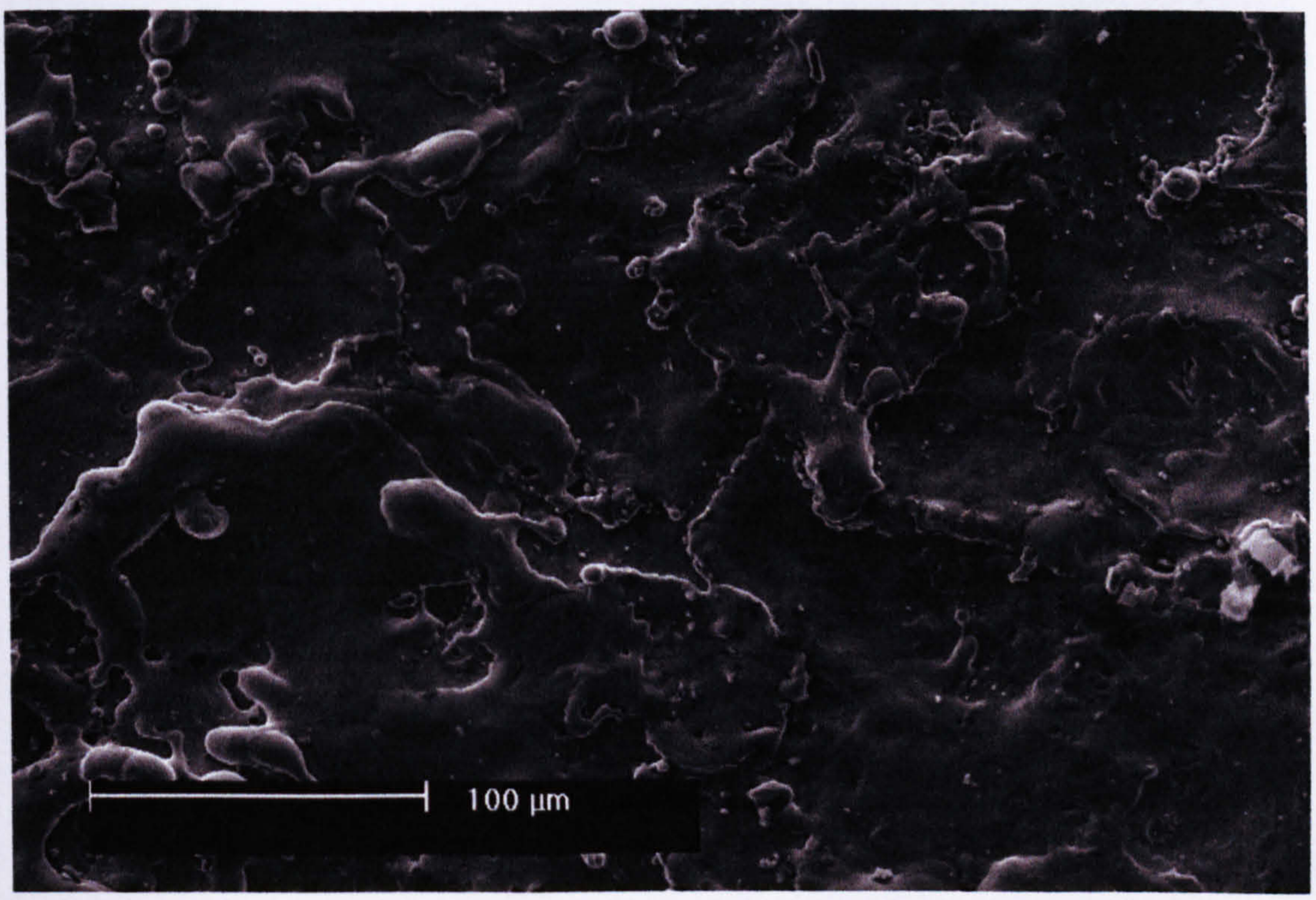

Figure 7-49 EDT surface finish using piezoelectric control system and operating parameters, current 6 amperes, 'on' time 50 µsec and duty cycle 2 µsec

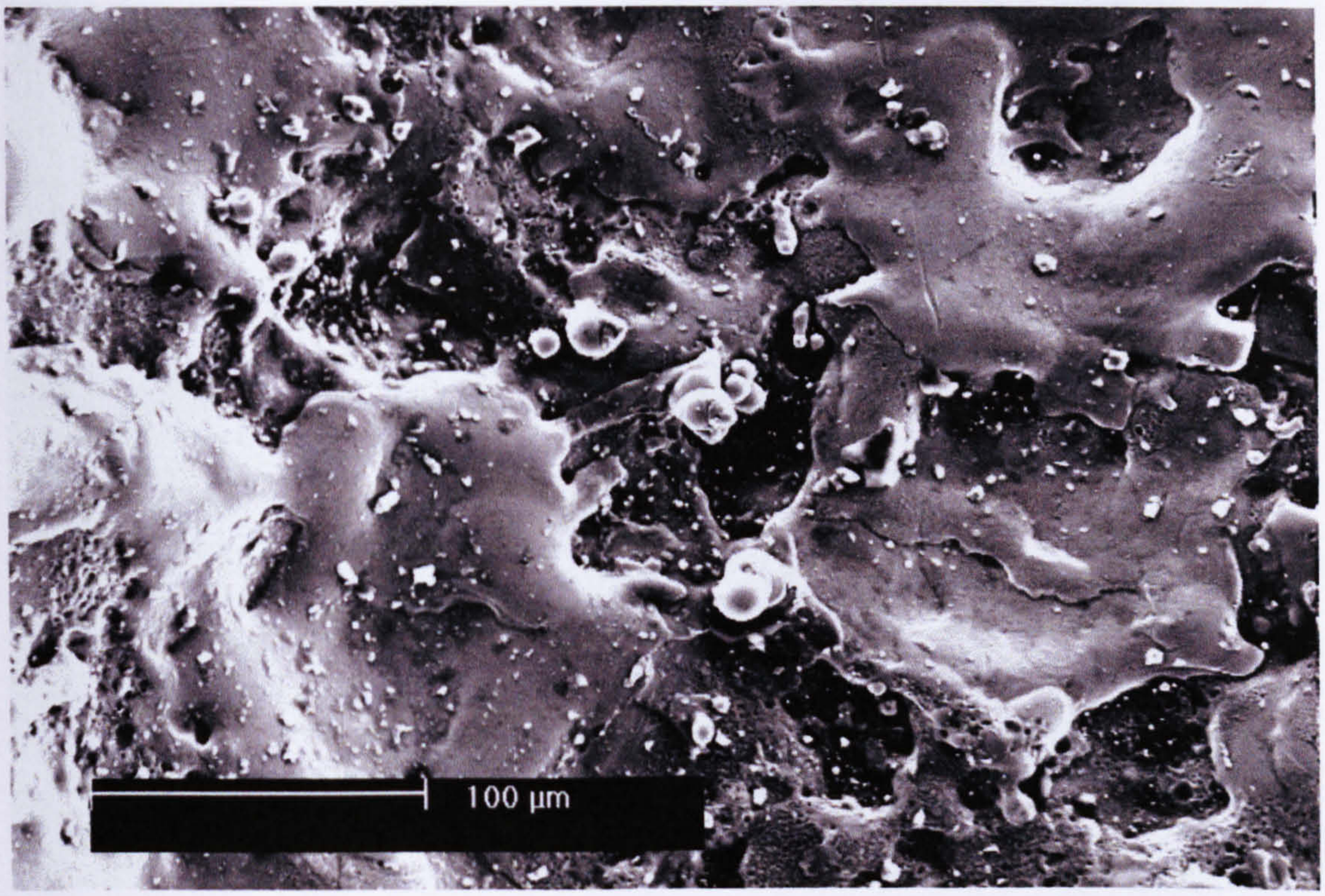

Figure 7-50 EDT surface finish using DC servo control system and operating parameters, current 6 amperes, 'on' time 50 µsec and duty cycle 4 µsec

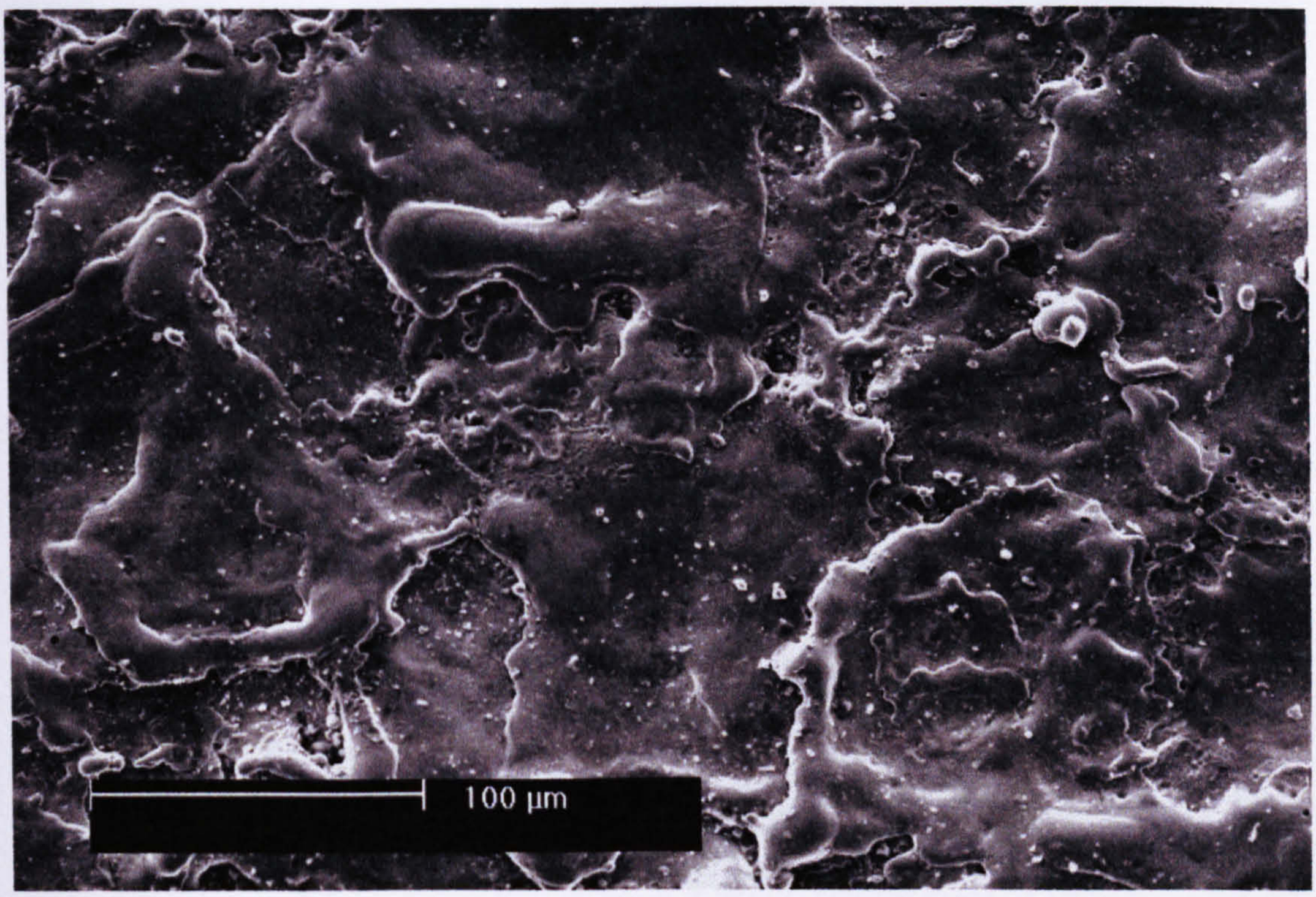

Figure 7-51 EDT textured surface finish using piezoelectric control system and operating parameters, current 6 amperes, 'on' time 50 µsec and duty cycle 4 µsec

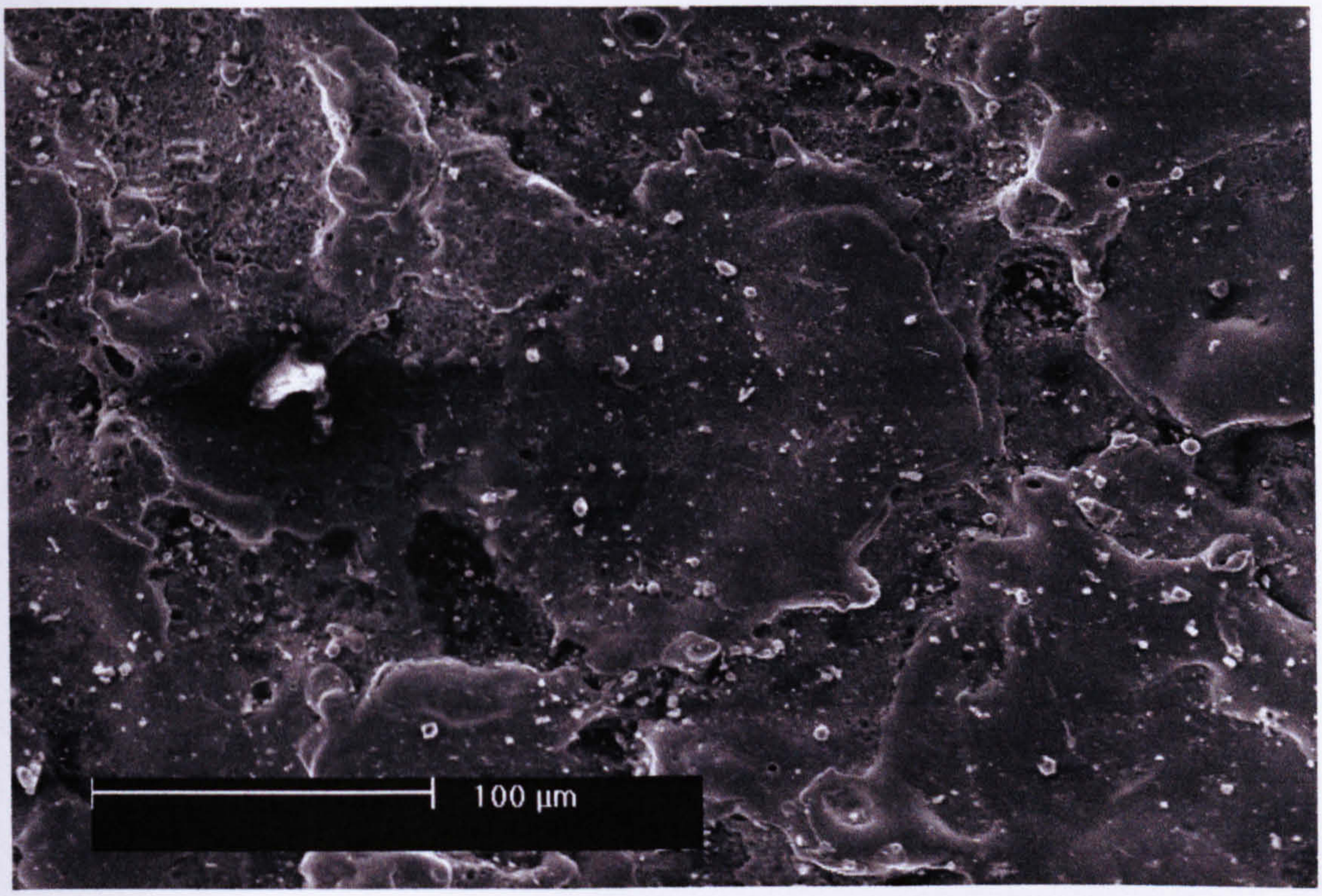

Figure 7-52 EDT surface finish using DC servo control system and operating parameters, current 6 amperes, 'on' time 50 µsec and duty cycle 6 µsec

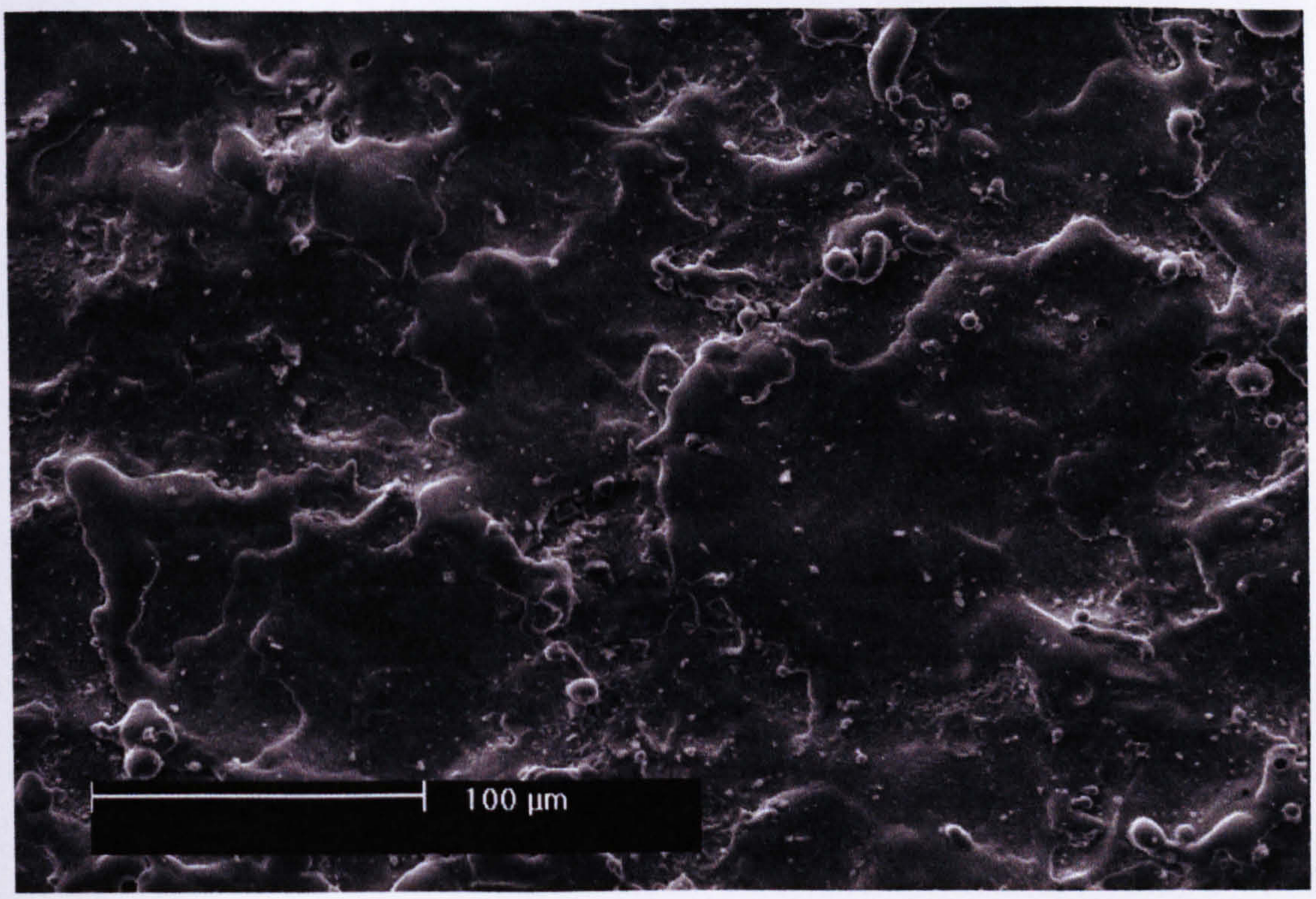

Figure 7-53 EDT surface finish using piezoelectric control system and operating parameters, current 6 amperes, 'on' time 50 µsec and duty cycle 6 µsec

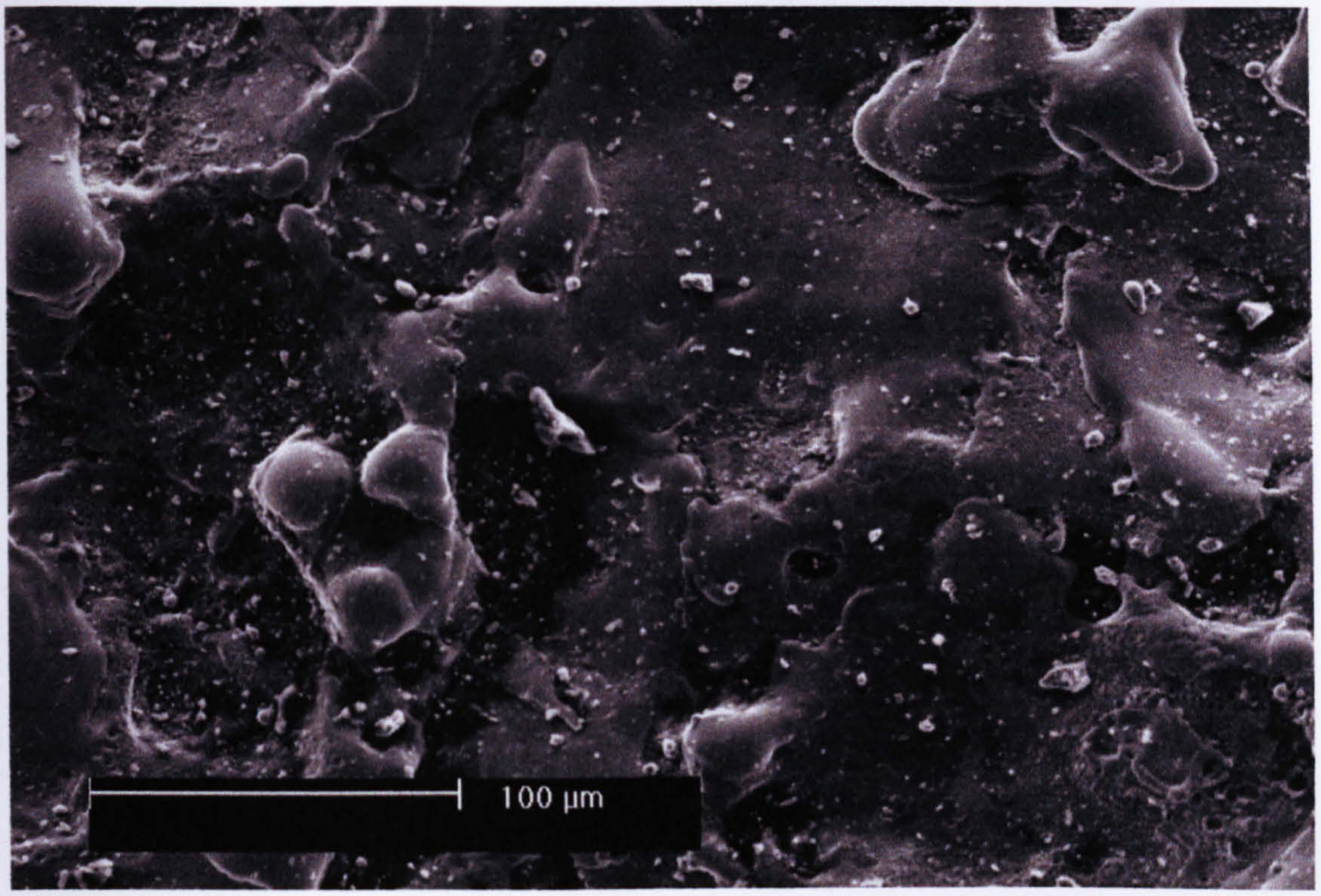

Figure 7-54 EDT surface finish using DC servo control system and operating parameters, current 6 amperes, 'on' time 50µsec and duty cycle 8 µsec

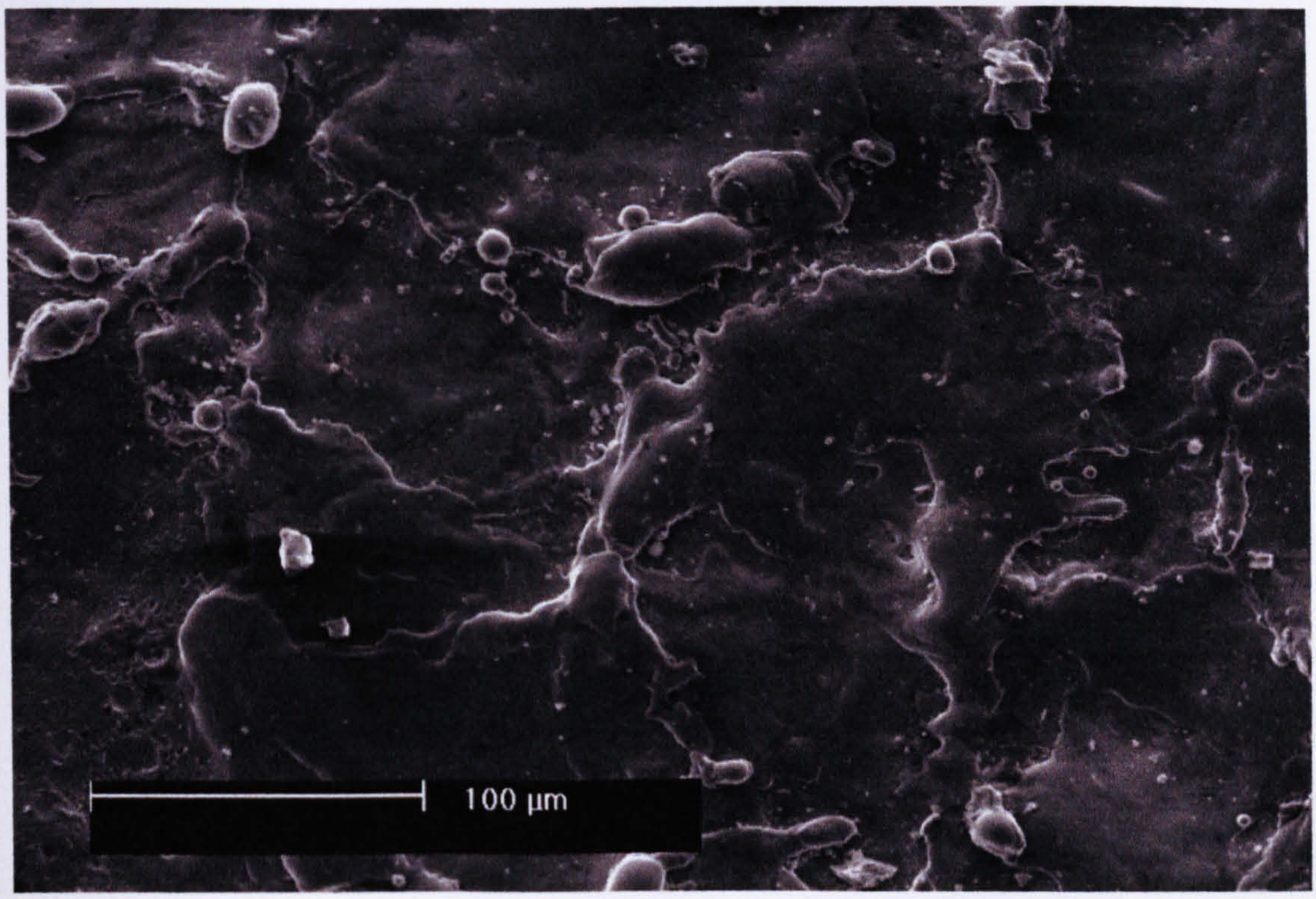

Figure 7-55 EDT surface finish using piezoelectric control system and operating parameters, current 6 amperes, 'on' time 50µsec and duty cycle 8 µsec

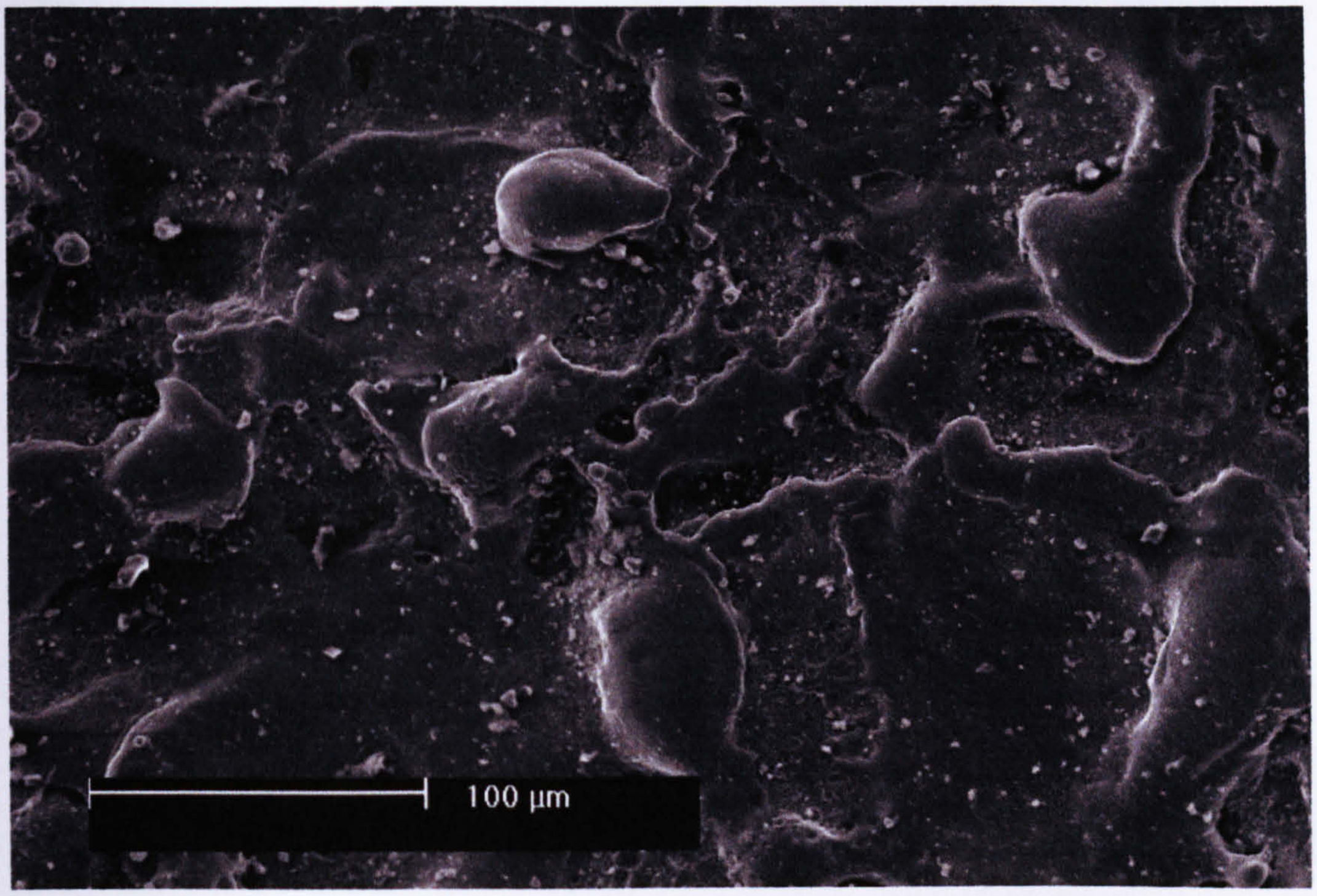

Figure 7-56 EDT surface finish using DC servo control system and operating parameters, current 6 amperes, 'on' time 50 µsec and duty cycle 10 µsec

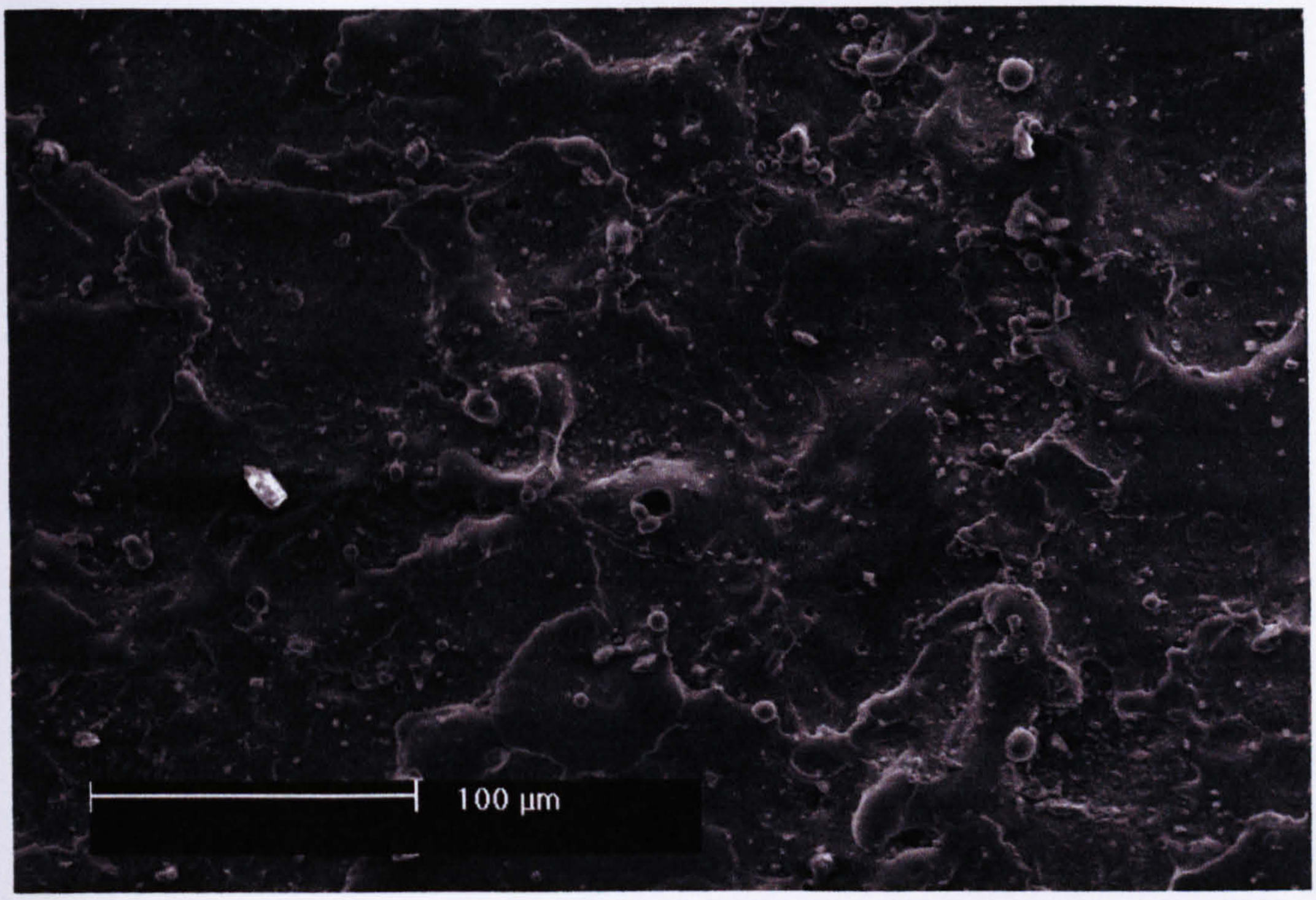

Figure 7-57 EDT surface finish using piezoelectric control system and operating parameters, current 6 amperes, 'on' time 50 µsec and duty cycle 10 µsec

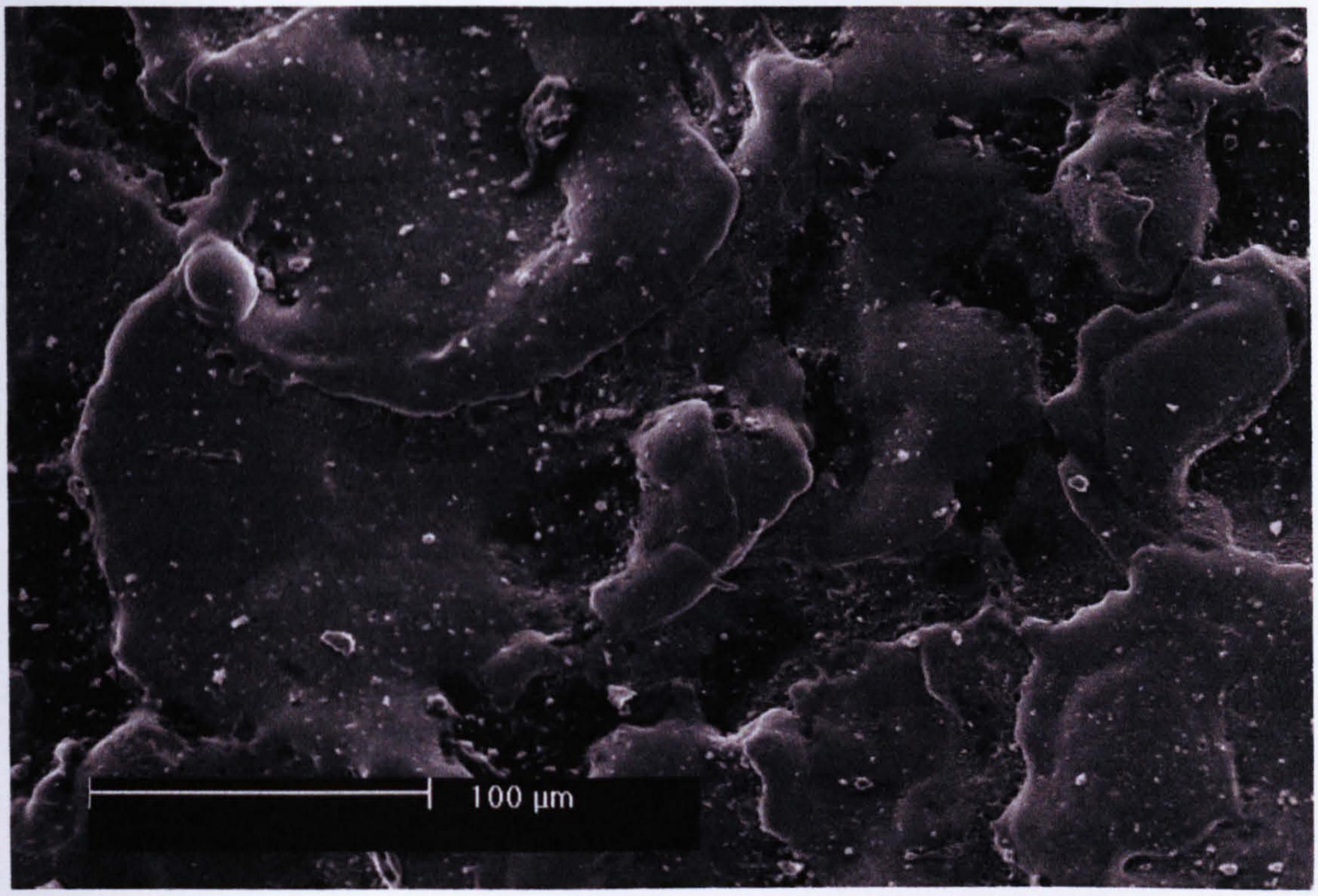

Figure 7-58 EDT surface finish using DC servo control system and operating parameters, current 6 amperes, 'on' time 50 µsec and duty cycle 12 µsec

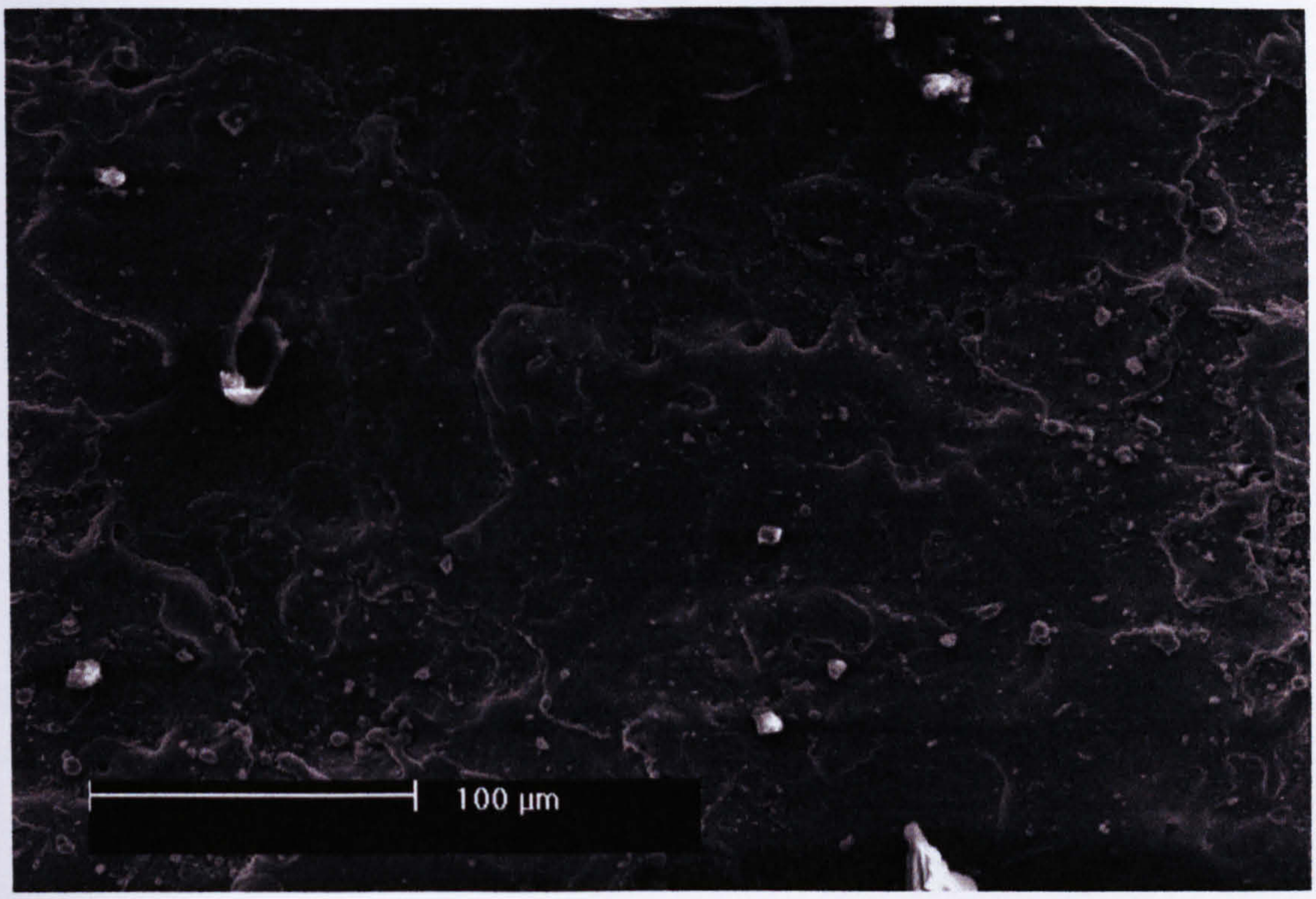

Figure 7-59 EDT surface finish using piezoelectric control system and operating parameters, current 6 amperes, 'on' time 50 µsec and duty cycle 12 µsec

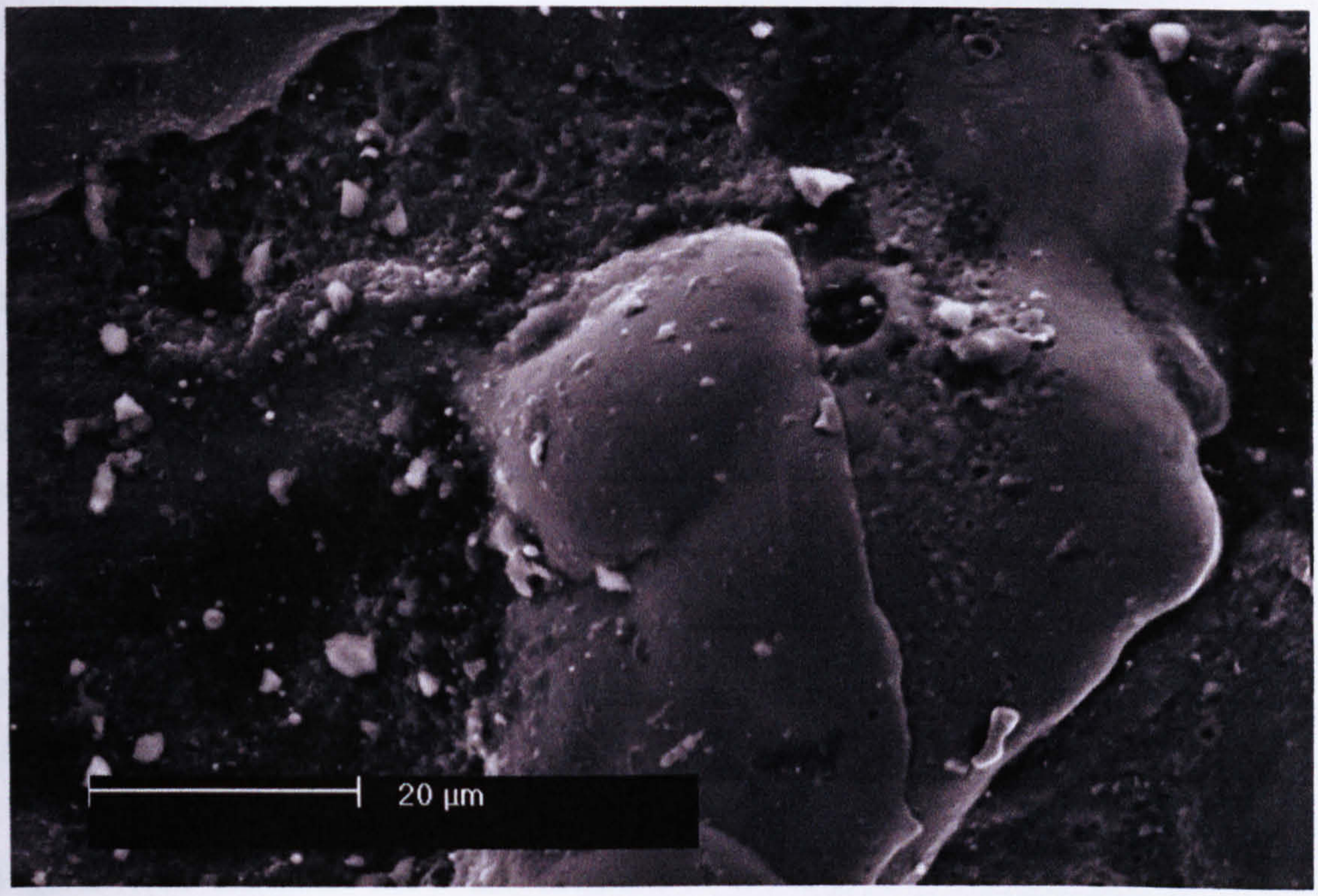

Figure 7-60 EDT surface finish using DC servo control system and operating parameters, current 6 amperes, 'on' time 50 µsec and duty cycle 12 µsec

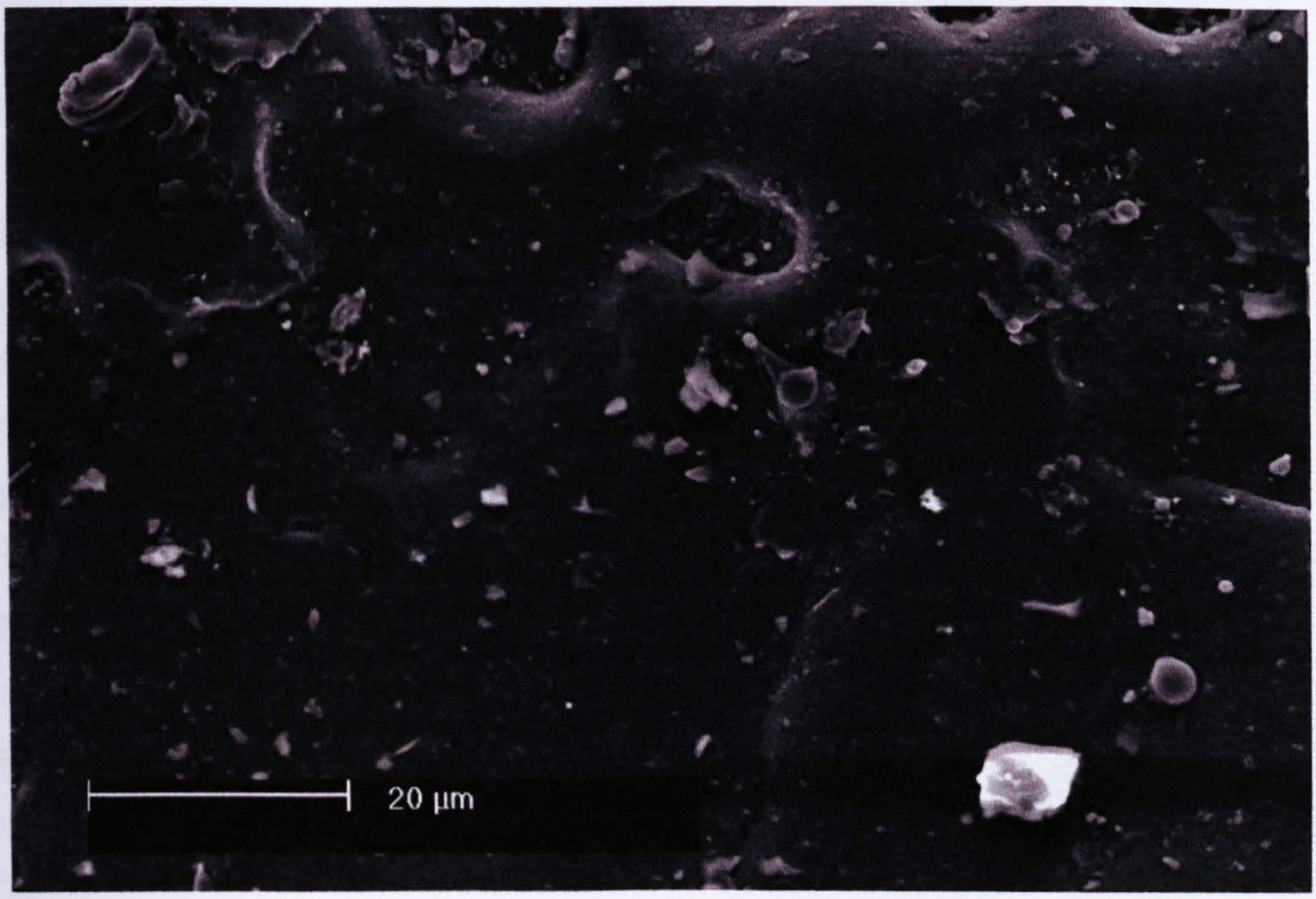

Figure 7-61 EDT surface finish using piezoelectric control system and operating parameters, current 6 amperes, 'on' time 50 µsec and duty cycle 12 µsec

7.5.1.3 Roughness and Peak Count

Various electro-machining parameters were used to texture different samples using both systems for control, current system and developed system. Taylor Hobson measuring equipment for surface finish was used to measure the roughness and peak count of these samples. This was carried out few times for each sample and the average of the degree of texture was determined. This was necessary to ensure of the accuracy of measurements.

The relationships between measured degree of roughness and peak count of the textured surfaces using both systems of control and various electro machining parameters are shown in Figures 7-62, 7-63, 7-64 and 7-65.

Figures 7-62 and 7-64 show the variation of the degree of roughness against peak current and on-off time. This shows clearly a close agreement with the work carried out in this area of application (appendix (C)).

Figures 7-63 and 7-65 show the variation of the peak count against peak current and on-off time.

These Figures show that the degree of roughness of the textured surface using both systems of control is increased with increasing the peak current and the on-off time. The developed control system using piezoelectric USM shows a little change in the degree of roughness in comparison to the current control system using DC servomotor. It also shows that the peak count decreased with increasing the peak current and on-off time. Small reduction in the peak count appeared in the case of the developed system of control which is obvious with increased the degree of roughness of a roll. Figures 7-63 and 7-65 showed the peak count variation of the textured surface obtained using both systems of control and measured using Taylor Hobson equipment.

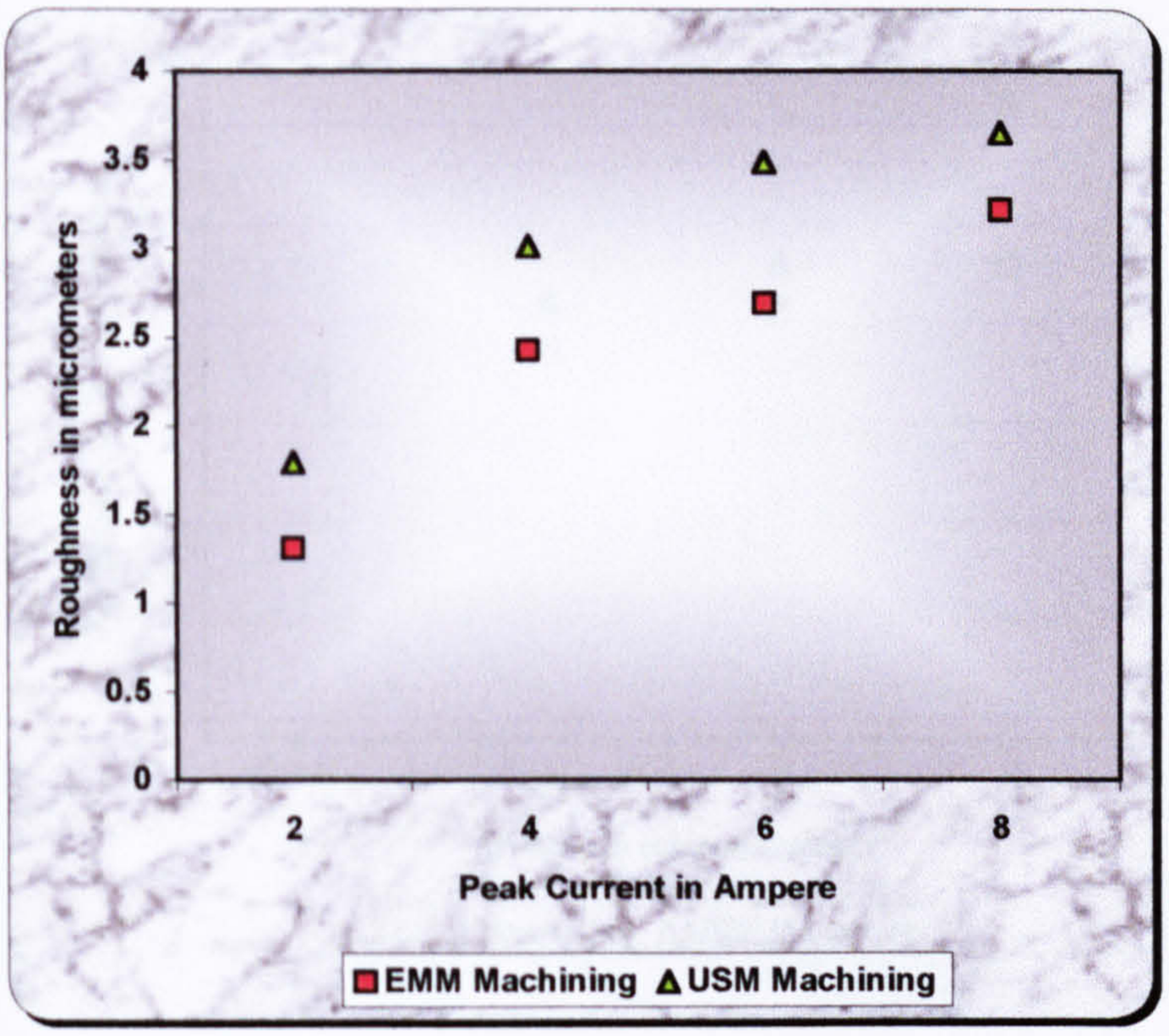

Figure 7-62 Relationship between the variation of the roughness against various peak current for both systems of control using DC servomotor and USM

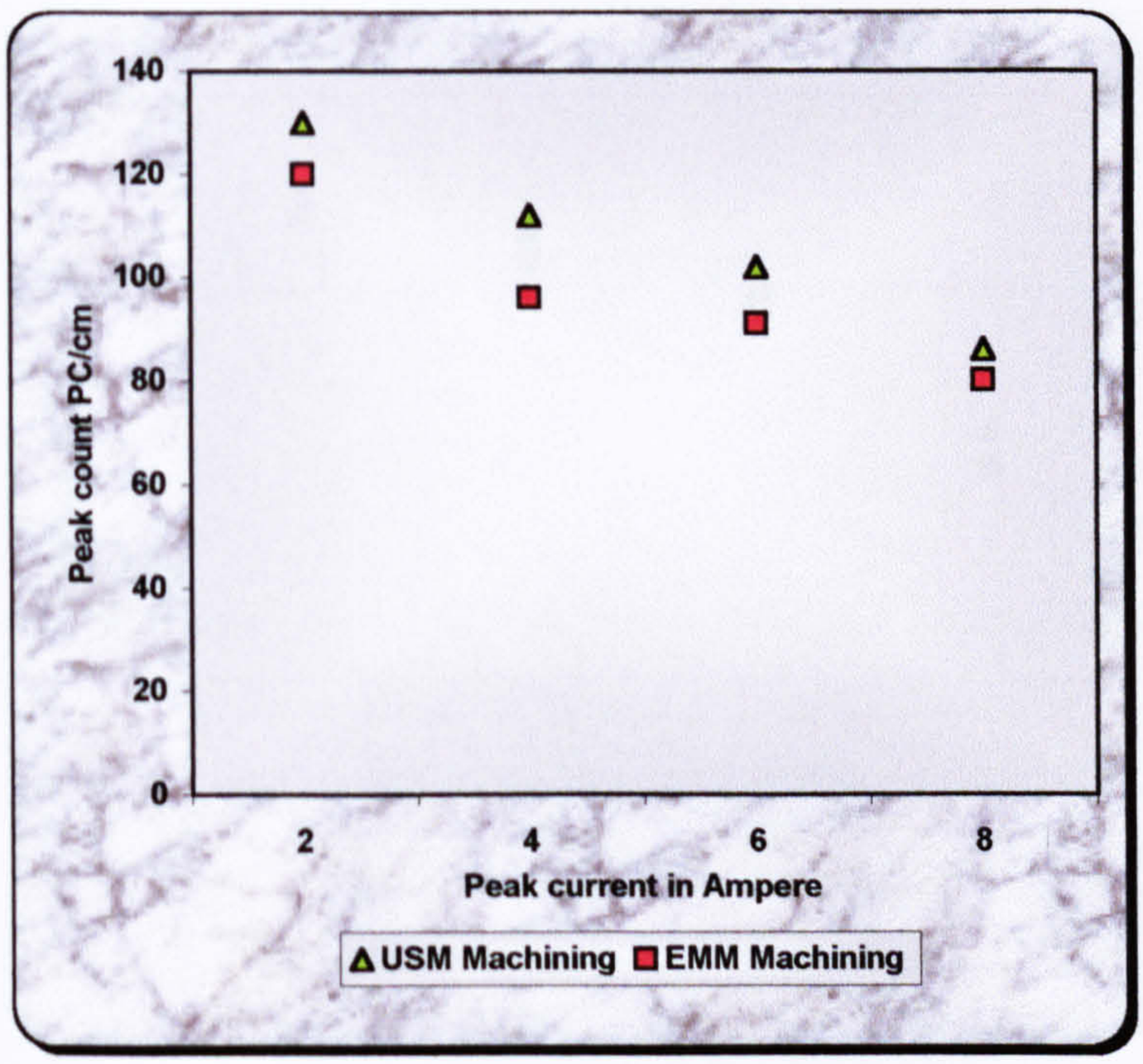

Figure 7-63 Relationship between the variation of the peak count against various peak current for both systems of control using DC servomotor and piezoelectric USM

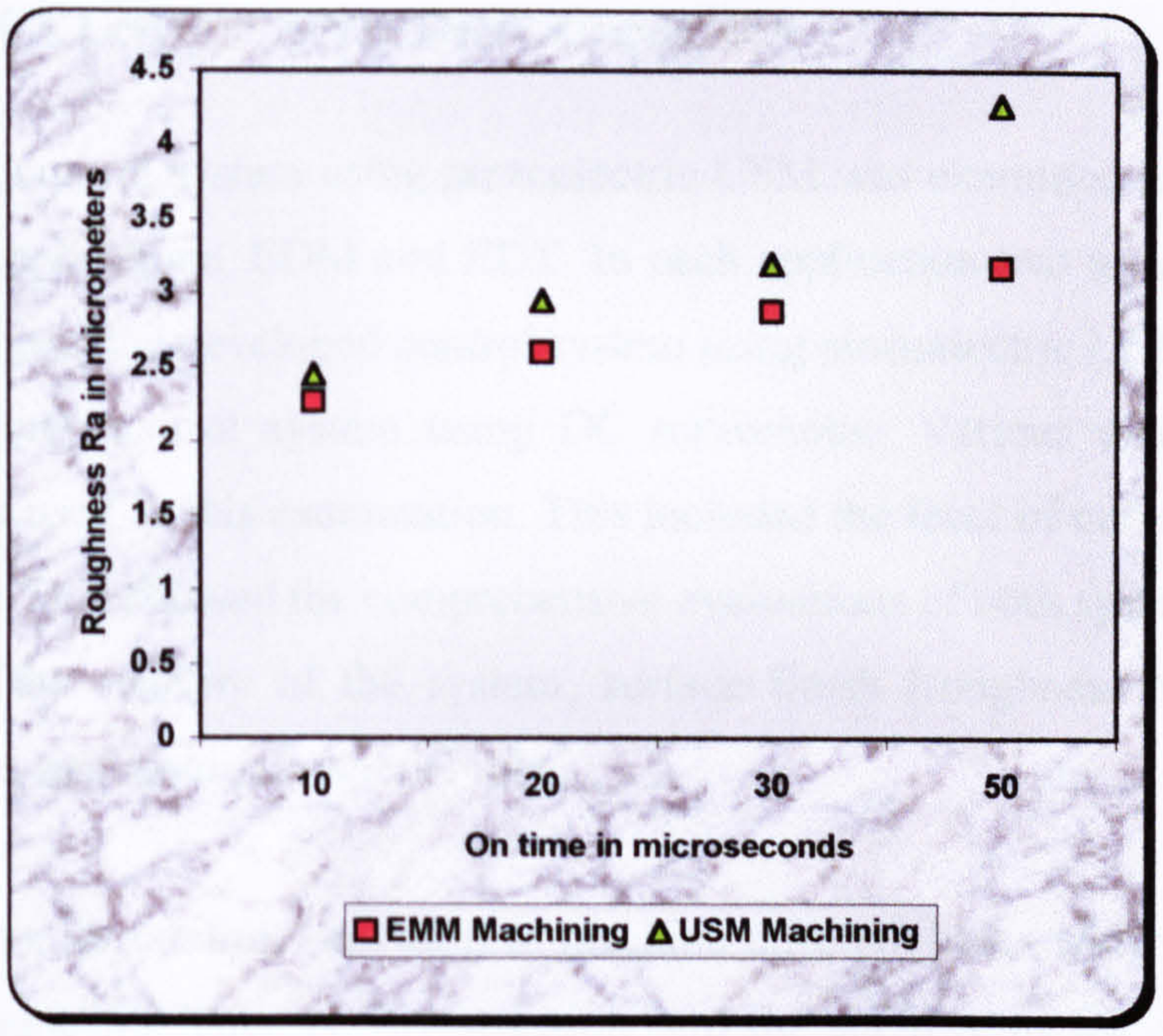

Figure 7-64 Relationship between the variation of the roughness against on-off time for both systems of control using DC servomotor and piezoelectric USM

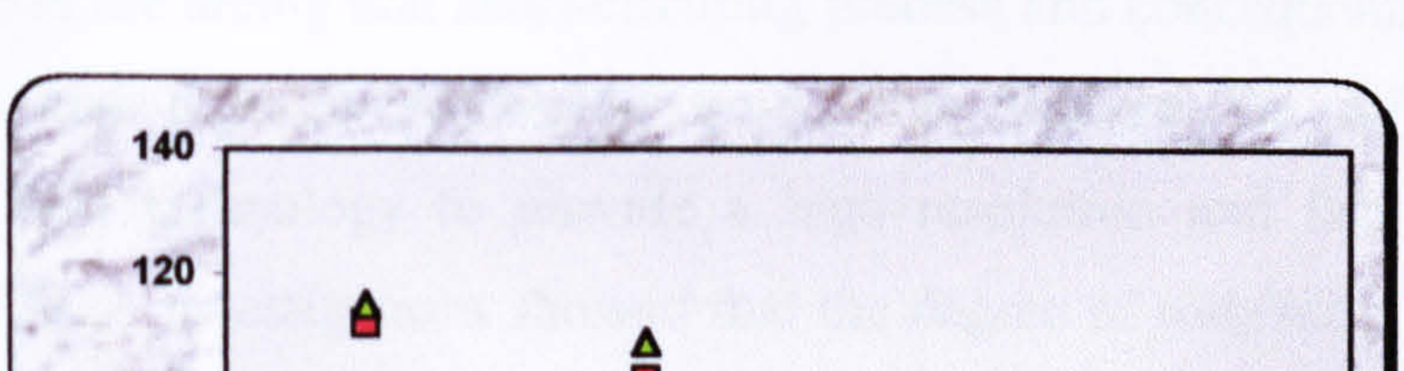

Figure 7-65 Relationship between the variation of the peak count against on-off time for both systems of control using DC servomotor and piezoelectric USM

7.6 CONCLUSION AND DISCUSSIONS

The developed control system using piezoelectric USM was examined and evaluated in two different applications, EDM and EDT. In each application two arrangements were used. The first used the developed control system using piezoelectric USM and the other was used existing control system using DC servomotor. Various electro machining paramters were used in this examination. This included the level of current, on-off time and duty cycle. This allowed the comprehensive evaluations of both systems for control. This included the stability of the system, surface finish (roughness & peak count), machining time, and material removal rate.

The two systems for control were used to machine different holes with various electro-machining parameters. Then an investigation into the stability of the system, surface finish of the machined products, material removal rate and machining time was carried out. The developed control system using pizoelectric USM showed an enhanced stability compared with the existing control system using DC servomotor. There was a clear reduction in the arcing and short-circuting process and concequently an improved surface finish and reduced processing time. This showed the influence of the piezoelectric USM technology to provide a high resolution and fast response. The relationship of these investigations showed that the degree of roughness increased with increasing the peak current and on-off time and vice verse for the peak count. However, the degree of surface finish was controlled by level of current, on-off time and duty cycle of the spark.

The two systems for control were also used to texture different surfaces using various electro-machining parameters. An investigation into the stability of the system, capability of control, surface finish of the textured surfaces and machining time was carried out. The developed control system using piezoelectric USM shows a good stability in comparsion to the current control system. The investigation into the surface finish machined using both systems of control showed that there was an improvement in the surface finish machined using piezoelectric ultrasonic control system. The degree of roughness and peak count of the textured surfaces using both system were measured. The relationship between the surface profile parameters (roughness and peak count) were obtained. These showed a little change in the degree of roughness in comparsion to

the current system using DC servomotor. The relationship obtained using both system showed that there is an improvement in the stability of the system, surface finish, and machining time of the main machining processes. It also demonstrated ability of the developed system using piezoelectric USM to be implemented in various application wherever, fast response, a high level of prescion, and micro-resoltion is required.

CHAPTER 8

8 GENERAL CONCLUSIONS AND DISCUSSIONS

A novel servo control feed drive system that uses piezoelectric USM was developed. The developed drive offers a micro dynamic response, micro resolution, and a compact size. The drive was examined in two industrial applications, EDM and EDT. The initial results showed the capability of the developed drive to improve EDM and EDT machining systems: Dynamic response, level of precision, stability of machining, surface finish of machined products, and material removal rate.

The development process for the developed piezoelectric servo control drive system passed various stages. These included:
An investigation into the piezoelectric USM system of control was carried out. This showed that: Piezoelectric actuators offer the fastest dynamic response time available. The piezoelectric effect directly converts electrical energy into motion only absorbing electrical energy during movements. The piezoelectric actuator has neither gears nor rotating shafts. Its displacement is based on solid state dynamic. Piezo actuators are ceramic elements that do not need any lubricants and show little wear.

A piezoelectric USM using a single flexural vibrating bar was developed. A methodology for design was established and implemented successfully. This methodology for design emphasizes capability to prevent the technical problems of the previous design. This was considered industrial application needs such as, motor configuration, type of motion, load capacity, output force, compactness, travelling speed, methodology for fabrication and performance.

This design methodology also focused on developing a flexure frame that should be designed to function as: A linear motion mechanism with an unlimited travel range, a mechanical transmission of the vibrational force into motion free of jerking effect, a structure frame easy to configure the parts, a vibrating bar housing which does not interfere the bar modes of vibration, a pre-load pressing force which does not influence the motor main characteristics, piezoelectric USM system with an optimised component

for compactness, a linear motion created without any mechanical joint which could suffer from external loads, and a mechanical system having only the surface type contact, which provide high stiffness.

A methodology for analysis and modelling using FEA was established. This methodology enabled the: Selection and identification of the piezoelectric material required, investigation of material deformation, investigation of the material modes of vibration, and Optimisation of the motor signal response parameters.

The developed motor was examined. This showed that the developed motor system could be controlled using either the frequency or amplitude of the driving signal. It also showed that the developed motor has an acceptable load capacity, travelling speed on the range of 28 mm/sec, response on the order of microseconds and a positioning resolution of order of micrometers. This showed the ability of the developed motor to be used in fast response and high precision control applications. The developed prototype suffered from asymmetrical characteristics in both directions of motion. This was result of small deviations in the resonant frequencies of the sub-surfaces. This was overcome using different techniques such as selecting an operating frequency to match the two modes of vibration of both sub-surfaces of the bar, or the design of resonant cavities which enabled adjustment of the deviations in the two sub-surfaces operating frequencies.

A piezoelectric USM drive was developed. The drive design passed through various stages. A methodology for design was established and implemented. This was optimised in the early stages of the design process using methodology for modelling and analysis using finite element analysis. This allowed optimising the signal response parameters of the motor. A practical optimisation of the motor operating conditions was also carried out. This was necessary to establish the maximum travelling rate of the motor that controls the processing time of main machining process of the system. The basic configuration of the developed drive was carried out based on the motor operating parameters and applications needs. The major factors considered in the design process, were the operating frequency, voltage variations and phase. However, it was noticed that the optimum operating condition for the developed piezoelectric USM was to set the motor at resonant frequency, use the amplitude to control the speed and phase of the

two modes of vibration to control the direction of motions of the motor. The developed prototypes using bipolar transistor, and operational power amplifier were suffered from un-ability to provide the motor with the necessary operating parameters in a wide range.

The developed piezoelectric feed drive was integrated successfully into the EDM system to carry out various examinations to test the drive capability of control. The necessary modification into the existing EDM system units was carried out. This is included control unit, motor driving unit and power switching unit.

An electro discharge control unit based on the piezoelectric USMs technology was built. The unit methodology for design, the structure, the principles of operation, the computer simulation and the modelling was conducted and presented. Computer simulation and modelling for the unit was carried out using various packages such as VIEWLOGIC, and VHDL. An examination of the unit capability to monitoring and control the main machining process was carried out. The required modification was added to the EDM-control unit, such as a tolerance unit, a fire protection circuit, an audible and visible circuit.

The main units of the developed system (piezoelectric USM, piezoelectric drive, control unit) were integrated successfully. An examination for the system characteristics was carried out. This showed that:

The developed prototype suffered from a slow travelling rate. This was a result of the slow motion provided from the source of motion of the drive. The equivalent circuit of the source of motion was developed and an investigation into the motor characteristics was carried out. This showed that, the active electrode operating frequency and surface finishing of the parts of the motor were the major parameters affecting the motor travelling speed, and resolution. These results were implemented successfully and a modification to the source of motion was carried out. The source of motion reintegrated into the drive frame and successful measurements were conducted including resolution, response time and travelling speed. These showed that an improvement to the source of motion travelling speed, and response time.

The developed control system using piezoelectric USM was examined and evaluated in two different applications, EDM and EDT. For each examination both systems of

control were used, the current system using DC servomotor and developed system using piezoelectric USM.

In EDM applications, both control systems were used to machine different holes. An investigation into the stability of the system, surface finish, and material removal rate were carried out. These showed:

- An improvement in the stability of machining was obtained when compared to the current system using DC servomotor. This was verified by examining the electrode movements, the variations in the inter-electrode gap voltage, current and feedback control signals.
- The investigation into the surface finish machined using both systems for control, showed that there was a clear improvement in the surface finish machined using piezoelectric ultrasonic system of control. A reduction in the arcing and short circuit process was also observed.
- The relationship between the electro machining parameters of the system and surface finish paramters (roughness and peak count) was obtained. This showed a close agreement to the known relationship of this application. The degree of roughness increased with increasing peak current and on-off time and vice verse for the peak count.
- These improvements showed the influnce of piezoelectric USM technology in this field of electro machinery.

In EDT applications, both control systems were also used to texture different rolls. Again an investigation into the stability of machining, surface finish of textured surface, response time, level of precision and safety aspect of the main machining process was carried out. These showed:

- An improvement in the stability machining of the system.
- An improvement in the surface finish.
- A reduction in the arcing and short circuit process.
- The obtained relationship for the surface finish paramters and electro machining parameters showed a close agreement with the known relationship for these applications. The degree of roughness increased with increasing the peak current and on-off time and vice verse for the peak count.

- The capability of this control system to be implemented in such high precision applications.

The developed piezoelectric servo control system can be used in many different industrial applications using either open loop or close loop control. It has the flexibility to modify characteristics such as, load capacity, output force, travelling speed and resolution to match different applications. It is able to provide two directions of motion, two types of motion, rotary and linear motion. The developed system also presents flexible configuration that is easy to configure and maintain.

8.1 MAJOR CONTRIBUTIONS OF THIS RESEARCH WORK

The work discussed in this thesis presented contributions in the fields of servo control, electro machinery, piezoelectric USMs and power electronics. These are summarised as fellows:

- The development of a piezoelectric servo control feed drive using a piezoelectric USM for fast response and high precision positioning control industrial applications.
- An innovative servo control feed drive for EDM-system applications using piezoelectric USMs technologies.
- A novel linear piezoelectric USM using a single flexural vibrating bar that has a resolution and fast response of the order of microns, two directions of motion and wide capability of control using either amplitude or frequency of the input signal.
- Establishment and implementation of many innovative ideas that presents an entirely new perspective on the possible usage of piezoelectric material, power electronics, in particular power MOSFETs in EDM and EDT- applications.
- Comprehensive computer simulation and modelling for each part of the system control strategies using various packages and softwares including ANSYS, VHDL, and VIEWLOGIC.
- The thesis presents a new idea in the field of piezoelectric materials that offers the ability to use a three dimensions piezoelectric electrode to create a number of operating frequencies. It was well know that a three dimension piezoelectric electrode provides only one operating frequency. I.e. for one electrode that has

three dimensions, there are three-resonant frequencies. The dominant frequency, named operating frequency and this is normally used to create mechanical motion using friction principles between two surfaces in contact. The current research results showed:

- It was possible to establish a new technique that allows the creation of a number of operating frequencies from one electrode. The concept was to divide one surface of its two surfaces into a number of sub-surfaces. Exciting the sub-surfaces with enough voltage and current creates a number of operating frequencies that equals to the number of the sub-surfaces. This enables to organise and control direction of propagation of the same material for the same electrode using same phase input signal by control the phase of the modes of vibration. This concept was implemented successfully in this investigations and two direction of motion was developed using one piezoelectric electrode.
- It was possible to control and organise the particles direction of propagation for the same electrode using same phase input signal for different resonant frequencies over hundred of KHz.

8.2 LIMITATION OF THE CURRENT DESIGN

The limitations and technical problems faced development process of this servo control system were:

Low Structure Stiffness and Strength:

Due to the configuration of the developed motor and optimum pre-load pressing force the current design can be classified as low structure strength. The low structure strength does not provide a large pre-load on the piezoelectric actuators and the associated mechanical contact stiffness, a low structural stiffness, is a result of this design.

Slow Travelling Rate:

It is extremely difficult for a feed drive, with micrometer resolution to achieve high positioning speed. Positioning speed of the developed drive was considered and some modifications were presented. These modifications were implemented successfully and the initial results were quite acceptable but it still has to be considered for more

improvement to extend possible of usage of this type of technology in different fields of application.

Asymmetrical characteristic in the Two Directions of Motion:

It was observed that this asymmetrical characteristic was result of a deviation on the two-resonant frequencies, which arise results of asymmetrical sub-surfaces. This needs the design of two resonators that would enable tuning of the frequency in a narrow band. Consequently it would be possible to produce similar characteristics in both directions of motion. This was treated in the developed system in two different ways, manually or using a small variable capacitance inserted in the drive of the motor.

Frame Material:

The material of the frame of the motor was necessary to be carefully considered. In the current case only the cost and machining time was considered. Aluminium material was chosen for producing the frame of the motor, which is a conducting material. This creates problems such as short-circuiting the two plates of the piezoelectric electrode, discharging the piezo electric field and consequently it compensate the properties of the piezoelectric materials. This was overcome by depositing a layer of 0.01mm of insulating material (silicon) in front surface of the frame to avoid short circuit between two surfaces of the piezoelectric electrode.

Measurements:

The current area of research is one of a very sensitive area. It needs special equipment to measure the main characteristics of the developed system such as, resolution, pre-load pressing force, torque and so on. Most of the measurements carried out in this research were taken using available facilities and basic principles of measurement. This in fact was a major reason to carry out these measurements many times to ensure that high accuracy of measurements has been obtained.

CHAPTER 9

9 RECOMMENDATIONS AND FUTURE WORK

This research work has a significant contribution in the field of servo control, methodology for modelling and design, implementation of piezoelectric USMstechnologies and power electronics in EDM-applications. Concequently many technical points have been raised in this area of applications and the possibility to extend this system to cover different applications. Futher research work and experimental work is required to fully implement the capability of the developed control system. This showed the nessacity to:

- Create a microdynamic modelling for the motor to investigate the motor capability for positioning control for future applications.
- Investigate a new technique of machining that may enable to use vibrated electrode technique, which may improve flushing action of the system and machining process (Appendix (B)).
- Determine the rules to control the machining process, using vibrated electrode control technique. This should include:
  - Optimisation of the electrode vibrating degree using either open loop or close loop control, feedback unit and a new knowledge base system.
- An investigation into the machined surface finishes using piezoelectric USMs technologies and developed necessary control techniques.
- Investigation of a new surface profile measuring technique that would enable the creation of knowledge base system for the developed control system. This could extend and open a new area of research to create an intelligent EDM - system able to modify and optimise system-operating conditions automatically. This required more experimental work using various machining parameters such as level of current, on -off time, feeding rate, dielectric flushing, electrode material, workpiece material, speed of the roll, and so on. This would need a further analysis of the machined surface finish using various methodology of analysis and measurments.

REFERENCES

- **Ahmed, M. S. and Knight, J. A. G., (1988),** "Roll texturing by EDT", Mechanical Working and Steel Processing Proceeding", pp. 405-413.
- **Ahmed, M. S., (1987),** "Texturing of large surface area by EDM", Conf. EDM Clinic, Sept. 3-5, Chicago.
- **ANSYS software manuals, (1996),** (Reference, Element, Theory...) version 5.3.
- **Aoyagi, M. and Tomikawa, Y., (1999),** "New designed longitudinal and torsional vibrator combination-type USM", FERROELECTRICS, 232 (1-4): 1121-1126.
- **Aspinwall, D., Kasuga, Y. and Mantle, A., (2001),** "The use of ultrasonic machining for the production of holes in $\gamma - TiAl$", 13th international symposium for Electromachining, ISEM, Spain, May 9th to 11th.
- **Aspinwall, D., Wise, M., Stout, K., Goh, T., Zhao, F., and El-Menshawy, F., (1992),** "Electrical discharge texturing", Inter. J. of Machine tools & manufacture, Vol. 32. No. 1-2, pp. 183-193.
- **Aspinwall, D., Zhao, F., and El-Menshawy, F., (1989),** "Electrical discharge texturing (EDT) of steel rolls", Surface topography 2, pp.123-141.
- **Battacharyya, S. K., and El-Menshawy, F., (1980),** "Monitoring and controlling the EDM Process", Trans. ASME, J. Eng. Ind., paper 79-WA/Proc-2, pp. 1-6.
- **Battacharyya, S. K. and El-Menshawy, F., (1978),** "Monitoring the EDM Process by radio signal", Int. J. Prod. Res., 16 (5), 353-63.
- **Behrens, A., and Ginzel, J., (2001),** "A comparison of different input values for gap-width controllers used in electro-discharge machining", 13th international symposium for Electromachining, ISEM, Spain, May 9th to 11th.
- **Behrens, A., and Ginzel, J., (2001),** "An open numerical control architecture for electro discharge machining", 13th international symposium for Electromachining, ISEM, Spain, May 9th to 11th.
- **Behrens, A., Ginzel, J. and Bruhns, F., (2001),** "Arc detection in electro-discharge machining", 13th international symposium for Electromachining, ISEM, Spain, May 9th to 11th.

- **Bernard, G., (1997)** "Electronic circuit and application", McGraw-Hill, Inc. USA.
- **BP Dielectric (1982),** "Dielectric fluid for electro discharge machining", MP 639/82, UK.
- **Bragard, A., et al (1985),** "Texturing the roughness of work rolls of rolling mills by means of laser pulses: the process of tomorrow", Advances in cold rolling technology, the institute of metals, pp. 94-101.
- **Cabanes, I., Maidagan, X., Sanchez, J., Garcia, A. and Lamikiz, A., (2001),** "Electro discharge machining of boron carbide industrial components", 13th international symposium for Electromachining, ISEM, Spain, May 9th to 11th.
- **Chiharu, K., Yoshiro, T., Sadayuki, T. and Takehiro, T., (1998),** "Effect of pressing force applied to a rotor on disk-type piezoelectric USM driven by self-oscillation" Jpn. J. Appl. Phys. Vol. 37, pp. 2966-2969.
- **Dong, S., Wang, S., Shen, W., and Li, L., (2000)** "A miniature piezoelectric ultrasonic motor based on circular bending vibration mode", IEEE-ASME Trans. on Mechatronics, 5 (4): 325-330-Dec.
- **Dong, S., Wang, S. and Li, L., (1999)** "Piezoelectric ultrasonic motor and fine positioner with two freedoms", FERROELECTRICS, 232 (1-4): 1109-1114.
- **El-Menshawy, F. and Snaith, (1991),** "Advances in electrical-discharge texturing (EDT) for cold mill work rolls", Iron and Steel Engineer, pp. 57-58, August.
- **El-Menshawy, F., (1990),** "Electro-discharge machining apparatus", United States Patent, Patent No. 4950860, August.
- **El-Menshawy, F., (1988),** "Electro-discharge machining apparatus", European Patent Office, Patent App. No. 88302076.0, Sept. 21.
- **El-Menshawy, F., and Ahmed, M. S. (1985),** "Monitoring and control of the electrical discharge texturing process for steel cold mill work roll", Proc. of 13th North American Research Conference, pp. 470-5.
- **El-Menshawy, F. and Bhattacharyya, (1973),** "The use of acoustic techniques for monitoring and controlling the EDM process", Proceeding of the 19th International Machine Tool Design and Research Conference, UMIST, Manchester.

- **Ernest, R., (1995),** "Friction and wear of materials", 2rd edition, JohnWiley & Sons, Inc..
- **Fukunaga, et al (1989),** "Artificial heart using ultrasonic motor", Choonpa Techno, Vol. 1, No. 2, pp 42-45.
- **Furuya, S., Maruhashi, T., Izuno, Y. and Nakaoka, M., (1992),** "Load-adaptive frequency tracking control implementation of two-phase resonant inverter for ultrasonic motor", J. of IEEE Trans. Power Electron., Vol. 7, pp. 542-550, July.
- **Ghoreishi, M., and Atkinson, J., (2001),** "Vibro-rotary electrode, a new technique in EDM drilling-performance evaluated by statistical modelling and optimisation", 13th international symposium for Electromachining, ISEM, Spain, May 9th to 11th.
- **Godwin, M. J., (1985),** "Application of new type of electrical discharge texturing for surface preparation of cold mill work rolls", *Advances in cold rolling technology*, The Institute of Metals, pp. 102-107.
- **Gromakovskii, V., A. et al (1978),** On the possibility of using a piezoelectric motor for direct actuation of the drive shaft of a video tape recorder, Tekhnika Kino I Televideniya, (5), 33-43.
- **He, S., Chen, W., Tao, X., and Chen, Z., (1998),** "Standing wave bi-directional linearly moving ultrasonic motor", IEEE trans. On ultrasonics ferr. And freq. Control, Vol. 45, No. 5, pp. 1133-1139.
- **Hoshi, and Kawamura, (1994),** Analysis of slider-driven ultrasonic motors, and their use as many-degree-of-freedom actuators. Trans. IEE., Japan, D, Vol. 114, No. 11, pp. 1074-1082.
- **Hosoe, (1989),** "Ultrasonic motors for auto-focusing lenses" choonpa Techno, Vol. 1, No. 2, pp. 36-41.
- **Hu, J., Li, G., Chan, H., and Choy, C., (2001),** "A standing wave-type noncontact linear ultrasonic motor", IEEE Trans. on ultrasonics ferroelectrics and frequency control, 48 (3): 699-708, May.
- **Inoue, T., Myohga, O., Watari, N., Hashiguchi, T., and Ueha, S., (1997),** "Ultrasonic motor operating in longitudinal-torsional degenerate-mode" IEICE Transactions on Fundamentals of Electronics Communication and Computer Sciences, Vol. E80A, Iss 12, pp. 2540-25-47.

- **Ise, et al (1991),** "Three degree-of-freedom artificial forearm using ultrasonic motor", Keisoku Jido Seigyo Gakkai Ronbunshu, Vol. 27, No. 11, pp. 1281-1289.
- **Ishida, T., and Takeuchi, Y., (2001),** "Development of automatic discharge gap controller for curved hole machining", 13th international symposium for Electromachining, ISEM, Spain, May 9th to 11th.
- **Iwai, M., Ichinose, M., Bing, Q. H., Takeuchi, K., Uematsu, T. and Suzuki, K., (2001),** "Application of fluid-free EDM to on-machine trueing/dressing for superabrasive grinding wheels", 13th international symposium for Electromachining, ISEM, Spain, May 9th to 11th.
- **Izuno, Y., Izumi, T., Yasutsune, H., Hiraki, E. and Nakaoka, M., (1998),** "Speed tracking servo control system incorporating travelling-wave-type ultrasonic motor and feasible evaluations", IEEE Transactions on Industry Applications, 34 (1): pp. 126-132, January-February.
- **Izuno, Y., and Nakaoka, M., (1996),** "Ultrasonic motor actuated direct drive positioning servo control system using fuzzy reasoning controller", Electrical Eng. in Japan, Vol. 117, No. 6, pp. 74-84.
- **Izuno, Y., Takeda, R., and Nakaoka, M., (1992),** " New fuzzy reasoning-based high-performance speed/position servo control schemes incorporating ultrasonic motor", J. of IEEE Trans. on Ind. App., Vol. 28, No. 3, January. /February.
- **Izuno, Y., and Nakaoka, M., (1990),** "Adaptive control-based high performance drive system implementation of travelling-wave type ultrasonic motor", Trans. Inst. Elect. Eng. Jpn., Vol. 110-D., November.
- **Kato, K., Sase, T. and Chiba, M., (2000),** "An ultrasonic motor using an injection-moulded plastic rotor and its application to motor-driven potentiometers", Kato K, Sase T, Chiba M, Electronics and Communications in Japan part ii-Electronics, 83 (8): 8-17.
- **Kato, K. and Sase, T., (1997),** "Robust resonant frequency tracking control for ultrasonic-motor drive", IEICE Trans. Electron. Vol. J80-C-II, No. 1, pp. 31-39. June.
- **Klocke, F., Lung, D. and Nothe, T., (2001),** "Micro contouring by EDM with fine wires", 13th international symposium for Electromachining, ISEM, Spain, May 9th to 11th.

- **Kobayashi, Y., Kimura, E. and Yanabe, S., (1999),** "Robust speed control of ultrasonic motor based on H-infinity control with repetitive compensator", JSME international J. series c-mechanical systems machine elements and manufacturing, 42 (4): 884-890, Dec.
- **Koc, B., Dogan, A., and Xu, Y., (1998),** "An ultrasonic motor using a metal-ceramic composite actuator generating torsional displacement", Japanese J. of Applied Physics part 1-regular papers short notes & review papers, 37 (10): 5659-5662, Oct.
- **Koch, O., Ehrfeld, W., Michel, F. and Gruber, H., (2001),** "Recent progress in micro-electro discharge machining-part I: Technology", 13th international symposium for Electromachining, ISEM, Spain, May 9th to 11th.
- **Kusakabe, C., Tomikawa, Y., Takahashi, S., and Takano, T., (1998),** "Effect of pressing force applied to a rotor on disk-type ultrasonic motor driven by self-oscillation", Japanese J. of applied physics part 1-regular papers short notes & review papers, 37 (5B): 2966-2969, May.
- **Kuwamoto, H., Kawano, M., Koga, Y., Kachi, Y. and Hiasa, M., (1985),** "Development of a new roll texturing system: electrical discharge method, Advances in cold rolling Technology", The Institute of Metals, pp. 108-114.
- **Lebrun, L., et al (1999),** "A Low-cost piezoelectric motor using a (1,1) non-axisymmetric mode", Smart Mater. Struct. , Vol. 8, No. 4, pp. 469-475.
- **Lebrun, L., Petit, L., and Gonnard, P., (1996),** "Ultrasonic motor using a (1,1) non-axisymmetric mode", Ultrasonic 34, pp. 251-255.
- **Lin, F. J., Wai R. J. and Hong C. M., (2000)** "Recurrent neural network control for LCC-resonant ultrasonic motor drive", IEEE Trans. on ultrasonics ferroelectrics and frequency control, 47 (3): 737-749, May.
- **Lin, F. J., Duan, R., and Yu, J., (1999),** "An ultrasonic motor drive using a current-source parallel-resonant inverter with energy feedback", IEEE Transaction on Power Electronics, Vol. 14, No. 1, January..
- **Lin, F. J., Rong-Jong, W. and Rou-Yong, D., (1999)** "Neural-network controller for parallel-resonant ultrasonic motor", IEEE Transaction on Control Systems Technology, Vol. 7, No. 4, July.

- **Lin, F. J., Wai R. J., and Lin, H. H., (1999)** "An adaptive fuzzy-neural-network controller for ultrasonic motor drive using the LLCC resonant technique", IEEE Trans. on ultrasonics Ferr. and Freq., control, Vol.46, No.3, pp.715-727.
- **Lin, F. J., Wai, R. J. and Duan, R. Y., (1999),** "Fuzzy neural networks for identification and control of ultrasonic motor drive with LLCC resonant technique", IEEE Trans. on industrial electronics, 46 (5): 999-1011, Oct.
- **Lin, F. J., Wai, R. J. and Lee, C. C., (1999),** "Fuzzy neural network position controller for ultrasonic motor drive using push-pull DC-DC converter", IEE proc. -control theory and applications, 146 (1): 99-107, January.
- **Lin, F. J., Hwang, W., and Wai, R., (1998),** "Ultrasonic motor servo-drive with online trained neural-network model-following controller", IEE Proc.-electric power applications, 145 (2): 105-110 March.
- **Lin, M. W., Abatan, A. O. and Rogers, C. A., (1994),** "Application of commercial finite codes for the analysis of induced strain-Actuated structures", J. of Intelligent material systems and structures, 5, pp. 869-875.
- **Marian, K. and Robert, C., (1996),** "Current source parallel-resonant DC/AC inverter with transformer" IEEE Transaction on Power Electronics, Vol. 11, No. 2, March.
- **Marian, K. and Abdulkarim, A., (1995),** "Current source parallel-resonant DC/DC converter" IEEE Transaction on Industrial Electronics, Vol. 42, No. 2, April.
- **Masuzawa, T., (2001),** "Micro-EDM", 13th international symposium for Electromachining, ISEM, Spain, May 9th to 11th.
- **McGeough, J. and Rasmussen, H., (1992),** "A model for the surface texturing of steel rolls by electro discharge machining", Vol. 436, pp. 155-164.
- **McGeough, J., (1988),** *Advanced methods of machining*, Chapman and Hall, USA.
- **Millman, J., (1987),** "Microelectronics", 2nd ed, New York, London: McGraw-hill.
- **Ming, Y. and Que, P. W., (2001),** "Performance estimation of a rotary travelling wave ultrasonic motor based on two-dimension analytical model", ULTRASONICS, 39(2): 115-120, March.

- **Miyadani, (1994,** "Development of spherical ultrasonic motors", Omron Technics, Vol. 34, No. 3, pp. 195-200.
- **Morita, T., Kurosawa, M. K. and Higuchi, T., (2000),** "A cylindrical shaped micro ultrasonic motor utilizing PZT thin film (1.4 mm in diameter and 5.0 mm long stator transducer", sensors and actuators a-physical, 83 (1-3): 225-230 May.
- **Morita, T., Kurosawa, M. K. and Higuchi, T., (1999),** "Cylindrical micro ultrasonic motor utilizing bulk lead zirconate titanate (PZT)", Japanese J. of applied physics part 1-regular papers short notes & review papers, 38 (5B): 3347-3350, May.
- **Morita, T., Kurosawa, M. K. and Higuchi, T., (1998),** "A Cylindrical micro ultrasonic motor using PZT thin film deposited by single process hydrothermal method (phi 2.4mm, 110=mm stator transducer", IEEE Trans. on ultrasonics ferr. And freq. Control, Vol. 45, No. 5, pp. 1178-1187.
- **Muralt, P., (1999),** "Ultrasonic micro motors based on PZT thin films", J. of Electroceramics, Vol. 3. No. 2. pp. 143-150.
- **Nakamura, K., Kurosawa, M., and Ueha, S., (1993)** "Design of hybrid transducer type ultrasonic motor" IEEE trans. On ultrasonic, ferroelectric and frequency control, Vol. 40. No. 4, July.
- **Newton, D., Garcia, E., and Horner, G. C., (1997),** "A Linear piezoelectric motor", Smart Mater. Struct. 6, pp. 295-304.
- **Obara, H., Magota, T., Ohsumi, T. and Hatano, M., (2001),** "Development of surface damage monitoring system for EDM", 13th international symposium for Electromachining, ISEM, Spain, May 9th to 11th.
- **Obara, H., Ohsumi, T. and Hatano, M., (2001),** "Development of twin-type resistorless power supply for electrical discharge machining", 13th international symposium for Electromachining, ISEM, Spain, May 9th to 11th.
- **Okada, A., Uno, Y., Okamoto, Y., Nakashima, H., Hatano, H. and Okada, S., (2001),** "A new micro EDM technique of monocrystalline silicon using fine triangular section electrode", 13th international symposium for Electromachining, ISEM, Spain, May 9th to 11th.

- **Pawelski, O., (1994),** "The influence of different work-roll texturing systems on the development of surface structure in the temper rolling process of steel used in the automotive industry", J. Mater. Process. Tech. 45, pp. 215-222.
- **Pei, J., Gao, J. and Liu, Z., (2001),** "A multi-sensor integration and data fusion system application in discharge condition recognition and classification in micro-EDM", 13th international symposium for Electromachining, ISEM, Spain, May 9th to 11th.
- **Petit, L., et al (1999),** "A multi-mode piezomotor using a flextensional coupler", Smart material & Structures, Vol. 8, No. 2, pp. 167-174.
- **Ruszaj, A., et al (2001),** "Electrochemical machining supported by electrode ultrasonic vibrations", 13th international symposium for Electromachining, ISEM, Spain, May 9th to 11th.
- **Saigoh, H., Kawasaki, M., Maruko, N. and Kanayama, K., (1995),** "Multilayer piezoelectric motor using the first longitudinal and the second bending vibrations", Jpn. J. Appl. Phys. Vol. 34, pp. 2760-2764.
- **Sashida, T. and Kenjo, T., (1993),** "An introduction to ultrasonic motors", Clarendon press, Oxford, London, UK.
- **Satsuta, T. and Hirai, K., (2001),** "Surface modification using electrode transfer induced by discharge in gas", 13th international symposium for Electromachining, ISEM, Spain, May 9th to 11th.
- **Savant, C. J., et al (1987),** "Electronic Circuit Design", the Benjamin/Cummings Publishing Company, Inc..
- **Schulze, H. P., al (2001),** "Investigation of the pre-ignition stage in EDM", 13th international symposium for Electromachining, ISEM, Spain, May 9th to 11th.
- **Sedra, S. and Peter O., (1978),** "Filter theory and design: active and passive", Toronto, Canada.
- **Shafik, M., Knight, J. A. G., (2002),** "An investigation into electro discharge machining system applications using ultrasonic motor", Proceeding of International Manufacturing Conference, IMC-19, Queens Univ., Belfast, August 28th to 31st.

- **Shafik, M., Knight, J. A. G., (2002),** "An investigation into electro discharge machining applications using a linear piezoelectric ultrasonic motor", IMech Part B (Submitted).
- **Shafik, M., Knight, J. A. G., (2002),** "Computer simulation and modelling of an ultrasonic motor using a single flexural vibrating bar", Proceeding of ESM'2002 International Conference, Germany, June 3rd to 5th.
- **Shafik, M., Knight, J. A. G. and Abdalla, H. S., (2001),** "Development of New Generation of Electrical Discharge Texturing-System Using an Ultrasonic Motor", 13th international symposium for Electromachining, ISEM, Spain, May 9th to 11th.
- **Sheu, D. Y. and Masuzawa, T., (2001),** "Development of large scale production of microholes by EDM", 13th international symposium for Electromachining, ISEM, Spain, May 9th to 11th.
- **Shieh, Y. S. and Lee, A. C., (1995),** "A new sampled-data drive for CNC-Machine tools", Int., J. of Mach. Tools Manuf., Vol. 35, No. 6.
- **Simao, J., Aspinwall, D., El-Menshawy, F. and Meadows, K., (2001),** "Surface modification/alloying of electrical discharge textured (EDT) mill rolls using PM tool electrodes and various coatings", 13th international symposium for Electromachining, ISEM, Spain, May 9th to 11th.
- **Simao, J. and Aspinwall, D., (1999),** "Hard Chromium plating of EDT mill work rolls", J. of Material Processing Technology 92-93, pp. 281-287.
- **Simao, J., Aspinwall, D. and El-Menshawy, F., (1996),** "The effect of the EDT process on the surface integrity of cold mill work rolls", 37th MWSP Conf. Proc. ISS, Vol. XXXIII, pp. 197-204.
- **Simao, J., Aspinwall, D., Wise, M. L. H., and Subari, K., (1996),** "Surface texturing transfer in simulated tandem and temper mill rolling using electrical discharge texturing rolls", J. of Materials Processing Technology, 56, pp. 177-189.
- **Simao, J., El-Menshawy, H., Wise, M. L. H. and Kockott, L., (1994),** "Simulated laser texturing using a modified electrical discharge arrangement", Advancement of Intelligent Production, Vol. 123, pp. 558-563.
- **Simao, J., et al (1994)** "Mill roll texturing using EDT", J. of Materials Processing Technology, 45, pp. 207-214.

- **Snoeys, R., Dauw, D. F. and Kruth, J. P., (1983),** "Survey of adaptive control in electro discharge machining" J. of Manufacturing Systems, Vol. 2.
- **Solotykh, B., Postanogov, V. and Bathov, A., (2001),** "Calculation of EDM technological parameters for materials of space engineering", 13th international symposium for Electromachining, ISEM, Spain, May 9th to 11th.
- **Takano, T., Tomikawa, Y. and Kusakabe, C., (1999),** "Operating characteristics of a same-phase drive-type ultrasonic motor using a flexural disk vibrator", Japanes J. OF Applied physics part 1-regular papers short notes & review papers, Vol. 38, No. 5b, pp. 3322-3326.
- **Takezawa, II., Ito, Y. and Mohri, N., (2001),** "The behavior of thin electrode wear in electrical discharge machining", 13th international symposium for Electromachining, ISEM, Spain, May 9th to 11th.
- **Tamura, T., (2001)** "Surface modification of cemented carbides machined by electrical discharge machining using oxidizing treatment-explanation of removal mechanism of oxidized layer", 13th international symposium for Electromachining, ISEM, Spain, May 9th to 11th.
- **Tomikawa, Y. and Kusakabe, C., (1999),** Operating characteristics of a same-phase drive-type ultrasonic motor using a flexural disk vibrator, Japanese J. of applied physics part 1-regular papers short notes & review papers, 38 (5B): 3322-3326, May.
- **Tsai, Y., Masuzawa, T. and Fujino, M., (2001),** "Investigations on electrode wear in micro-EDM", 13th international symposium for Electromachining, ISEM, Spain, May 9th to 11th.
- **Tsujino, J., (1998),** "Ultrasonic motor using a one-dimension longitudinal vibration converter with diagonal slits", Smart material & Structures, Vol. 7, No. 3, pp. 345-351.
- **Uefa, S. and Tomikawa, Y., (1993),** Ultrasonic motor theory and applications, Oxford.
- **Vadium and Knight, J. A. G., (1997),** "Model of cylinder piezoelectric actuator with radial polarisation and harmonic excitation", SPA Cop. 1109, Dec.

- **Valentin, I. J. and Junkar, M., (2001),** "Monitoring of the effective size of the electrode in EDM", 13th international symposium for Electromachining, ISEM, Spain, May 9th to 11th.
- **Woo, S H. and Hyun, C. P., (1993),** "Finite element modelling piezoelectric sensors and actuators", AIAAJ, Vol. 31, No. 5.
- **Wu, J. and Li, M. H., (2001),** "The identification of the servo control state in wire electrical discharge machining process", 13th international symposium for Electromachining, ISEM, Spain, May 9th to 11th.
- **XU, W. and King, T. G., (1996),** "A new type of ultrasonic motor using a roller clutch mechanism", Mechatronics, Vol. 6, No. 3, pp. 303-315.
- **Yaakov, S., et al (1999),** "A resonant driver for a piezoelectric motor with single transistor direction switches", www.google.com.
- **Zhang, B. and Zhenqi, Z., (1997),** "Developing a linear piezomotor with nano-meter resolution and high stiffness", IEEE/ASME Transaction on Mech., Vol. 2, No. 1.
- **Zhenqi, Z., (1995),** "Design of a linear piezomotor for positioning feed drive", PhD University of Connectient.

APPENDIX (A)

PRINCIPLES OF PIEZOELECTRIC MATERIALS

PIEZOELECTRICITY:

When the piezoelectric elements are strained, using an external force, a displaced electrical charge accumulates on opposing surfaces ("Piezo" is a Greek term which means "to squeeze."). Figure A-1 shows the displacement of electrical charge due to the deflection of the lattice in a naturally piezoelectric quartz crystal. The yellow circles represent silicon atoms, while the red represent oxygen.

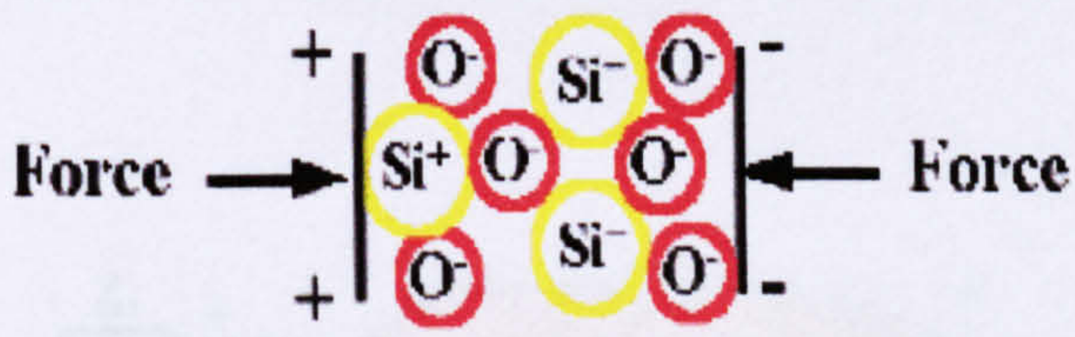

Figure A-1 Piezoelectric quartz

Most of the piezoelectric actuators rely on the use of the direct and inverse piezoelectric effect. These effects result in an electromechanical coupling, such that the deformation of a piezoelectric body results in the generation of an electric potential and vice versa. The typical situations are shown in Figures A-2 and A-3.

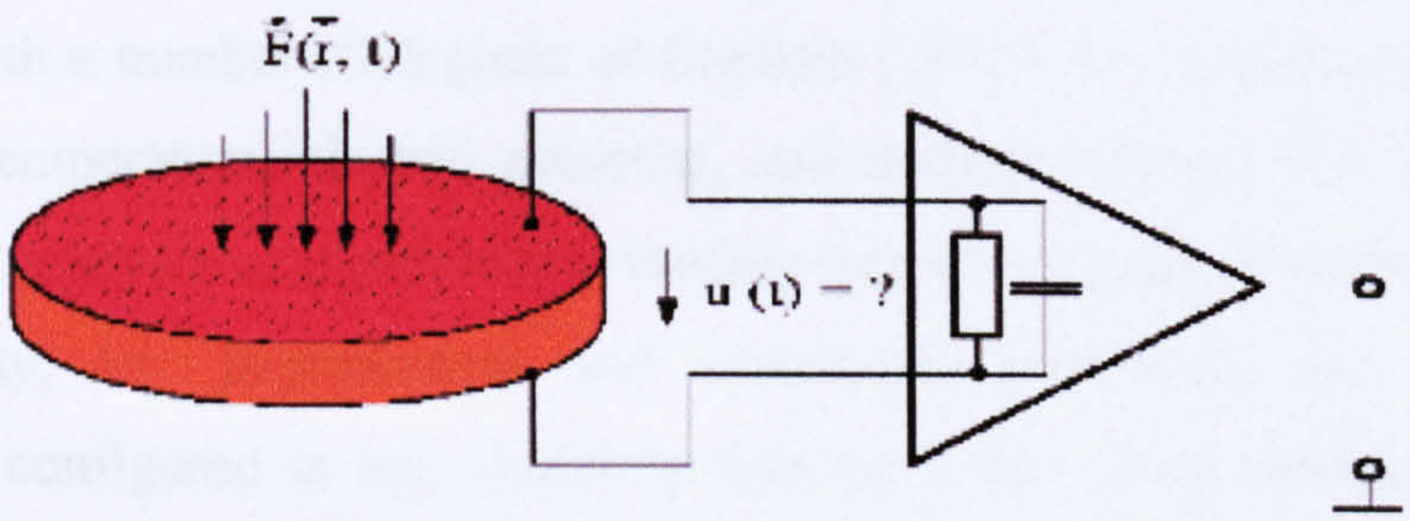

Figure A-2 Direct piezoelectric effect

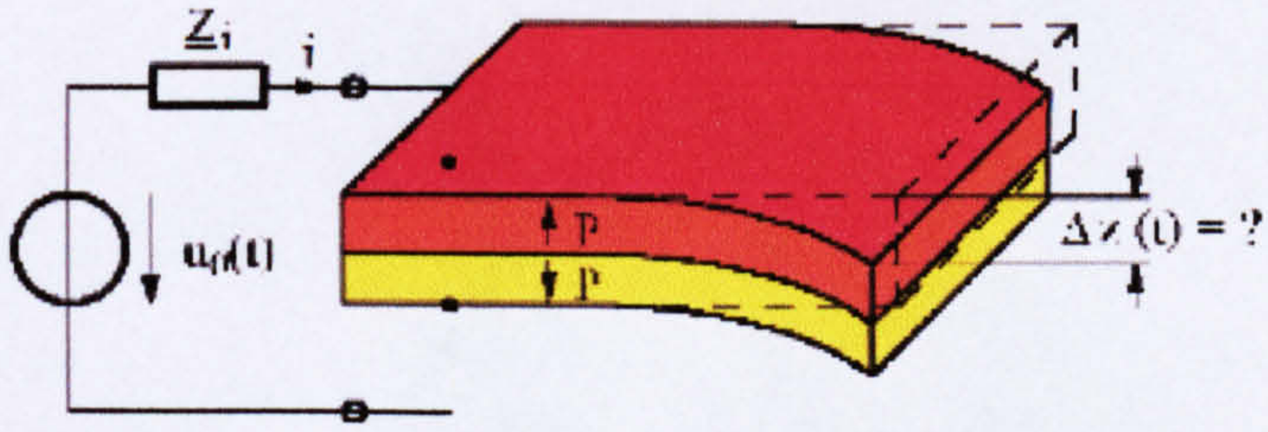

Figure A-3 Inverse piezoelectric effect

SOLID98 FE:

SOLID98 FE is a tetrahedron with ten nodes. Its geometry, nodal arrangements and the Cartesian co-ordinate system position are shown in Figure A-4. Each node on SOILD98 has been defined with a number of degrees of freedom (DOF) (i.e. displacement along global axis X, Y, Z, temperature, electric potential, and magnetic field). The SOILD98 allows direct combined analysis of piezoelectric models that have complex shapes. It also allows the non-linearity, i.e. piezoelectric and anisotropic properties and electromagnetic hysteresis. It is configured in any model by four keys that create influence on the nodal loads and characteristics. The key one is setting zero in the case of complex piezoelectric model, and the rest values depending on the type of the analysis. Thus this element incorporates the different nodal load combinations, determined by the keys. It is suitable for any type of load. Its solutions can be obtained in two different ways: a nodal DOF that includes all nodal solutions, and additional output element parameters [ANSYS 5.7-5.3 Manual, 2000, 1996].

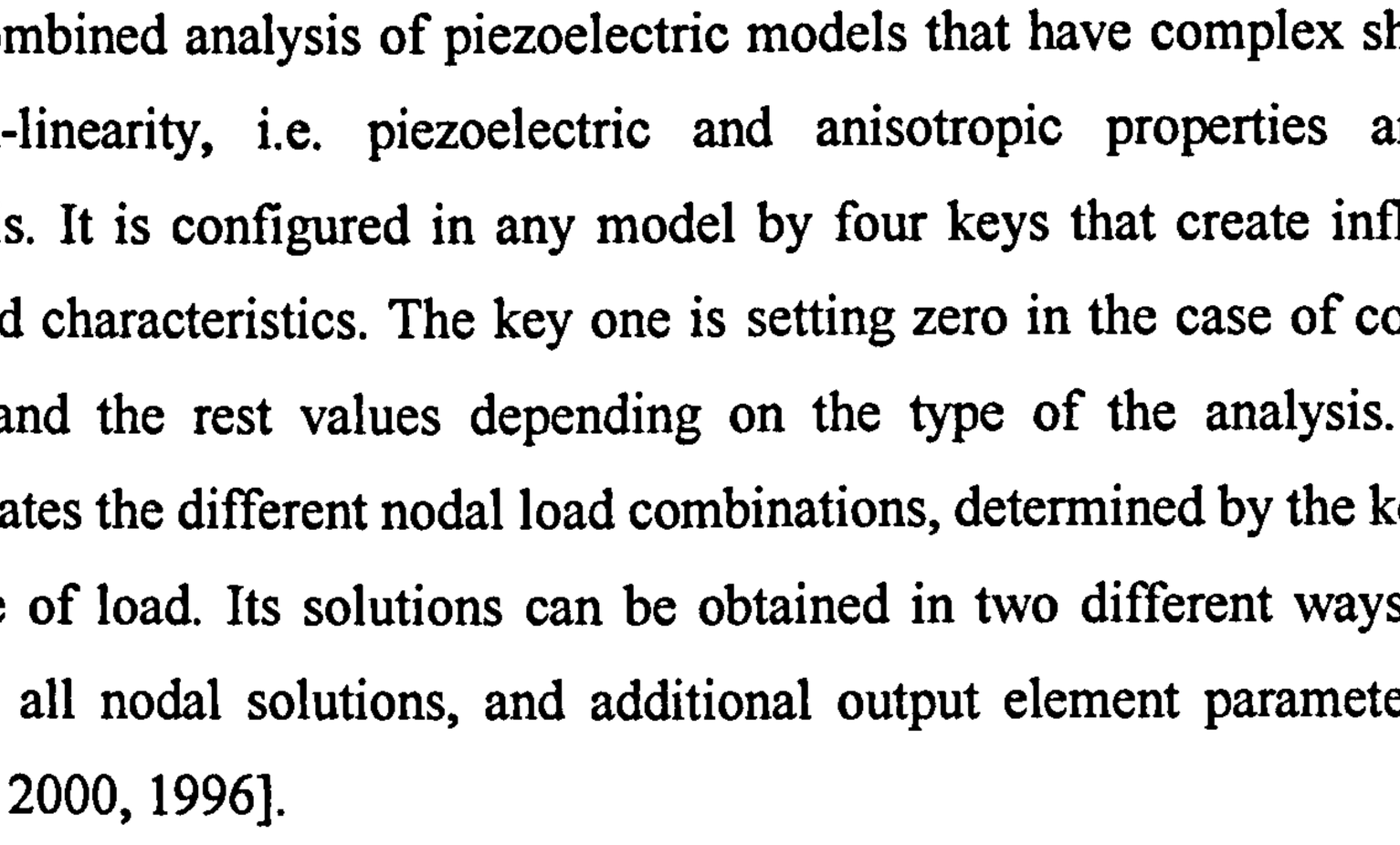

Figure A-4 Construction of the SOILD98 finite element used to define active element in the model of the developed piezoelectric USM

SOLID72 FE:

The SOLID72 is a 3-d 4-node tetrahedral structure solid finite element with rotation as shown in Figure A-5. It has four nodes with six degrees of freedom that define the element: translations and rotations of each node in the nodal X, Y and Z directions. The element has the stress stiffening capability. The density and the Young's modulus of the passive material were used to define this FE [ANSYS 5.7-5.3 Manual, 2000, 1996].

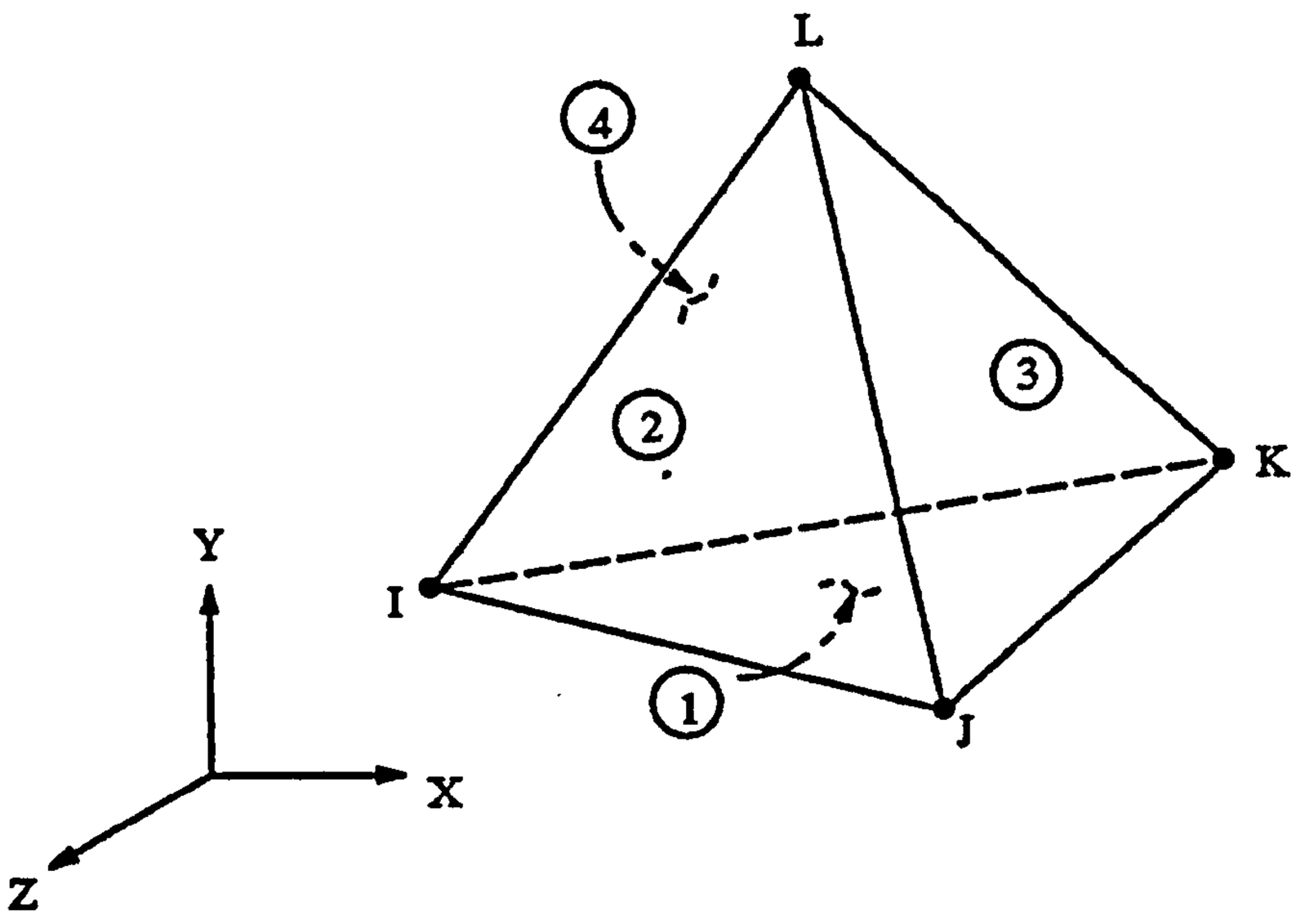

Figure A-5 The constructions of the SOILD72 finite element used to define passive element in the model of the developed piezoelectric USM

CONTAC49 FE:

The CONTAC49 3-D Point to Surface contact element was used to create the links inside the kinematics couple (between the passive and the active element) of the model of the motor. It may be used to represent the sliding between the two surfaces in three dimensions. The element has five nodes and three degrees of freedom at each node: translations in the nodal X, Y and Z directions. Links occurs when the contact node penetrates the target base. It allows for the elastic and the rigid Coulomb friction at sliding along the target base. The geometry and node locations are shown in Figure A-6. It takes a pyramid shape with the base a quadrilateral or triangular, vertices being nodes on one of the surfaces (called the target surface and in our case this is a passive element), and opposing vertex being a node on the other surface (called the contact surface, i.e. the active element in our case) [ANSYS 5.7-5.3 Manual, 2000, 1996].

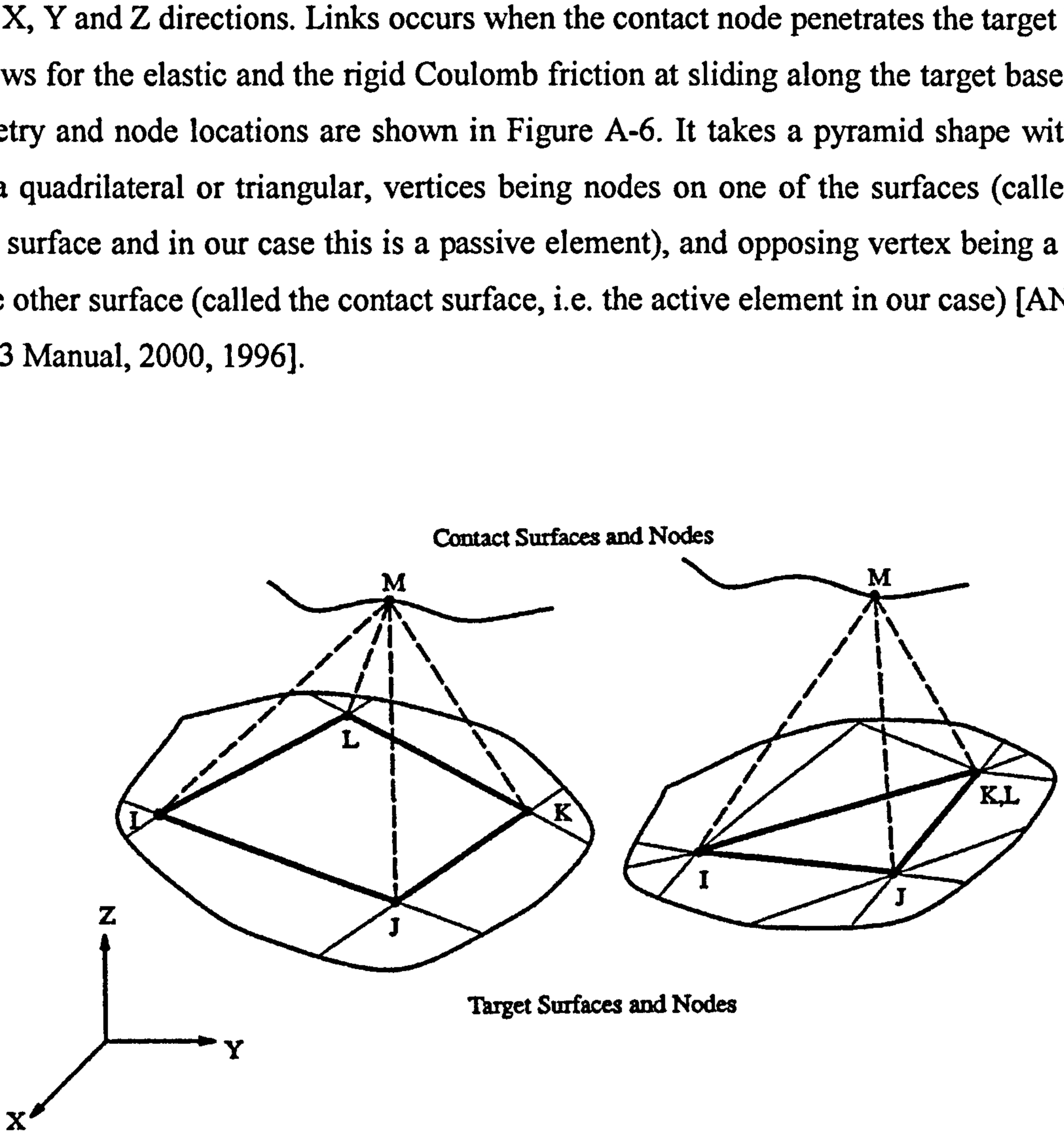

Figure A-6 The constructions of the CONTAC49 finite element used to define link element in the model of the developed piezoelectric USM

ELEMENT LOADS

Element loads include surface, body and inertial loads. Surface loads (i.e. pressure in structure analysis, heat exchange in a thermal analysis, etc) might be defined as nodal or element loads. Usually the surface loads are described with a help of the SF and SFE commands. Body loads (i.e. temperature in structure element, rates of heat source in thermal elements, etc) may be defined as nodal element or element loads. Temperature is not a constituent part of the load vector but it is used for material property appreciation. Nodal loads are converted to element loads and may be written by the BF, BFE and BFUNIF commands. However, inertial loads (i.e. gravity, rotation, etc) may be applied to all elements that have structure DOF and mass (i.e. the elements have mass as input real constant, or material density is defined for them). Inertial loads may be written by the ACEL and OMEGA commands [ANSYS 5.7-5.3 Manual, 2000, 1996].

APPENDIX (B)

MODIFIED DRIVE USING POWER MOSFETS

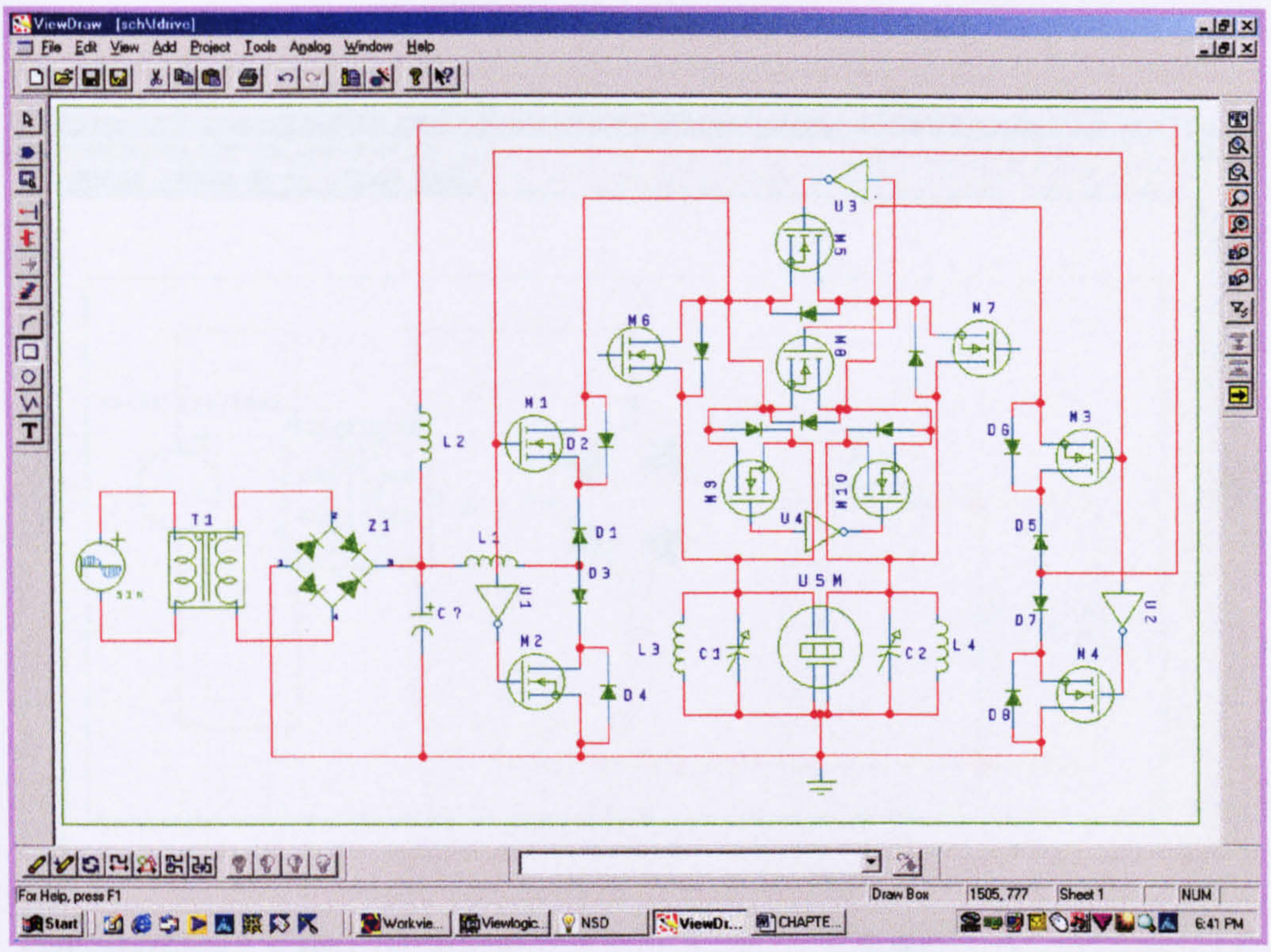

Figure B-1 Circuit for the USM drive using a push-pull DC-DC power converter and two-phase current source parallel-resonant capacitor-parallel load inverter

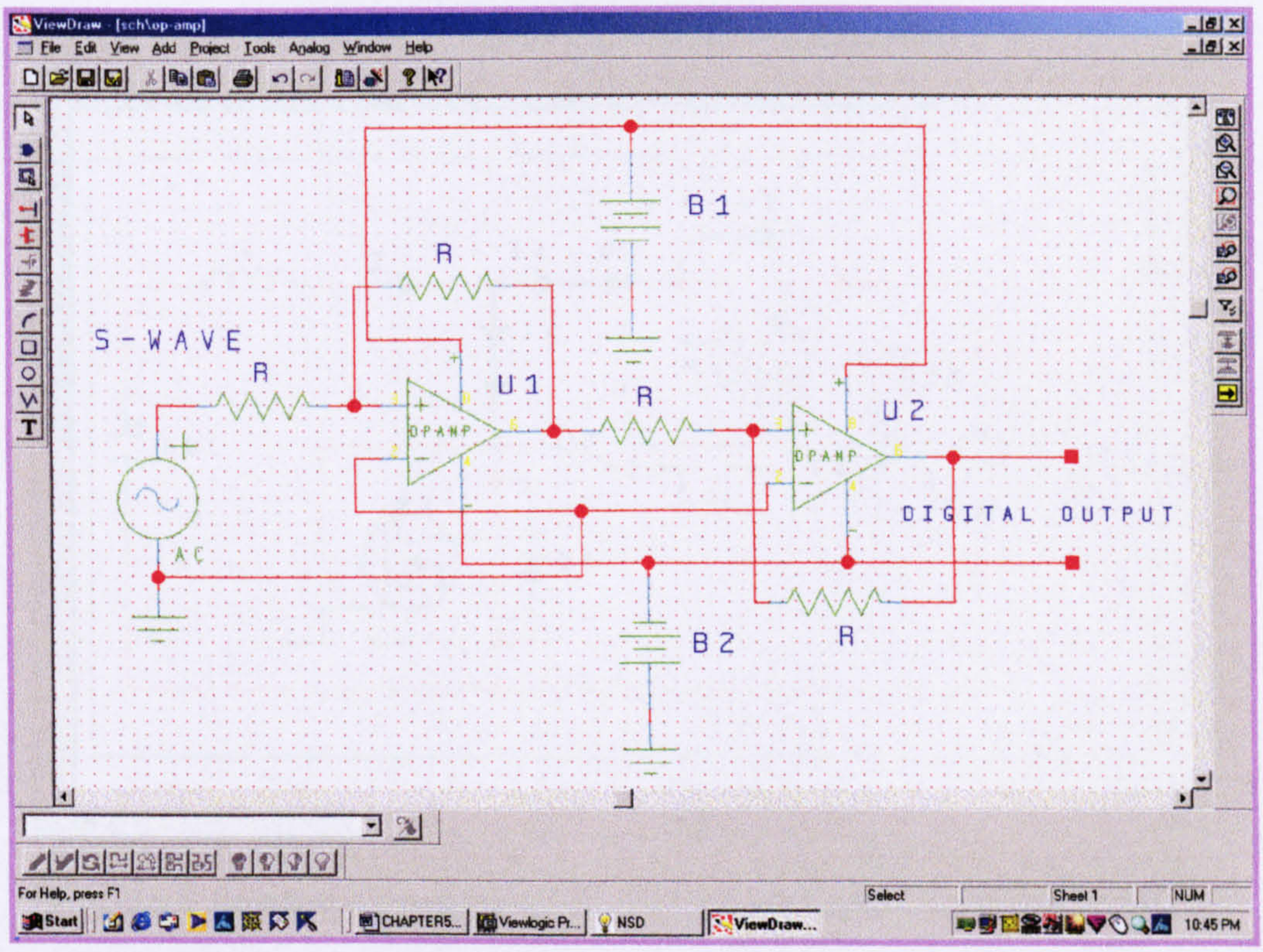

Figure B-2 MOSFETs driving circuit digital generator using two operational amplifiers

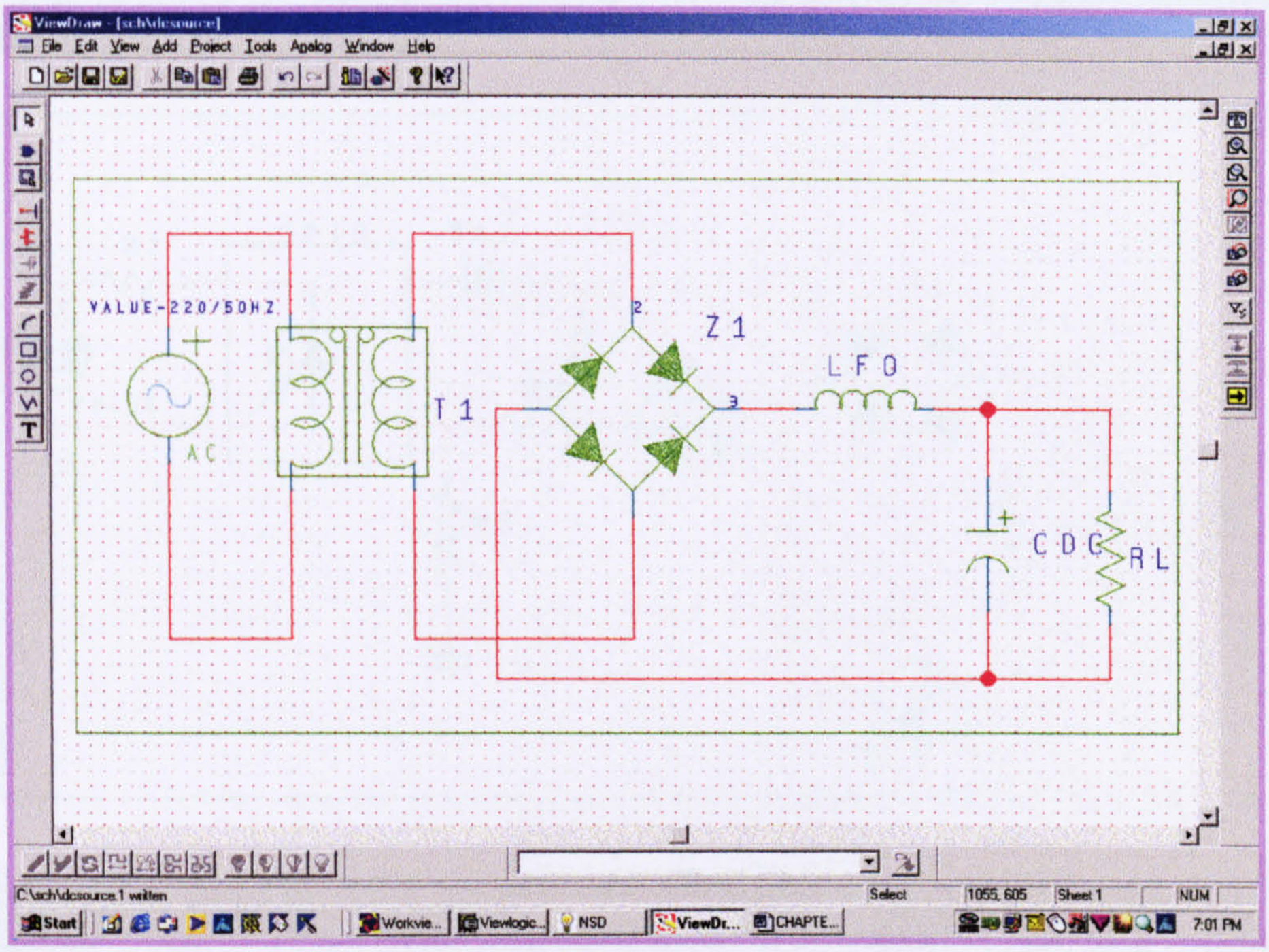

Figure B-3 Class D voltage driven rectifier using a bridge rectifier

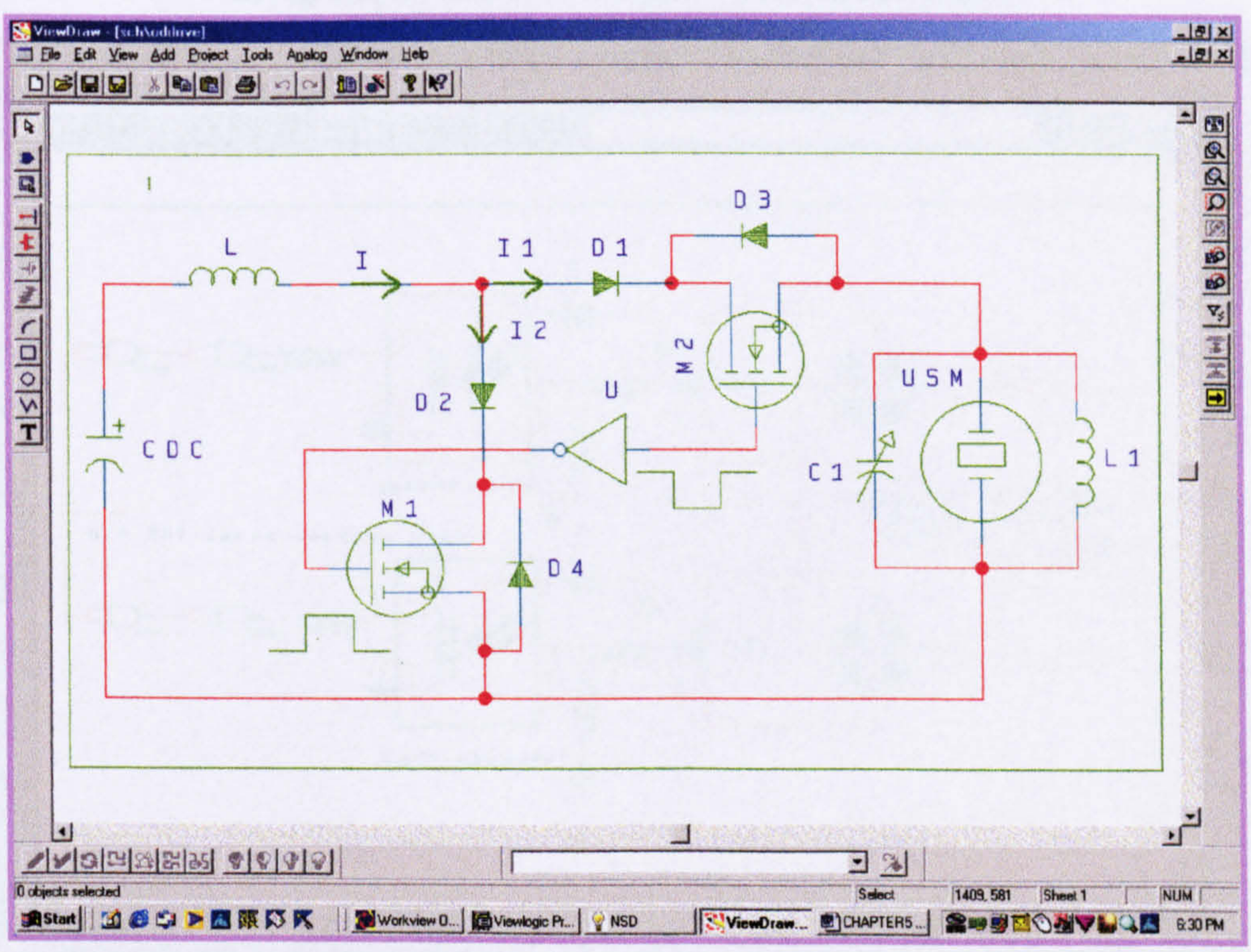

Figure B-4 Forward direction section of the USM drive using two power MOSFETs and a current source resonant circuit

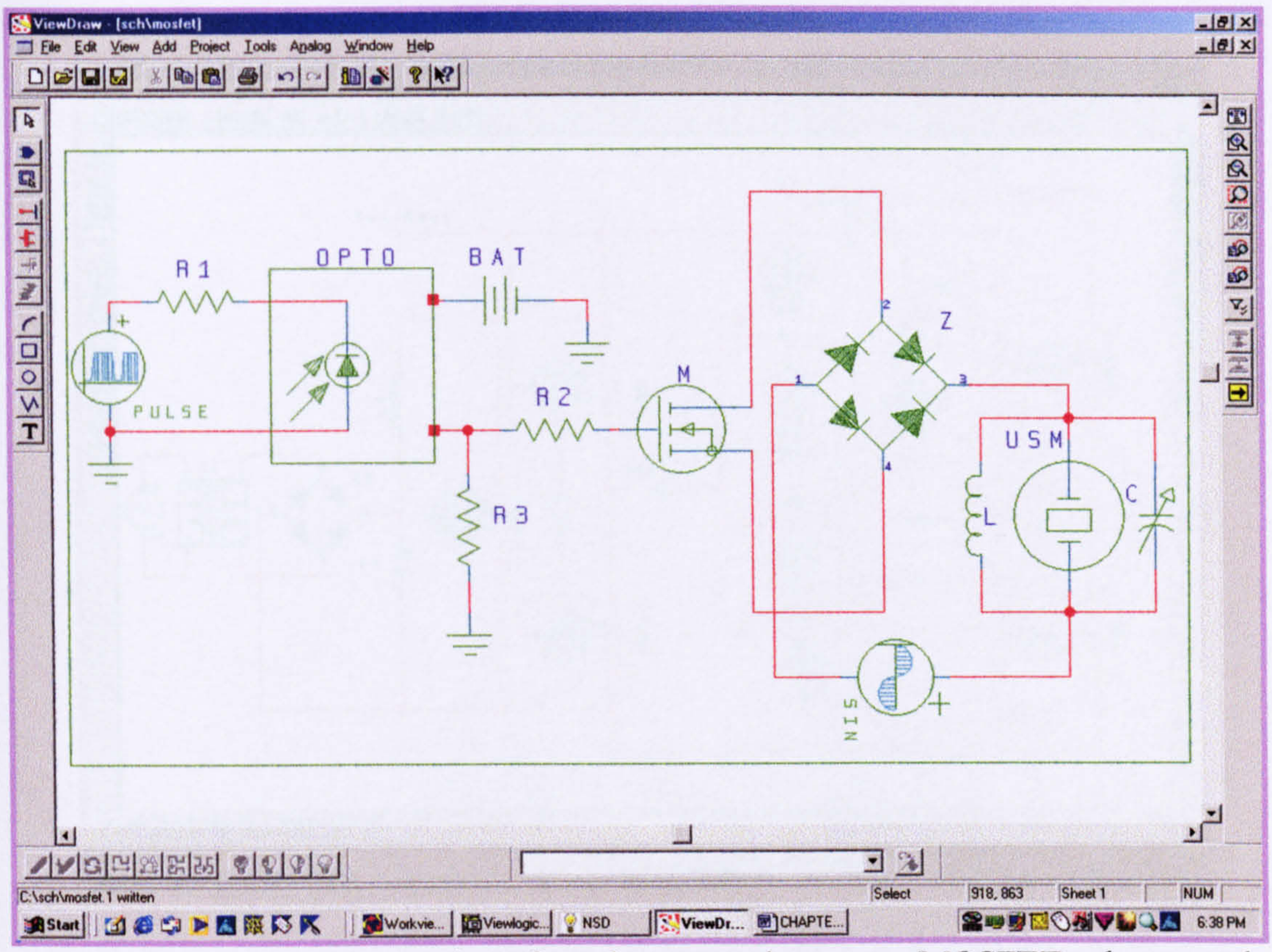

Figure B-5 Circuit construction of one inverter using power MOSFETs, the normal firing circuit and the resonant circuit load inverter

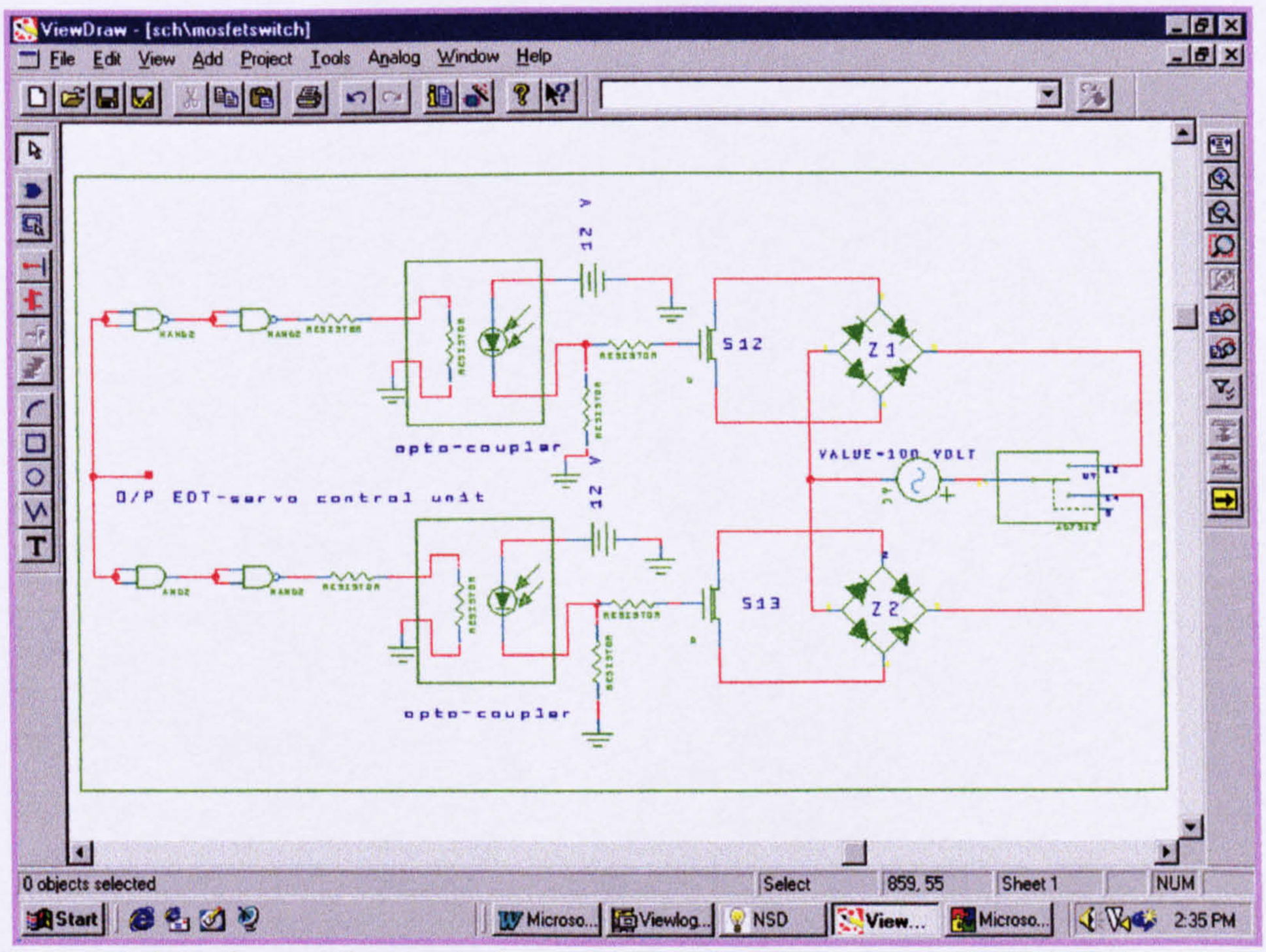

Figure B-6 An innovative texturing control unit using power MOSFETs based on an ultrasonic vibrating electrode for EDT-applications

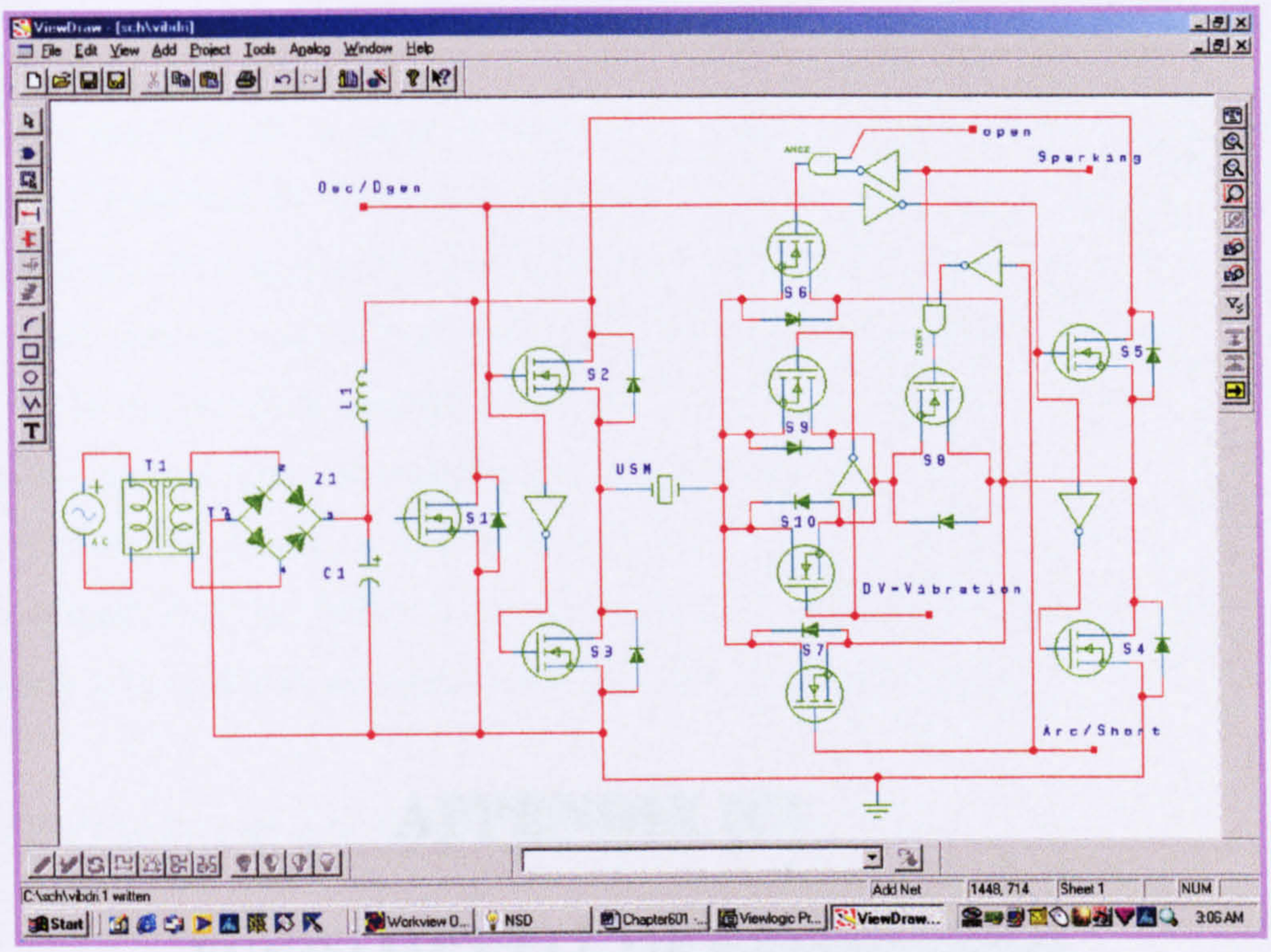

Figure B-7 Circuit of the vibro-control unit installed in the developed ultrasonic motor drive

APPENDIX (C)

FUNDAMENTAL OF EDM SYSTEM

EDM

EDM systems principle of operation is based on the creation of a spark discharge between two electrodes separated by dielectric oil [Shafik, M., et al., 2001, Simao, J., et al., 1996, McGeough, J. and Rasmussen, H., 1992]. The stored energy, between the two electrodes, was discharged into the form of heat that caused removal of tiny amounts of material from each surface of the electrode and the workpiece. These processes formed small craters in the workpiece surface. The material removal rate of machining was controlled by the spark discharge parameters [Simao, J. and Aspinwall, D., 1999, Simao, J., et al., 1994, Ahmed, M. S. and Knight, J. A. G., 1988]. It was found that this method was capable of producing surface finish with relatively acceptable degree of accuracy and lifetime.

COMPOSITION OF AN EDM-SYSTEM

A block diagram and equipment used in one of the EDM system industrial applications [El-Menshawy, F. and Ahmed, M. S., 1985] are shown in Figure 6-1 chapter 6. The workpiece to be machined fit in a tank and a dielectric fluid continuously covers it.
The dielectric fluid provides significant requirements that are:

Electrical Insulation

The dielectric oil insulates the eroded electrode and the workpiece from each other. Consequently, there is a very small gap for the spark to jump. Small gaps have the effect of raising the effectiveness of erosion from the discharge energy and improving the dimensional accuracy of the workpiece. The precise size of the gap, for a given discharge voltage, depends on the breakdown strength of this oil. This in turn is influenced by the presence of gas bubbles and solid contaminants that facilitate the creation of discharge channels. The inevitable presence of very small amounts of water (either dissolved or in the form of minute droplets) also encourages the initial spark by slightly reducing the insulating value of the fluid. The maximum breakdown resistance (or dielectric strength) is a critical feature in a dielectric performance. In service the selected gap is a compromise of high dielectric strength that gives a smaller spark gap and accurate machining. Too small a gap gives higher electrode wear and lower machining speed. A lower dielectric strength and a

wider gap can give increased discharge delay time that may result in poorer machining accuracy.

Restricting the Spark Area

The dielectric oil narrows the discharge channel and thereby produces a high energy density that concentrates heat energy over a smaller area of metal. This increases material removal rate. As the discharge channel becomes electrically conductive, by virtue of ionization, the viscosity of the fluid discourages diffusion of vapour and gas. The higher the viscosity is the higher resistance to diffusion and the narrower the discharge channel becomes. Thus the energy density is greater and the craters are deeper but of relatively small surface area. Reduced heat transfer into the workpiece, means less dissipation of thermal energy required for the melting and erosion processes.

Cooling

The dielectric fluid cools both the workpiece and the electrode. It helps to ensure that overheating does not occur. During a discharge process, the stored electrical energy is converted to heat that ultimately has to be removed by the fluid. Too low a rate of flushing and inadequate cooling, would lead to over heating to the workpiece and to excessive production of gas and vapour. Inadequate cooling could cause dimensional inaccuracies. The maximum generation of heat arises when uncontrolled discharging process takes place. If generation of heat reaches an extremely high rate, the dielectric fluid itself may have to be cooled. The temperature in the storage reservoir should not be allowed to exceed $50^0 c$, for reasons of dimensional control of the workpiece and the avoidance of oxidation in the fluid. Oxidation would reduce service life. On no account should the fluid in the working tank ever be allowed to rise to temperature within $15^0 c$ of its flash point. The flash point is the lowest temperature at which under closely specified laboratory conditions, vapour flashes momentarily when a source of ignition is applied. The term does not automatically involve any risk from spontaneous combustion or explosion.

Flushing and Filtration

An important function of the dielectric fluid is the continuous removal of eroded particles from the instantaneous sparking zone so that the erosion process can continue and the working gap is not bridged. If these particles are not removed these would be a short circuit

which in turn would create a cracks in the machined surface. Finely dispersed impurities from machining are often too small to be removed by filtration. They enhance the fixed residual conductivity of the fluid, facilitate ionization and formation of discharge channel. However, coarse metallic and carbonaceous particles, larger than about 10 μm, must be filtered out. If the rate of fluid circulation is very low, such particles can accumulate and cause bridging of the inter-electrode gap that would lead to arcing and a short circuit.

Ionization

The dielectric oil used in ED-system must ionise and de-ionise quickly, so that the sparking can be proceeded within a short pulse interval. This ensures that pulses can follow at high frequency that in turn leads to higher productivity, consistent rate of erosion and low electrode wear. It has been recognized that at all machining settings, irrespective of polarity and material, a short interval time leads to less electrode wear a short pulse interval also has the effect of improving the surface finishing of workpieces. A finite pulse interval is essential to allow for de-ionization of the fluid.

The conductivity of the fluid influences the development of the discharge channels and consequently the formation of electrically conducting ions. The dielectric fluid should preferably have a conductivity of between 1 and $1000x10^{-13}$ S/metre. Conductivity and dielectric strength are strongly influenced by contamination from dirt arising from unfiltered erosion debris and breakdown products from the fluid. The dirt level and hence conductivity, is affected by the capability of filtration and flushing rate.

The servo control drive system is to:

- Drive the electrode into the workpiece during an "open circuit" process where there is no current between the electrode and workpiece.
- Drive the electrode with a predetermined feed rate during the "spark discharge process".
- Retract the electrode away from the roll during the arcing process and stops the system when the short circuit process takes place.
- The main feature of the servo control feed drive is to:
- Provide a response time that should be shorter than one period of the sparking pulse,
  - ° Have a high resolution which enable the system to travel in many different feeding rates,

- Gives the system the flexibility to react quickly with different machining situation on order of microsecond.

An electronic oscillator unit provides:

- An electronic pulse depending on the operator requirements and a control signal from the control unit.
- It generates two signals, the first is the on-off machining signal and the second the test signal which has the property of very short 'on' period and long 'off' period.

The operators identify and select the current level and the 'on-off' signal through a keypad unit. The power unit controls the electrical power supply from the DC source to the gap between the two electrodes. The gap sensor unit detects the spark parameters (voltage, current and RF signal emitted) for the close loop control. Finally, a servo control unit is to ensure, that the servo feed drive moves the electrode with its determined feed rate and controls the inter-electrode gap of the whole system during system main machining processes. It is also retracts the electrode away from the rolls when the gap is bridged.

PRINCIPLES OF OPERATION OF EDM SYSTEM

The principles of operation of EDM system are based mainly on the voltage and current variation between the electrode and the roll. There are four main processes that are called the open circuit, the sparking, the arcing and the short circuit process. In the open circuit process, no current flows between the two electrodes. In this case the servo control drive, drives the electrode into the roll. With reducing the inter-electrode gap size between the two electrodes the electric field increases. When the gap size becomes very small, the dielectric oil is broken down and the stored energy is discharged into localised heat and approaches $20{,}000^0 c$. This leads to melting the local surfaces of the two electrodes, producing small craters in the surface. Figures C-1, C-2, C-3 and C-4 show the sub processes for a life of one pulse cycle. This shows the reaction between the two surfaces and the intensity of the charged particles for each sub-process. This is ended by the decay of the current and voltage for the current pulse and initiation of a new pulse.

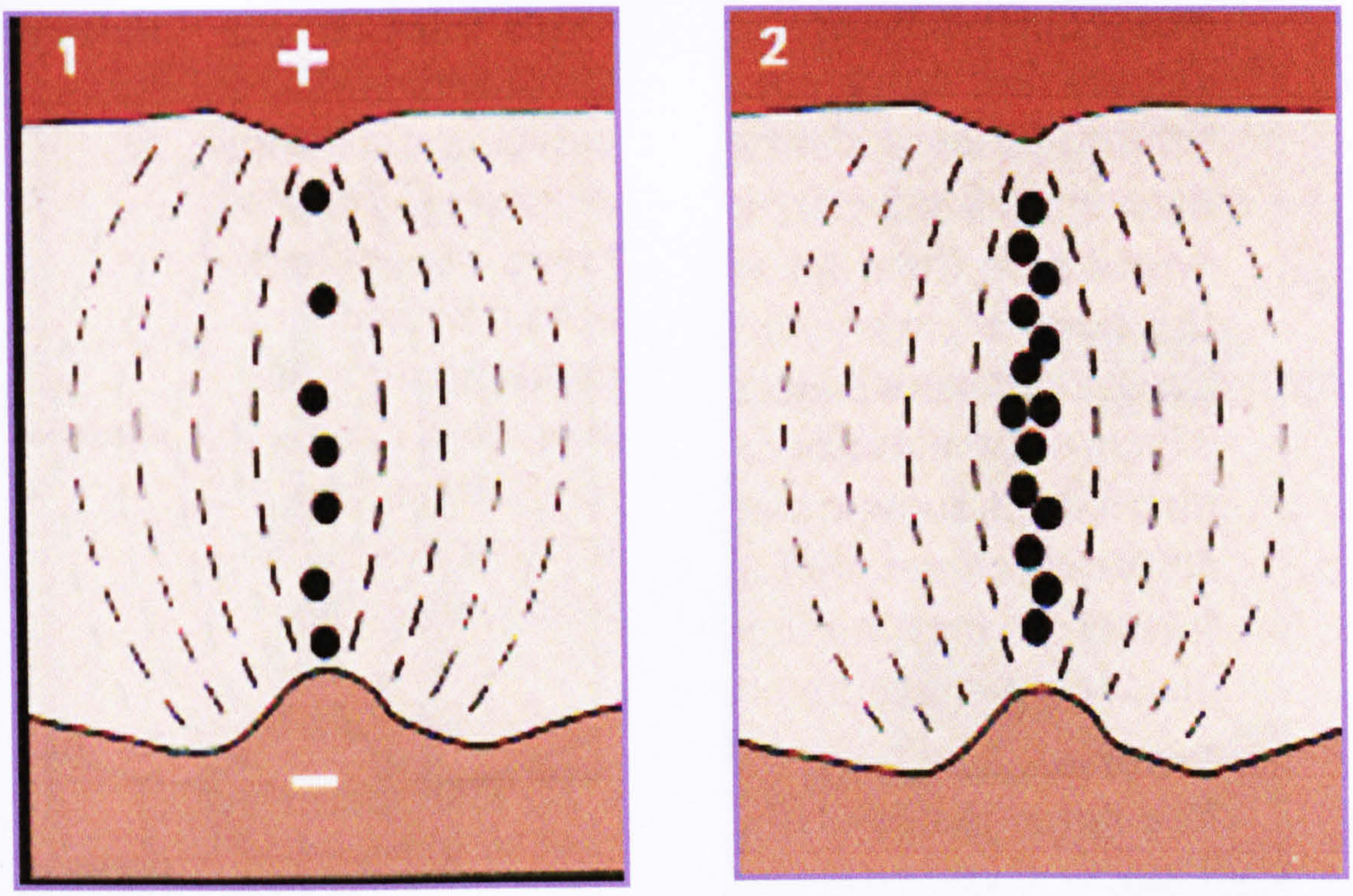

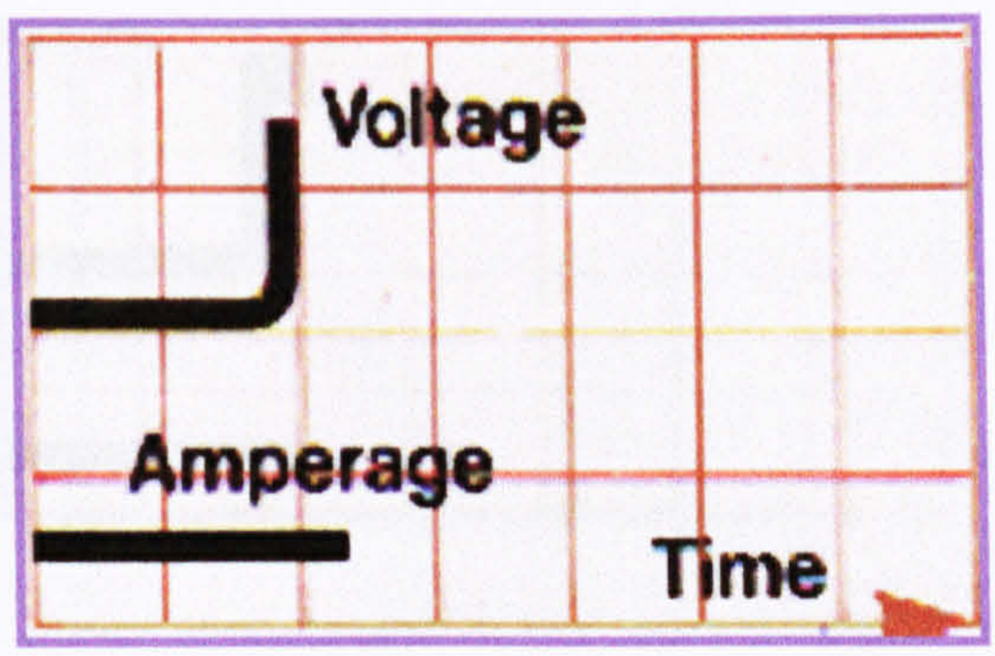

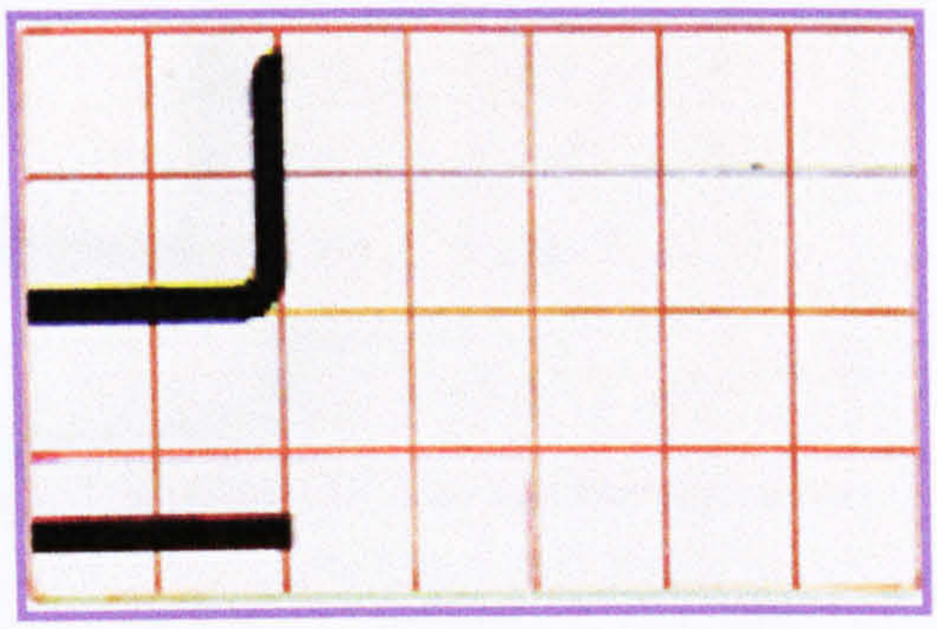

Open circuit process

Initiate of bridge of charged particles

Figure C-1 Open circuit process and its major sub-processes 'electric field, dielectric oil resistant and discharging channel' [BP Dielectric, MP 1982]

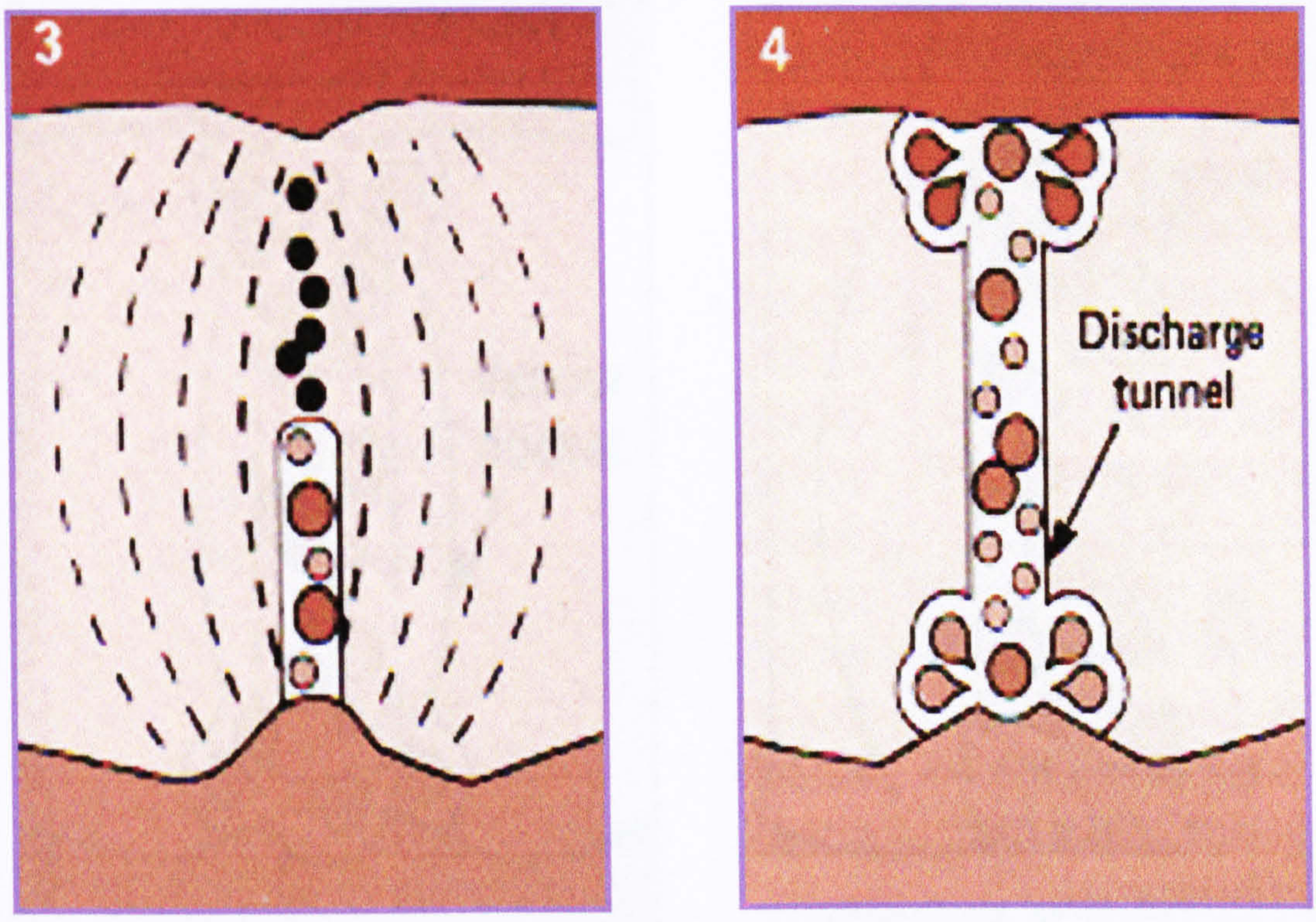

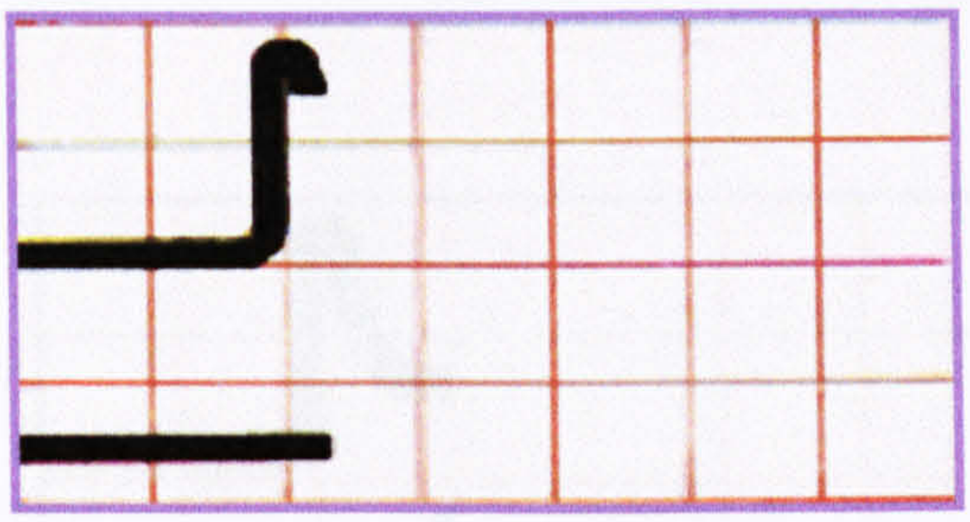

Dielectric oil breakdown and initiation of discharging process starting

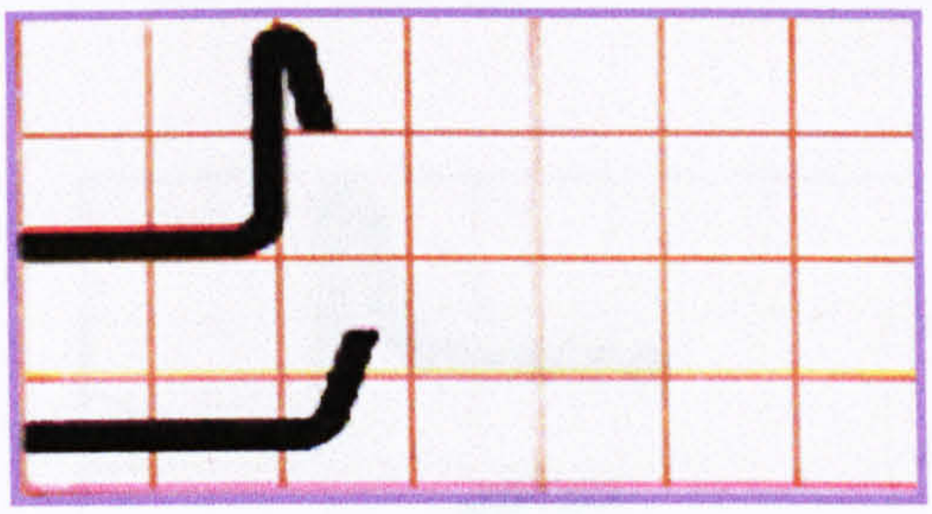

Voltage, current, discharging energy and influences of the gap capacitance

Figure C-2 Discharging process and its major sub-processes 'dielectric oil broken down, current, discharging channel and removal rate' [BP Dielectric, MP 1982]

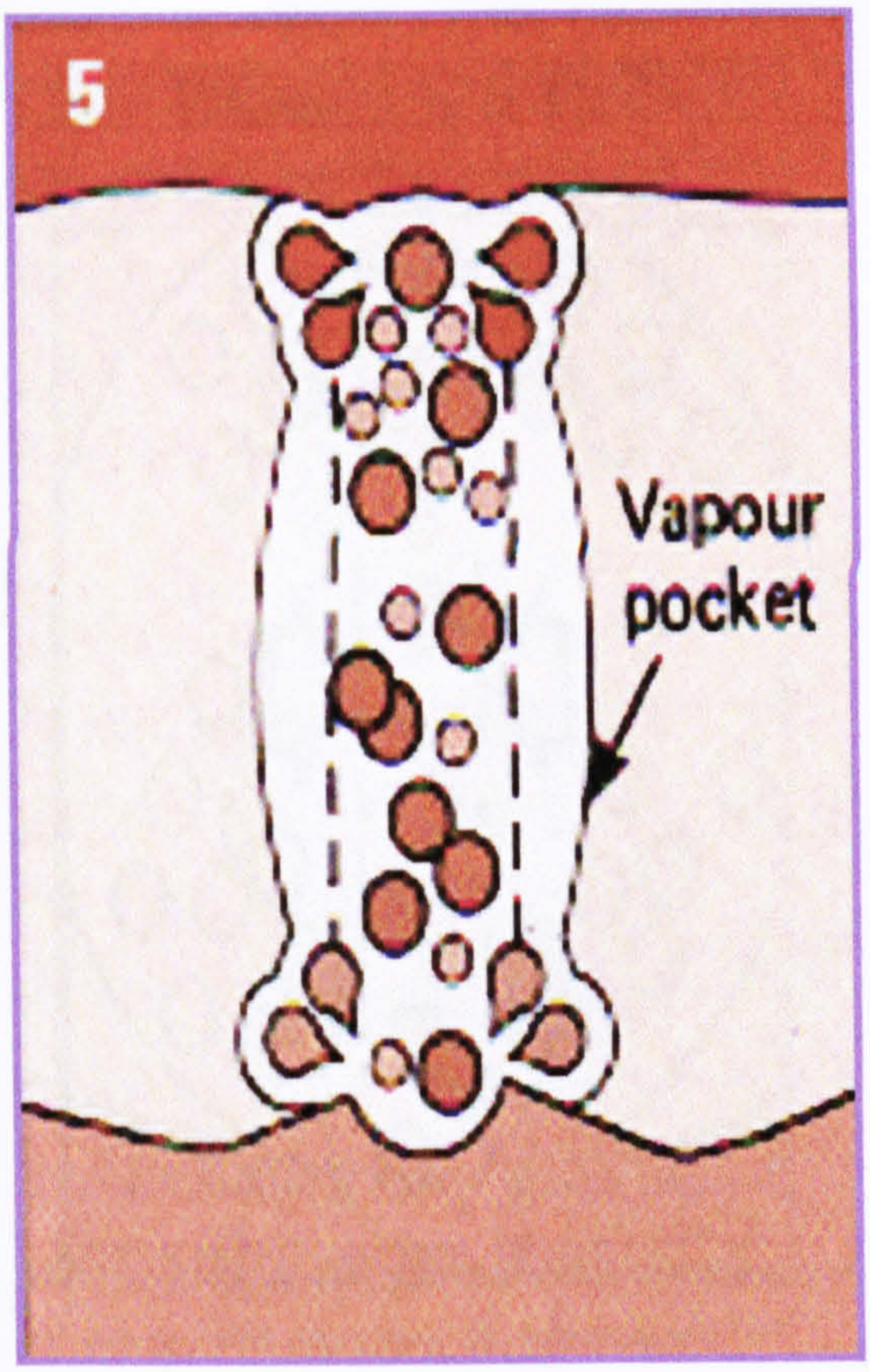

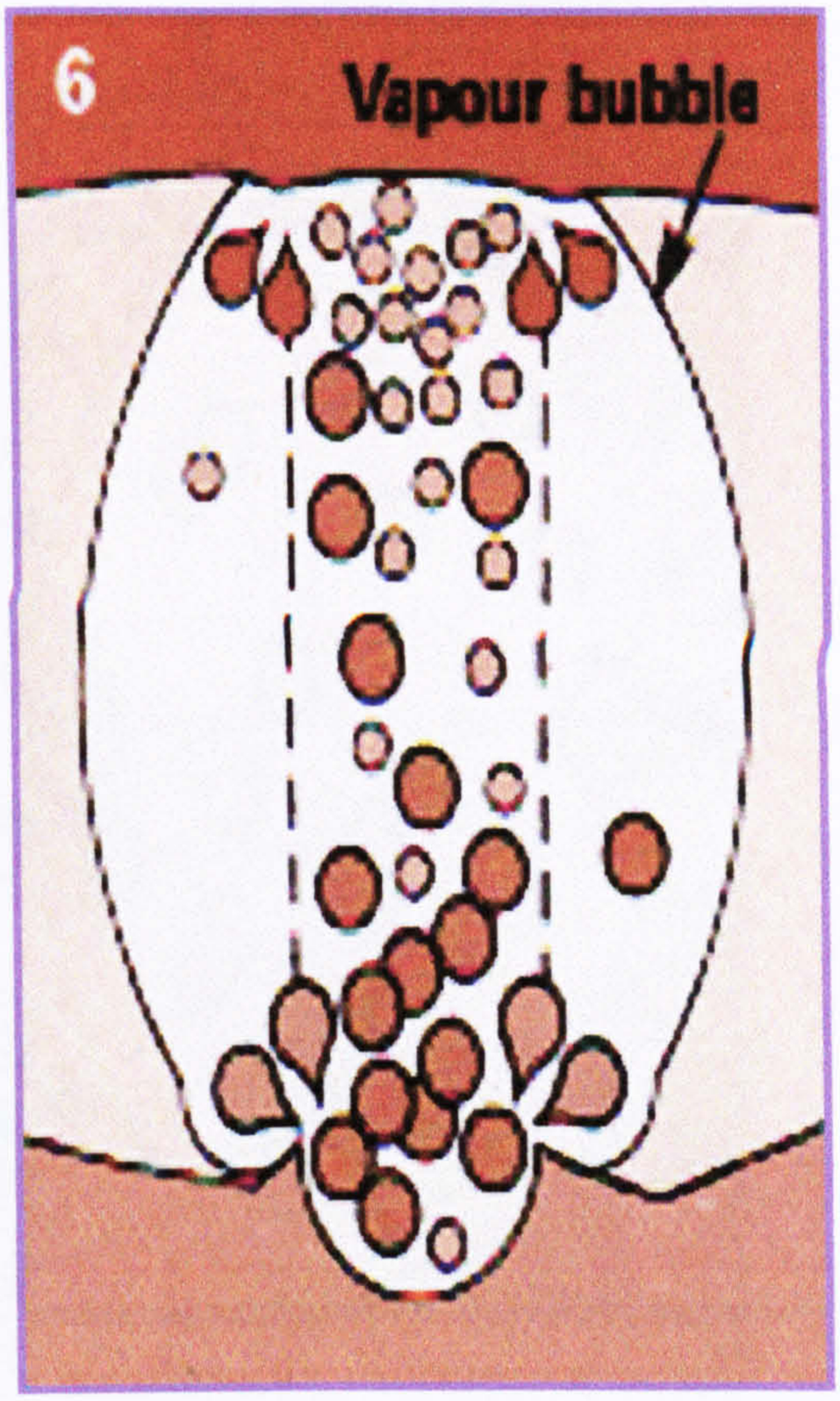

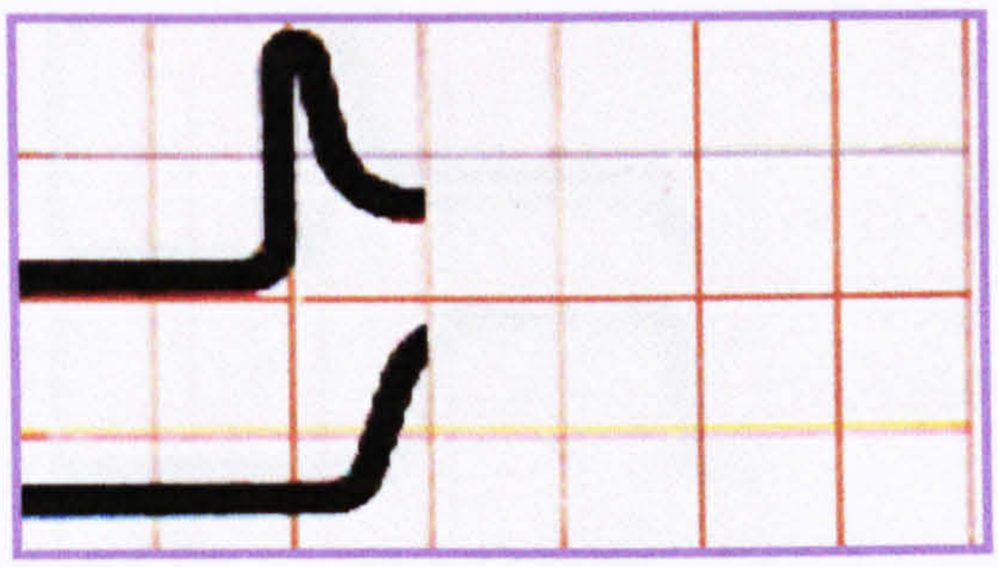

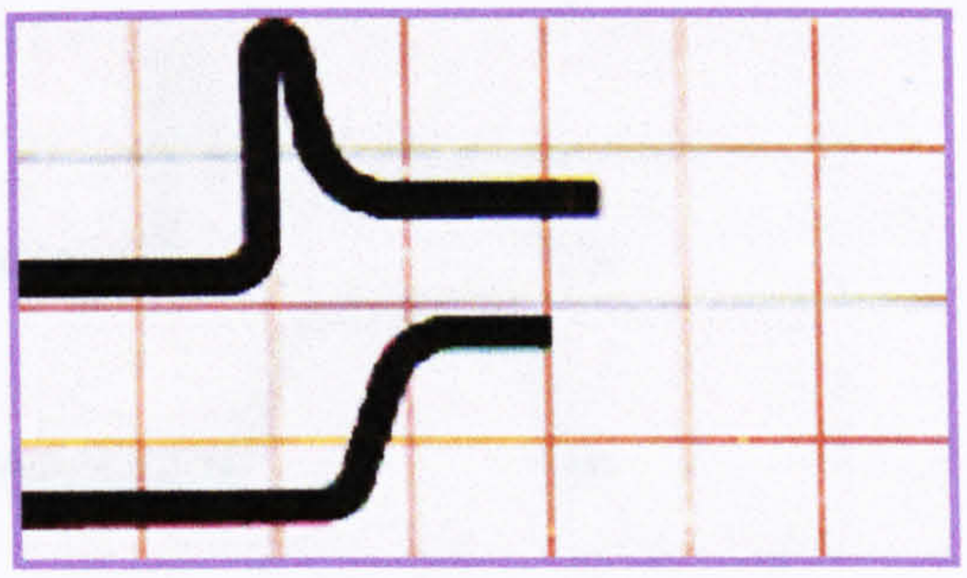

Start of stable discharging and removal rate	Fixed current, voltage and ending of the process

Figure C-3 Continuation of sparking process and main essentials sub-processes 'variation of the current, voltage, removal rate and vapour bubble' [BP Dielectric, MP 1982]

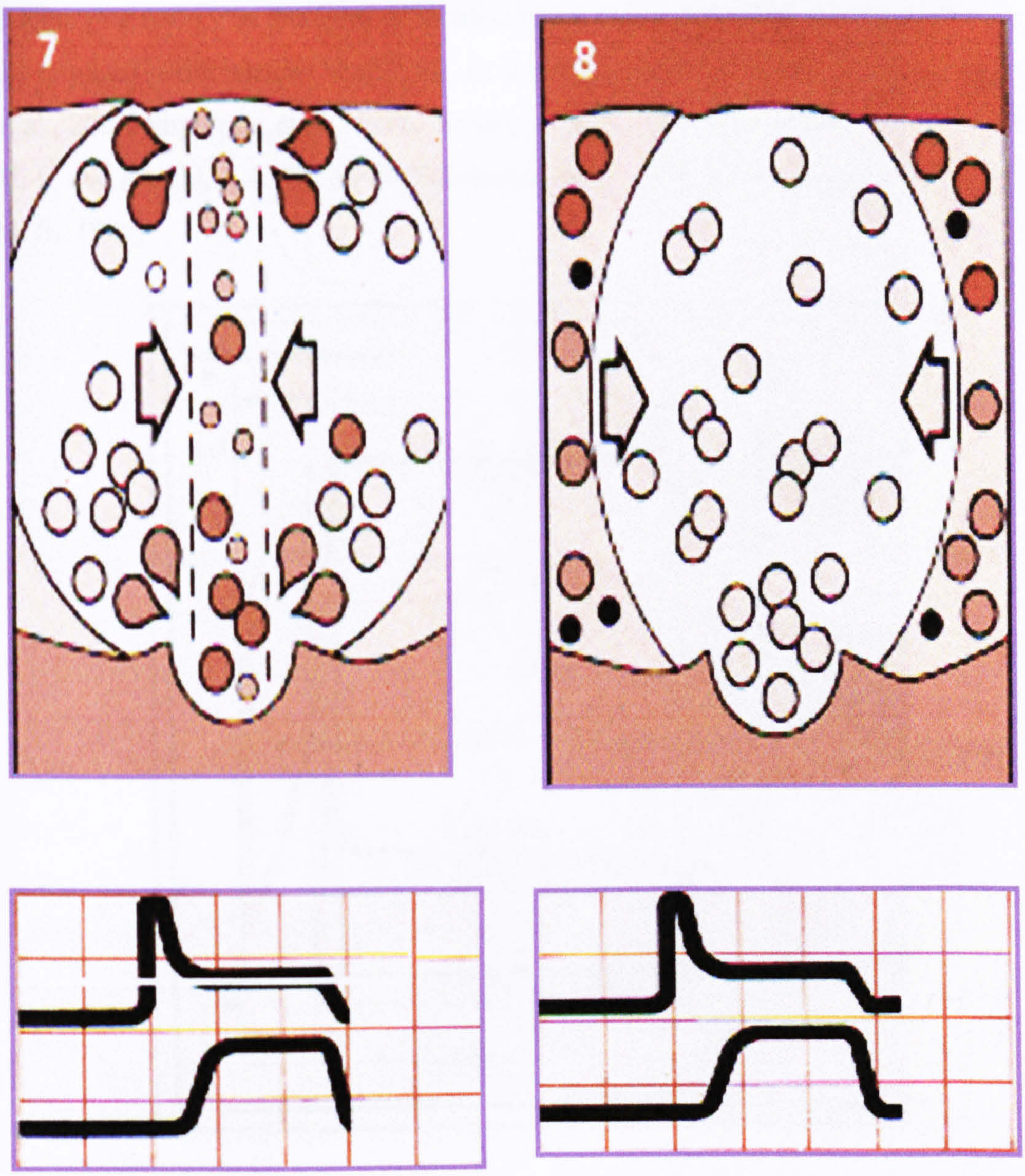

Decay in the current and voltage at the end of one activated pulse

End of one activated pulse

Figure C-4 Ending of the sparking process and its major sub-process 'variation of the vapour bubbles and flushing the product of machining' [BP Dielectric, MP 1982]

Figure C-5 illustrates the physical action of the electrical discharge and sub-process of the dielectric oil in terms of change in conductivity that occurs in one completed pulse cycle. The repetition of this discharging process at a high frequency produces stable discharging energy in the form of localised heat and provides the texturing surface with the required performance [Shafik, M., et al., 2001, Simao, J., *et al.*, 2001, Aspinwall, D., et al., 2001, Simao, J., et al., 1996, Simao, J., et al., 1994, McGeough, J., 1988, Ahmed, M. S. and Knight, J. A. G., 1988, Kuwamoto, et al., 1985, El Menshawy, F. and Ahmed, M. S., 1985].

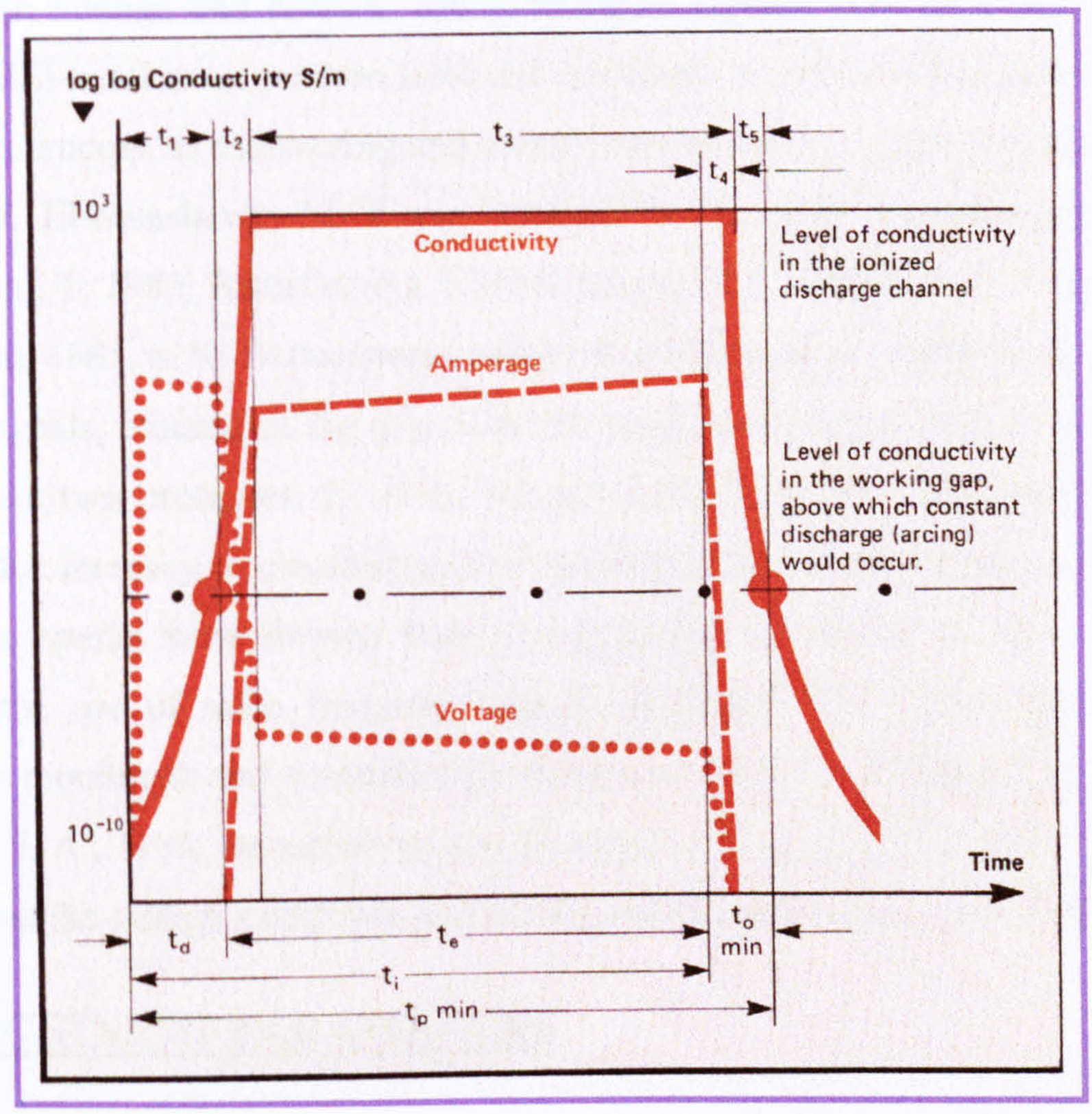

Figure C-5 Physical action of the electrical discharge and conductivity of the dielectric oil against the time for one complete pulse cycle [BP Dielectric, MP 1982]

Here t_1 and t_2 are the formation of discharge channel, t_3, t_4, t_5, t_d, t_e, $t_{0\min}$, t_i, $t_{p\min}$ are the period in which the discharge channel is in existence, the implosion of the discharge channel, the de-ionisation of the discharge channel, the initial delay until the resistance of the dielectric fluid is overcome, the period of discharge, the minimum pulse interval

that allows sufficient de-ionisation to prevent arcing process, the duration of energy pulse and the minimum cycle pulse (pulse time plus de ionisation), respectively.

EDT SYSTEM MONITORING AND CONTROL

Much research has been successfully carried out into electro discharge texturing monitoring and control [Shafik et al, 2001, Ahmed M. S. 1987, El-Menshawy M. F and Ahmed M. S., 1985, McGeough J. A., 1988, Battacharyya, and El-Menshawy, M. F, 1980, Battacharyya, and El-Menshawy, M. F, 1978]. The main technique for control was based on voltage and current. Many technical reports indicate that voltage and current in EDS-machining process were not sufficient to differentiate between arcing and sparking process, as monitoring and control was based on average voltage [Ahmed, M. S., 1987, El-Menshawy, M. F and Ahmed, M. S., 1985, Battacharyya, and El-Menshawy, M. F, 1980, Battacharyya, El-Menshawy, M. F, 1978]. M. F. El-Menshawy, M. S. Ahmed, 1985, S. K. Battacharyya and M. F. El-Menshawy, 1980, found that radio frequency signals, emitted in the gap could be used more successfully to differentiate between these two processes. In 1980, Battacharyya, S. K. and El-Menshawy, M. F found that, the intensity of electromagnetic radiation from the discharge gap was much higher when sparks were formed than during arcing, in the range 15 to 30 MHz. Therefore, the use of radio frequency signals facilitated ED system process to be successfully monitored and controlled [El-Menshawy M. F and Ahmed M. S., 1985, McGeough, J. A., 1988, Battacharyya and El-Menshawy M. F, 1980, 1978]. There was concern about the system's response and surface profiles of the machined products.

EDT MACHINING PARAMETERS

EDM-system machining performances are dependent on eight major factors. Four of them are called 'planning parameters', in which they are dependent on the kind of machining operation and whether the machining is a roughing or fine operation. These factors include polarity, open-circuit or no load voltage, discharge current and pulse duration.

The remaining parameters are adjusted to give the best operating conditions for the machine used and the results required. These are electrode material, pulse interval, gap control and circulation rates. However, the pulse interval, gap control and circulation rates are called 'operating parameters', which in much more sophisticated machines are

automatically monitored and corrected. The knowledge and experience of a skilled machine operator play a valuable part in electro discharge machining, especially in older and less sophisticated equipment.

Polarity

The polarity of the electrode selected is aimed at minimizing the electrode wear rate and for obtaining the required material removal rate. The materials of the electrode and workpiece influence the choice of polarity. Usually the polarity of any EDM operation is quoted in terms of the electrode's polarity, in which negative operation means that the tool electrode is connected to the negative side.

No-Load Voltage

This is the open circuit voltage established in the period before the current flows. It is usually selected on the basis of the machine manufacturer's recommendations. It takes into account the workpiece material and the electrode material. The no-load voltage lies usually between 60 and 120 volts, but in extreme cases it may be chosen to be of the order of 300 volts.

Discharge Current

A small discharge current gives low rates of material removal. High current produces a high removal rate but also a higher rate of electrode wear which depends on the type of electrode material. Higher discharge current means higher erosion rates, but at each level of discharge current there is particular discharge energy where the erosion rate is a maximum. Although higher discharge current leads to higher electrode wear, the rates of electrode wear fall with increasing discharge energy. This was dependent on the materials used for the electrode.

Pulse Duration

Short pulse durations normally give higher rates of electrode wear than long pulses. Experimentally it was observed that maximum erosion rate does not coincide with the maximum electrode wear. Therefore, in some machining cases, where roughing operations are on steel workpiece where either a copper or a graphite electrode was

required, the pulse duration lay between the maximum erosion and minimum electrodes wear.

Pulse Interval

In general a short pulse interval provides a high erosion rate and reduced electrode wear. In the interests of fully developed de-ionisation and adequate fall of conductivity, it is desirable not to exceed a certain minimum pulse interval and a limiting pulse interval/duration.

Gap Control

Frontal and lateral working gaps are determined and controlled by the pulse generator's characteristics and settings. Rising discharge energy and lengthening pulse duration have the effect of widening the working gap. The main consequence of a wider gap is that the surface roughness becomes more obvious. Figures 2-11 and 2-12 show the relationship between the erosion rates, electrodes wear, working parameters and gap size. It was observed that when the dielectric oil was fed onto the work area at constant pressure, any variation of the gap caused a variation of flow rate. This had an unpleasant effect not only on flushing but also on the erosion rate and electrode wear.

Electrode Materials

Among the factors, that influence the choice of electrode materials is the cost, ease of shaping, service life, workpiece material, fineness of finish and dimensional accuracy required [BP Dielectric, MP 639/82]. The best materials are those of lowest electrical resistively, highest melting point and highest stability.

Immersion

It is important that the workpiece should remain fully covered by dielectric fluid throughout an electro discharge machining operations. Generally, there should be at least 40 mm depth of fluid above the highest part of the workpiece. Less than this level is likely to cause inadequate flushing and in extreme cases arcing and inaccurate machining.

Flow Rates, Pressure, and Temperature

The material removal rate is significantly influenced by the conditions for fluid circulation. In any application where the flow is controlled by pressure, a change should be made to control by volume flow rate. If for example, in the case of EDM machining applications, a deep hollow is being machined in a workpiece the pressure that provides adequate flow at the start of the cut may be totally insufficient when the electrode has sunk into the cavity. Only by the measurement of differential pressure or of volume throughput can ascertain that the flow velocities in the working zone are adequate for removing machining debris and heat generated during the machining process. Both a low and high a circulation rate could result in lower material removal rates and higher electrode wear. Attention to the circulation is just as important as attention to electrical factors and the machining of electrode and workpiece materials. Wear, in particular, is influenced by the circulation rate of the fluid.

If the density of the eroded particles becomes too high at point in the working gap, bridges are formed which create conductive paths. This leads to abnormal discharging and ultimately arcing in which some cracks are produced in the machined product surface profiles and a reduction in the life. Adequate flushing can prevent resultant damage to the electrode and workpiece. Very low flushing rates can cause overheating of the fluid, which in turn leads to loss of dimensional accuracy. High temperatures also lead to higher vaporisation losses in the fluid. Poor flushing can give rise to fuming, which is not only unpleasant for the operator but can create fire and health hazards.

In the automotive industry, particular attention has been devoted to EDT-systems to enhance the relation between the electrical machining parameters, system performance, surface profiles and lifetime of the machined products. A number of technical reports have examined the electrical operating parameters and their influence on surface finish (roughness & peak count) and surface profiles [Simao J., et al 2001, Aspinwall D., et al 2001, Simao J. and Aspinwall D., 1999, Simao J., et al, 1996, Everett V. et al, 1995, Simao J. et al, 1994, Aspinwall D., et al, 1992, McGeough J. and Rasmussen H., 1992, El Menshawy M. F. et al, 1991, Aspinwall D., et al, 1989, Ahmed M. S. and Knight J. A. G., 1988, McGeough J., 1988, Ahmed M. S., 1987, Kuwamoto et al, 1985, El Menshawy M. F. and Ahmed M. S. 1985, Kuwamoto et al, 1985, Bhattacharyya S. K. and El-Menshawy M. F., 1980, Bhattacharyya and El-Menshawy M. F., 1978]. The

current level, 'on-off' time, electrode polarity, electrode materials, rotational speeds of roll, flushing method and spark energy were the main parameters considered.

The results demonstrated that:

- Increasing of the current level and 'on' time increased the surface roughness [Simao J., et al 1994, Aspinwall D., et al, 1989 Ahmed M. S. and Knight, J. A. G., 1988, El-Menshawy, M. F., 1988, Ahmed M. S., 1987] as shown in figures 2-19 and 2-20.
- Electrode polarity did not have a major effect on surface texturing [Aspinwall D., et al, 1989].

Aspinwall D., et al, (1989) considered the influence of the roll rotational speed and the flushing method on the roll's texture specifically surface roughness and peak count. The results of this study showed, that as the rotational speed of the roll increased, for a particular peak current and time, the surface roughness increased to a certain point and it became almost constant irrespective of the spark energy. However, it was observed that when the through electrode flushing technique was used, higher values of surface roughness, peak count and better texturing conditions were achieved, especially at low roll rotational speed (including stationery rolls) and low level of discharge energy.

APPENDIX (D)

INSTALLATION OF THE DEVELOPED SYSTEM ON EDM

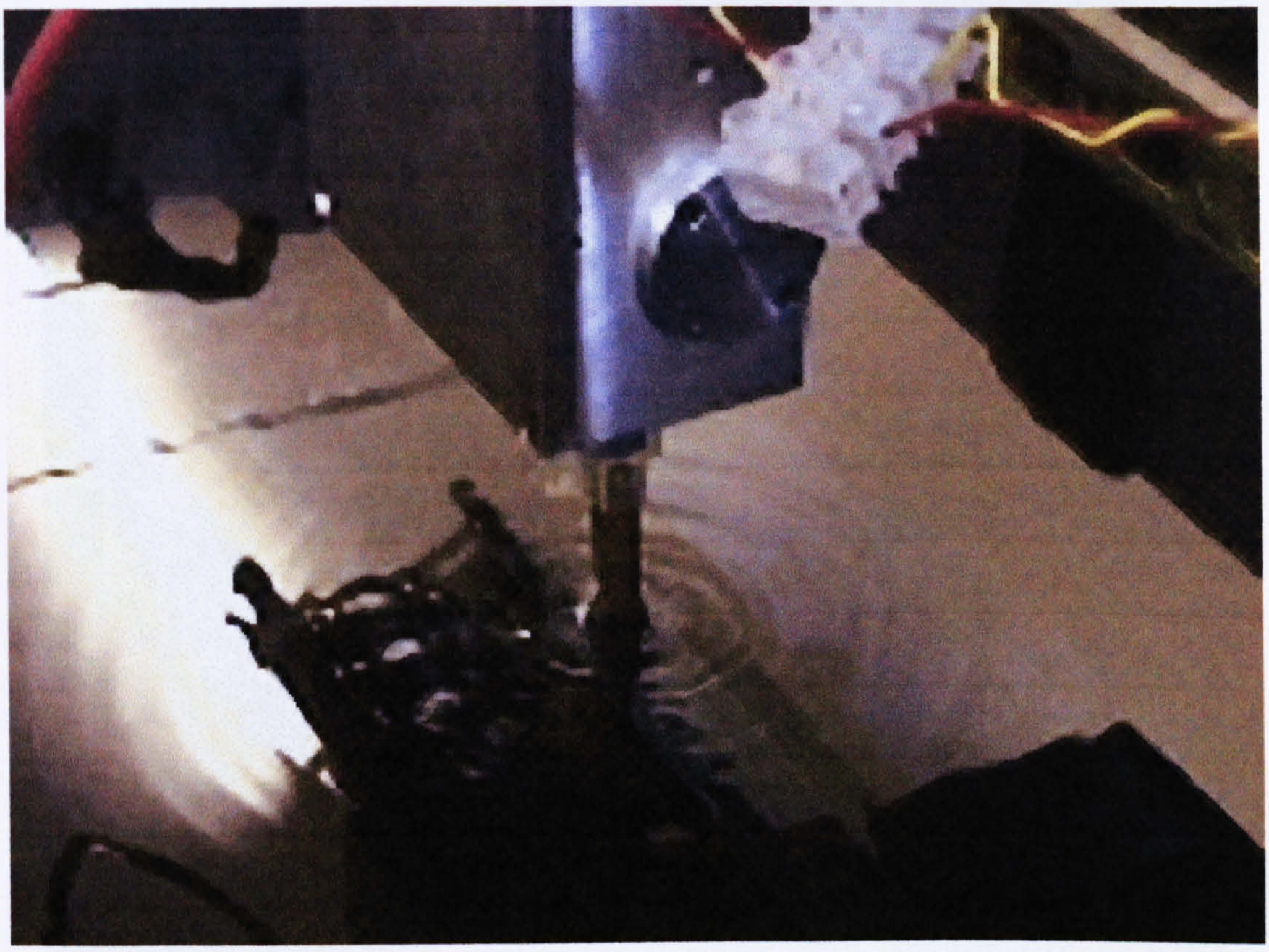

Figure D-1 Discharging process of one spark using developed piezoelectric USM drive for EDM- machining process

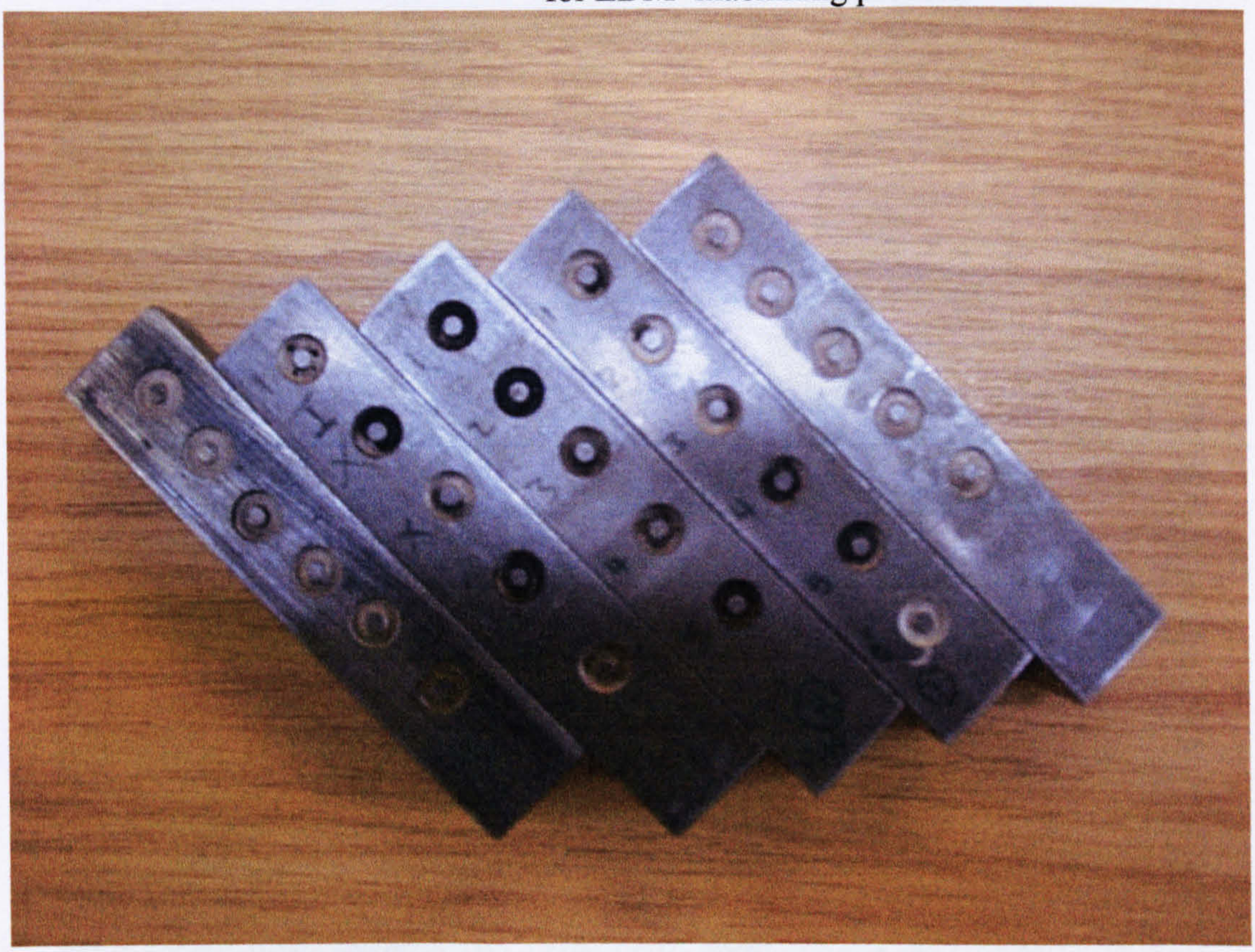

Figure D-2 Different holes machined using developed system of control and existing system using various electrical machining parameters

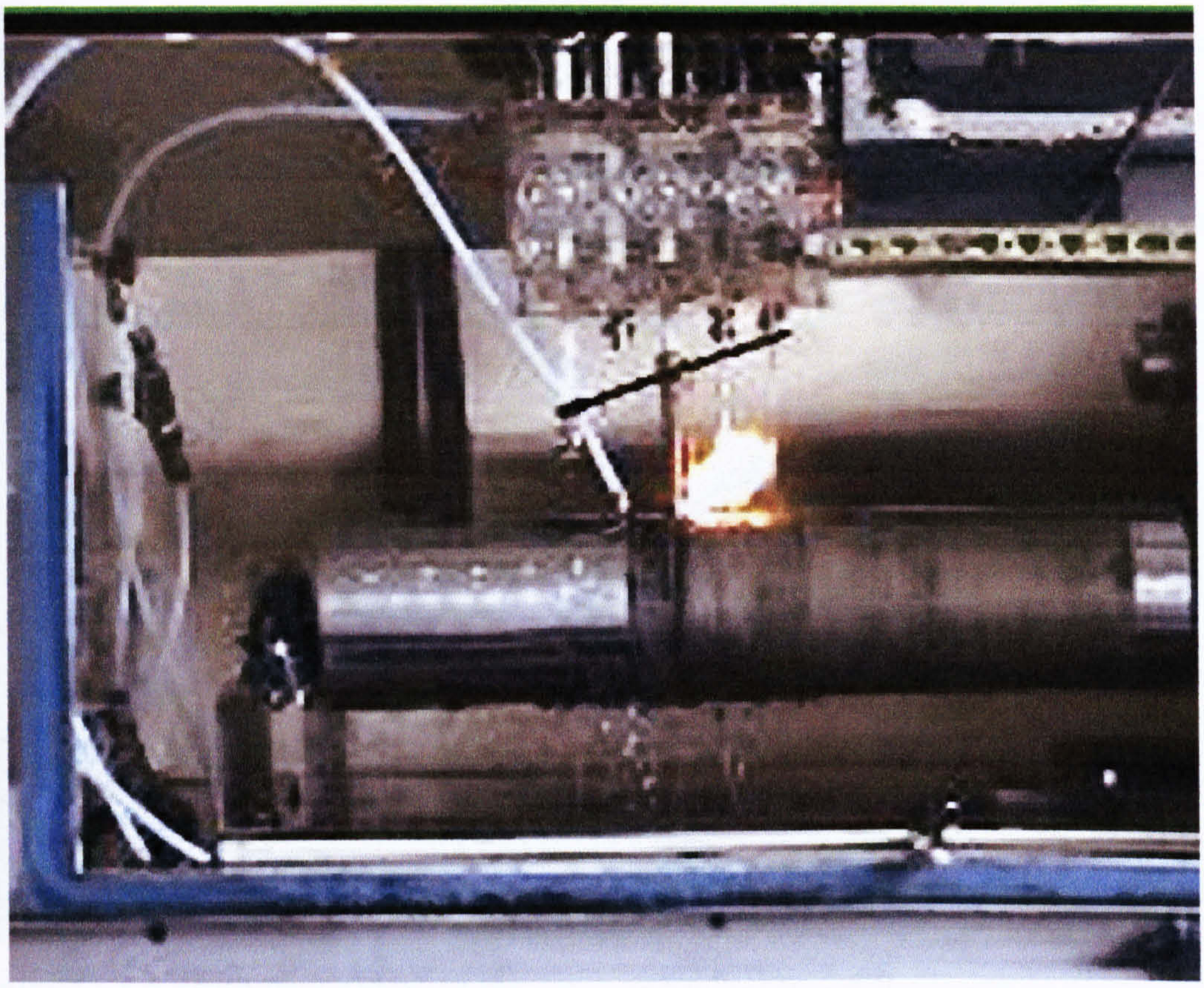

Figure D-3 Machining using existing electromagnetic system of control using EMM

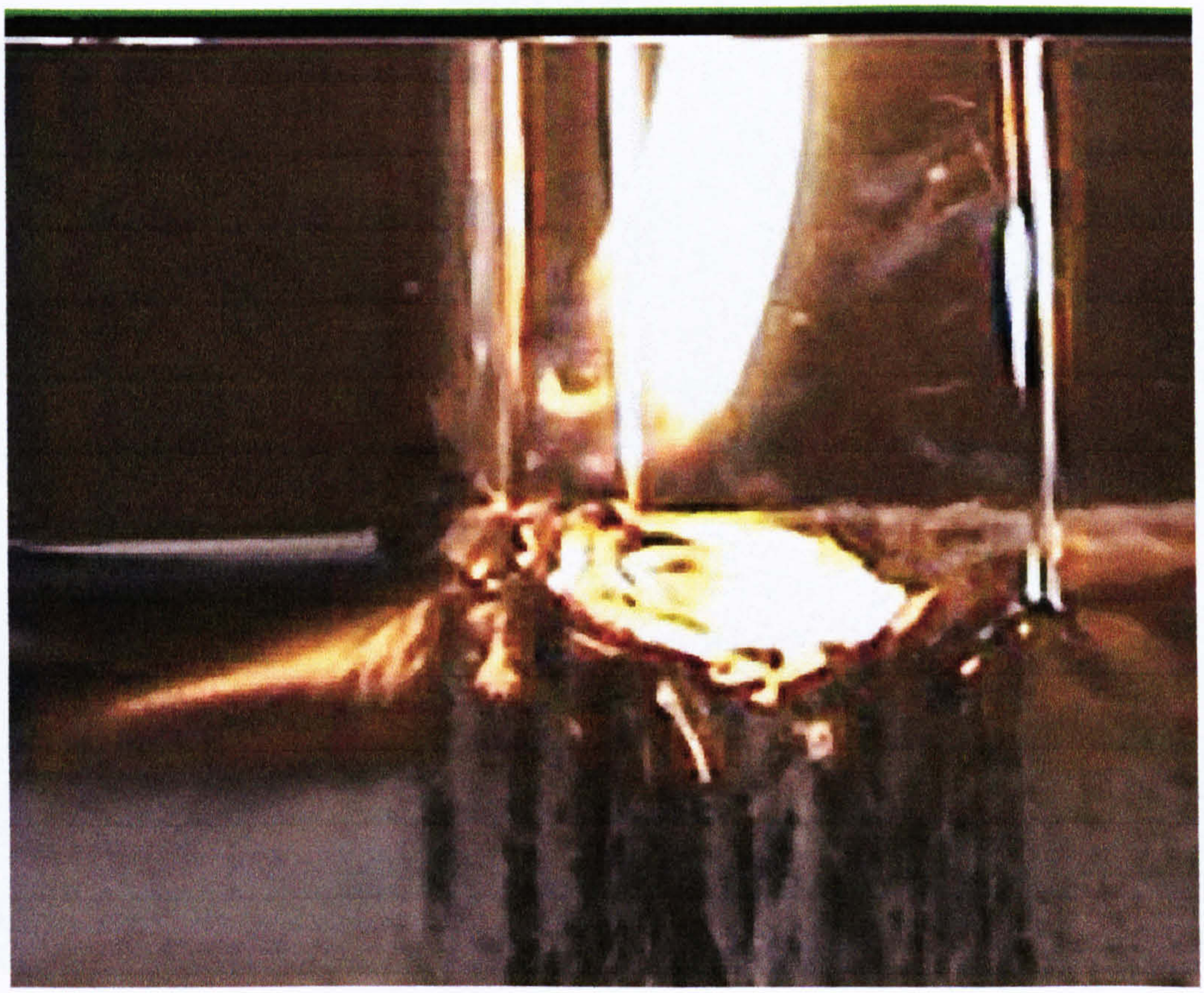

Figure D-4 Existing electromagnetic system of control under fire due to unstable machining process

Figure D-5 A close photograph to the discharging process of one spark in EDT-system using developed system of control

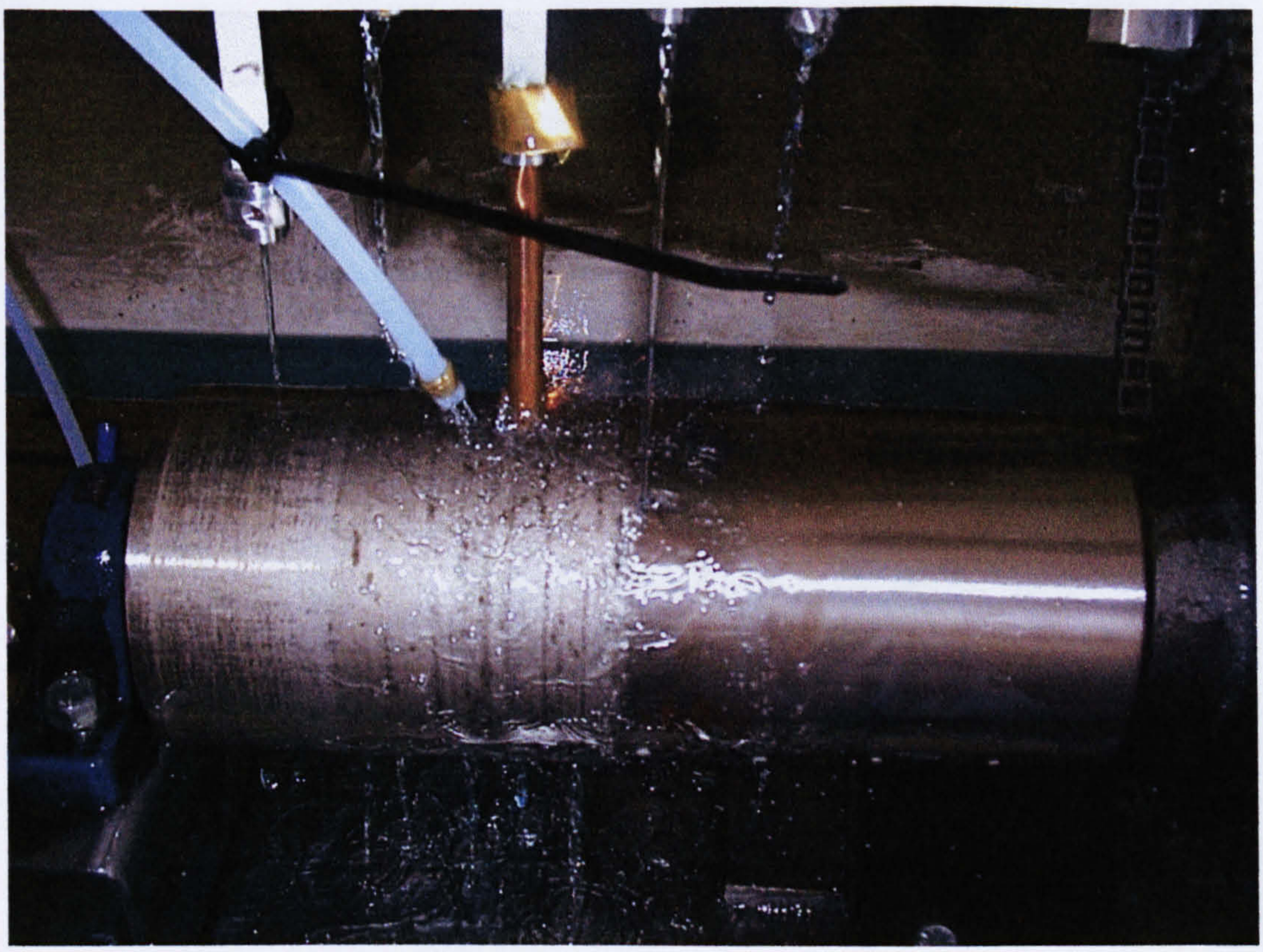

Figure D-6 Discharging process of one spark in EDT-system using developed piezoelectric USM drive (one channel activated)

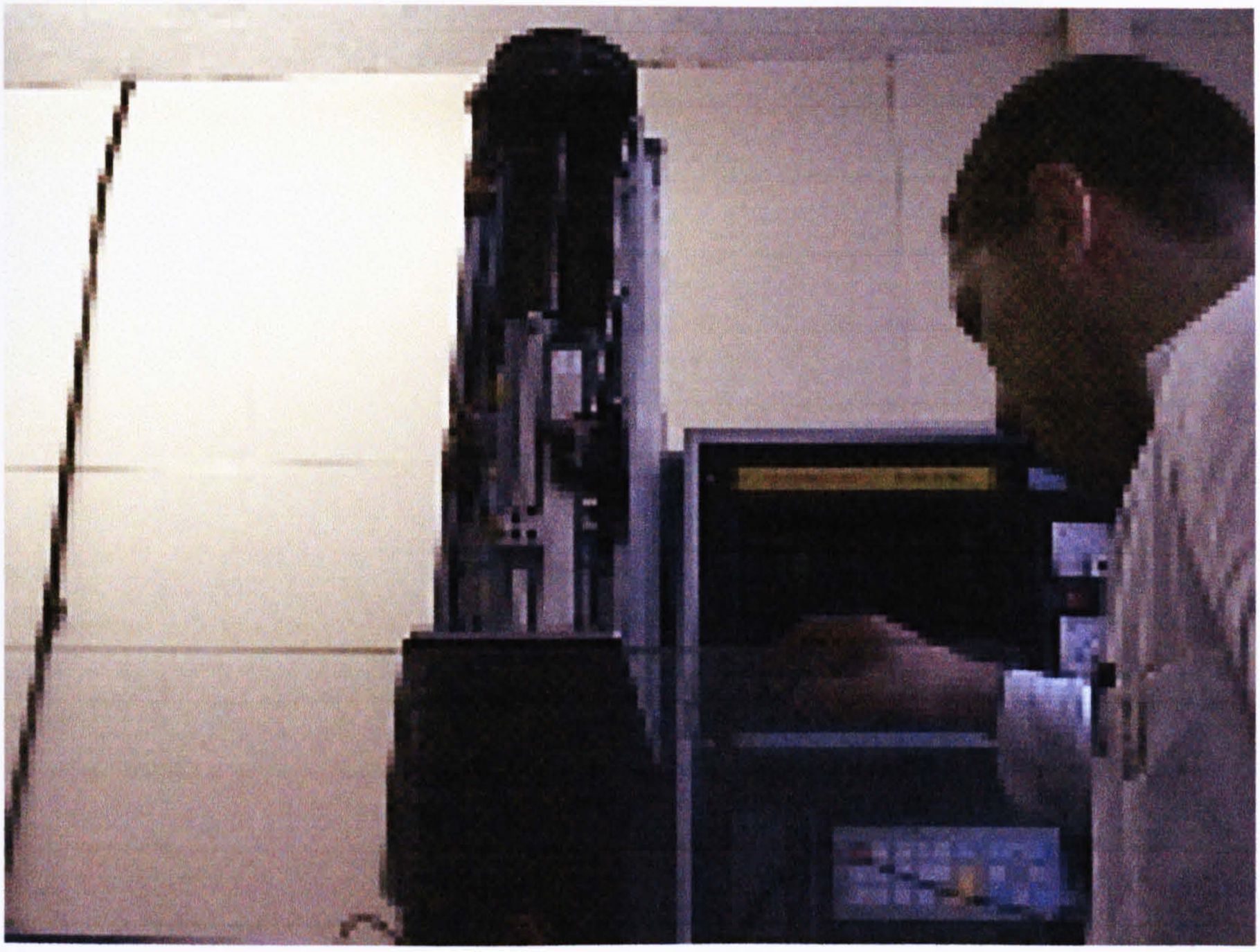

Figure D-7 Developed system of control under examination, evaluation, control and supervision

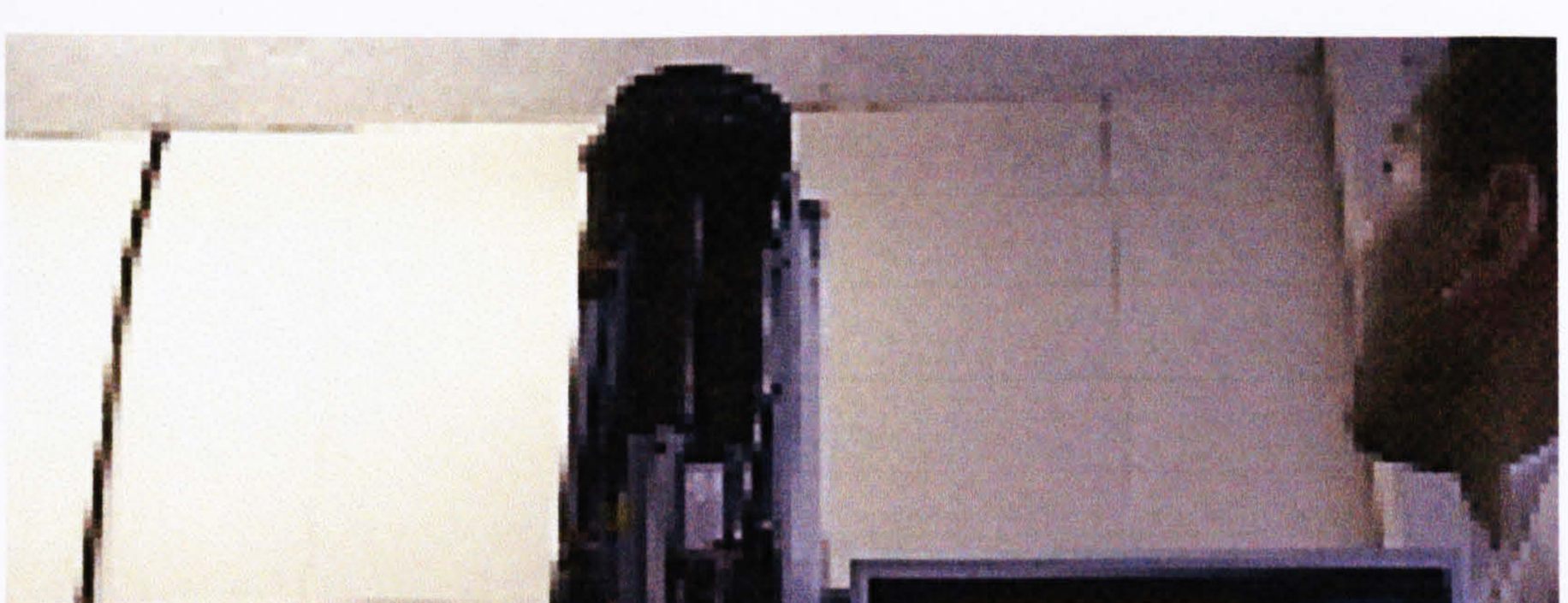

Figure D-8 Sensitivity and antiarc adjustment during EDT-system machining process under supervision